Organisation and dynamics of amphiphilic systems at the air - water interface

Stella Kirsten Peace

Organisation and Dynamics of Amphiphilic Systems at the Air - Water Interface

September 1996

Stella Kirsten Peace

Grey College

University of Durham

A thesis submitted to the University of Durham in partial fulfilment of the regulations for the Degree of Doctor of Philosophy.

Declaration

The work reported in this thesis has been carried out at the Interdisciplinary Research Centre in Polymer Science and Technology, Department of Chemistry, Durham University and at the Rutherford Appleton Laboratory in Oxfordshire between October 1993 and September 1996. This work has not been submitted for any other degree in Durham or elsewhere and, unless stated otherwise, is the original work of the author.

Statement of Copyright

Financial Support

The provision of a CASE award from the Engineering and Physical Science Research Council and ICI Paints, Slough to support this work is gratefully acknowledged.

Organisation and Dynamics of Amphiphilic Systems at the Air-Water Interface

Stella Kirsten Peace

Ph.D. Thesis September 1996

Abstract

The behaviour of polymeric amphiphiles, specifically systems containing poly(methyl methacrylate), PMMA, and poly(ethylene oxide), PEO, spread at the air water interface is reported. An amphiphilic graft copolymer containing a PMMA backbone and PEO side chains forms the main subject of the study. Films of PMMA spread onto a 0.1 wt.% solution of PEO have also been considered. Due to the presence of a surface excess, both PEO and PMMA populate the surface and the latter system provides a model of the graft copolymer.

Monolayer behaviour has been characterised by recording surface pressure isotherms. It has been demonstrated that the behaviour of the graft copolymers is highly composition dependent, exhibiting characteristics associated with the constituent homopolymers. In contrast the surface pressure isotherm for PMMA on PEO solution is quite unlike that for PMMA on water.

Details of the structural organisation in these systems have been determined using neutron reflectometry. The surface organisation adopted by the graft copolymers varies as the surface concentration increases. The PEO side chains penetrate the subphase and stretch increasingly whereas the PMMA backbone behaves much like the homopolymer. This is in contrast to the behaviour of PMMA on PEO solution where the PMMA occupies a wider region of the interface. The structure of the adsorbed PEO differs from that of the bare solution but maintains a constant surface excess.

Dynamic behaviour has been studied using surface quasi elastic light scattering. For the graft copolymers surface wave evolution is very unusual. The dilational parameters provide evidence, e.g. a negative dilational viscosity, indicating that surface wave propagation is complex and not described fully by current theories. Similar behaviour is exhibited by PMMA on a PEO solution. These features are believed to be associated with subphase penetration and are discussed in this context.

Acknowledgements

Many thanks are due to Randal Richards who has made the past three years great fun. His tireless enthusiasm, whether for SQELS, neutron reflectivity or gin and tonic is something I can only aspire to. His encouragement, patience and even nagging, 'pace yourself' etc.. will not be forgotten!

A big thank you is also due to Mark Taylor who has not only rebuilt the SQELS apparatus but has been a great help in discussing all aspects of the work.

Much of the work in this thesis has involved trips to the Rutherford Lab. This work would not have been so enjoyable, or so successful, without the much appreciated help of the instrument scientists, Jeff Penfold, David Bucknall and John Webster. I also thank all those from Durham who have given up their home comforts to help with these experiments, Helen Thompson, Antonio Brunacci, Mark and Randal.

The past three years would not have been so enjoyable without the many people who have been part of the IRC in Durham. I thank all those in both offices, particularly those who have been on the receiving end of my chatter (too numerous to mention). The synthetic lab has always been a good place to hide away for a chat and I thank Lian Hutchings and Tom Kiff for this, and for their help, advice and patience during my attempts at synthesis. I must also thank Julia Say and Alan Kenwright for their help with NMR, Gordon Forrest, the GPC king and Terry Harrison, the resident computer whiz.

Finally I must thank all my nearest and dearest. Richard whose support, patience and enviable calmness, not to mention cooking skills, have contributed much to my happiness. My tribe of chinchillas and guinea pigs have provided endless amusement and I thank Richard for putting up with us all! I also thank my family for all the encouragement and support they have given Richard and I over the last three years.

Preface: Units and Symbols

In this thesis standard SI units have been used where appropriate. However, in several of the areas of the work non - SI units are generally used. These conventions have been followed in the text, the following list provides conversions between these units and their SI equivalents

Unit	SI Equivalent
1 Å	10^{-10} m
1 mg	10^{-6} kg
1MHz	10^{6} Hz = 10^{6} s^{-1}
1 mm	10^{-3} m
1 µl	10^{-6} l = 10^{-9} m^{3}
1 µm	10^{-6} m
1 nm	10^{-9} m
1 mW	10^{-3} W = 10^{-3} J s^{-1}

Abbreviations

PMMA	poly(methyl methacrylate)
PEO	poly(ethylene oxide)
dPMMA	perdeuterated poly(methyl methacrylate)
dPEO	perdeuterated poly(ethylene oxide)
iPMMA	isotactic poly(methyl methacrylate)
sPMMA	syndiotactic poly(methyl methacrylate)

where i is used as a subscript this infers that the quantity may be expressed explicitly in terms of component i.

i	Component
MA	PMMA
EO	PEO
W	Water

Greek symbols

α	expansion coefficient
β	phase shift on traversing the layer
γ_{sub}	surface tension of subphase
γ_{oST}	surface tension of film covered subphase
γ	shear tension modulus
γ_o	SQELS surface tension
γ'	transverse shear viscosity
Γ	wave damping
Γ_s	surface concentration in mg m^{-2}
Γ^*_{sD}	surface concentration at the onset of the semi dilute regime
Γ^{**}_{SD}	surface concentration at the onset of concentrated regime
Γ_{si}	surface concentration of component i.
Γ^*_{brush}	surface concentration at the onset of brush type behaviour, from scaling laws.
Γ_{sLIM}	maximum surface concentration without subphase penetration, from area considerations.
$\Delta\rho$	difference in the scattering length density of air and subphase, $\Delta\rho = \rho_{-\infty} - \rho_{\infty}$
δ	separation of number density distributions along z axis
$\delta\theta$	scattering angle, SQELS
ε	static dilational modulus, also given by ε_{oST}
ε_o	dilational modulus
ε'	dilational viscosity
η	viscosity
θ	for neutrons the glancing incident angle
θ	for SQELS the incident angle measured relative to the normal to the surface
λ	neutron or capillary wavelength, depending on the context
ν	critical scaling exponent.
ν_θ	critical scaling exponent for theta conditions
ξ	'blob' dimension
$\xi(x,t)$	displacement

Π surface pressure, $\gamma_{sub} - \gamma_{oST}$

π osmotic pressure

ρ_i in the context of neutrons, scattering length density of layer or component i.

ρ in the context of SQELS, density of the subphase

Ω_i frequency of free, uncoupled, oscillator

σ_r root mean square amplitude of roughness

σ full width of Gaussian at n_i/e

τ_r relaxation time for Rouse movement

ϕ_i volume fraction of component i

χ_D displacement transfer function

χ_V velocity transfer function

χ interaction parameter

ω complex capillary wave frequency

ω_o wave frequency

Roman Symbols

A_2 second virial coefficient

A_{22} two dimensional second virial coefficient

b_i the scattering length of species i.

$D(\omega)$ dispersion equation

d_i thickness of the layer occupied by component i.

d_m dimensionality of the system

c solution concentration

c* solution concentration at the onset of semi dilute regime

d layer thickness

d_i thickness of layer i

$G^*(\omega)$ complex dynamic modulus

$G'(\omega)$ storage modulus

$G''(\omega)$ loss modulus

$g(\tau)$ correlation function in the time domain

$\hat{g}(\tau)$	generated correlation function
$h_{ii}(Q)$	self partial structure factor
$h_{ij}(Q)$	cross partial structure factor
I_o	incident intensity, neutrons
I	reflected intensity, neutrons
I_r	reflected intensity, SQELS
I_s	scattered intensity, SQELS
K	scattering vector for SQELS
k_B	Boltzmann's constant
k_i	incident wavevector
k_f	reflected wave vector
L	brush thickness
M_i	molecular weight of component i
M_j	matrix for layer i
M_{ij}	element ij of the matrix M
M_n	number average molecular weight
M_w	weight average molecular weight
m	coupling coefficient
N	number of segments, i.e. degree of polymerisation.
N_A	Avogadro's Number
n	neutron refractive index
n_i	number density of species i
n_{W0}	number density of bulk water
N	in the context of neutron theory the atomic number density
P_v	velocity power response
P_D	displacement power response
$P(\omega)$	power spectrum of the scattered light
Q	scattering vector
q	wavenumber
R	Rydberg constant
R_g	radius of gyration
R_{go}	unperturbed radius of gyration

R(Q)	reflectivity
r_{ij}	Fresnel coefficient between layers i and j
R(Q)	reflectivity
$R_s(Q)$	reflectivity of a sharp interface
R_{exp}	experimental reflectivity
R_f	Fresnel reflectivity
T	absolute temperature
T*	oscillatory strain modulus
T_g	glass transition temperature
w_i	weight fraction of component i
X_j	represents the four surface parameters
X	number of PEO side chains per chain of graft copolymer

Contents

Chapter One

Introduction

1.1 Polymers at Interfaces

Interfaces and related phenomenon play an important role in daily life. By varying the chemical nature and configuration of the molecules which populate an interface its properties may be modified. The behaviour of polymers at 'wet' interfaces, i.e. solid-liquid, liquid-liquid and liquid-gas, is of particular interest. There has been a significant amount of research in this field motivated, at least in part, by the many applications to commercial systems, for example colloidal dispersions.[1] Dispersions consist of a continuous phase, the dispersion medium, and a dispersed phase; the latter may be particulate or a fluid. To form a stable dispersion it is often necessary to add stabilisers. Such moieties reside at the interface between the dispersion medium and the dispersed phase and, by virtue of long range repulsive forces, maintain the dispersion. Due to their size polymer molecules provide ideal stabilisers. Although this field of science has only been quantified, and studied systematically, over the last 50 years the results of such phenomenon have been exploited for centuries. Egyptian ink, where carbon particles were retained in an aqueous dispersion by addition of carbohydrates, is an ancient example.

Although homopolymers may be used as stabilisers in most applications copolymers are used. Copolymers whose comonomers have very different solubilities exhibit a 'dual nature', a quality making them ideal for interfacial applications. For the specific case of emulsions, liquid-liquid dispersions, copolymers in which one component is insoluble in the disperse phase, while the other is soluble, are ideal stabilisers. In the case of aqueous emulsions such systems are termed 'amphiphilic'. An example of such a system being a poly(ethylene oxide) - poly(styrene), PEO - PS, diblock copolymer, where the PS forms the insoluble, hydrophobic block.

Polymers at the air - liquid interface may be viewed as providing model systems for the more complex interfacial behaviour of polymers in dispersions. In addition these systems comprise films of molecular dimensions, the properties and behaviour of which may be modified by controlling copolymer composition. This area is attracting increasing interest as such monolayers have possible applications in fields as diverse as electronic devices, bio sensors and microlithography. These applications are offered by films prepared at the air - water interface and then deposited onto a different substrate, so called Langmuir - Blodgett films. It follows that polymer monolayers at the air water interface constitute important

systems to study. A detailed understanding of behaviour and properties of the film at the air liquid interface is required, not only to predict behaviour in dispersions but also in regard to the formation of Langmuir - Blodgett films.

The remainder of this discussion is concerned with the study of polymers at the air water interface, the type of system studied in this work. There are two ways in which polymer molecules may populate this interface. A number of water soluble polymers, for example poly(vinyl methyl ether), PVME, and PEO,[2] exhibit considerable surface activity. As a result of this such polymers have a tendency to adsorb at interfaces and in aqueous solution form a surface excess, i.e. a region where the polymer concentration is greater than the bulk solution. Such systems are in a dynamic equilibrium as molecules adsorb and desorb from the interfacial region. By modifying the properties of the subphase[3] it may be possible to influence the structure, and hence properties, of the film. For soluble diblock copolymers behaviour may be controlled via composition, although there may be only a narrow window of compositions that remain soluble and form a surface excess.

The alternative method of obtaining films at the air water interface is to spread the films at the interface. In addition to water soluble systems, many of which also form spread films,[4] this enables monolayer properties of amphiphilic, insoluble copolymers to be studied. Films formed by this method may be compressed in a Langmuir trough so that properties can be studied as a function of surface concentration.

Films prepared by either of the methods outlined above may be studied in situ using a variety of techniques. Some of the major techniques which may be applied to the study of these films are mentioned briefly below. Particular emphasis is given to the methods used in this study.

The standard means of characterising the behaviour of spread films is to measure the surface pressure isotherm. This involves measuring the reduction in the surface tension of the water, the surface pressure, as the film is compressed. The technique was developed over a century ago, the first reports of its application to polymers go back as far as 1891.[5] Since Kawaguchi[6] has published an extensive review of the application of this technique to polymer films at the air water interface only brief details are given here. In principle surface pressure measurements provide information regarding molecular orientation which may enable details of the film structure to be inferred. A major advance in interpreting the surface pressure isotherm for polymeric systems has been the application of scaling laws. Developed by de

Gennes[7] these theories enable the thermodynamic interactions between the polymer and subphase to be quantified.[8] These theories have been applied to a number of studies and have also been utilised in this study.[9,10,11,12,13]

Although surface pressure isotherms are sensitive to very slight differences in spread film behaviour they provide little direct information regarding the structure adopted by polymers. To characterise monolayer behaviour fully and correlate properties to structural features requires additional techniques. Specific forms of microscopy have been developed for direct application to the air water interface. Fluorescent microscopy relies on the presence of a fluorophore; which may be added to a monolayer if not naturally present. Monitoring the fluorescence across the surface area provides details regarding in plane inhomogeneities. Recently monolayers of an insoluble lipid, dipalmitoylphosphatidylchloine, DPPC, spread on an aqueous solution of a PS - PEO diblock copolymer were studied in this way.[14] From the variation in the fluorescence across the surface it was shown that the spread films are inhomogeneous forming both condensed and expanded phases. In addition time resolved studies using this technique have enabled the lateral diffusion coefficient of fluorescent polymers to be determined.[15] The major disadvantage with this technique is the requirement of a fluorescent species, where this is added to the system there is always the possibility that behaviour is also modified. Brewster angle microscopy is a technique that has been developed relatively recently and offers comparable information to fluorescent microscopy without the need to have additional species in the system. The principle of the technique is that at the Brewster angle, 53.1°, light polarized parallel to the incident plane is not reflected; where the water is covered by a film the reflectivity increases. By exploiting this behaviour in-plane inhomogeneities, greater than 1 μm in dimension, can be identified.[16]

Ellipsometry may be applied to the study of many types of interfaces, the air water interface being a specific case. The technique relies upon changes in the ellipticity of polarised light caused by reflection at an interface and has been extensively reviewed.[17] Most workers have confined such studies to determining the difference in the ellipticity of clean water and the film covered surface.[16,18] One such study of PMMA[19] demonstrated that in plane inhomogeneities can be identified by this technique. The experiment is sensitive to both the film thickness and the refractive index but because these parameters are coupled they cannot be determined in a single experiment. Many workers have interpreted data by making

an assumption about one of the parameters.[16] In most cases there is no evidence to support this assumption.

Attenuated total reflection infrared spectroscopy has also been applied to the study of wet surfaces. Recently the results of a 'real time' study of the kinetics of polymers adsorbing onto a preformed layer has been published.[20] In addition there are studies of more conventional Fourier transform IR where by using polarised light the orientation of groups at the interface has been successfully determined. [21]

Despite all the valuable information offered by the techniques which have been mentioned they supply only limited information about film structure at a molecular level. The resolution of the microscopy techniques is not sufficient to provide information at a molecular level. Although the results of ellipsometry and surface pressure measurements may be interpreted in terms of structure the information is indirect and may rely on gross assumptions. In contrast the recent advent of reflectivity experiments can offer such information enabling the details of surface structure to be probed. The essence of these experiments is to monitor changes in the intensity of a reflected beam of X-rays or neutrons as a function of the scattering vector, Q. The variation in the reflectivity depends on the layer composition normal to the interface and is therefore rich in structural information. Although X-ray reflectivity has the advantage of high flux its neutron equivalent has been much more widely applied. While X-ray reflectivity has been shown to be successful in determining surface structure, due to the different processes which underlie the scattering interaction the two experiments exhibit distinct features (see a recent review by Penfold and Thomas[22] for further details). By exploiting isotopic substitution, generally H / D, neutron reflectivity offers the potential to determine the contributions of individual species to the reflectivity. In principle neutron reflectivity can enable a complete number density profile to be constructed for all the species at the interface. There is currently no other technique which can provide this information.

As neutron reflectivity is one of the major techniques used in this work a brief review of the applications are given. This is by no means intended to be a comprehensive review of the literature but rather highlights major work in the field.

Total reflection of neutrons was first reported in 1946 by Fermi and co workers.[23] The phenomenon was exploited in neutron optics for sometime and it was only relatively recently, in the 1980s, that the potential to study interfacial structure was realised. Since this time the technique has been developed considerably, the major pioneers being Penfold and Thomas.

Since the comissioning of CRISP[24] the U.K's first dedicated reflectometer in 1986 the technique has been applied to a wide range of systems and interfaces. The early studies, notably by Thomas, mainly involved the study of surfactants.[25,26] Selective deuteration was exploited and the experimental profiles analysed by modelling the surface structure, generating the reflectivity for this model and subsequently modifying the model as required. In 1990 Crowley et al[27] applied the kinematic approximation to the problem of neutron reflectivity and showed that, in principle, the reflectivity could be broken down into contributions from the separate components. Subsequently they demonstrated that the reflectivity could be expressed in terms of the separate contributions from the species at the interface.[28] In fact this depended, not only upon the number density of the species at the surface, but also on the separations of the different distributions. This method of analysis is rather more direct, and certainly more rapid, than modelling of the profiles directly. However, to extract the full information selective deuteration of all the components at the interface is necessary. For more complex systems this may not be possible.

Neutron reflectivity has been extensively applied to polymeric systems, see a review by Thomas.[29] The water soluble polymer PEO has been much studied in the form of both adsorbed[30] and spread layers.[31] These experiments proved that, contrary to popular belief, the two films do exhibit different structural behaviour. Different tacticity samples of poly(methyl methacrylate), PMMA, have also been widely studied.[32,33,34] The results were able to quantify the previous reports of different surface pressure isotherms associated with the different microstructures.[35,36] These studies have recently been extended to the study of copolymeric systems. A diblock copolymer of PEO and PMMA has been studied[37] and, by virtue of selective deuteration, the distributions of the two blocks and the water in the interfacial layer elucidated fully. Other recent studies include adsorbed films of poly(dimethyl siloxane) from toluene solution[38] and films spread on surfactant solutions.[16] The application of neutron reflectivity to polymers at liquid surfaces looks set to continue with the recent commissioning of a new reflectometer, SURF, designed specifically for experiments on liquids. With the additional features available on this instrument the next major stage in the development is expected to be application to polymers at liquid-liquid interfaces.

The other major technique used in this work is surface quasi elastic light scattering, SQELS. This technique, unlike all those described up to now, provides information on the dynamic behaviour and responses of monolayers to perturbations. The perturbations are

caused naturally by the thermal excitation and have frequencies in the range 10^3 - 10^6 s^{-1}. The experiment exploits the fact that these waves scatter light. The spectrum of the scattered light reflects the temporal evolution of the surface waves and depends upon the properties of the bulk subphase and, more importantly, certain surface parameters. The surface parameters which can be determined using this experiment can only be accessed by a limited number of techniques. Related experiments are those in which the surface roughening is generated by mechanical methods.[39] The major problem with this approach is that the surface is being unnaturally perturbed. By using only the thermally generated capillary waves one can be sure that the system is in a 'natural' state.

Like neutron reflectivity the SQELS experiment is a relatively recent development. Much of the development can be attributed to Earnshaw and co workers who have not only optimised the experimental technique[40] but have also developed a novel method of data analysis.[41] Earnshaw has demonstrated that by fitting a theoretical correlation function, the Fourier transform of the power spectrum of the scattered light, to the experimental data the four surface parameters which influence the surface wave propagation can be determined. There are two surface modes of interest to this experiment, the capillary waves and the dilational waves. Only the capillary waves scatter light; their evolution is governed by the surface tension, γ_o, and the transverse shear viscosity γ'. The latter term represents dissipative effects as the waves propagate across the surface. Because the capillary waves couple to the in-plane modes, the dilational modes, the analogous terms which influence their evolution ε_o and ε', the dilational modulus and viscosity respectively, also influence the capillary wave evolution. It has been demonstrated that inclusion of all these parameters is required to describe the surface wave propagation on monolayer covered surfaces.[41] In spite of this one of the major bodies of work which exists on polymer films includes analysis based on the fact that $\gamma' = 0$.[42,43,44] Such assumptions were necessary prior to the development of the direct fitting data analysis and unfortunately are still encountered. This makes comparison to the results of different studies, certainly those presented here, very difficult as the influence of neglecting γ' on the other surface parameters is not obvious.

In the last five years Richards and co workers have published a number of studies on polymeric systems.[45,46,47,48] The direct spectral fit pioneered by Earnshaw to determine all four surface parameters simultaneously has been applied to this data. Thus for the first time it is possible to compare the values of the parameters for low molecular weight surfactants, as

studied by Earnshaw, to those for macromolecular systems. The major difference is in γ' which appears to be larger for polymeric systems.

Recently unusual behaviour has been observed for certain systems: the dilational viscosity, ε', has been found to be negative. These effects were first observed for low molecular weight materials surfactants [49,50]and have subsequently been reported for polymeric systems,[47] up until now soluble systems. The current consensus is that negative dilational viscosities indicate that there are additional processes influencing surface wave propagation which are not understood fully and therefore not included in the theories. Work is currently in progress to modify the theories for wave propagation to account for this behaviour with an emphasis on polymeric systems.

1.2 Objectives

The objective of the work reported here was the elucidation of the surface organisation of polymeric amphiphiles using a combination of surface pressure isotherms and neutron reflectivity. By application of SQELS dynamic behaviour was investigated and where possible these properties are correlated to structural details. Two systems have been studied in this way. One system was an amphiphilic graft copolymer containing a PMMA backbone and PEO side chains. By preparing a series of these graft copolymers the dependence of surface behaviour on composition was investigated. The study of this copolymer, which is used commercially as a stabiliser, expands on previous studies of homopolymer PMMA[33,34] and PEO[30,31] and their diblock copolymer.[37,46] In addition this study extends the application of these surface techniques to polymeric systems of industrial relevance. The behaviour of films of PMMA spread on a solution of PEO was also studied. The surface organisation adopted by these polymers was studied at two concentrations, and the dynamic properties investigated using SQELS. The motivation for studying this system was to provide a model between the behaviour of the homopolymers and more complex copolymers. Thus the results of this study are compared and contrasted with the separate homopolymers and the graft copolymers.

1.3 References

1. D. H. Napper, *Polymeric Stabilization of colloidal dispersions*, Academic Press, (1989).
2. J. E. Glass, *Journal of Physical Chemistry,* **72**, 4459, (1968).
3. D. D. Eley, M. J. Hey, J. M. Speight, *J. Chem. Soc., Faraday Trans.*, **84**, 2069, (1988).
4. R. L. Shuler, W. A. Zisman, *J. Phys. Chem.*, **27**, 4459, (1970).
5. A. Pockels, *Nature,* **43**, 437, (1891).
6. M. Kawaguchi, *Progress in Polymer Science,* **18**, 341, (1993).
7. P. G. de Gennes, *Scaling Concepts in Polymer Physics,* Cornell University Press, (1979).
8. M. Daoud, G. Jannink, *Journal de Physique (Paris),* **37**, 973, (1975).
9. R. Vilanove, F. Rondelez, *Physical review Letters,* **45**, 1502, (1980).
10. D. P. R. Vilanove, F. Rondelez, *Macromolecules,* **21**, 2880, (1988).
11. A. Y. M. Kawaguchi, A. Takhashi, *Macromolecules,* **16**, 956, (1983).
12. A. Takahashi, A. Yoshida, M. Kawaguchi, *Macromolecules,* **15**, 1196, (1982).
13. Q. Jiang, Y. C. Chiew, *Macromolecules,* **27**, 32, (1994).
14. J. R. Charron, R. D. Tilton, *J. Phys.l Chem.*, **100**, 3179,(1996).
15 F. Caruso, F. Gruieser, P. J. Thistlewaite, D. N. Furlong, *Macromolecules,* **27**, 77, (1994).
16. E. K. Mann, L. T. Lee, S. Henon, D. Langevin, J. Meunier, *Macromolecules,* **26**, 7307, (1993).
17. R. Reiter, H. Motschmann, R. Lawall, M. Stamm, W. Knoll, preprint.
18. C. Amile, M. Sikka, J. W. Schneider, Y. H. Tsao, M. Tirrel, J. W. Mays, *Macromolecules,* **25**, 3125, (1995).
19. B. B. Sauer, H. Yu, M. Yazdanian, G. Zografi, M. W. Kim, *Macromolecules,* **22**, 2232, (1989).
20. K. Miyano, K. Asano, *Langmuir,* 7, 444, (1991).
21. R. A. Dluhy, D. G. Cornell, *J. Phys. Chem.*, **89**, 3195, (1985).
22. R. K. Thomas, J. Penfold, *Current Opinion in Colloid and Interface Science*, **1**, 23, (1996).

23. E. Fermi, W. Zinn, *Phys. Rev.*, **173**, 189, (1946).

24. J. Penfold, R. C. Ward, W. G. Williams, *J. Phys. E: Sci. Instrum.*, **20**, 1411, (1987).

25. E. M. Lee, R. K. Thomas, *J. Phys. Chem.*, **93**, 381, (1989).

26. J. Penfold, E. M. Lee, R. K. Thomas, *Mol. Phys.*, **68**, 33, (1989).

27. T. L. Crowley, E. M. Lee, E. A. Simister, R. K. Thomas, J. Penfold, A. R. Rennie, *Colloids and Surfaces,* **52**, 85, (1990).

28. T. L. Crowley, E. M. Lee, E. A. Simister, R. K. Thomas, *Physica B,* **174**, 143, (1991).

29. R. K. Thomas, in *Scattering Methods in Polymer Science,* Ed. R. W.Richards, Ellis Horwood, 1995.

30. J. R. Lu, T. J. Su, R. K. Thomas, J. Penfold, R. W. Richards, *Polymer,* **37**, 263, (1996).

31. J. A. Henderson, R. W. Richards, J. Penfold, R. K. Thomas, J. R. Lu, *Macromolecules,* **26**, 4591, (1993).

32. J. A. Henderson, R. W. Richards, J. Penfold, C. Shackleton, R. K. Thomas, *Polymer,* **32**, 3284, (1991).

33. J. A. Henderson, R. W. Richards, J. Penfold, R. K. Thomas, *Macromolecules,* **26**, 65, (1993).

34. J. A. Henderson, R. W. Richards, J. Penfold, R. K. Thomas, *Acta Polymerica,* **44**, 184, (1993).

35. R. H. G. Brinkhuis, A. J. Schouten, *Macromolecules,* **24**, 1487, (1991).

36. R. H. G. Brinkhuis, A. J. Schouten, *Macromolecules,* **25**, 2725, (1992).

37. R. W. Richards, B. R. Rochford, J. R. P. Webster, *Faraday Discussions,* **98**, 263, (1994).

38. L. T. Lee, O. Guiselin, B. Farnoux, A. Lapp, *Macromolecules,* **24**, 2518, (1991).

39. K. Tamada, K. Miyano, *J. Appl. Phys.*, **33**, 5012, (1994).

40. C. J. Hughes, J. C. Earnshaw, *Rev. Sci. Instrum.*, **64**, 2789, (1993).

41. J. C. Earnshaw, R. C. McGivern, A. C. McLaughlin, P. J. Winch, *Langmuir,* **6**, 649, (1990).

42. M. Kawaguchi, M. Sano, Y. L. Chen, G. Zografi, H. Yu, *Macromolecules,* **19**, 2606, (1986).

43 M. Kawaguchi, B. B. Sauer, H. Yu, *Macromolecules,* **22**, 1735, (1989).

44. F. E. Runge, H. Yu, *Langmuir,* **9**, 3191, (1993).

45. S. K. Gissing, J. A. Henderson, R. W. Richards, *Journal of Macromolecular Science-Pure and Applied Chemistry,* **A31**, 1109, (1994).

46. R. W. Richards, B. R. Rochford, M. R. Taylor, *Macromolecules,* **29**, 1980, (1996).

47. R. W. Richards, M. R. Taylor, *Journal of the Chemical Society-Faraday Transactions,* **92**, 601, (1996).

48. R. W. Richards, M. R. Taylor, In preparation.

49. J.C Earnshaw, E. McCoo, *Langmuir*, **11**, 1087, (1995)

50. J.C. Earnshaw, D. J. Sharpe, *J. Chem Soc. Faraday Trans*, **92**, 611, (1996)

Chapter Two

Theory

Section 2.1 Monolayer Behaviour

Surface tension is defined as the work required to create unit area of surface. The phenomenon arises due to the unbalanced molecular attractions at the surface.[1] When a liquid surface is covered by a film this balances some of the forces and the surface tension falls. The surface pressure, Π, exerted by the film is defined as the reduction in the surface tension of the fluid due to the presence of a film

$$\Pi = \gamma_{sub} - \gamma_{oST}$$

Equation 2.1.1

where γ_{sub} is the surface tension of the pure liquid and γ_{oST} is the surface tension of the film covered surface.

By studying the variation in surface pressure as a spread film is compressed information regarding the orientation of the molecules can be accessed. Depending on the strength of the lateral cohesive forces the film may exist in different states.[2] Classically three states have been defined to interpret the behaviour exhibited, these are gaseous, G, liquid condensed, LC, and liquid expanded, LE. A surface pressure isotherm for a system exhibiting these states is represented schematically in figure 2.1.1 where Π is given as a function of surface concentration, Γ_s. For low molecular weight substances Π is generally expressed as a function of molecular area. This convention is not used in this thesis as, for polymers, Γ_s can be interpreted more directly.

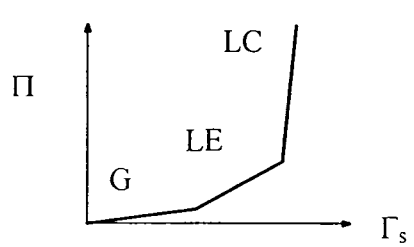

Figure 2.1.1 Schematic representation of the effect of changing monolayer states.

The isotherms of polymer monolayers do not exhibit as many features as smaller molecules. Generally the surface pressure increases more smoothly than for smaller molecules with no marked discontinuities. Polymer monolayers fall into two states,

condensed and expanded. Like liquid expanded films of smaller molecules these types of polymer films exhibit only a gradual increase in the surface pressure on compression. In contrast liquid condensed films are identified by their high rigidity. The lateral cohesive forces within the films, as well as the film subphase interactions, determine the characteristics exhibited by the monolayers.

It is conventional to extrapolate the region of the sharpest increase in the surface pressure to $\Pi = 0$ to determine a minimum area per molecule. In the case of simple molecules this value may provide information on the orientation of molecules. For polymers interpretation of this minimum area may be ambiguous as chain segments may be desorbed or partially coiled on the surface.

2.1.1 Equations of State

Equations of state provide mathematical models to describe monolayer behaviour using parameters which have physical significance. Fitting such models to experimentally determined surface pressure isotherms can yield information on the film interactions and consequently provide a greater insight into monolayer behaviour.

Quantitative theories to describe the behaviour of polymer monolayers in terms of molecular interactions have been much sought after.[3,4,5] Recent developments in scaling theories have contributed greatly to the understanding of surface pressure data. De Gennes[6] initially formulated scaling theories for homopolymers in three dimensions and these have subsequently[7] been extended expressing d_m, the dimensionally, explicitly. These advances have enabled scaling laws to be applied to behaviour in two dimensions.

2.1.2 Scaling Theory

Scaling laws are based on the fact that the physical properties of a polymer can be expressed as simple power laws of molecular weight and concentration. Such approaches have been developed in the last 15 years, notably by de Gennes.[6] Using this theory a description of behaviour in polymer solutions has been formulated. For a polymer in a good solvent, where the monomers repel one another, three separate concentration regimes exist, dilute, semi-dilute and concentrated. These treatments can be extended successfully to the

behaviour of polymer monolayers as these constitute two-dimensional solutions. The application of such theories enables the nature of the thermodynamic interaction between the subphase and chains to be investigated. A brief description of the pertinent points of the application of scaling theory to polymer solutions is given here with emphasis on the applications to two dimensional systems.

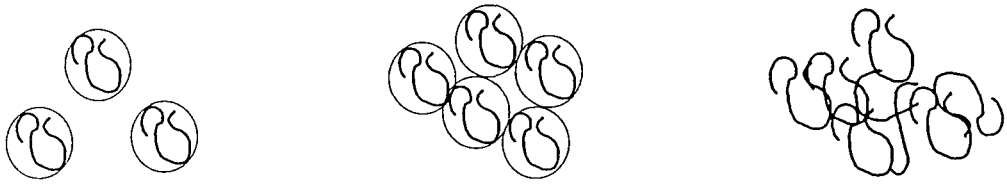

Dilute **Onset of semi-dilute** **Semi-dilute**

Figure 2.1.2 Schematic representation of the dilute regime and the onset of 'semi-dilute' behaviour where the chains first come into contact with one another. The final picture represents the significant chain contact in a semi-dilute solution.

2.1.2.1 The Dilute Regime.

In this regime the polymer chains are isolated from one another and only intrachain interactions are important. In a good solvent these interactions are repulsive and the chains swell. Each chain, of N monomers, behaves as a single chain with excluded volume and a radius of gyration, R_g, given by:

$$R_g \propto N^{\nu}$$

Equation 2.1.2

The quantity ν is an excluded volume exponent depending on the dimensionality, d_m, of the system. For a good solvent the exponent can be defined using the general Flory formula

$$\nu = \frac{3}{d_m + 2}$$

Equation 2.1.3

where d_m is the dimensionality of the system

By modelling the coils as impenetrable spheres, and applying a pseudo gas law an equation of state for the osmotic pressure, π, as a function of solution concentration, c, can be obtained:

$$\frac{\pi}{T} \propto \frac{c^2}{N} + A_2 c^2$$

Equation 2.1.4

where A_2 is the second virial coefficient and depends on the nature of the polymer solvent interaction, the better the interaction the larger A_2. In a theta solvent the interactions cancel out and the chains adopted their unperturbed dimensions so that $A_2 = 0$. This parameter, A_2, has been explicitly defined in terms of the degree of polymerisation, the dimensionality and ν by Daoud and Jannik.[7] Incorporating the dimensionality into this coefficient has enabled equation 2.1.4 to be translated to monolayer behaviour. The surface pressure, Π, of a dilute film is the two dimensional osmotic pressure and is given to a first approximation by:

$$\frac{\Pi}{RT} = \frac{\Gamma_s}{M_n} + \Gamma_s^2 A_{22}$$

Equation 2.1.5

where Γ_s is the surface concentration and A_{22} is the two dimensional virial coefficient, M_n is the number average molecular weight.

2.1.2.2 The Semi Dilute Regime

As the solution concentration increases the polymer chains are forced closer together and interchain interactions becoming increasingly significant. The onset of interchain interactions, occurring at c*, marks the transition from dilute to semi-dilute behaviour. As a consequence of this interpenetration the thermodynamic behaviour of the solution changes. Rather than view chains as separate entities, 'blob' theory is introduced. This involves modelling the chains as a succession of blobs of size ξ, rather like beads on a necklace. At distances less than ξ the chain does not interact with other chains and the behaviour is that of a single chain with excluded volume. In this concentration regime the thermodynamic properties reach a limit and are dependent on c but independent of N. In this situation the osmotic pressure is given by:

$$\frac{\pi}{T} \propto \frac{c^*}{M} \propto (c^*)^m \times \text{constant}$$

Equation 2.1.6

where $m = \nu d_m / (\nu d_m - 1)$

Once again this equation can be related to a similar transition in a monolayer, although it is hard to visualise a two dimensional equivalent of chain entanglement whilst all the monomers are maintained in the same plane. Despite this conceptual problem an equation equivalent to 2.1.5 can be written. This treatment applies for film concentrations at and above Γ_{SD}^*, where this concentration marks the onset of interchain interactions. The relation is given by equation 2.1.7.

$$\Pi \propto \Gamma_s^y \qquad \text{where } y = \frac{2\nu}{2\nu - 1}$$

Equation 2.1.7

The critical exponent, ν, depends on the dimensionality of a system, see equation 2.1.3; for a good solvent, $d_m = 3$, $\nu = 3/5$. In contrast for a theta solvent ν remains close to 0.5 for all dimensions.[8] There has been a substantial amount of work published reporting theoretical calculations of ν in two dimensions for these extreme situations. It is generally agreed that for a good solvent $\nu = 0.75$, the value predicted by Flory's mean field equation. There is more controversy about the value under theta conditions, ν_θ. Theoretical and computational simulations give values in the range 0.51 - 0.59,[9] the current consensus is agreed on $\nu_\theta = 0.55$. It follows that values of ν determined from experiments are expected to fall somewhere in the range 0.75 - 0.55, the higher the value the more favourable the polymer - subphase interaction.

2.1.2.3 The Concentrated Regime

As the concentration increases the 'blob' size decreases, eventually becoming comparable to the monomer dimensions. At this point behaviour is as for Gaussian chains with a radius $R = N^{0.5}$. It is no longer possible to describe behaviour in terms of the interactions between the different components and properties are universal. As a consequence of this there are no relations comparable to equations 2.1.5 and 2.1.7.

Section 2.2 Neutron Reflectometry

An interface has a number of unique properties associated with it. One of these is the boundary in refractive index which causes the reflective properties generally associated with light. A beam of neutrons exhibits behaviour analogous to that of light and may also be reflected an interface.

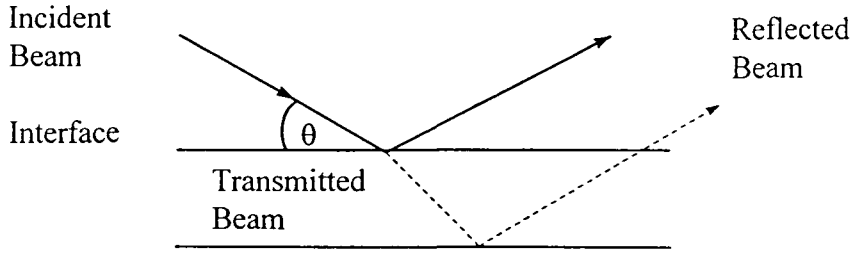

Figure 2.2.1 Representation of the processes

When a neutron beam impinges on a surface as illustrated in figure 2.2.1 the dominant processes are specular reflection, transmission and scattering from the bulk. Specular reflection occurs when the angle of reflection and incidence are equal. The reflectivity is defined as the ratio of the intensity of this specularly reflected beam to that of the incident beam. The essence of a neutron reflectivity experiment is to monitor changes in the reflectivity as a function of the scattering vector and relate these to structural variations normal to the interface.

The analogy between the reflection of light and neutrons also has a quantitative basis. It has been shown that the intensity of neutrons reflected across an interface follows the same laws as the s component of electromagnetic radiation.[10] The corollary of this is that the results of standard optics can be applied to neutron reflection with only minor modifications. Whereas in conventional optics behaviour is expressed in terms of refractive indices and scattering angles, in neutron optics it is usual to work in terms of wavevectors and scattering length densities. Ignoring the effects of absorption the neutron refractive index is given by:

$$n = 1 - \frac{\lambda^2 N b}{2\pi}$$

Equation 2.2.1

where λ is the neutron wavelength, N is the atomic number density and b is the scattering length of the atom.

The scattering length is a nuclear property and determines the amplitude of the reflected wave. Values of b for common nuclei are given in Table 2.2.1 Where the values are negative the beam experiences a phase change on interacting with these species. The most notable feature of Table 2.2.1 is the large difference in b for H and D. As a consequence of this D reflects neutrons strongly whereas H barely contributes to the coherent signal. In fact due to a large incoherent scattering cross section H mainly contributes to the incoherent background.

Nucleus	b / 10^{-4} Å
C	0.67
O	0.58
H	-0.37
D	0.68

Table 2.2.1: Scattering lengths for some commonly encountered nuclei.

The scattering length density, ρ, is related to b by

$$\rho = \sum_i n_i b_i$$

Equation 2.2.2

where n_i is the number density of the ith nucleus in the unit.

From equation 2.2.1 and 2.2.2 it follows that the neutron refractive index is related to ρ and the refractive index profile normal to the interface depends directly on the species populating the interface. From Table 2.2.1 it follows that by manipulating the H / D content of systems the reflective index, and therefore the reflecting properties of the system, can be modified whilst maintaining the same interfacial structure. This feature, which is common to neutron techniques, is one of the major advantages of neutron reflectivity. Table 2.2.2 contains examples of Σb_i and ρ for the species important to this work. Notice that for D_2O and H_2O ρ has different signs. Thus by mixing these materials in the correct proportion a

subphase which is 'invisible' to neutrons, $\rho = 0$, can be prepared. This is called null reflecting water, NRW.

Unit	Σb_i /10^{-4} Å	ρ /10^{-6} Å^{-2}
H_2O	-0.17	-0.56
D_2O	1.92	6.35
air	0	0
methyl methacrylate	1.49	0.90
methyl methacrylate - d_8	9.82	6.02
ethylene oxide	0.41	0.56
ethylene oxide - d_4	4.58	6.33

Table 2.2.2: Scattering lengths and scattering length densities

The scattering vector, Q, is the fundamental variable in neutron reflectivity, $Q = (4\pi/\lambda)\sin\theta$. The origin of Q becomes clear if the wavevectors of the incident and reflected light are considered, see figure 2.2.2. These have wavevectors k_i and k_f respectively, for reflection $k_i = k_f = 2\pi/\lambda$.

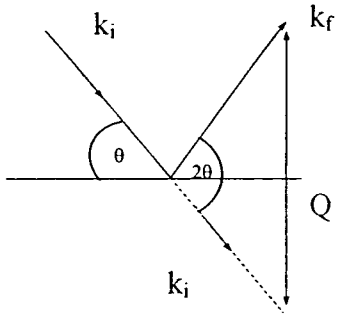

Figure 2.2.2 Wavevector diagram

The term 'scattering vector' is technically incorrect as Q only relates to the magnitude of the scattering vector. Despite this ambiguity this terminology is commonly accepted and is used throughout this work.

Full details of the theory of neutron reflectivity are provided in a number of texts.[11,12] As a consequence only a limited description of the more pertinent points are provided here.

Specular Reflection

From Snell's law, $n_1 \cos\theta_1 = n_2 \cos\theta_2$, the critical angle for total reflection, θ_c, at an interface between two bulk media of refractive indices n_1 and n_2 is:

$$\cos\theta_c = \frac{n_2}{n_1}$$

Equation 2.2.3

For the case of a neutron beam incident at an air - liquid interface $n_1 \approx 1$ and n_2 is close to 1 making θ_c small. The cosine term can be expanded and using equations 2.2.1 and 2.2.2 it can be shown that:

$$\theta_c \approx \lambda\sqrt{\rho/\pi}$$

Equation 2.2.4

Thus the critical glancing angle for total reflection at any interface depends on the scattering length of the interfacial media. For air / D_2O interface, using the values for ρ in Table 2.2.2 it can be shown that $Q_c = 0.0179$ Å^{-1}.

Standard multilayer optical methods provide the exact reflectivity for a system of discrete layers with differing refractive indices. Consider specular reflection from a single layer on a substrate, as illustrated in figure 2.2.3.

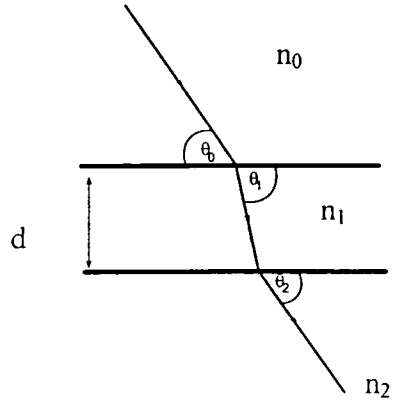

Figure 2.2.3 Thin film of thickness d and refractive index n_1 between two bulk media of refractive indices n_0 and n_2.

The reflectivity R is given by:

$$R = \left| \frac{r_{01} + r_{12} \exp(2i\beta)}{1 + r_{01} r_{12} \exp(2i\beta)} \right|^2$$

Equation 2.2.5

The quantity β is the phase shift on traversing the layer, $\beta = (2\pi/\lambda) n_i d \sin\theta_i$, r_{ij} are the Fresnel coefficients at the i - j interface and are given by:

$$r_{ij} = \frac{n_i \sin\theta_i - n_j \sin\theta_j}{n_i \sin\theta_i + n_j \sin\theta_j}$$

Equation 2.2.6

Equation 2.2.5 can be expanded to give:

$$R = \frac{r_{01}^2 + r_{12}^2 + 2 r_{01} r_{12} \cos 2\beta}{1 + r_{01}^2 r_{12}^2 + 2 r_{01} r_{12} \cos 2\beta}$$

Equation 2.2.7

Below the critical value of Q for either interface, R is constant at 1. However, as equation 2.2.7 shows, above this Q value the reflectivity exhibits maxima and minima when $\cos 2\beta = \pm 1$. To appreciate the implications of equation 2.2.7 fully it is helpful to express β in terms of the fundamental parameters of neutron reflectivity, namely Q. Thomas[11] has shown that:

$$\beta = \frac{Qd}{2} \left(1 - \frac{Q_c^2}{Q^2} \right)^{0.5}$$

Equation 2.2.8

Equation 2.2.8 indicates that β, and therefore the separation of the maxima, is determined by the thickness of the layer and value of Q_c. The latter quantity depends on the scattering length profile normal to the interface and thus the surface composition.

The major problem encountered with neutron reflectometry is extracting structural information from experimental profiles. There are two approaches to overcome this problem. In one the reflectivity profiles are fitted directly using modelling techniques. The other, the kinematic approximation, enables the contributions to R(Q) from the different species at the interface to be determined. Both have been applied in this study and are outlined below.

2.2.1 Direct Modelling of the Reflectivity Profiles

As has been outlined the reflectivity of a single layer can be described by standard optical methods, see equation 2.2.5. In theory the reflectivity of any number of layers can be calculated in this way although the computation rapidly becomes complex. Born and Wolf[13] pioneered a method which has proved very powerful for multilayer systems. They defined a characteristic matrix for each layer such that for the jth layer:

$$M_j = \begin{bmatrix} \cos\beta_j & -(i/n_j \sin\theta_j)\sin\beta_j \\ -in_j \sin\theta_j \sin\beta_j & \cos\beta_j \end{bmatrix}$$

Equation 2.2.9

The product of these matrices gives the resultant reflectivity matrix, M_r.

$$M_r = M_1 \times M_2 \times M_3 \ldots\ldots \times M_n = \begin{bmatrix} M_{11} & M_{12} \\ M_{21} & M_{22} \end{bmatrix}$$

Equation 2.2.10

The elements of this matrix then combine to give the final reflectivity.

$$R = \left| \frac{(M_{11} + M_{12}p_n)p_a - (M_{21} + M_{22})p_s}{M_{11} + M_{12}p_n)p_a + (M_{21} + M_{22})p_s} \right|$$

Equation 2.2.11

where $p_i = n_i \sin\theta_i$, the subscripts a and s represent air and subphase respectively.

Surface roughness reduces the reflected intensity.[14] Such effects can be accounted for by introducing a Debye Waller type factor of the kind:

$$I = I_o \exp(-Q^2\sigma_r^2)$$

Equation 2.2.12

where σ_r is the root mean square amplitude of the surface roughness.

Although this factor can be incorporated into equation 2.2.9 the additional complexity is such that for more than three or four layers the computation becomes unwieldy. It has been shown that dividing the interface into more layers is equivalent to incorporation of surface

roughness and the preferred approach is that of Abeles, as described by Heavens.[15] Once again a characteristic matrix is defined for each layer, in this instance the elements are expressed in terms of Fresnel coefficients and phase factors.

$$M_j = \begin{bmatrix} \exp(i\beta_{j-1}) & r_j \exp(i\beta_{j-1}) \\ r_j \exp(-i\beta_{j-1}) & \exp(-i\beta_{j-1}) \end{bmatrix}$$

Equation 2.2.13

As in equation 2.2.10 the resultant matrix, M_r, is given by the product of the matrices for the individual layers. The elements of this resultant matrix are related to the exact reflectivity by:

$$R = \frac{M_{21}M_{21}^*}{M_{11}M_{11}^*}$$

Equation 2.2.14

In practice the most common application of this approach, the optical matrix analysis, is to calculate the reflectivity for a system with n layers each with a thickness, d, and composition, ρ. This is then compared to the experimental reflectivity profiles and the model is adapted until the generated reflectivity profile reproduces the experimental data satisfactorily.

There are certain problems associated with this approach, the most significant is the question of the uniqueness of a model. Although this always remains an issue it can be addressed by collecting reflectivity profiles for a variety of different isotopic combinations or subphase and polymer, referred to as contrasts. In addition it is possible to use the fitted parameters to calculate the surface concentration.

The scattering length density of a layer is related to the scattering length density of each component,ρ_i, and their volume fractions,ϕ_i, by:

$$\rho = \sum \rho_i \phi_i$$

Equation 2.2.15

Once the volume fraction is known the number density can be determined using:

$$\phi_i \rho_i = b_i n_i$$

Equation 2.2.16

The calculation of the surface concentration of each component is given by:

$$\Gamma_s = \frac{n_i M_i d}{N_A} \times 10^{20} \quad \text{mg m}^{-2}$$

Equation 2.2.17

where M_i is the mass of a monomer unit, N_A is Avogadro's number and d is in Å.

Thus an additional constraint which can be imposed on the model is that it not only reproduces the reflectivity profiles for all the contrasts, but also the known surface concentration of the interfacial species. Although these constraints may not be sufficient to ensure that a truly unique model is found they do combine to provide additional confidence in any model of the surface structure.

2.2.2 The Kinematic Approximation

In principle application of the kinematic approximation to neutron reflectometry enables the different contributions to the reflectivity to be identified.[16] Assuming there is only weak elastic scattering the specular component of the reflectivity is given by:

$$R(Q) = \frac{16\pi^2}{Q^2}|\rho(Q)|^2$$

Equation 2.2.18

where $\rho(Q)$ is the one dimensional Fourier transform of $\rho(z)$, the scattering length density normal to the interface.

$$\rho(Q) = \int_{-\infty}^{\infty} \exp(iQz)\rho(z)dz$$

Equation 2.2.19

An equivalent expression in terms of the gradient of the refractive index profile, $d\rho/dz$ is

$$R(Q) = \frac{16\pi^2}{Q^4}|\rho'(Q)|^2$$

Equation 2.2.20

where $\rho'(Q) = \int_{-\infty}^{\infty} \exp(iQz)(d\rho/dz)dz$

Equation 2.2.21

When Q = 0 equation 2.2.21 becomes: $\rho'(0) = \Delta\rho$

$\Delta\rho$ is the step in the scattering length density between the two bulk materials. The reflectivity can then be written as:

$$R(Q) = R_s(Q)h'(Q)$$

Equation 2.2.22

where $R_s(Q) = \Delta\rho^2(16\pi^2/Q^4)$ and is the kinematic expression for the reflectivity of the sharp interface and h'(Q) is a structure factor that modulates $R_s(Q)$ according to the shape of the scattering length density profile across the interface. Notice that $R_s(Q)$ depends on the square of $\Delta\rho$ which expresses the phase problem associated with neutron reflectivity. Basically because $\Delta\rho = \rho_2 - \rho_1$ and only $\Delta\rho^2$ can be accessed the determination of ρ_2 and ρ_1 is subject to ambiguities. These effects are considered in more detail in chapter 4.

In principle with knowledge of R(Q) it should be possible to determine $|\rho(Q)|^2$ or $|\rho'(Q)|^2$ and perform Fourier transform to determine $\rho(z)$. In practise this is not possible because of the limited Q range available. The maximum Q value is limited by the incoherent background and is typically about 0.3 $Å^{-1}$.

As equation 2.2.22 demonstrates it is possible to access the structure factor, h'(Q). This structure factor depends on the whole scattering length density profile. Crowley et al[17] have shown by exploiting isotopic substitution it is possible to determine the contribution of the separate components to h'(Q). Substitution of equation 2.2.2 into equation 2.2.18 gives:

$$R(Q) = \frac{16\pi^2}{Q^2}\sum b_i b_j h_{ij}(Q)$$

Equation 2.2.23

When i = j, $h_{ii}(Q)$ the self partial structure of species i is obtained. This is related to the Fourier transform of the number density distribution, $n_i(Q)$, by:

$$h_{ii}(Q) = |n_i(Q)|^2$$

Equation 2.2.24

The cross partial structure factors $h_{ij}(Q)$ are given by a similar relation.

$$h_{ij}(Q) = \mathrm{Re}\{n_i(Q)n_j(Q)\}$$

To exploit this approach isotopic labelling is used so that n_i refers to the different groups in the system. The resolution of the experiment is too low for exploration of very fine detail and substitution is generally confined to large groups of atoms. Consider an A - B copolymer spread at the air water interface. The species of interest are blocks A and B and the water, W. Using these labels to describe the interface equation 2.2.2 becomes:

$$\rho = b_A n_A(z) + b_B n_B(z) + b_W n_W(z)$$

which gives, omitting (Q) in $h_{ii}(Q)$ for clarity:

$$R(Q) = \frac{16\pi^2}{Q^2}\left(b_A^2 h_{AA} + b_B^2 h_{BB} + b_W^2 h_{WW} + 2b_A b_B h_{AB} + 2b_A b_W h_{AW} + 2b_W b_B h_{WB}\right)$$

Equation 2.2.25

Clearly there are six unknowns in equation 2.2.25, knowledge of which constitutes a complete description of the distribution of species at the interface. To extract the structure factors six different reflectivity profiles are required so that simultaneous equations can be set up and solved at each Q. This can be achieved by deuterating species selectively. In the case of the diblock copolymer the problem is solved by deuterating each block selectively, then the entire polymer. Along with the fully hydrogenous version this provides four different isotopic composition copolymers. To collect six reflectivity profiles two different subphases are used, D_2O, and null reflecting water. Three profiles are collected for the part and fully deuterated copolymers on NRW, $b_w = 0$. Similarly the part deuterated copolymers and fully hydrogenated versions are spread on D_2O. Thus six reflectivity profiles can be generated each being driven by a different combination of deuterated polymer / subphase.

When the subphase is highly reflecting Crowley[18] has shown that the experimentally determined reflectivity must be corrected for multiple scattering events as these will limit the application of the kinematic approximation. To account for this the experimental reflectivity, R_{exp}, is scaled by the reflectivity for a smooth interface using the kinematic reflectivity, $R_s(Q)$, and R_f, the Fresnel reflectivity calculated by optical matrix methods. The so called Crowley correction gives the reflectivity as:

$$R(Q) = \left[\frac{1+(1-Q_c^2/Q^2)}{2}\right]\frac{R_{exp}-R_f}{1-R_f} + R_s$$

Equation 2.2.26

Having corrected the reflectivity data as required equation 2.2.25 is solved to yield the partial structure factors.

Interpretation of the partial structure factors requires models to be adopted to describe n(z) which on Fourier transform gives n(Q). There are certain requirements of any model of n(z): it is necessary that any model for n(z) will Fourier transform, ideally to give a relatively simple well behaved function for n(Q). Profiles which satisfy these requirements, and have been extensively used, are the uniform layer, the Gaussian distribution and the tanh profile. The details, and application of these models are best described by specific examples and are given in chapter 5.

The cross terms contain information about the relative positions of the distributions at the interface. When a distribution is moved a distance from the origin its Fourier transform is changed by a phase factor,

if $\quad n'(z) = n(z-\delta)$

then $\quad n'(Q) = n(Q)\exp(iQ\delta)$

The cross term between the two shifted distributions becomes:

$$h_{ij}(Q) = \mathrm{Re}\{n_i(Q)n_j(Q)\exp(iQ\delta)\}$$

Equation 2.2.27

When n(z) is totally even, generally true for species confined to the interface, its Fourier transform, n(Q), is real. Where n(z) is odd, generally true for subphase distributions n(Q) is imaginary.

For two even functions equation 2.2.27 simplifies to:

$$h_{ij}(Q) = \pm(h_{ii}h_{jj})\cos Q\delta$$

Equation 2.2.28

where ± represents the uncertainty in the phase.

For the cross term of an odd and even distribution:

$$h_{ij}(Q) = \pm(h_{ii}h_{jj})\sin Q\delta$$

Equation 2.2.29

Thus not only can the number density distributions of the individual species be determined by this analysis, but also their separations of these distributions. Combining this information enables a number density profile of all the species at the interface to be constructed.

Section 2.3 Surface Quasi Elastic Light Scattering, SQELS

The surface of a fluid is not flat but continually agitated due to thermal excitation. These surface fluctuations are only a few Ångstroms in amplitude and are governed by the restoring force of surface tension. Such fluctuations are essentially transverse to the surface and are referred to as capillary waves. Despite the microscopic dimensions of these waves they scatter light, the intensity of which reflects the temporal evolution of the surface waves. The evolution of the waves depends on the physical properties of the system, i.e. density, viscosity and surface tension. It follows that monitoring the intensity of the scattered light provides a non perturbative method of probing these properties.

When a monolayer is spread, or adsorbed, at this surface behaviour becomes rather more complex. As described by Goodrich[19] up to five modes of motion can be supported by a monolayer surface. In fact only two of these modes, the transverse shear and surface dilational are important to this study, these are illustrated below.

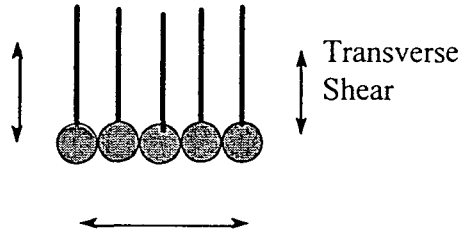

Figure 2.3.1 Surface modes of interest

Only the capillary modes, the transverse shear modes, scatter light significantly. While the dilational modes also cause fluctuations of dielectric constant the scattered intensity is negligible. Treatment of the surface fluctuations can be simplified by Fourier decomposition into complete sets of capillary and dilational modes. Consider the surface plane defined as the x-y plane. A two dimensional wave propagating in the x direction gives rise to an interfacial disturbance, ξ:

$$\xi(x,t) = \xi_0 \exp(i(qx + \omega t)$$

Equation 2.3.1

where ω is the wave frequency and can be expressed in terms of the spatial fluctuation which oscillates with frequency ω_0 and decays at a rate Γ, $\omega = \omega_0 + i\Gamma$. The quantity q is the wavenumber, given by

$$q = \frac{2\pi}{\lambda}$$

Equation 2.3.2

This interfacial disturbance acts as a weak phase grating, diffracting light incident on the surface. The angle of scatter, $\delta\theta$, can be related to q and the incident angle θ, in fact $q = 2k_0 \sin(\delta\theta/2)\cos\theta$, see figure 2.3.2.

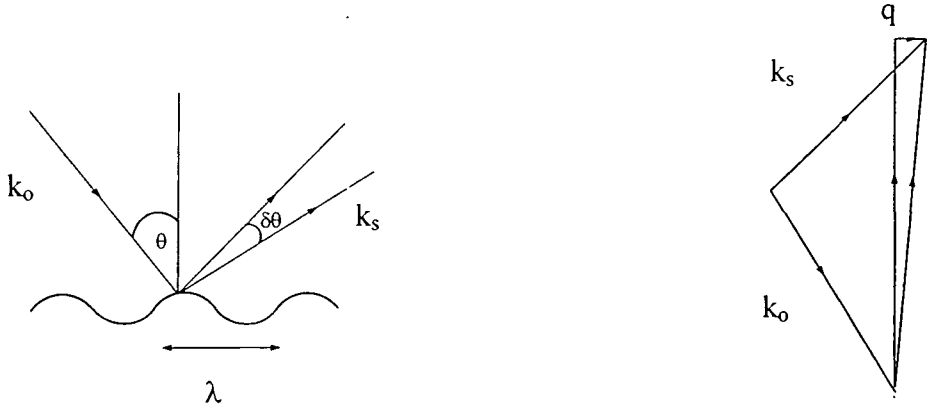

Figure 2.3.2 Scattering of light by a capillary wave. Also shown is the resultant vector diagram for the incident wavevector, k_o, and the scattering vector k_s.

The mathematical expression relating the physical properties of a system and q to the propagation characteristics of the surface modes, $\omega = \omega_0 + i\Gamma$, is called the dispersion equation. The general form for a monolayer at an air liquid interface,[20] where the superphase viscosity and density are essentially zero, is:

$$D(\omega) = \left[\varepsilon q^2 + i\omega\eta(m+q)\right]\left[\gamma q^2 + i\omega\eta(m+q) - \omega^2\rho/q\right] - \left[i\omega\eta(q-m)\right]^2 = 0$$

Equation 2.3.3

where $m = \sqrt{q^2 + \frac{i\omega\rho}{\eta}}$

There are two physically realistic roots to the dispersion equation, these correspond to the capillary and dilational waves. To a first order approximation the propagation characteristics of these modes are given by equations of the form $\omega = \omega_0 + i\Gamma$:

For the capillary waves:[21]

$$\omega = \sqrt{\frac{\gamma q^3}{\rho}} + i\frac{2\eta q^2}{\rho}$$

Equation 2.3.4

For the dilational waves:[22]

$$\omega = \tfrac{1}{2}(\sqrt{3} + i)(\varepsilon^2 q^4 / \eta\rho)^{1/3}$$

Equation 2.3.5

Despite the schematic representation in figure 2.3.1 the surface modes do not correspond to transverse and longitudinal waves, their motion is coupled, the coupling coefficient being $\eta(q - m)$. Only when the two modes are decoupled is it correct to refer to the modes as transverse and longitudinal. This is possible, under certain circumstances, for a liquid-liquid interface and has been discussed in number of texts, notably by Lucassen.[20]

Two surface moduli are also incorporated in equation 2.3.3. These are ε and γ which are familiar in the low frequency limit as the surface tension and the dilational modulus. The dilational modulus corresponds to the Gibbs static elasticity and is defined as $\Gamma_s \, d\Pi/d\Gamma_s$. This term influences the evolution of the dilational waves directly, γ influences the capillary waves. To account for loss processes within the surface layer these moduli are expanded to include dissipative effects:

$$\gamma = \gamma_0 + i\omega\gamma'$$

Equation 2.3.6

$$\varepsilon = \varepsilon_0 + i\omega\varepsilon'$$

Equation 2.3.7

where γ' is called the transverse shear viscosity and is a surface viscosity governing response to shear transverse to the surface. The quantity ε' is the dilational viscosity and is a surface viscosity associated with dilation in the surface plane. There is no clear consensus on the nature of these quantities. In the context of the results presented in this thesis, it is most informative to think of them as being directly related to the damping of the surface modes, γ'

being associated with the capillary modes, ε' with the dilational waves. Approximate equations for the influence of γ' and ε' on the appropriate modes are given in chapter 4.

The characteristics of the capillary waves, which actually cause the light to be scattered, depend predominantly on γ_o and γ'. However, because of the coupling to the dilational modes they are also influenced, albeit weakly, by ε_o and ε'. It is this coupling that makes it possible to extract information about all the surface parameters, γ_o, γ', ε_o and ε' despite the fact that only the capillary waves scatter light.

The spectrum of the light scattered by the capillary waves, $P(\omega)$, reflects their temporal evolution. The relationship between the spectrum of the scattered light and the dispersion equation is:

$$P(\omega) = \frac{-kT}{\pi\omega} \mathrm{Im}\left\{\frac{i\omega(q+m)+\varepsilon q^2}{D(\omega)}\right\}$$

Equation 2.3.8

where k is Boltzmann's constant and T is the absolute temperature.

Equation 2.3.8 approximates to a skewed Lorentzian with a central frequency ω_o and line width Γ. In the experiment, rather than record the power spectrum of the light its Fourier transform, $g(\tau)$, is collected.

$$g(\tau) = FT[P(\omega|X_j)]$$

Equation 2.3.9

where X_j represents the four surface parameters, γ_o, γ', ε_o and ε' and $P(\omega|X_j)$ is its value at a particular q.

The frequency shifts caused by the scattering are low, typically 10-100 kHz. To detect these small changes it is necessary to employ heterodyne detection. This method of detection involves mixing the scattered light with a reference beam so that the photomultiplier tube detects the scattered light beating against the reference frequency. The output of this detection is analysed in the time domain to give $g(\tau)$. The correlation function which is measured experimentally is related to the intensity of the scattered and reference intensities, I_s and I_r. To ensure that heterodyne detection dominates, the ratio I_s/I_r is maintained below 10^{-3}. Under

these circumstances the homodyne, or 'self beat' term is negligible and any spurious effects from the scattered light beating against itself are avoided.

2.3.1 The Cosine Fit

If the power spectrum, P(ω), were a true Lorentzian the Fourier transform would take the relatively simple form:

$$g(\tau) = B + A\cos(\omega_0\tau)\exp(-\Gamma\tau)$$

Equation 2.3.10

where A and B are the amplitude and background factors respectively.

In principle by fitting experimental data with equation 2.3.10 it should be possible to determine ω_0 and Γ. In fact it has been demonstrated[23] that this function does not reproduce the experimentally observed correlation functions and large non random residuals result. To improve on the fit significantly a number of additional terms must be incorporated into the fitting function. The full form becomes:

$$g(\tau) = B + A \times \cos(\omega_0|\tau| + \phi) \times \exp(-\beta^2\tau^2/4) + C\exp(-\alpha\tau) + D\tau^2$$

Equation 2.3.11

The phase term, ϕ, accounts for the fact that the power spectrum is a skewed Lorentzian. The term $\exp(-\beta^2\tau^2/4)$ is an instrumental function whose inclusion is necessary to correct for broadening of the intensity distribution of the scattered light. This arises because a finite number of waves are illuminated and more than a single surface fluctuation scatters the light.

The first few points of a measured correlation function follow an exponential decay, an effect attributed to after pulsing in the photomultiplier.[24] At sufficiently long sample times this only influences the first point of the function and by dropping this point the effect can be eliminated. It has been established that neglecting the first point of the function in this way does not bias the results of the fits. When the sample times are short, typically less than 2 μs, the effect influences more points and an additional term, $C\exp(-\alpha\tau)$, is incorporated into the fitted function to account for this.

The final term in equation 2.3.11, $D\tau^2$, accounts for the effects of external vibrations which cannot be completely eliminated. Such vibrations are slow and manifest as a low frequency oscillation or 'droop' superimposed on the correlation function.

By fitting equation 2.3.11 to the experimentally obtained correlation function it is possible to ascertain the frequency and damping of the capillary wave scattering light at that q.

2.3.2 The Spectral Fit

Although the cosine fit provides values of ω_o and Γ it provides no information on the surface parameters, γ_o, γ', ε_o and ε'. To determine the surface parameters a fitting technique is again employed but, due to the complex nature of the dependences, a more powerful routine is required. The four surface parameters all have a separate effect on the spectrum of the scattered light.[24] Relying on this fact a method of extracting these parameters without making any a priori assumptions has been developed.

This method, the direct spectral fit, involves fitting the experimental data with a generated correlation function. A 'model' correlation function is generated from values provided for the surface parameters. In the first step a power spectrum is generated according to equation 2.3.10. This spectrum is Fourier transformed, to give $\hat{g}(\tau)$, and is then fitted to the experimental autocorrelation function. The data are non-linear least squares fitted by varying the parameters and repeating the cycle until F, given by equation 2.3.12 reaches a minimum.

$$F = \sum_{i=2}^{128} [g(\tau_i) - \hat{g}(\tau_i)]^2$$

Equation 2.3.12

The fitted form of the correlation function is similar to equation 2.3.11, the damped cosine having been replaced by the Fourier transform of the spectrum:

$$\hat{g}(\tau) = B + A \times FT[P(\omega|X_j)] \times \exp(-\beta^2\tau^2/4) + C\exp(-\alpha\tau) + D\tau^2$$

Equation 2.3.13

2.4 References

1. A. W. Adamson, *Physical Chemistry of Surfaces,* Wiley-Interscience, (1990).
2. G. L. Gaines, *Insoluble Monolayers at Liquid -Gas Interfaces,* Wiley - Interscience, (1966).
3. S. J. Singer, *J. Chem. Phys.,* **16**, 872, (1948).
4. H. L. Frisch, R. Simha, *J. Chem. Phys.*, **27**, 702, (1957).
5. K. Motomura, R. Matuura, *Journal of Colloid Science,* **18**, 52, (1963).
6. P. G. de Gennes, *Scaling Concepts in Polymer Physics,* Cornell University Press, (1979).
7. M. Daoud, G. Jannink, *Journal de Physique (Paris),* **37**, 973, (1975).
8. P. Vidakovic, F. Rondlez, *Macromolecules*, **16**, 253, (1983).
9. R. Vilanove, D. Poupinet, *Macromolecues*, **21**, 2880, (1988).
10. M. L. Goldberger, F. Seitz, Phys. Rev., **71**, 294, (1947).
11. R. K. Thomas, in *Scattering Methods in Polymer Science,* Ed. R. W.Richards, Ellis Horwood, (1995).
12. J. Penfold, R.K. Thomas, *J. Phys.: Condens. Matter*, **2**, 1369, (1990).
13. M. Born, E. Wolf, *Principles of Optics,* Pergamon, (1980).
14. L. Nevot, P. Croce, *Phys. Appl*, **15**, 761, (1980).
15. O. S. Heavens, *Optical Properties of Thin Films,* Butterworths, (1955).
16. T. L. Crowley, E. M. Lee, E. A. Simister, R. K. Thomas, J. Penfold, A. R. Rennie, *Colloids and Surfaces,* **52**, 85, (1990).
17. T. L. Crowley, E. M. Lee, E. A. Simister, R. K. Thomas, *Physica B,* **174**, 143, (1991).
18. T.L. Crowley, *Physica A*, **195**, 354, (1993).
19. F. C. Goodrich, *Journal of Physical Chemistry,* **66**, 1858, (1962).
20. E.H. Lucassen-Reynders, J. Lucassen, *Adv. Colloid. Interf Sci.*, **2**, 347, (1969).
21. H. Lamb, *Hydrodynamics,* Dover, (1945).
22. L. Kramer, *J. Chem. Phys*, **55**, 2097, (1971).
23. J. C. Earnshaw, R. C. McGivern, *Journal of Colloid and Interface Science,* **123**, 36, (1988).
24. J. C. Earnshaw, R. C. McGivern, A. C. McLaughlin, P. J. Winch, *Langmuir,* **6**, 649, (1990).

Chapter Three

Experimental Techniques

Section 3.1 Surface Pressure - Surface Concentration Measurements

Two Langmuir troughs were available for measurement of surface pressure - surface concentration isotherms. The troughs were purchased from Nima Technology, Coventry, UK and are illustrated below. The essential details of the troughs were the same; both were fabricated out of teflon, mounted on a metal support and had motorised barriers.

In figure 3.1.1 the large circular trough is shown. This trough contained approximately 900 cm^3 of subphase and had two barriers which closed symmetrically around the pressure sensor. The enclosed area could be varied from 980 cm^2 to a minimum of 40 cm^2.

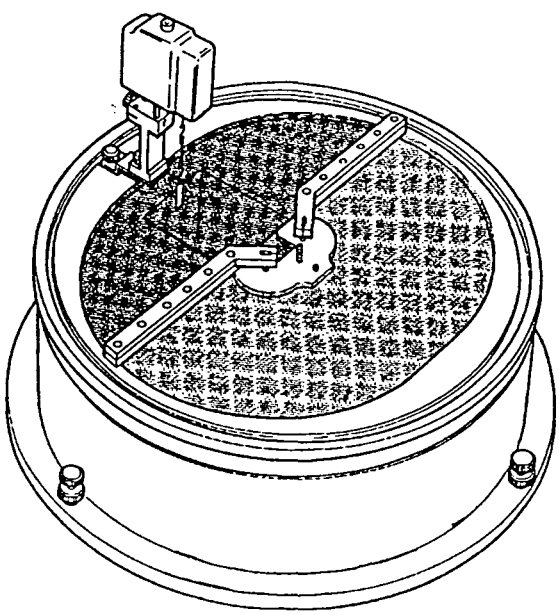

Figure 3.1.1 Circular Nima trough, figure reproduced with the permission of Nima.

The other trough was rectangular and as illustrated in figure 3.1.2 had only one barrier. Due to its size this trough covered a more limited surface area range, 550 cm^2 to 60 cm^2.

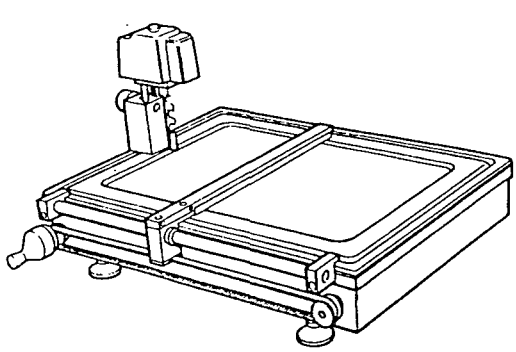

Figure 3.1.2 Rectangular Nima trough, figure reproduced with the permission of Nima.

The two troughs gave equivalent results and both have been used in the work reported here. For all measurements the trough being used was installed on a JRS electronic vibration isolation unit which was placed on a heavy optical table. Control of the subphase temperature was obtained by circulation of water through a network of tubes in the underside of the trough using a Haake thermostat water circulator. The subphase temperature could be maintained within ± 2 K of the set temperature using this arrangement.

3.1.1 Measurement of Surface Pressure

Surface pressure measurements were obtained using a Wilhelmy plate sensor attached to a displacement transducer. The Wilhelmy plate consisted of a 10 mm wide 20 mm long piece of high grade filter paper, Whatmans number 1. When suspended at an air water interface the plate is pulled into the bulk of the subphase by the surface tension of the subphase. In addition to the force of surface tension the weight of the plate provides a downward force, although the upthrust cancels this out slightly. By setting the sensor to zero with the plate in contact with the water the weight, upthrust and surface tension are compensated for. If, subsequently, the surface tension of the system decreases due to the presence of a surface active material the forces on the plate will change and the pressure sensor will detect a resultant force on the plate. This force depends on the difference between the surface tension of the bare and film covered subphase, i.e. the surface pressure.

3.1.2 Recording Surface Pressure - Surface Concentration Isotherms

The procedure for recording surface pressure isotherms and general film preparation, was as follows. Prior to use the trough was cleaned using swabs of Kimwipe tissue and chloroform. Once clean the trough was filled using water that had been distilled and passed through an Elgastat ultra high quality purification system, UHQ. The water surface was cleaned rigorously by closing the barriers of the trough to the minimum area and aspirating the enclosed surface. This method was continued until compressing the surface led to a surface pressure of 0.2 mN m^{-1} or less and the surface tension of water was reproduced, ~ 72.8 mN m^{-1}.

The films were formed by spreading a known volume of the polymer solution onto the desired subphase using a 100µl gas tight Hamilton syringe. For films of PMMA spread on

PEO solution following brief aspiration of the surface the PEO solution was left to equilibrate for ten minutes before spreading the PMMA film. Films were spread from 0.5 - 1 mg ml^{-1} solutions in chloroform.

Depending upon the subphase temperature a delay of 10 or 15 minutes was allowed to enable the solvent to evaporate. The films were then compressed under computer control using a specified barrier speed, the surface pressure was monitored every 0.02 s. The raw output from the transducer was converted to a display of surface pressure against surface area on a PC using Nima's software. Knowing the amount of material spread on the water surface enables the output to be converted to surface pressure against surface concentration, in mg m^{-2}, which is the format of the isotherms presented here.

3.1.3 Film Relaxation

Film relaxation processes can also be studied by setting the compression rate to zero, the surface pressure is then monitored as a function of time.

Section 3.2 Neutron Reflectometry

All neutron reflectometry results presented in this work were obtained at the ISIS pulsed neutron source at the Rutherford Appleton Laboratories, Oxfordshire. The majority of the work was performed using CRISP, the critical reflection spectrometer at ISIS. Some of the later work was performed using SURF a recently commissioned reflectometer dedicated to the study of fluid interfaces. Since the majority of the data presented was collected using CRISP this instrument is described in detail. A brief description of the advantages that SURF offers is given.

The neutrons at ISIS are produced by spallation. Protons are accelerated to high energies in a synchrotron and then bombard a tantalum target resulting in neutrons being 'chipped off' or spalled from the target. The protons do not bombard the target continually but are pulsed with a frequency of 50 Hz.

3.2.1 Experimental Details

The basic principle of these experiments was to monitor the neutron reflectivity, R(Q), as a function of Q, the scattering vector given by:

$$Q = \frac{4\pi}{\lambda}\sin\theta$$

Equation 3.2.1

where λ is the neutron wavelength and θ is the incident angle which, in neutron reflectivity, is defined from the horizontal.

Clearly the scattering vector, Q, may be varied either by using different incident angles or by using a range of neutron wavelengths. The particular method employed depends on the instrument and neutron source used. CRISP is a variable wavelength instrument enabling a range of Q to be covered while θ remains fixed.

3.2.2 CRISP

Figure 3.3.1 is a schematic of the CRISP instrument. Before emerging on the instrument illustrated the neutrons travel from the target station through the hydrogen moderator. The moderator reduces the energy of the incident neutrons so that the beam that emerges on CRISP is inclined at 1.5° to the horizontal and contains a wide range of neutron energies, hence wavelengths.

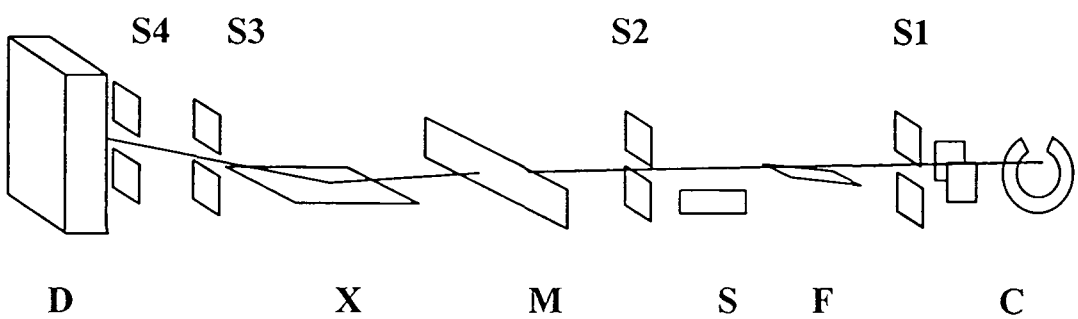

Figure 3.3.1 Schematic of CRISP

CRISP uses neutron wavelengths over the range 0.5 - 6.5 Å which, given an incident angle of 1.5°, enables a Q range from 0.05 to 0.65 $Å^{-1}$ to be accessed. Neutrons with wavelengths outside this range are excluded from the incident beam by a beam chopper, C in figure 3.3.1. The beam chopper is basically a disc that has a segment cut out of it rotating in synchronisation with the arrival of a neutron pulse from the target. The chopper is rotated so that neutrons of the correct velocity coincide with the gap and therefore pass straight through. Neutrons with velocities outside this range miss the gap and are stopped. By operating the beam chopper at the same frequency as the source, 50 Hz, every pulse of neutrons is used by CRISP.

Slow neutrons, i.e. long λ, have the potential to corrupt the specified wavelength range as they may reach the beam chopper coincidentally with fast neutrons of the succeeding pulse. Such out of sequence neutrons will pass through the beam chopper but are rejected by the nickel coated frame overlap mirrors, F in figure 3.3.1, which selectively reflect long wavelength neutrons. Thus by a combination of the beam chopper and the frame overlap mirrors the beam incident on CRISP at any one time will contain only neutrons from a single pulse with the desired wavelength range.

Collimation of the neutron beam is vital and, although this is effected crudely between the instrument and the moderator, fine adjustment is performed on the instrument. The slits S1 and S2 collimate the incident beam. For studies of liquid surfaces where $\theta = 1.5°$ these slits are generally set at 4 mm and 3 mm respectively. The incident beam flux, I_o, is measured following beam collimation just before the beam impinges on the sample using a beam monitor, M. The sample is placed at point X and the reflected neutrons pass through further slits, S3 and S4, onto the detector, D. In all work reported here a single scintillation detector was used.

CRISP uses time of flight detection thus exploiting the different arrival times of the different wavelength neutrons. The raw signal at the detector is converted to reflectivity by dividing the intensity of reflected neutrons by the intensity of the incident beam as monitored at M. The scattering vector, Q, is calculated by regrouping the time analysed data packages into corresponding wavelength data sets and combining these with the incident angle.

All the systems studied in this work contained poly(ethylene oxide) in some form. It is known that this polymer displays substantial subphase penetration[1] and low Q reflectivity data have been shown to be essential to characterise the behaviour of such systems fully. It is possible to access Q values below 0.05 $Å^{-1}$ by changing the incident angle, θ. Clearly for a solid sample it is trivial to tilt the sample and therefore vary θ. In the case of liquid surfaces it is necessary to alter the incident angle of the beam. This can be achieved by use of the supermirror, S, an additional component available on CRISP. The supermirror deflects the incident beam so that it strikes the sample at a lower incident angle; in this work θ was reduced to 0.8°. By using this incident angle a Q range 0.025 - 0.08 $Å^{-1}$ can be accessed. For $\theta = 1.5°$ the Q range covered was 0.05 - 0.65 $Å^{-1}$ so that combination of the two geometries not only enabled access to low Q but also provided a good region of overlap between the two data sets. Data at the higher angle extended far enough in Q to estimate the level of the flat isotropic background.

3.2.2.1 Operation

The geometry of CRISP was controlled by a command file which, following initial alignment of the optics at the two angles, moved the slits, detector and supermirror as required

for all subsequent runs. Alignment of CRISP is performed using a laser beam which is exactly coincident with the neutron beam.

A rectangular Langmuir Trough of exactly the same dimensions as that shown in figure 3.1.2 was used for all the reflectometry experiments. A perspex lid, with quartz windows to allow passage of the neutron beam, covered the trough during all experiments. The trough was placed on a height adjustable table mounted on a heavy anti vibration concrete plinth at point X in figure 3.3.1.

Alignment of the neutron beam depended on the height of the liquid surface. Whilst the position of all the other components in the flight path could be controlled on a command file this alignment was performed manually. The height of the water surface varied following the cleaning and deposition cycle so it was not possible to automate this stage of the alignment. The procedure following each sample and / or angle change was to check that the laser beam, and hence the neutrons, passed without obstruction onto the centre of the detector. When necessary the alignment was changed using the adjustable height table. The general method used was to monitor the reflectivity of each sample first of all at $\theta = 0.8°$ which was the most difficult angle to align. The geometry was then changed to $\theta = 1.5°$, the alignment optimised and then data collection was started. Typical data collection times were just under 1 hour at the low angle and 2 - 3 hours at the high angle.

3.2.3 SURF

SURF is the new reflectometer at ISIS designed specifically for the study of liquid surfaces. Its main advantage over CRISP is an increased neutron flux, achieved by placing the instrument closer to the target. When used in this study the components, and operation, of this instrument were essentially as for CRISP.

3.2.4 Data Analysis

The raw reflectometry data were reduced using data analysis software available at RAL. The reflectivity was placed on to a scale of absolute reflectivity following calibration of the instrument with D_2O. Calibration was performed at each angle by recording the

reflectivity profile for D_2O and using a fitting program to determine the factor required to convert the reflectivity onto an absolute scale.

Once all the profiles were placed on an absolute reflectivity scale the low and high angle data sets were combined to give a single data set covering the Q range 0.025 - 0.65 $Å^{-1}$. A flat background was subtracted from each profile by taking an average of the reflectivity at Q values above circa. 0.4 $Å^{-1}$ by which point the reflectivity has reached a stable level and no longer exhibits a Q dependence. Combined data files both with and without background subtraction, were written out as ASCII files for subsequent analysis.

3.2.4.1 Data Reduction: Kinematic Approximation

Where the data were to be analysed in terms of partial structure factors using the kinematic approximation additional data reduction was required. For profiles recorded on D_2O the background subtracted data sets were corrected according to the method suggested by Crowley.[2] This was performed using CORRECT a program available at the RAL. All data were then converted to the format $Q^4 \times R(Q)$ against Q using the program CONVERT, also at RAL. These files formed the input to the program which solved the kinematic equation and calculated the partial structure factors. Two such programs were available, PARTIAL2 and PARTIAL3. PARTIAL2 is used for two component systems, PARTIAL3 for three component systems.

3.2.4.2 Data Analysis: Optical Matrix Analysis

The reflectivity profiles have been fitted directly by application of the optical matrix modelling technique. The fitting program, PCMULF, an adapted version of a program available at RAL, was used throughout. The general procedure for fitting the profiles is described below.

A single layer model was applied initially and fitted to every contrast. The parameters of this layer, the scattering length density, ρ, and layer thickness, d, were varied to obtain the best fit. The fitting program returned a goodness of fit parameter, χ^2, the layer parameters were varied until the best fit was achieved. Any reasonable model of a system was expected to provide consistent layer dimensions for all the contrasts and to reproduce the spread surface concentration. Additional layers were incorporated in the model as required.

Section 3.3 Surface Quasi Elastic Light Scattering

3.3.1 Apparatus

Surface Quasi Elastic light scattering experiments were performed on an apparatus constructed in Durham which is shown schematically in figure 3.3.1. It was possible to vary the Langmuir trough used on the apparatus. Generally the large circular trough was used for surface concentration dependent studies as this enabled a wide Γ_s to be covered using a single film. In contrast, where the film concentration was fixed the rectangular trough was used.

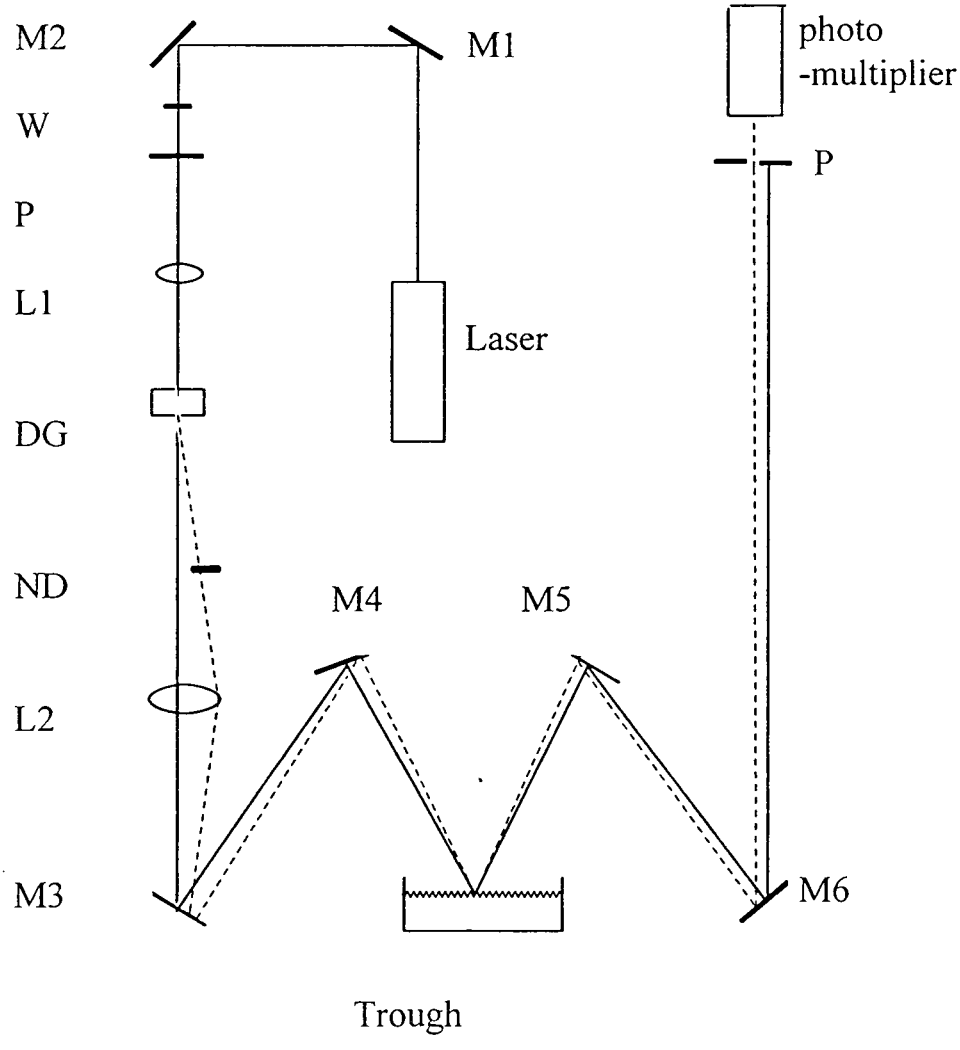

Figure 3.3.1 Schematic representation of the SQELS apparatus

The apparatus consists of a number of lenses and mirrors which periscope and focus the light onto the water surface and then collect the scattered light for detection. Under most

conditions, and certainly in this case, the frequency range accessible is limited by the intensity of the light source. The initial experiments were performed using a 30 mW He/Ne Laser, λ = 633 nm. Latterly this laser was replaced with a 100 mW diode pumped, continuous wave, YAG laser, λ = 532 nm. Both lasers gave equivalent data and results except that, by virtue of the additional power, the YAG laser enabled higher frequency measurements to be performed as well as significantly reducing data collection time and increasing the signal to noise. In both instances the light was polarised normal to the plane of incidence. The details of the experiment and apparatus are presented below and are independent of the laser used.

The laser was positioned parallel to the optical path so that the light beam had to be deflected up, across, and finally down the optical path. This was achieved using the mirrors M1 and M2 in figure 3.3.1. This series of reflections changed the polarisation of the light with respect to the incident plane so a half wave plate, W, was used to correct the polarisation. A polaroid filter was placed after the wave plate to ensure that only light of the correct polarisation was used, P.

Having passed through these components the light was now of the required polarisation for the experiment. Lens L1 focused the beam before it passed through a diffraction grating. Thereafter the diffracted beams diverged increasingly from the main beam as they travelled along the optical path. Those which constitute the reference beams were passed through a neutral density filter, ND, to attenuate the intensity. This was necessary to maintain a suitable ratio of the scattered beam intensity, I_s, to the reflected beam intensity, I_r, for heterodyne detection to occur. Neutral density filter 2 was generally used, although at the highest scattering angles it was sometimes necessary to increase the attenuation. This is because the scattered intensity decreases as the scattering angle increases and thus to maintain a suitable value of I_s/I_r for detection it sometimes became necessary to reduce I_r.

The diffracted beams are reconverged by lens L2 such that they are perfectly focused by the time the beam reaches the water surface where a single spot is formed. This reconverging beam is directed onto the water surface by a periscope arrangement of mirrors, M3 and M4. The light is reflected through 90° by M3 so that it follows a vertical path until it strikes the second mirror, M4, which reflects it down onto the liquid surface. The reflected light is collected in an analogous manner by mirrors M5 and M6 so that after reflection the light once more travels parallel to the optical path towards the photomultiplier. As the beam makes this journey, approximately 2 m long, the diffracted beams diverge so that by the time

they reach the photomultiplier tube, PMT, they appear as a horizontal row of spots. The most intense spot was the main undiffracted beam, the intensity falling off quite markedly as the diffracted order increases. Each of the spots about the main beam corresponded to a specularly reflected beam with a particular wavenumber, q. In addition to the specularly reflected light there was also a contribution from any light scattered from the main beam which fell at the same angle. A pinhole was placed in front of the PMT so that only one diffracted beam was incident on the PMT at any one time. The required beam was directed through the pinhole by tilting the final mirror M6, which was mounted on a motorised mount making fine adjustments possible.

The output of the photomultiplier tube was analysed using a 128 channel correlator, Malvern, Model K7025. The evolution of the correlation function was displayed during data collection on an oscilloscope linked to the correlator. The correlator was controlled by a PC using purpose written software, experimental data were also stored on this PC. The general procedure was to record ten correlation functions under constant conditions, be it fixed q or fixed Γ_s. Each was analysed separately and the results averaged.

Calibration of the instrument using water enabled the q values for each diffraction beam to be determined. Basically this involved recording ten correlation functions for pure water using each diffraction order of interest. This calibration procedure was performed at the start of an experiment before any films were spread. The correlation functions were analysed separately using the damped cosine fit and the results averaged to give the frequency and damping of the waves. The dispersion equation was then solved using the physical properties of water. A computer program, CANICE,[3] was available to solve the dispersion equation as a function of q, or one of the surface viscoelastic parameters. The predicted surface wave frequencies were plotted as a function of q. The q value of each diffraction beam was determined by reading off the q value corresponding to the frequency of the experimentally observed wave.

3.3.2 Experiments

There are three basic types of experiment which have been performed with this apparatus.

In one experiment a single reference beam was used while the surface concentration of polymer on the surface was varied. Generally a low value of q was used, ~ 220 cm^{-1}, as the signal to noise ratio was large and correlation functions could be collected in about 30 s. The general procedure, having calibrated this spot, was to spread the polymer film onto the Langmuir trough and, as previously, allow 10 mins for the solvent to evaporate. Correlation functions were then recorded at a number of surface concentration increments. Basically this entailed compressing the film, allowing the system to settle for 2 - 3 mins and then recording ten correlation functions, then repeating the cycle. In this way correlation functions corresponding to different points on the surface pressure isotherm were recorded.

In the alternative approach the spread film was compressed to a single, specified surface concentration. Correlation functions were then recorded using successive diffraction spots which had been calibrated previously. Once again ten correlation functions were recorded at each q value and were analysed separately. This experiment provides insight into the frequency dependence of the film's response.

A final experiment which has also been performed is that where both Γ_s and q are fixed. This experiment is used to investigate any time dependent behaviour in the system and its influences on surface wave propagation. Generally a low q spot was used, 200 - 300 cm^{-1}, so that correlation functions could be collected in 30 - 60 s. The experiment was set up to collect a large number of correlation functions and each was analysed individually. In contrast to previous experiments, the results of each analysis, not the averages, were plotted as a function of time.

3.3.4 Data Analysis

All correlation functions were analysed using both the damped cosine analysis and the spectral fit technique. The theory underlying these methods has already been presented, see

chapter 2, and it suffices here to mention briefly the details of the operation of the programs which perform these analyses. All data analysis programs ran on a PC.

3.3.4.1 Damped Cosine Analysis

The program FITS[3] performed this analysis using a least squares fitting routine. The correlation function formed the input to the fitting program along with initial estimates for the parameters of the fits. These were entered into a file which the program read automatically. In general this method of fitting the data were extremely robust and quick to implement, however as with any fitting process it was important that reasonable starting parameters were used. This is particularly true of the frequency and damping and whilst all other parameters were kept constant these were changed for each diffraction spot.

The quality of all the fits were examined by overlaying the fit onto the experimental data. Any fits which failed to reproduce the experimental data were excluded from the averaging process. An example of a typical fit is presented in figure 3.3.2.

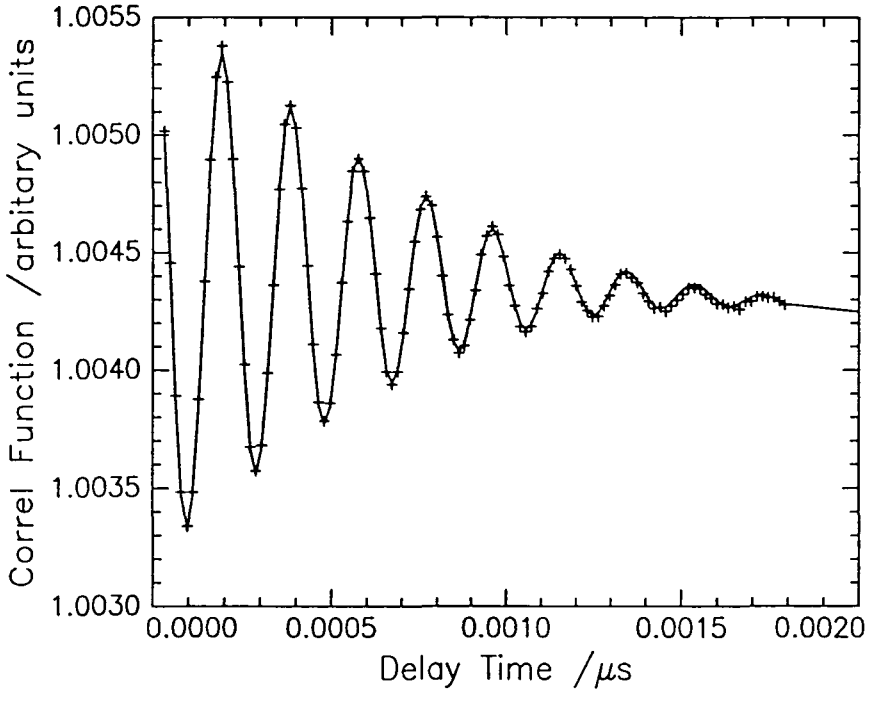

Figure 3.3.2 Experimental correlation function, crosses, with damped cosine fit overlaid, solid line. These data were recorded for graft copolymer 60CP at 0.2 mg m^{-2}, q = 220 cm^{-1}

3.3.4.2 Spectral Fit

The fitting function implemented to fit the correlation function directly is rather more sophisticated than the FITS program. Basically the program, HERMAN,[3] generates a theoretical spectrum using user defined starting points for the four surface parameters. This spectrum is then Fourier transformed to give the correlation function. The generated correlation function is compared to the experimental correlation function and a sum of squares obtained. The surface properties and other parameters of the fit are varied and the cycle is repeated until the sum of squares falls to a minimum. Once again it is important that reasonable starting parameters are supplied for the surface parameters. Initially the only information available for many of the systems was the static surface tension and dilational modulus. These were generally used in the initial attempts to fit the data. As no estimates existed for ε' or γ' the general procedure was to start these parameters at various values, ranging from 1×10^{-3} mN s m^{-1} to 1×10^{-5} mN s m^{-1}. In addition to defining starting values for these parameters boundary conditions to confine these parameters were specified. For γ_o and ε_o the search was made in the range 0 - 100 mN m^{-1}, for ε' and γ' the range was -1×10^6 - $+1 \times 10^6$ mN s m^{-1}. There were no a priori reasons for restricting the parameters to a narrower range.

The procedure for fitting data in this way was to start the parameters at the static values and guesses for ε' and γ'. The fits were started a number of times using different values for all the parameters. Depending on the quality of the fits extracted the parameters were started at different values in an attempt to ensure that the same fit was returned whether the parameters were started above or below the returned value. After much experimentation it was found that the following parameters were the most successful starting combination, γ_o = 60 mN m^{-1}, $\gamma' = 1 \times 10^{-4}$ mN s m^{-1}, ε_o = 5 mN m^{-1} and $\varepsilon' = -1 \times 10^{-4}$ mN s m^{-1}. As will be discussed the value of ε' was consistently returned as negative despite the fact that the initial value was positive. Attempts were made to fit the data by limiting ε' to positive values but the quality of the fits clearly decreased. All fits were examined by overlaying the experimental data and the fit. As can be seen in figure 3.3.3. once the optimum fit was achieved all the features of the data were reproduced successfully.

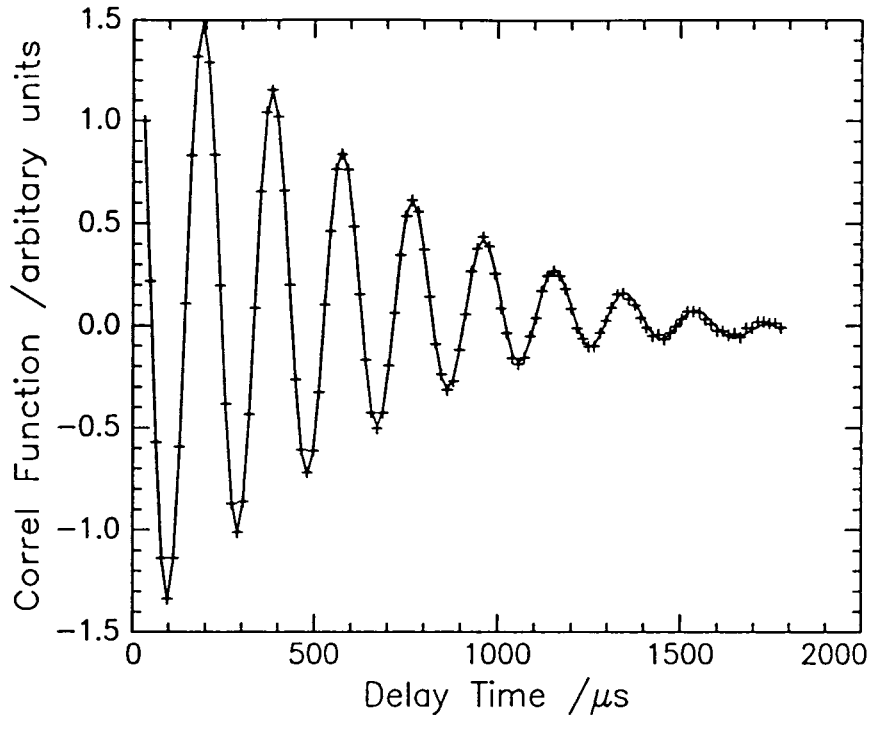

Figure 3.3.3 Experimental correlation function, crosses, with spectral fit overlaid, solid line. Same data as for figure 3.3.2.

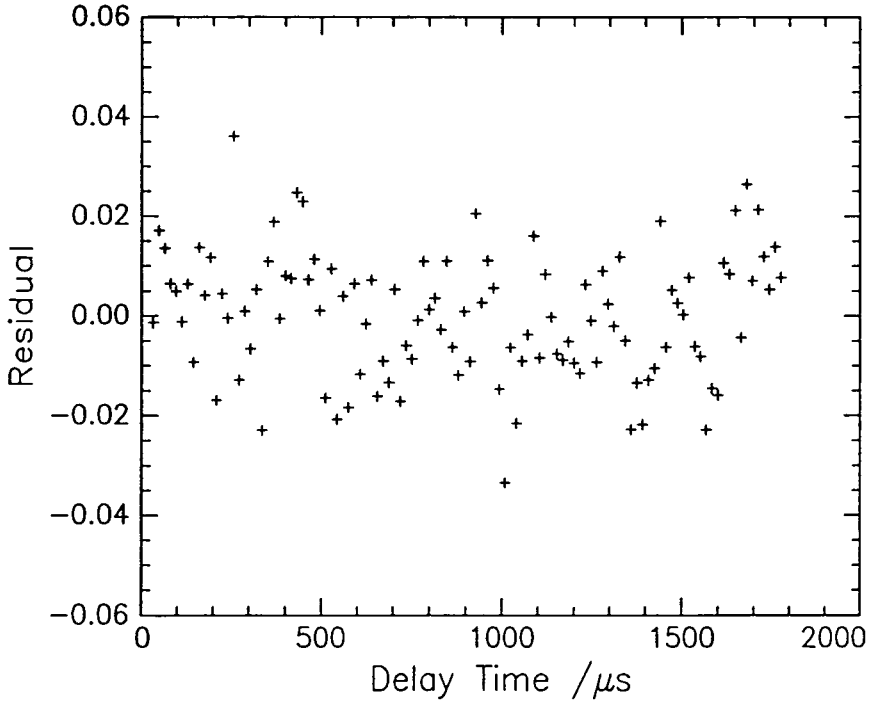

Figure 3.3.4 Residuals for the direct spectral fit given in figure 3.3.3.

3.4 References

1. J.A. Henderson, R.W. Richards, J. Penfold, J.R. Lu, R.K. Thomas, *Macromolecules*, **26**, 4591, (1993).
2. T. L. Crowley, *Physica A*, **195**, 354, (1993).
3. SQELS data analysis software was kindly made available by Professor John Earnshaw, Queen's University, Belfast.

Chapter Four

Graft Copolymers of Poly(methyl methacrylate) and Poly(ethylene oxide)

Section 4.1: Introduction

The number of homopolymers which display amphiphilic behaviour is limited. This can be attributed to the fact that to exhibit such behaviour a balance of hydrophobic and hydrophilic characteristics is necessary, requirements which are rarely met in homopolymers. In contrast, by preparing copolymers, species which exhibit these different types of behaviour can be incorporated into the same chain leading to the formation of amphiphilic polymers. By exploiting different architectures and controlling the composition of the copolymers there is scope for an enormous variety of different amphiphiles. The only disadvantage with such copolymers are the synthetic and characterisation problems which may be encountered.

There a wide variety of molecular architectures which may be exploited to form copolymers, for example stars, hyperbranched systems, diblocks and grafts. The subject of the study reported in this chapter is an amphiphilic graft copolymer and therefore the discussion is limited to such systems.

A graft copolymer is a polymer which differs from linear systems due to the presence of pendant side chains connected to the main chain backbone. Generally the side chains have constitutional properties different to those of the main chain and may even be composed of different blocks. The simplest case of a graft copolymer with a backbone comprised of monomer units A and side chain of units B is represented in the figure below.

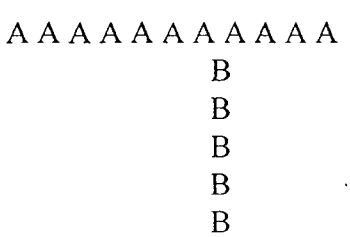

Figure 4.1.1: Representation of a simple graft copolymer

Due to the presence of two types of structural units graft copolymers have an intrinsic capacity for ordering. Crystallisation of long side chain polymers has been observed and was first suggested by Rehberg and Fisher.[1] Increases in T_g, the glass transition temperature, with increasing side chain length can be explained as arising from crystallisation of the side chain. This was later confirmed by X-ray work.[2]

As has been implied, graft copolymerisation is a common method for modifying polymer properties. In the case where the main chain and the backbone are thermodynamically incompatible, graft copolymers may form a multiphase solid state, analogous to polymer blends and block copolymers. Such phase separated systems can exhibit many unique thermal and mechanical properties which are highly composition dependent. Like block formation, grafting can improve tolerance to non-solvents and similarly graft copolymers are expected to exhibit micellisation behaviour.

Studies on a poly(methyl methacrylate) graft poly(styrene) copolymer[3] illustrated how the presence of grafts can radically alter the properties of polymer systems. With only two poly(styrene) grafts per hundred methyl methacrylate units the copolymer was soluble in pure cyclohexane unlike random or block copolymers of similar compositions.[3] Clearly, the solubilising effects of the side chains becomes operative at very low degrees of grafting. In a solvent mixture of dioxane and cyclohexane the same macromolecule was found to form intramolecular micelles in which the backbone and side chains are segregated. The backbone occupies the core of the micelle and the side chains wrap around it protecting from precipitation and association. This is behaviour more familiar with block copolymers.

Graft copolymers are not ideally suited to industrial applications due to problems associated with purification and characterisation. Despite this graft copolymers currently have a number of applications. The performance of natural rubber can be improved by effectively reinforcing the system with styrene grafts.[4] The hardness and modulus of elasticity are increased by the addition of only 30 parts of grafted material to 100 of ungrafted material without appreciable loss in tensile strength or elasticity. Dye retention can also be improved by grafting with a monomer which readily accepts the desired dye.[4] Strength, abrasion resistance, and crease resistance of cotton has also been increased by graft copolymerisation with vinyl monomers using gamma radiation.[4] The graft copolymer studied here is a commercial system which is used as a stabiliser in paints.

The graft copolymer system studied contains a poly(methyl methacrylate) backbone and grafts of poly(ethylene oxide). The constituent homopolymers, PMMA and PEO, exhibit very different behaviour, the former being a predominantly hydrophobic polymer whereas the latter is hydrophilic. As a result their graft copolymer, like a PMMA - PEO diblock,[5] exhibits amphiphilic properties. The aim of this study was to characterise the spread monolayer behaviour of these copolymers at the air water interface and to investigate how this varied

with copolymer composition. The monolayer properties of particular interest were the surface organisation adopted by these copolymers and the dynamic properties associated with the films. To perform this study and characterise these features of behaviour three major techniques have been employed. These are surface pressure measurements, neutron reflectivity and surface quasi elastic light scattering.

The following chapter reports the results of this study and is broken into six sections. Preparation and characterisation of the graft copolymers is discussed in section 4.2. Having prepared the copolymers their monolayer behaviour was characterised by recording the surface pressure isotherms, section 4.3. Section 4.4 reports the results of neutron reflection experiments and details of the surface organisation adopted by each of the copolymers. The results and implications of the surface light scattering study are presented in section 4.5. The influence of each composition graft copolymer on surface wave propagation at a single q has been studied and reported. In addition a frequency study of two of the three graft copolymers at fixed film concentrations is also reported. Conclusions inferred from application of the different techniques are summarised in section 4.6.

4.1.1 Abbreviations

The following abbreviations are used in this Chapter

PMMA	poly(methyl methacrylate)
PEO	poly(ethylene oxide)
MPEG	methoxy poly(ethylene glycol) macromonomer
Γ_s	Surface Concentration in mg m^{-2}
Γ_{sEO}	Surface concentration of PEO in mg m^{-2}
Γ_{sMA}	Surface concentration of PMMA in mg m^{-2}
ϕ_{MA}	Volume fraction of PMMA component.
ϕ_{EO}	Volume fraction of PEO component.
ϕ_W	Volume fraction of water.
d_w	Thickness of water layer in Å
n_w	Number density of water layer in $Å^{-3}$
d_{MA}	Thickness of PMMA layer in Å
n_{MA}	Number density of PMMA layer in $Å^{-3}$

4.2: Synthesis and Characterisation of the graft copolymers

Graft copolymers containing a poly(methyl methacrylate) backbone and poly(ethylene oxide) side chains have been prepared using a macromonomer. The macromonomer contained the PEO side chain capped by a methyl methacrylate monomer unit and was copolymerised with methyl methacrylate to form the PMMA backbone of the graft copolymer. The aim was to prepare a series of graft copolymers to enable the composition dependence of monolayer behaviour to be studied.

To obtain the maximum information from a neutron reflectivity experiment it is advantageous to deuterate the different components selectively. Attempts to prepare copolymers in which either the PEO side chain and / or the PMMA backbone are deuterated are also reported.

4.2.2 Synthesis of the Graft Copolymers

4.2.2.1 Monomer Purification

MPEG Macromonomer

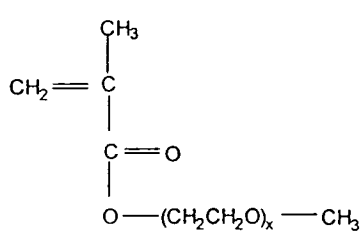

Figure 4.2.1 Structure of MPEG macromonomer

The methoxy poly(ethylene glycol) methacrylate macromonomer, MPEG, was supplied by ICI Paints contained in a propylene glycol / water solution. The monomer was extracted by removing the water by evaporation and then cooling to 273 K, at which point the monomer precipitated out. The MPEG was then washed in ice cold ethanol and dried under vacuum at room temperature.

The proton NMR spectra of MPEG dissolved in deuterated chloroform was recorded on a 400 MHz Varian machine. Proton NMR confirmed that the structure is of the form given in figure 4.2.1. The value of x was determined by NMR and was found to be 54 ± 2. This result was confirmed by aqueous Size Exclusion Chromatography measurements which gave $M_w = 2500$ and a polydispersity of 1.05.

To obtain the maximum information from neutron reflectometry experiments a perdeuterated version of this macromonomer was required. Polymer Labs attempted this synthesis but on receiving their product it became obvious that it contained a number of species. The final step of the reaction performed by Polymer Labs involved capping single end terminated methoxy PEG chains with methacryloyl chloride to provide the methacrylate functionality. This reaction appeared to be incomplete and was repeated at Durham in an attempt to complete the 'capping'. Unfortunately these attempts were not totally successful. On analysis it became clear that there was a significant distribution of PEG chain lengths. This had such a marked influence on the monolayer behaviour that the synthesis of perdeuterated copolymers was abandoned.

Methyl Methacrylate

Methyl methacrylate, MMA, was purchased from Aldrich chemical company. The hydroquinone monomethyl ether stabiliser was removed by washing with aqueous sodium hydroxide solution then water. Final purification was effected by reduced pressure distillation, the monomer was subsequently stored at 268 K.

Perdeuterated methyl methacrylate, dMMA, was purchased from Cambridge Isotopes. Like the hydrogenous version dMMA contained a considerable amount of stabiliser which was only removed immediately prior to use.

4.2.3 Polymerisation

The aim of the polymerisation was to prepare graft copolymers of different compositions and analogous part deuterated versions. The details of the synthetic procedure are given below. The basic structure of all copolymers prepared is given below in figure 4.2.2.

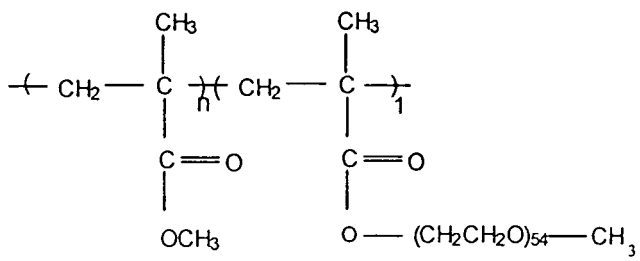

Figure 4.2.2 General Structure of the graft copolymers. By varying n different composition graft copolymers may be prepared.

4.2.3.1 Experimental Details

The polymerisation of the MPEG and MMA was effected by using a free radical reaction and azoisobutyronitrile, AIBN, as initiator. The reactants were mixed together in ethanol to form the feed and placed in a pressure equalised dropping funnel. Although the ratio of MPEG : MMA was altered to make the different copolymers the overall molar ratio of AIBN to total number of moles of monomer was kept the same at 1:221 in all experiments.

The reaction apparatus was thoroughly purged with nitrogen and a small amount of ethanol was placed in the reaction flask and taken to reflux. Once at reflux the feed was added dropwise over approximately one hour. On addition of the feed bubbling was observed and the solution became slightly yellow and viscous. Once all the feed had been added the system was refluxed for a further hour. The reaction product, a pale yellow viscous liquid, was poured into chilled hexane and a sticky, white product formed on precipitation. The precipitate was then dried under vacuum at room temperature. Further purification was required to remove residual unreacted MPEG.

The MPEG : MMA ratios aimed at were of the form 1 : n, where n is as given in figure 4.2.2 and took the values 60, 20, 10 , 5 and 1. Preparation of the MPEG homopolymer was

also attempted. The products were all labelled and referred to as nCP, the analogous part deuterated polymers are labelled nDP.

4.2.4 Purification of the Polymers

Unreacted MPEG monomer was found to be present in all samples after reprecipitation from 2-butanone into hexane. For the water insoluble polymers, namely 60CP and 20CP, the MPEG was removed by stirring the polymer in water then drying in vacuum at room temperature.

Fractionation was necessary to remove MPEG from 10CP. Although not water soluble this polymer was water sensitive and on exposure to water was observed to swell forming a gel like substance. Given this behaviour 10CP was purified by fractionation using ethanol as solvent and hexane as precipitant. The polymer rich lower phase which settled out following fractionation was poured into cool hexane, a white powder settled out immediately. This was removed by filtration and dried under vacuum.

The methods for purifying the part deuterated copolymers were as described above. The syntheses of the 1 : 5, 1 : 1 and MPEG homopolymers were unsuccessful. Further attempts were made to prepare the homopolymer of MPEG but even increasing the initiator concentration tenfold and refluxing for 24 hours failed to produce a polymer.

4.2.5 Characterisation of the Polymers: Composition determination

Introduction

Proton NMR and elemental analysis were used to characterise the polymers once prepared. An outline of the methods used and the results is given below.

4.2.5.1 Proton NMR

Proton NMR were recorded in deuterated chloroform on a 400 MHz Varian machine. The ^{1}H NMR spectra for all the polymers contained a broad band in the 3.5-3.7 ppm region, see the example in figure 4.2.3. The protons in the PEG chain and the terminal ester methyl protons in the MMA fall in this region. The peak at 3.4 ppm arises from the terminal methyl

on the MPEG monomer. By equating this integral to three protons the number at resonance between 3.5 - 3.7 ppm can be determined. From this information the number of MMA protons at resonance can be calculated providing the copolymer composition.

This method was applied to all the polymers but was less successful with increasing MPEG content. There were some problems in calculating the integral for the broad band in the spectra as it is difficult to approximate correctly to the base line. The error on the integrals was estimated to be ± 2% and becomes increasingly significant as the MMA content falls. Thus, although ^{1}H NMR was used to characterise the 1:20 and 1:60 polymers it was not suitable for the 1:10 version.

The part deuterated copolymers were also characterised using ^{1}H NMR. The method used was to weigh accurately approximately 4 mg of tetramethylsilane and 40 mg of deuterated polymer into a dried NMR tube. The composition was obtained from calculating the number of moles of TMS added and therefore the number of protons at resonance at ~ 1 ppm, the only signal from TMS. The integrals could then be normalised and the composition of the polymer calculated since the total mass added was known. This treatment assumes that all the ^{1}H present in the part deuterated polymers were from the MPEG macromonomer.

4.2.5.2 Elemental Analysis

Elemental analysis was also used to calculate composition. The percentage carbon in a sample of graft copolymer is related to n as shown below.

$$\%C = \frac{(113 \times 12) + (5 \times 12 \times n)}{2476 + 100n}$$

In determination of composition the percentage of carbon, % C, was used since being the larger figure it should be less subject to errors from background etc. It can be shown that provided n is less than 20 there is a rapid change in % C and such compositions can be distinguished. However, when n > 20 the limit of reproducibility of the method, which is ±0.4% for carbon content, corresponds to a composition change of n = 56 to n = 83.

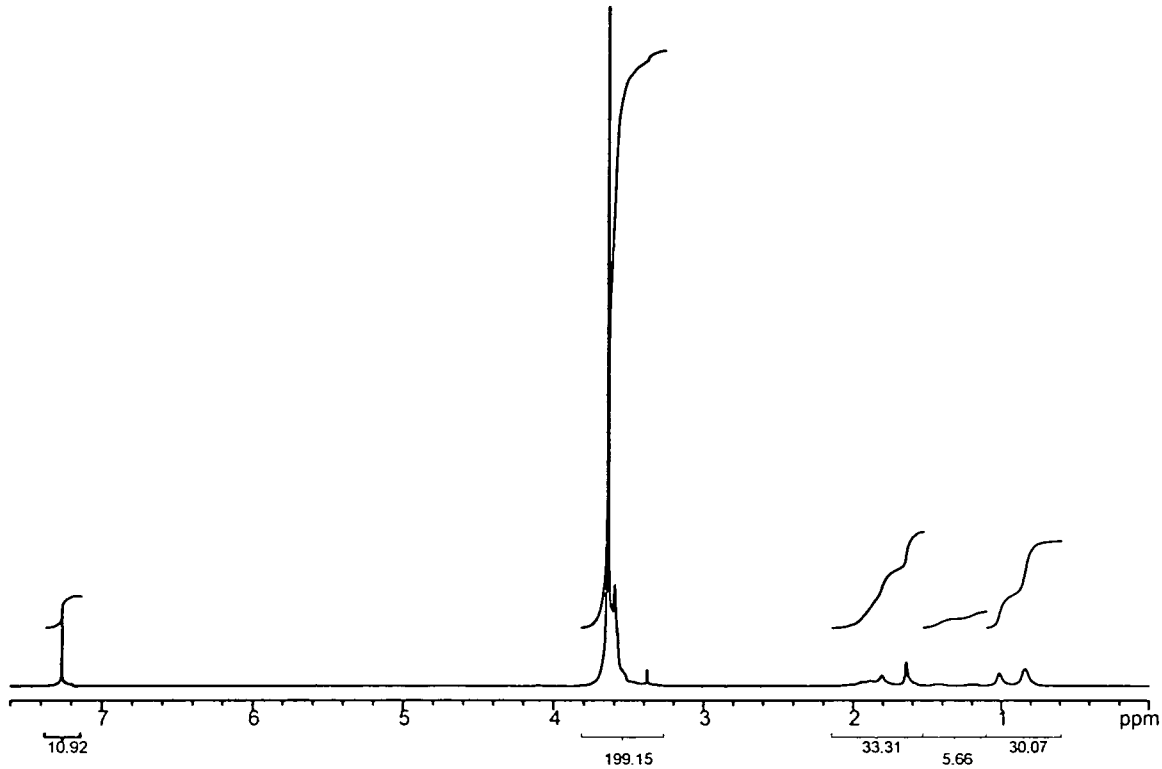

Figure 4.2.3 Example of 1H NMR spectra for 20CP. The integrals were expanded to determine composition.

4.2.5.3 Results of Composition Determination

Proton NMR

A ^{1}H spectrum representative of those obtained for all the hydrogenous polymers is given in figure 4.2.3. The only change in spectra with composition are the values of the integrals. The results of the composition determination are presented table 4.2.1.

Sample	MPEG : MMA	EO : MMA units
60CP	1:56 ± 2	54 : 57
60DP	1:59 ± 3	54 : 60
20CP	1:19 ± 2	54 : 20
20DP	1:16 ± 3	54:17
10CP	1:7 ± 4	54 : 8
10DP	1:5 ± 4	54 : 6

Table 4.2.1: Copolymer composition as determined using ^{1}H NMR.

Elemental Analysis

Samples of 10CP and 10DP were submitted for elemental analysis. The results are given in Table 4.2.2.

Sample	% of C	% of H	n
10CP	56.40 ± 0.16	9.05 ± 0.05	12 ± 2
10DP	56.52 ± 0.10	9.10 ± 0.10	11 ± 2

Table 4.2.2: Results of Elemental Analysis. Given that 10DP is deuterated it is unlikely that the value of %H can be linked in a simple way to composition.

4.2.6 Conclusion

The copolymer compositions were determined successfully using a combination of ^{1}H NMR and elemental analysis. The results are given below in Table 4.2.3.

Polymer	MPEG : MMA	Mass % EO
60CP	1 : 56 ± 2	30 ± 1
60DP	1 : 59 ± 3	29 ± 1
20CP	1 : 19 ± 2	55 ± 3
20DP	1 : 16 ± 3	60 ± 4
10CP	1 : 12 ± 2	70 ± 4
10DP	1 :11 ± 1	66 ± 2

Table 4.2.3: Copolymer composition

In addition to the copolymer composition there is also the question of the tacticity of the samples, as well as the distribution of the PEO side chains. To characterise these features ^{13}C NMR is required. Although attempts were made to extract ^{13}C spectra problems were encountered due to the signal from the PEO side groups which essentially swamped more subtle influences associated with the features mentioned. However, it is known that free radical polymerisation of MMA gives rise to a predominantly syndiotactic polymer.[6] This is attributed to repulsion between the methyl group at the polymer end and that of the approaching monomer. Similar behaviour is anticipated in the presence of the macromonomer and thus the graft copolymers prepared are expected to contain predominantly syndiotactic PMMA.

To determine the distribution of the side chains fully required a sample of homopolymer MPEG. Despite forcing conditions, attempts to prepare this polymer failed. This is attributed to the steric bulk of the side chains. This result in itself implies that the formation of a sequence of MPEG units is unfavourable and it is concluded that the copolymers are predominantly random, although the extent of the 'randomness' remains unknown.

4.2.7 Molecular Weights: Size Exclusion Chromatography

4.2.7.1 Experimental

All the polymer samples were submitted for size exclusion chromatography using chloroform as solvent and toluene as flow marker. The instrument used had three gel columns with pores sizes 10^5, 10^3 and 100 Å and 5μm gel beads. A Waters differential refractometer (model R401) was used for detection and the system was calibrated using polystyrene standards.

4.2.7.2 Results

The following results were obtained from SEC. To obtain reproducible results the solutions had to be prepared in dry solvents and left to stand for 2 - 3 days. The results are presented below in Table 4.2.4.

Polymer	M_w / g mol^{-1}	M_n / g mol^{-1}	M_w/M_n
60CP	83600	55400	1.5
60DP	56800	24000	2.4
20CP	96900	62400	1.6
20DP	71100	43200	1.7
10CP	120400	87200	1.4
10DP	82700	39400	2.1

Table 4.2.4: SEC results for the graft copolymers.

4.2.8 Thermal Analysis

4.2.8.1 Introduction

The glass transition temperature, T_g, is a characteristic parameter of a particular polymer. At a molecular level the glass transition temperature corresponds to the temperature at which all long range molecular motion ceases.

As one would anticipate from the molecular phenomenon which underlay the glass transition, it is characterised by marked changes in physical properties. These range from the modulus, heat capacity and specific volume of a polymer. Due to a discontinuous change in many characteristics of behaviour there is therefore a variety of ways in which T_g can be monitored. Experimentally determined T_g values are found to depend on both the method of measurement and the thermal history of the sample.

4.2.8.2 Experimental

The glass transition temperature for all the polymer samples was determined using a power compensated Perkin Elmer DSC7. The instrument operates in the range 173 - 950K and can use heating rates between 0.1 - 200 K min^{-1}. Samples for analysis were weighed, sealed into aluminium capsules and placed in the heavily insulated DSC head. The basic principle of the machine is to vary the temperature of the sample and reference material during controlled heating or cooling cycles, whilst maintaining zero temperature gradient between the two. The energy flow in / out of the sample cell is compared to the inert reference, usually an empty cell, as a function of temperature. The resultant thermogram represents the amount of energy supplied to maintain zero temperature gradient across the cells as a function of temperature. Clearly the area under any maxima or minima in this thermogram will be proportional to the enthalpy changes exhibited by the sample.

All data were recorded using heating runs and a heating rate of 5 K min^{-1}. The temperature range used was 203 K to 373 K. All samples were run on a thermogravimetric analysis machine, TGA, before performing DSC to ensure that there was no degradation over the temperature range used.

4.2.8.3 Results

The DSC traces are given overleaf, figure 4.2.4. The glass transition temperatures for each copolymer are given in table 4.2.5.

Sample	T_g / K
MPEG	-
60CP	308
20CP	222
10CP	222

Table 4.2.5: Glass Transition Temperatures

There was no observable T_g for MPEG. The sample was even taken to the melt and quenched immediately to 77 K in an attempt to lock in an amorphous structure. Despite all efforts no T_g was observable.

The sample 10CP gave a clear trace with a well defined glass transition occurring at 222 K. As the temperature increased separate crystallisation and melting transitions were identifiable. The area under the melting peak, ~ 316 K, is larger than the area under the crystallisation peak, ~ 250 K, indicating that the sample contains crystalline regions before thermal treatment. Similar behaviour is observed for 20CP which also exhibits the same T_g as 10CP. As for 10CP the area under the melting endotherm is greater than that under the crystallisation exothermic. From these observations it can be concluded that there is some inherent crystallinity in both 10CP and 20CP.

The trace for the copolymer 60CP does not exhibit such well defined transitions. The trace is noisy with considerable expansion being required to identify a rather broad T_g.

10CP

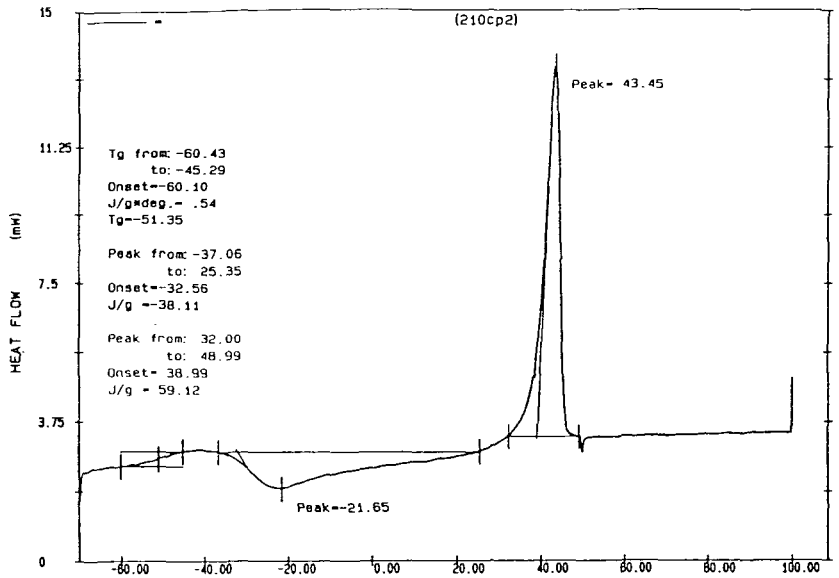

20CP

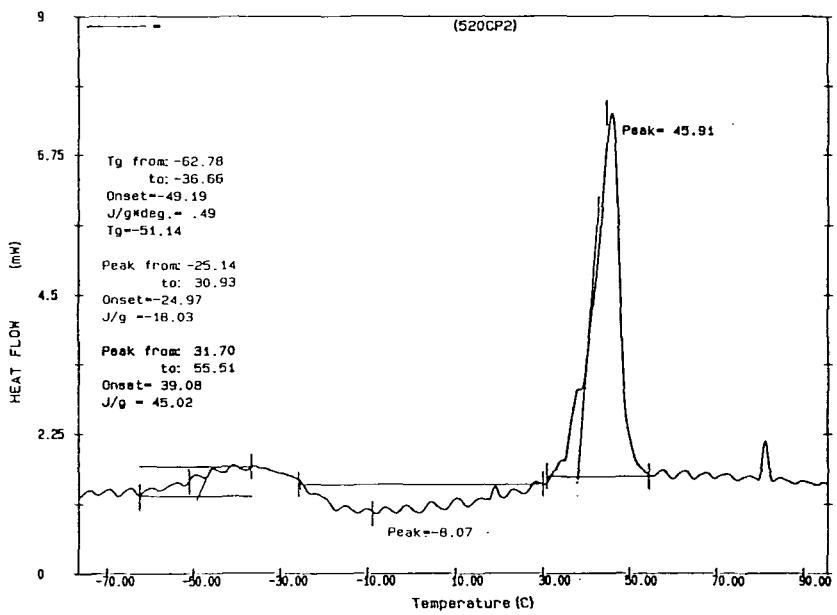

60CP

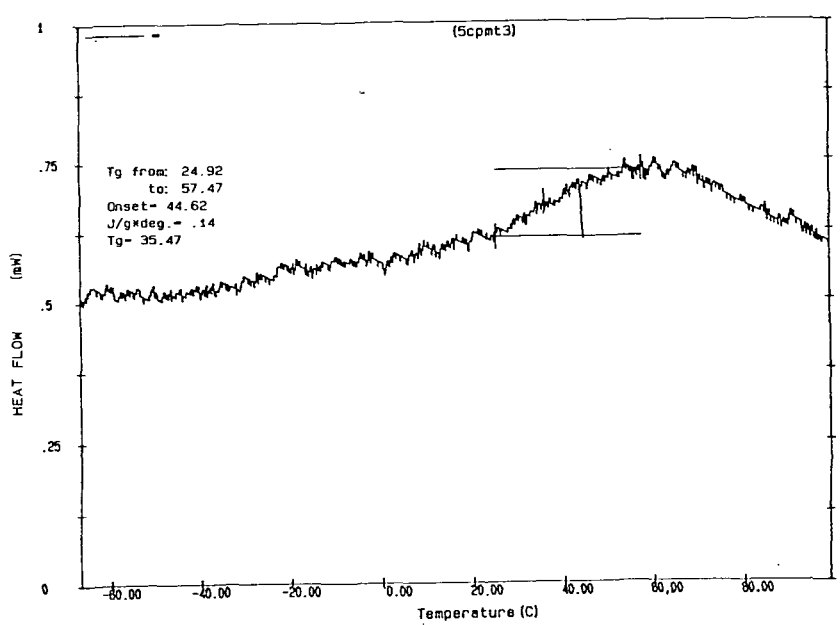

Figure 4.2.4 DSC traces for the graft copolymers, as labelled.

4.2.8.4 Discussion

A number of empirical relationships have been proposed to relate the T_gs of random copolymers and compatible polymer blends to their composition. One of the more simple approaches developed by Fox[7] has been considered and applied to this study.

Fox[7] proposed a relationship for the dependence of T_g on the composition of a copolymer. The limiting form is given below in terms of w_1, w_2 the weight fraction of components 1 and 2 and the T_gs of their homopolymers, T_{g1}, T_{g2}.

$$\frac{1}{T_g} = \frac{w_1}{T_{g1}} + \frac{w_2}{T_{g2}}$$

Equation 4.4.1

Equation 4.4.1 applies to compatible systems that are not strongly polar and from these simple considerations would be expected to have applications to the present system.

To apply Fox's equation values of T_g for the homopolymers were taken from the literature. The value for PMMA was 378K.[8] The value for PEO is somewhat more complicated because of the low molecular weight of the PEO side chains. The molecular weight dependence of T_g has been shown to have the general form[9]

$$T_g = T_g(\infty) - \frac{K}{M}$$

Equation 4.4.2

where $T_g(\infty)$ is the limiting value of the glass transition temperature, K is a constant of the order of 10^5 and M is the molecular weight.

Despite the predictions of equation 4.4.2 studies have shown that for PEO the molecular weight dependence of T_g is rather different. Read[10] showed that rather than reaching an asymptotic limit over the molecular weight range 500 - 1000, which would be predicted from equation 4.4.2, the T_g for PEO exhibits a maximum of 269 K at a molecular weight of 10^4. This behaviour is believed to arise from the variation in the degree of crystallinity with molecular weight.[11]

Given the unusual behaviour exhibited by PEO it is clear that determining T_g for this component and applying it directly to these graft copolymers, which exhibit a varying degree

of crystallinity, may be questionable. The value for T_g of the PEO chains was eventually determined from data reported by Faucher et al.[12] This group reported a detailed study of the molecular weight dependence of T_g for a variety of ethylene oxide polymers ranging in molecular weight from 62 to 7800000. The value of T_g for PEO used in application of Fox's equation was extracted from this study. Faucher's data[12] covering the molecular weight range 600 - 10000 were plotted and fitted using a linear least squares fit. The T_g for molecular weights of 2500 was then read from this line and found to be 232 K.

The results and theoretical expectations given by equation 4.4.1 are given below in the Table 4.2.6.

Sample	Predicted T_g / K	Observed T_g /K
60CP	328	308
20CP	278	222
10CP	268	222

Table 4.2.6: Measured and predicted T_gs.

Clearly the values of T_g predicted from Fox's equation differ from the experimental values. In all cases the experimental values for T_g are considerably lower then those predicted. These discrepancies may arise from a combination of factors. One of the major failings of Fox's equation is the assumption that the individual components of the copolymers are not affected by the presence of one another. Clearly there will be some instances in which this may be valid but it seems unlikely to be so for this system. Not only are the PEO side chains short but they are also separated from one another by varying lengths of PMMA. Although the latter factor will vary with copolymer composition, its influence is such that the environment occupied by the PEO in the graft copolymers may be quite different to that in bulk PEO. The crystallinity in the systems may cause further deviations from the behaviour predicted by equation 4.4.1. This suggestion is supported by the fact that the experimentally determined T_g for the least crystalline sample, 60CP, exhibits the smallest deviation from values predicted by equation 4.4.1. The T_gs observed for the samples 10CP and 20CP are very similar. This behaviour is reproduced by equation 4.4.1 indicating that it is due to the similarity in the composition of these two systems.

4.2.8.5 Conclusion

Due to presence of the two different structural units in the graft copolymers it was feasible that two distinct T_gs would be exhibited by the polymers, one for the backbone and one for the side chains. In reality a single T_g was observed for each polymer sample. This is consistent with the observation that the MPEG macromonomer, i.e. the side chain, did not exhibit a T_g. This behaviour would not be expected to change on polymerisation.

The inherent crystallinity observed in the graft copolymers using DSC has been confirmed by wide angle X-ray scattering. At room temperature untreated samples of 10CP showed considerable crystalline regions as did 20CP, although to a lesser extent. In contrast 60CP was mainly amorphous. These results are in qualitative agreement with those reported here. Alfrey and coworkers[2] have published a study on alkyl comb polymers suggesting that the side chains of these species can crystallise. From the evidence available it is therefore concluded that the PEO side chains in the graft copolymers crystallise in the solid state. The observed behaviour indicates that a critical concentration of PEO side chains is required for crystallisation in the graft copolymers.

Section 4.3: Surface Pressure Surface Concentration Isotherms

4.3.1 Introduction

The characteristics of the spread monolayer behaviour of the graft copolymers are reported and discussed here. Surface pressure - surface concentration isotherms have been recorded and are reported for each graft copolymer. The influence of compression rate and subphase temperature have also been investigated.

This section contains brief details of the general experimental procedure as well as results of the various studies. The results for the compression dependence are presented first. This enabled the optimum compression rate for recording isotherms to be determined and, having specified this parameter a series of isotherms were measured. The temperature dependence of the isotherms has also been investigated and is discussed. The thermodynamic properties of the monolayers have been investigated by application of scaling laws.

4.3.2 Experimental

Surface Pressure isotherms were recorded using the Langmuir troughs described in Chapter 3. Films of the graft copolymers were spread by depositing about 25 μl of ~ 0.05 mg ml^{-1} solutions on the water surface. The films were compressed at a specified barrier speed, the surface pressure was logged every 0.02 s.

4.3.3 Compression Rate Dependence

4.3.3.1 Introduction

The copolymer 20CP was used to investigate whether the isotherms exhibited a dependence on compression rate. Being the intermediate composition graft copolymer this system was chosen as it was expected to represent the properties of the series of graft copolymers. Isotherms were recorded at 298 K using compression rates of 10, 20, 30, 40 and 50 $cm^2\ min^{-1}$.

4.3.3.2 Results

The results of this study are presented in terms of the surface pressure at a given compression rate at fixed surface concentration. Four surface concentrations were considered 1.0, 1.5, 2.0 and 2.5 mg m^{-2}. These values were chosen to cover the low surface concentration range of the isotherm which is generally found to be the most reproducible. The results for Γ_s = 1.5 mg m^{-2} are presented in figure 4.3.1 and are representative of the general behaviour exhibited at each surface concentration considered. Each data point in figure 4.3.1 is the mean value of the surface pressure obtained from at least two consecutive isotherms.

It is evident from figure 4.3.1 that the surface pressure exhibits a dependence on the compression rate. At the slowest compression rate the surface pressure is found to be low, this is representative of behaviour at each surface concentration considered. At higher rates of compression there is less variation in the surface pressure and, as illustrated in figure 4.3.1, the values are almost the same within error for rates in the range 20 - 50 cm^2 min^{-1}.

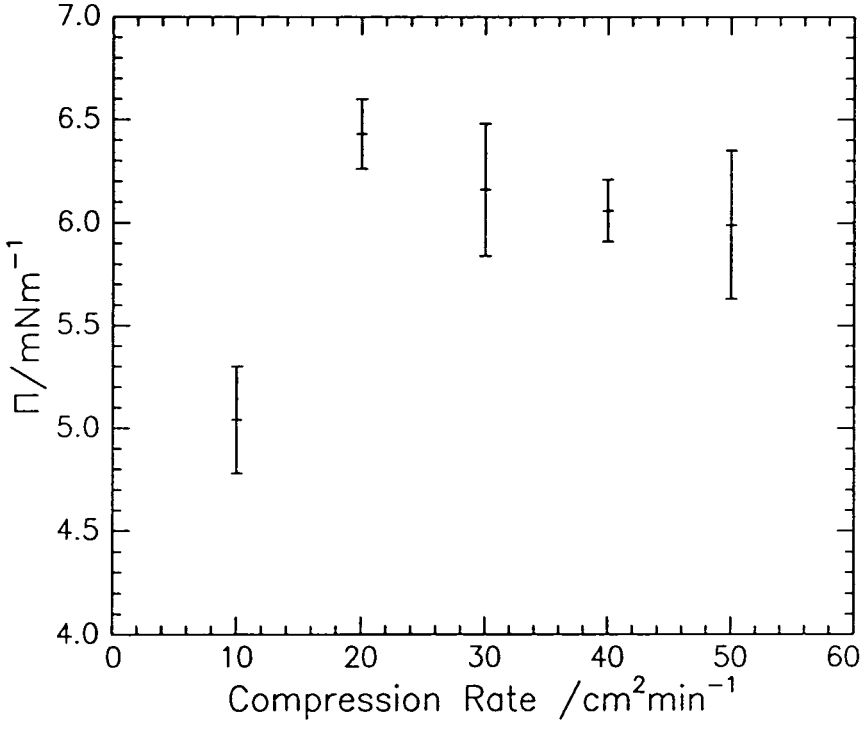

Figure 4.3.1 Surface pressure for Γ_s = 1.5 mg m^{-2} as a function of compression rate.

4.3.3.3 Discussion

The data clearly indicate that the surface pressure at fixed Γ_s depends on the compression rate, although the dependence is less for compression rates of 20 cm^2 min^{-1} and above. Presumably the reason for this behaviour lies in the ageing of the film. The slower the compression speed the longer the film has been on the surface before reaching a specific surface concentration and the longer it has had to relax to the preferred conformation.

The aim of this experiment was to determine what compression speed to use in recording subsequent isotherms. Clearly the decision was whether to use 10 cm^2 min^{-1} as this would cause the largest differences. It was decided that a compression rate of 30 cm^2 min^{-1} would give the optimum conditions. A compression rate of 10 cm^2 min^{-1} is rather slow and would make the process of recording an isotherm lengthy. Wherever possible it is best to reduce the time of the measurement and hence reduce the chance of contamination. It was found that the isotherms recorded in this way were perfectly reproducible indicating that, if there were any film relaxations occurring over the duration of the experiment, they were perfectly reproducible.

4.3.3.4 Conclusion

There appears to be a slight dependence on the compression rate. It was decided to record all subsequent isotherms at 30 cm^2 min^{-1} eliminating a possible variable and making all subsequent isotherms comparable.

4.3.4 Surface Pressure Isotherms

4.3.4.1 Introduction

Surface pressure - surface concentration isotherms were recorded for each copolymer over the temperature range 286 - 310 K at approximately 5 K intervals. At each temperature at least two consecutive isotherms were recorded.

4.3.4.2 Results

The reproducibility of the surface pressure isotherms is illustrated by comparing two representative data sets for the copolymer 20CP, figure 4.3.2. There is good agreement over the entire surface concentration range.

Surface pressure surface concentration isotherms for the three copolymers at 296 K are given in figure 4.3.3. It is clear that the films all exhibit different behaviour suggesting that surface behaviour is highly composition dependent. The features of the isotherms are very similar, initially the surface pressure is low but increases sharply with Γ_s once a critical value is reached. Following this increase there is a knee in the isotherms and a subsequent change in the gradient.

The isotherms were found to show some temperature dependence, although this was not a linear effect. Over the range 286 - 300 K there was no change and the isotherms for each composition copolymer remained essentially coincident. However, when the temperature of the subphase was increased to around 305 K the isotherm behaviour changed. Each system, while giving approximately the same behaviour at low Γ_s, exhibited a significant deviation as Γ_s increased. This is illustrated in figure 4.3.4 for 20CP which is representative of the behaviour observed.

As figure 4.3.4 illustrates the isotherms diverge increasingly with increasing Γ_s, so much so that at Γ_s above 0.75 mg m^{-2} the shapes are very different. In marked contrast to these observations there was no change in the behaviour when the subphase temperature was lowered.

Deuterated Counterparts

Versions of each graft copolymer were also synthesised using deutero-methyl methacrylate. As has been shown analysis indicated that the composition of these polymers was close to the hydrogenous versions. The real test of whether deuteration influences the thermodynamics of the polymer - water interactions is a comparison of the surface pressure isotherms.

With this aim surface pressure isotherms were recorded for all the part deuterated copolymers using the same method as outlined above. The surface pressure isotherms were

found to be in good agreement, particularly over the concentration range 0 - 1.5 mg m^{-2}. The isotherms for 20CP and 20DP are presented in figure 4.3.5 and are representative of the consistency observed between copolymers which differ only in isotopic composition. As can be seen generally there is excellent agreement. From this it was concluded that the part deuterated versions of the copolymers adopt the same surface organisation as the hydrogenous versions and thus provide adequate models of behaviour.

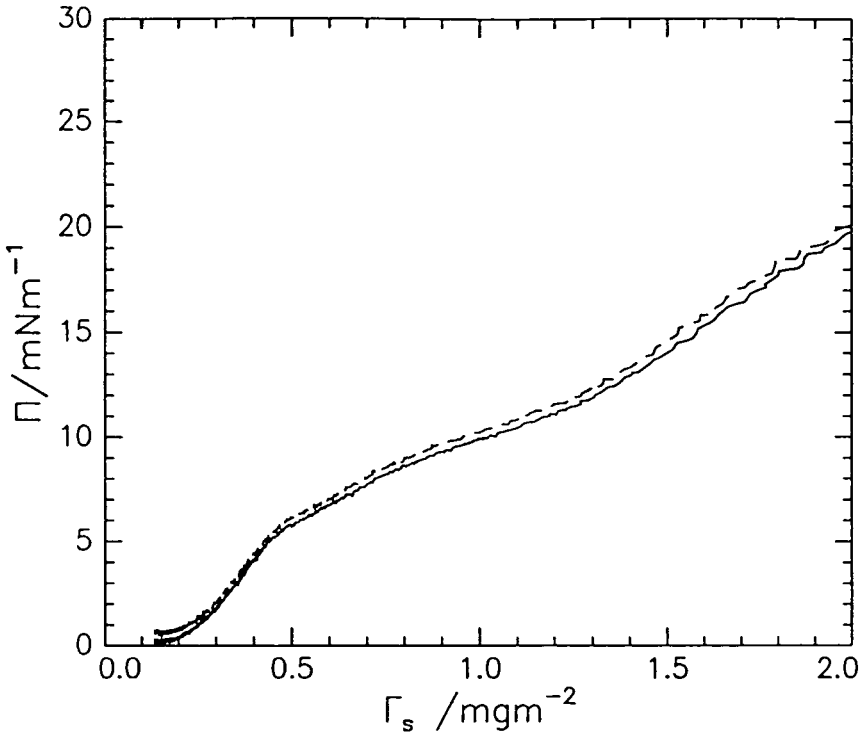

Figure 4.3.2 Two consecutive isotherms for 20CP at 296K. This is typical of the reproducibility of the surface pressure isotherm data.

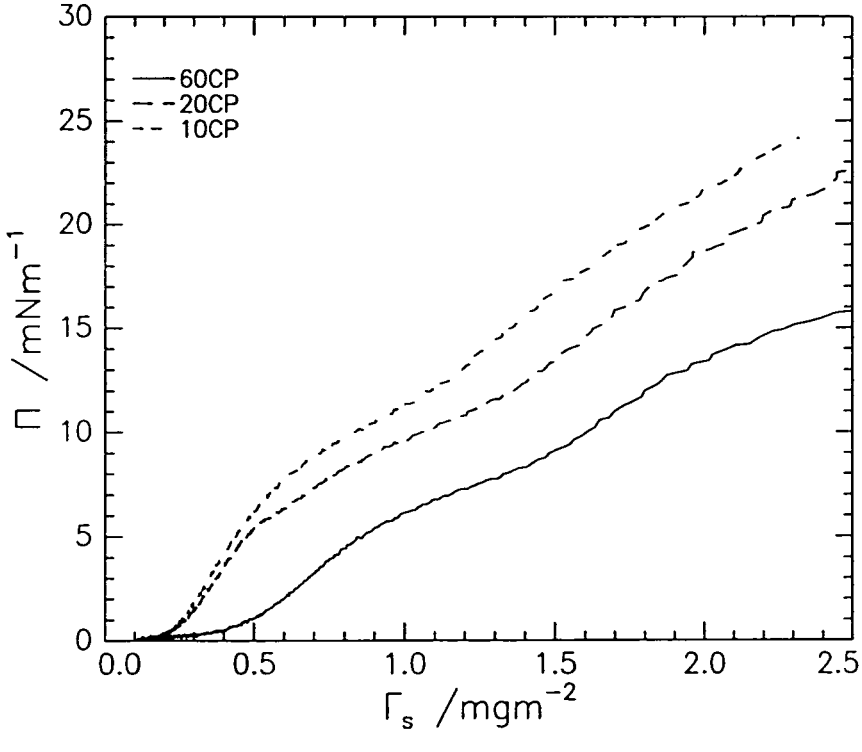

Figure 4.3.3 Surface pressure - surface concentration isotherms for the graft copolymers at 296 K.

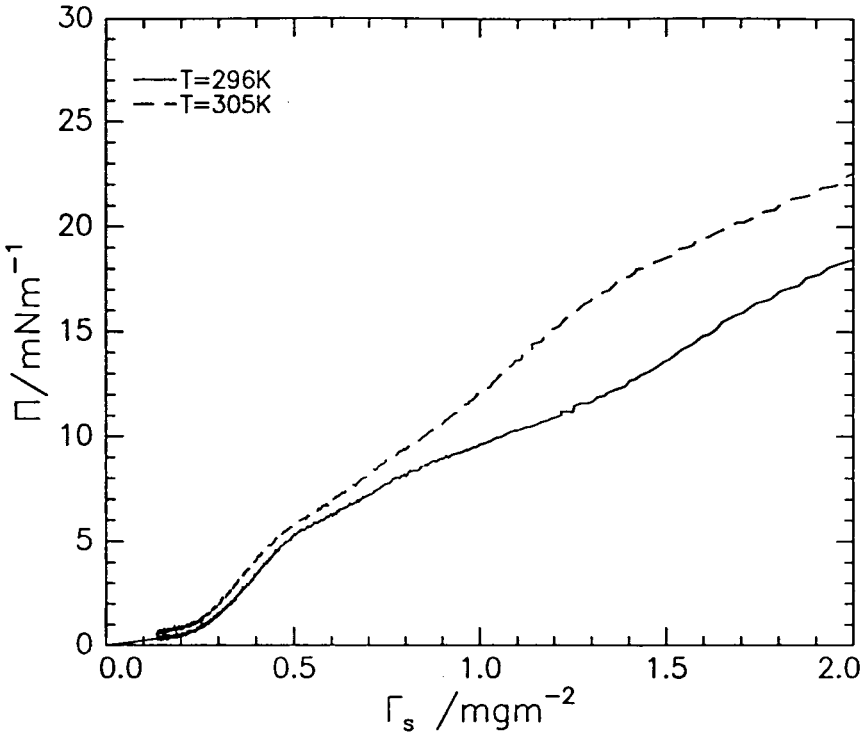

Figure 4.3.4 Isotherms for 20CP at 296K and 305K.

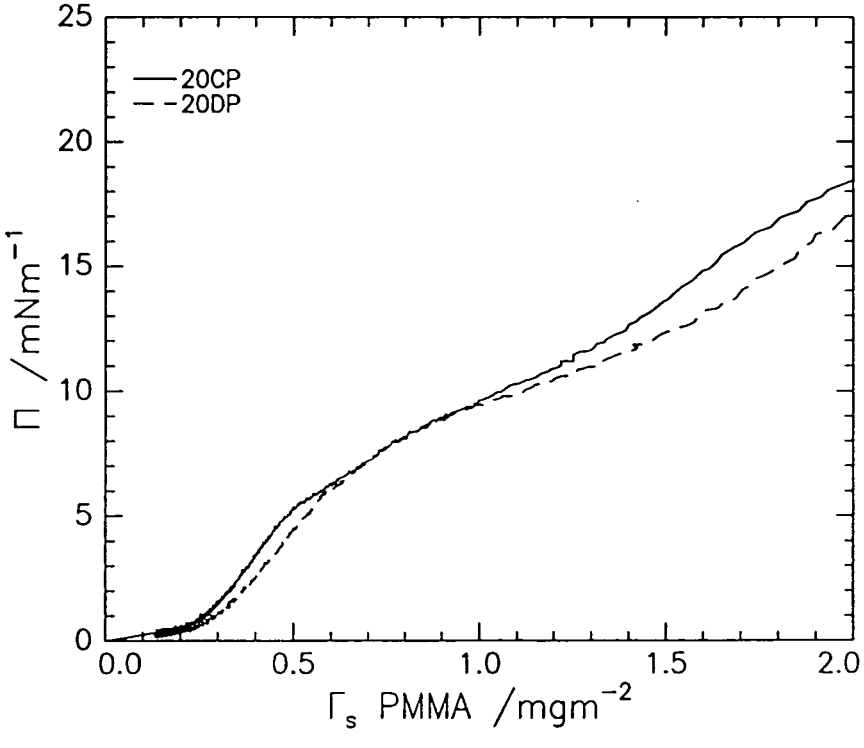

Figure 4.3.5 Surface pressure isotherms for 20CP at 296 K and the part deuterated counterpart, 20DP.

4.3.4.3 Discussion

The small discrepancies observed in figure 4.3.2 are associated with experimental errors and processes within the films. At higher surface concentrations as the film becomes highly compressed, non reproducible local deformations can occur leading to film collapse or faults in the monolayer. Other non reproducible events which may influence behaviour at high surface concentrations include surface contamination. Divergence of the experimental data at high surface concentrations, in general, does not present a problem. The theories that are used to infer the characteristics of the subphase - film interactions from the isotherm data apply to the low surface concentration region only and this is well within the reproducible part of the isotherm.

It is clear then that the isotherms for each system are reproducible and that the differences between the isotherms for the different composition copolymers at 296 K are outside experimental error. A glance at figure 4.3.3 illustrates that as the PEO content in the copolymer increases, from 60CP to 20CP to 10CP, the surface pressure at a given surface concentration increases. This is entirely consistent with the increasing PEO content of the copolymers, and easily rationalised. The more PEO there is in the copolymer the more favourable the interactions with the subphase, leading to a greater reduction in the surface tension and thus a greater surface pressure.

Given that the monolayer behaviour appears to be closely correlated to the copolymer composition the isotherms have been replotted in the form of surface pressure against surface concentration of PEO, Γ_{sEO} . The results are given in figure 4.3.6.

As can be seen in figure 4.3.6 when the surface pressure is expressed as a function of PEO surface concentration the isotherms for each of the graft copolymers converge. Over the range 0 - 0.4 mg m^{-2} of PEO the isotherm for 60CP and 20CP are coincident, that for 10CP falls slightly below. At higher surface concentrations the isotherms for 10CP and 20CP are remarkably similar, remaining coincident right up to the highest surface concentrations. In comparison the isotherm for 60CP peels away and exhibits different characteristics. Given the uncertainty on the composition of the copolymers it is suggested that over the concentration range 0 - 0.4 mg m^{-2}, within the errors due to this uncertainty, the isotherms in figure 4.3.6 are essentially the same. This implies that over the low surface concentration range the monolayer behaviour is dominated by the PEO in the polymer. The range of surface

concentration of copolymer referred to here is up to 1.3 mg m^{-2} for 60CP, 0.7 mg m^{-2} for 20CP and 0.6 mg m^{-2} for 10CP. These figures are in terms of the total spread surface concentration of graft copolymer.

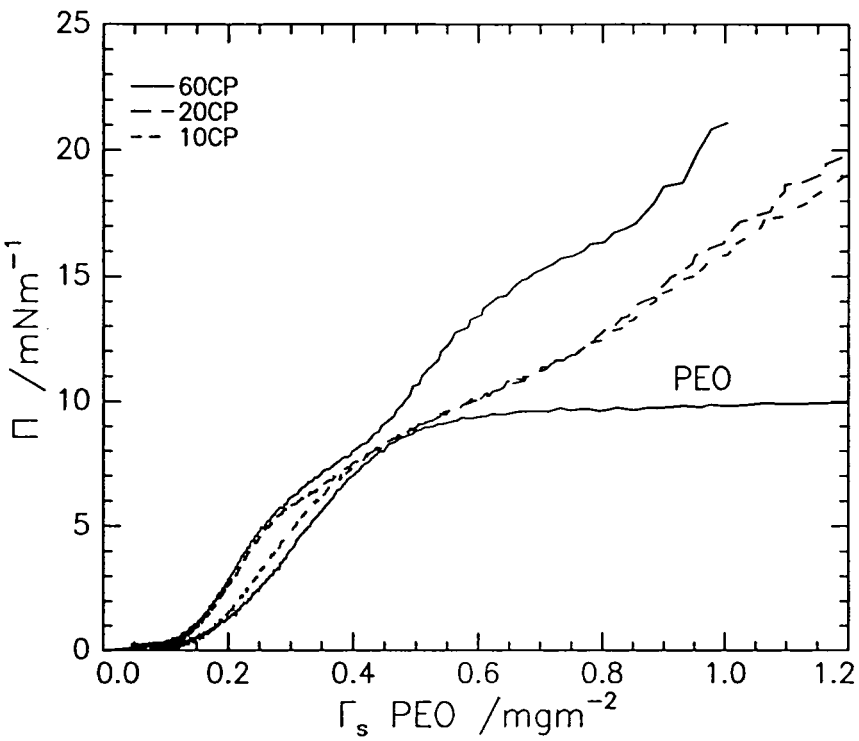

Figure 4.3.6 The variation in the surface pressure for the graft copolymers as a function of PEO surface concentration. The isotherm for homopolymer PEO is overlaid for comparison.

In the discussion above it is clearly implied that the behaviour of the PEO side chains dominates the initial rise in the surface pressure isotherm. In addition to this the side chains appear to behave in a manner akin to that of homopolymer PEO. This leads to the suggestion that on increasing compression of the monolayers, just as for spread films of pure PEO, the side chains penetrate the subphase. Clearly, such behaviour will be modified by the insoluble backbone in the polymer. In an attempt to estimate when such effects become dominant the occupied surface area has been considered. On compression the available surface area decreases, this may be relieved by the PEO side chains penetrating the subphase rather than remaining at the uppermost surface. The minimum surface areas required by a segment of syndiotactic PMMA and PEO have been shown to be 16 $Å^2$ and 43 $Å^2$ respectively.[13] These values have been used to calculate the limiting surface area occupied by one chain of each

graft copolymer. From this the number of chains of graft copolymer per unit area can be determined and this is then converted to the mass of polymer per unit area. This value is denoted Γ_{sLIM} and is given in Table 4.3.1.

Polymer	Γ_{sLIM} / mg m^{-2}
60CP	0.41 ± 0.03
20CP	0.25 ± 0.02
10CP	0.23 ± 0.02

Table 4.3.1: Limiting surface concentration

From the values in Table 4.3.1 the PEO side chains are anticipated to penetrate the subphase at low surface concentrations. Although it may be useful to consider these figures in regard to other features of behaviour, it is noted that they are subject to the assumption that the graft copolymer exhibits behaviour which is adequately predicted assuming additivity of the corresponding homopolymer behaviour. Whilst providing a first approximation for the behaviour this may not be correct.

When the surface pressure isotherms are expressed in terms of PEO concentration the results are very similar up to 0.4 mg m^{-2} of PEO. From this result it is concluded that, over this concentration range, the surface organisation and behaviour of the PEO side chains are independent of any changes in the PMMA backbone. In addition it is clear that the behaviour of the PEO side chains is not correlated directly to the PMMA content over the low surface concentration range. This result follows from the fact that, although the surface concentration of PEO may be the same for each copolymer, the corresponding surface concentration of PMMA is not and varies from 0.2 mg m^{-2} to 0.9 mg m^{-2} over the series. Despite these changes in PMMA content all the systems exhibit similar behaviour.

The suggestion that, at low Γ_s, the isotherms are dominated by the PEO side chains can be confirmed by comparing the isotherms in figure 4.3.6 with that for a spread film of PEO. The isotherm is overlaid and labelled in figure 4.3.6. The behaviour of the graft copolymers is remarkably similar to that of PEO up to around 0.5 mg m^{-2} after which the isotherm for PEO plateaus out, behaviour associated with the onset of subphase penetration.

If, as a comparison, the surface pressure isotherms are expressed as a function of PMMA surface concentration no correlations are observed. The differences between the isotherms are magnified and no trends can be identified, see figure 4.3.7.

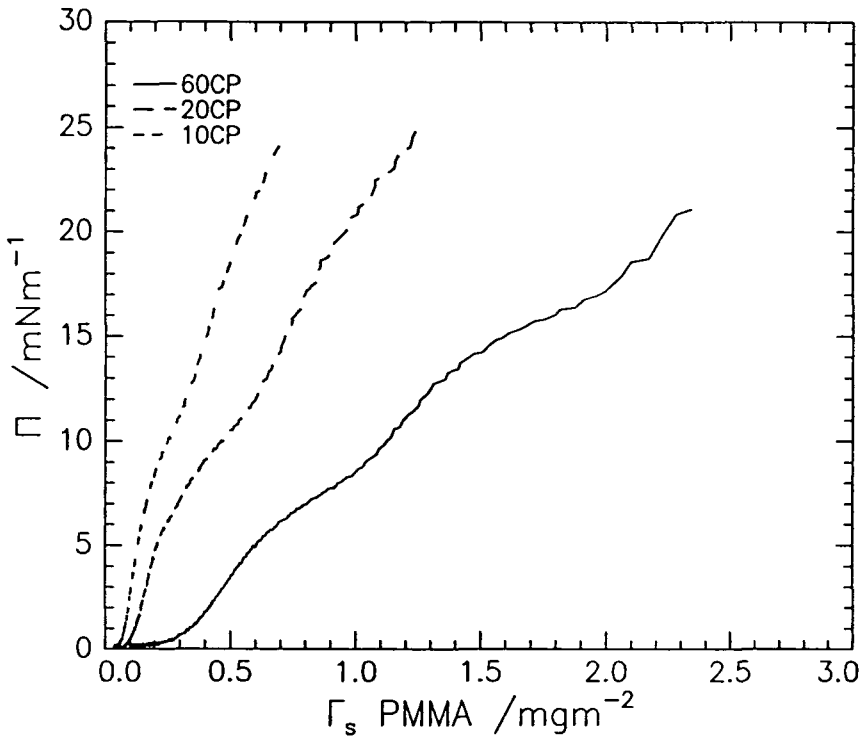

Figure 4.3.7 Surface Pressure as a function of surface concentration of PMMA for each of the copolymers.

This provides further evidence that, at low surface concentrations, the surface pressure is markedly influenced by the PEO in the polymer. If the behaviour of the homopolymer films is considered this seems quite logical. It is known that for films of syndiotactic PMMA, sPMMA, the surface pressure remains negligible until a surface concentration of 1.0 mg m^{-2} is reached. Given that the maximum PMMA content of any of the copolymers is 70% by mass by applying a direct analogy it would be predicted that the PMMA parts of the graft copolymers would not contribute significantly to the surface pressure until a minimum concentration of 1.4 mg m^{-2} of 60CP is reached. In contrast for 10CP and 20CP respective surface concentrations of 3.3 mg m^{-2} and 2.3 mg m^{-2} are required. To test this hypothesis a method of subtracting the contribution to the surface pressure from the PEO in the copolymer is required.

A crude way of doing this is to assume that the contribution from the PEO is essentially constant once the concentration of PEO exceeds 0.5 mg m^{-2} and to subtract 10 mN

m^{-1} from the surface pressure at each Γ_s. The result of this calculation is that at low surface concentration the surface pressure becomes negative. Since this only applies to the regions where the concentration of PEO is not sufficient to give a surface pressure of 10 mN m^{-1} this can be ignored. Only the contribution from the PMMA is of interest and it is assumed that this is not significant until the surface concentration of PEO exceeds 0.5 mg m^{-2}. At this point the surface pressure always exceeds 10 mN m^{-1} and finite values will be returned.

By using the methods outlined above, subtracting 10 mN m^{-1} from the isotherms and expressing the variation of the surface pressure in terms of PMMA concentration, the data presented in figure 4.3.8 is obtained. Comparison with the behaviour of homopolymer films of PMMA may also be of use and to this end the isotherm for syndiotactic PMMA is overlaid in this figure. At a glance it is clear that the behaviour is more complex than that of a simple film of PMMA. As figure 4.3.9 illustrates the isotherm of 20CP appears to be rather more like that for isotactic PMMA, iPMMA. In contrast the behaviour of 10CP and 60CP is no nearer that of iPMMA than sPMMA.

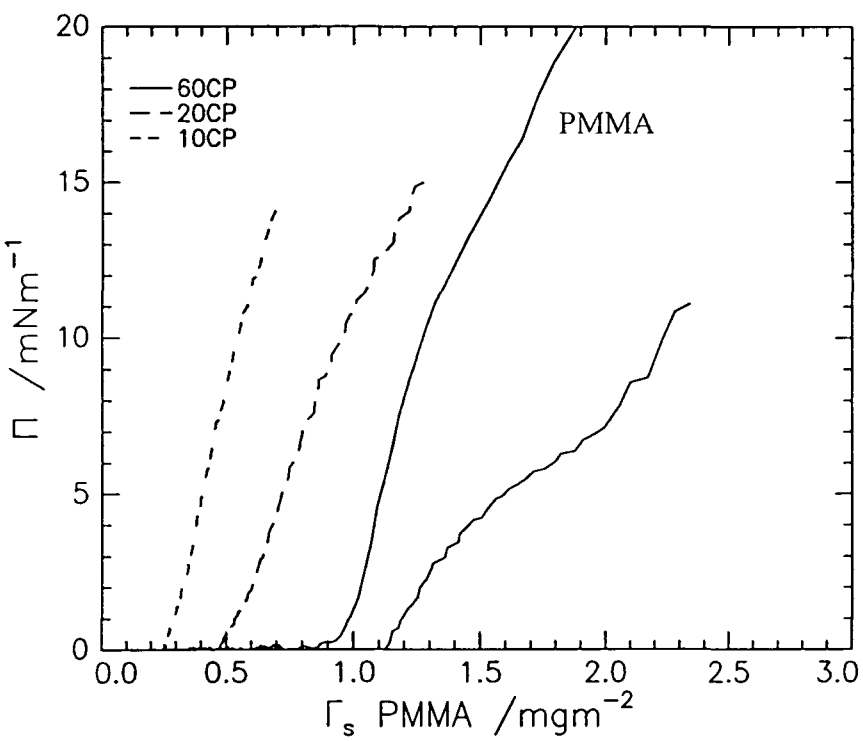

Figure 4.3.8 The variation in the 'residual' surface pressure for the graft copolymers following subtraction of the contribution from the PEO as a function of surface concentration of PMMA. The isotherm for syndiotactic PMMA is overlaid for comparison.

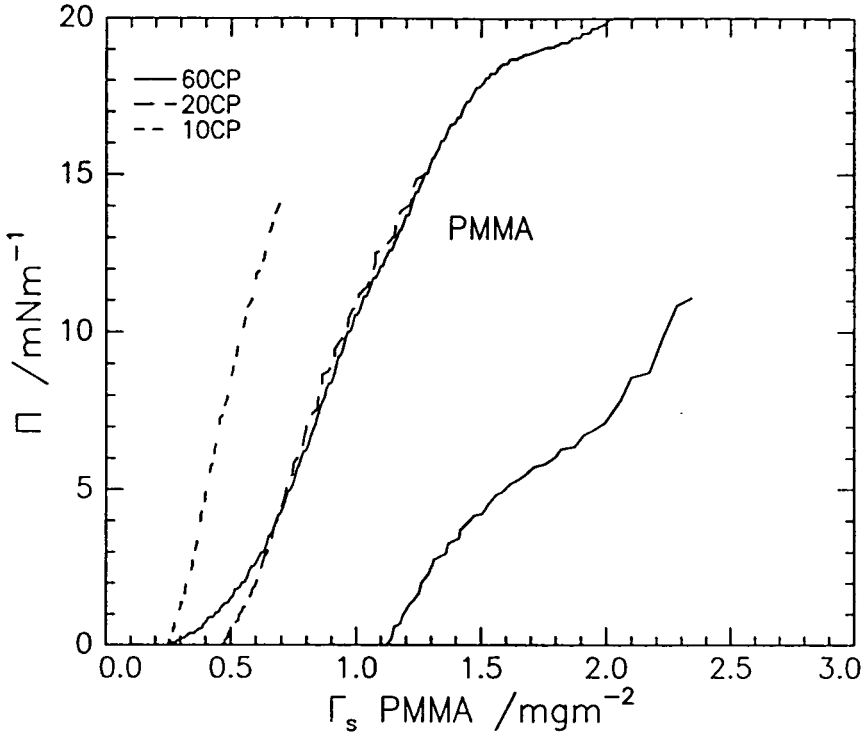

Figure 4.3.9 As for figure 4.3.8 except that the isotherm for isotactic PMMA is overlaid for comparison. This isotherm was taken, with permission, from reference 15.

Given the number of assumptions that have been used to determine the 'PMMA' contribution to the isotherms of the graft copolymers the observed similarity to isotactic PMMA may be coincidental. There is no evidence to suggest that this actually indicates the predominant tacticity of the sample, which as discussed in section 4.2 is expected to be mainly syndiotactic. Despite these possible problems it is believed that the analogy with the behaviour exhibited by homopolymer PMMA can be carried usefully one step further. Differences in the behaviour of isotactic and syndiotactic PMMA have been rationalised by considering the probable orientation of the chains at the interface.[14,15,16] It is feasible that by applying a similar logic to the 'PMMA part' of the isotherms of the graft copolymers analogous information may be extracted.

There have been a number of studies on homopolymer films of stereoregular PMMA samples[14,15,16] and it is clear that films of isotactic and syndiotactic PMMA exhibit quite different behaviour. For isotactic PMMA the film formed may be classified as exhibiting behaviour typical of a liquid expanded monolayer. The surface pressure rises gradually from a

relatively low onset concentration. In contrast sPMMA forms a liquid condensed film. The surface pressure is first observed at a higher surface concentration than for iPMMA and rises steeply in the first instance. The differences in behaviour have been attributed, at least in part, to the strength of the lateral cohesive forces in the films. These interactions are contributed to by dipolar interactions between the ester groups. In isotactic PMMA the interactions are shielded due to the conformation of the chains which forces the ester groups into the subphase. The different surface organisation adopted by sPMMA means that there is no such shielding and therefore the in plane interactions are stronger.

It follows from this brief discussion that one parameter which may help in quantifying behaviour is the gradient of the isotherm at the initial increase in the surface concentration. A straight line has been fitted to this region and the gradients are presented in Table 4.3.2.

System	Gradient /N m g^{-1}
iPMMA	21 ± 1
sPMMA	35 ± 1
60CP	14 ± 2
20CP	24 ± 1
10CP	34± 1

Table 4.3.2: Gradient of initial rise in Π for PMMA contribution

It seems that as the PMMA content of the copolymers decreases the behaviour shifts from that associated with expanded monolayers to that of condensed systems. This can be rationalised if the PEO side chains are considered to act as anchors acting on the backbone of PMMA chains. The lengths of PMMA between the side chains are greatest for 60CP and are expected to have the most freedom. Given that PMMA is a predominantly hydrophobic polymer it is anticipated that, if possible, these chains will minimise their interactions with the aqueous subphase. Although PMMA is known to spread on water it is stressed that this occurs in the absence of any other component. In the case of the copolymers it is feasible that the hydrophilic PEO groups will interact preferentially with the water. These groups alone may minimise the surface tension of the water sufficiently so that there is no longer any advantage in PMMA - water interactions. As a consequence of this the PMMA groups may

have more freedom to adopt conformations in which subphase interactions are minimised, for example forming loops above the water. It is evident that in this model the longer the length of PMMA between the side chains the smaller the fraction of the total content which will be constrained to remain in contact with the water.

On compression, those films where the PMMA loops above the subphase are expected to exhibit a gradual change in surface pressure. In contrast, where there are many PEO side chains the relatively short lengths of PMMA will not get too far from the subphase before they are forced to return to the water surface by an anchoring PEO chain. A specific example is afforded by 10CP where the lengths of PMMA between side chains are, on average, only 10 units long. It is imagined that due to their length they will be constrained to remain at the surface. The larger the number of species confined to the surface plane, the more rapidly the lateral interactions are expected to increase and correspondingly the more rapid the increase in surface pressure. From this argument it follows that as the number of MMA units between side chains decreases, i.e. from 60CP to 10CP, the lateral interactions should increase and the films become more like condensed type monolayers. The behaviour of such systems manifests itself with a more rapidly increasing surface pressure following onset, i.e. a larger gradient, behaviour consistent with the data in Table 4.3.2.

The discussion above provides a qualitative rationalisation of the isotherm behaviour. At low surface concentrations the graft copolymers exhibit behaviour typical of PEO and, as shown by expressing the variation in surface pressure in terms of the surface concentration of PEO, the behaviour appears to converge to that of PEO. Given this, and knowing the behaviour of spread PEO, namely that the surface concentration remains constant at Γ_s above 0.5 mg m^{-2}, subtracting a constant contribution from the total surface pressure to account for the contribution from the PEO appears to be justified. Of course there may be features of the isotherm linked to more complex, although subtle, effects due to PEO / PMMA water interactions but in this first approximation these are ignored. This is a possible source of error particularly for 60CP and 20CP for which the behaviour diverges most from that of PEO. Expressing the surface pressure isotherms in terms of the surface concentration of PMMA shows that there is no correlation between the different systems even at a particular surface concentration of PMMA. This observation leads to the conclusion that the PEO side chains adopt a similar organisation in all the graft copolymer films which influences, possibly even

dominates, the behaviour of the PMMA backbones. This latter feature appears to be correlated with the length of the backbone between successive side chain units.

This leads to a discussion of the temperature dependence exhibited by the isotherms. Although PEO is water soluble, and has a high affinity for water, it is known that as the temperature increases its solubility decreases. The effect is such that while water is a good solvent for PEO at 298K at 369K it is a theta solvent.[8] This behaviour is attributed to changes in the nature of the hydrogen bonding between water and the polymer. As the temperature increases the hydrogen bonding structure of the water decreases and so too will the water - polymer hydrogen bonding. It is believed that it is this interaction which maintains the PEO in solution, consequently as it breaks down the solubility of the PEO falls. Although such behaviour is strictly a property of the bulk solution the effects may be expected to extend to any solvated PEO at the water surface.

Whilst the surface pressure isotherms for all the polymers were consistent over the temperature range 286 - 300 K at the highest temperatures studied a change was observed. The largest change in the isotherm occurred at high surface concentrations where the contribution from the PEO side chains is anticipated to be constant. This is not as surprising as it may seem at first. Once the surface concentration of a spread film of PEO reaches about 0.5 mg m^{-2} the surface pressure remains constant despite large increases in the surface concentration. This is attributed to the onset of subphase penetration which is more favourable than increasing the density of species at the interface. By direct analogy, when the surface concentration of the graft copolymers is such that the surface concentration of PEO exceeds 0.5 mg m^{-2}, the side chains are envisaged to penetrate the subphase co-operatively. This suggestion is consistent with the maximum surface concentration before subphase penetration as given in Table 4.3.1. Following subphase penetration the chains are envisaged to adopt a highly solvated, expanded coil structure. Given this model it is quite possible that any changes in the polymer - water interaction, assuming they are mainly attributable to the PEO side chains, will not be observed until higher Γ_s. This follows because the PEO / water interactions become most significant when the surface concentration of PEO exceeds 0.5 mg m^{-2} following the onset of subphase penetration. It is evident that this suggestion is consistent with the behaviour exhibited in figure 4.3.4.

It is not known whether the surface pressure isotherm for spread monolayers of PEO exhibits a temperature dependence. The surface pressure for spread films of PEO changes

only at low surface concentrations, up to 0.5 mg m^{-2}, at which point the value reaches a plateau level. If the model proposed above is correct the most marked temperature dependence would be anticipated following the onset of subphase penetration. However, it is possible that as homopolymer PEO chains are soluble they will be able to exploit their increased freedom reducing unfavourable interactions in a manner not available to the insoluble graft copolymers.

It is quite possible that changes in the structure and conformation of the PEO side chains due to increases in the subphase temperature will cause associated changes in the organisation of the PMMA backbone. Such behaviour would require a rather more sophisticated model than that proposed earlier in which the PEO side chains simply act as anchors on the backbone. To consider these changes in more detail the surface pressure isotherm has been analysed as previously. The contribution from the PEO has been subtracted and the surface concentration expressed in terms of PMMA content. The isotherms recorded at 296K and 305K are presented in this way in figure 4.3.10, the parameters are presented in Table 4.3.3.

System	T /K	Gradient / N m g^{-1}
20CP	296	25
20CP	302	35

Table 4.3.3: Gradient of initial rise in Π for PMMA contribution

Table 4.3.3 clearly demonstrates that as the subphase temperature increases the film characteristics change, becoming increasingly like a liquid condensed film. Applying the same logic as previously it is suggested that at 302 K the PMMA chains are forced to interact more with the subphase than at 296 K. This is consistent with the suggestion that water becomes a poorer solvent for PEO as the temperature increases. If the water - PEO interaction becomes less favourable, to compensate for this the PMMA may be forced to become more involved in interacting with the water and reducing the surface tension. The counter argument is that the surface tension of water will also fall as the temperature increases. Doubtless the behaviour exhibited, and the surface organisation adopted, will be a balance of a number of effects. Not only is there the surface tension of water in the two environments to consider but

there is also the change in the PEO - water interactions and any PMMA - PEO interactions. From work done on bulk solutions a significant change in the PEO - water interaction would not be anticipated over the 6 K from 296 - 302 K.[8] However, it is generally acknowledged that phenomena quantified for bulk behaviour may exhibit quite different behaviour when occurring at a surface. Basically, there are too many unknowns to confirm or discount the suggested model although it does appear to reconcile the general observations.

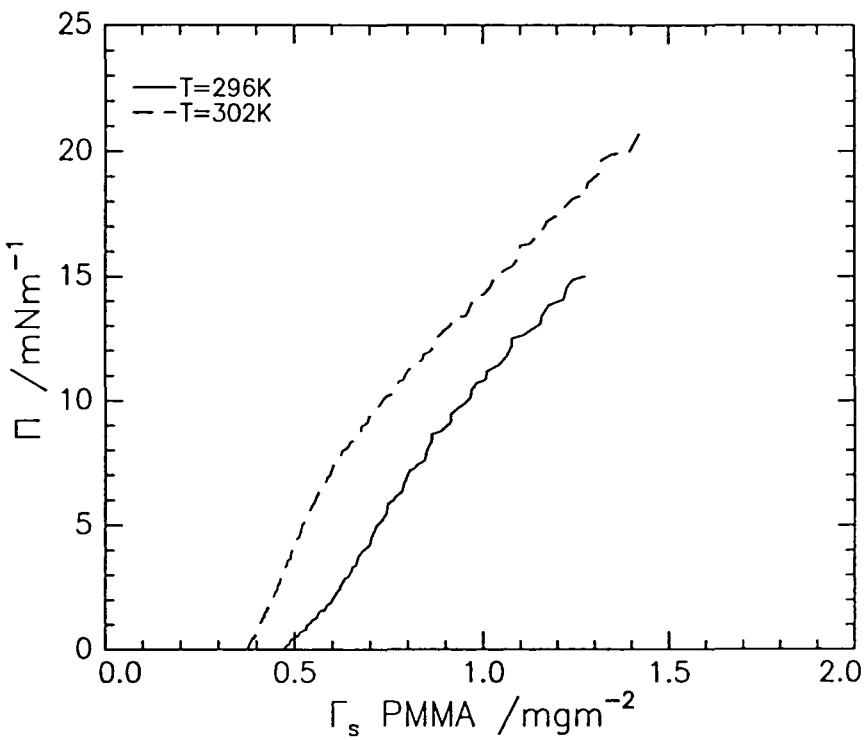

Figure 4.3.10 The variation in the 'residual' surface pressure for 20CP as a function of surface concentration of PMMA, the contribution from the PEO has been subtracted.

4.3.4.4 Analysis of Isotherms

The application of scaling laws to the surface pressure isotherms of homopolymer films has already been outlined. Strictly these scaling laws apply only to homopolymer films and their extension to copolymers, where there may be a number of different interactions between the separate entities comprising the copolymer and the subphase, is not necessarily straightforward. Despite these problems the theories have been applied to interpret the isotherms for the graft copolymers. In view of the limitations any values extracted may not have a direct physical significance, but should stand up to cross-comparison through the series of copolymers studied.

Dilute Regime

The behaviour of polymer monolayers in the dilute regime, where the chains are modelled as completely non-interacting, is given by an equation of state with a virial expansion of the form:

$$\frac{\Pi}{\Gamma_s} = RT\left[\frac{1}{M_n} + A_{22}\Gamma_s\right]$$

Equation 4.3.1

Assuming that further terms are negligible a plot of Π/Γ_s should enable A_{22} and M_n to be determined.

The data for 20CP collected at 296 K are plotted in this way in figure 4.3.11. These data are representative of all that collected and are subject to a high level of noise, so much so that they do not justify fitting. The data quality in this regime is attributed to the fact that the surface pressure remains low being only a fraction of a mN m^{-1}, thus approaching the limits of the sensitivity of the pressure balance. Vilanove et al[17] reported work in which they successfully characterised behaviour in this low concentration regime but their apparatus was considerably more sensitive than that used here. They were able to measure successfully surface pressures down to 1 μN m^{-1} whereas the lowest value which could be confidently measured here was 0.2 mN m^{-1}.

Although the data presented cannot be analysed in a quantitative form qualitative conclusions can be inferred. The slopes of Π/Γ_s against Γ_s are directly proportional to A_{22} and show that there is a change in gradient at around 0.2 mg m^{-2} for all the polymers. The data below this surface concentration range are believed to correspond to the dilute regime. For 60CP the gradient in this region is negative, indicating a negative A_{22}. This indicates that the chains tend to be compact rather than in the expanded conformation one would expect in a good solvent. It is concluded that these chains are subject to unfavourable chain - solvent interactions. As the PEO content of the copolymers increases the interactions between the graft copolymer chains and the subphase become more favourable. This is entirely consistent with the behaviour of the homopolymer films, under the same conditions, whereas PEO is in good solvent conditions PMMA is in poor solvent conditions.[13] From this it appears that the interactions between the chains and the subphase scale with copolymer composition as one would anticipate.

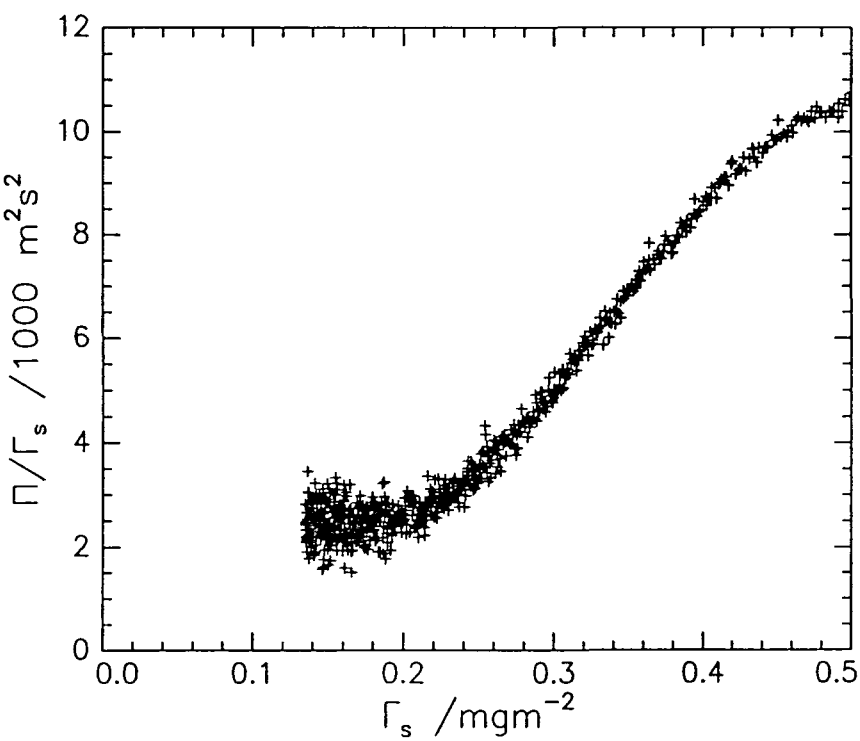

Figure 4.3.11 Surface pressure isotherm data for 20CP plotted in the form of equation 4.3.1.

Semi Dilute Regime

The behaviour of the graft copolymers in the semi dilute regime is considered next. Behaviour in this surface concentration range is correlated to the chains starting to overlap and entangle. The following expressions apply

$$\Pi \propto \Gamma_s^y$$

Equation 4.3.2

where $y = \frac{2\nu}{2\nu - 1}$

By plotting the data in the form $\log \Pi$ against $\log \Gamma_s$ y, and therefore ν, the critical exponent, can be extracted. All data were plotted in this way and the linear region fitted using a least squares fitting routine. A representative plot of the data plotted in this way is given in figure 4.3.12.

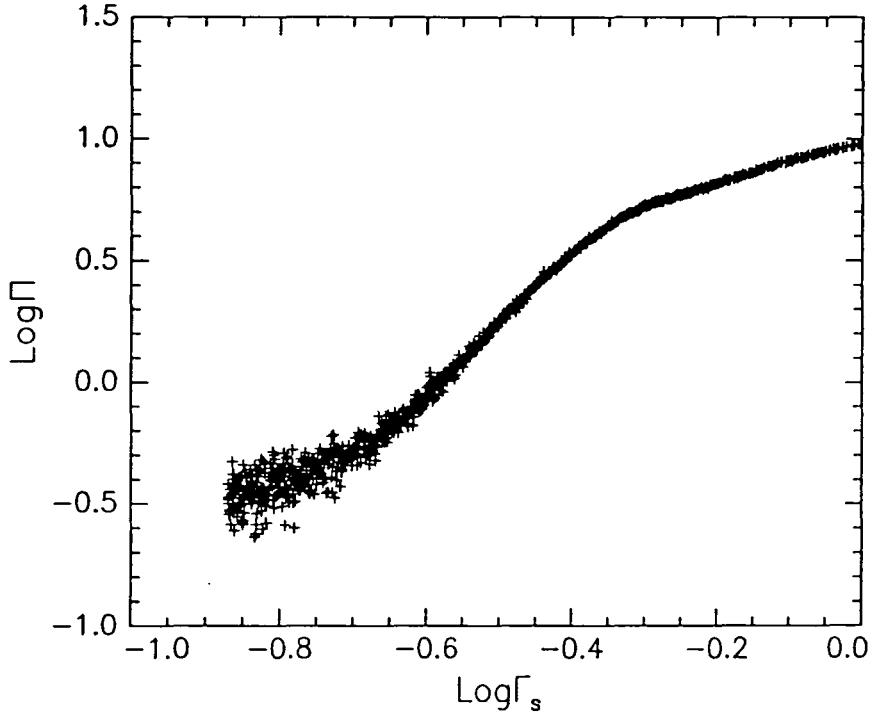

Figure 4.3.12 The surface pressure isotherm data for 20CP plotted in accordance with theories for the semi dilute regime.

The values extracted at 296 K are given in Table 4.3.4. Taking the values of ν which have been previously reported for PEO and PMMA[13] at room temperature, 0.76 and 0.55

respectively, predicted values for the graft copolymer calculated from the copolymer composition are also given.

As shown in Table 4.3.4 ν increases with PEO content and is in good agreement with the calculated values. For a good solvent $\nu = 0.75$, whereas for a theta solvent $\nu = 0.55$. Given that all the values of ν are close to 0.7 it is concluded that the interactions between the water and copolymer chains are predominantly favourable. As the PEO content increases this interaction becomes more favourable.

System	ν calc	ν
60CP	0.64	0.64 ±0.01
20CP	0.70	0.68 ±0.02
10CP	0.72	0.71 ±0.01

Table 4.3.4: Experimental ν values of compared to predictions.

The calculated ν values were noted to be in excellent agreement with experimental values. This may be because, at a thermodynamic level and within the accuracy of this experiment, the behaviour of the grafts is like that of the simple mixtures of the two homopolymers, although this assumes that the mixing is athermal. It should also be remembered that in the graft copolymers the PEO side chains are low molecular weight whereas the value of ν for the homopolymer was determined by studies on a higher molecular weight sample.[13] There were no values of ν available for lower molecular weight samples of PEO, although it is feasible that deviations are very small and are therefore lost in the experimental error. From the information available it is concluded that the nature of the interaction between the chain and the subphase varies with copolymer composition, becoming more favourable with increasing PEO content.

Logarithmic plots of the data enable the surface concentration at the transition from dilute to semi dilute behaviour, Γ_{SD}^*, and semi dilute to concentrated behaviour, Γ_{SD}^{**}, to be identified. These points define the extremes of the linear behaviour of the log plots. The values determined for the graft copolymers at 296 K are listed in Table 4.3.5.

Polymer	Temp / K	Γ_{SD} * / mg m^{-2}	Γ_{SD}**/ mg m^{-2}
60CP	296	0.23	0.58
20CP	296	0.20	0.44
10CP	295	0.16	0.37

Table 4.3.5: Surface concentrations for dilute - semi dilute and dilute - concentrated regime

The values of Γ_{SD}* and Γ_{SD}** increase with decreasing PEO content. This behaviour would seem to suggest that it is the PEO side chains on different graft copolymer chains which come into contact on compression of the monolayers

4.3.6 Conclusion

The surface pressure isotherms clearly indicate that the spread monolayer behaviour of the graft copolymers is highly composition dependent. It was clearly demonstrated in figure 4.3.6 that when the surface concentration is expressed in terms of the PEO surface concentration the isotherms diverge exhibiting characteristics associated with PEO, predominantly over the low surface concentration range. In contrast an analogy with the behaviour of PMMA films does not lead to any similar correlations. From these results it is concluded that the PEO side chains dominate behaviour at low Γ_s. In addition the results in figure 4.3.6 show that the PEO side chains exhibit similar behaviour despite very different PMMA contents. This demonstrates that, at low surface concentrations, the behaviour of the side chains does not scale continuously with PMMA content.

There is substantial evidence to suggest that as the surface concentration of the polymers increases the PEO side chains experience a structural change analogous to the subphase penetration and dissolution exhibited by spread films of PEO above a critical surface concentration. This is supported by considerations of occupied area from which it was implied that subphase penetration would occur at relatively low Γ_s, see Table 4.3.1. Further evidence is supplied by the temperature dependence exhibited by the isotherms. At increased temperatures the isotherms diverged from those at ambient temperatures but only at surface concentrations above the point at which subphase penetration is substantial. This behaviour can be rationalised with changes in the thermodynamic environment experienced by the heavily solvated PEO side chains.

To conclude, it is clear that the PEO side chains in the graft copolymers have a significant influence on the surface pressure isotherms and therefore monolayer properties. There is evidence to suggest that the side chains interact with the subphase over much of the surface concentration range studied and influence the behaviour exhibited by the PMMA backbone.

Section 4.4: Neutron Reflectivity Study

4.4.1 Introduction

The surface organisation adopted by the graft copolymers when spread at the air water interface has been studied using neutron reflectometry. The films have been studied at constant surface concentration which, in all cases, corresponded to constant surface pressure. Films of 10CP and 60CP have been studied at two fixed surface concentrations whereas 20CP was studied at three surface concentrations.

The reflectivity profiles have been analysed mainly by application of the optical matrix analysis. Rather than repeat the details of the modelling for each graft copolymer studied full descriptions have only been provided for films of 20CP. The principles of modelling the data this way are general and so the results of the analysis are presented for 10CP and 60CP without such extensive details.

As has been discussed, it was not possible to deuterate the separate components of the copolymers selectively. As a result of this all the contrasts required to perform a rigorous analysis using the kinematic approximation were not available. Despite this certain assumptions have enabled a truncated analysis of the data using the latter method, the results of which can be cross checked with information extracted from the optical matrix analysis for each particular system.

4.4.2 Experimental

Two versions of each graft copolymer were available for reflectivity measurements. One was a fully hydrogenous polymer whilst the other was prepared with dMMA and contained a deuterated backbone. To obtain the maximum information from a neutron reflectometry experiment it is necessary to collect data for as many different contrasts as possible. In this case three different contrasts could be accessed, the fully hydrogenous polymer on D_2O and the part deuterated polymer on D_2O and null reflecting water, NRW.

Films of all the copolymers were studied at two surface concentrations corresponding to surface pressures of approximately 5 mN m^{-1} and 10 mN m^{-1}. In addition 20CP was studied at a higher surface concentration corresponding to 16 mN m^{-1}. Details of the films studied are given in Table 4.4.1.

Polymer	Γ_s studied / mg m^{-2}		
60CP	0.65	1.60	-
20CP	0.50	1.50	2.00
10CP	0.40	1.10	-

Table 4.4.1: Film Concentrations studied using neutron reflectometry

4.4.3 Results

Rather than reproduce the reflectivity profiles for each of the systems studied this discussion is based on the results obtained for the graft copolymer 20CP. The behaviour of this system is representative of the general trends exhibited by the different composition graft copolymers. As a consequence of this all the remarks made in the following discussion, although made in reference to the graft copolymers 20CP and 20DP, are general.

The reflectivity profiles recorded for 20CP and 20DP on D_2O, as the surface concentration increases from 0.5 to 2 mg m^{-2}, are presented in figures 4.4.1 to 4.4.3. The reflectivity profile for clean D_2O is overlaid on all the figures for comparison.

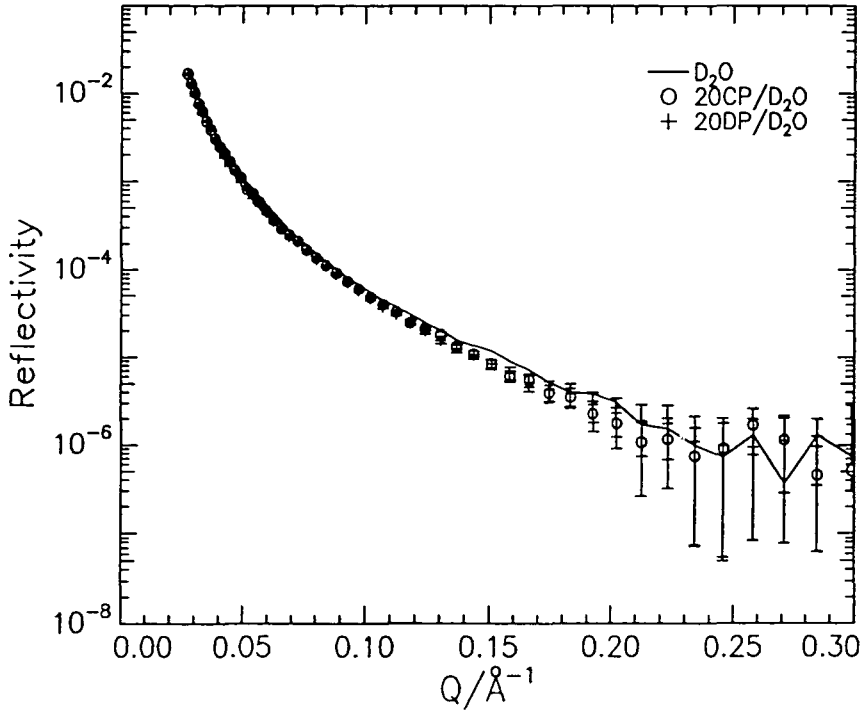

Figure 4.4.1 Reflectivity profiles on D_2O for Γ_s = 0.50 mg m^{-2}.

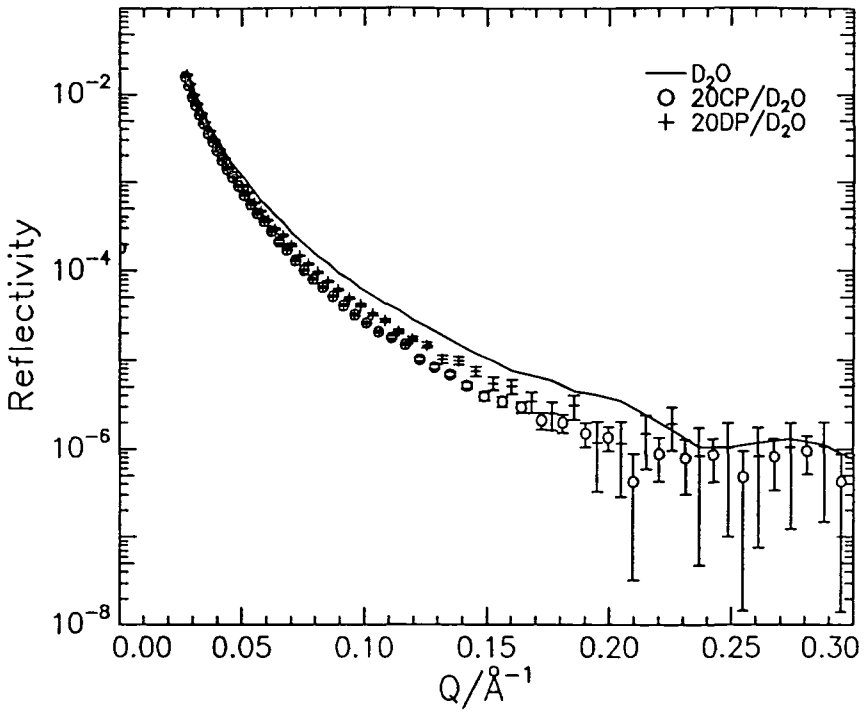

Figure 4.4.2 Reflectivity profiles on D_2O for $\Gamma_s = 1.50$ mg m^{-2}.

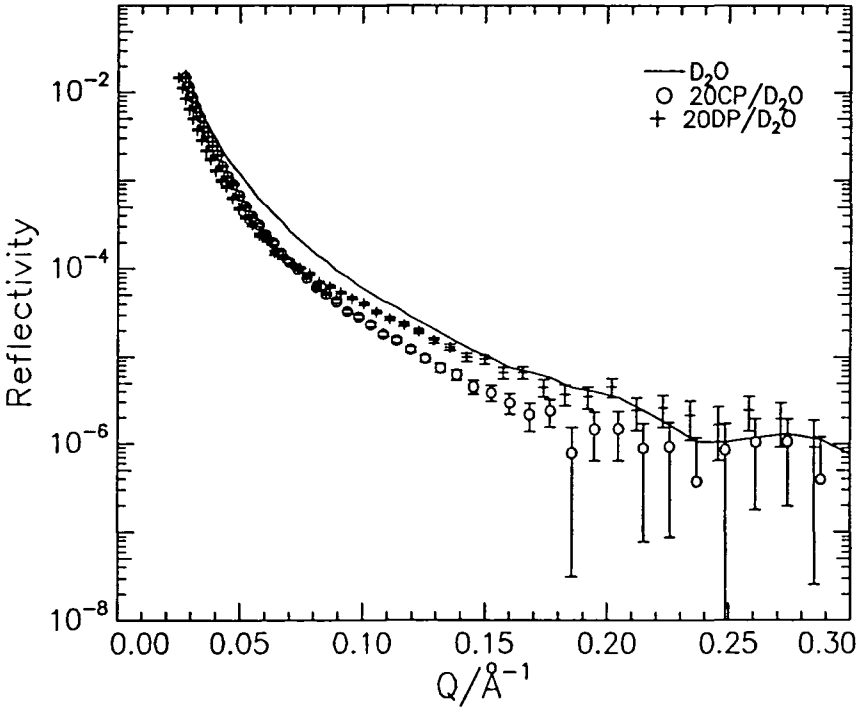

Figure 4.4.3 Reflectivity profiles on D_2O for $\Gamma_s = 2.00$ mg m^{-2}.

All the profiles have had a flat background signal subtracted and consequently are only presented over the Q range 0 - 0.30 $Å^{-1}$. Examination of the profiles indicates that the background becomes dominant between 0.20 - 0.25 $Å^{-1}$, at this Q value the profiles become coincident and the errors are significant.

Before the detailed characteristics of the data are considered, behaviour universal to all the profiles is discussed. The overwhelming trend displayed by all the profiles is the rapid fall off in the reflectivity with increasing Q. Such behaviour is typical of this experiment and reflects the fact that the reflectivity exhibits an inverse dependence on Q, because $R(Q) \propto Q^{-4}$ the rapid fall off in R(Q) as Q increases is a general phenomenon. It is because of this rapid fall off in the coherent reflected signal that by Q values as low as 0.2 - 0.4 $Å^{-1}$ the signal is lost in the incoherent background. Although there are a number of contributions to the background, the predominant effect is attributable to the hydrogen in the system and arises from the high incoherent scattering cross section of the hydrogen nucleus. As a consequence the background signal is larger for an NRW subphase, which is predominantly H_2O, than for D_2O. The difference is such that for data collected using CRISP when the subphase was D_2O the background signal was around 2×10^{-6} whereas for NRW the background was over twice this at approximately 5×10^{-6}.

It is clear that films of either 20CP or 20DP depress the reflectivity below that for clean D_2O. The effect is small at the lowest surface concentrations and the depression appears the same for both 20CP and 20DP with the profiles being basically coincident, see figure 4.4.1. When the surface concentration increases to 1.5 mg m^{-2} the depression of the reflectivity of the D_2O due to presence of polymer is more marked, see figure 4.4.2. At the very lowest Q the profiles are coincident with those for D_2O but as Q increases the profiles diverge and the reflectivity is observed to be lower in the presence of 20CP than 20DP. At the highest surface concentration similar behaviour is observed, see figure 4.4.3. The reflectivity of 20CP on D_2O is the lowest, that for 20DP on D_2O although depressed below that of D_2O over the range 0.04 - 0.10 $Å^{-1}$, does not fall away as rapidly as for D_2O and the reflectivity of these two systems converges at around 0.15 $Å^{-1}$.

The reflectivity data collected for the part deuterated copolymer, 20DP, on NRW have been overlaid and are presented in figure 4.4.4. The reflectivity at a given Q increases as the surface concentration of polymer increases, this is consistent with the increased amount of deuterated species. On NRW only the deuterated parts of the copolymers contribute to the

reflectivity, and therefore it does not fall off as rapidly, nor is it as high as that on a D_2O subphase. The signal for the lowest concentration film rapidly becomes lost in the background such that by 0.15 $Å^{-1}$ there does not appear to be any subsequent dependence of R(Q) on Q. As the concentration of polymer increases, the coherent signal remains distinguishable to slightly higher Q values of around 0.2 $Å^{-1}$. To emphasise that 20CP is representative of the general behaviour of the graft copolymers the data for 60DP / NRW at Γ_s = 0.65 mg m^{-2} and Γ_s = 1.6 mg m^{-2} have also been presented in this way, see figure 4.4.5. On comparison of the two data sets it is clear that the general trends exhibited by either polymer on increasing Γ_s are the same.

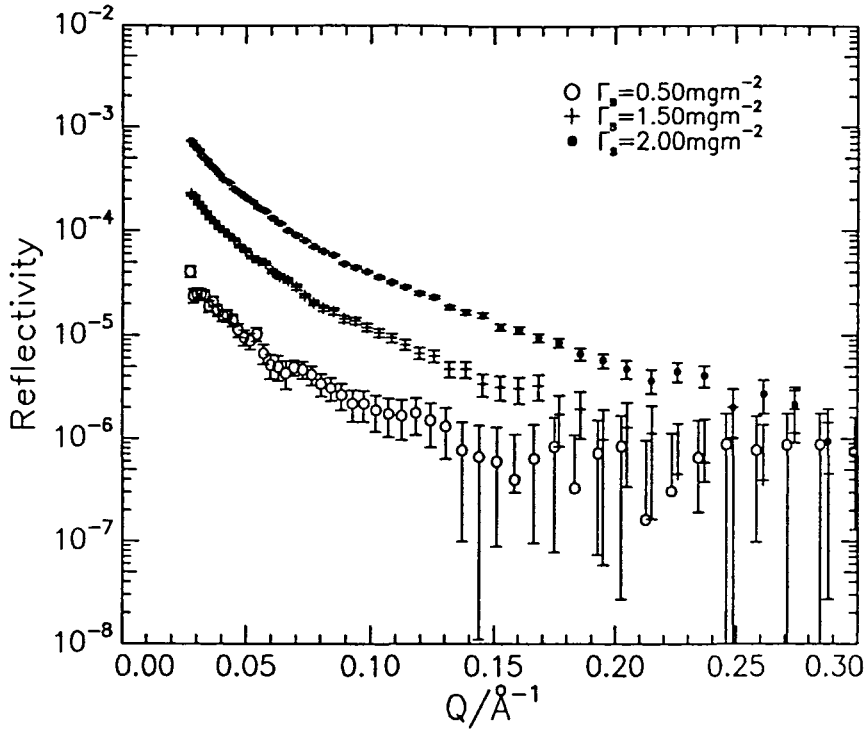

Figure 4.4.4 Reflectivity profiles for 20DP on NRW.

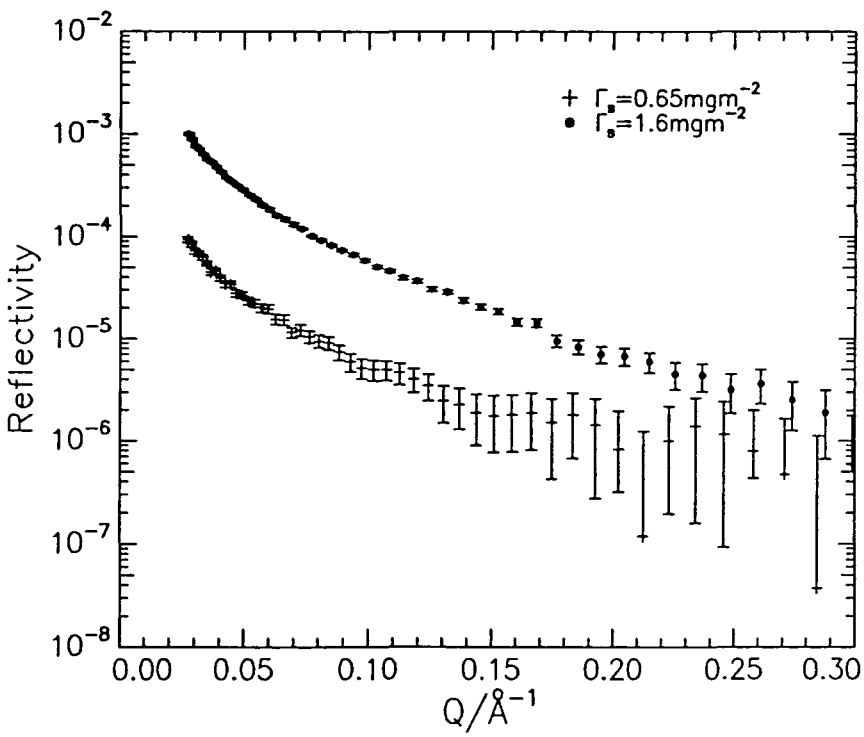

Figure 4.4.5 Reflectivity profiles for 60DP on NRW.

4.4.4 Discussion

It was observed that the reflectivity of D_2O was depressed to a larger extent by the same surface concentration film of 20CP than 20DP. Clearly a layer of hydrogenous polymer will cause the scattering length density of the surface to be reduced below the values for a deuterated polymer. However, it does not necessarily follow that the reflectivity will scale in the same manner. Where the subphase is D_2O the reflectivity depends on the difference between the scattering length density of the clean subphase and the film covered surface. The dependence is not straight forward and is best expressed in the kinematic approximation by:

$$R(Q) = \frac{16\pi^2}{Q^4}\left(\Delta\rho^2 - 4\rho_d(\Delta\rho - \rho_d)\sin^2(Qd/2)\right)$$

Equation 4.4.1

where $\Delta\rho = \rho_{-\infty} - \rho_{\infty}$, i.e. the difference in the scattering length density of air and subphase respectively, ρ_d is the scattering length density of the surface layer.

When $Q = \pi/d$ this reduces to:

$$R(Q) = \frac{16\pi^2}{Q^4}(2\rho_d - \Delta\rho)^2$$

Equation 4.4.2

The loss of phase is a problem inherent to the neutron reflectometry experiment. As a direct result of this it is not always possible to determine ρ_d unambiguously from R(Q), this is demonstrated in Equation 4.4.2 by the presence of the squared term. Although there are cases where one root may be discounted, the two solutions can lead to ambiguities which are not readily resolved.

Since the scattering length density of D_2O is 6.35×10^{-6} Å^{-2} and that of air is zero, $\Delta\rho$ is 6.35×10^{-6} Å^{-2}. It is clear from Equation 4.4.2 that where the subphase is D_2O the maximum reduction in reflectivity occurs when the scattering length density of the surface layer is half that of the subphase, i.e. 3.18×10^{-6} Å^{-2}. The simulated reflectivity for this system is presented in figure 4.4.6. Incidentally although according to Equation 4.4.2 one would expect $R(Q) = 0$ at $Q = \pi/d$, in this case 0.157 Å^{-1}, only a minima is observed and the reflectivity remains at a finite level. This behaviour is due to the fact that this equation derives from the kinematic approximation which does not give a exact description of the system. It is also instructive to consider behaviour for steps in the scattering length density

profiles both above and below 3.18×10^{-6} Å^{-2}. When the ρ is 2.18×10^{-6} Å^{-2} or 4.18×10^{-6} Å^{-2} as predicted by Equation 4.4.2 the reflectivity profiles are identical and greater than for ρ = 3.18×10^{-6} Å^{-2}, see figure 4.4.6.

It follows from the discussion above that although the scattering length density of the surface layer will undoubtedly increase on going from a film of 20CP to 20DP when the subphase is D_2O, this increase will not necessarily be accompanied by an increase in the reflectivity. Depending on the amount of water incorporated into the surface layer the scattering length density may increase from say 2.18×10^{-6} Å^{-2} for 20CP on D_2O to 3.18×10^{-6} Å^{-2} for 20DP in which case the reflectivity would fall. This discussion illustrates the need to exercise caution when attempting to make qualitative inferences from reflectivity profiles.

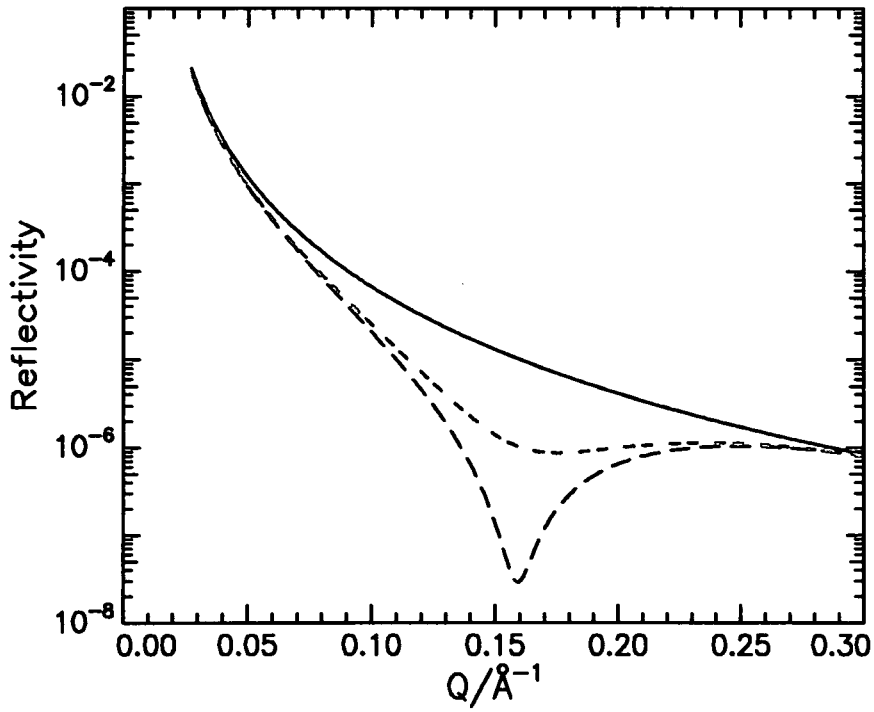

Figure 4.4.6 Simulated reflectivity profiles for $\rho_d = 3.18 \times 10^{-6}$ Å^{-2}, d = 20 Å, broken line. The solid line is the profile for clean D_2O while the broken red line is for $\rho_d = 2.18 \times 10^{-6}$ Å^{-2}.

Despite the ambiguities associated with interpretation of the profiles discussed above there is certainly some qualitative information that can be inferred directly from the profiles. It can be shown, with simulations, that the thicker the layer at the interface the more rapid the fall off in reflectivity. This is demonstrated by the simulations in figure 4.4.7 and provides a means of rationalising the behaviour exhibited by the reflectivity profiles of 20CP and 20DP

on D_2O. It is noted that a broader interfacial region particularly affects the data at low Q which corresponds to longer penetration depths, see figure 4.4.7.

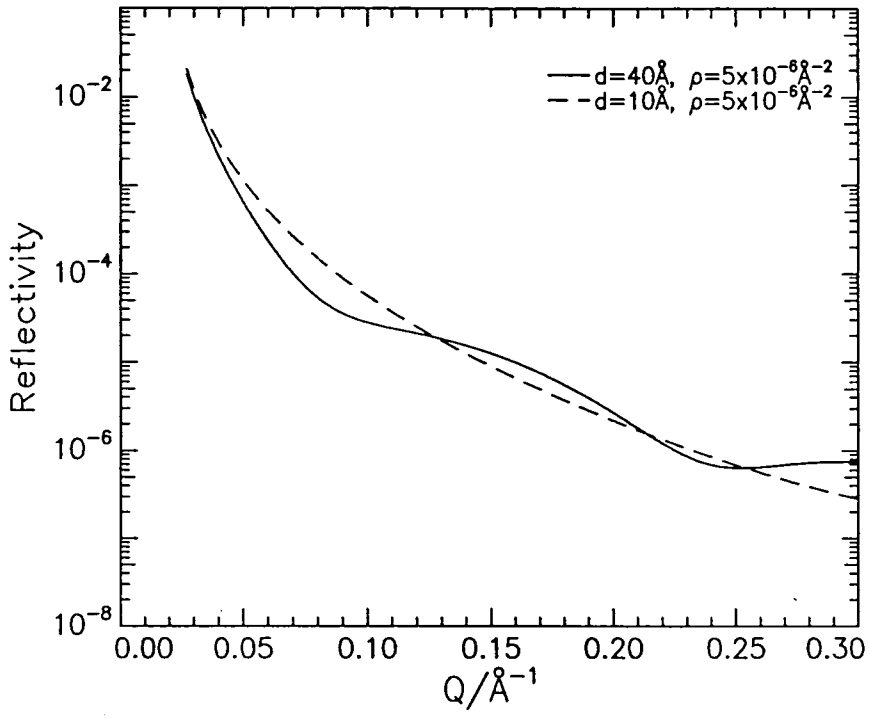

Figure 4.4.7 Simulated reflectivity profiles on D_2O for films with the parameters as indicated.

To compare and rationalise any analogous features exhibited in the reflectivity profiles collected on D_2O it is helpful to replot the data in figures 4.4.1, 4.4.2 and 4.4.3. To this end the reflectivity profiles collected for a single contrast at different values of Γ_s have been overlaid and are given in figures 4.4.8 and 4.4.9.

When the data are plotted in this way it soon becomes clear that at low Q the reflectivity falls off more rapidly as Γ_s increases. This indicates that the film formed at the interface is becoming thicker as the surface concentration of polymer increases. The profiles for 20CP on D_2O imply that the film thickness increases most markedly between 0.5 mg m^{-2} and 1.50 mg m^{-2}, this corresponding to the largest depression in the reflectivity.

The behaviour of films spread on NRW differs from that on D_2O; because the scattering length density of both continuous phases is zero the reflectivity correlates more intuitively to the scattering length density and layer thickness. It is observed that the profiles recorded on NRW exhibit a very similar decrease in R(Q) with increasing Q and just appear to be offset from one another along the y axis, see figures 4.4.4 and 4.4.5. This behaviour

indicates that the thickness of the layer which is contributing most directly to the reflectivity is similar for all the systems and appears to be independent of Γ_s over the range studied. Figure 4.4.10 demonstrates that as d increases the reflectivity is observed to fall off more rapidly with Q. In contrast where the scattering length density of the film is varied but the film thickness is fixed behaviour is much more like that observed here, compare figures 4.4.4 and 4.4.5 with figure 4.4.11

The profiles in figure 4.4.11 maintain the same general shape but give a higher reflectivity at any Q value as the scattering length density increases. From the results of these simulations it is suggested that the thickness of the surface layer which is contributing to the profiles collected on NRW remains essentially constant despite increasing Γ_s. This implies that when Γ_s increases from 0.5 - 1.5 mg m^{-2} the dominant effect is an associated increase in the scattering length density of the layer whilst the thickness remains essentially constant. Although initially this statement may appear to contradict the suggestion made, earlier that the thickness of the film increases with Γ_s, this is not necessarily so. The vital point to appreciate is that the surface film may be composed of different layers and that those dominating the reflectivity on NRW and D_2O may differ. In the situation where the subphase is NRW only the deuterated sections of the polymers will contribute to the reflectivity. The PEO side chains are hydrogenous and may be so heavily diluted by the null scattering subphase that their contribution to the reflectivity is negligible. In contrast, where the subphase is D_2O the reflectivity is driven by the subphase and is depressed from that of clean D_2O due to the presence of polymer. The reflectivity profile for such a system will reflect the scale over which the scattering length density of D_2O is reduced below 6.35×10^{-6} $Å^{-2}$. For the graft copolymers the available evidence indicates that the interfacial width occupied by the dPMMA backbone does not increase significantly with Γ_s. This leads to the suggestion that the effects observed in the profiles recorded on D_2O, which were attributed to increases in the film thickness, are predominantly due to changes in the organisation of the PEO side chains. It therefore appears, from this simplistic interpretation of the reflectivity profiles, that as Γ_s increases the PEO side chains stretch into the suphase. Such effects will be described in more quantitative detail by direct fitting of the profiles.

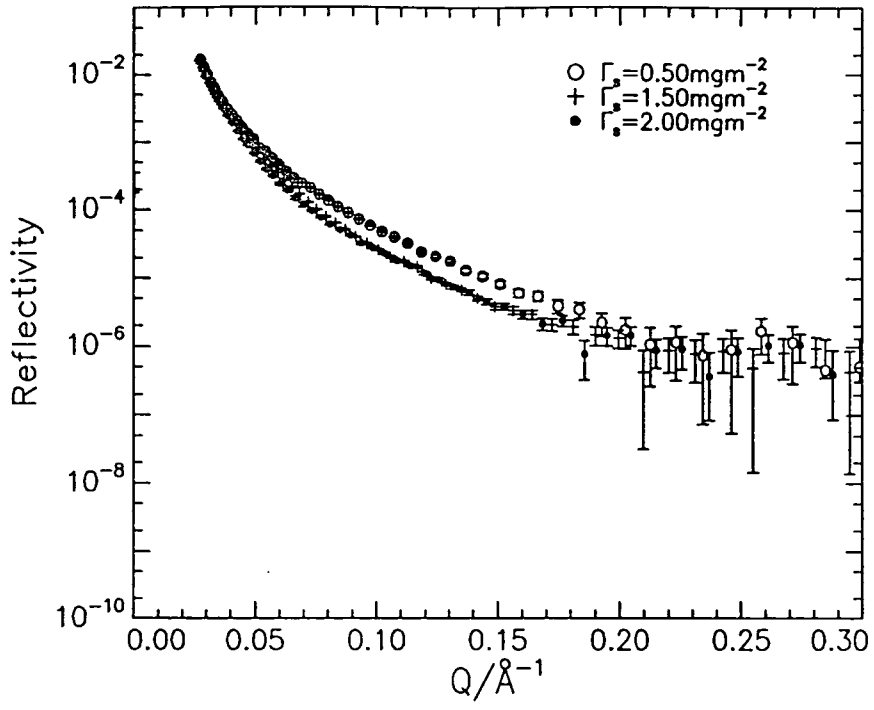

Figure 4.4.8 Reflectivity profiles for 20CP on D_2O.

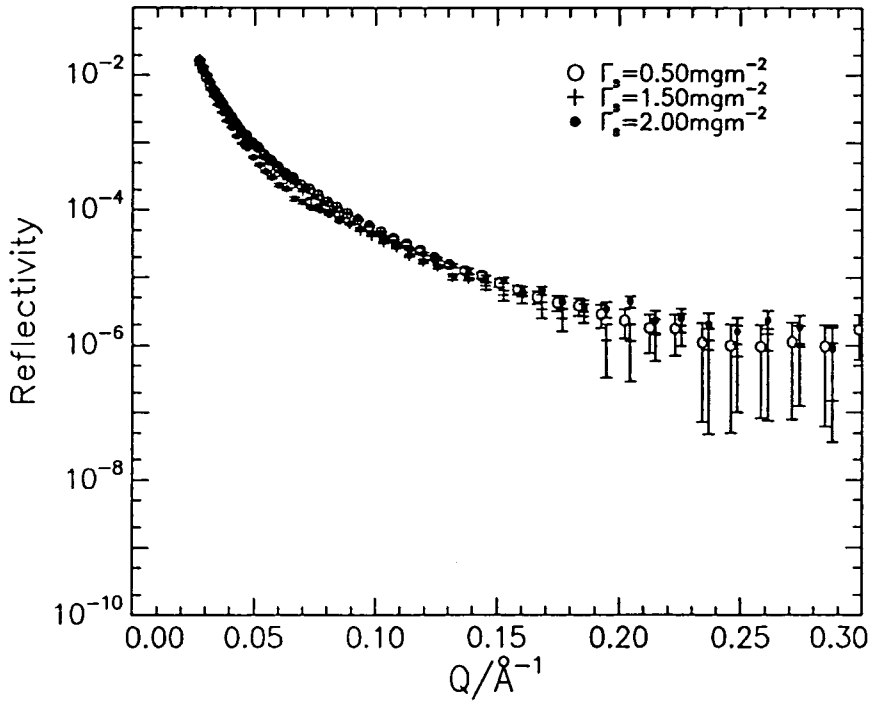

Figure 4.4.9 Reflectivity profiles for 20DP on D_2O.

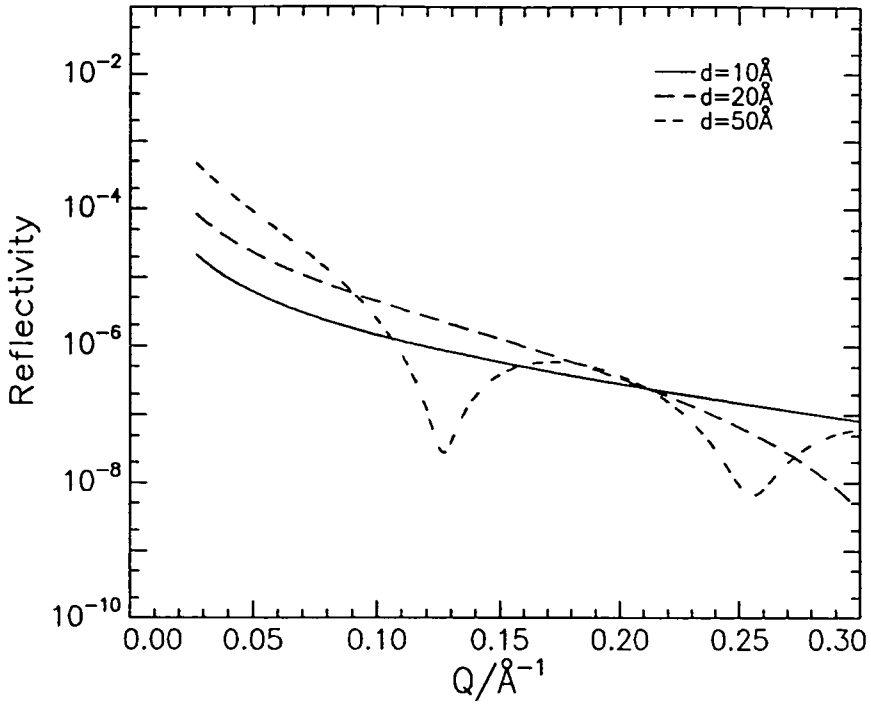

Figure 4.4.10 Simulated reflectivity profiles for a film on NRW where $\rho = 1 \times 10^{-6}$ Å^{-2} and the thickness, d is as given.

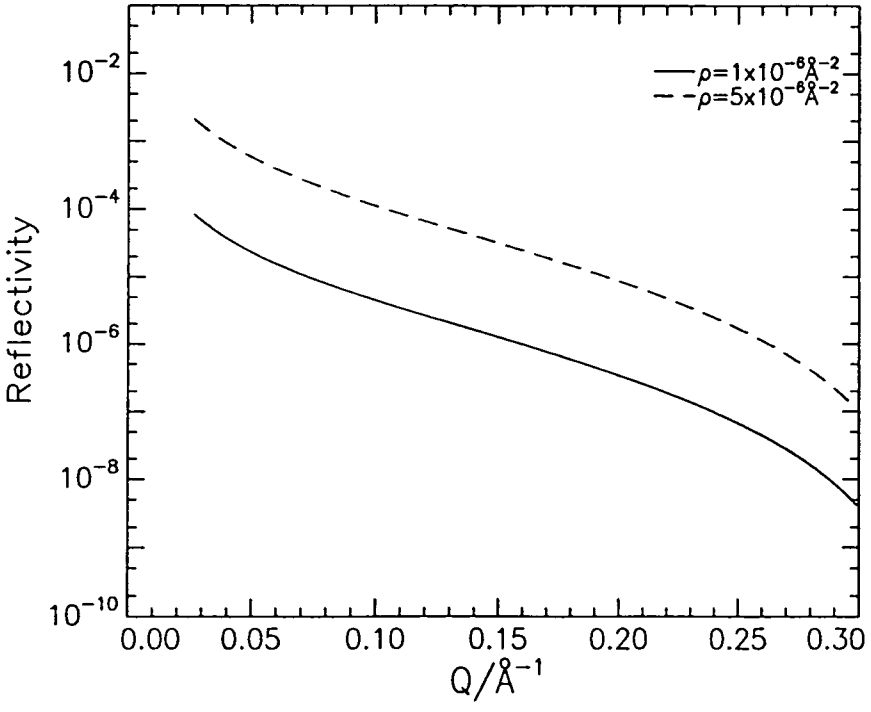

Figure 4.4.11 Simulated reflectivity profiles for a surface film 20 Å thick spread on NRW, the scattering length density is as indicated.

4.4.5 Data Analysis: Optical Matrix Analysis

4.4.5.1 Introduction

In the following discussion the application and results of fitting the reflectivity profiles for 20CP / 20DP are presented. Each surface concentration has been considered in turn with the most simple model applied initially, any modifications to this model are discussed as required. Application of the optical matrix analysis to the data for the other two graft copolymers, 10CP and 60CP, is exactly the same as given here and the results for these systems are presented in a more concise form following this Section.

The equations given in chapter 2, section 2.2, are central to the discussion and are repeated here.

The scattering length density of the layer, ρ, is related to the volume fraction, ϕ_i, and scattering length density of each component, ρ_i, by:

$$\rho = \sum \rho_i \phi_i$$

Equation 4.4.3

The number density, n_i, of each component is given by:

$$\phi_i \rho_i = b_i n_i$$

Equation 4.4.4

Giving an overall surface concentration:

$$\Gamma_s = \frac{n_i M_i d}{N_A} \times 10^{20} \quad \text{mg m}^{-2}$$

Equation 4.4.5

where M_i is the molecular weight of a monomer unit and d is the layer thickness.

4.4.5.2 Films of 20CP: $\Gamma_s = 0.50$ mg m^{-2}

As remarked earlier, the reflectivity profiles collected for both 20CP and 20DP on D_2O when $\Gamma_s = 0.5$ mg m^{-2} are almost identical. In addition the reflected signal for 20DP spread on NRW at this surface concentration was very low and subject to relatively large errors. It is clear that the contribution of the polymer to the reflectivity of these systems at this surface concentration is small.

A single layer model fitted the data for 20DP on NRW well giving the fit shown in figure 4.4.12 and the parameters shown in Table 4.4.2.

Contrast	d_1 / Å	ρ_1 / 10^{-6} Å^{-3}
20DP / D_2O	12 ± 1	4.00 ± 0.03
20CP / D_2O	10 ± 1	2.64 ± 0.01
20DP / NRW	11 ± 1	1.10 ± 0.02

Table 4.4.2: Parameters of a single layer fit, Γ_s = 0.5 mg m^{-2}

As a first approximation it is assumed that only the dPMMA contributes to the fitted ρ for this system. Given that for hPEO the scattering length density is small, at only 0.57 × 10^{-6} Å^{-2}, this seems a valid approximation. Using equation 4.4.3:

$$1.10 = 6.02\phi_{MA}$$

So that ϕ_{MA} = 0.18 which gives a number density of 1.10 × 10^{-3} Å^{-3} and Γ_{sMA} = 0.22 mg m^{-2}

The spread surface concentration of graft copolymer is 0.5 mg m^{-2}, of this 0.2 mg m^{-2} is PMMA. Clearly, the surface concentration calculated from the parameters of the single layer fit is consistent with the spread surface concentration .

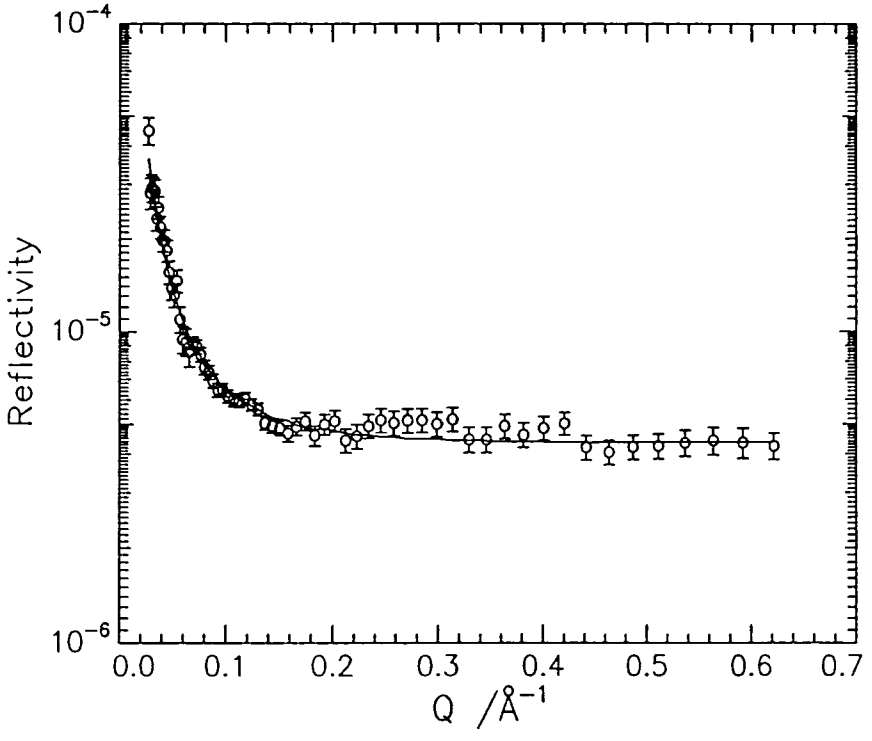

Figure 4.4.12 Single layer fit to reflectivity profile for 20DP on NRW.

However, when the single layer model was applied to the data on D_2O it was not possible to obtain reasonable quality fits to the data. Despite repeatedly starting the fit with different values for ρ and d the 'best' fits were found to be poor. The fitted parameters are also given in Table 4.4.2, an example of a fit is given in figure 4.4.13.

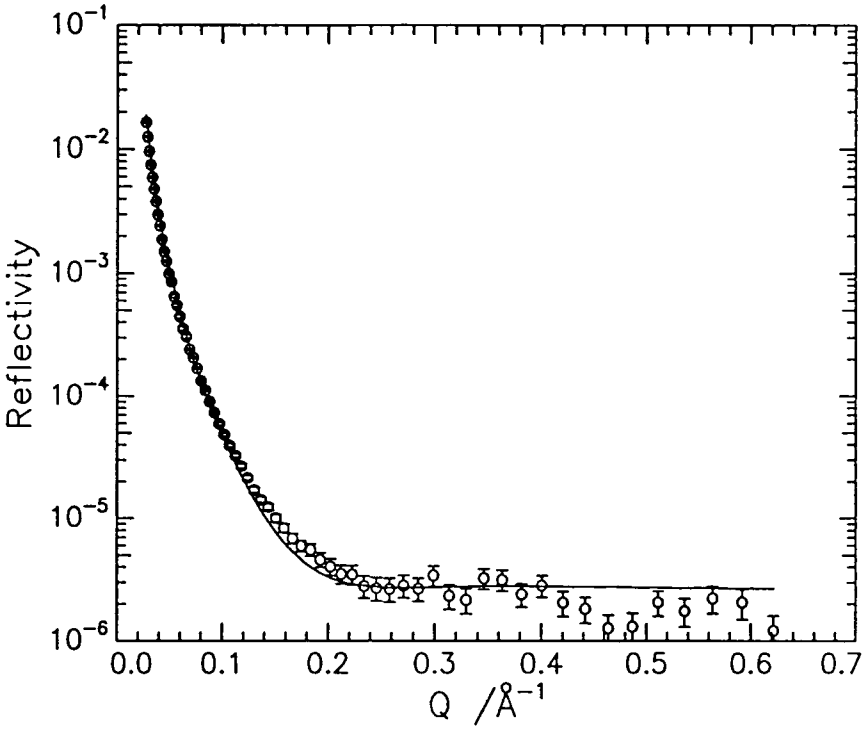

Figure 4.4.13 Single layer fit to reflectivity profile for 20DP on D_2O.

On examination of figure 4.4.13 it becomes clear that the single layer model does not reproduce the features of the data, particularly when Q exceeds 0.1 $Å^{-1}$. From this result it is concluded that where the subphase is D_2O the model is not sufficiently sophisticated to reproduce the behaviour of the system.

When 20DP is spread on NRW the contribution of the hPEO side chains to the reflectivity is likely to be negligible, especially if they are heavily solvated. Assuming that this contribution is negligible, the fact that a single layer model fitted the data adequately implies that the PMMA backbone of the graft copolymer remains at the uppermost surface forming a single layer. In comparison, when the polymers are spread on D_2O the PEO side chains contribute to the reflectivity, albeit indirectly. The influence of PEO on R(Q) is identified as indirect because, rather than causing reflection of the neutrons, its presence reduces the reflectivity of the D_2O. The observation that extra layers need to be incorporated

into the model to improve the quality of the fits to the D_2O data implies that the PMMA and PEO occupy different regions at the interface. Such behaviour is consistent with the suggestion that the PEO side chains are penetrating the subphase. A surface organisation of the kind intimated, with the PEO residing below a layer of PMMA, would lead to a lower layer which, although not contributing significantly to the overall reflectivity where the subphase is NRW, would depress the reflectivity of the D_2O and therefore contribute to profiles collected on this subphase.

Following from the discussion above, in an attempt to improve the quality of the fit to the reflectivity profiles on D_2O, a second layer was incorporated into the model. The parameters giving the best fits to the data are given in Table 4.4.3 and have been used to determine the layer composition.

Contrast	d_1 / Å	ρ_1 / 10^{-6} Å^{-2}	d_2 / Å	ρ_2 / 10^{-6} Å^{-2}
20DP / D_2O	10	5.94 ± 0.02	20 ± 2	5.79 ± 0.05
20CP / D_2O	11	5.52 ± 0.02	20 ± 1	6.13 ± 0.02

Table 4.4.3: Parameters of the two layer fit, Γ_s = 0.5 mg m^{-2}

Assuming the upper layer consists of PEO, PMMA and water two simultaneous equations can be constructed:

$$5.94 = 6.02\phi_{MA} + 0.57\phi_{EO} + (1 - \phi_{MA} - \phi_{EO})6.35$$

Equation 4.4.6

$$5.52 = 0.90\phi_{MA} + 0.57\phi_{EO} + (1 - \phi_{MA} - \phi_{EO})6.35$$

Equation 4.4.7

Using the equations above ϕ_{MA} was found to be 0.08, Γ_{sMA} = 0.10 mg m^{-2}, again rather low. On substitution of ϕ_{MA} = 0.08 into equation 4.4.6 it can be shown that ϕ_{EO} = 0.07 and, assuming that the remainder of the space is occupied by water, gives ϕ_W = 0.85. When the surface concentrations are computed this gives Γ_{sMA} = 0.1 mg m^{-2} and Γ_{sEO} = 0.08 mg m^{-2}. Given that the reflectivity profile for 20DP / NRW was fitted well with a single layer model it was assumed that the PMMA primarily occupies the upper layer. It follows from this that the lower layer contains only PEO and water. The fact that the scattering length density of this

layer does not increase at all between 20CP and 20DP, rather it actually decreases, supports this assumption.

Since the lower layer contains only two components the volume fraction of PEO can be computed from the scattering length densities obtained from fits to the profiles for both 20CP and 20DP on D_2O.

Basically, $$\rho_2 = 0.57\phi_{EO} + 6.35(1 - \phi_{EO})$$

In this way it was found that for 20DP / D_2O ϕ_{EO} = 0.10 and Γ_{sEO} = 0.12 mg m^{-2} whereas for 20CP / D_2O ϕ_{EO} was found to be 0.04 and Γ_{sEO} = 0.08 mg m^{-2}. The discrepancies exhibited by these two models may appear alarming. In fact this behaviour is believed to reflect the very high dilution of the PEO and the relatively large penetration depths that the chains extend to. If the PEO is heavily diluted the difference between the reflectivity of this layer and bulk D_2O may be only small, making the parameters of this layer difficult to identify. Added to this is the fact that the effects are occurring relatively deep into the subphase. Since Q correlates to $2\pi/d$ this infers that the Q range of interest will be around 0.2 - 0.25 $Å^{-1}$ where the reflected signal is approaching background and as a consequence the errors become more significant. These effects combine to hamper efforts to get a full characterisation of the lower layer.

Summing the surface concentration in each layer gives a total surface concentration of 0.33 mg m^{-2}, where 0.1 mg m^{-2} is PMMA and 0.23 mg m^{-2} is PEO. The overall ratio of PEO : PMMA by weight is 2.3 : 1. In fact the spread surface concentration was 0.5 mg m^{-2} which, given the uncertainty on the copolymer composition, indicates a PMMA content varying from 0.22 - 0.18 mg m^{-2}. The spread surface concentration is rather higher than that inferred from the models fitted to the reflectivity profiles recorded on D_2O. In contrast the value is in good agreement with the surface concentration extracted following a single layer fit to 20DP / NRW contrast for which Γ_{sMA} = 0.22 mg m^{-2}. Using the average volume fraction of PEO in the lower layer it can be shown that on NRW a layer 20 Å thick with a scattering length density of 0.04 × 10^{-6} $Å^{-2}$ would be anticipated. Given the large background inherent to data recorded on a null reflecting subphase, as well as the heavy dilution of the side chains and very low ρ, detection of this layer will be beyond the sensitivity of the experiment.

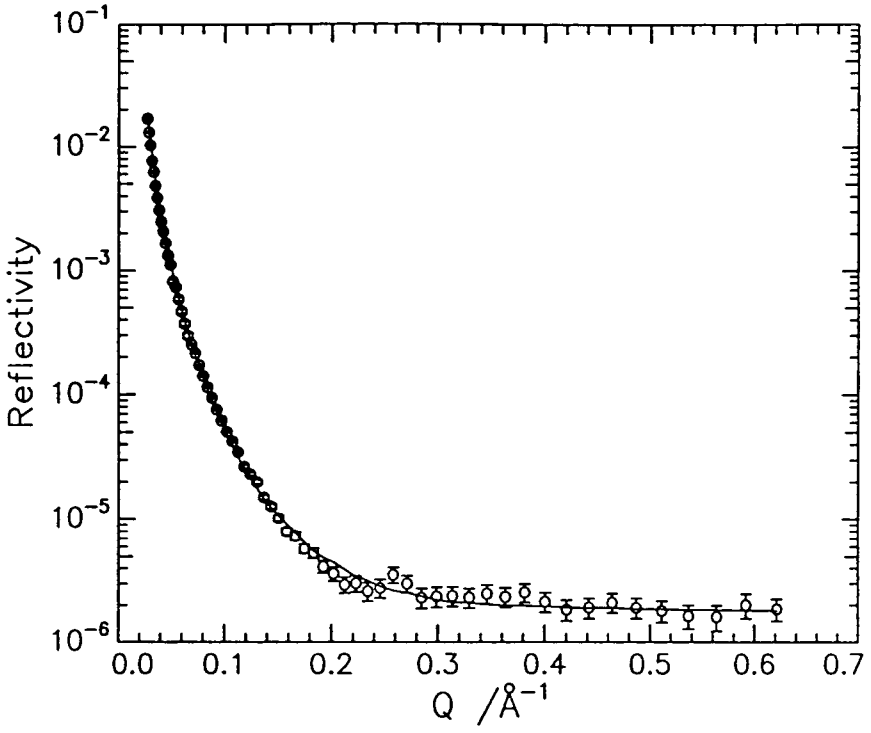

Figure 4.4.14 Two layer fit to reflectivity profile for 20DP on D_2O.

Having rationalised the model adopted for 20DP / NRW, attention is turned to the details of the two layer models. The two layer model fits the reflectivity data well, see figure 4.4.14. Despite the reasonable fits obtained the fitted parameters imply surface concentrations rather lower than the known spread amount. Assuming that layer 1 contains PMMA, PEO and water, whereas layer 2 contains just PEO and water, the layer compositions have been determined. The values are given in Table 4.4.4.

The surface concentration of each constituent in the graft copolymer can be calculated from these values and it can be shown that whilst Γ_{sMA} = 0.1 mg m^{-2}, Γ_{sEO} = 0.23 mg m^{-2}. From these results it appears that the surface concentration of PEO was reproduced rather better than PMMA. A number of possible reasons for such behaviour can be suggested. Although the error in determining the copolymer composition is likely to be the greatest source of error other possibilities include not only the solution concentration and preparation, but also deposition of the solution. Even slight errors in each of these steps may combine to give errors which, given the very dilute film studied here, may have a significant effect. Other ways in which PMMA may be 'lost' include the fact that the polymer may be so dilute that its influence on the reflectivity is marginal.

Given the results presented in figure 4.4.1, where it is clearly demonstrated that R(Q) is barely changed from that of D_2O, this suggestion appears to be feasible. Considering the behaviour illustrated in figure 4.4.1 it is also clear that the profiles are not only very like D_2O, but in addition they are essentially identical to one another and are coincident over much of the Q range. This accounts for some of the difficulties encountered in fitting and interpreting this data and leads to the suggestion that, at such low concentrations of polymer, the limits of experimental sensitivity are approached.

Behaviour associated with experimental sensitivity, and the very slight depression in R(Q) for D_2O due to the dilute nature of the film, caused other problems. It was observed that a number of different layer compositions and layer thicknesses in addition to those given here provided good quality fits to the reflectivity data. In particular, it was observed that the lower layer had a tendency to return a very high layer thickness. Although such parameters gave excellent fits to the experimental reflectivity data the extracted surface concentrations were found to be at least twice the spread amount. Given this result the fits were discounted but for compleness these tendencies are noted.

Despite the problems encountered and outlined above it has been illustrated that the PMMA backbone remains predominantly at the uppermost surface. The PMMA in this layer is mixed with both water and the PEO side chains. The latter groups exhibit a tendency to penetrate the subphase, requiring a second layer to be incorporated into the model wherever the subphase is highly reflecting. The overall layer dimensions and parameters given by this model are presented in Table 4.4.4.

Layer No.	d / Å	ϕ_{MA}	ϕ_{EO}	ϕ_W
1	10 ± 1	0.08	0.07	0.85
2	20 ± 1	-	0.07	0.93

Table 4.4.4: Layer composition and dimensions, Γ_s = 0.5 mg m^{-2}

4.4.5.3 Films of 20CP: Γ_s = 1.50 mg m^{-2}

At a first glance the data for Γ_s = 1.5 mg m^{-2} appear to be fitted relatively successfully by a single layer model. The fitted parameters are reported in Table 4.4.5 and, as can be seen, the model gave consistent layer thicknesses for the data recorded on D_2O.

Contrast	d / Å	$\rho \times 10^{-6}$ Å^{-2}
20DP / D_2O	27 ± 1	5.42 ± 0.03
20CP / D_2O	27 ± 1	5.16 ± 0.02
20DP / NRW	12 ± 1	2.66 ± 0.02

Table 4.4.5: Parameters of single layer fits where Γ_s = 1.5 mg m^{-2}.

As observed when Γ_s = 0.50 mg m^{-2} the layer thicknesses for an NRW subphase are very much less than on D_2O. Again this is attributed to the fact that, where the subphase is null scattering, only the dPMMA contributes to the reflectivity. Clearly, much thicker layers were required to fit the single layer model to the reflectivity profiles recorded on D_2O, behaviour attributed to the contribution of the hPEO side chains. It follows, from the parameters of the single layer fit, that the reflectivity of the D_2O is depressed over larger length scales than those occupied by the main chain backbone of the graft copolymer. This result implies substantial subphase penetration by the side chains. The fitted parameters thus provide evidence to suggest that the PMMA and PEO exhibit a tendency to occupy different spatial regions where possible.

Considering the parameters for 20DP on NRW, and ignoring any contribution to the reflectivity from the hPEO, gives:

ϕ_{MA} = 0.44 $\qquad$ Γ_s = 0.58 mg m^{-2}

It is known that the total spread film concentration was 1.5 mg m^{-2} which, given the uncertainty on the composition, indicatesa surface concentration of PMMA in the range 0.59 ± 0.05 mg m^{-2}. Thus the surface concentration calculated from the parameters of the single layer model is clearly in good agreement with the spread surface concentration. When attention is turned to consider the quality of the fits obtained using the single layer model some discrepancies can be identified. Generally it is observed that the fitted reflectivity is a little high over the Q range 0.1 - 0.2 Å^{-1}. This feature is particularly noticeable when the fits to the profiles recorded on D_2O are considered, see figure 4.4.15.

Reflectivity data for both these contrasts is only fitted successfully up to Q values around 0.14 Å^{-1}, implying that additional layers are required to reproduce the reflectivity profiles satisfactorily.

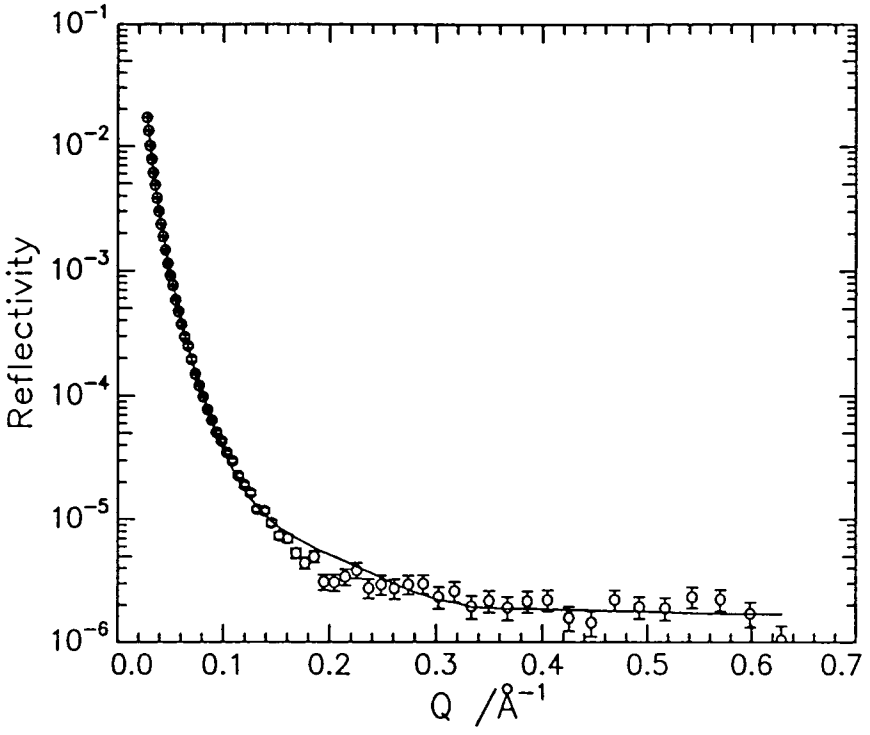

Figure 4.4.15 Single layer fit to 20DP / D_2O.

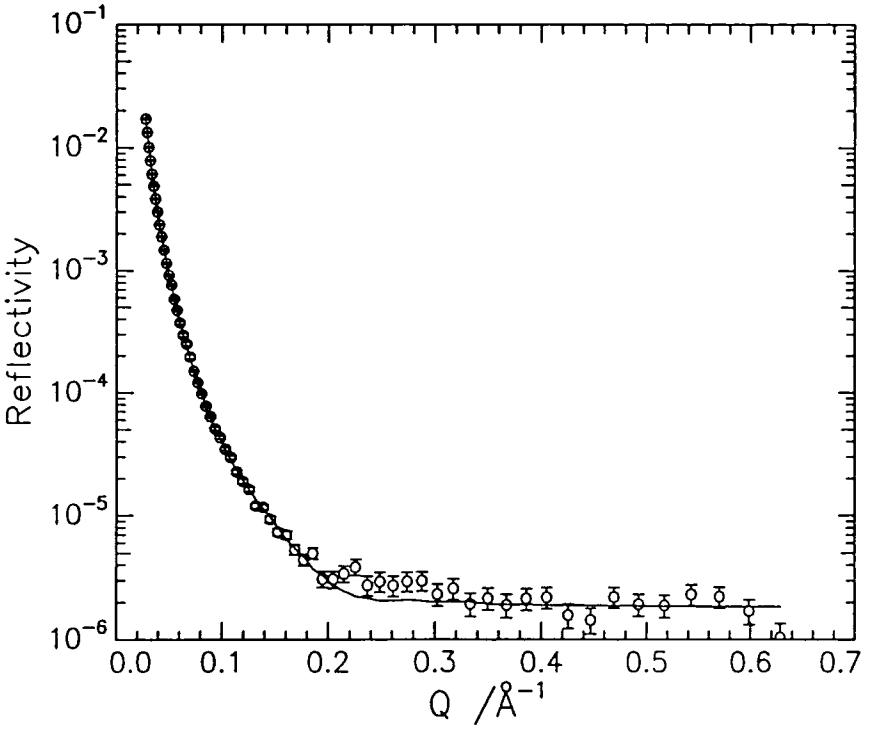

Figure 4.4.16 Two layer fit to 20DP / D_2O.

In response to this result a two layer model was fitted to the data. The quality of the fits are much improved over those for a single layer model. This is illustrated in figure 4.4.16 where the same raw data as presented in figure 4.4.15 is given with the results of fitting a two layer model. The features of the experimental reflectivity have been reproduced well up to Q values of 0.2 $Å^{-1}$.

The parameters of the two layer fits are given in Table 4.4.6.

Contrast	d_1 / Å	ρ_1 / 10^{-6} $Å^{-2}$	d_2 / Å	ρ_2 / 10^{-6} $Å^{-2}$
20DP / D_2O	13 ± 2	4.82 ± 0.25	28 ± 2	5.94 ± 0.03
20CP / D_2O	13 ± 1	2.69 ± 0.06	29 ± 1	5.87 ± 0.03
20DP / NRW	11 ± 1	2.68 ± 0.04	28 ± 1	0.16 ± 0.03

Table 4.4.6: Parameters of two layer fit, Γ_s = 1.5 mg m^{-2}

The parameters of the fit to 20DP / NRW are the most straight forward to interpret and are considered first. The reflectivity of the upper layer is assumed to be due to the presence of dPMMA giving ϕ_{MA} = 0.44 and Γ_{sMA} = 0.53 mg m^{-2} . This value is in good agreement with the known spread surface concentration of PMMA, 0.59 ± 0.05 mg m^{-2}.

To see how this result compares to the fits to the R(Q) data for 20CP / D_2O and 20DP / D_2O attention is turned to the parameters of the two layer fits to these systems. By combining the fitted parameters for layer 1, and assuming that this layer contains only graft copolymer and water, it can be shown that:

$\phi_{MA} = 0.42$ $\phi_{EO} = 0.24$ $\phi_W = 0.34$

There is good agreement between the volume fraction of PMMA inferred from these models and that for 20DP / NRW. This is despite the fact that the contribution of PEO to the top layer was ignored for the latter system. Given the result above, which indicates that the top layer contains both polymer backbone and side chains, the parameters of the fit to the NRW data are reconsidered. Using the volume fractions given above the scattering length density for layer 1 for 20DP / NRW is predicted to be 2.67 × 10^{-6} $Å^{-2}$. This value is in excellent agreement with the fitted ρ for this contrast, see Table 4.4.6. Thus it is clear that the fitted ρ for layer 1 for each contrast is consistent with the composition given above. This result, combined with the fact that all the fits indicate layers of essentially the same

dimensions, suggests that a two layer fit is the most appropriate model for the surface organisation adopted by this concentration of 20CP.

The surface concentration of each component in the upper layer has been computed:

$\Gamma_{sMA} = 0.59$ mg m^{-2}

$\Gamma_{sEO} = 0.35$ mg m^{-2}

Using the parameters fitted to the profiles recorded on D_2O and assuming that the lower layer contains only PEO and water, the volume fraction of PEO has been calculated:

For 20CP / D_2O

$\phi_E = 0.08$ $\Gamma_{sEO} = 0.26$ mg m^{-2}

For 20DP / D_2O

$\phi_E = 0.07$ $\Gamma_{sEO} = 0.22$ mg m^{-2}

Indicating that the surface concentration of PEO in the lower layer is 0.24 ± 0.02 mg m^{-2} giving an overall surface concentration of 0.57 mg m^{-2}.

$0.24 + 0.35 = 0.57$ mg m^{-2}

This is low compared to the known spread concentration of PEO which was 0.91 ± 0.05 mg m^{-2}. When the fitted parameters for 20DP / NRW are considered a rather different picture emerges. Assuming that the layer contains only PEO and water implies a far higher PEO content with $\phi_{EO} = 0.28$ and a surface concentration of 0.87 mg m^{-2} in this layer alone. This indicates an overall surface concentration of 1.22 mg m^{-2} considerably more than the spread amount.

There is clearly some ambiguity associated with determining the PEO content of the lower layer. Assuming that the parameters of the fits to the D_2O data are representative of the system, the scattering length density of this lower layer on NRW is anticipated to be 0.04×10^{-6} $Å^{-2}$, considerably lower than the fitted value. The only other component which may be contained in this layer, and thus contributing to ρ, is dPMMA. The 'residual' scattering length density of 0.12×10^{-6} $Å^{-2}$ indicates a volume fraction of PMMA of only 0.02. Such a low PMMA content may pass unnoticed where the scattering length density of the subphase is high, i.e. D_2O. To illustrate this consider the situation of either polymer on D_2O, making the

assumption that the lower layer is composed of PMMA backbone, PEO side chains and water. The volume fractions of the polymeric components being 0.02 and 0.07 respectively. Where the polymer 20CP is spread on D_2O the scattering length density of such a layer is 5.84×10^{-6} $Å^{-2}$. Given the uncertainty on the fitted parameters it follows that this layer composition is consistent with the results of the two layer fit. In the case of 20DP on D_2O the scattering length density of a layer of the same composition is 5.94×10^{-6} $Å^{-2}$, exactly the value returned by the optical matrix model fitting.

From the discussion above it becomes clear that whilst the bulk of the dPMMA resides in the upper layer a very small amount penetrates into the lower layer. Given that the side chains are believed to be distributed fairly randomly along the backbone, the length of the sections of PMMA between side chains may differ. Where two side chains are close together it is feasible that, as the side chains penetrate the subphase, the backbone will also be dragged down into the subphase beyond the confines of layer 1. An alternative mechanism for incorporation of PMMA into this lower layer is that of chain ends just dipping below layer 1. Only a very small amount of PMMA, 0.05 mg m^{-2}, behaves in this way.

The only remaining reservation regarding adoption of this model is the fact that the surface concentration of PEO implied by the fitted parameters is considerably lower than the spread amount, 0.57 ± 0.02 mg m^{-2} as opposed to 0.91 ± 0.05 mg m^{-2}. Following careful consideration it is believed that the discrepancy arises due to the high dilution of the PEO side chains occurring at increasing depths from the surface, as a result of which some of the chains appear to be 'lost'. To investigate and characterise such behaviour requires selective deuteration of the side chains, unfortunately as already mentioned synthesis of these polymers has proved difficult.

Layer No.	d / Å	ϕ_{MA}	ϕ_{EO}	ϕ_W
1	12 ± 1	0.42	0.24	0.34
2	28 ± 1	0.02	0.07	0.91

Table 4.4.7: Layer composition and dimensions, Γ_s = 1.5 mg m^{-2}

From the above discussion it is concluded that, at this surface concentration of the graft copolymer 20CP, the surface organisation adopted can be adequately described by a two layer model. The PMMA backbone of the polymer resides mainly in the upper layer which is 12 ± 1 Å thick. In contrast the PEO side chains are contained in both layers, about 60%

remaining in the upper layer mixed with PMMA and water. The lower layer is considerably thicker and contains mainly water with heavily diluted side chains and a small amount of PMMA backbone which is believed to be looping down from the uppermost layer. The details of the layer compositions and dimensions are summarised in Table 4.4.7.

4.4.5.4 Films of 20CP: $\Gamma_s = 2.0$ mg m^{-2}

On increasing the surface concentration of graft copolymer to 2 mg m^{-2} it was observed that the reflectivity profiles exhibited many more features than at low surface concentrations. It was evident that at Q values greater than 0.06 Å^{-1} the profiles were not only quite distinct from one another, but also from that of D_2O. Initially the simplest single layer model was applied to describe this system.

Contrast	d /Å	$\rho \times 10^{-6}$ Å^{-2}
20DP / NRW	14 ± 1	4.40 ± 0.04
20DP / D_2O	49 ± 1	5.26 ± 0.02
20CP / D_2O	33 ± 2	4.92 ± 0.01

Table 4.4.8: Parameters of a single layer fit to the data, $\Gamma_s = 2.0$ mg m^{-2}

From Table 4.4.8 it is clear that the layer thicknesses returned by fitting a single layer model to the data are not consistent for the different contrasts. As might be expected from behaviour observed for lower surface concentrations of polymer, the single layer model reproduces the profile for 20DP / NRW most successfully, see figure 4.4.17. This is also observed to be the narrowest layer at the interface being only 14 Å thick, in contrast for 20DP / D_2O the layer is 49 Å, for 20CP / D_2O 33 Å. By making the assumption that a single layer, although a crude model of the system, describes the region of the interface over which the scattering length density differs from that of the bulk, these apparent variations in layer thickness may be rationalised, albeit only qualitatively. As mentioned in regard to previous profiles collected on NRW, only the region occupied by the dPMMA backbone of the copolymer is anticipated to contribute to this profile. This indicates that, as seen at lower Γ_s, the main backbone of the graft copolymer occupies a fairly narrow region of the interface.

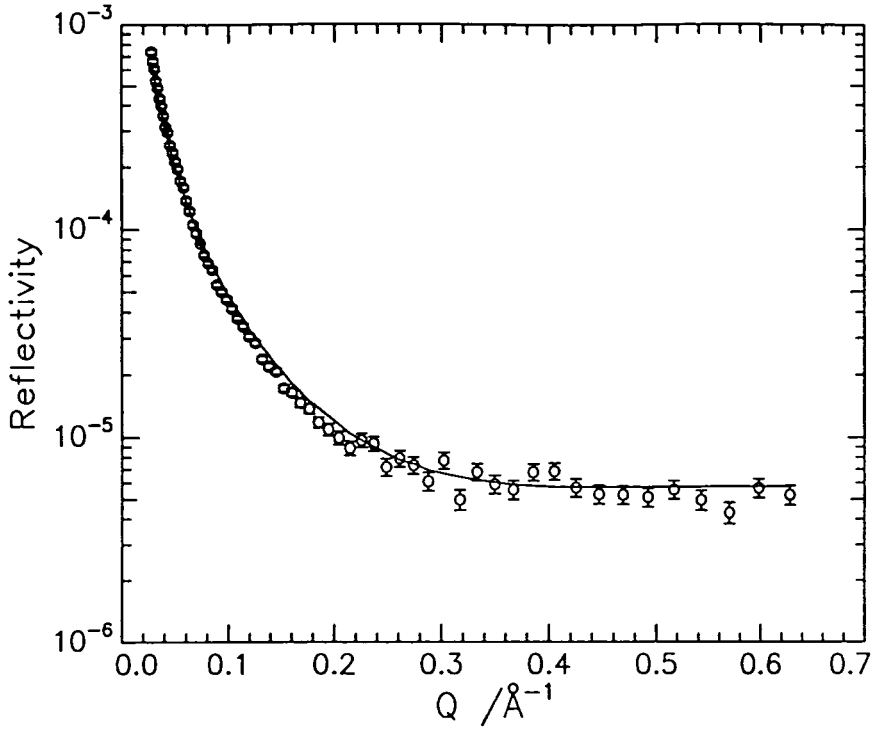

Figure 4.4.17 Single layer fit to 20DP / NRW.

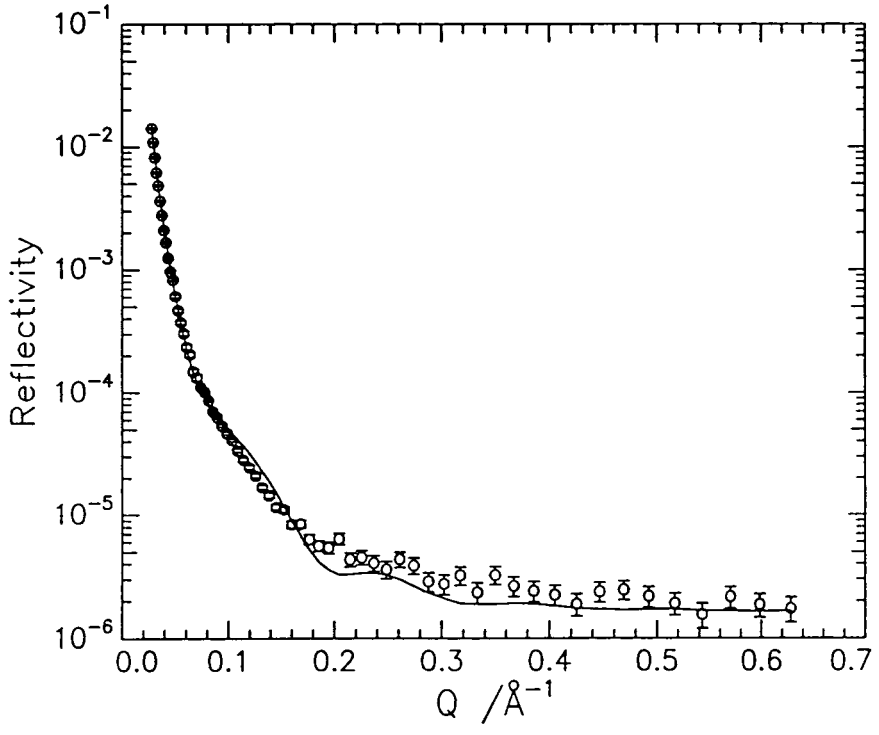

Figure 4.4.18 Single layer fit to 20DP / D_2O.

Conversely, when the polymer is spread on D_2O since all the components depress the reflectivity of the subphase the apparent layer thickness may change. An increase in the apparent layer thickness is indicative of the side chains and polymer backbone occupying different regions at the interface

The parameters of the single layer fit to the NRW data imply that the backbone occupies an interfacial region 14 Å wide. If this layer is in the subphase then it should contribute to the reflectivity of both 20CP and 20DP on D_2O. Under these circumstances although the layers fitted to these profiles may appear considerably thicker than 14 Å, the values for each contrast should be essentially the same. In fact the fitted layer thickness for 20CP on D_2O is 16 Å less than for a film of 20DP. This is believed to indicate that the layer occupied by the PMMA is not in contact with the subphase. A hydrogenous layer of PMMA mixed with air would have a negligible influence on R(Q). In contrast where the backbone is deuterated, because the scattering length density of dPMMA is quite high, it would be expected to influence R(Q). As a result of these effects the film formed by 20DP on D_2O would appear thicker than that formed by 20CP. The latter statement will only be true if the PMMA is not heavily diluted by air, which would cause a considerable reduction in the scattering length density of the layer. The evidence supporting a significant contribution from this layer is provided by the parameters of the fit to the profile for 20DP on NRW which indicate a high volume fraction of PMMA concurrent with a thin, dense layer.

Although the arguments outlined above rationalise the discrepancies in the layer thicknesses, to account fully for the surface organisation adopted by the copolymer requires incorporation of additional layers into the model. This can be confirmed by considering the quality of the fits to the reflectivity data in more detail. It becomes clear that the single layer model does not reproduce the experimental data satisfactorily. The model provides a poor fit to the data for 20DP / D_2O, see figure 4.4.18. On examination of the single layer fit to the NRW data it is evident that when $Q > 0.1$ Å^{-1} the reflectivity is very slightly overestimated by the model clearly indicating that a more sophisticated model is required to improve on the quality of the fit.

As illustrated in figure 4.4.19 the reflectivity profiles for 20DP / NRW is reproduced successfully by the two layer model. However, despite this success the model fails to fit the profiles collected on D_2O satisfactorily. Problems are encountered, mainly at $Q > 0.12$ Å^{-1}, where the reflectivity data exhibits some characteristic features, which are clearly real effects, and as such must be reproduced by any reasonable model of the system.

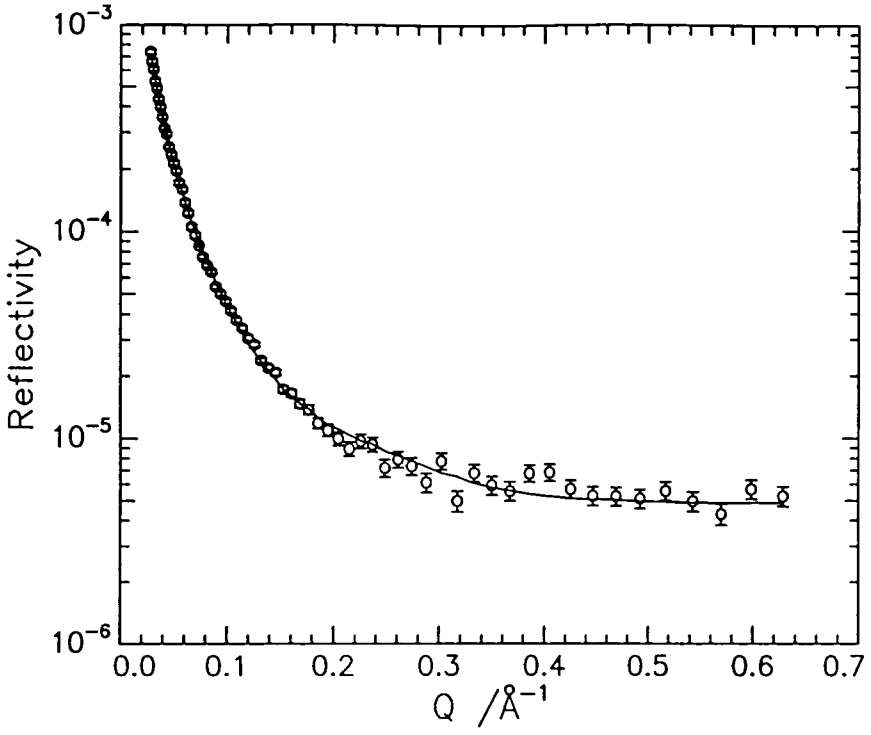

Figure 4.4.19 Two layer model fitted to the reflectivity profile for 20DP / NRW

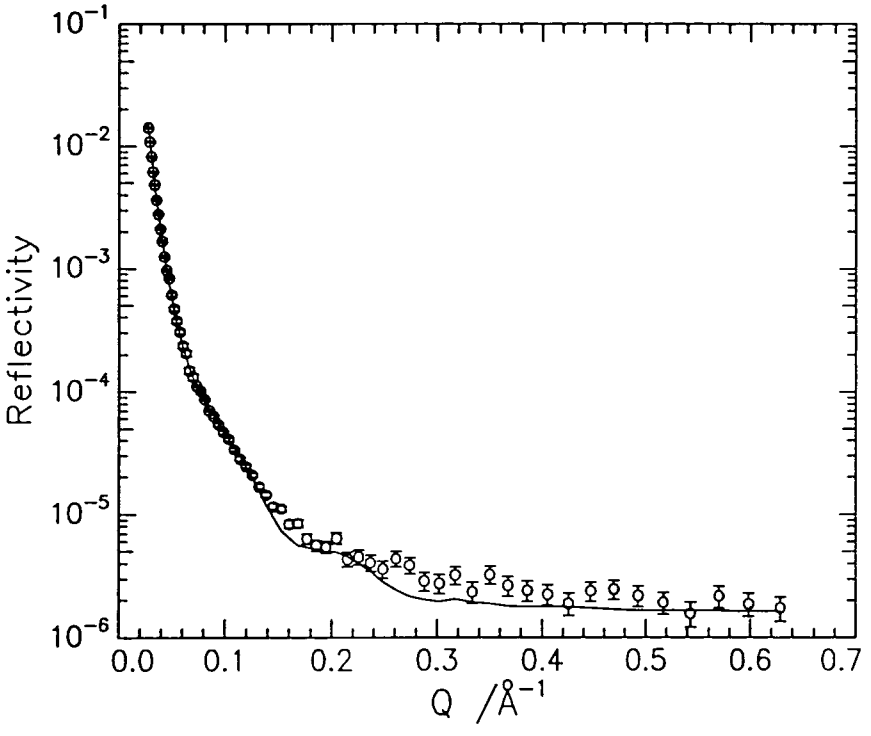

Figure 4.4.20 Two layer model fitted to the reflectivity profile for 20DP / D_2O.

This is illustrated by careful comparison of the data in figure 4.4.20 and the 'best fit' as given by the two layer model. The failure of this model is confirmed by the fitted parameters given in Table 4.4.9. Although there is better agreement than for the single layer fits to the profiles collected on D_2O, the layer thicknesses required to fit the data with this model are still far from consistent. In addition, the surface concentration calculated from the parameters, given in Table 4.4.9 assuming a top layer of PMMA, PEO and water and a lower layer of just PEO and water, is low at only 1.3 mg m^{-2}.

Contrast	d_1 / Å	$\rho_1 \times 10^{-6}$ Å^{-2}	d_2 / Å	$\rho_2 \times 10^{-6}$ Å^{-2}
20DP / NRW	10 ± 1	5.17 ± 0.02	23 ± 1	0.37 ± 0.04
20DP / D_2O	30 ± 1	5.11 ± 0.03	27 ± 2	5.58 ± 0.02
20CP / D_2O	22 ± 1	4.57 ± 0.01	25 ± 1	5.53 ± 0.03

Table 4.4.9: Fitted parameters for a two layer model, Γ_s = 2.0 mg m^{-2}

Given the failure of both the single layer and two layer models to fit the reflectivity data, particularly that recorded on D_2O a third layer was introduced into the model.

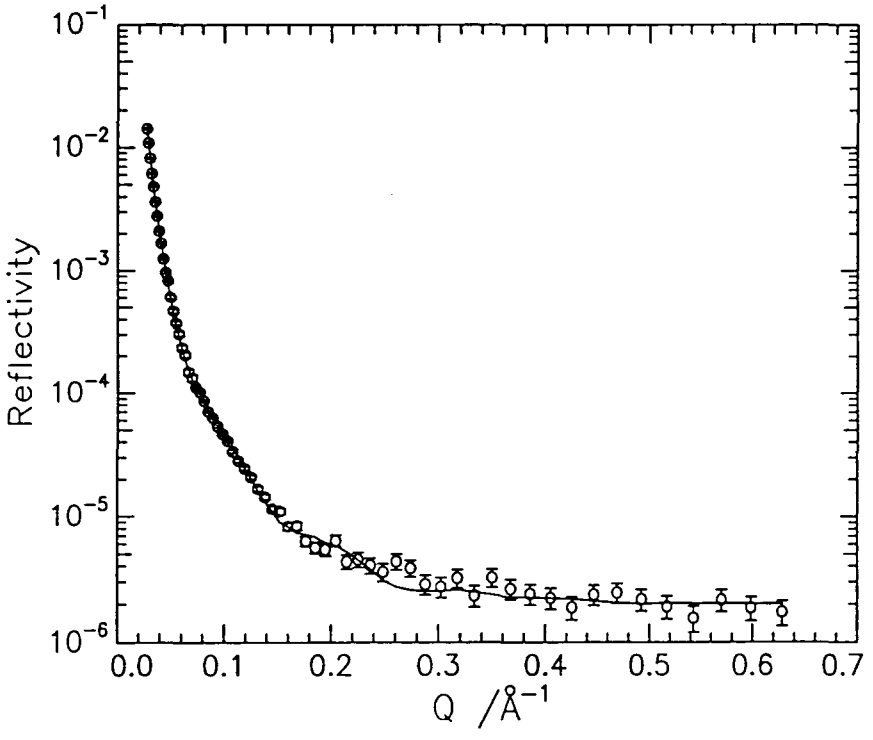

Figure 4.4.21 Three layer model fitted to the reflectivity profile for 20DP / D_2O.

Fitting a three layer model to the data improved the quality of the fit greatly. As illustrated in figure 4.4.21 all the features of the reflectivity profiles collected on D_2O are reproduced by the model. The parameters of the fits to the D_2O data are presented in Table 4.4.10.

Contrast	d_1 / Å	$\rho_1 \times 10^{-6}$ Å^{-2}	d_2 / Å	$\rho_2 \times 10^{-6}$ Å^{-2}	d_3 / Å	$\rho_3 \times 10^{-6}$ Å^{-2}
20DP/D_2O	10 ± 1	5.51 ± 0.03	23 ± 1	5.14 ± 0.02	24 ± 1	5.61 ± 0.01
20CP/D_2O	9 ± 1	0.80 ± 0.02	23 ± 1	4.87 ± 0.04	25 ± 1	5.78 ± 0.03

Table 4.4.10: Fitted parameters for a three layer model, $\Gamma_s = 2.0$ mg m^{-2}

Both the profiles collected on D_2O are fitted well by this model and a direct comparison between the fitted parameters demonstrates clearly, that the thicknesses returned by fitting the reflectivity data for the two contrasts are in good agreement. To establish whether the scattering length densities of the two layers are consistent requires a somewhat more detailed analysis. The scattering length density for layer 1 is high for 20DP but low for 20CP. This is clearly correlated to the presence of the deuterated backbone in the graft copolymer. Given the low scattering length density of this layer for the contrast 20CP on D_2O it follows that the layer is predominantly PMMA and air. Assuming that this top layer contains only PMMA and air the volume fraction of PMMA can be determined from the parameters of each contrast:

For 20DP / D_2O $\phi_{MA} = 0.89$

For 20CP / D_2O $\phi_{MA} = 0.90$

The parameters fitted to the second layer indicate a relatively high scattering length density independent of deuteration of the backbone of the graft copolymer. This suggests that the layer contains a significant amount of water. Assuming that this layer contains PEO, PMMA and water the volume fraction of each component can be computed. The presence of PMMA in this layer is evident since ρ is slightly higher for 20DP than 20CP. It can be shown that $\phi_{MA} = 0.06$, $\phi_{EO} = 0.20$ and $\phi_W = 0.74$. The scattering length density of the third layer is observed to be independent of deuteration of the backbone indicating that the layer contains only water and PEO. Calculating the volume fraction of PEO and water in this layer shows

that the PEO is very heavily diluted occupying a volume fraction of only 0.11 as opposed to 0.89 occupied by the water.

Having determined the composition of each layer the surface concentration of each component can be calculated. The details of the layer compositions are summarised below in Table 4.4.11.

Layer No.	d / Å	ϕ_{MA}	ϕ_{EO}	ϕ_{W}
1	10 ± 2	0.90	-	-
2	23 ± 1	0.06	0.20	0.74
3	24 ± 2	-	0.11	0.89

Table 4.4.11: Layer compositions as calculated for a three layer model, $\Gamma_s = 2.0$ mg m^{-2}

The overall calculated surface concentration is 1.75 mg m^{-2} which is in reasonable agreement with the spread surface concentration, 2 mg m^{-2}. On examination it transpires that the discrepancy lies mainly in the surface concentration of PEO which was 0.8 mg m^{-2} rather than that calculated from the spread volume, which was in the range 1.1 - 1.2 mg m^{-2}. This result is consistent with observations made for the more dilute films where any discrepancies in the calculated Γ_s, compared to the spread amount, were mainly attributable to 'lost' PEO. As discussed previously this is believed to be a symptom of the high dilution of PEO occurring at increasing depths from the surface.

Referring to the parameters of the two layer fit for 20DP / NRW given in Table 4.4.9, it becomes clear that the thickness of each layer is consistent with those for layers 1 and 2 of the three layer fits to the contrasts on D_2O. In addition to this the quality of the fit to the 20DP / NRW data obtained using a two layer fit was good. Before introducing a third layer to the model, consideration was given as to whether the reflectivity profiles for 20DP / NRW would be sensitive to the presence of a lower layer of heavily diluted PEO. The scattering length density of this layer on NRW would be 0.06×10^{-6} Å^{-2}, barely outside the uncertainty encountered on the fitted ρ values. Simulations show that, given the high background which all the profiles recorded on NRW are subject to, the influence of a layer with $\rho = 0.06 \times 10^{-6}$ Å^{-2} on the reflectivity profile will be negligible. With these considerations in mind it was decided that for this contrast a two layer fit is consistent with the overall model adopted to describe the surface organisation of the graft copolymer. The scattering length densities of the

two layers are both consistent with the layer composition reported in Table 4.4.11, a result that provides further evidence for the applicability of this model.

It is evident from the discussion above that a three layer model is required to describe and account for the behaviour of this system when Γ_s = 2 mg m^{-2}. The model indicates that the backbone of the graft copolymer occupies a layer above the subphase which is devoid of the PEO side chains. A small amount of the backbone protrudes into the second layer, probably just due to the physical links between the side chains and the backbone. The PEO side chains exist in the lower two layers populating a region around 47 Å thick, the dilution of the side chains is considerable and increases with depth.

4.4.5.5 Results of Optical Matrix Analysis for 10CP and 60CP

Neutron reflectometry profiles for 10CP and 60CP at two different surface concentrations have been fitted using the same technique as outlined for 20CP, consequently only the results of the fits are presented here. In general it was observed that, as for 20CP, the data at the lowest surface concentration were particularly difficult to fit. The choice between a number of possible fits was made on the Γ_s values calculated, otherwise it was not possible to differentiate between the quality of the fits.

4.4.5.5A 10CP

Neutron reflectometry profiles were collected for 10CP at two surface concentrations, $\Gamma_s = 0.4$ mg m^{-2} and $\Gamma_s = 1.1$ mg m^{-2}. A two layer model was required to fit the reflectivity data for the low concentration whereas at the higher surface concentration it was necessary to incorporate a third layer into the model. The results of the fits are presented in tables 4.4.12 and 4.4.13.

$\Gamma_s = 0.4$ mg m^{-2}

Contrast	d_1 / Å	ρ_1 / 10^{-6} Å^{-3}	d_2 / Å	ρ_2 / 10^{-6} Å^{-3}
10DP / D_2O	16 ± 1	5.62 ± 0.04	47 ± 2	6.17 ± 0.02
10CP / D_2O	16 ± 1	5.58 ± 0.04	51 ± 2	6.10 ± 0.02
10DP / NRW	16 ± 1	0.53 ± 0.03	-	-

Table 4.4.12: Fitted Parameters for 10CP, $\Gamma_s = 0.40$ mg m^{-2}

At $\Gamma_s = 0.40$ mg m^{-2} the profile recorded on NRW was not sensitive to the lower diffuse layer and was adequately fitted by a single layer model. As seen for 20CP the upper layer of the surface film was composed of water, PEO and PMMA whereas the lower layer contained PEO heavily diluted by water and a small amount of PMMA. The presence of PMMA in this lower layer is attributed to similar processes as discussed previously, i.e. the PEO side chains 'dragging' some of the backbone into the subphase. Since there are more side chains in this graft copolymer, and therefore shorter lengths of PMMA between them, such behaviour would be anticipated.

The details of the film composition are presented in Table 4.4.13, although it is noted that the surface concentration of PMMA calculated from these values was about half of the value spread, i.e. 0.05 mg m^{-2} as opposed to 0.11 ± 0.02 mg m^{-2}. The discrepancy is believed to be due to heavy dilution of the backbone such that its influence on the reflected signal was very small.

Layer No	d / Å	ϕ_{MA}	ϕ_{EO}	ϕ_{W}
1	16 ± 1	0.02	0.13	0.86
2	49 ± 2	0.01	0.03	0.94

Table 4.4.13: Layer composition and dimensions, 10CP Γ_s = 0.4 mg m^{-2}

As is illustrated by figure 4.4.22 this model reproduces the reflectivity of the system well.

Γ_s = 1.1 mg m^{-2}

At Γ_s = 1.1 mg m^{-2} a three layer fit was required to fit the reflectivity data collected on D_2O. Once again the profile recorded on NRW was not sensitive to the deepest layer and could be fitted adequately by a two layer model.

Contrast	d_1 / Å	ρ_1 / 10^{-6} $Å^{-3}$	d_2 / Å	ρ_2 / 10^{-6} $Å^{-3}$	d_3 / Å	ρ_3 / 10^{-6} $Å^{-3}$
10DP / D_2O	10 ± 1	4.12 ± 0.02	24 ± 2	5.86 ± 0.03	46 ± 3	6.30 ± 0.03
10CP / D_2O	11 ± 1	3.47 ± 0.03	28 ± 3	5.61 ± 0.05	44 ± 3	6.00 ± 0.10
10DP / NRW	14 ± 2	1.20 ± 0.10	20 ± 1	0.34 ± 0.02	-	-

Table 4.4.14: Parameters of three layer fit, 10CP Γ_s = 1.1 mg m^{-2}

The layer compositions have been computed from the parameters in Table 4.4.14. In comparison with the results for Γ_s = 0.40 mg m^{-2} the PMMA backbone occupies the uppermost 20 - 30 Å of the surface. The top two layers contain PEO, PMMA and water

whereas the final layer is composed of heavily diluted PEO. An example fit for this system is given in figure 4.4.23.

Layer No	d / Å	ϕ_{MA}	ϕ_{EO}	ϕ_{W}
1	12 ± 2	0.13	0.38	0.49
2	24 ± 4	0.05	0.08	0.87
3	45 ± 3	-	0.02	0.9

Table 4.4.15: Layer compositions and dimensions, 10CP Γ_s = 1.1 mg m^{-2}

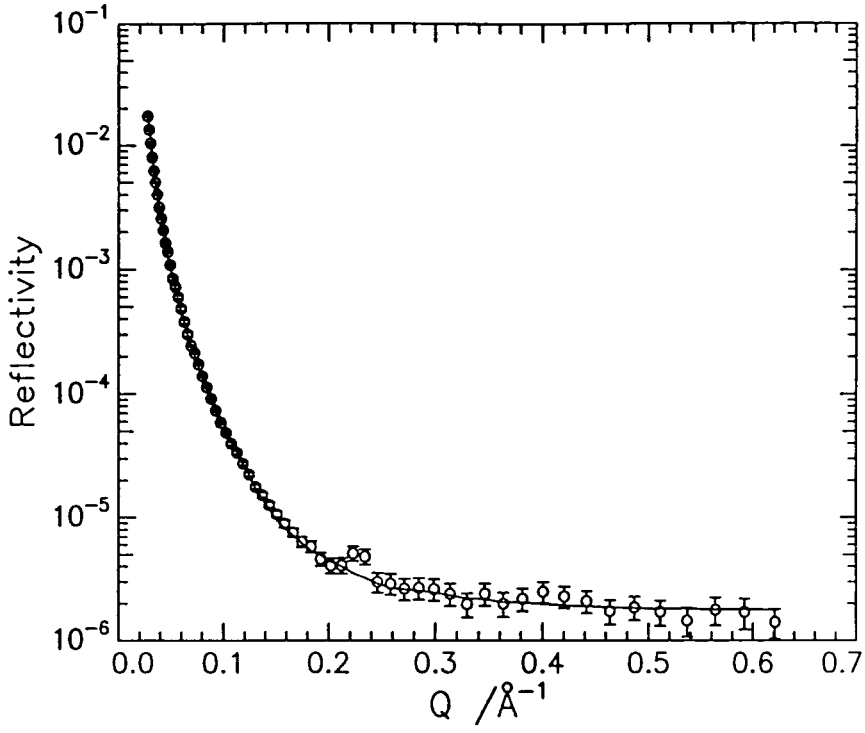

Figure 4.4.22 Reflectivity Profile for 10DP / D_2O, Γ_s = 0.4 mg m^{-2}. Open circles are data points, solid line is the fit with the parameters given in Table 4.4.12.

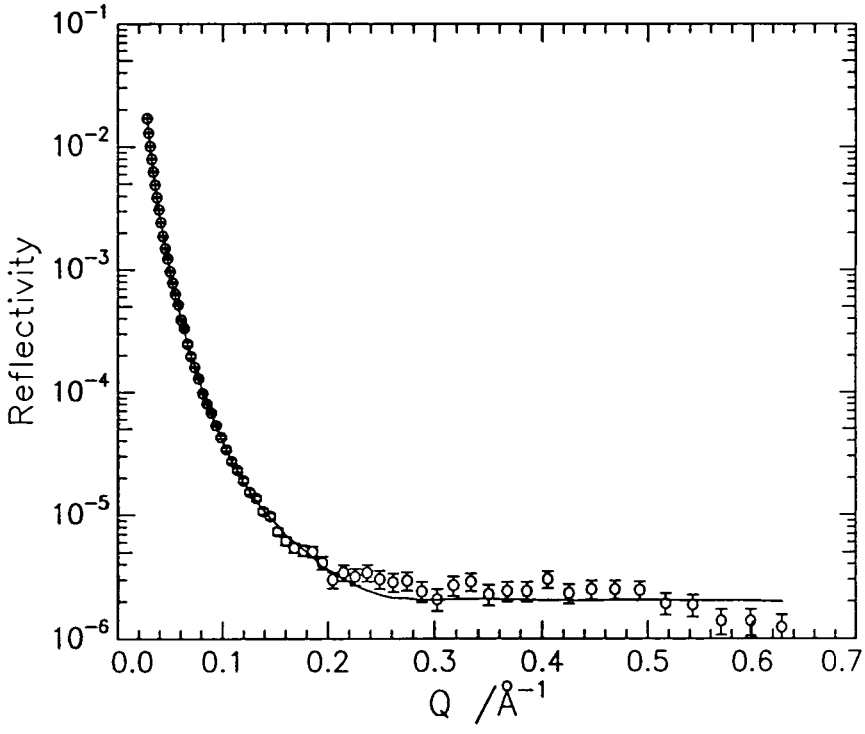

Figure 4.4.23 Reflectivity Profile for 10DP / D_2O, Γ_s = 1.1 mg m^{-2}. Open circles are data points, solid line is the fit with the parameters given in Table 4.4.14.

4.4.5.5B 60CP

At Γ_s = 0.65 mg m^{-2} a two layer model is required to fit the data for 60CP. A three layer model is required to model the interfacial structure at the higher concentrations. The fitted parameters of the two models described are given below.

Γ_s = 0.65 mg m^{-2}

Contrast	d_1 / Å	ρ_1 / 10^{-6} $Å^{-3}$	d_2 / Å	ρ_2 / 10^{-6} $Å^{-3}$
60DP / D_2O	9 ± 1	5.05 ± 0.02	21 ± 2	6.33 ± 0.01
60CP / D_2O	10 ± 1	3.31 ± 0.04	20 ± 2	6.33 ± 0.01
60DP / NRW	8 ± 1	2.70 ± 0.03		

Table 4.4.16: Fitted parameters for a two layer model for 60CP , Γ_s = 0.65 mg m^{-2}.

The parameters in Table 4.4.16 give an excellent fit to the reflectivity data as is illustrated in figure 4.4.24. The layer compositions are given in Table 4.4.17.

Layer No	d / Å	ϕ_{MA}	ϕ_{EO}	ϕ_W
1	9 ± 2	0.34	0.21	0.45
2	20 ± 2	-	0.01	0.99

Table 4.4.17: Layer Compositions for 60CP Γ_s = 0.65 mg m^{-2}

Γ_s = 1.6 mg m^{-2}

A three layer fit was required to fit the data collected for films spread at 1.6 mg m^{-2}. The layer compositions are similar to those for 20CP when Γ_s = 2 mg m^{-2}. The top layer is attributed to PMMA looping above the aqueous subphase. The second layer contains PEO, PMMA and water whereas, as always, the lower layer appears to be heavily diluted PEO chains.

As can be seen from Table 4.4.18 the NRW contrast was only sensitive to the dPMMA. Both the subphase and air have ρ = 0 and, unless the organisation of the polymer changes radically, it is not possible to differentiate between a polymer / air or polymer /

subphase layer. In contrast when the subphase is D_2O the uppermost surface is split into two layers. This observation implies that ϕ_{MA} is similar for the layers 1 and 2 on D_2O. As Table 4.4.19 demonstrates this is found to be the case.

Contrast	d_1 / Å	ρ_1 / 10^{-6} Å^{-3}	d_2 / Å	ρ_2 / 10^{-6} Å^{-3}	d_3 / Å	ρ_3 / 10^{-6} Å^{-3}
60DP / D_2O	9 ± 1	4.50 ± 0.04	8 ± 1	5.61 ± 0.03	29 ± 2	6.00 ± 0.03
60CP / D_2O	9 ± 1	0.67 ± 0.02	8 ± 1	2.10 ± 0.05	32 ± 3	5.98 ± 0.02
60DP / NRW	17 ± 2	4.01 ± 0.10	-	-	-	-

Table 4.4.18: Parameters of three layer fit, 60CP Γ_s = 1.6 mg m^{-2}

The parameters of the three layer model give the layer compositions presented in table 4.4.19. The reflectivity data is reproduced successfully by this model, see figure 4.4.25.

Layer No	d / Å	ϕ_{MA}	ϕ_{EO}	ϕ_W
1	9 ± 1	0.75	-	-
2	8 ± 1	0.69	0.08	0.23
3	30 ± 2	-	0.06	0.94

Table 4.4.19: Layer Compositions for 60CP Γ_s = 1.6 mg m^{-2}

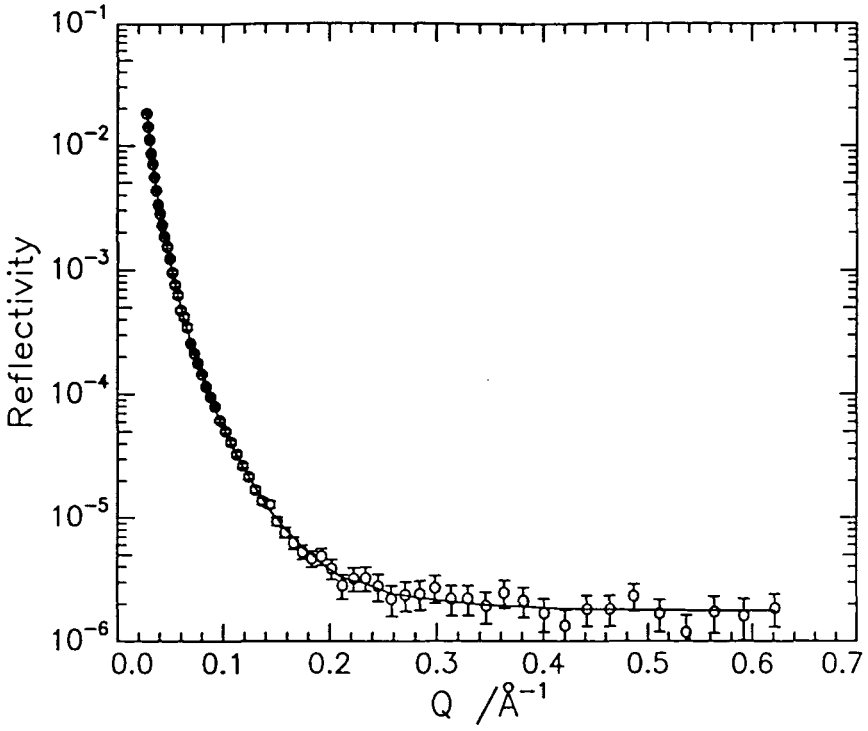

Figure 4.4.24 Reflectivity Profile for 60CP / D_2O, Γ_s = 0.65 mg m^{-2}. Open circles are data points, solid line is the fit with the parameters given in Table 4.4.16.

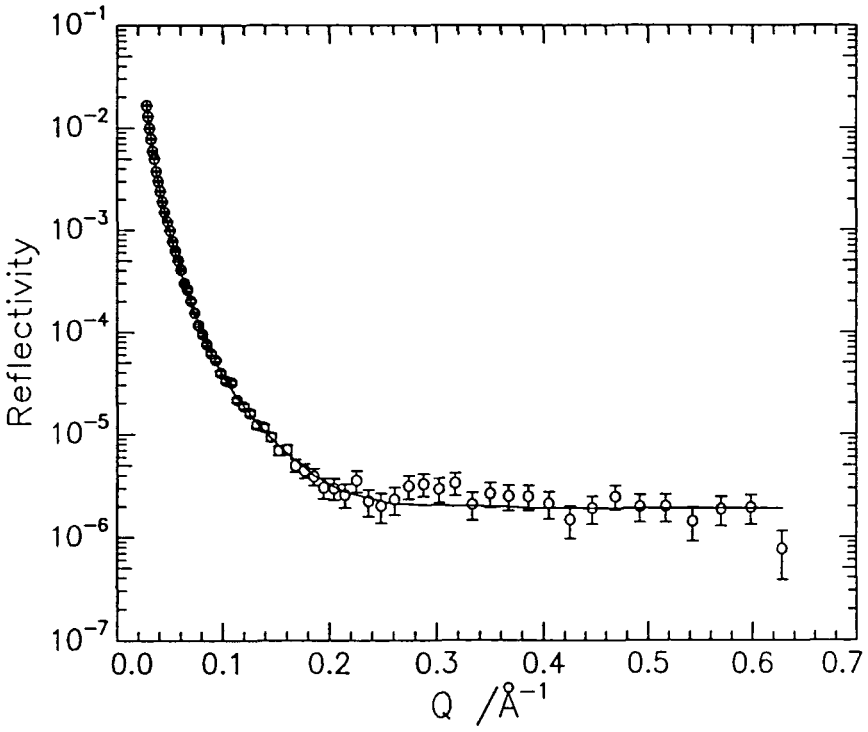

Figure 4.4.25 Reflectivity Profile for 60CP / D_2O, Γ_s = 1.6 mg m^{-2}. Open circles are data points, solid line is the fit with the parameters given in Table 4.4.18.

4.4.5.6 Summary

The results of the optical matrix analysis exhibit a number of trends, see the schematic block profiles in figure 4.4.26. It is clear that none of the profiles recorded can be adequately fitted by a single layer model, even the lowest concentrations studied require two layer models. If the parameters of the two layer models are compared a number of observations can be made:

Polymer	Layer No	d / Å	ϕ_{MA}	ϕ_{EO}	ϕ_{W}
60CP	1	9 ± 2	0.34	0.21	0.45
20CP	1	10 ± 1	0.08	0.07	0.85
10CP	1	16 ± 1	0.02	0.13	0.86
60CP	2	20 ± 2	-	0.01	0.99
20CP	2	20 ± 1	-	0.07	0.93
10CP	2	49 ± 2	0.01	0.03	0.94

Table 4.4.20: Two layer fit parameters for the most dilute films studied, 60CP Γ_s =0.65 mg m^{-2}, 20CP Γ_s = 0.50 mg m^{-2}, 10CP Γ_s = 0.40 mg m^{-2}.

It is clear, from the parameters of the two layer models in Table 4.4.20, that the PMMA backbone of the graft copolymers is situated predominantly at the uppermost surface. Other than for 10CP, where the low concentration of PMMA may cause erroneous results, the layer occupied by PMMA has similar dimensions of circa 10 - 12 Å. In all systems the PEO occupies both layers. The dimensions, and composition, of the lower layer show that these groups exhibit a tendency to form a diffuse lower layer indicating significant subphase penetration. These characteristics of the behaviour become more marked at higher surface concentrations. As the surface concentration of each graft copolymer increases the layer dimensions increase and, in a number of cases, it was necessary to incorporate additional layers into the model. As the surface concentration of 20CP increased to 1.5 mg m^{-2} a two layer model fitted the data successfully. The layer dimensions indicated that while the thickness of layer 1 was much the same as at Γ_s = 0.5 mg m^{-2} the lower layer was circa 10 Å thicker. This is consistent with the PEO side chains extending into the subphase on compression.

On a further increase in surface concentration of 20CP to 2 mg m^{-2} a three layer model was required to fit the data. Likewise a three layer fit was required for the high concentration data of both 10CP and 60CP. In all cases the dimensions of the layers 1 and 2 were found to be very similar. The thickness of layer 1 fell in the range 10 - 12 Å, that of layer 2 was 24 - 23 Å, see Tables 4.4.11, 4.4.15 and 4.4.18. In all instances the PMMA in the system was contained in these layers, predominantly in layer 1. Data for both 20CP and 60CP indicated that the PMMA backbone loops above the subphase, such that this top layer contains only PMMA and air. The dimensions of the lower layers, containing PEO and water, were found to vary from circa 45 Å for 10CP, 24 Å for 20CP and 30 Å for 60CP. Such dimensions indicate substantial subphase penetration by the PEO side chains and a tendency of the side chains to extend on compression of the film.

To summarise the above, it seems that the PMMA backbone of the graft copolymers occupies the uppermost surface forming a layer 12 - 16 Å thick. At higher surface concentrations the PMMA backbone exhibits a tendency to pull out of the subphase and mix with the air whilst the PEO side chains remain buried in the subphase. These tendencies can be identified in figure 4.4.26. Clearly the backbone and side chains occupy different spatial regions over the entire surface concentration range studied. This is entirely consistent with the different characteristics of these components.

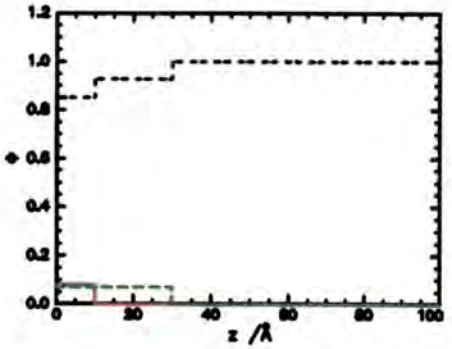

20CP, $\Gamma_s = 0.5$ mg m^{-2}

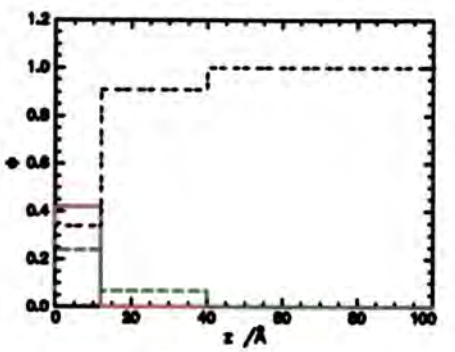

20CP, $\Gamma_s = 1.5$ mg m^{-2}

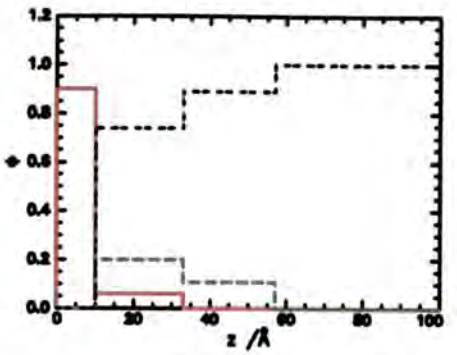

20CP, $\Gamma_s = 2.0$ mg m^{-2}

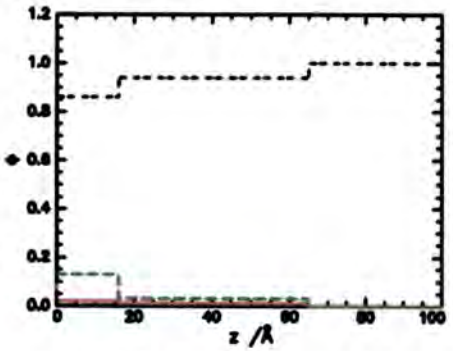

10CP, $\Gamma_s = 0.4$ mg m^{-2}

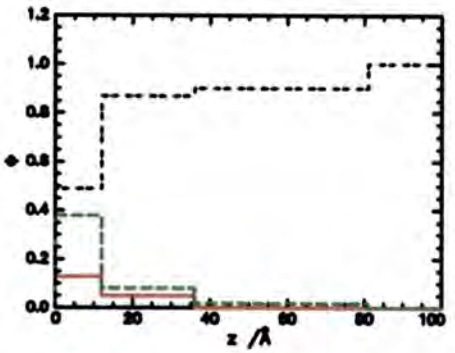

10CP, $\Gamma_s = 1.1$ mg m^{-2}

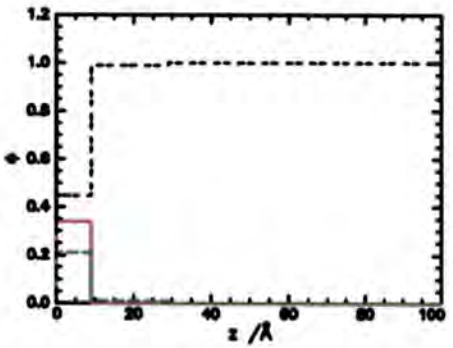

60CP, $\Gamma_s = 0.65$ mg m^{-2}

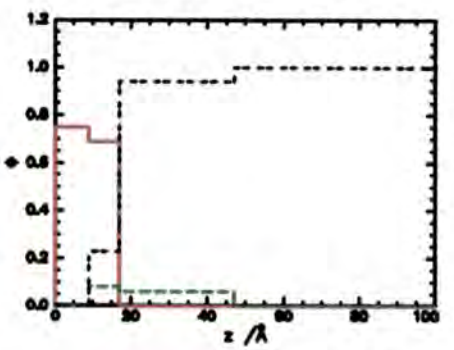

60CP, $\Gamma_s = 1.6$ mg m^{-2}

Key

PMMA	**Solid red line**
PEO	**Broken green line**
Water	**Broken black line**

Figure 4.4.26 Volume fraction block profiles for the interfacial layers determined using the optical matrix analysis.

4.4.6 The Kinematic Approximation

Using the kinematic approximation the reflectivity of a system can be linked to the distribution of the various species at the interface via partial structure factors, h_{ii} and h_{ij}. In the current system there are three species of interest, PEO side chains, PMMA backbone and water. For a three component system applying the kinematic approximation gives the reflectivity as:

$$R(Q) = \frac{16\pi^2}{Q^2}\left[b_1^2 h_1 + b_2^2 h_2 + b_3^2 h_3 + 2b_1 b_2 h_{12} + 2b_1 b_3 h_{13} + 2b_2 b_3 h_{23}\right]$$

Equation 4.4.6

where h_{ii} are the self partial structure factors and h_{ij} are the cross partial structure factors. The subscripts, 1, 2 and 3, represent the different species in the system. To solve this equation and determine all the partial structure factors requires reflectivity profiles for six different contrasts. Unfortunately, only a limited number of contrasts were available for the graft copolymers and consequently a rigorous analysis of the reflectivity data in terms of the kinematic approximation is not possible. Despite these problems a less rigorous form of the analysis can be applied to two of the three reflectivity profiles recorded at each Γ_s thus enabling two of the self partial structure factors to be estimated.

Consider first the reflectivity profile collected for 20DP spread on NRW. Assuming that in equation 4.4.6 species 1 is PEO, 2 is PMMA and 3 is water. For 20DP, on NRW $b_3 = 0$ and the expression simplifies to:

$$R(Q) = \frac{16\pi^2}{Q^2}\left[b_1^2 h_1(Q) + b_2^2 h_2(Q) + 2b_1 b_2 h_{12}(Q)\right]$$

Equation 4.4.7

Assuming that the scattering length density of PEO is so small that b_1 approximates to zero:

$$R(Q) = \frac{16\pi^2}{Q^2} b_2^2 h_2(Q)$$

Equation 4.4.8

enabling the PMMA self partial structure factor to be estimated directly from the reflectivity profile. It should be noted that, given the approximations applied in determining the relation above, self terms extracted in this way are subject to being overestimated. This follows

simply because all the reflectivity is assumed to originate from the dPMMA in the polymer, even though there may be contributions from the PEO present. Although this effect is acknowledged the results of the model fitting clearly indicated that the side chains are heavily diluted. This implies that the contributions from the PEO to the reflectivity of this contrast are likely to be negligible. It follows that, in this case, the extracted self term is expected to be in good agreement with the 'true' values from a full kinematic analysis.

The reflectivity profile for 20CP on D_2O can be analysed in a similar manner to give the self partial structure factor for water. In this approach the scattering lengths of both hPEO and hPMMA are approximated as zero and equation 4.4.6 becomes:

$$R(Q) = \frac{16\pi^2}{Q^2} b_3^2 h_3(Q)$$

Equation 4.4.9

This approximation is more likely to lead to overestimated structure factors than equation 4.4.8. Neglecting the scattering length of the polymeric species, although probably valid for the PEO, not only because b is small but also due to the heavy dilution of the chains, may be less valid for PMMA.

It follows, from the preceding discussion, that multiplication of the background subtracted, and where necessary Crowley[18] corrected, reflectivity data by $Q^4/16\pi^2 b^2$ yields $Q^2 h_{ii}$. Having extracted the self partial structure factors for water and PMMA in this way a means of interpreting the values is required. As has been mentioned analysis of self partial structure factors involves adopting a suitable model to describe the number density profile of the species, n(z). On Fourier transformation this gives n(Q) which can be linked to the self partial structure factor thus:

$$h_i = |n_i(Q)|^2$$

Equation 4.4.10

A number of models, for which well behaved Fourier transforms exist, are available for n(z). In this instance only one model is used; more sophisticated models and their application are discussed in Chapter 5. Due to the approximations inherent in determining $Q^2 h_{ii}$ comparison of the results with the optical matrix analysis was the only justifiable discussion of the data. In the optical matrix analysis the surface organisation adopted by the polymer was described using block profiles. For consistency, and to make comparison between the two methods straight forward, only a single uniform layer model has been used to describe n(z).

For a polymer distribution:

$$n(z) = n_{MA} \qquad 0 < z < d_{MA}$$

$$n(z) = 0 \qquad \text{for all other } z$$

Following Fourier transform this gives the self partial structure factor, h_{PP}:

$$Q^2 h_{pp}(Q) = 4n_{MA}^2 \sin^2(Qd_{MA}/2)$$

Equation 4.4.11

The behaviour of a subphase distribution differs marginally from that of a spread film. Rather than the number density falling to zero either side of the interface below the surface the value must increase to the bulk number density, n_{WO}, over some length scale The number density profile for such circumstances is represented in figure 4.4.27 for d_W = 20 Å and n_W = 0.02 $Å^{-3}$.

The number density profile is described by:

n(z)	d
0	$z < -d_W/2$
n_W	$-d_W/2 < z < d_W/2$
n_{W0}	$z > d_W/2$

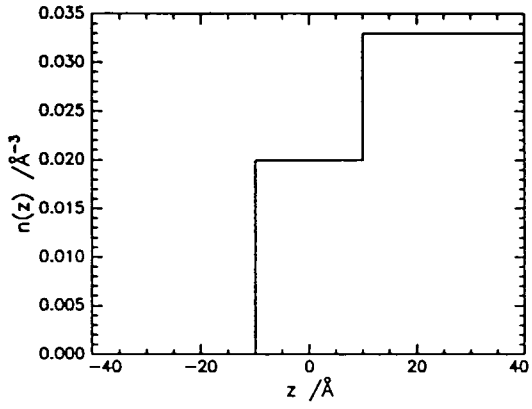

Figure 4.4.27 Representation of a uniform layer of water.

And the partial structure factor becomes:

$$Q^2 h_{ww}(Q) = n_{W0}^2 + 4n_W(n_W - n_{W0})\sin^2(Qd_W/2)$$

Equation 4.4.12

Clearly it is relatively straightforward to fit Equation 4.4.11 or 4.4.12 to the appropriate self partial structure factor, using both the thickness and the number density of the interfacial layer as variables.

4.4.6.1 The PMMA Self Partial Structure Factor

Wherever possible the PMMA self partial structure factor has been estimated from the reflectivity profile and fitted using equation 4.4.11; for certain systems the self terms were so scattered that it was not possible to fit the values. This tended to be the case for dilute, low PMMA content films where the reflected signal was very low, i.e. 10DP. A representative example of the self partial structure factors obtained and fitted using the uniform layer model is given in Figure 4.4.28. Clearly, experimental self partial structure values are reproduced well by the single uniform layer model.

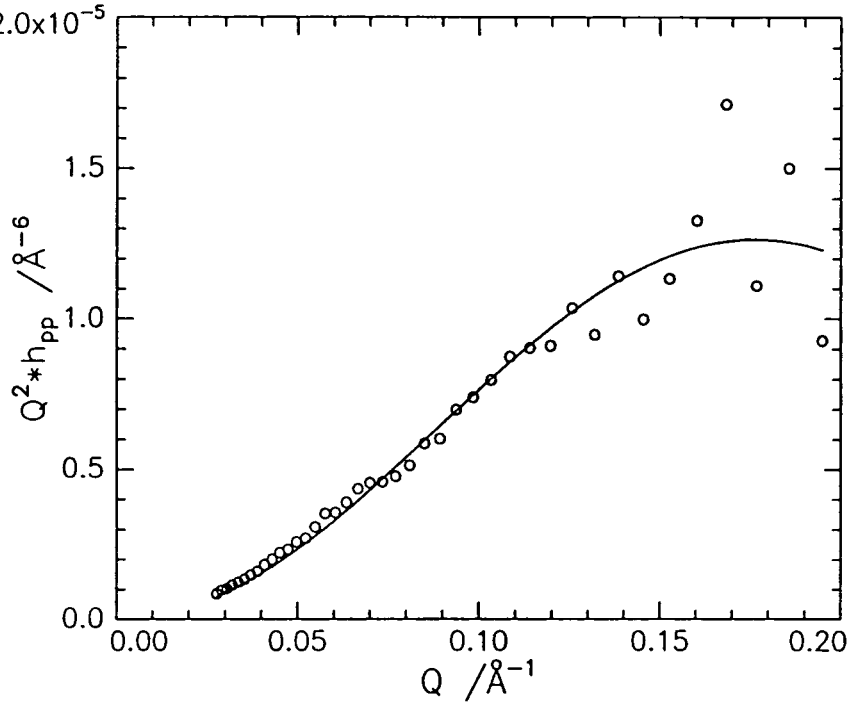

Figure 4.4.28 PMMA self partial structure factor for 20CP at Γ_s = 1.5 mg m^{-2}, open circles, with the best fit using a single uniform layer model overlaid, solid line.

The parameters obtained by fitting the PMMA self partial structure factor with a single uniform layer model are presented in Table 4.4.21. Where it was not possible to fit the self term the entry is left blank in the table. Since the number density of PMMA and the thickness of the interfacial layer are obtained in this fit the surface concentration of PMMA can be calculated using Equation 4.4.5. The applicability of the model can be tested by comparing the calculated surface concentration with the spread value and for this reason these values are also presented in Table 4.4.21.

Polymer	Γ_s / mg m^{-2}	Γ_{sMA} / mg m^{-2}	d_{MA} / Å	$n_{MA} \times 10^{-2}$ Å^{-3}	Γ_{sMAC} /mg m^{-2}
10CP	0.40	0.11 ± 0.01	-	-	
	1.10	0.33 ± 0.03	14 ± 1	0.16 ± 0.01	0.40 ± 0.10
20CP	0.5	0.20 ± 0.02	-	-	
	1.5	0.60 ± 0.05	18 ± 1	0.18 ± 0.01	0.58 ± 0.05
	2.0	0.80 ± 0.06	15 ± 1	0.37± 0.01	1.00 ± 0.20
60CP	0.65	0.46 ± 0.05	10 ± 1	0.19 ± 0.01	0.34 ± 0.09
	1.60	1.12 ± 0.10	17 ± 1	0.41 ± 0.01	1.25 ± 0.21

Table 4.4.21: Parameters of the single layer fits to the PMMA partial structure factors

It is clear from Table 4.4.21 that the fitted parameters give surface concentrations, Γ_{sMAC}, which, within experimental uncertainty, are consistent with the known spread surface concentration. At a PMMA surface concentration of around 0.60 mg m^{-2}, and above, the width of the layer falls in the range 15 - 18 Å. At the lowest surface concentration the layer appears rather narrower at 10 Å. It is difficult to ascertain whether this is a true feature of the system or whether it is correlated to the weak signal, and hence greater relative error inherent to the more dilute systems. Although only a limited data set is available it is concluded that, as the surface concentration of the PMMA increases the width of the layer formed at the surface barely changes. The greatest change in the layer characteristics as Γ_{sMA} increases manifests in an increasing number density rather than changes in the layer dimensions.

4.4.6.2 The water Self Partial Structure Factor

As for the PMMA self term the single uniform layer model has been fitted successfully to the estimated water self partial structure factor, see figure 4.4.29.

The parameters of the fits are presented in Table 4.4.22. Comparing the values in Table 4.4.22 with those in Table 4.4.21 shows that the parameters of the water layer, particularly the thickness, exhibit much greater variations with Γ_s than the PMMA layer. Considering the values for 20CP alone it is clear that as Γ_s increases the width of the interfacial region formed by the water increases. Similar results are observed for 60CP, although over a more limited concentration range.

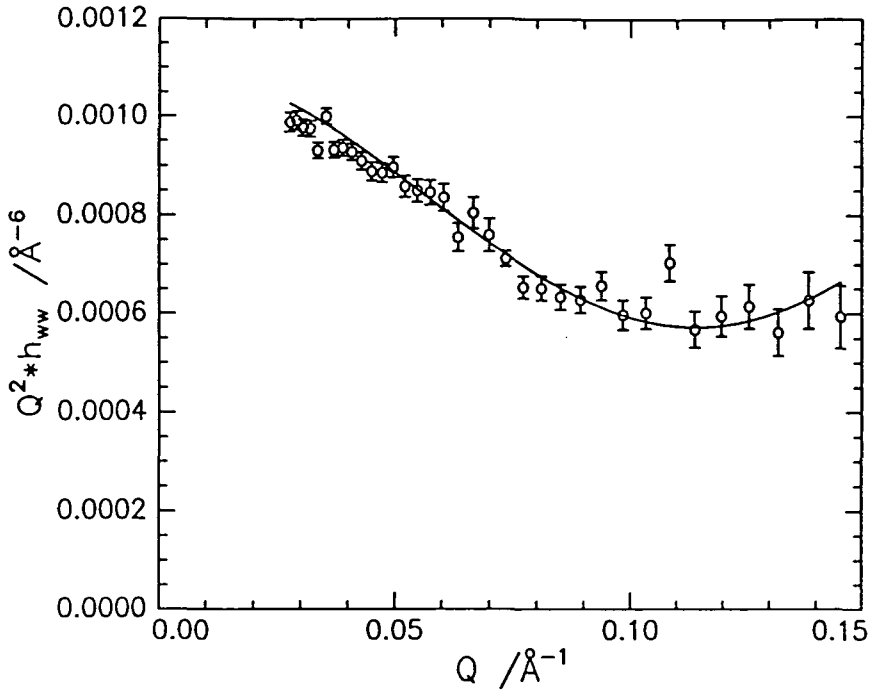

Figure 4.4.29 Example of the fit to the water self partial structure factor for 20CP at $\Gamma_s = 1.5$ mg m^{-2}.

It should be noted that the water self partial structure factor for 10CP, at both concentrations studied, was not fitted adequately by the model applied. The self terms exhibited marked downturns at the lowest Q value, behaviour totally at odds with the model of a single uniform layer. Such behaviour has been observed for other systems[5] with a high PEO content and its origin is not fully understood. Suggestions such as long range structuring of the water have been proposed. Another possibility is that it is associated with the formation of a diffuse, pseudo rough water layer. This point is considered, and discussed, in more detail in Chapter 5.

Polymer	Γ_s / mg m^{-2}	d / Å	$n_{pl} \times 10^{-2}$ Å^{-3}
20CP	0.5	19 ± 2	0.31 ± 0.03
	1.5	33 ± 1	0.48 ± 0.02
	2.0	40 ± 1	0.67 ± 0.01
60CP	0.65	16 ± 1	0.37 ± 0.03
	1.60	28 ± 1	0.46 ± 0.01

Table 4.4.22: The parameters of a single layer fit to the water self partial structure factor.

4.4.6.3 Discussion

Clearly, application of this truncated form of the kinematic approximation analysis to the reflectivity data yields self partial structure factors which can be fitted successfully using a single uniform layer model. Only a few data sets could not be fitted in this way. Rather than implying a problem with the model used, such behaviour arose where the reflected signal was very weak. For such systems the extracted self term exhibited a very scattered dependence on Q, so much so that the values could not be fitted reliably.

It was observed that the thickness of the PMMA layer did not exhibit a systematic variation with either Γ_s or Γ_{sMA}. This can be further emphasised by plotting the values as a function of Γ_{sMA}. The variation in the layer thickness, d_{MA}, with Γ_{sMA} is scattered, as expected, see figure 4.4.30. It is instructive to compare this behaviour with that of spread films of syndiotactic PMMA. Henderson et al[14] have reported a neutron reflectivity study of spread films of syndiotactic PMMA in which films covering a range of surface concentrations were studied. The kinematic analysis was in its infancy at the time of the work and the self partial structure factors were obtained using the same truncated analysis as applied here, then fitted using the single uniform layer model. The results of the fit have been plotted in figure 4.4.30 to serve as a comparison to the behaviour exhibited by the graft copolymers.

It is clear from figure 4.4.30 that the thickness of the layer formed by homopolymer PMMA does not exhibit any systematic variation with Γ_{sMA} and the values are rather scattered. It is also noticeable that for Γ_{sMA} in the range 0.5 - 1.0 mg m^{-2} the dimensions of the layer occupied by the PMMA backbone of the graft copolymers are essentially the same as for the homopolymer. Likewise the values of the fitted number densities of the layers, n_{MA}, have also been considered and compared to PMMA. As intimated earlier whilst the layer thickness appears essentially independent of Γ_{sMA} the number density is not. This variation in the number density can be inferred from the fact that the thickness of the PMMA layer remains constant despite increases in the spread concentration of PMMA. In figure 4.4.31 the reported variation in n_{MA} with Γ_{sMA} for homopolymer PMMA is overlaid with the analogous data obtained for the graft copolymers. Although there is some scatter at the lowest surface concentrations studied it is evident that the two sets of data exhibit a similar dependence on Γ_{sMA}.

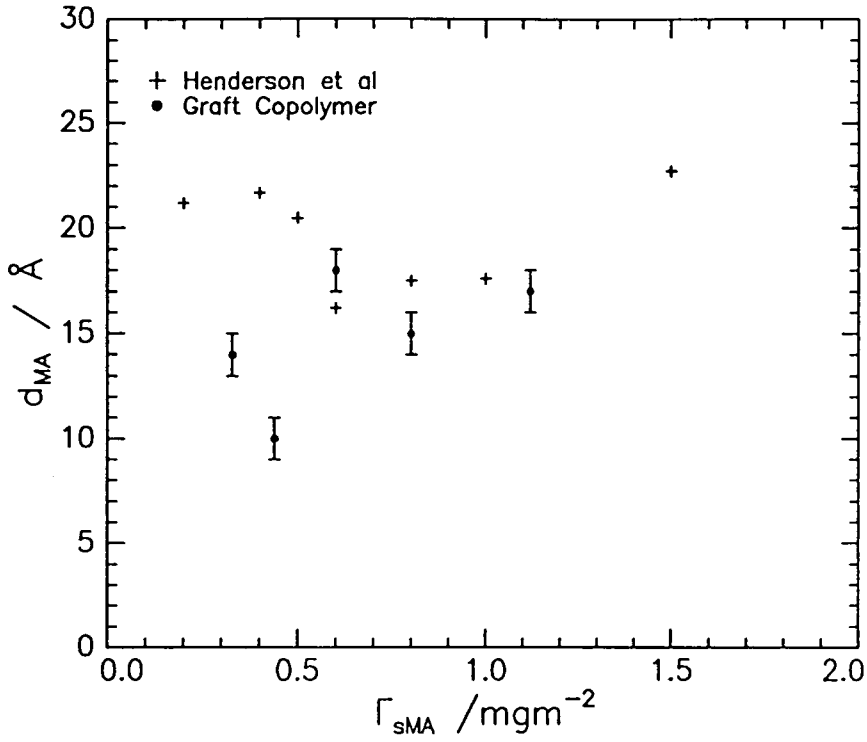

Figure 4.4.30 Fitted thickness of the PMMA layer as a function of Γ_{sMA} for the graft copolymers. Data for PMMA is overlaid.

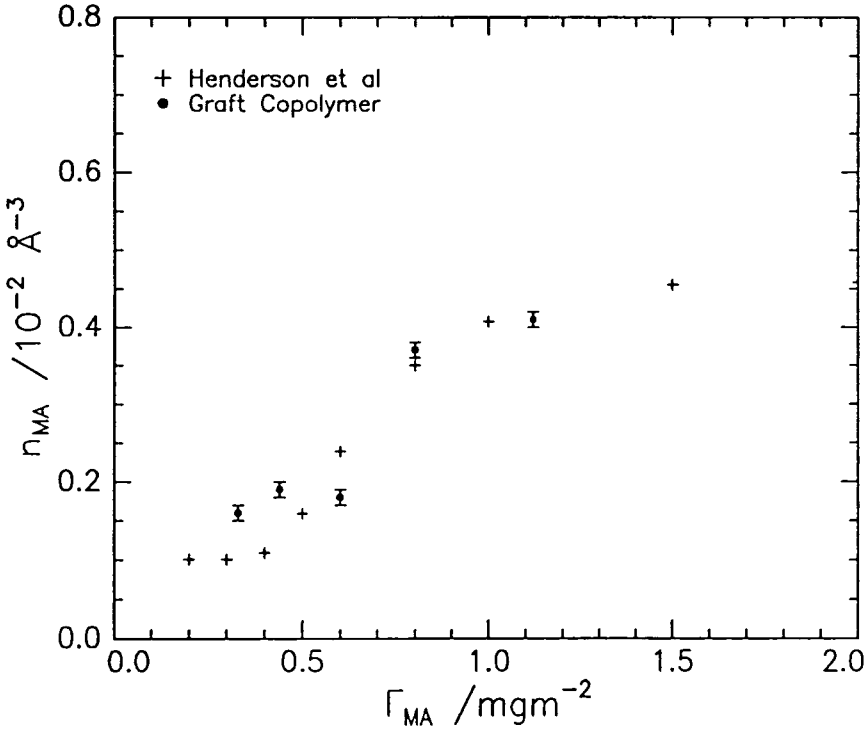

Figure 4.4.31 Fitted number density of the PMMA layer as a function of Γ_{sMA} for the graft copolymers. Data for PMMA is overlaid.

The comparisons outlined above illustrate that the characteristics of the organisation adopted by the PMMA, when modelled by a single uniform layer, are much the same as those exhibited by homopolymer PMMA. This implies that, over the concentration and copolymer composition range studied here, the structural organisation adopted by the PMMA backbone in the graft copolymer does not differ significantly from that of homopolymer PMMA.

One of the more unusual features exhibited by this system is the parameters obtained by fitting the water self partial structure factor. It is clear from the results of the fits that, as the concentration of the graft copolymer increases, the width of the water layer at the interface also increases to values which, in comparison to other systems are very large, up to 40 Å. This behaviour is believed to be associated with the presence of PEO at the interface.

To investigate these effects further the fitted parameters of the water layer for the different graft copolymers have been combined and plotted as a function of Γ_s and Γ_{sMA}. However, no systematic variation emerged. The observation that the thickness of the water layer is not correlated to changes in Γ_{sMA} is consistent with the results of Henderson et al.[14] From their data it is clear that neither d_W or n_W are directly correlated to changes in Γ_{sMA}. From this result it is concluded that the parameters of the water layer are essentially independent of changes in the surface organisation of the backbone of the graft copolymer.

When the thickness of the water layer is plotted as a function of Γ_{sEO} a linear relationship between the quantities is clearly evident, see figure 4.4.32. Similar results are observed for the variation in the number density of the water layer, see figure 4.4.33. Since the data points presented in these figures are collated from all the different composition graft copolymers this behaviour is universal to all the systems studied. From the preceding discussion it becomes evident that the linear relationships between the parameters of the water layer and Γ_{sEO} must reflect changes in the organisation of the graft copolymer. It was clear from the results of the model fitting that as Γ_s increases the total thickness of the interfacial film also increases. Such behaviour has tentatively been associated with the idea of the side chains extending on compression of the film, behaviour analogous to a polymer brush. It transpires that this analogy provides a useful model for behaviour which will be developed later in the discussion.

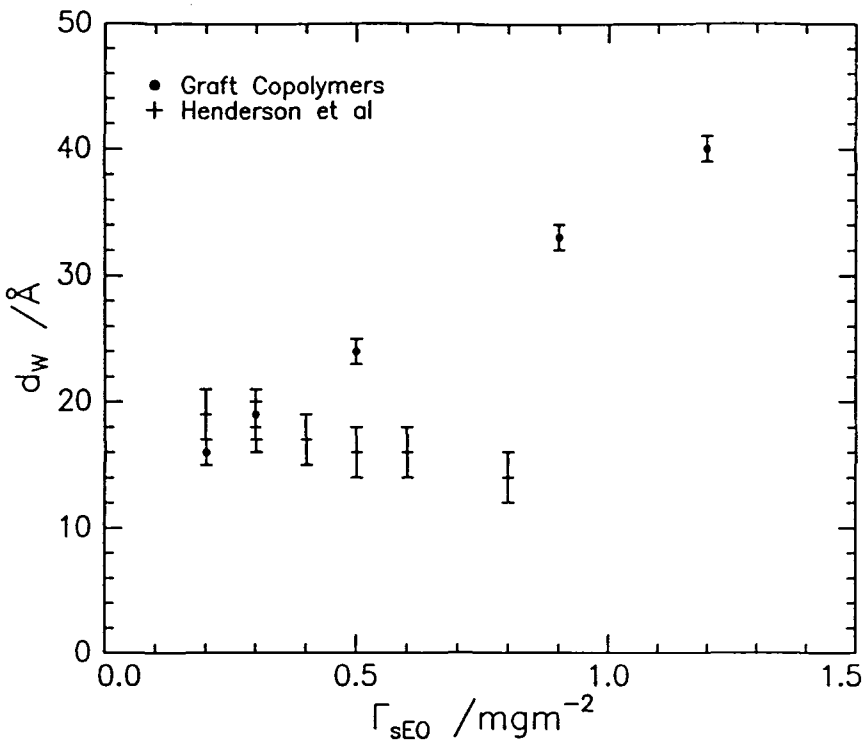

Figure 4.4.32 Fitted thickness of the water layer as a function of Γ_{sEO} for the graft copolymers. Data for PEO from reference 19 is overlaid.

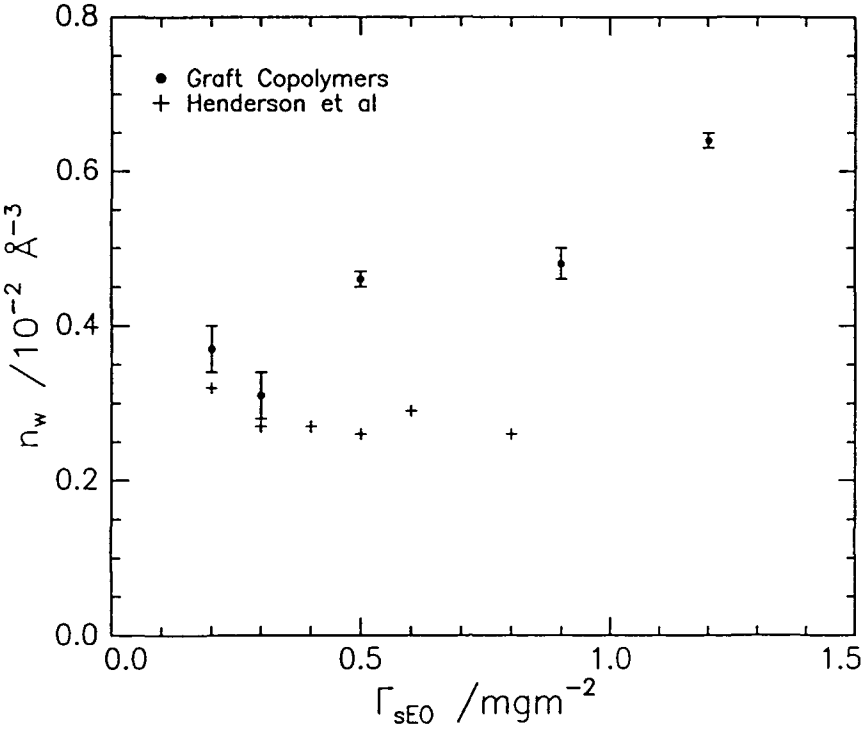

Figure 4.4.33 Fitted number density of the water layer as a function of Γ_{sEO} for the graft copolymers. Data for PEO from reference 19 is overlaid.

As for the behaviour associated with the PMMA in the graft copolymer, it is instructive to establish a comparison between the parameters which exhibit a systematic dependence on Γ_{sEO} and any analogous behaviour observed for films of PEO. Data enabling such a comparison to be made is available in the literature, once again having been reported by Henderson et al.[19] This publication reports the results of a neutron reflectivity study on spread films of PEO over a range of surface concentrations. It is stressed that the decision to compare the behaviour of the graft copolymers to that of spread films of PEO does not represent any particular behaviour exhibited by the graft copolymers. Spread films of PEO do not necessarily constitute a better parallel to the behaviour associated with the graft copolymer than adsorbed films, in fact the comparison is enforced simply by the lack of data available for adsorbed films of different concentrations. The thickness of the water layer as a function of Γ_{sEO} was presented in figure 4.4.32 and the data reported for spread PEO is overlaid in this figure for comparison. Clearly, the thickness of the water layer exhibits a much more marked dependence on Γ_{sEO} for the graft copolymers than films of PEO. As the spread surface concentration of homopolymer PEO increases the thickness of the water layer barely changes. In contrast, for the graft copolymers the thickness of the layer appears to be inherently linked to the surface concentration of PEO, exhibiting a linear dependence. Likewise, when the variation in the number density of water in the layer is considered as a function of Γ_{sEO} similar behaviour is observed. For spread films of homopolymer PEO the number density of this layer remains essentially the same, despite the surface concentration of PEO increasing from 0.2 - 0.8 mg m^{-2}. In comparison the number density of the water layer increases linearly with Γ_{sEO} for the graft copolymers.

Initially, given the previously observed correlations between the behaviour of the graft copolymers on homopolymer PMMA, the marked differences between the behaviour of the graft copolymers and PEO may appear quite remarkable. However, when figures 4.4.32 and 4.4.33 are compared it is clear that behaviour of the PEO side chains diverges from that of the PEO homopolymer only at surface concentrations of 0.5 mg m^{-2} and above. It so happens that at this surface concentration spread films of homopolymer PEO exhibit a structural change. This behaviour was identified by an extensive analysis of the neutron reflectivity data for film concentrations over the range 0.2 - 0.8 mg m^{-2}.[19] It was observed that the number density of PEO segments in the uppermost layer remains constant once a surface concentration of 0.5 mg m^{-2} is reached. This also coincides with the region of the isotherm where the surface pressure attains an almost constant value, even though the apparent surface concentration is increasing.

These observations were rationalised by the suggestion that at surface concentrations exceeding 0.5 mg m^{-2} no more PEO can be accommodated at the surface. As a consequence of this any further addition of polymer taking the spread surface concentration above 0.5 mg m^{-2} results in loss of polymer into the bulk subphase such that a surface film of constant concentration, Γ_s around 0.5 mg m^{-2}, is maintained.

Given that spread films of PEO behave in this way it is feasible to anticipate that an analogous structural transition may exist in films of the graft copolymer, although behaviour exhibited by the grafts will be subject to slight modifications due to the constraint of being attached to an insoluble backbone. The major modification, in comparison to homopolymer PEO, is that complete dissolution of the graft copolymer chains will not be possible. As the nearest analogy to dissolution of the chains a model mentioned earlier is reconsidered. It is suggested that as the graft copolymers are compressed, so that the surface concentration of PEO increases above 0.5 mg m^{-2}, the side chains begin to stretch into the bulk subphase. By stretching the chains can extend further into the subphase and away from the surface thereby reducing the number density at the immediate surface. Such behaviour may manifest itself in a number of ways, one being an increasingly thick near surface water layer. This follows because the number density of water over the interfacial region penetrated by the PEO will be depleted compared to the bulk. Basically then, in this model the width of the interfacial water layer is believed to be directly proportional to the penetration depth of the PEO side chains. Clearly, the characteristics of the water layer are consistent with the hypothesis that the side chains stretch on compression of the film. To test this model further details of side chain conformation and dimensions are considered.

4.4.6.3A The Side Chains: Dimensions and Pseudo Brush type behaviour

Linear polymers end grafted in some way to an interface exhibit changes in behaviour as a function of their surface density. The particular case of interest here is chains which are attached by one end to a surface such that the rest of the molecule is surrounded by solvent. At low enough surface concentrations the chains do not overlap but, as the crowding of the surface increases, the chains are forced to stretch anisotropically away from the surface, adopting configurations which may be quite different from those exhibited in the bulk. This stretching enables the chains to minimise their free energy and the layer formed is akin to a brush. Although the grafting density, the number of chains per unit area, may be high the low

molecular weight solvent will still penetrate into the brush layer so that the chains remain solvated. There exists a large volume of work on this area, including a number of theories of varying complexity to describe and predict behaviour. Work in this field has been fuelled not only by academic interest but also the applications of polymer brushes into industrially important areas such as colloidal stabilisation.

The hypothesis which has been suggested to account for the results of the neutron reflectometry for the graft copolymer clearly incorporates some features which fall under the general guise of polymer brushes. It is therefore logical to treat the PEO side chains as brushes to see whether such theories can account for the behaviour exhibited. A vast literature exists in this field but only the more basic treatments are considered here.

Alexander[20] and de Gennes,[21] have applied a scaling law approach to the problem which has the benefit of yielding relatively simple results and is considered initially. In this model a block profile of chains is assumed. When the distance between neighbouring molecules is large each polymer occupies a half sphere comparable to its radius of gyration in a good solvent, R_g. As the distance between the grafted chains decreases and becomes less than R_g the chains begin to stretch and in the theoretical treatment are subdivided into 'blobs', a concept discussed previously in regard to the behaviour of semi-dilute solutions. In this situation the chains are stretched and the layer thickness is given by:

$$L = Na\sigma^{\frac{1}{3}}$$

Equation 4.4.13

where N is the number of statistical steps of length a in the molecule and σ is the grafting density. Clearly, the concept of a grafting density will be central to any treatment in which polymers are viewed as forming a brush layer. The grafting density can be determined relatively simply for the graft copolymers at any surface concentration by calculating the number of chains of copolymer per unit area and knowing the average number of side chains per chain. The relation between σ and Γ_s is given by:

$$\sigma = \frac{\Gamma_s N_A X}{M_n} \times 10^{-23} \text{ chains per Å}^2$$

Equation 4.4.14

where X is the average number of side chains per chain of graft copolymer. For 10CP X = 24, for 20CP X= 15 and for 60CP X = 7.

It follows from Equation 4.4.14 that the calculation of the grafting density for the graft copolymers is straight forward. By application of Equation 4.4.14 the variation in σ as a function of Γ_s has been determined for each of the graft copolymers. It is relatively simple to calculate the layer thickness which would be anticipated from this model using Equation 4.4.13. The statistical step length can be calculated provided that R_g is known. A value for R_g was computed in the following manner. For PEO it is known[8] that:

$$\frac{r_o}{M^{\frac{1}{2}}} \times 10^4 = 750 \text{ nm}$$

Therefore for M = 2376, r_o = 37 Å

$$R_{go} = \frac{r_o}{\sqrt{6}}$$

Thus R_{go} = 14.9 Å

For a macromolecule in solution, due to molecular interactions with the surroundings, the real radius of gyration will be greater than the unperturbed value. The expansion factor α links these two values, R_g and R_{go}. Although α is not explicitly known for this system a plateau value of $\alpha^2 = 2.5$ is typical and is used here:

$$R_g^2 = \alpha^2 R_{go}^2$$

Giving R_g = 24 Å enabling a to be determined from: $R_g^2 = Na^2/6$

Taking this value for R_g and knowing N = 54 it transpires that a = 8 Å. Substituting the values into equation 4.4.13 the layer thickness which would be anticipated using this model can be calculated as a function of σ, basically Γ_s. From the discussion above it is clear that the thickness of the water layer scales with Γ_{sEO} and it is therefore this property that should be compared to the brush thickness. By combining Equations 4.4.13 and 4.4.14 it is possible to express the variation in L as a function of Γ_{sEO}. It can be shown that when σ is expressed as a function of Γ_{sEO} the values for all the different graft copolymers converge. This reflects the fact that σ is ignorant of the means by which the chains are attached to the surface. Thus, although the values of L presented were explicitly calculated for 20CP by expressing them in terms of Γ_{sEO} the results are 'normalised'. The calculated variation in L is overlaid with the layer thickness of the water layer and is given in figure 4.4.34. On

examination of figure 4.4.34 it is clear that the theory, whilst predicting the dependence of the layer thickness on Γ_{sEO}, overestimates the layer thickness considerably. Given the various approximations made whilst calculating L, and the fact that this theory may not be strictly applicable to this situation, it is difficult to identify the source of the discrepancies. In addition to these problems it is feasible that the thickness of the water layer although representative of the behaviour of the PEO side chains does not have exactly the same dimensions. This behaviour could go some way in explaining the discrepancies observed in figure 4.4.34, albeit only at a qualitative level.

Given the results obtained by application of Equation 4.4.13 a slightly more sophisticated treatment has been applied. In contrast to the treatment of Alexander[20] and de Gennes[21] where the volume fraction profile described by the polymer was presumed Milner, Witten and Cates[22] have developed an approach in which the profile can be derived and is found to be parabolic. In this manner they successfully extracted an analytical expression for the thickness of the polymer brush, L:

$$L = \left(\frac{12}{\pi^2}\right)^{\frac{1}{3}} \left(\frac{1}{2} - \chi\right)^{\frac{1}{3}} N\sigma^{\frac{1}{3}} a^{\frac{5}{3}}$$

Equation 4.4.15

The only new parameter in this equation is χ, the polymer solvent interaction parameter. The interaction parameter, χ, characterises the interactions between polymer and solvent. An early study of poly (ethylene glycol) in water gave $\chi = 0.4$.[23] It was decided to take two values of χ, 0.4 and 0.45, to observe the effect of χ and see whether the experimental data could be reproduced more successfully than equation 4.4.13. As previously, L was calculated as a function of the surface concentration of PEO and is presented in this format in figure 4.4.35 with the layer thickness for water overlaid. This approach is less successful at reproducing the observed water layer thickness than equation 4.4.13.

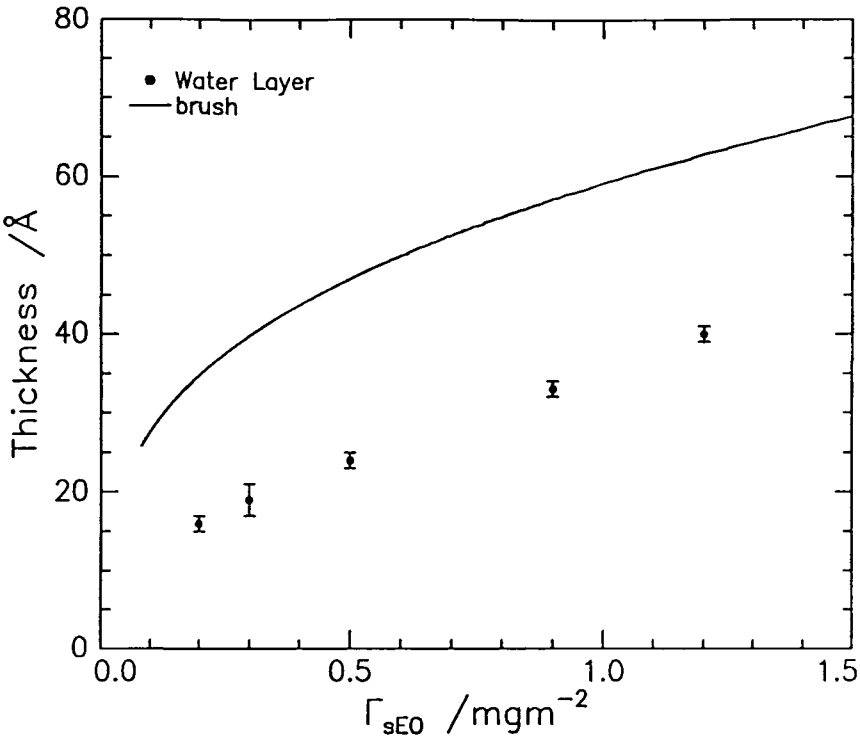

Figure 4.4.34 Layer thickness for interfacial water layer compared to brush thickness given by Equation 4.4.13.

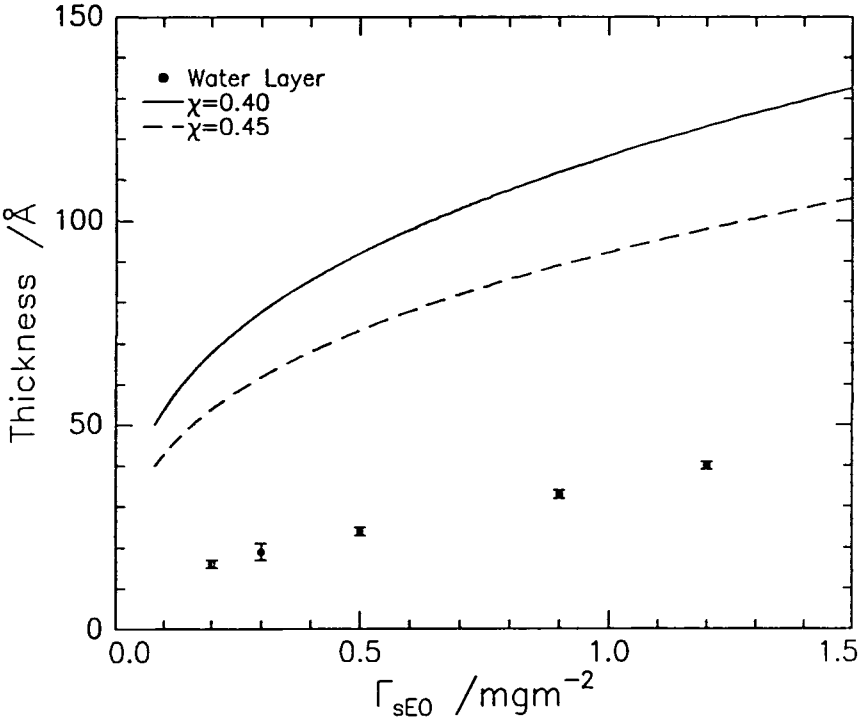

Figure 4.4.35 Layer thickness for interfacial water layer compared to brush thickness given by Equation 4.4.15.

It is clear that equation 4.4.14 reproduces the variation in the water layer thickness most successfully. This indicates that the profile of the side chains, which is represented by the water layer, is more block like than parabolic. Given that the water layer was modelled as a uniform layer this result may not seem surprising. However, it should be remembered that although the water layer was modelled as a block there was no assumption made about the way the dimensions would scale with Γ_{sEO} and parabolic characteristics may have lead to different behaviour. To summarise, it is concluded that the thickness of the water layer and, more importantly, its variation with Γ_{sEO} is sufficiently similar to that predicted by brush theory that the existence of such behaviour cannot be ruled out.

A rather more simplistic approach to the phenomenon of chain stretching can be developed by reconsidering the observation that the variation in the thickness of the water layer with Γ_{sEO} is linear. The best straight line fit to the data can be described by:

$$d_W = 24\Gamma_{sEO} + 12 \text{ Å}$$

Equation 4.4.16

Clearly, the width of the water layer cannot increase indefinitely as the side chains can only extend a finite amount. In an attempt to determine the maximum extension of the PEO side chains, assuming that they penetrate the subphase in a manner akin to a brush, calculations have been performed assuming an all trans configuration. Taking standard values for the PEO[24] bond angles as 110° and the bond lengths as C - C 1.53 Å and C - O as 1.43 Å the length of a repeat unit in the all trans configuration is 3.7 Å indicating that, for a chain of 54 units, the maximum extension would be 200 Å. Placing this into Equation 4.4.16 gives Γ_{sEO} = 4.5 mg m^{-2} which is well beyond the concentration range covered here. Even for the highest PEO content graft copolymer this implies a total spread concentration of 6.4 mg m^{-2}. It is highly unlikely that monolayers of this surface concentration could be maintained and problems associated with collapse are predicted. Whatever the nature of behaviour at these surface concentrations it is clear that the experimentally observed behaviour is consistent with expectation, and over the concentration range studied the PEO side chains are not anticipated to reach their maximum extension.

The main points of the various treatments considered here are briefly summarised below. Clearly, although none of the models adopted have provided good quality fits to the observed variation in d_W with Γ_{sEO}, rationale may be offered to account for the discrepancies. The discrepancies are not sufficient to negate the original suggestion that d_W represents

stretching of the PEO side chains. To identify the processes occurring more fully requires not only more data points but also a wider range of Γ_s.

4.4.6.4 Summary

The results and implications of the kinematic analysis are summarised briefly below. From the application of a truncated form of the kinematic analysis it appears that the behaviour of the backbone of the graft copolymer is very similar to that of homopolymer PMMA. Assuming that the single uniform layer model is an adequate model of both systems the thickness of the layer formed by the PMMA appears independent of Γ_{sMA}, certainly over the concentration range studied in this work. In both systems, homopolymer and graft copolymer, a layer around 17 ± 2 Å thick is formed with the film parameters changing only slightly at the extreme concentrations studied. The most significant change in the film parameters as Γ_{sMA} increases is the associated increase in the number density of the layer.

There is indirect evidence, via. the water self partial structure factor, to suggest that as Γ_{sEO} increases and, most significantly exceeds 0.5 mg m^{-2}, the PEO side chains stretch. This behaviour is interpreted as an attempt to reduce the increasing number density at the immediate surface.

4.4.7 Conclusion

Application of neutron reflectivity to the study of spread monolayers of the PMMA - PEO graft copolymers has enabled the surface organisation to be elucidated successfully. One of the main conclusions drawn from fitting the neutron reflectivity profiles directly is that the PEO side chains are penetrating the subphase. The conformation of these side chains appears to change on compression of the films. The models implied that the diffuse layer of heavily diluted PEO became thicker on compression, consistent with the side chains stretching, see sections 4.4.5.5 and 4.4.5.6. In contrast the PMMA backbone of the graft copolymer appears to be situated at the uppermost surface occupying a fairly constant interfacial width. At low surface concentrations the backbone remains in contact with the subphase but, as the polymer concentration increases, it exhibits a tendency to pull out of the subphase and form a layer mixed with air. This is evident in the series of studies on films of 20CP, compare Tables 4.4.4, 4.4.7 and 4.4.11.

These results are entirely consistent with the analysis of the profiles using a truncated form of the kinematic approximation, Section 4.4.6. This analysis showed that if the PMMA backbone is considered to occupy a single uniform layer at the interface, the dimensions of this layer barely change with surface concentration whereas the number density increases steadily. By a comparison with a study of spread films of PMMA it has been shown that the behaviour of the graft copolymer backbone is essentially the same as for PMMA. This leads to the conclusion that, not only is the behaviour of this section of the copolymer very like the corresponding homopolymer, but in addition it adopts what appears to the same structure irrespective of copolymer composition and the differing amounts of PEO in the systems. From this it is concluded that, as far as this technique can determine, the structure adopted by the PMMA backbone of the graft copolymers is not influenced by the presence of the PEO side chains.

The conclusion that the thickness of the layer formed by the PMMA backbone is independent of the surface concentration over this range is in agreement with the inferences made in section 4.4.4. From a qualitative consideration of the reflectivity profiles for the part deuterated copolymers on NRW it was suggested that changes were consistent with a layer of constant thickness and varying layer composition. It is clear that the quantitative analyses have confirmed this.

The thickness of the water layer determined by application of the kinematic analysis has been taken as a model of the layer formed by the PEO side chains. Analysis, and a

comparison with the behaviour of spread films of PEO, has demonstrated that this layer becomes thicker with increasing surface concentration of graft copolymer, see figure 4.4.32. It appears that this occurs only when the concentration of PEO on the surface exceeds 0.5 mg m^{-2}, this being the critical surface concentration which, for homopolymer PEO, heralds the onset of subphase penetration. Once this surface concentration of PEO is exceeded the side chains of the graft copolymers appear to stretch and the layer thickness increases linearly with Γ_{sEO}. As discussed above this is consistent with the observations of the model fitting. This is also consistent with the trends observed and noted in the reflectivity profiles of the fully hydrogenous polymers on D_2O in section 4.4.4. Consideration of these profiles and simulations illustrated that the variations observed with increasing Γ_s were consistent with an increasingly thick layer, possibly even brush formation. This, combined with the fact that the PMMA layer thickness appeared to remain constant, lead to the suggestion that the PEO side chains were forming an increasingly thick layer. This has been confirmed by both the model fitting and kinematic approximation analysis.

It is evident that both the kinematic analysis and direct model fitting of the profiles demonstrate that the width of the interfacial region occupied by the PEO increases with surface concentration of PEO. In fact the behaviour exhibited in figure 4.4.32 and identified using the kinematic approximation analysis, was fitted with a straight line giving the equation:

$$d_W = 24\Gamma_{sEO} + 12 \text{ Å where } \Gamma_{sEO} > 0$$

Equation 4.4.16

By using this equation to predict the layer thickness of the PEO layer formed by 20CP it is possible to compare the predictions of the kinematic approximation with the results of the model fitting. The result of this comparison are given below in Table 4.4.23

System	Γ_{sEO} / mg m^{-2}	d_w / Å (eq. 4.4.16)	d / Å (model fitting)
20CP 0.5 mg m^{-2}	0.3	19	30
20CP 1.5 mg m^{-2}	0.9	34	40
20CP 2.0 mg m^{-2}	1.2	41	47

Table 4.4.23: Comparison of PEO layer thickness from the kinematic analysis and the optical matrix model fitting analysis.

It is clear from Table 4.4.23 that, whilst the values scale in the same manner, the layer thicknesses determined from model fitting are systematically larger than the kinematic approximation would predict. The discrepancies are likely to arise from a combination of effects. Clearly the kinematic analysis involved a number of approximations which may cause some error in the results of the analysis. In fact the main problem, that both analyses are subject to, is that all information regarding the PEO side chains is unfortunately indirect. Information about the surface organisation adopted by the PEO side chains is in terms of the reduction in the reflectivity of the D_2O due to the presence of the hydrogenous side chain. This is because it was not possible to prepare a suitable sample containing dPEO side chains. This accounts for some of the discrepancies in Table 4.4.23 although fortunately these limitations are not sufficient to obscure all information regarding the side chains. It is evident that the two analyses are consistent with the side chains penetrating the subphase increasingly as the surface concentration of PEO increases. This is envisaged to be the nearest parallel to the dissolution of homopolymer PEO when the spread films exceed a critical surface concentration, circa. 0.5 mg m^{-2}.

It is concluded that whilst the behaviour of the graft copolymer is not unlike that of the corresponding homopolymers, there are certain modifications to behaviour. These arise due to the structure of the graft copolymers and lead to behaviour quite unique from that of the homopolymers.

Section 4.5: Surface Quasi Elastic Light Scattering

4.5.1 Introduction

This Section details the results of two kinds of surface quasi elastic light scattering experiments. In the first experiment the behaviour of a surface wave mode of fixed q, q = 220 cm^{-1} throughout, was studied as a function of the spread polymer concentration, Γ_s. All three different composition graft copolymers have been studied and the data have been analysed using the damped cosine fit to give the propagation characteristics of the capillary waves. In addition the data have been analysed using the spectral fitting method. The results from the different analyses are presented separately but discussed in a single Section. In this way the interrelations between the surface viscoelastic parameters and the surface wave propagation become a little more transparent.

As will be shown, the surface wave propagation and surface viscoelastic parameters for each of the graft copolymers exhibited a similar dependence on Γ_s. Due to this behaviour, whilst the results and discussion are general to all the copolymers, only the data for the graft copolymer 10CP are presented.

Having completed this study the properties of fixed concentration films have been investigated as a function of q, i.e. the frequency dependence of the film behaviour has been studied. Four concentrations of 60CP have been studied and three of 10CP. The results of both the damped cosine fit and direct spectral fit are presented and discussed also.

4.5.2 Results: Capillary Wave Frequency, ω_o and damping, Γ.

The variation in the capillary wave frequency, ω_o, with Γ_s for 10CP is presented in figure 4.5.1. All the polymers behave in a similar manner to 10CP with ω_o exhibiting a significant dependence on Γ_s. The capillary wave frequency is observed to increase with surface concentration from the value for a pure water surface to a maximum, which for all the systems, corresponds to a frequency of approximately 2.85×10^4 s^{-1}. The actual surface concentration at which ω_o reaches this maximum is denoted Γ_s^* and varies for the different copolymers suggesting that it is linked to composition. Examination of the data reveals that as the PEO content of the copolymer increases Γ_s^* shifts to lower total surface concentrations. This can be seen by comparing the behaviour of 10CP, the system containing the most PEO, for which $\Gamma_s^* \approx 0.25$ mg m^{-2} to 60CP, the system containing with the lowest PEO content, where $\Gamma_s^* \approx 0.45$ mg m^{-2}. The values of Γ_s^* for all the systems are given in Table 4.5.1.

Polymer	Γ_s^* / mg m^{-2}	Γ_{sEO} / mg m^{-2}	Γ_{sMA} / mg m^{-2}
10CP	0.25 ± 0.05	0.20 - 0.13	0.17 - 0.05
20CP	0.30± 0.03	0.20 - 0.16	0.17 - 0.07
60CP	0.45 ±0.05	0.16 - 0.12	0.33 - 0.28

Table 4.5.1: Characteristics of the dependence of ω_o on Γ_s.

The value of Γ_s^* shows a dependence on copolymer composition and it is informative to consider whether the values actually correspond to the same surface concentration of either component, i.e. PEO or PMMA. The partial surface concentrations of PEO and PMMA in the copolymer at Γ_s^* have also been determined and are reported in Table 4.5.1.

It is evident from Table 4.5.1 that the surface concentration of PEO at the critical surface concentration, Γ_s^*, is similar for all the polymers. Due to the error on evaluating Γ_s^* and the uncertainty in the polymer composition, the calculated surface concentration of PEO covers a relatively broad range. However, this range is in good agreement for both 10CP and 20CP, falling on the low end of this range for 60CP. A comparison with the surface concentration of PMMA indicates that the position of Γ_s^* would appear to be determined by a critical surface concentration of PEO rather than PMMA.

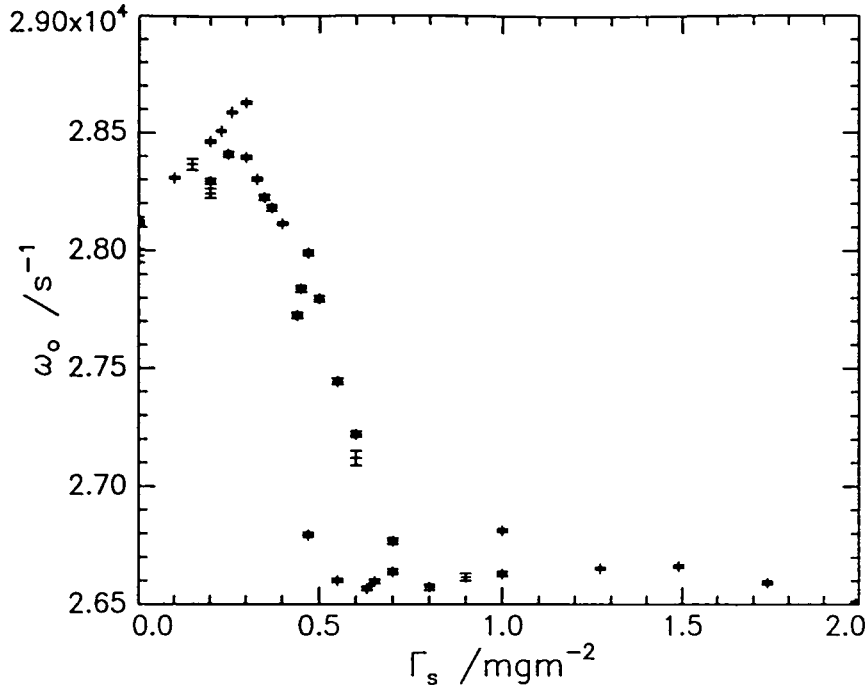

Figure 4.5.1 ω_o **vs.** Γ_s **for 10CP.**

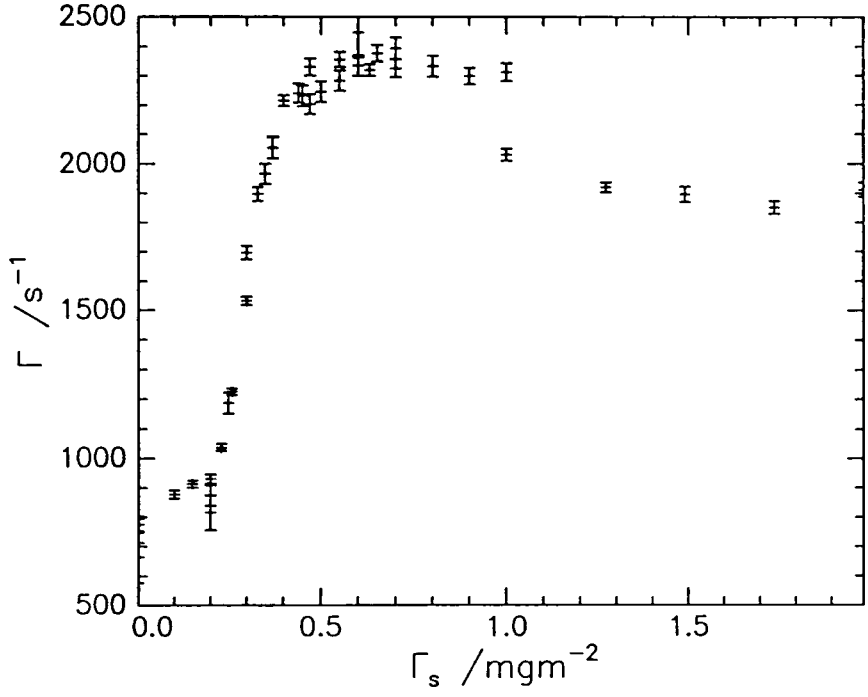

Figure 4.5.2 Γ **vs.** Γ_s **for 10CP. The maximum value of** Γ **reached,** Γ_{max}**, being 2330** s^{-1}**.**

As the surface concentration of polymer increases above Γ_s^* the capillary wave frequency decreases quite abruptly to a constant value. A pseudo 'rate' can be determined for this decrease in ω_o:

$$\frac{\delta\omega_o}{\delta\Gamma_s}$$

Equation 4.5.1

The rates calculated in this way are found to be very similar for all the copolymers, see Table 4.5.2. The similarities between a number of the characteristics of the capillary wave frequency, including this rate, indicate that the processes influencing wave propagation are very much the same for all the copolymers. However, it should be stressed that the calculation of the 'rates' given is dependent on the determination of the positions of the maxima and plateau which are rather subjective.

Polymer	$\frac{\delta\omega_o}{\delta\Gamma_s}$	Γ_s^* / mg m^{-2}
10CP	- 7000 ± 400	0.25 ± 0.05
20CP	- 6900 ± 200	0.30± 0.03
60CP	- 6700 ± 250	0.45 ±0.05

Table 4.5.2: Characteristics of the ω_o vs. Γ_s variation.

The capillary wave damping, Γ, like the frequency is very sensitive to Γ_s, see figure 4.5.2. At low surface concentrations Γ is of the same order as that for pure water when $\Gamma_s = \Gamma_s^*$ Γ increases in a single step to about three times the initial value. This behaviour is exhibited by all the copolymers, each system reaching essentially the same value of Γ at the maximum, 2200 - 2400 s^{-1}. For $\Gamma_s > \Gamma_s^*$ the damping remains predominantly high, for 60CP the value reached at the step is maintained over the entire surface concentration range. There is a slight decline in the damping for both 10CP and 20CP when the surface concentration exceeds 0.75 mg m^{-2}. This downturn in the damping is most marked for 10CP, but even for this system the values only fall by circa 20 % indicating that the decrease in Γ remains fairly small over this Γ_s range. Comparison of the variation in both the capillary wave damping and frequency for each polymer indicates that the step in Γ occurs at the same concentration as the maximum in ω_o, i.e. Γ_s^*. It appears that this is a critical surface concentration where the dynamic behaviour of the graft copolymers changes.

4.5.3 Results: Spectral Fits

Four surface parameters have been successfully extracted from the correlation functions recorded as described earlier. The variation of each parameter with Γ_s has been determined and the results are presented below.

4.5.3.1 Surface Tension

The dependence of the surface tension, γ_o, on Γ_s is similar for all the polymers and reflects the variation of ω_o with Γ_s, see figure 4.5.3. This behaviour is due to the relationship between γ_o and ω_o which was given in chapter 2, equation 2.3.4 and is of the form; $\omega_o^2 \propto \gamma_o$.

Thus, like the capillary wave frequency, γ_o increases from the value for water at low Γ_s, passes through a maximum then decreases rapidly to a constant value. All the polymers exhibit the same general behaviour with the maximum value of γ_o falling in the range 75 - 80 mN m^{-1} and occurring at $\Gamma_s = \Gamma_s^*$. Data collected at Γ_s^* were found to be particularly difficult to fit as the surface parameters extracted from consecutive fits of a set of correlation functions, recorded under the same conditions, were found to vary considerably despite good quality fits being obtained in all cases. This was attributed to the fact that Γ_s^* appears to represent a sudden transition in the dynamic behaviour and consequently at this concentration, where the systems are on the edge of this change, the fitted parameters may go either way. The best fits were achieved by using a variety of different starting parameters and careful comparison of fits and residuals.

At surface concentrations above Γ_s^* , generally above 0.70 mg m^{-2}, the surface tension was found to be constant and for all the copolymers was 65 ± 1 mN m^{-1}. This is in contrast to the dependence of the static surface tension which is given in figure 4.5.4. The static surface tension continues to fall over the entire concentration range and for 10CP, for example, at Γ_s = 1.5 mg m^{-2} whereas the dynamic surface tension has stabilised at 65 mN m^{-1} the static surface tension is considerably lower at 55 mN m^{-1}. A direct comparison between the static, γ_{oST}, and dynamic values for the surface tension shows that although the first transition in γ_{oST} corresponds approximately to similar behaviour in γ_o there are some marked differences. Generally over the entire surface concentration range, the value of γ_o is higher than the corresponding static value at the same surface concentration implying that the surface tension is subject to some kind of relaxation process, the equilibrium value being represented by γ_{oST}.

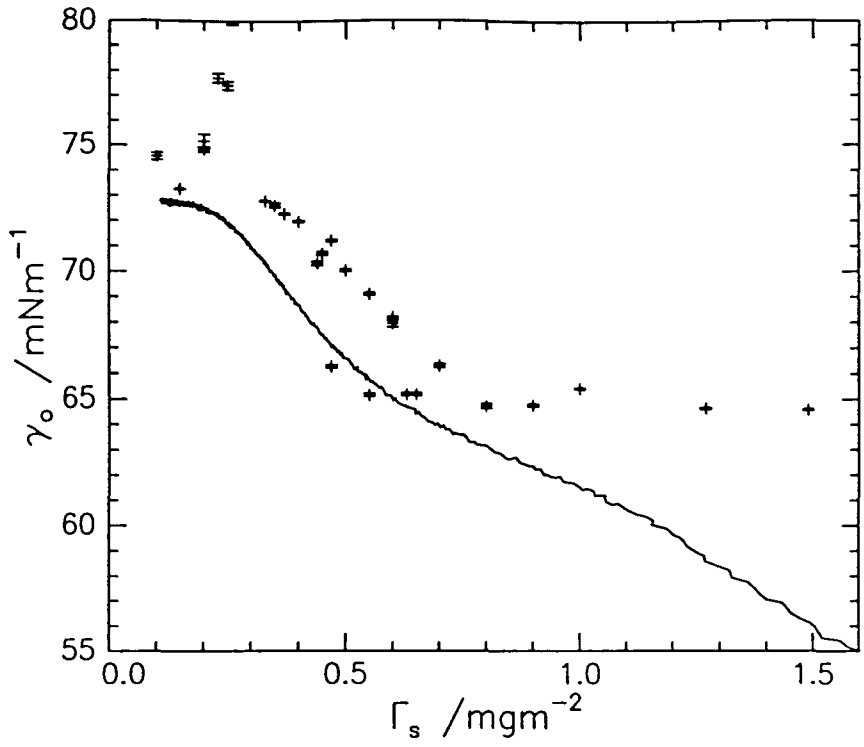

Figure 4.5.3 **A comparison between the static, solid line, and dynamic surface tension values, crosses, for 10CP.**

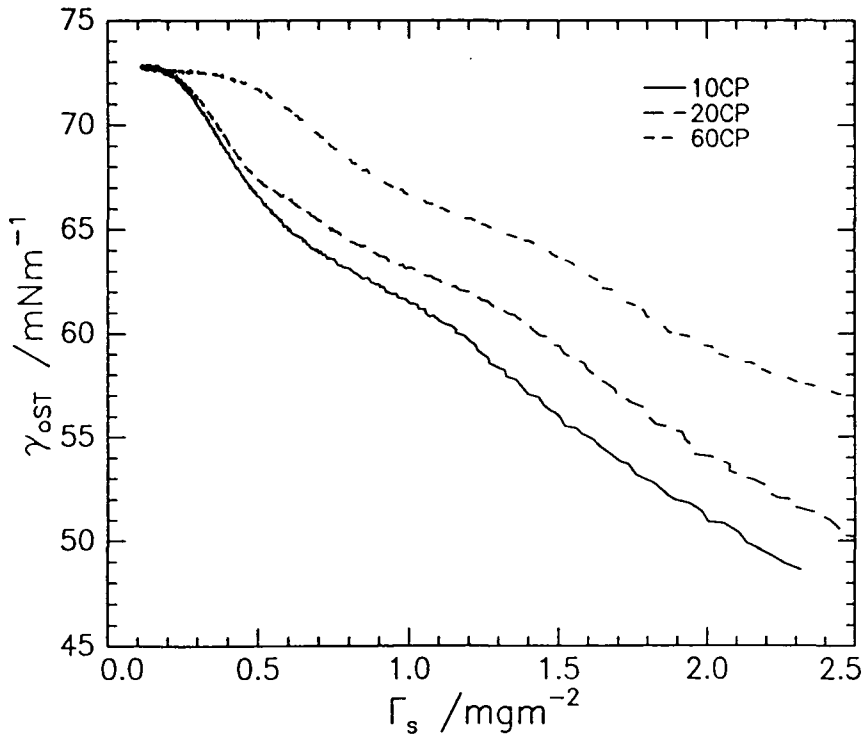

Figure 4.5.4 **The static surface tension as measured using the Wilhelmy plate method.**

4.5.3.2 Transverse Shear Viscosity

The transverse shear viscosity, γ', is the parameter that has the most direct influence on the capillary wave damping. As a consequence γ' not surprisingly exhibits the same dependence as the capillary wave damping on Γ_s, see figure 4.5.5. At the lowest polymer surface concentration γ' is found to be in the region of 3×10^{-4} mN s m^{-1}, as the surface concentration increases to Γ_s^* the value increases a to maximum of around 5×10^{-4} mN s m^{-1}. For water $\gamma' = 0$ which implies that the process of spreading even a very dilute film on water leads to a larger increase in γ' than is caused by subsequent compression of the film. Given that the greatest increase in γ' occurs below Γ_s^* it is rather remarkable that the wave damping barely changes. The capillary wave damping is essentially the same as for water until Γ_s^* where there is a rapid increase. At Γ_s^* the increment in γ' is 2×10^{-4} mN s m^{-1}, less than that on spreading the film, but despite this is accompanied by a marked increase in the capillary wave damping. It follows from these observations that the influence of γ' alone is not sufficient to explain the behaviour of the wave damping.

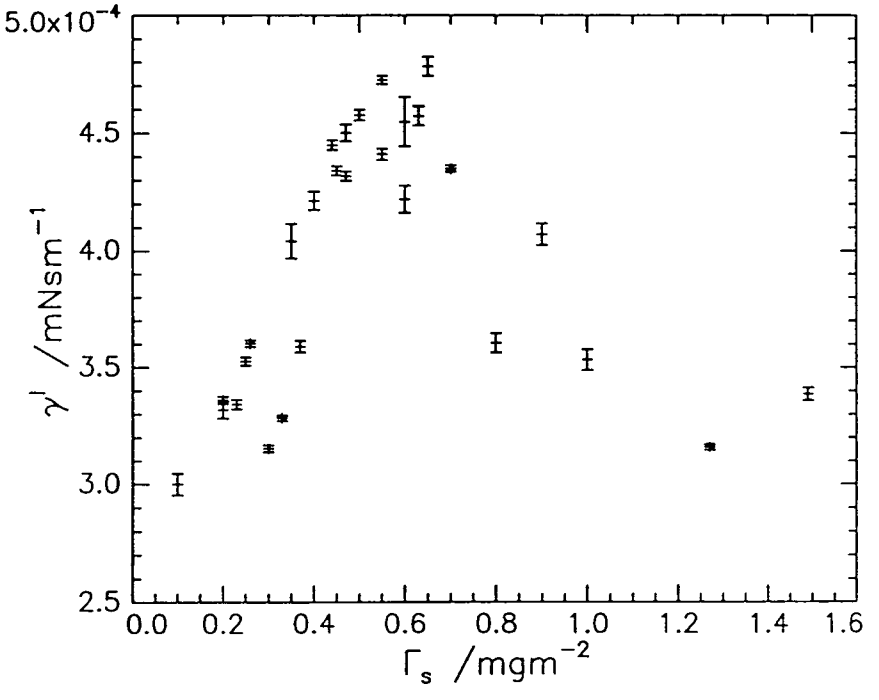

Figure 4.5.5 The variation in γ' with Γ_s for 10CP.

In addition to the behaviour discussed it was observed that the maximum in γ' occurs at ~ 0.5 mg m^{-2} for all the systems. As for Γ at surface concentrations above this value γ' decreases, the decrease is greater as the PEO content of the copolymer increases.

4.5.3.3 Dilational Modulus

Reliable determination of ε_o was found to be rather difficult and large variations were found for a set of correlation functions recorded under the same conditions for which the remaining three surface parameters were entirely consistent. All the values of ε_o were found to be very low and the errors tended to be relatively large. In spite of this systematic variations in ε_o with Γ_s are evident, see figure 4.5.6. The values of the dilational modulus are low for all the polymers and exhibit a similar variation with Γ_s tending to a minimum at Γ_s*. For $\Gamma_s = \Gamma_s$* consistent values of ε_o were particularly hard to determine. This is believed to be due to the reasons mentioned above combined with the effect of being so close to a transition. The overall result being that spurious values of ε_o were often returned.

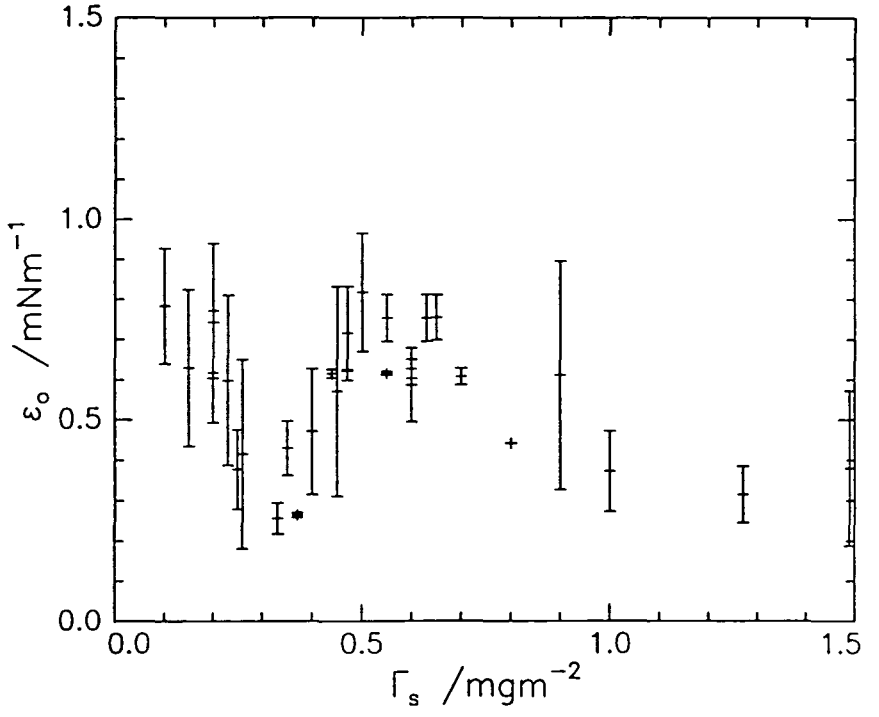

Figure 4.5.6 The variation in ε_o with Γ_s for 10CP.

Static values of ε_{oST}, the Gibbs static elasticity, can be determined from the surface pressure isotherm according to:

$$\varepsilon_{oST} = \Gamma_s \frac{d\pi}{d\Gamma_s}$$

Equation 4.5.2

To determine ε_{oST} a least squares fitting routine was used to fit a polynomial to the experimental surface pressure - surface concentration data. The derivative of this function was evaluated over the entire surface concentration range and thus ε_{oST} was determined using Equation 4.5.2. It was found that a linear 6th order polynomial was generally required to fit the surface pressure isotherm satisfactorily.

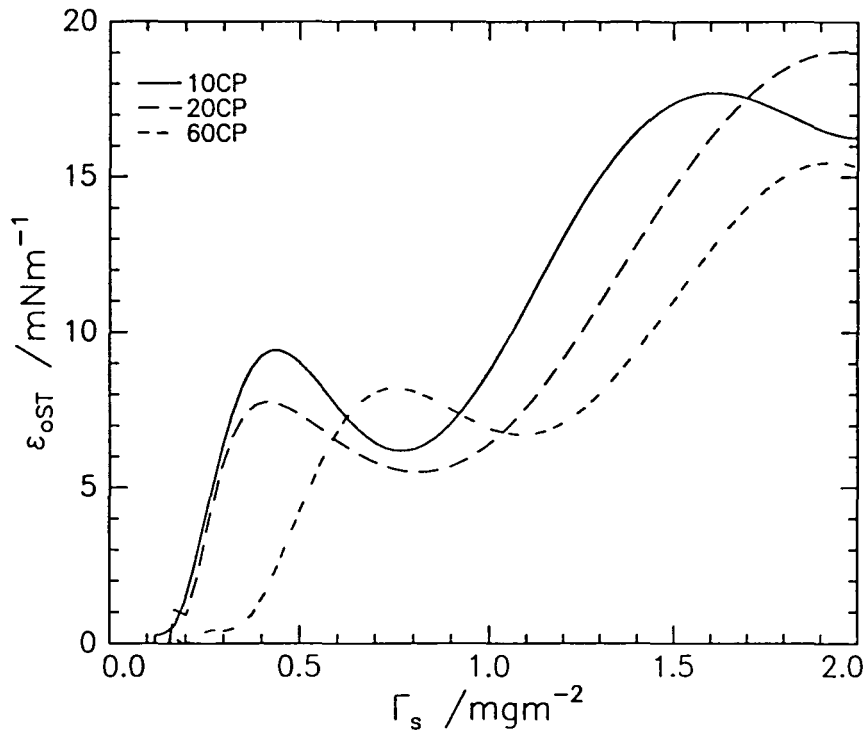

Figure 4.5.7 Gibbs elasticity for 10CP, 20CP and 60CP.

The values of ε_{oST} are given in figure 4.5.7 and are found to be significantly higher than ε_o and exhibit a quite different dependence on surface concentration. The marked differences between the dynamic and static elasticity can be highlighted by considering the behaviour at Γ_s^* where ε_o falls to a minimum whilst the static elasticity rises to its first maximum.

4.5.3.4 Dilational Viscosity

The fitted values of the dilational viscosity, ε′, were found to be systematically negative, see figure 4.5.8. Considerable care using a variety of different starting parameters in the fitting routine indicated that ε′ was negative and that this was not simply an artefact of the fitting process. It was found that starting ε′ from both positive and negative values, while varying the surface tension and elastic modulus, always gave the best fits with $\varepsilon' < 0$.

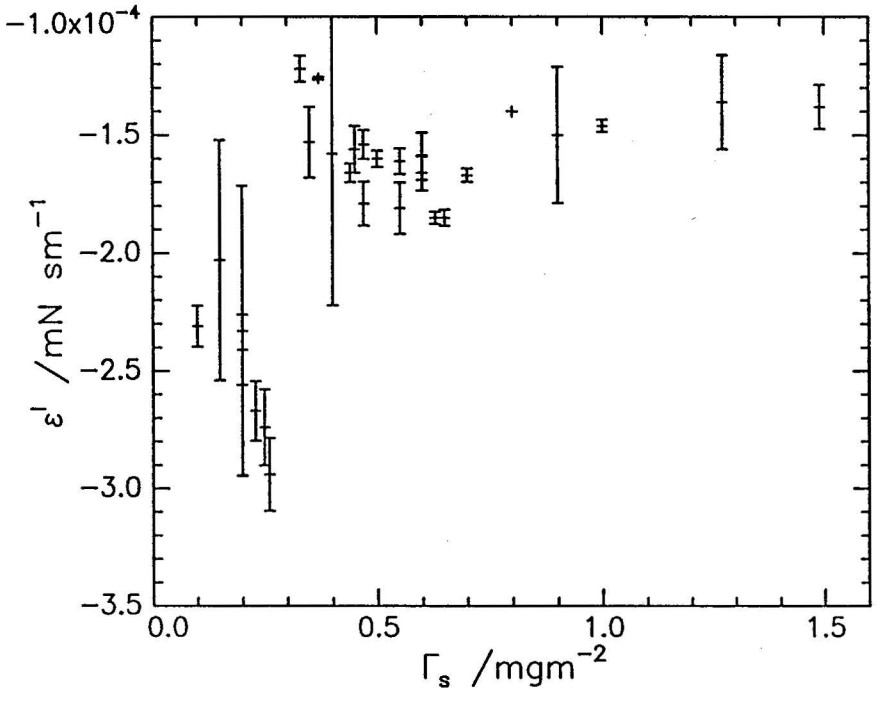

Figure 4.5.8 The variation in ε′ with Γ_s for 10CP.

A marked dependence of ε′ on Γ_s is evident for all the copolymers. At low surface concentrations ε′ decreases in a parabolic manner with increasing Γ_s. There is a marked change in the behaviour at Γ_s^* where ε′ exhibits a discontinuous change and on further increases in Γ_s falls slightly and thereafter exhibits little further variation. The value which ε′ tends to at high surface concentrations is similar to the value found for very dilute films, this is particularly so for 60CP. This behaviour and almost identical values of ε′, are observed for all the polymers. This point can be emphasised by overlaying the data for all the different copolymers, see figure 4.5.9.

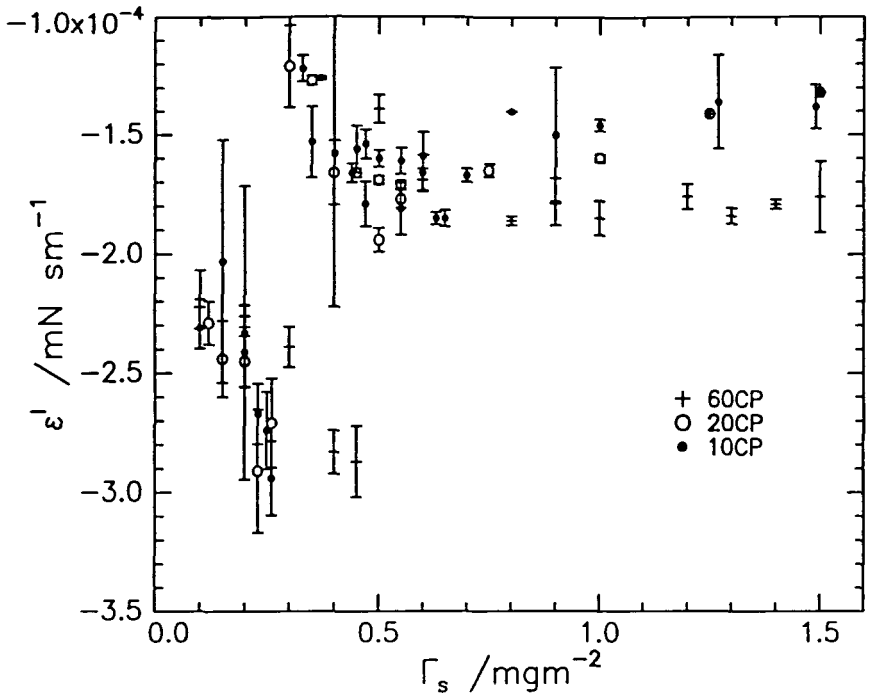

Figure 4.5.9 The variation in ε′ with Γ_s for 10CP, 20CP and 60CP.

4.5.4 Discussion: Fixed q, Variable Surface Concentration Study

The discussion of the results of the constant q, variable surface concentration study is presented here and falls into two major Sections. Section 4.5.4.1 of the discussion comprises a detailed consideration of the propagation characteristics of the surface waves. It transpires that by considering the surface modes as coupled oscillators the features of the behaviour can be reconciled in terms of the physical processes underlying them. By comparing behaviour to that of the relevant homopolymers, PMMA and PEO, attempts have been made to relate the propagation characteristics to composition and surface organisation.

The surface viscoelastic parameters are considered in the section 4.5.4.2. The unusual features exhibited by both ε_o and ε' are discussed and rationalised at a qualitative level, although this treatment does not explain the observation of negative ε'. The observation and implications of negative ε' are discussed with reference to similar recent reports in the literature. The discrepancies between the surface tension determined by light scattering and that given by static methods are also considered. Finally, to complete the discussion, attention is turned to the surface viscosities, ε' and γ', and their combined influence on the capillary wave propagation.

4.5.4.1 Capillary Wave Propagation

The major feature of the variation in ω_o for each system is the maximum observed at low surface concentrations. This is typical of resonant behaviour whereby energy can be fed into the capillary waves from another oscillation in the system. The obvious candidate for the origin of this oscillation is the dilational mode and indeed a resonance between the two surface modes is documented in the literature.[25] First order approximations for the propagation of the dilational and capillary modes are valid at relatively low q and give:

For the dilational waves $$\omega_D = \tfrac{1}{2}(\sqrt{3} + i)(\varepsilon^2 q^4 / \eta\rho)^{1/3}$$

Equation 4.5.3

For the capillary waves $$\omega_C = \sqrt{\frac{\gamma q^3}{\rho}} + i\frac{2\eta q^2}{\rho}$$

Equation 4.5.4

where $\gamma = \gamma_o + i\omega\gamma'$ and $\varepsilon = \varepsilon_o + i\omega\varepsilon'$

These equations are of the general form: $\omega = \omega_0 + i\Gamma$

At the resonance the real frequencies of the modes coincide, the q value at which resonance occurs is:

$$q = \left(\frac{3}{4}\right)^3 \varepsilon^4 \rho / \gamma^3 \eta^2$$

Equation 4.5.5

At each value of q the resonance condition is satisfied by a particular value of the ratio ε_0 / γ_0 . It has been shown that as ε_0 increases relative to a fixed γ_0 the resonance condition occurs at $\varepsilon_0 / \gamma_0 \approx 0.16$ at $q \approx 200$ cm^{-1}. Figure 4.5.10 shows how the ratio ε_0 / γ_0 changes for the copolymers with surface concentration at $q = 220$ cm^{-1}.

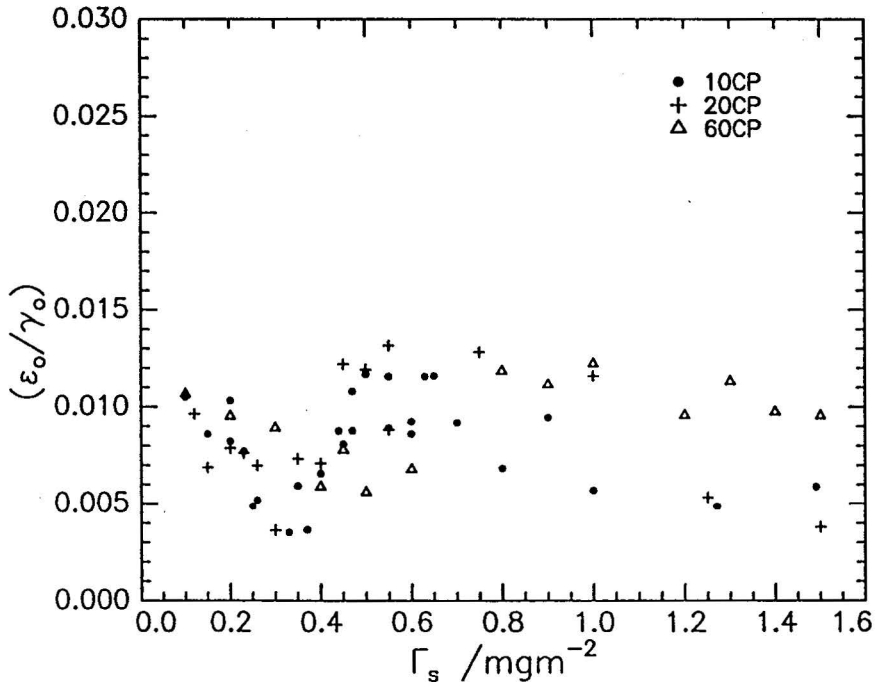

Figure 4.5.10 The variation in ε_0 / γ_0 for all the copolymers with surface concentration, Γ_s.

The value of ε_0 / γ_0 for each polymer is very low over the whole concentration range, always below 0.16, and falls to a minimum at $\Gamma_s = \Gamma_s^*$ in each case. From this it can be concluded that the resonance is not of the 'classical' type predicted above. In fact from the light scattering data $\varepsilon_0 / \gamma_0 = 0.16$ is only attained at surface concentrations far higher than Γ_s^*.

Given that the classical conditions for resonance are not satisfied at Γ_s^* other processes must be contributing to the observed phenomena. There are a number of possibilities which should be considered. The capillary waves may be at resonance at Γ_s^* but with some other surface wave, wave X, rather than the dilational waves. Although not scattering light this wave may couple to the capillary waves and hence influence their evolution.

If there are 'extra' wave modes on the surface which are presently unaccounted for, then mechanisms for their evolution must be considered. Assuming that the maximum in the capillary wave frequency is due to a resonance, then the frequency of wave X must be around 2.85×10^4 s^{-1}, although of course this may change with Γ_s. The existence of other surface modes is not predicted by the dispersion equation and so by suggesting such a process the validity of this equation is automatically being called into question. The possibility of other surface modes has been acknowledged, notably by Kramer,[26] who discussed the theory of light scattering from monolayers in a variety of situations. Kramer[26] includes the presence of compression, transverse and shear modes, the transverse modes being capillary, the compression modes being the dilational modes. The shear modes do not couple to any fluctuations of the dielectric tensor and therefore do not scatter light, but it is acknowledged that if the film is anisotropic these modes may mix with others and new modes could appear. These effects may be relevant to this study, accounting for the existence of a hitherto unnoticed mode coupled to the capillary mode. Quantifying such an effect is not straight forward and would involve modification of current theories, a new dispersion equation and detailed examination of the behaviour. Alternatively, rather than being a discrete surface wave there may be dynamic processes at the interface that occur at frequencies of about 2.85×10^4 s^{-1}. Molecular motion of the PEO side chains or motion of the polymer backbone are possible contenders, although are likely to be too rapid. These motions are considered to be analogous to the molecular motion of polymers in dilute solution and are considered in more detail later.

Although the values of the surface parameters at the maximum in ω_o are not consistent with a classical resonance where $\varepsilon_o / \gamma_o = 0.16$, this ratio is actually predicted by applying approximations rather than by solving the full dispersion equation. The fundamental evidence of a resonance between the capillary and dilational modes will be found in the variation of the dilational mode frequency. Thus in order to elucidate the behaviour at $\Gamma_s = \Gamma_s^*$ it was considered helpful to determine how the dilational mode is propagating in this regime. By using the surface parameters extracted from the spectral fits it was possible to solve the

dispersion equation in terms of the wave frequency and damping, enabling the experimentally inaccessible dilational wave frequency and damping to be determined at each value of Γ_s studied. This method of extracting information about the propagation of the dilational mode is discussed in more detail in section 4.5.7. At this point it is simply noted that in this approach the tacit assumption is made that the dispersion equation does describe the propagation of the surface modes correctly, as will be discussed this may not be the case.

The variation in the frequency of the two different surface modes is given in figure 4.5.11 and clearly shows that the modes are not at resonance. The frequency of the capillary mode is much higher than that of the dilational mode over the entire surface concentration range studied. The dilational wave frequency falls to a minimum value at the 'resonance' surface concentration, Γ_s*, whilst there is a maximum in the capillary wave frequency. As a consequence at $\Gamma_s = \Gamma_s$* the difference between the frequencies of the two modes rather than being small / zero as required for the 'classical' resonance is actually a maximum. The 'classical' resonance is that referred to earlier for which $\varepsilon_o/\gamma_o = 0.16$.

This type of behaviour is exhibited by two coupled oscillators which provides a valid way of conceptualising the characteristics exhibited by the surface waves. In reality, of course, behaviour at the water surface is much more complex. Despite the possible complications modelling the system using this simple approach provides a successful means of explaining a number of observations.

Consider the situation of two oscillators, pendula for example, both of which have different free frequencies of oscillation, Ω_1 and Ω_2. If these oscillators are linked in some way their behaviour will change.

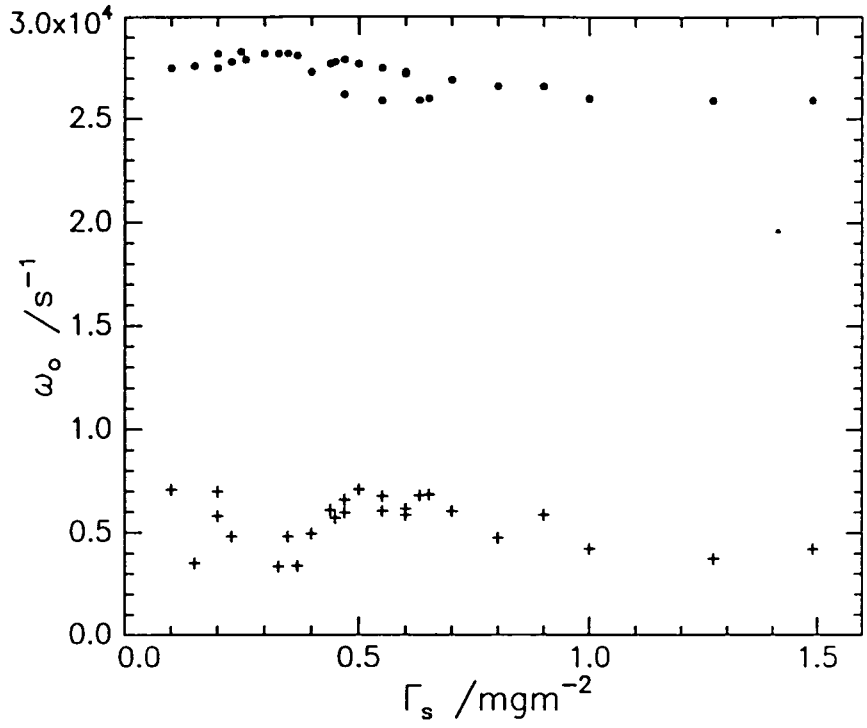

Figure 4.5.11 Variation in the dilational wave frequency, crosses, and the capillary wave frequency, filled circles for 10CP with Γ_s.

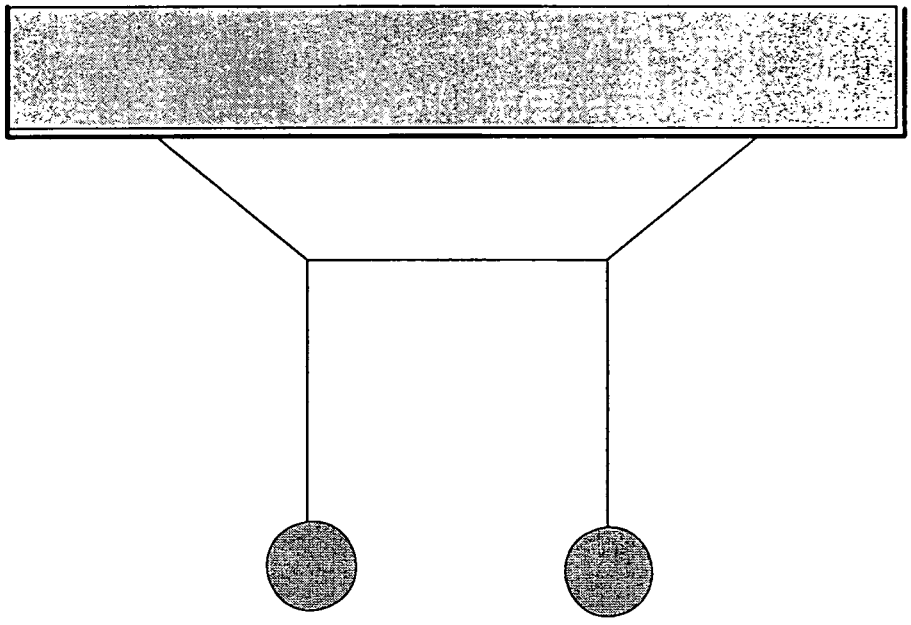

Figure 4.5.12 Two pendula coupled by a piece of string. See text for further discussion.

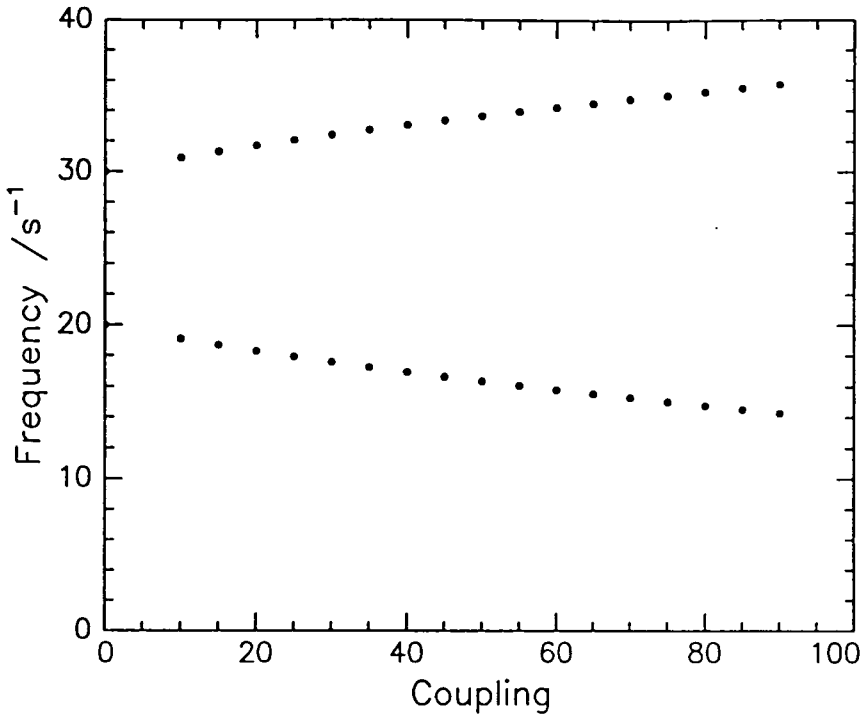

Figure 4.5.13 Demonstrating the change in the frequency of the normal modes with coupling constant using Equation 4.5.6, $\Omega_1 = 20\ s^{-1}$, $\Omega_2 = 30\ s^{-1}$.

Rather than consider the motion of each pendulum separately one must now consider the system, where both oscillators constitute the system. An example of this is given in figure 4.5.12 where two pendulum bobs have been linked horizontally by a string. Due to this link, the coupling, neither pendulum can move separately from the other and the motion of one imposes motion on the other. In systems of this nature the vibration frequencies exhibited by the normal modes can be linked to the free oscillation frequencies and the coupling strength K by:

$$(\omega - \Omega_1)(\omega - \Omega_2) = K^2$$

Equation 4.5.6

This equation is quadratic in ω and has solutions ω_1 and ω_2, the normal modes of the system. The uncoupled oscillations have frequencies Ω_1 and Ω_2 and are coupled with a coupling constant K. Clearly the frequency of the normal modes depends explicitly on K; at K = 0 the oscillations are uncoupled, i.e. have frequencies Ω_1 and Ω_2. However, as K increases the frequencies of the modes diverge from these values, ω_1 increases above Ω_1 whereas ω_2 falls below Ω_2. Thus if the coupling were to increase to a maximum value one

would expect to observe an associated maximum in the high frequency mode and a minimum in the low frequency mode, this is illustrated in figure 4.5.13.

This result can be translated directly to the behaviour of the surface wave modes. In this situation the capillary and dilational waves are coupled oscillators and their frequencies are the normal modes of the system. The dilational mode constitutes the low frequency vibration, the capillary mode is the high frequency vibration. Following the logic presented above, it is clear that if the coupling between these surface modes were to gradually increase behaviour analogous to that described above would be observed. The high frequency vibration, the capillary mode, would increase in frequency, conversely the frequency of the other, dilational, mode would fall. Thus it follows that an increase in the capillary mode frequency may be observed due to changes in the strength of the coupling between the surface modes. If at some point, the coupling between the waves reached a maximum value one would expect to see a minimum in the low frequency vibration, the dilational mode, and a maximum in the high frequency vibration, the capillary mode. Examination of figure 4.5.11 illustrates that this is indeed the case. At Γ_s = 0.30 mg m^{-2} the capillary mode reaches a maximum value whereas the dilational mode frequency falls to a minimum. In fact all the different composition graft copolymers exhibit this behaviour at Γ_s^*. This observation indicates that this surface concentration corresponds to some kind of transition in the films which leads to particularly strong coupling between the surface wave modes. Presumably this behaviour is linked to a structural transition in the films which occurs at a discrete surface concentration. However, at this point there is no molecular rationale for the behaviour.

It follows from the preceding discussion that the observed variation in the frequency of the two surface modes may be attributed to changes in the coupling between the dilational and capillary waves. Consider the coupling in more detail. The quantity which is associated with the coupling in the specific case of surface modes is m where:

$$m = (q^2 + i\omega\rho/\eta)^{0.5}$$

Equation 4.5.7

The coupling coefficient for the air-water interface is given by:

$$[\eta(q - m)]^2$$

Equation 4.5.8

The values of q, ρ and η are constant during the experiment but ω is not and changes with Γ_s. Through m the coupling will alter in the same manner as the propagation characteristics because, $\omega = \omega_0 + i\Gamma$. If the solution to $D(\omega)$ corresponding to capillary modes is considered at Γ_s^*, it is known from experiments that the damping and frequency both achieve their highest values and consequently the coupling will be a maximum. From the model behaviour of two classic coupled oscillators we would expect the dilational wave frequency, being the lower frequency mode, to be at a minimum at this point and this is indeed observed, see figure 4.5.11. Thus, it can be concluded that by viewing the surface modes as coupled oscillators with a variable coupling, the frequency variation for both modes can be rationalised.

The decrease in ω_0 with Γ_s is similar for all the systems indicating that the processes which influence the wave frequency are similar for all the polymers once $\Gamma_s > \Gamma_s^*$. There is no marked variation in $\delta\omega_0/\delta\Gamma_s$ with copolymer composition although there a significant change at $\Gamma_s = \Gamma_s^*$. There is insufficient neutron reflectivity data to ascertain whether this corresponds to a structural change in the layer. In fact the most dilute films studied were, in most cases, just above Γ_s^*. These experiments were performed before the implication of Γ_s^* was realised fully but, given that such dilute films are very weakly reflecting and the failure to deuterate the PEO side chains, it seemed unlikely that performing the experiments at Γ_s^* would provide much more information. In addition it may be that the two experiments, being on different timescales, would not both be sensitive to the same processes. Whereas SQELS measurements are complete in a matter of minutes neutron reflectivity profiles take up to 4 hours to collect. Despite the lack of neutron reflectometry data at this Γ_s it transpires that these surface concentrations, very close to Γ_s^* for each of the copolymers, have already been considered in terms of some kind of structural change in the layer. In section 4.3.4.3 where the surface pressure isotherm data was presented, a rough calculation was performed to determine the maximum concentration of each graft copolymer which could be accommodated on the water surface. Using the minimum surface areas for the homopolymers values for Γ_{sLIM} were determined. These are presented below in Table 4.5.3 along with Γ_s^*.

It is clear from the values in Table 4.5.3 that Γ_{sLIM} and Γ_s^* are almost identical for all the different composition graft copolymers. It is believed that the similarity in these values is not just coincidence and that this result has significant implications on the physical interpretation of Γ_s^*. The implication of Γ_{sLIM} is that above this surface concentration the

species are so cramped on the surface that to relieve this the side chains penetrate the subphase. In the absence of any other evidence it seems that the structural transition most likely to correspond to Γ_s^* is co-operative subphase penetration by the PEO side chains. This is not to say that there is no subphase penetration below Γ_s^* and it is expected that rather than occurring sharply this is a gradual transition that becomes complete at Γ_s^*. Clearly, this transition causes marked changes in the surface wave propagation and characteristics of the behaviour. A molecular rationale for these effects is not forthcoming. Understanding at this level is hampered by the fact that certain features of the behaviour are specific to Γ_s^*. In the model adopted it is supposed that while co-operative subphase penetration only occurs at Γ_s^* at all surface concentrations thereafter the system remains in this state. Given this behaviour it is difficult to rationalise a number of features exhibited by the system which have been identified as unique to this concentration. This result implies that the behaviour is specific to a system undergoing structural reorganisation.

Polymer	Γ_{sLIM} / mg m^{-2}	Γ^*_{brush} / mg m^{-2}	Γ_s^* / mg m^{-2}
10CP	0.23 ± 0.02	0.33 ± 0.01	0.25 ± 0.05
20CP	0.25 ± 0.02	0.38 ± 0.01	0.30 ± 0.03
60CP	0.41 ± 0.03	0.73 ± 0.03	0.45 ± 0.05

Table 4.5.3: Comparison of Γ_{sLIM}, Γ^*_{brush} and Γ_s^*.

In addition to Γ_{sLIM} Table 4.5.3 also contains the quantity Γ^*_{brush}. This is the surface concentration when, from scaling laws[20,21] for polymer brushes, the side chains are expected to stretch. Such behaviour occurs when the distance between the brushes becomes equal to R_g. To determine Γ^*_{brush} the side chains have been envisaged to occupy cylinders with a radius equal to R_g, 24 Å. The surface concentration corresponding to this occupation of the surface was then computed and is given for comparison in Table 4.5.3. Although the values scale in the same manner as Γ_s^* they are systematically higher. This is consistent with the discrepancies observed when brush theory was compared to the results of the neutron reflectometry study, see section 4.4.6. It was found that the thickness of the water layer, which was assumed to be representative of the brush thickness, was always less than predicted by brush theory, i.e. the theories overestimate observed behaviour. Assuming these systems do exhibit brush type behaviour, co-operative stretching would be anticipated to occur at

slightly higher Γ_s than observed; unfortunately it is not possible to quantify these effects. However, it is concluded that, from the discussion above, the most likely origin of Γ_s* appears to be a co-operative change in the behaviour of the PEO side chains most probably associated with subphase penetration.

A sudden increase in the capillary wave damping also occurs at Γ_s*. In fact the variation in the Γ with Γ_s provides further evidence that the maximum in ω_o is not a resonance phenomenon. If the capillary mode was at resonance one would expect to see a resonance maximum in Γ since , like the wave frequency, it may be viewed as a measure of the response of the capillary waves. The wave damping does not exhibit such behaviour for 60CP and although the other systems do demonstrate maxima in Γ they are far broader than that observed in the frequency variation. The position of Γ_s* shifts with copolymer composition but the magnitude of Γ at this point is, within experimental error, the same. This indicates that the processes which influence the damping of the capillary waves are similar for all the polymers and are, most probably, intimately linked with copolymer composition and monolayer structure.

As mentioned earlier γ' has the most direct influence on the wave damping and so at $\Gamma_s = \Gamma_s$* the values of γ' for 60CP, 20CP and 10CP are very similar. In terms of surface parameters it is known that γ' influences the capillary wave damping according to:[39]

$$\Delta\Gamma \approx \frac{\gamma' q^3}{2\rho}$$

Equation 4.5.9

Thus γ' increases the capillary wave damping and, due to the coupling, will also cause the dilational wave damping to decrease, see figure 4.5.14. Increases in the dilational viscosity predominately influence the dilational wave damping, Γ_D, causing it to increase whereas the capillary wave damping, only indirectly influenced via the coupling, decreases. The equation analogous to that above, expressing the effect of ε' on the dilational wave damping is:[40]

$$\Delta\Gamma = \tfrac{1}{3}(\varepsilon'\varepsilon_o q^8 \Big/ \eta^2\rho^2)^{\frac{1}{3}}$$

Equation 4.5.10

In the case of $\varepsilon' < 0$, the implications of which will be discussed later, the behaviour is reversed and the dilational wave damping falls as ε' becomes more negative, concurrently the capillary wave damping increases.

In the discussion above the influence of each of the viscosities on the wave damping was considered independently, however when both viscosities are non zero the influence of each on the system becomes more complex especially when $\varepsilon' < 0$. The effect of introducing $\varepsilon' < 0$ is, provided that $\gamma' = 0$, a reduction in Γ_D but an increase in Γ_C. Using simulations and taking typical values for the surface parameters, $\gamma_o = 65.4$ mN m^{-1} at q= 220 cm^{-1} setting $\varepsilon_o =$ 10.5 mN m^{-1}, it transpires that the effect of $\varepsilon' < 0$ on the capillary wave damping actually depends on the value of γ', see figure 4.5.15. Setting $\varepsilon' = -1.46\times 10^{-4}$ mN s m^{-1}, a typical value for the systems studied, and varying γ' from 0 to 5×10^{-4} mN s m^{-1} , which broadly encompasses the range of values found in experimental studies, the magnitude of the damping relative to the same situation with $\varepsilon' = 0$ is observed to alter with γ'. When $\gamma' < 3.4 \times 10^{-4}$ mN s m^{-1} introduction of $\varepsilon' < 0$ causes the capillary wave damping to increase, however at higher values of γ' the behaviour is reversed and the capillary wave damping is decreased by $\varepsilon' < 0$.

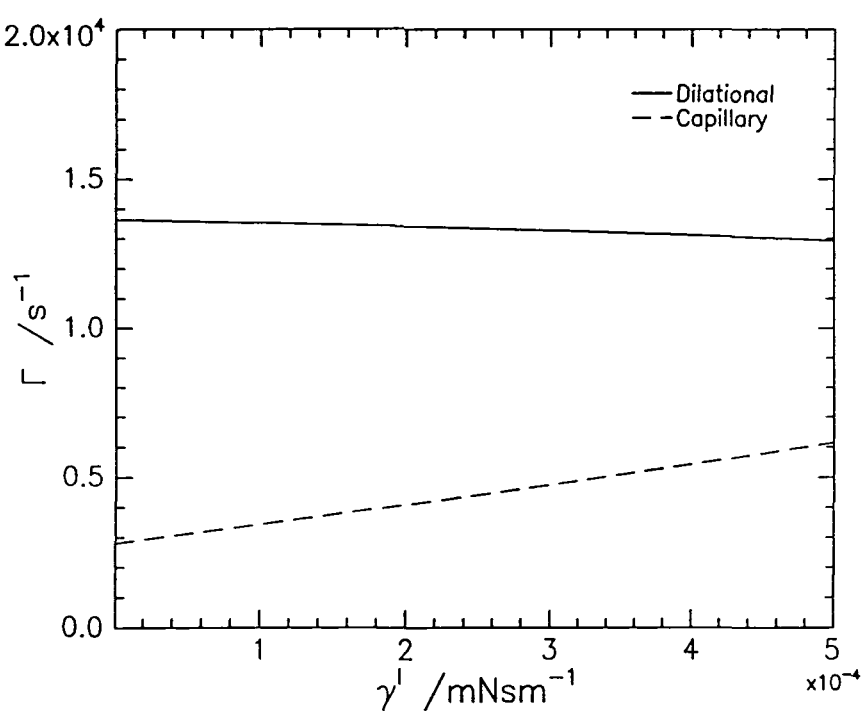

Figure 4.5.14 Influence of γ' on the capillary and dilational wave damping for $\gamma_o = 65.4$ mN m^{-1}, $\varepsilon' = 0$ and γ' as given at q = 220 cm^{-1}.

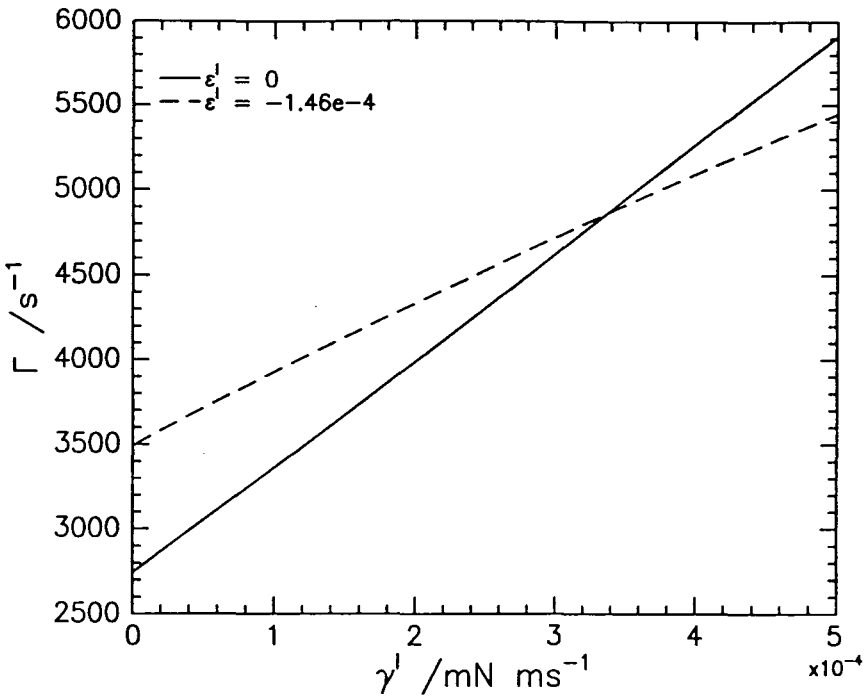

Figure 4.5.15 Influence of γ' on the capillary wave damping at $q = 220\ cm^{-1}$, $\gamma_o = 65.4\ mN\ m^{-1}$, ε' and γ' as given.

In the case of the graft copolymers the dilational modulus is very low and this also influences the wave damping. Simulations show that when ε_o is low and γ' falls in the range 0 to 5×10^{-4} mN s m^{-1}, exactly as observed for this study, introducing a negative dilational viscosity leads to a reduction in the capillary wave damping. From simulations it becomes clear that the precise behaviour of the system will depend not only on the balance of γ' and ε' but also the elastic moduli. It is informative to compare the propagation of the capillary waves in the presence of the graft copolymer films to that for films of the homopolymers PEO and PMMA.[27] Previous work has shown that for PMMA ω_o remains at that of water until Γ_s = 1.00 mg m^{-2} then falls slowly over the remaining surface concentration range. In contrast, for spread layers of PEO ω_o decreases rapidly from the outset to a value below that for water and remains essentially constant when $\Gamma_s > 0.4$ mg m^{-2}. The behaviour of the graft copolymers is a hybrid of these two extremes. At low Γ_s the capillary wave frequency remains high then decreases to a constant value when $\Gamma_s > \Gamma_s^*$, suggesting that behaviour in the range $\Gamma_s > \Gamma_s^*$ is dominated by the PEO parts of the copolymers.

The variation in the capillary wave damping also shows characteristics of the homopolymers. The wave damping for a spread film of PMMA[27] increases abruptly at low

surface concentrations then remains essentially constant at 2330 s^{-1} at q = 220 cm^{-1}. The behaviour of 60CP is very similar to this and remarkably the value of Γ reached is essentially the same. The implications of this observation are not clear, suffice to say that at low surface concentrations, $\Gamma_s < \Gamma_s^*$, the wave propagation appears to be dominated by the PMMA in the molecule. As the PEO content of the copolymer increases the damping exhibits a downturn at $\Gamma_s > \Gamma_s^*$. Similar behaviour is exhibited by PEO where Γ is observed to increase rapidly, reach a maximum at surface concentrations circa 0.4 - 0.6 mg m^{-2} then fall slightly. It follows that the behaviour of the copolymers is predominantly PEO like above Γ_s^*. The basic corollary of the comparison with the homopolymers is that at $\Gamma_s < \Gamma_s^*$ the graft copolymer's behaviour is dominated by the PMMA parts, whereas at surface concentrations above Γ_s^* the behaviour changes becoming increasingly like that of PEO.

At a simplistic level the fall in Γ for the PEO rich copolymer, 10CP, at $\Gamma_s > \Gamma_s^*$ means that as a waves passes over the surface less energy is dissipated by this motion. It seems that the presence of PEO can be correlated to this reduction in energy dissipation. If the PEO side chains are considered to penetrate the subphase, which the neutron reflectometry data indicates, then one might expect the hydrogen bonding structure of water to be disrupted. When a wave passes across a liquid surface any processes which retard the motion of the molecules at the surface must contribute to the damping. The hydrogen bonding structure of water may contribute to this but, if it can be disrupted, the molecules may be able to move more easily causing the damping to fall. If penetration of the subphase by the side chains can have this effect then an increasing reduction in Γ with increasing Γ_s would be predicted and indeed such behaviour is observed. In addition hydrogen bonding between submerged PEO and water molecules may lead to increasingly co-operative motion between the film and subphase which could also contribute to a reduction in the damping. Studies indicate that three water molecules are associated with each EO unit in solution[28] and a similar co-ordination is expected here.

To test the extent to which the water structure is disrupted it is helpful to get an idea for the ratio of EO units to water molecules in the surface layer.

For 10CP 1 side chain to 12 units of MMA

54 EO units : 12 MMA units

M_n = 87200

From these figures it is found that on average each chain contains 1296 EO units and 288 MMA units.

At Γ_s =1.0 mg m^{-2} each unit of surface area contains 8.95×10^{18} units of EO.

Using the bulk density of water and taking a typical layer thickness determined from neutron reflectivity as 40Å, a ratio of 1 EO unit to 15 water molecules is calculated. This figure indicates that any reduction of the hydrogen bonding will be unlikely to be significant.

Attention is now turned to consider whether molecular motion may be occurring at a frequency comparable to that of the capillary waves and therefore influencing the observed behaviour. In the Rouse model[29] a polymer chain is modelled as being a number of beads linked by springs. For polymer chains in solution rotation and deformation have the same characteristic relaxation time given using this model by:

$$\tau_r = 0.325\eta_s \frac{(\sqrt{N}a)^3}{k_B T}$$

Equation 4.5.11

where N is the number of units with a statistical step length a and η_s is the viscosity of the solvent. At this stage only motion of the side chains is considered, the step length is taken as being 6 - 10 Å and N = 54. Substituting these values into Equation 4.5.11 suggests that the relaxation time for this motion is in the range 0.007 - 0.03 μs giving a frequency range of 3 10^7 - 1.5×10^8 s^{-1}. Thus the side chains are likely to be moving very rapidly, their frequency being considerably higher that that of the capillary waves. It is anticipated that on the timescale of this experiment these contributions will be smeared out by averaging and will not have a significant influence on the dilational wave propagation.

4.5.4.2 Surface Viscoelastic Parameters

The behaviour of the surface viscoelastic parameters is complex, there is substantial disagreement with the static surface tension and γ' is found to be relatively large, ε_o rather small and ε' negative. In addition ε' and ε_o exhibit a unique dependence on Γ_s and it is this behaviour that is considered first.

In order to account for the behaviour of the dilational parameters attention is turned to the propagation of the dilational waves. The variation in the frequency of these waves was presented in figure 4.5.11 for 10CP and clearly show that the minimum value of ω_{oD} at Γ_s* is similar for all the polymers, 2000 - 3000 s^{-1}. At this surface concentration the dilational parameters, ε_o and ε', exhibit a very distinct dependence on Γ_s, ε' exhibits a bifurcation, ε_o a minimum. This behaviour can be reproduced if the dilational waves are considered to be behaving as forced oscillators. Following standard treatments[30] a sinusoidal oscillating force is considered to act on an oscillator, say a spring, which has a natural resonant frequency ω_o. When a force $F_o \exp(i\omega t)$ acts on the spring, which represents the dilational waves, the system will respond and the resulting 'output' will be in a mechanical component of the system, the displacement or velocity. Consider first the displacement, $\xi(t)$, given by:

$$\xi(t) = \frac{-F_o \exp(-i\omega t)}{m(\omega^2 - \omega_o^2 + 2i\omega''\omega)}$$

Equation 4.5.12

where m is the mass of the oscillator, ω is the frequency of the motion described by the spring following the input of the force, ω_o is the resonance (natural) frequency of the system and ω'' is the complex component of the frequency, i.e. the damping. Equation 4.5.12 can be written in terms of the displacement transfer function $\chi_D(\omega)$. A transfer function describes the relationship between the input force and resulting output exhibited by the system. The general equation being of the form:

Output = Input × Transfer Function.

Previously the displacement caused by the force acting on the spring was considered. The displacement can be related to the input force via.:

$$\xi(t) = \chi_D(\omega) F \exp(-i\omega t)$$

Equation 4.5.13

where $\chi_D(\omega)$ is the displacement transfer function,

$$\chi_D(\omega) = \frac{-1}{m(\omega^2 - \omega_o^2 + 2i\omega''\omega)}$$

Equation 4.5.14

To investigate the behaviour of $\chi_D(\omega)$ it is necessary to consider the real and imaginary parts separately. Multiplying Equation 4.5.14 through by the complex conjugate of the denominator, $\omega^2 - \omega_o^2 - 2i\omega''\omega$ gives:

$$\chi_D(\omega) = \frac{\omega_o^2 - \omega^2 + 2i\omega''\omega}{m((\omega^2 - \omega_o^2)^2 + 4\omega''^2\omega^2)}$$

Equation 4.5.15

The real and imaginary parts can easily be separated out of Equation 4.5.15 and give:

$$\mathrm{Re}\,\chi_D(\omega) = \frac{\omega_o^2 - \omega^2}{m((\omega^2 - \omega_o^2)^2 + 4\omega''\omega^2)}$$

Equation 4.5.16

$$\mathrm{Im}\,\chi_D(\omega) = \frac{2\omega''\omega}{m((\omega^2 - \omega_o^2)^2 + 4\omega''\omega^2)}$$

Equation 4.5.17

By taking general values for the parameters, m = 1 kg, $\omega_o = 10^5$ s^{-1} and $\omega'' = 10^4$ s^{-1}, the variations in the real and imaginary parts can be plotted and are shown in figure 4.5.16. It is observed that the variation of $\mathrm{Im}\,\chi_D(\omega)$ is like that of ε_o whereas the variation of $\mathrm{Re}\,\chi_D(\omega)$ has the same form as ε'. This implies that the dilational parameters represent the response of the system to an applied force. On examination however it becomes clear that if ε_o and ε' do represent the response of the system then ε_o must be related to the real part of the transfer function and ε' with the imaginary part. Clearly the real and imaginary parts of the transfer function must be swapped round somehow. This can be achieved by taking the time differential of Equation 4.5.13, i.e. considering the velocity response of the spring given by:

$$\dot{\xi}(t) = \chi_V(\omega) F \exp(-i\omega t)$$

Equation 5.18

where $\chi_V(\omega) = \dfrac{i\omega}{m(\omega^2 - \omega_o^2 + 2i\omega''\omega)} = -i\omega\chi_D(\omega)$

Equation 4.5.19

Following exactly the same the method outlined above the real and imaginary parts of $\chi_V(\omega)$ may be separated to give:

$$\mathrm{Im}(\chi(\omega)) = \frac{\omega(\omega^2 - \omega_o^2)}{m((\omega^2 - \omega_o^2)^2 + 4\omega''^2\omega^2)}$$

Equation 4.5.20

$$\mathrm{Re}(\chi(\omega)) = \frac{2\omega''\omega^2}{m((\omega^2 - \omega_o^2)^2 + 4\omega''^2\omega^2)}$$

Equation 4.5.21

Using the same values for the parameters as given previously we find that the variation of ε' with Γ_s is reproduced by the behaviour of the imaginary part of $\chi_V(\omega)$, see figure 4.5.17. However, in order to reproduce the form of ε_o with Γ_s -Re($\chi_V(\omega)$) must be taken, figure 4.5.18. The reason for this is not clear, although it implies that ε_o represents an absorption resonance. The discontinuous behaviour exhibited by both the real and imaginary part of the velocity transfer function at an particular value of ω occurs due to a resonance, which is termed a velocity resonance. Basically this behaviour arises because the driving force has caused the system to vibrate at its natural frequency, the system is at resonance.

From the treatment above it is clear that by considering the velocity response of the dilational waves the variation of ε_o and ε' can be qualitatively accounted for. In this system the term $\varepsilon = \varepsilon_o + i\omega\varepsilon'$ represents the response of the dilational waves to an external driving force. It is stressed that the dilational parameters do not represent the output of the dilational waves, the output is the rate of change of some parameter of the dilational waves. If this parameter is displacement then the output becomes the velocity of the waves. Despite the terminology used here it is not necessarily the velocity of the waves which constitutes the output, but more generally the rate of change of some parameter associated with them.

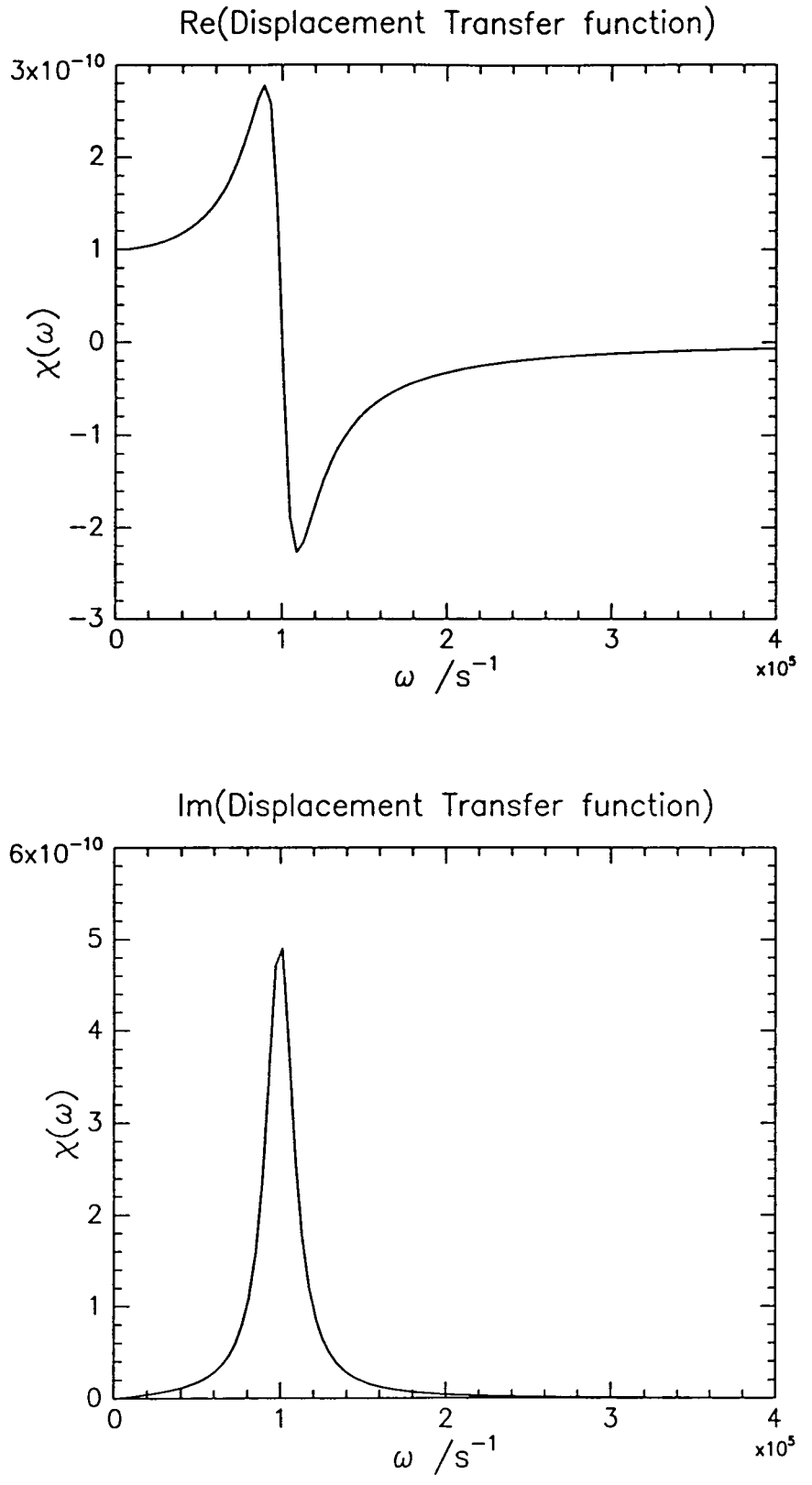

Figure 4.5.16 Real and imaginary parts of the displacement transfer function, see text for further details.

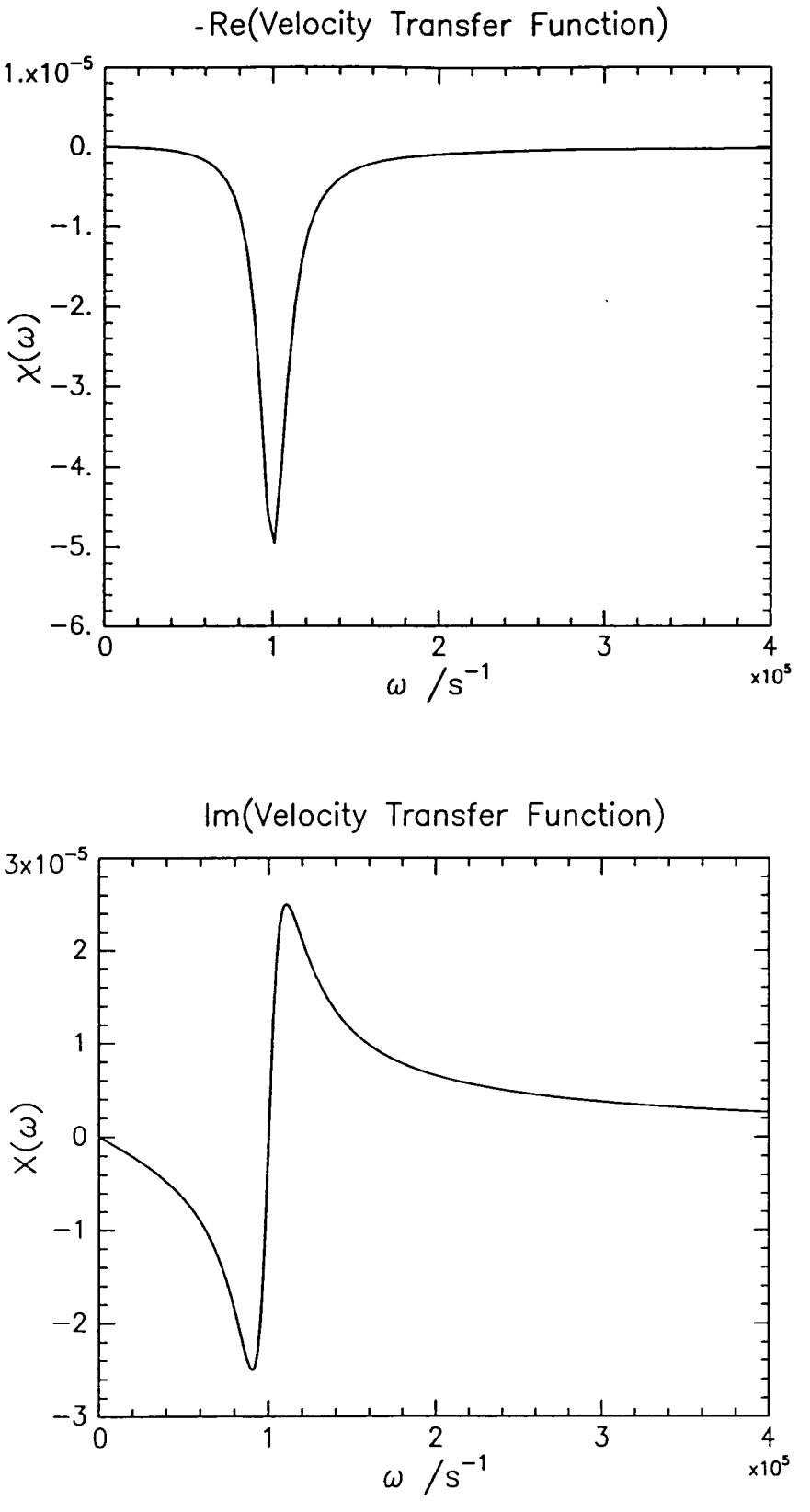

Figure 4.5.17 Real and imaginary parts of the velocity transfer function, see text for further details.

To summarise the above, it is clear that modelling the dilational waves as forced oscillators reproduces qualitatively the form of ε_o and ε', see figures 4.5.6 and 4.5.9. The major problem with the treatment is that theory predicts that such behaviour would be observed as a function of ω although experimentally the variable was Γ_s. This anomaly may be accounted for by reference to the behaviour of the dilational mode frequency determined earlier, figure 4.5.11 It was observed that the frequency of this mode varied with Γ_s. This is consistent with expectations, since the properties of the surface will vary with Γ_s and in turn the parameters influencing wave propagation will change. Clearly the vital point is that the dilational wave frequency varies with Γ_s, although this variation may or may not be linear. In essence then, by varying the surface concentration of polymer a window of dilational wave frequencies is being sampled. At low surface concentration, $\Gamma_s < \Gamma_s^*$ the frequency of the driving force is below that of the dilational mode. At $\Gamma_s = \Gamma_s^*$ the coupling between the dilational and capillary waves reaches its maximum value and consequently the frequency of the dilational mode falls to a minimum. The frequency of the dilational mode falls to the same value as that of the sinusoidal force and resonance is established leading to a transfer of energy between the two oscillators.

The above discussion illustrates that the behaviour of ε_o and ε' is consistent with the model proposed and the observation of such behaviour as a function of Γ_s may be reconciled. Given this result the model adopted for this system is that of the dilational waves with an external force constantly acting on them, thus supplying energy to this wave mode. Clearly this force may cause not only a velocity 'output' but also a displacement, both quantities can clearly be viewed as 'output signals'. If this were the case one would expect to observe a displacement resonance in the system whereas only a velocity resonance is observed. This may be simply because the experiment is not sensitive to any of the parameters which represent the displacement response. Alternatively further consideration of the theory of forced oscillators enables this, and other points, to be rationalised.

Consider the power response of the displacement P_d, and the velocity, P_v, of a forced oscillator. These take the form:

$$P_d = \chi_d \chi_d^*$$

Equation 4.5.22

$$P_v = \chi_v \chi_v^*$$

Equation 4.5.23

The maximum of P_d occurs at frequency ω_d which can be manipulated into the form:

$$\omega_d \approx \omega_o(1 - 1/Q^2 + ...)$$

Equation 4.5.24

where ω_o was the natural frequency of the oscillator being 'forced'. The quantity Q is called the 'quality factor' and is defined as the number of radians through which a damped system oscillates as the energy decays to 1/e of its original value.

In comparison to the above the maximum in P_v occurs at ω_o and consequently it follows from equation 4.5.24 that if Q is sufficiently small $\omega_o > \omega_d$ the resonances will occur at different frequencies. Clearly, the smaller the value of Q the greater the damping in the system and the greater the discrepancy between ω_o and ω_d. Thus, one way to explain the absence of a displacement resonance in this system is Q is sufficiently small to separate ω_o and ω_d.

Consideration of the damping may also explain why resonant responses may not have been observed previously. The width of the resonance response is determined by the ratio ω_o / Q and in this study Q appears to be relatively small so the resonance is reasonably wide. However, if the system passes through a resonance but the damping is only small, i.e. Q is large, the resonant peak will be very sharp and narrow, possibly within the sensitivity limits of the experiment. For the graft copolymers it appears that quite fortuitously a particular combination of parameters have been obtained such that a velocity resonant response can not only be observed, but is also separated from the displacement resonance.

At this stage it is perhaps useful to set out the description of the surface waves in order to clarify the main points. All the polymers were observed to exhibit a maximum in ω_o at a discrete surface concentration, Γ_s^*. By comparing behaviour to that of a classical coupled oscillator it has been established that the coupling between the capillary and dilational waves reaches a maximum at this point. The observed variation in the mode frequency, figure 4.5.11, is consistent with this model. Due to the maximum in the coupling the dilational wave frequency falls to a minimum at Γ_s^*. The dilational parameters exhibit behaviour consistent with that of a forced oscillator. This indicates that an additional force, not previously anticipated, is influencing surface wave propagation. The dilational parameters, ε_o and ε', have been shown to represent the velocity response of the dilational waves. The absence of a displacement resonance has been interpreted as indicative of relatively high damping in the

system which causes the frequencies of the resonances to differ. To summarise then, the capillary and dilational waves are strongly coupled at Γ_s^* and do not exhibit the 'classical resonance' at this point. The dilational waves exhibit behaviour typical of a driven oscillator. At Γ_s^* resonance exists between the dilational waves and this extra driving force, hence the discontinuous nature of ε_o and ε' at this point.

The frequency of the dilational waves when resonant behaviour is exhibited is quite low at circa 2500 s^{-1}, a number of possible origins for the driving force acting on this wave will be presented as the discussion broadens. The first thought is of any possible molecular motion with a relaxation time in the order of 400 μs. Such a time scale is actually rather slow for molecular motion and is almost certainly too slow to be associated with molecular motion at the level of a single chain. The Rouse equation, equation 4.5.11, can be used to get an estimate of the longest relaxation time for a single chain. The parameters for an entire chain of 10CP where N = 1584 and a ~ 10 Å are used giving a relaxation time of 5 μs. Clearly, this is too fast to be the origin of the driving force and attention is therefore focused on any possible co-operative motion of the film which will occur over longer times. This is specifically referred to in the section regarding film viscoelasticity.

It is informative to compare the fact that ε_o and ε' represent the transfer function of the dilational waves to more familiar bulk, rather than surface, properties. If a system is placed under some kind of strain, the input, the output will be a stress. It transpires that in such a system the transfer function is given by the elastic modulus of the system. Clearly this is analogous to the behaviour observed here, suggesting that the input force acting on the dilational waves is straining the system. Strain is defined as the extension of unit length and it is not immediately obvious as to which parameters of the system which could be extended. Clearly, the passage of a capillary wave causes the surface, and possibly the polymer chains, to stretch and extend. One particular component of the copolymers which may be considered in this way is the PEO side chains. To continue this analogy the output exhibited by the system should be a stress, a force per unit area. Basically then, by causing some component of a system to extend the output, or stress, should be proportional to the input, the proportionality constant being the elastic modulus. Thus it is perhaps not surprising to see the ε_o and ε' representing the transfer function of the system. The feature which is not obvious is why the strain and stress should be related via. a 'rate of change' transfer function. A time dependent strain, sinusoidal, would be anticipated to result in a time dependent stress but this does not rationalise the observed velocity response. In addition it is hard to envisage any origin for this

strain other than the capillary waves which appear to be of the wrong frequency range. Unfortunately the analogy with 'bulk' behaviour does not appear to be particularly satisfying in this instance. As a consequence it is simply concluded that for the dilational terms to represent a transfer function of the system seems consistent with the behaviour exhibited in the bulk, although rationalising the details is not straightforward.

One of the most remarkable observations is that of negative dilational viscosities and although the treatment above reproduces the variation of ε' with surface concentration there is no attempt to predict, or explain, the absolute values. From intuitive perceptions of bulk viscosities one would always predict that a viscosity either had to be zero or positive. A positive dilational viscosity implies that there is energy dissipation associated with the dilational waves, i.e. they are being damped. Logically it follows that a negative viscosity indicates that the waves are being propagated, i.e. destabilised. It has already been mentioned that dilational waves have their origin in the concentration fluctuations which occur in the plane of the surface when amphiphilic molecules are either spread or adsorbed there. It follows that any processes which affect either the motion, or the number of molecules at the surface, will directly influence the dilational wave motion, and in certain cases to a lesser extent the capillary waves. Such processes include the Marangoni effect[31] which is associated with local variations in surface tension which give rise to movement in a fluid interface. The variations in surface tension are caused by differences in composition or temperature, i.e. chemical potential or thermal gradients. Thus the Marangoni effect represents the conversion of chemical or thermal energy to mechanical energy. The relevance of this effect to the specific case of surface films is that if a chemical potential or thermal gradient is set up either across or in the plane of the interfacial region, mechanical energy will be generated and will cause spatial fluctuations of surfactant concentration at the surface. Fluctuations in the plane of the surface will be in addition to the motion associated with dilational waves and will contribute to any other motion and may act to drive the dilational waves. Clearly if the rate of supply of energy from such effects exceeds the energy dissipated by these waves then they will propagate. Studies have indicated that the threshold for destabilisation of the dilational waves is actually rather high and it is unlikely that the effects outlined above will markedly alter their propagation.[32]

The discussion of Marangoni type effects causing destabilisation of the dilational waves is most suited to the case of surfactant solutions.[33,34] In this scenario the surface layer is in a constant dynamic state as molecules adsorb from and desorb into the bulk. In this

situation it has been shown that destabilisation of the dilational waves can be enhanced by any processes that slow down adsorption. A concept called the Marangoni number has been introduced and provides a way of quantifying the Marangoni effect. Its value is influenced by the dependence of the surface tension on the surface excess concentration, the viscosities of the fluids at the interface and the solute diffusivity. It transpires that it is only when the Marangoni number reaches a critical value that the waves will be significantly destabilised.[35] This critical value depends predominantly on competition between bulk diffusion and convective effects along the interface. If a potential barrier exists just below the interfacial layer transfer of matter will be slowed down somewhat, becoming a two step process. Firstly, a solute molecule must adsorb from the bulk through diffusion to a sublayer from where it must overcome the potential barrier to adsorb at the surface. The origin of such a barrier is not clear although it has been suggested[35] that the energy required to overcome the surface pressure at an interface may represent a potential barrier. In the case of electrolytes a molecule approaching the surface layer will be subject to electrostatic repulsion which may constitute a potential barrier. Whatever its exact origin the presence of an adsorption barrier leads to a reduction in the rate of adsorption and causes the critical Marangoni number to fall and the dilational waves may be destabilised. Thus certainly in the case of surfactant solutions observations of $\varepsilon' < 0$ can be rationalised, albeit rather qualitatively, by chemical potential gradients being established across the interface as molecules adsorb and desorb.[35] An adsorption barrier may arise if the local surface concentration variations are out of phase with the adsorption process. To understand this fully consider the perturbations caused by the passage of a capillary wave. Due to these effects the local surface concentration at a given point will vary. If this reaches a maximum just as a molecule attempts to adsorb at the surface a barrier to this adsorption will be encountered. These barriers may slow the adsorption process down, reducing the Marangoni number required for destabilisation of the dilational waves.

The discussion above, although perfectly plausible for adsorbed films, does not translate well to the current study where the films are insoluble. The nearest parallel between the graft copolymers and the behaviour of adsorbed films is intramolecular motion which encounters a barrier. The compressive and stretching motion of the PEO side chains has been considered previously and was predicted to have a frequency of 10^7 - 10^8 s^{-1}. This value may be a little high given that the model assumes free linear chains whereas the molecules are effectively tethered to the backbone of the polymer. In fact rather than considering the motion

of the side chains as individual units it would perhaps be more accurate to consider the influence of the backbone on this motion and whether tethering the side chains to a 'wall' will slow down their movement. As the side chains move they will exert a force on the backbone and depending on the inertia of the backbone this may result in movement of the backbone. Given that the backbone is predominantly hydrocarbon, and therefore hydrophobic, any motion causing the backbone to increase its contact with the subphase will be unfavourable, possibly representing a pseudo potential barrier. The polymer backbone is therefore predicted to slow down the motion of the side chains, although to what extent and by what order the associated frequency is affected is not quantifiable. Other processes may contribute to a 'potential barrier' such as repulsion between the side chains as they are compressed and approach the backbone. This behaviour would be in accord with the predicted behaviour of polymer chains in good solvents.

The form of the dependence of both ε_o and ε' on Γ_s has been reproduced by considering the response of the dilational mode to a driving force. This driving force may also contribute to $\varepsilon' < 0$, a suggestion that is certainly consistent with the observed variation of ε' with Γ_s. The values of ε' at surface concentrations sufficiently far removed from Γ_s^* either above or below, show a tendency to stabilise at almost the same value indicating that the dilational waves are equally destabilised. The most marked variation in ε' is in the vicinity of Γ_s^* where, due to the resonance, there will be the greatest exchange of energy between the dilational waves and the driving force and consequently the waves are even more destabilised.

From the discussion above it follows that negative values of ε' provide a computational method of incorporating the effect of currently unknown processes which somehow influence the propagation of the dilational surface modes. These processes may be due to molecular motion or behaviour associated with co-operative motion of the film that manifests itself in the form of a sinusoidal force acting. Under such circumstances ε' is an effective parameter and, presumably if the additional processes could be identified and quantified then the stability reducing role would not necessarily be played by $\varepsilon' < 0$. In essence the problem appears to be caused by the use of an inappropriate functional form, i.e. the dispersion equation, being fitted to the data. Thus in order to quantify the behaviour of the current and similar systems it appears that modification of dispersion equation is required.

Although the variation in ε_o with Γ_s has been reproduced this does not rationalise the fact that the values are rather low compared to those determined from static measurements. In

fact the dilational modulus determined by light scattering is an order of magnitude lower than the static measurement whereas in other studies of polymers the static and dynamic values compared well.[5] Although there is only limited data currently available it appears that for polymeric systems when $\varepsilon' < 0$ the dilational modulus is always found to be unexpectedly low. This statement is supported by the present study and also by preliminary results for PEO - PMMA diblock copolymers.[36] It was suggested previously that ε' is an effective parameter due to the presence of an additional process which influences the evolution of the dilational waves, supposedly reducing the damping. Such effects are unlikely to influence only ε' and it is suggested that ε_o is also effective, and that the large discrepancies between dynamic and static measurements arise because ε_o does not represent a simple parameter associated with a single process. Presumably the values for both ε' and ε_o which have been extracted contain information about the true dilational properties of the system but, in addition, are affected by the process which appears to modify dilational wave propagation.

Significant differences between the static surface tension, $\gamma_{oST,}$ and γ_o were observed. At low surface concentrations γ_o is very high, exceeding the value for pure water, 72.3 mN m^{-1} at 296K. At first glance this may not seem physically realistic. However, γ_o has a frequency dependence whereas the value for water is the static value. Discrepancies between the static and dynamic values may be due to relaxation processes occurring in the film, this point is discussed in more detail in section 4.5.6.

The more alarming difference between the dynamic and static surface tensions is the plateau in γ_o while γ_{oST} is still decreasing. The plateau in γ_o is reminiscent of the behaviour of PEO[27] where above a critical surface concentration both the dynamic and static surface tension moduli have the same constant value of 65 mN m^{-1}. The similarity to the data presented here is quite striking; the magnitude of γ_o at the plateau is also 65 mN m^{-1}. This may indicate that for some reason at these surface concentrations only the PEO parts of the copolymer are influencing the capillary wave evolution. The surface concentration of homopolymer PEO when γ_o reaches a constant value is ~0.5 mg m^{-2} and is associated with the point at which no more polymer can be accommodated on the surface. From neutron reflectometry studies it is known that this surface concentration coincides with the onset of significant subphase penetration. In comparison the surface concentration of PEO in the graft copolymers is in the range 0.18 - 0.42 mg m^{-2}, but of course the PMMA in the copolymer also occupies the surface. Forcing the PEO into the subphase would increase the favourable PEO -

water interactions, leaving more space for the PMMA backbone on the surface. This is consistent with the comparison made earlier between Γ_s^* and Γ_{sLIM} implying that subphase penetration does occur at Γ_s^* and is mainly influenced by the surface area available to the different components.

The absolute values of γ' that have been determined are high compared to studies of low molecular weight surfactants, for example for cetyltrimethylammonium bromide,[33] CTAB, γ' is circa. 10^{-5} mN m s^{-1}. However, the values extracted for other polymers do vary considerably and range as high as the values found here. For example for spread layers of PMMA[27] γ' is around 5×10^{-5} mN s m^{-1} at q = 220 cm^{-1}, those for PEO[27] falling in the range 1 - 4×10^{-4} mN s m^{-1}. The values obtained for the graft copolymers are clearly of the order of those observed for PEO, certainly for $\Gamma_s > \Gamma_s^*$. This observation lends more weight to the suggestion that different parts of the copolymers dominate behaviour in the two surface concentration regimes, i.e. above or below Γ_s^*.

It was noted that for water $\gamma' = 0$ and that there is a relatively large increase in γ' on spreading the film but little correspondence in the capillary wave damping. This can be accounted for by using simulations to investigate the influence of the viscosities on the capillary wave propagation, specifically the damping. Values typical of those found for the graft copolymers were used for ε_o, γ' and ε'. Initially the capillary wave damping was determined at q = 220 cm^{-1} with only the surface tension set at a non zero value, γ_o = 72 mN m^{-1}. The dilational modulus was introduced and following this γ', then finally ε'. The variation in the capillary wave damping is given in Table 4.5.4 along with the parameters corresponding to each situation.

The data in Table 4.5.4 indicates that, if on spreading the film the only change was ε_o and γ' becoming non zero and positive, one would expect Γ to rise markedly. However, in addition to these effects a large negative dilational viscosity is introduced and acts to offset the increase in Γ bringing the value down from 2485 s^{-1} when $\varepsilon' = 0$ to 1967 s^{-1}. Thus by considering both γ' and ε' the unexpectedly low values of Γ observed for $\Gamma_s < \Gamma_s^*$ can be rationalised. This is perhaps counter-intuitive as generally it suffices to consider γ' which has the most direct influence on the capillary wave damping. Given that the values of γ' extracted using the spectral fit are correct then the behaviour of the wave damping, which is of course directly observable, provides additional confirmation that ε' must be negative. It was also observed that at $\Gamma_s = \Gamma_s^*$ although the increment in γ' is less than on spreading the film the

capillary wave damping exhibits a marked increase. This is entirely logical since ε' also increases in magnitude, but remains negative, at this concentration and therefore will offset the increase in Γ, caused by the increment in γ', by a lesser amount. For further increases in the surface concentration above Γ_s* the variation of Γ reflects the balance of ε' and γ' which changes for each system.

γ_0 / mN m^{-1}	γ' / mN s m^{-1}	ε_0 / mN m^{-1}	ε' / mN s m^{-1}	Γ / s^{-1}
72	0	0	0	823
72	0	1	0	885
72	3×10^{-4}	1	0	2485
72	3×10^{-4}	1	-1×10^{-4}	1967
72	3×10^{-4}	1	1×10^{-4}	3775
72	3×10^{-4}	1	-2×10^{-4}	1128

Table 4.5.4: The variation in the capillary wave damping at q = 220 cm^{-1} with surface viscoelastic parameters.

4.5.5 Frequency Dependence

The capillary wave propagation and the surface parameters for films of 60CP and 10CP at fixed concentrations have been determined over a range of q values. For 60CP films have been studied at fixed surface concentrations of 0.20 mg m^{-2}, 0.50 mg m^{-2}, 0.70 mg m^{-2} and 1.25 mg m^{-2}. These concentrations were chosen as they fall shortly before, after and at the maximum in ω_0. For similar reasons films of 10CP at 0.15 mg m^{-2}, 0.30 mg m^{-2} and 1.00 mg m^{-2} were studied.

The results are presented below, first the characteristics of the capillary wave propagation are presented then the surface parameters determined using spectral fitting. The surface viscoelastic parameters are discussed in terms of their variation with the capillary wave frequency. In general representative data sets are presented for both 60CP and 10CP to illustrate the behaviour exhibited by these systems.

4.5.5.1 Results: Capillary Wave Propagation; frequency and damping

The dependence of the light scattering dispersion data (ω_0 and Γ) on q is presented in figures 4.5.18 and 4.5.19. The lines represent the theoretical predictions found by solving the dispersion equation taking η and ρ equal to those for water at 296 K and using the average value of γ_0 extracted for each film across the frequency range. All the other surface viscoelastic parameters, namely γ', ε_0 and ε', were taken as zero so that any differences between the experimental data and theoretical lines reflect the effects of the surface viscosities and ε_0 on the evolution of the capillary waves. This comparison has been applied to all the experimental data, the results are discussed below.

The capillary wave frequency and damping behave broadly as expected for capillary waves, $\omega_0 \propto q^{3/2}$ and $\Gamma \propto q^2$. This is particularly true of the capillary wave frequency, ω_0, which for most of the films coincides with the theoretical line, the exception being the 0.30 mg m^{-2} film of 10CP for which the data is slightly lower than that predicted. In contrast experimental values for the capillary wave damping show significant deviations from predictions. Such behaviour is anticipated because the surface viscosities, which contribute

significantly to the damping, have been neglected. Generally the experimental values of Γ are higher than predicted due to the influence of the viscosities although for the most dilute film of 60CP, Γ_s = 0.20 mg m^{-2}, Γ is found to be consistent with theory indicating that the viscosities are small or cancel each other out, see figure 4.5.18.

The dispersion data for 10CP at 0.30 mg m^{-2} exhibits some unusual features, see figure 4.5.20. The frequency is slightly lower than the theoretical prediction but otherwise unremarkable whereas the damping exhibits very unusual behaviour as q increases. The damping is higher than predicted at low q and, as previously, this is attributed to the neglect of γ' and ε'. However, at higher q values Γ falls below the theoretical line exhibiting a unique and reproducible discontinuity indicating that there is something unusual in the behaviour of 10CP at this surface concentration.

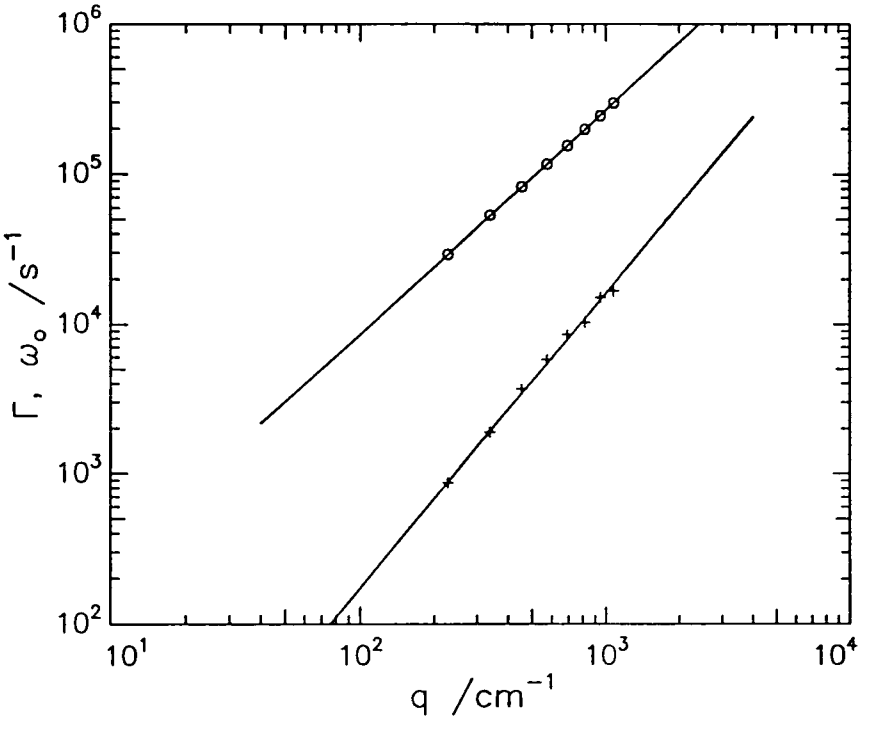

Figure 4.5.18 Capillary wave damping, crosses, and frequencies, open circles, for 60CP at Γ_s =0.20 mg m^{-2}. The lines are theoretical predictions for a fluid of tension 73 mN m^{-1}, other properties being as for water at 296K.

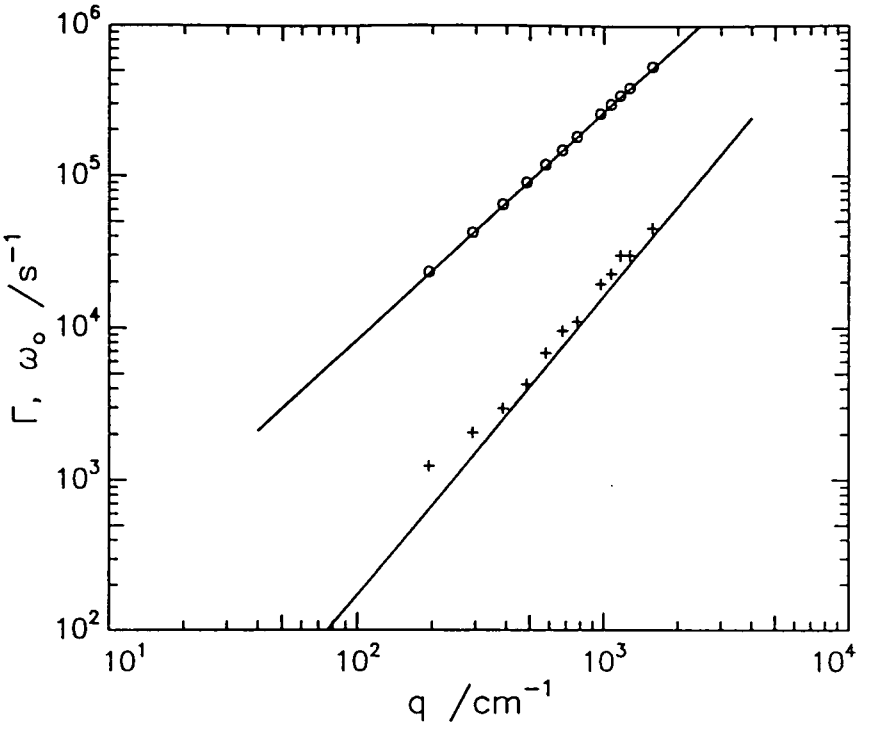

Figure 4.5.19 Capillary wave damping, crosses, and frequencies, open circles, for 10CP at Γ_s =0.15 mg m^{-2}. The lines are theoretical predictions for a fluid of tension 70 mN m^{-1}, other properties being as for water at 296K.

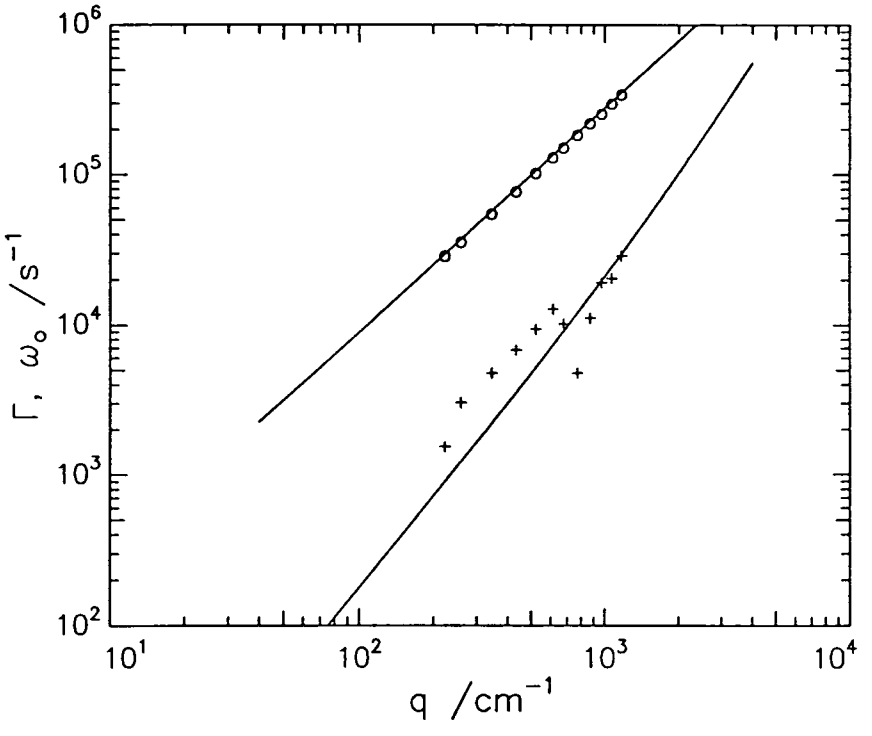

Figure 4.5.20 Capillary wave damping, crosses, and frequencies, open circles, for 10CP at Γ_s =0.30 mg m^{-2}. The lines are theoretical predictions for a fluid of tension 80 mN m^{-1}, other properties being as for water at 296K.

4.5.5.2 Results of direct spectral fit

The results of applying the direct spectral fit to the experimental data are presented here. The characteristics exhibited by each of the four surface viscoelastic parameters are reported separately.

4.5.5.2A Surface Tension

The surface tension data for the different concentration films are presented in figures 4.5.21 and 4.5.22. The data for the films of 60CP are considered first and clearly do not exhibit a marked frequency dependence. There is no frequency dependence of γ_o for the most dilute film, 0.20 mg m^{-2}, and the data are rather scattered, see figure 4.5.21. However, at higher concentrations γ_o appears to exhibit a tendency to decrease to a minimum value then subsequently increase. The position of the minimum in γ_o shifts to higher frequencies with increasing Γ_s, for Γ_s = 0.70 mg m^{-2} the minimum occurs at $\omega_o = 0.65 \times 10^5$ s^{-1}, shifting to 1.1 $\times 10^5$ s^{-1} for a 1.25 mg m^{-2} film.

The films of 10CP exhibit a much more marked frequency dependence than those of 60CP. The behaviour is actually very similar to that of 60CP but rather more pronounced, γ_o decreasing quite markedly to a minimum as ω_o increases, see figure 4.5.22. The position of the minimum in γ_o cannot be determined for Γ_s = 0.15 mg m^{-2}, see figure 4.5.22, but for Γ_s = 0.30 mg m^{-2} occurs at approximately 2.2×10^5 s^{-1} and shifts to a higher frequency, $\omega_o \approx 2.4 \times 10^5$ s^{-1}, for the most concentrated film, Γ_s = 1.00 mg m^{-2}.

4.5.5.2B Transverse Shear Viscosity

The values of γ' for 60CP are found to be rather scattered at all the concentrations studied, for example see figure 4.5.23. It is anticipated that γ' will decrease with ω_o otherwise the dissipative term, $\omega\gamma'$, will become prohibitively large at high frequencies. The data for 10CP does exhibit a downward trend with increasing ω_o. Given the scatter of γ' for each film of 60CP it is not possible to establish whether there is any significant downward trend over this frequency range.

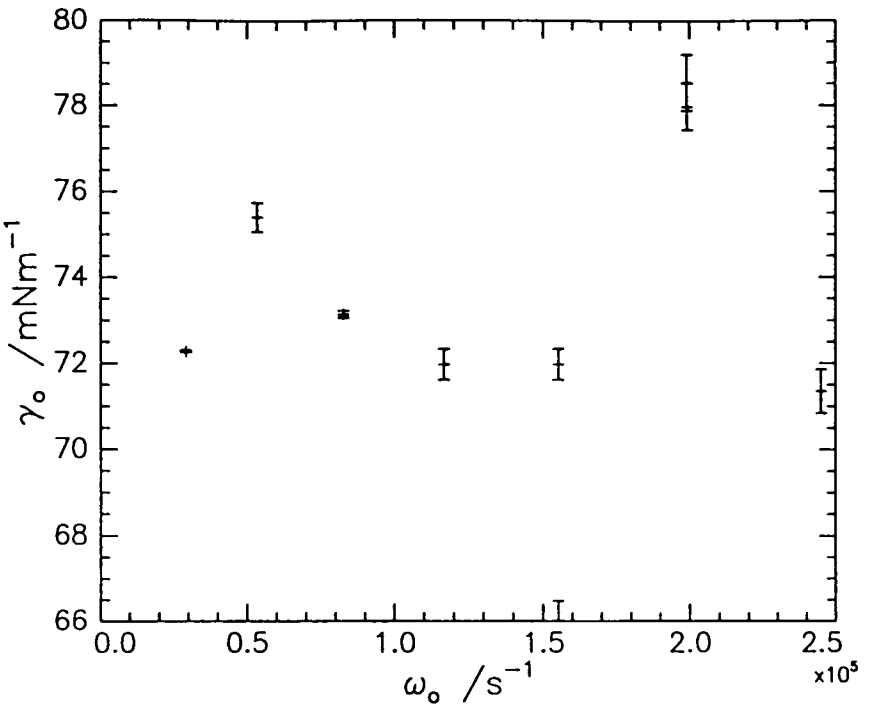

Figure 4.5.21 Variation in γ_o with ω_o for 0.20 mg m^{-2} film of 60CP.

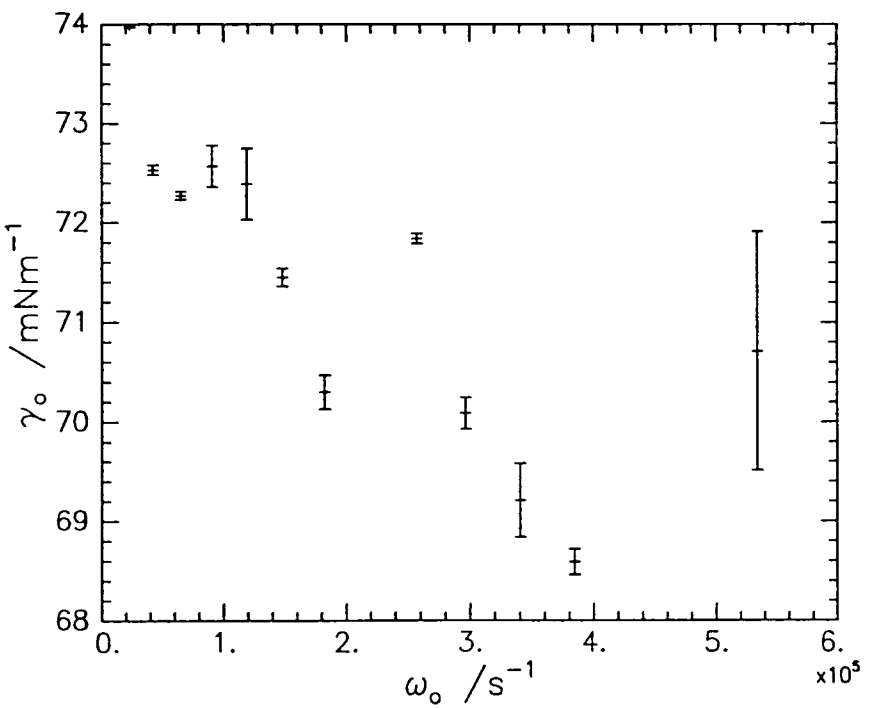

Figure 4.5.22 Variation in γ_o with ω_o for 0.15 mg m^{-2} film of 10CP.

A particular feature of the data which is worth noting is that for the 1.25 mg m^{-2} film γ' becomes negative. This behaviour was found to be reproducible and does not appear to be an artefact of the fitting process, especially given the fact that the raw data was repeatedly refitted using a variety of different starting parameters, none of which involved negative γ'. Despite this the analysis systematically returned negative values for γ' and gave good fits. It was not possible to get a fit of comparable quality to the data by constraining γ' to be positive.

Further negative values of γ' are observed in the data for films of 10CP and in contrast to 60CP the data for each film studied displays a marked decrease in γ' to a minimum value as ω_o increases, see figure 4.5.24. For the lowest film concentration studied, Γ_s = 0.15 mg m^{-2}, γ' decreases in a linear manner with increasing ω_o, at the highest frequencies becoming negative. For the 0.30 mg m^{-2} film the data are slightly more scattered but exhibit a similar variation in γ' and negative values are again found at high ω_o.

The behaviour of γ' for the 1.00 mg m^{-2} film is rather like that for the highest concentration 60CP film, both show a similar dependence of γ' on ω_o and in addition the values of γ' fall in the same range. However, the data are much less scattered for the 10CP film and the minimum in γ' occurs at higher frequencies, 1.40 × 10^5 s^{-1} rather than 1.05 × 10^5 s^{-1} in the case of the 1.25 mg m^{-2} film of 60CP.

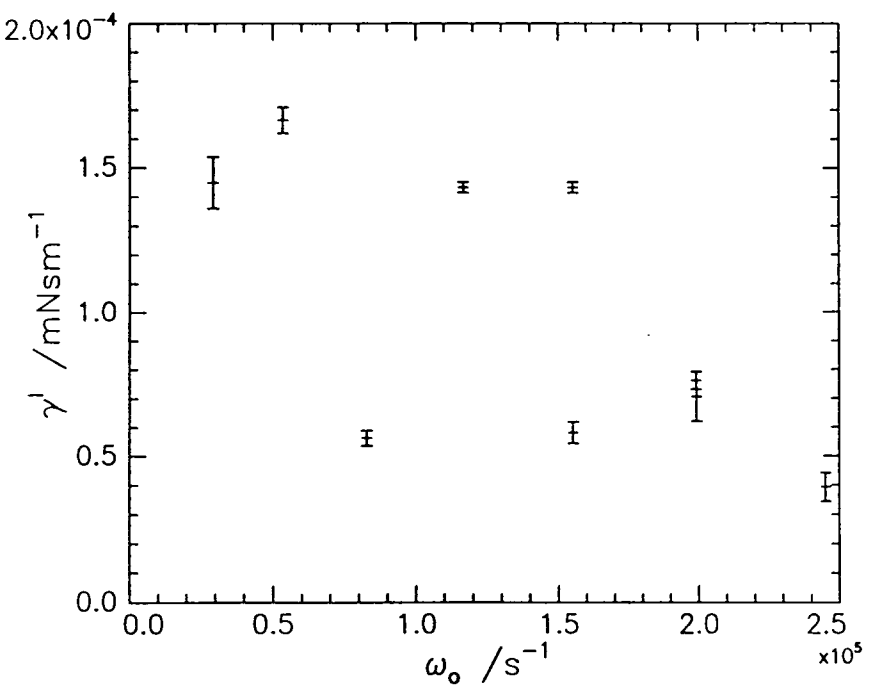

Figure 4.5.23 Variation in γ' with ω_o for 0.20 mg m^{-2} film of 60CP.

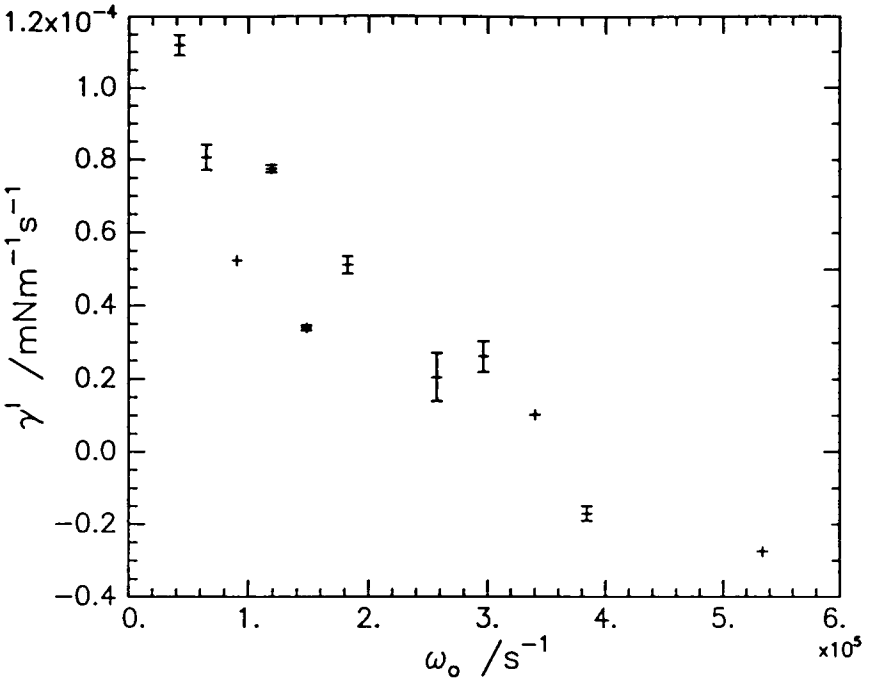

Figure 4.5.24 Variation in γ' with ω_0 for 0.15 mg m^{-2} film of 10CP.

4.5.5.2C Dilational Modulus

The frequency dependent behaviour of ε_0 is no less difficult to elucidate than its variation with surface concentration. Comparing the values obtained for 60CP and 10CP over all the film concentrations studied a number of points emerge, see figures 4.5.25 to 4.5.26. The values of ε_0 are very low, on the whole not exceeding 5 mN m^{-1}, and seem to exhibit a general trend of increasing with ω_0. This statement is certainly true for 10CP at 1.00 mg m^{-2}, 60CP at 0.70 mg m^{-2} and for the lower frequency region of the most dilute films. In comparison the data for 60CP at 1.25 mg m^{-2} is scattered and does not exhibit any systematic variation with ω_0.

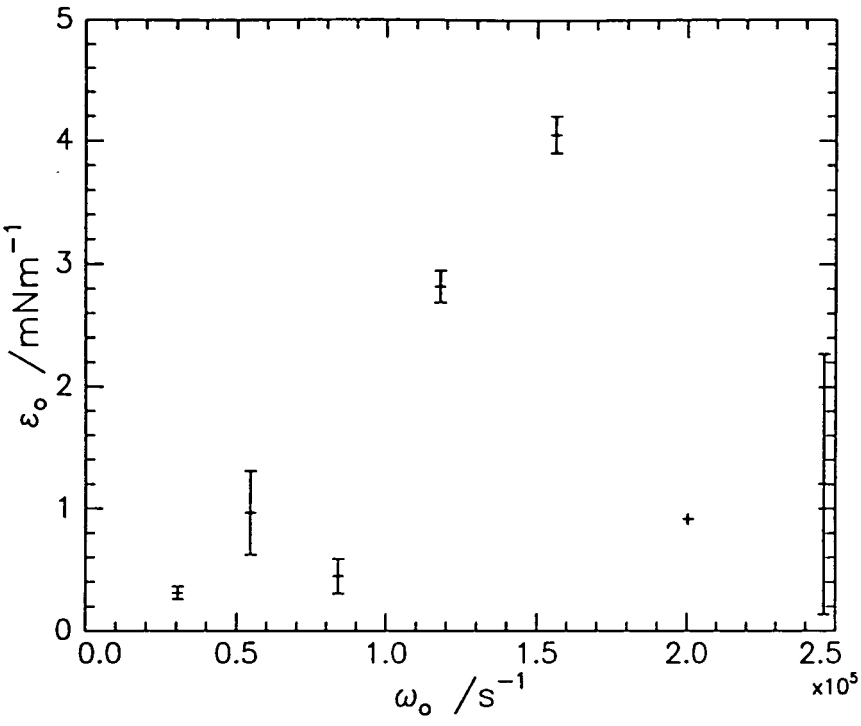

Figure 4.5.25 Variation in ε_o with ω_o for 0.20 mg m^{-2} film of 60CP.

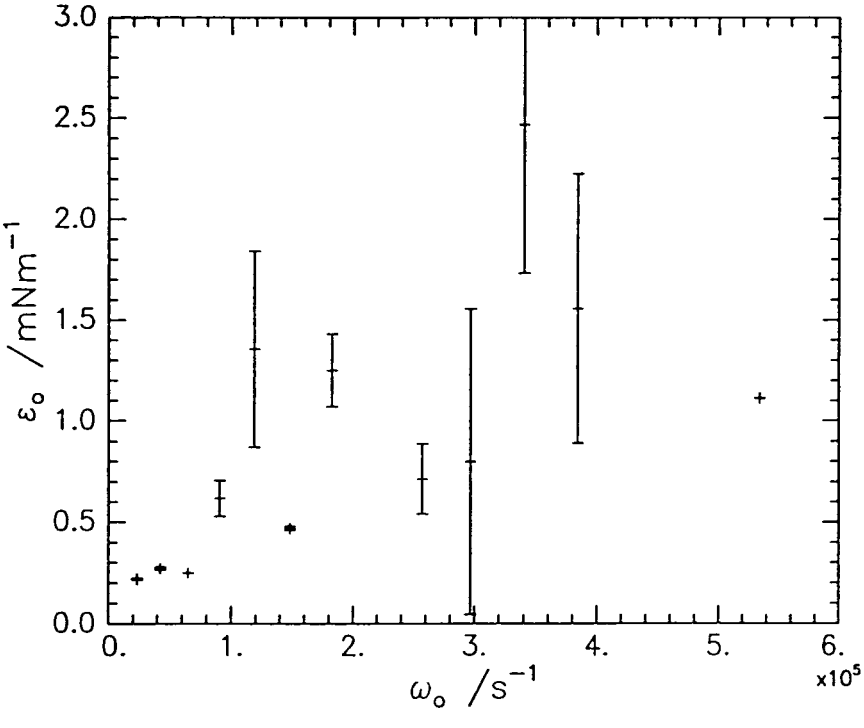

Figure 4.5.26 Variation in ε_o with ω_o for 0.15 mg m^{-2} film of 10CP.

4.5.5.2D Dilational Viscosity

The dilational viscosity, ε', displays a remarkable frequency dependent behaviour, especially in the light of the rather poor determination of the other dilational parameter, ε_o. The data for both 60CP and 10CP are presented in figures 4.5.27 and 4.5.28, clearly the variation of ε' with ω_o is the same for both systems. The dilational viscosities remain negative over the entire frequency range studied, increasing steadily from round -1.7×10^{-4} mN s m^{-1} at the lowest frequency to -0.2×10^{-4} mN s m^{-1} as the frequency increases. Subsequently the values show little change maintaining this value, despite further increases in frequency displaying no tendency to become positive.

The magnitude of ε' at a given ω_o is, within error, the same for all the films of both copolymers the exceptions being the 0.30 mg m^{-2} film of 10CP and the 0.50 mg m^{-2} film of 60CP. This is illustrated in figures 4.5.29 and 4.5.30 where the data for each copolymer film are plotted on the same graph. From these rather busy plots one can see that there is no discernible difference in the values obtained except, as mentioned, those recorded at Γ^*_s for each graft copolymer, which intriguingly follow the same variation with ω_o as all the films but are consistently more negative over the entire frequency range studied.

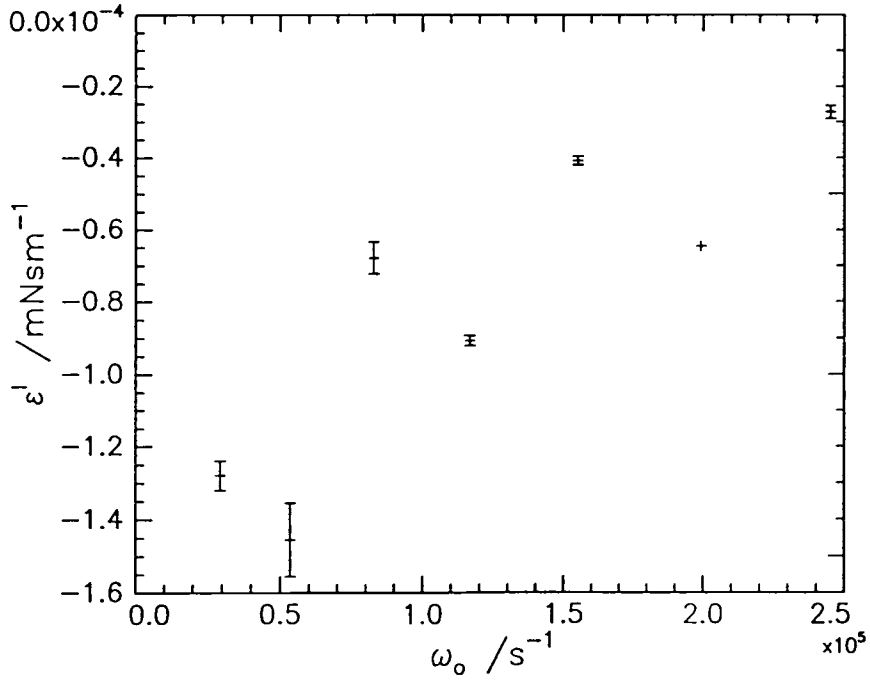

Figure 4.5.27 Variation in ε' with ω_o for 0.20 mg m^{-2} film of 60CP.

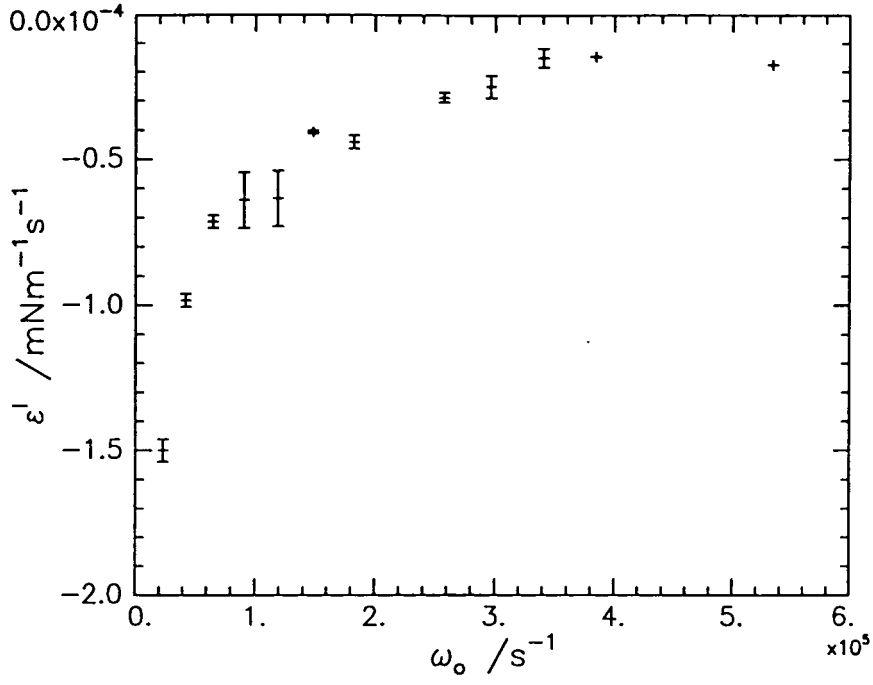

Figure 4.5.28 Variation in ε′ with ω_0 for 0.15 mg m^{-2} film of 10CP.

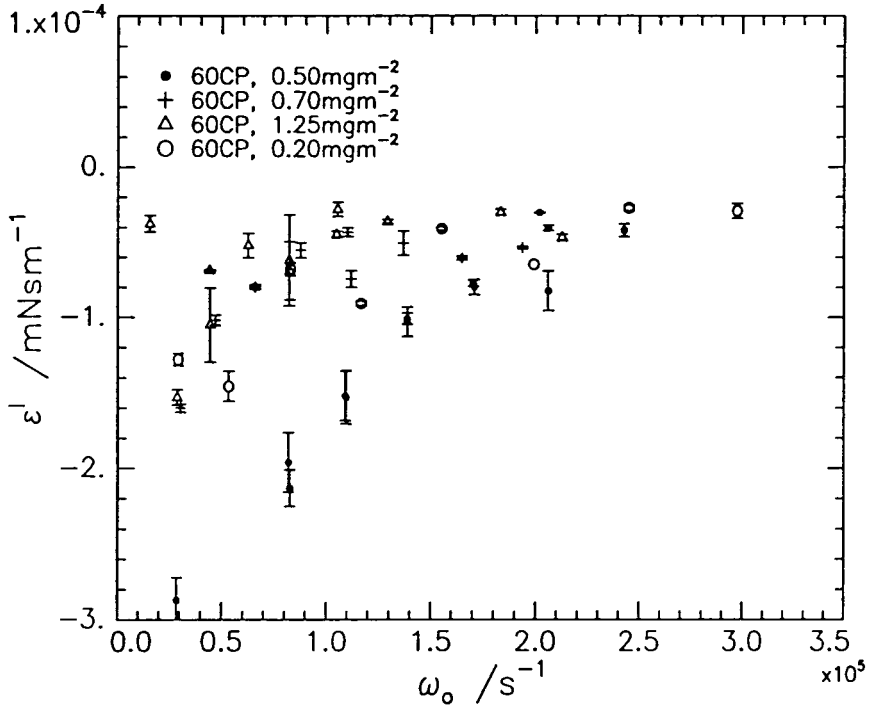

Figure 4.5.29 Variation in ε′ with ω_0 for all the films concentrations of 60CP.

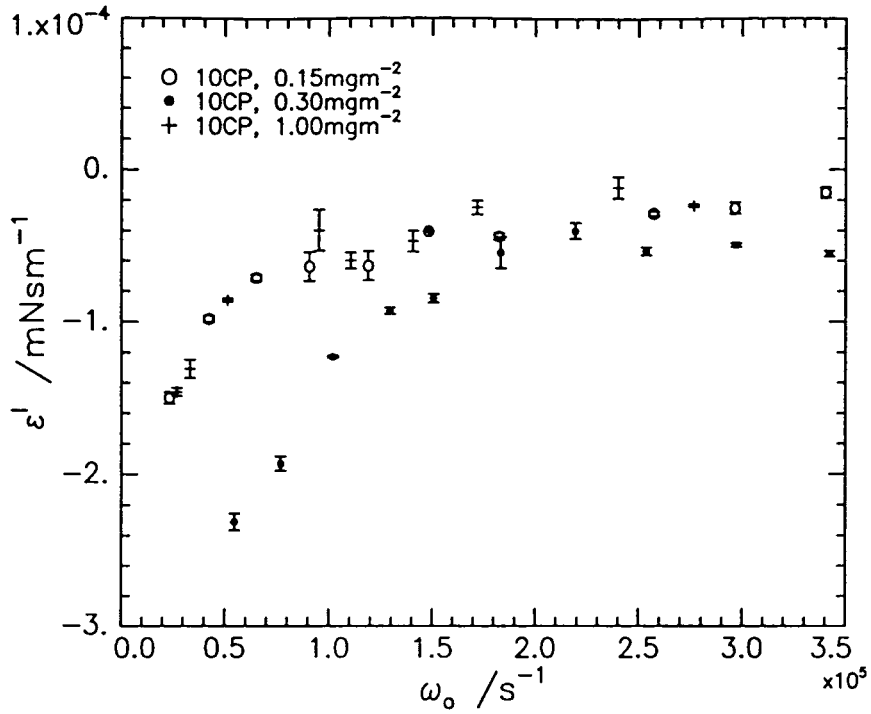

Figure 4.5.30 Variation in ε′ with ω_o for all the films concentrations of 10CP.

4.5.6 Viscoelastic Relaxation

Conventional viscoelastic treatments[37] for relaxation processes can be, and have been, applied to the behaviour of films at interfaces.[38,27] As will be discussed such treatments have been used to interpret the frequency dependent behaviour of the surface viscoelastic parameters of both PMMA and PEO.[27] Given the success with which the models have been applied to the component homopolymers of this graft copolymer a similar analyses of the behaviour of the copolymer has been attempted. It was evident from the preceding discussion, Section 4.5.4, that the behaviour exhibited by the graft copolymer films is rather unusual and differs quite markedly from that of the homopolymers. Despite this observation this analysis has been pursued but, as will be discussed, many of the results should be treated with extreme caution and on further development it appears that behaviour is more complex than can be accounted for by these simple models.

Assuming that spread monolayers exhibit a linear viscoelastic response an oscillatory stress $T(t) = T^* \exp(i\omega t)$ and strain, $u = u^* \exp(i\omega t)$, can be related via a complex dynamic modulus, $G^*(\omega)$:

$$T^* = [G'(\omega) + iG''(\omega)]u^*$$

Equation 4.5.25

where $G'(\omega)$ is the storage modulus and is associated with the storage and release of energy in the periodic deformation; in the present situation this corresponds to the elastic moduli, γ_o or ε_o. The term $G''(\omega)$ is the loss modulus and represents processes by which energy is dissipated; in the case of a spread monolayer $G''(\omega)$ is equivalent to $\omega\varepsilon'$ or $\omega\gamma'$.

Viscoelastic behaviour can be imitated using mechanical models with a sufficient number of elastic and viscous elements. The elastic contribution is represented by a spring, the viscous element by a dashpot, which is simply a piston moving in oil. Each spring element is assigned a stiffness analogous to a shear modulus and each dashpot is associated with a frictional resistance, analogous to a viscosity contribution. Such terminology allows the distinctions between two commonly used models, the Voigt solid and Maxwell Fluid, to be highlighted; no other models will be considered here.

The behaviour associated with a Maxwell fluid is represented by the so called Maxwell element which is a spring and dashpot in series, see figure 4.5.32. When a number

of such elements are placed in series a generalised Maxwell fluid is modelled. Each element relaxes exponentially in response to an applied stress, and consequently a discrete spectrum of relaxation times will exist.

In the case of a single Maxwell element the storage and loss modulus are given by:

$$G'(\omega) = G_e + \frac{G\omega^2\tau^2}{1+\omega^2\tau^2}$$

Equation 4.5.26

$$G''(\omega) = \frac{G\omega\tau}{1+\omega^2\tau^2}$$

Equation 4.5.27

Where G_e is the equilibrium (static) elastic modulus and G is the strength of the relaxation process with a relaxation time τ. The equilibrium modulus, G_e, is added to the Maxwell model to incorporate 'solid like' behaviour in the material which, in the case of a spread film, corresponds to the static surface tension.

In the Voigt solid model the basic element is a dashpot and spring in parallel such that the extension of the spring is exactly counterbalanced by the dashpot, see figure 4.5.33.

In the Voigt solid the storage modulus is given by:

$$G'(\omega) = G$$

Equation 4.5.28

and the loss modulus by,

$$G''(\omega) = G\omega\tau$$

Equation 4.5.29

Using this model it is noted that no frequency dependence is predicted for either γ_0 or γ'.

The viscoelastic models mentioned above may be applied to data obtained from both types of SQELS experiment, i.e. where either Γ_s or ω_0 is varied. The frequency dependence of the surface parameters can, in principle, be fitted allowing G_e, G and τ to be determined. Alternatively the variation in the surface parameters with Γ_s at $q = 220\ cm^{-1}$ enables values for G and τ to be extracted. For simplicity it is assumed that there is only one relaxation characterised by a single relaxation time. Both of the approaches describe the same viscoelastic phenomenon and therefore should return consistent parameters.

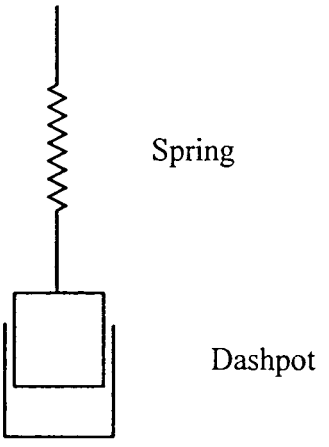

Figure 4.5.32 Maxwell element consisting of a spring and dashpot in series

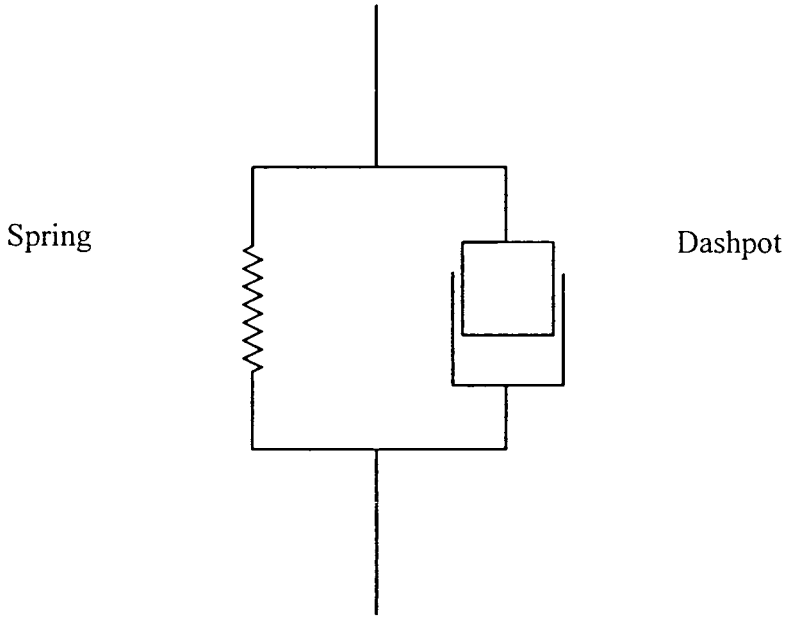

Figure 4.5.33 Voigt element consisting of a spring and dashpot in parallel

Data collected at q = 220 cm^{-1} has been analysed and examined using both the Voigt solid and the Maxwell fluid model. Consider initially the determination of τ assuming a Voigt solid, from equation 4.5.29 τ is given by:

$$\tau = \frac{G''(\omega)}{G\omega}$$

Equation 4.5.30

It is known that a system will relax following a perturbation which causes oscillatory stress and strain in the layer. Presumably this may be imparted by perturbations caused by both the capillary and dilational modes.* If the effect of the capillary mode is considered $G''(\omega)$ will be equivalent to $\omega_o \gamma'$ and $G'(\omega)$ to γ_o. Thus it follows that;

$$\tau = \frac{\gamma'}{\gamma_o}$$

Equation 4.5.31

In an analogous manner for any relaxation arising due to the perturbation caused by the dilational mode τ is given by:

$$\tau = \frac{\varepsilon'}{\varepsilon_o}$$

Equation 4.5.32

Clearly since $\varepsilon' < 0$ but $\varepsilon_o > 0$ the values of τ extracted using equation 4.5.31 are physically unrealistic. Thus only the values of τ associated with relaxation following a capillary wave are reported, see figure 4.5.33. Similar relaxation times are found for all the systems and fall in the range 5 - 10 μs. The relaxation times for all the graft copolymers are observed to increase to a maximum value of circa. 7 μs over the surface concentration range 0.4 - 0.6 mg m^{-2}. Subsequently the values fall to ~5 μs.

* It is clear that the values of ε_o and ε' have only been determined at the capillary wave frequencies. Using the same values combined with computed dilational wave frequencies will not necessarily be valid and this discussion should be treated with caution.

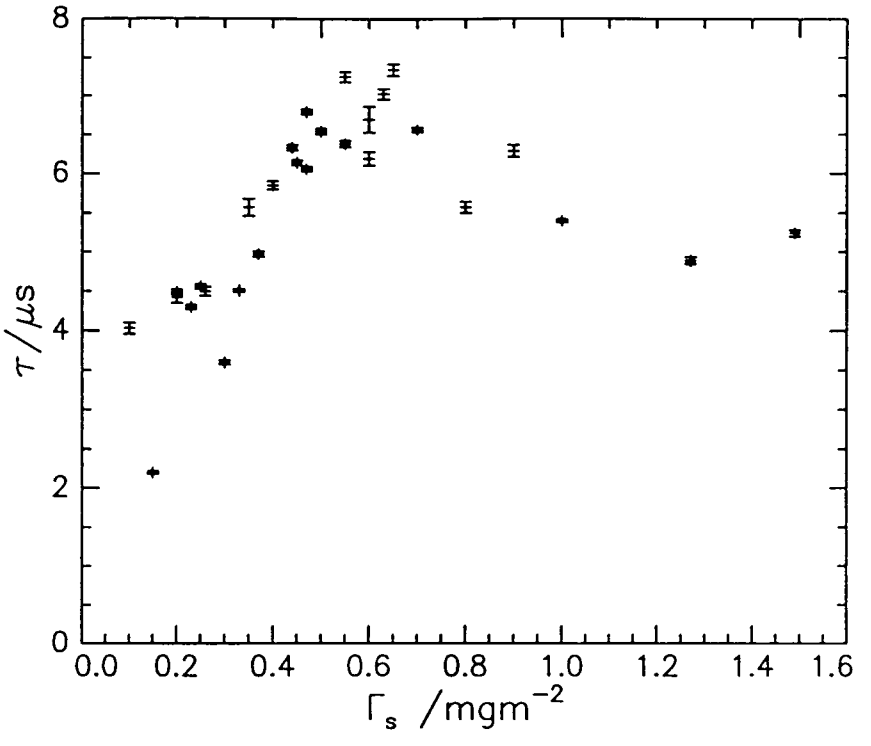

Figure 4.5.33 Relaxation times following the passage of a capillary wave for 10CP assuming Voigt behaviour.

A Maxwell model can also be applied to the same data and using equation 4.5.26 and 27 with the appropriate surface parameters in place of the moduli τ can be expressed by:

$$\tau_C = \frac{\gamma_o - \gamma_{o,st}}{\omega_o^2 \gamma'}$$

Equation 4.5.33

An equivalent expression can be used to determine the relaxation process associated with the perturbations caused by a dilational mode:

$$\tau_D = \frac{\varepsilon_o - \varepsilon_{o.st}}{\omega^2 \varepsilon'}$$

Equation 4.5.34

Where ω is the frequency of the dilational mode which has been extracted by solving the dispersion equation using the values of the surface parameters determined from the spectral fit. In contrast with the physically unrealistic values of τ extracted when a Voigt solid model was applied, equation 4.5.34 yields positive values of τ_D; although $\varepsilon' < 0$, it also transpires that $\varepsilon_o < \varepsilon_{oST}$ and thus $\tau_D > 0$. Typical values of τ_C and τ_D obtained by applying the above equations are given in figures 4.5.34 and 4.5.35.

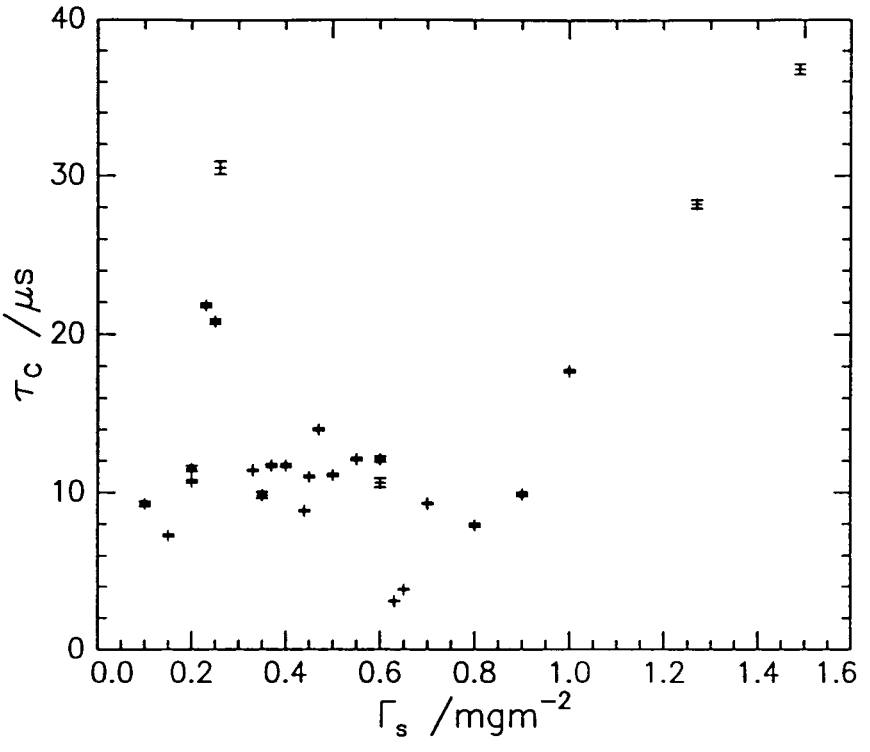

Figure 4.5.34 Relaxation times following the passage of a capillary wave for 10CP assuming a Maxwell fluid behaviour.

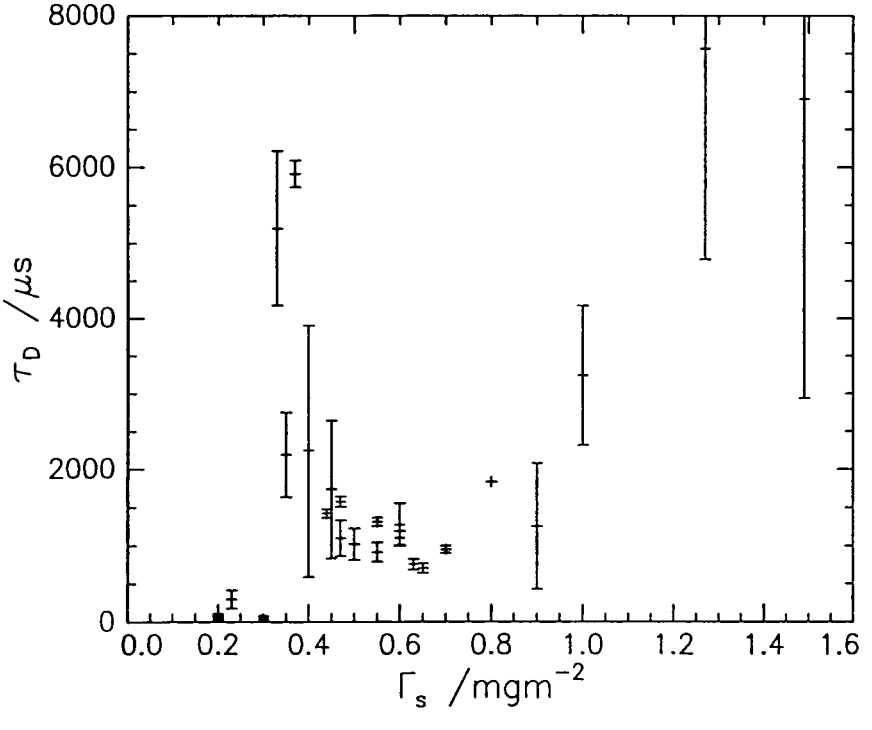

Figure 4.5.35 Relaxation times following the passage of a dilational wave for 10CP assuming a Maxwell fluid relaxation model.

The relaxation times, τ_C, determined assuming the perturbation arises from a capillary mode fall in the range 0 - 30 μs, being rather scattered at low surface concentrations but increase with Γ_s to a local maximum at Γ_s*. Thereafter the values fall to a local minimum then following a further increase in the surface concentration τ_C increases linearly. The gradient of the linear regime was determined using a least squares fitting routine and decreases from 0.29×10^{-4} mg m^{-2} s for 60CP to 0.20×10^{-4} mg m^{-2} s for 10CP. The implication of this is that the relaxation process occurs more slowly with compression, increasingly so as the PEO content increases. This appears to indicate that the relaxation mechanism is impeded by compression of the film, possibly due to changes in the film structure.

The relaxation times determined for the response to the perturbation due to the dilational modes, τ_D, are much longer than for the capillary modes. This is consistent with the dilational modes being the more heavily damped, consistent with a stiff damped spring relaxing slowly following a perturbation. At surface concentrations around, and below, Γ_s* for each system the relaxation time, τ_D, falls in the range 500 - 1000 μs and thereafter increases in a linear fashion with Γ_s to about 3000 μs.

The value of τ_D is two orders of magnitude larger than τ_C, suggesting that as well as the relaxations being highly dependent on frequency very different molecular mechanisms may underlie the processes. It is also informative to compare the values of G, the strength of the relaxation process given by:

$$G = \frac{G''(\omega)(1+\omega^2\tau^2)}{\omega\tau}$$

Equation 4.5.35

The relaxation response of the film to a capillary mode gives values of G predominantly in the range 0 - 60 mN m^{-1}, although the values for each system appear to pass through a sharp maximum where the value of G suddenly increases to 150 ~ 200 mN m^{-1}, see figure 4.5.36. Although these values may appear spurious each graft copolymer exhibited this behaviour implying that there values do correspond to 'real' behaviour. The position of the maximum occurs at increasing values of Γ_s for the series 10CP, 20CP and 60CP and does not appear to be related to Γ_s*, being above this for all the systems. The dependence of G on Γ_s alters at Γ_s* from a negative gradient to positive and thereafter increases to the maximum

value. This implies that the strength the relaxation process alters markedly with Γ_s and is weakest at the point where the surface modes appear to be most strongly coupled, i.e. when $\Gamma_s = \Gamma_s^*$.

The strength of the relaxation process, G, has also been calculated using τ_D and in this case the values were found to be negative. The physical processes underlying what appears to be a negative relaxation are not clear and there is no way that viscoelastic elements could be arranged to exhibit such behaviour. It is concluded that this result is attributable to failures of these models to account properly for the behaviour of this system.

The suggestion that the graft copolymer does not exhibit a simple viscoelastic relaxation is confirmed by considering the frequency dependence of the surface parameters. It was noted that in the Voigt solid neither γ_o or γ' will exhibit any frequency dependence. It has already been mentioned that for 60CP γ_o does not exhibit a marked ω_o dependence, indicating a slight tendency to lower values as ω_o increases. Similarly γ' does not show a systematic dependence on ω_o, although again there are indications of γ' falling at high ω_o. In comparison the data for 10CP clearly shows that both γ_o and γ' decrease with increasing ω_o. Given the marked similarities in the viscoelastic behaviour of the copolymers generally it is likely that they all relax in the same manner and thus will be described by the same model. The Voigt solid predicts that γ_o and γ' are independent of frequency whereas in the Maxwell fluid model γ_o is predicted to increase with frequency, γ' to decrease. Clearly neither model describes the observed variations in the surface parameters. The viscoelastic behaviour appears to be more complex than can be accounted for and it is not intuitively clear how springs and dashpots could be arranged to mimic it. Therefore it appears that we cannot adequately describe the viscoelastic relaxation processes in the films using phenomenological approaches.

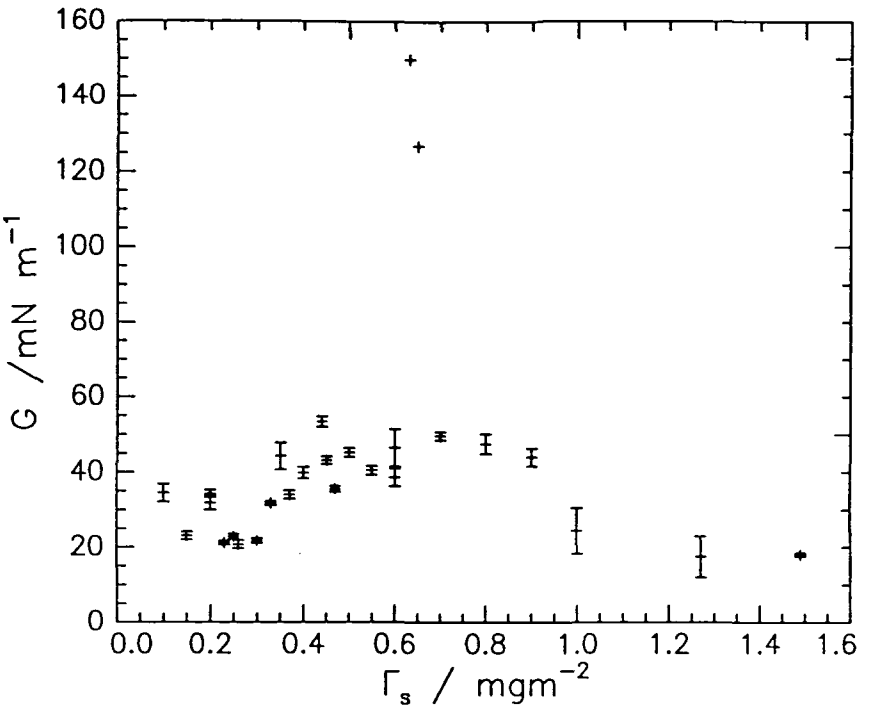

Figure 4.5.36 Strength of the relaxation following the passage of a capillary wave for 10CP assuming a Maxwell model.

As has been mentioned this failure of the phenomenological models is not general to the study of polymers. Such treatments have been applied successfully to the spread film behaviour of both PEO and PMMA.[27] The surface viscoelasticity data for PEO exhibited a dependence on frequency, albeit weak. A Maxwell model was successfully fitted to the data and the relaxation times at q = 220 cm^{-1} were found to vary in the range 10 - 80 μs over the surface concentration range studied. Preliminary analysis of data for surface excess layers of PEO also indicates viscoelastic behaviour following a Maxwell type model. In comparison, films of PMMA do not exhibit frequency dependent viscoelastic behaviour and are described well by a Voigt solid. Given that the homopolymers exhibit conventional behaviour the results of this applying this analysis to the graft copolymers are totally unexpected and not easily rationalised.

Although application of this type of analysis is clearly under question there are certain features which are worth noting. In particular, application of the Maxwell fluid model to the film's response to perturbation arising from the dilational mode indicated a relaxation mechanism with a characteristic time in the order of 500 - 1000 μs. On referring back to section 4.5.4 it is clear that this is of the same magnitude as that predicted for the oscillatory

force that is acting on the dilational waves. The frequency inferred for this driving force was circa 2500 Hz with an associated relaxation time of 400 μs. Otherwise the models clearly fail to reproduce the behaviour of the graft copolymer and care should be exercised in the interpretation of the observation given above. Although it is possible that the force supplying energy to the dilational mode originates from a low frequency relaxation in the film there is no way to account for this currently and the noted similarity may be a coincidence. However, if nothing else this result does seem to support the suggestion made in section 4.5.4 that an oscillatory force with a frequency of ~ 2500 s^{-1} would have to be associated with co-operative molecular motion rather than at the level of a single chain. The latter process would occur at much higher frequencies. In the absence of other evidence it seems feasible to suggest that, an as yet unquantified relaxation process provides a possible candidate for the origin of the driving force that appears to act on the dilational waves.

To conclude, it is clear that phenomenological models fail to account for the behaviour exhibited by the graft copolymers and therefore an alternative interpretation of the data is required. In an attempt to meet this demand the results of the previous Section are discussed at a more fundamental level in the following discussion.

4.5.7 Discussion: Variable Frequency Study

It has already been mentioned that dilational and capillary waves are coupled and in fact it is only because of this coupling that any information about the dilational parameters can be extracted from the capillary waves. Since capillary and dilational waves are coupled they essentially constitute a pair of coupled oscillators and the classic standard results[30] for such systems may be applied as described previously. The fundamental equation governing behaviour has been given previously but, being vital to much of the subsequent discussion, is repeated below:

$$(\omega - \Omega_1)(\omega - \Omega_2) = K^2$$

Equation 4.5.36

where Ω_1 and Ω_2 are the natural frequencies of the uncoupled free oscillators, ω is the frequency of a normal mode of the system and K is the coupling constant.

Capillary waves on a free liquid surface, $\varepsilon_o = 0$, are taken as an 'uncoupled' reference states, the wave frequency being Ω_1. Similarly for dilational waves a reference is defined as the state where $\gamma_o = 0$ and the waves have a frequency, Ω_2. In fact the motions involved in these states are not purely transverse or longitudinal, which is the strict definition of uncoupled waves, but are sufficiently close for the current purpose.

The quadratic equation above has two solutions, $\omega = \omega_1$ and $\omega = \omega_2$, the normal modes of the system. Clearly as K decreases towards zero the normal modes have frequencies almost the same as those of the uncoupled oscillators.

Expressing Equation 4.5.36 in terms of $\Delta\Omega = \frac{1}{2}(\Omega_1 - \Omega_2)$ and $\overline{\Omega} = \frac{1}{2}(\Omega_1 + \Omega_2)$ gives:

$$\left(\omega - \overline{\Omega}\right)^2 = K^2 + \Delta\Omega^2$$

Equation 4.5.37

which demonstrates clearly that, in addition to the coupling, the difference between the frequencies of the uncoupled oscillations, $\Delta\Omega$, is also important in quantifying the behaviour of the normal modes.

Provided that K is small and constant, increasing $\Delta\Omega$ leads to normal modes with frequencies almost the same as in the uncoupled oscillators, i.e. an oscillation in one of the oscillators is so far off the resonance of the other that it will excite little response. However, at the other extreme the maximum effect of coupling is achieved when the oscillators are perfectly tuned and $\Omega_1 = \Omega_2$ so that $\Delta\Omega = 0$ and $\omega = \overline{\Omega} \pm K$. In this case the normal modes will exhibit 'mixed' characteristics, i.e. a combination of the behaviour associated with the uncoupled oscillators, and are therefore referred to as mixed modes. This type of behaviour can only be identified by a detailed study of dispersion behaviour and so the consideration of such effects is most important in the context of frequency dependent studies where such information is available.

One of the most documented aspects of the coupling between the capillary and dilational waves is a resonance[25], which has been alluded to already, and according to the discussion above may lead to mixed modes. This resonance occurs when the real frequencies of the dilational and capillary waves coincide, i.e. $\Omega_1 = \Omega_2$, which at relatively low q follow the established first order approximations. These have the general form $\omega = \omega_0 + i\Gamma$ and are:

For the dilational waves:

$$\omega_D = \tfrac{1}{2}(\sqrt{3} + i)(\varepsilon^2 q^4 / \eta\rho)^{1/3}$$

For the capillary waves:

$$\omega_C = \sqrt{\frac{\gamma q^3}{\rho}} + i\frac{2\eta q^2}{\rho}$$

The resonance occurs when the real frequencies of the modes coincide which occurs at a q given by:

$$q = \left(\tfrac{3}{4}\right)^3 \varepsilon^4 \rho / \gamma^3 \eta^2$$

resonance occurs when $\varepsilon_o / \gamma_o = 0.16$.

To consider the implications of mode mixing on surface waves the discussion of classical coupled oscillators must be extended slightly. The results given so far are for loss free coupled oscillators whereas in the real system there are processes leading to energy dissipation and the behaviour is actually that of coupled lossy oscillators. Equations 4.5.36

and 4.5.37 apply to lossy oscillators with the simple modification that the frequencies will be complex and consequently K^2 may now be positive or negative. If $K^2 > 0$ then the system is said to be reactively coupled, if $K^2 < 0$ the coupling is resistive. It is important to identify which is occurring in a system since the type of coupling will influence the way in which the normal modes of the system are split. The particular case of $K^2 > 0$, reactive coupling, is of relevance here.

Consider a system which exhibits reactive coupling, where the frequencies of the free oscillations are constant but the strength of the coupling changes. It can be shown that as the coupling increases the imaginary parts of the normal modes, the damping constants, converge, eventually coalescing at a particular K^2. Any subsequent increase in K^2 causes the real parts of the normal modes, the frequencies ω_o, to separate and thereafter the normal modes exhibit mixed characteristics, neither exhibits only capillary or dilational characteristics but elements of both.

Generally, dilational and capillary waves are only weakly coupled and the normal modes are clearly identifiable, exhibiting solely dilational or capillary characteristics. However, as has been mentioned, a resonance may occur between the capillary and dilational waves when $\varepsilon_o / \gamma_o = 0.16$, and clearly in this situation mode mixing may arise. Since the surface waves constitute reactively coupled lossy oscillators in order for mode mixing to occur the imaginary components of each of the normal modes, the damping, must converge. Generally the dilational modes are more heavily damped than the capillary modes, the surface viscosities ε' and γ' representing the predominant dissipative processes for each mode. The first order approximations relating the viscosity to the change in the damping of the relevant mode have been given previously, see equation 4.5.9 and 4.5.10.

Earnshaw and McLaughlin[39] have shown that the primary effect of non zero γ' when $\varepsilon' = 0$ is to increase the damping of the capillary waves and, due to the coupling, to reduce the dilational wave damping, see figure 4.5.14. Thus the net effect of high values of γ' will be an increase in the capillary wave damping and reduction in the dilational wave damping causing the damping of the two modes to converge. This route to mode mixing was reported in 1991 and more recently in a subsequent publication[40] it has been shown that certain values of ε' may also bring about the conditions required for mode mixing. In the absence of γ' the effect of $\varepsilon' > 0$ is to increase the damping of the dilational waves. However, if $\varepsilon' < 0$ then the opposite occurs, the dilational wave damping is reduced and the capillary wave damping is

increased, causing the damping to converge, leading to a situation which may also lead to mode mixing.

When the surface modes mix each of the resultant modes will exhibit both capillary and dilational wave like behaviour, with the different characteristics being dominant over different q ranges. Thus if mode mixing is occurring in a system it will only be identified by studying the dispersion behaviour of the modes, i.e. a frequency dependent study.

The two routes to mode mixing documented above give rise to very different behaviour. Initially a system where mode mixing occurs as γ' increases with $\varepsilon' = 0$ is considered. The dispersions are given in figure 4.5.37 normalised by the first order approximations for the capillary wave damping and frequency given in equation 4.5.4, taking $\gamma_o = 65.4$ mN m^{-1} and $\varepsilon_o = 15$ mN m^{-1}. When $\gamma' = 0$ the capillary and dilational modes are clearly identifiable. The capillary mode originates at (1,1) then loops slightly left and down. The dilational mode sweeps characteristically across the top left of the figure from right to left. As γ' increases from zero the capillary mode which originates at (1, 1) and is initially purely capillary in nature, begins to exhibit dilational characteristics, 'looping' up rather than down until at $\gamma' = 3 \times 10^{-4}$ mN s m^{-1} mode mixing occurs. The branch originating at (1, 1) now approaches dilational like behaviour asymptotically at the left of the figure. In comparison the branch which at low q exhibits dilational behaviour becomes capillary wave like at higher q, looping to the right and approaching (1, 1).

Figure 4.5.38 demonstrates the dispersions that arise when mode mixing originates from $\varepsilon' < 0$. In these simulations the value of ε' is maintained constant and ε_o is varied until the classical resonance value is achieved. Far from resonance the dilational and capillary branches are identifiable, the dilational branch sweeping down the right hand side of the figure, almost vertically, due to the inappropriate normalisation.

The capillary mode starts at approximately (1, 1) then follows a nearly semicircular arc down and left. Increasing ε_o brings the modes close at intermediate q but they still retain their separate characteristics. When the resonance condition is reached at $\varepsilon_o = 12$ mN m^{-1} mode mixing occurs and unique dispersions are observed. Mode 1 originally appears to be dilational, sweeping vertically down to the left of the figure but then hooks round to the right, behaviour typical of a capillary mode. The initially capillary mode at (1, 1) adopts an increasingly dilational wave like trajectory at higher q.

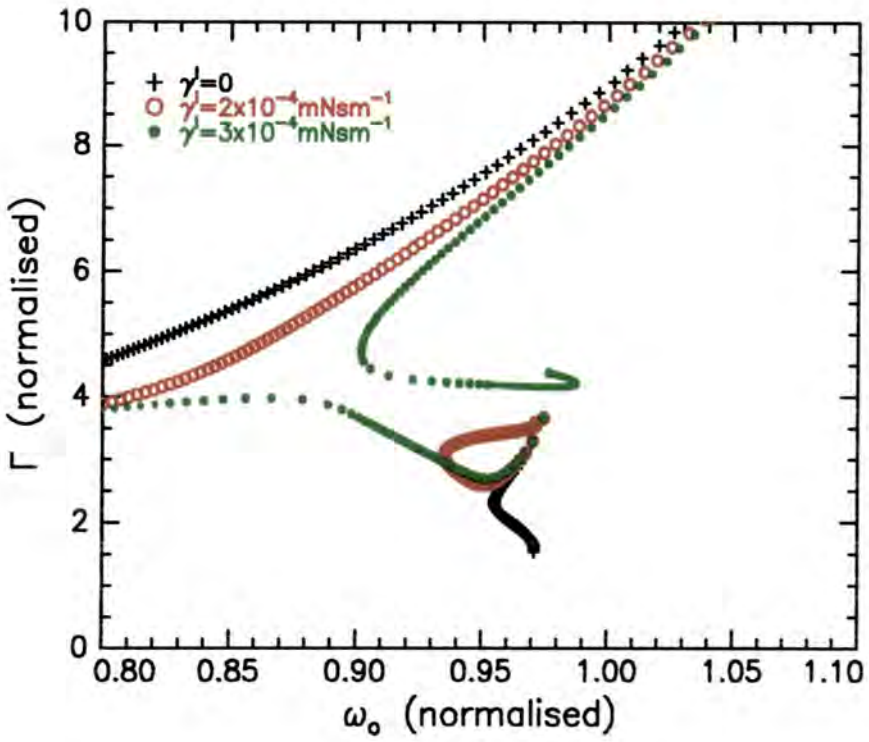

Figure 4.5.37 Theoretical surface wave dispersions for γ_o = 65 mN m^{-1}, ε_o = 15 mN m^{-1}, ε' =0 and γ' as given. See text for discussion.

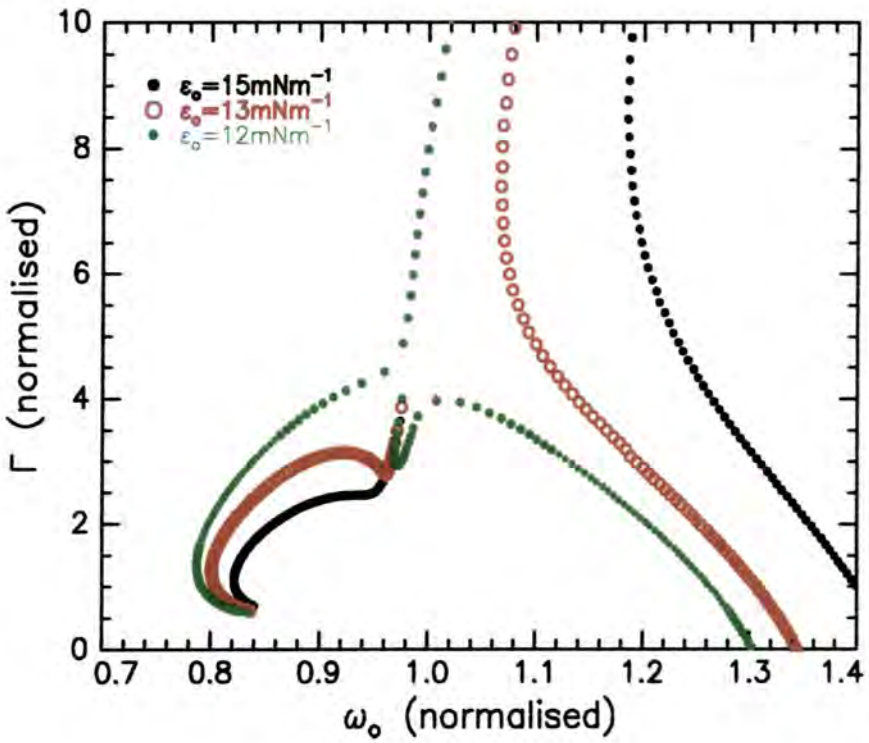

Figure 4.5.38 Theoretical surface wave dispersions for γ_o = 65 mN m^{-1}, γ' =0, ε' = -2 × 10^{-4} mN s m^{-1} and ε_o as given. See text for discussion.

The dispersion behaviour is clearly very different depending on the route to mode mixing and in principle examination of the experimentally determined dispersions should enable the origin of any mode mixing to be determined. However, the generation of these dispersions is highly idealised, the viscoelastic parameters are assumed to be independent of frequency and γ' or ε' are incorporated individually, not both. Unfortunately experimental data is rarely so well behaved. Examination of the data reported here indicates that the present system has the rather unusual situation of exhibiting relatively high values of γ' and large, but negative, values of ε'. The implications of this on the dispersions and any possible routes to mode mixing when both viscosities contribute is not immediately obvious.

It has been stated that $\varepsilon' < 0$ will reduce Γ_D while increasing Γ relative to the values when $\varepsilon' = 0$. However, as has been mentioned this behaviour is specific to $\gamma' = 0$ as demonstrated in figure 4.5.15. Further simulations using experimental values for the surface parameters illustrate the variation of Γ with γ' and ε', although not at the classical resonance ratio of $\varepsilon_o / \gamma_o = 0.16$ which was the case in section 5.5.4. Using the experimental data for a 1.00 mg m^{-2} film of 10CP the wave damping and frequency for both the capillary and dilational waves were computed at each q value studied. The experimental values of γ_o varied from 63 - 59 mN m^{-1}, γ' from 3×10^{-4} - 1×10^{-5} mN s m^{-1} dipping to a negative value at q = 675 cm^{-1}. The dilational modulus, ε_o varied from 4 - 0.6 mN m^{-1}, ε' from -1.3×10^{-4} - 1.2×10^{-5} mN s m^{-1}.

Values for the capillary wave damping and frequency were calculated using γ_o and ε_o only and these act as a reference state for descriptions of any subsequent variations in the wave damping. The surface viscosities γ' and ε' were introduced separately at first to assess their influence and then finally all four parameters were included, the data are presented in figure 4.5.39. Introduction of γ' increased Γ_C with a negligible effect on Γ_D, whereas $\varepsilon' < 0$ reduces both Γ_C and Γ_D. The overall effect of incorporating γ' and ε' is a reduction in the dilational wave damping and an increase in the capillary wave damping. Thus the overall effect of $\varepsilon' < 0$ and γ' in systems studied will cause the damping of the two modes to converge and the possibility of observing mixed modes should be considered.

There are certain features in the variation of damping and frequency which can be identified with mode mixing and have already been mentioned, in addition there is also specific behaviour associated with $\varepsilon' < 0$.

4.5.39a.

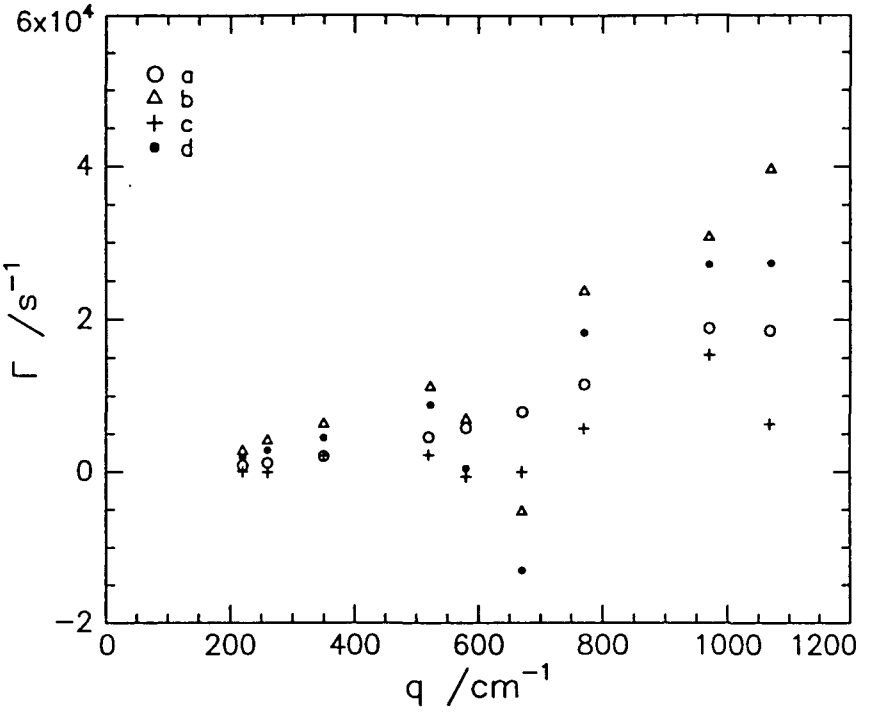

4.5.39b

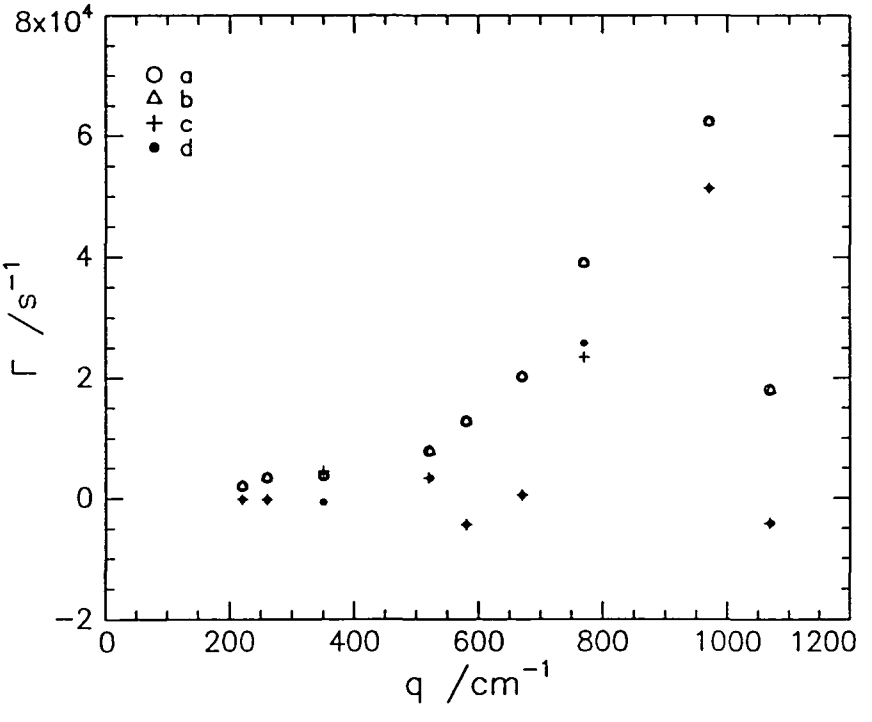

Figure 4.5.39 a)The calculated capillary wave damping using experimental data for 1.00 mg m^{-2} film of 10CP with progressive introduction of γ' and ε'. Data set a: $\gamma' = \varepsilon' = 0$, b: $\varepsilon' = 0$, γ' incorporated, c: $\gamma' = 0$, ε' incorporated, d: both γ' and ε' are incorporated. b): The calculated dilational wave damping otherwise as for 65a. Note that in 4.5.39a the values for c and d are essentially coincident.

The variation in the capillary wave damping, normalised using the first order approximation, $\Gamma = 2\eta q^2/\rho$, with increasing q is unique in systems where $\varepsilon' < 0$ and exhibits an abrupt downturn as q increases. This behaviour cannot be reproduced in any other way and is associated with the collapse of the dilational waves which will eventually occur in the case of $\varepsilon' < 0$. The dilational mode collapses because, as q increases, the destabilisation indicated by $\varepsilon' < 0$ has an increasing influence until eventually the waves grow rather than decay. As the dilational wave approaches collapse the capillary wave damping falls to the value it would have in the absence of the dilational waves and hence exhibits a downturn.

It follows from the preceding discussion that plotting the normalised damping as a function of q will serve a number of purposes. In the first instance a clear downward trend with increasing q will be vindication of $\varepsilon' < 0$, further evidence that the values are real and not simply an artefact of the fitting process. Additionally, the behaviour of the modes immediately after the downturn will exhibit specific characteristics depending on their nature and origin, these are illustrated in figure 4.5.40. In the absence of mode mixing the capillary mode damping reaches a finite essentially constant value following the downturn. In contrast in the mode mixed system the capillary like mode vanishes and almost simultaneously the originally dilational like mode assumes capillary wave character and exhibits normalised damping values typical of a capillary mode. Thus in the case of mode mixing one would anticipate a discontinuity in the damping associated with a 'jump' from observing one mode to the other.

The experimentally determined wave damping is plotted in this form in figures 4.5.41 to 4.5.42. For 60CP the data for the most dilute film is rather scattered and does not exhibit any noticeable trend, whereas for the 0.70 and 1.00 mg m^{-2} films there is a marked downturn with increasing q, see figure 4.5.41. The data obtained for the most dilute film of 10CP, similar to 60CP, shows no significant downturn in the normalised damping, whereas the higher concentration films do. The 0.30 mg m^{-2} film exhibiting a remarkable dependence. The normalised damping for this film actually falls to values far below those predicted by the first order approximations, then increases at higher q. It is not clear whether a so-called mode jump is occurring at this point but it is quite clear that the behaviour of the damping is consistent with $\varepsilon' < 0$. The underlying processes governing the specific behaviour will be considered in more detail later.

4.5.40a.

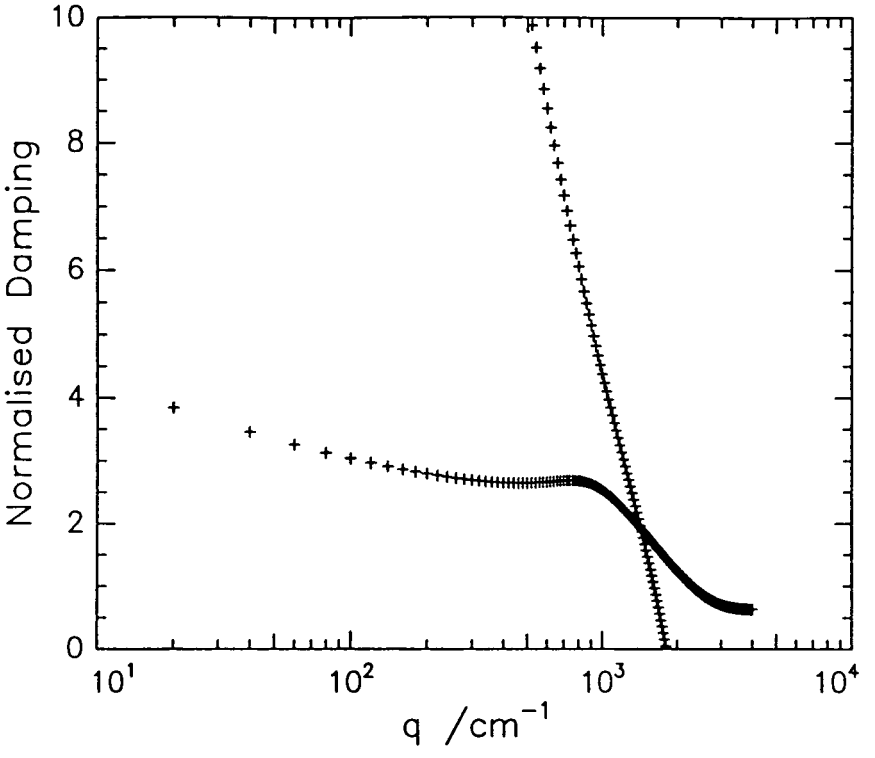

4.5.40b.

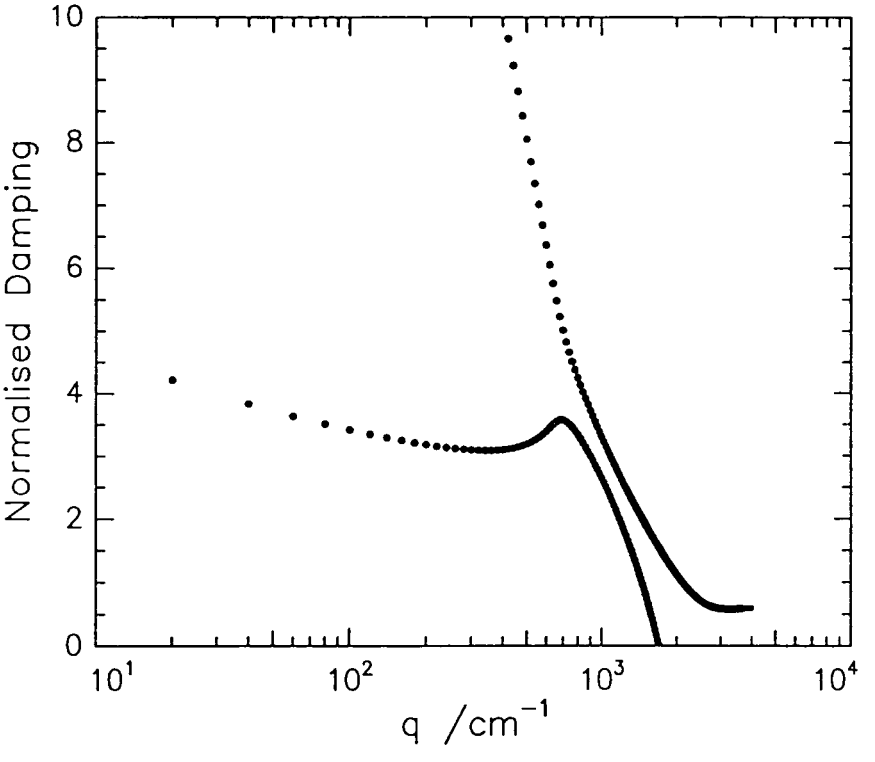

Figure 4.5.40 Normalised wave damping for $\gamma_o = 70$ mN m^{-1}, $\gamma' = 0$, $\varepsilon' = -2 \times 10\text{-}5$ mN s m^{-1}. For 40a. $\varepsilon_o = 15$ mN m^{-1}. For 40b. $\varepsilon_o = 12$ mN m^{-1} and the modes are mixed. See text for further discussion.

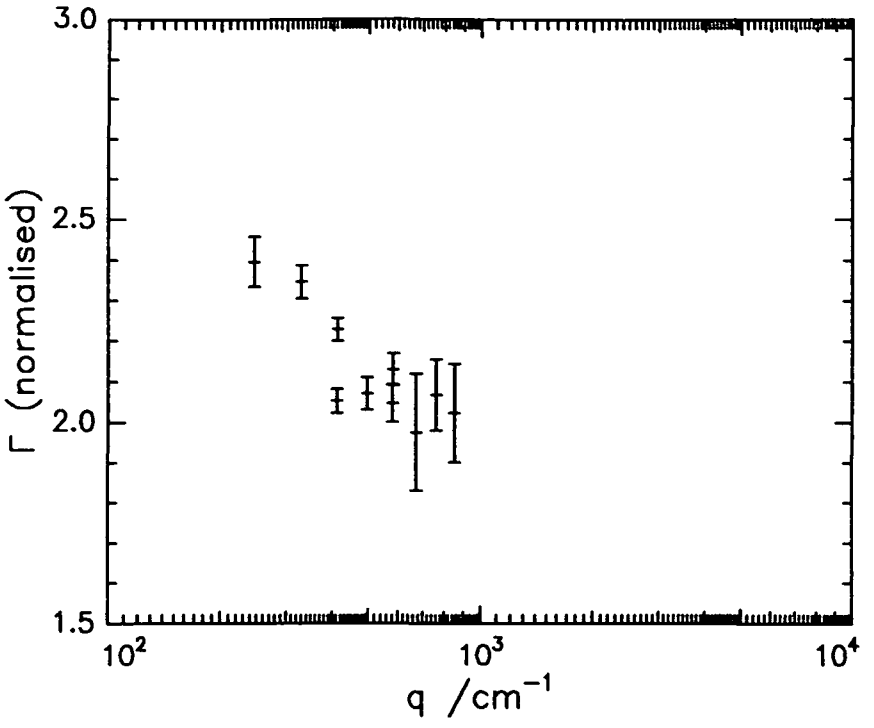

Figure 4.5.41 The normalised capillary wave damping for the 0.70 mg m^{-2} film of 60CP.

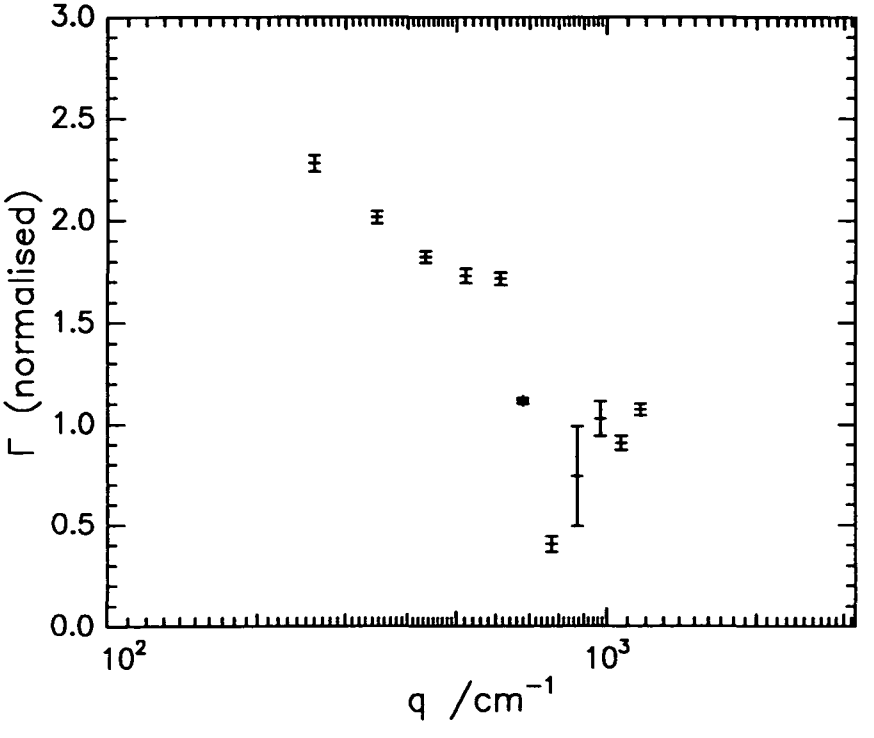

Figure 4.5.42 The normalised capillary wave damping for the 0.30 mg m^{-2} film of 10CP.

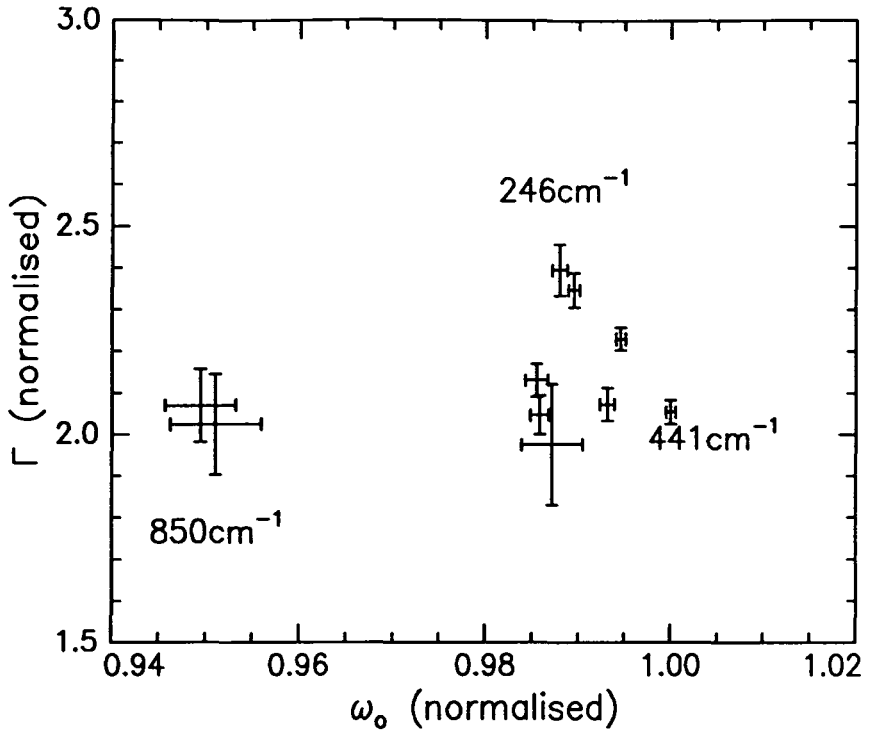

Figure 4.5.43 Dispersion data for 0.70 mg m^{-2} of 60CP plotted in the complex plane.

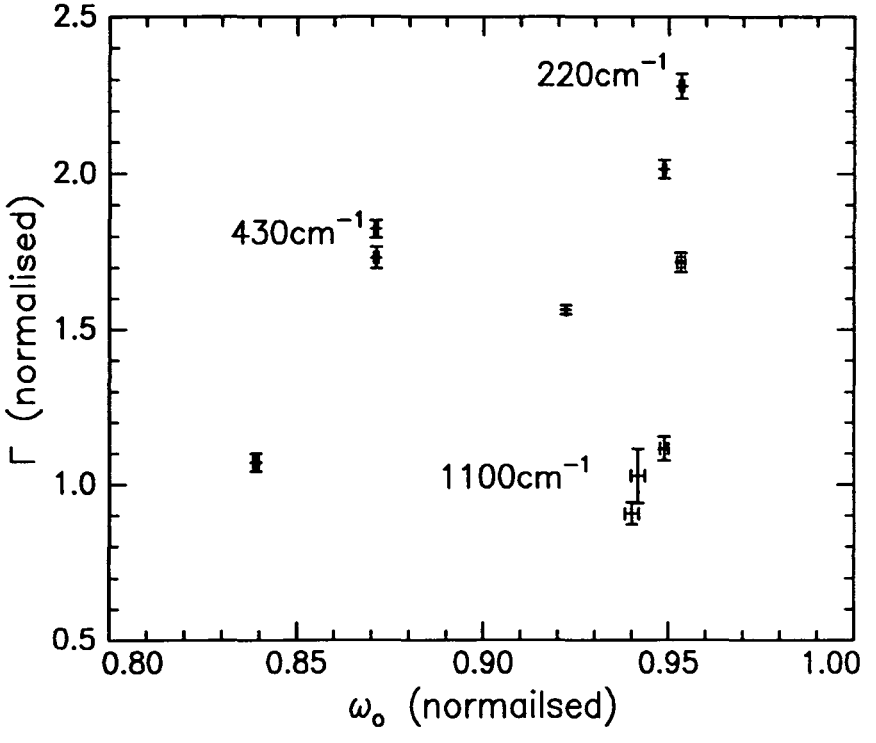

Figure 4.5.44 Dispersion data for 0.30 mg m^{-2} of 10CP plotted in the complex plane.

The capillary wave propagation data is also presented in the form of a complex plane plot where normalised damping is plotted against normalised frequency. The normalising factors are simply the first order capillary wave approximations with γ_o taken as the experimentally determined value at each q. In general the dispersions plotted in this way are of the same form as the examples given in figures 4.5.43 and 4.5.44 and are more like those generated where $\varepsilon' < 0$ in figure 4.5.38 than those for which γ' is high. This feature is considered worth noting since not only is it further confirmation of $\varepsilon' < 0$ but it is not necessarily expected. This is because γ' is relatively large which could modify behaviour significantly from the ideal case.

Considering the dispersions in more detail it is found that for the 0.25 mg m^{-2} film of 60CP in the form of a complex plane plot gives data points scattered around (1, 1) suggesting that there is no significant deviation from capillary wave behaviour. The damping is not being significantly altered from the classical value indicating that the viscoelastic parameters have only a small influence. At 0.70 mg m^{-2} the data describes a hook like trajectory, sweeping left with increasing q, behaviour characteristic of a capillary wave. As well as comparing the experimental data to figure 4.5.38 where $\varepsilon' < 0$ but $\gamma' = 0$ dispersions for $\gamma_o = 70$ mN m^{-1}, $\gamma' = 0.4 \times 10^{-5}$ mN s m^{-1}, $\varepsilon_o = 1$ mN m^{-1} and $\varepsilon' = -0.5 \times 10^{-4}$ mN s m^{-1} are given in figure 4.5.45. The general behaviour of the dispersions is similar to those where $\gamma' = 0$ except that the dilational mode falls at significantly lower frequencies mainly due to the smaller ε_o, although both ε' and γ' also influence this. The similarity between the general behaviour of the capillary modes indicates that the idealised dispersions when $\gamma' = 0$ can be of use as a comparison to this data. At 1.25 mg m^{-2} the trajectory given by the data is broadly vertical, again typical of a capillary mode.

By plotting the experimental data for the capillary wave damping and frequency in the form of a complex plane plot it is clear that 10CP behaves similarly to 60CP, see figures 4.5.43 and 4.5.44. At the lowest surface concentration, $\Gamma_s = 0.15$ mg m^{-2}, the data describes an almost straight line moving to the right with increasing q and seems characteristic of a capillary mode. For the more concentrated films the points are somewhat more scattered. At $\Gamma_s = 0.30$ mg m^{-2} the data are very scattered and rather ambiguous, possibly describing a hook to the right. For $\Gamma_s = 1.00$ mg m^{-2} there is a more defined hook to the right and the data is broadly consistent with the dispersion behaviour of capillary modes. This is true for most of the data but only a limited frequency range is available with the normalised values sometimes

only covering 0.99 - 1.03. This is a very narrow 'window' and may not be sufficient to identify the dispersion behaviour unambiguously and in addition to this there is also uncertainty about how the viscoelastic parameters modify dispersion behaviour relative to the idealised models. Although the latter consideration has been addressed by careful comparisons, with not only idealised data but also the dispersions in figure 4.5.45 where both γ' and ε' are incorporated, the effect of the quite marked variation of the viscosities with q cannot be so readily modelled.

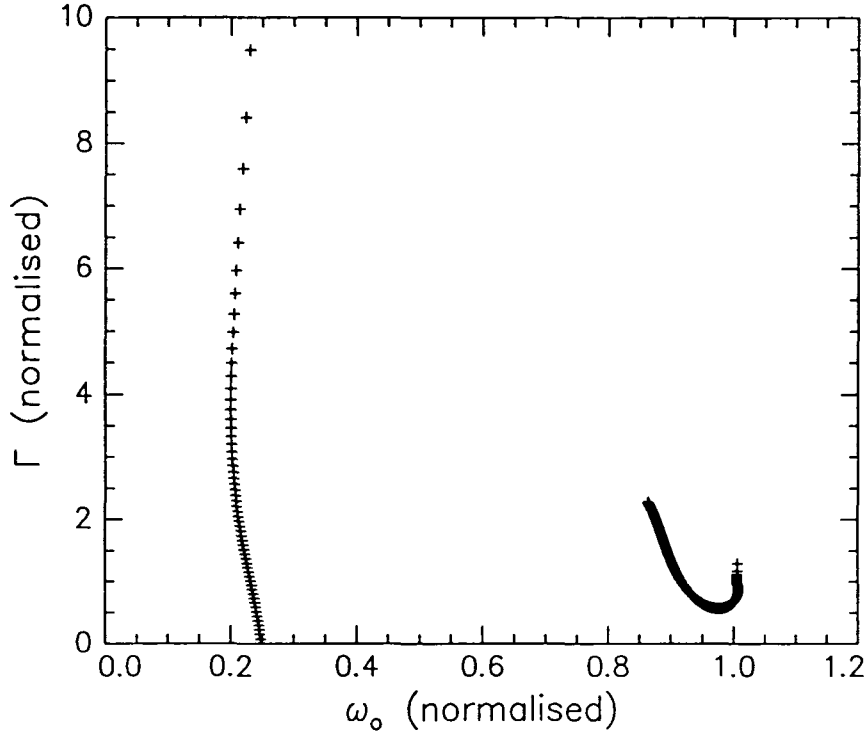

Figure 4.5.45 Dispersions for average values of surface viscoelastic parameters exhibited by the graft copolymers, namely $\gamma_0 = 70$ mN m^{-1}, $\gamma' = 0.4 \times 10^{-4}$ mN s m^{-1}, $\varepsilon_0 = 1$ mN m^{-1}, $\varepsilon' = -0.5 \times 10^{-4}$ mN s m^{-1}.

At this stage the various methods of manipulating the data indicate that although the systems all exhibit behaviour typical of $\varepsilon' < 0$ the surface modes do not appear to be mixed. The exception to this is 10CP at 0.30 mg m^{-2} for which it has been noted that ε' exhibits particularly low values, and the behaviour of the normalised damping is rather ambiguous.

In an attempt to elucidate the behaviour of the 0.30 mg m^{-2} film of 10CP a number of simulations have been used. The initial aim was to determine whether mode mixing is occurring in the system and if the behaviour observed in the normalised damping is indeed

associated with mode jumping. As has been demonstrated, in order for mode mixing to occur the capillary and dilational waves must be at resonance and then, due to appropriate values of either ε' and γ', the damping of the modes converge and mixed modes result. To investigate any possibility of mode mixing experimental values of γ_o, ε_o, γ' and ε' can be taken and the dispersions generated and examined to see whether resonance occurs. It is clear that the surface parameters extracted for this particular film do exhibit some frequency dependence and so the discrete values extracted at each q value were used to determine whether resonance conditions were satisfied at that q.

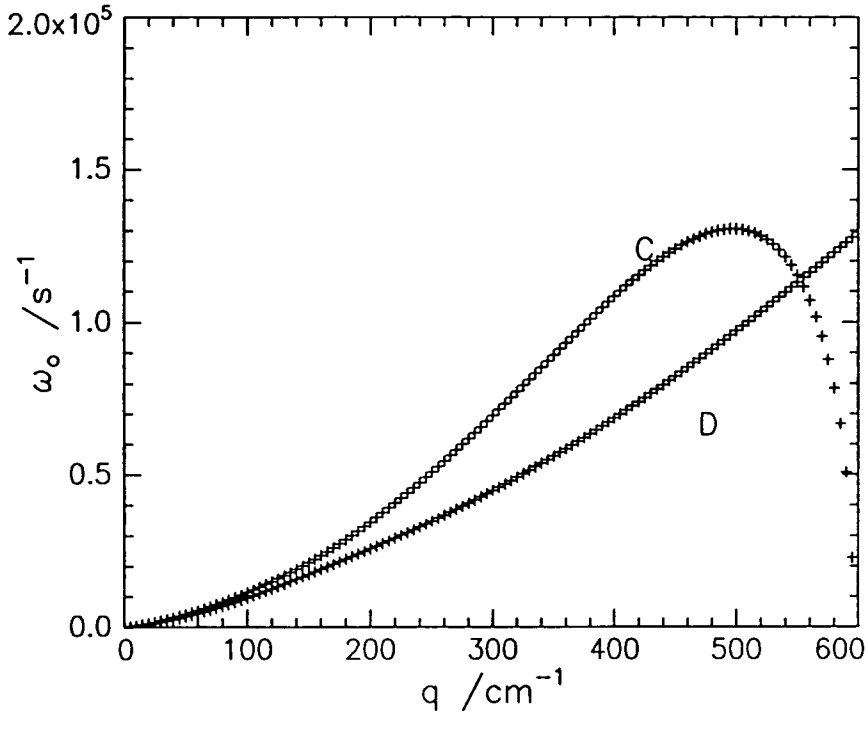

Figure 4.5.46 The frequencies of the surface modes for 10CP at 0.30 mg m^{-2} at q = 434 cm^{-1}, the mode labelled C is the capillary mode, D the dilational mode. It is evident that for these surface parameters resonance is not achieved until q = 550 cm^{-1}.

The dispersions generated were not generally found to exhibit resonances and the few that did occurred at q values significantly different to those of interest. For example taking the surface parameters extracted at q =434 cm^{-1} led to the frequencies given in figure 4.5.46 with a resonance at q = 548 cm^{-1}. The discrepancy between the q value where resonance occurred and the experimental q value was generally at least 200 / 100 cm^{-1}. Experimental data confirms that q values differing by this amount gave viscoelastic parameters which vary

considerably and therefore the resonances were not considered significant. It was concluded from this that a resonance between the dilational and capillary mode frequencies does not occur and therefore the modes are predicted to be purely capillary and dilational in nature.

Proceeding from this treatment the question of what conditions would be required for resonance arises. Taking experimental values for γ_o, γ', ε' and q dispersions were generated as a function of ε_o and it was observed that a resonance occurred at each value of q and quite unexpectedly corresponded to ε_o/γ_o =0.07. This ratio did not appear to exhibit any q dependence, certainly over the q range 220 to 1100 cm^{-1}. This resonance is not predicted by the first order approximations, equation 4.5.3 and 4.5.4, indicating that it has been modified by the relatively large viscosities which are not incorporated in the approximations. This is confirmed by simulations taking the surface tension as 70 mN m^{-1} and q = 300 cm^{-1}. It was considered important to use a low value of q to establish that the failure of the first order approximation to predict this 'new' resonance is not associated with their limitations which become increasingly relevant at high q values. These simulations show that with the viscosities set at zero the surface modes resonate at $\varepsilon_o/\gamma_o = 0.16$, with the introduction of $\gamma' = 1 \times 10^{-4}$ mN s m^{-1} the position is barely shifted, see figure 4.5.47. However, when the dilational viscosity is introduced, $\varepsilon' = -3 \times 10^{-4}$ mN s m^{-1}, the resonance shifts markedly down to ε_o/γ_o =0.07 indicating that it is specific to $\varepsilon' < 0$. Further simulations demonstrate that if ε' is varied whilst maintaining γ_o = 70 mN m^{-1} and $\gamma' = 1 \times 10^{-4}$ mN s m^{-1} the resonance shifts, see figure 4.5.48. For $\varepsilon' = -4 \times 10^{-4}$ mN s m^{-1} resonance occurs at ε_o/γ_o =0.16 in accordance with classical predictions but as ε' increases to -3.5×10^{-4} mN s m^{-1} the position of the resonance shifts to significantly lower values of ε_o/γ_o. When $\varepsilon' = -3 \times 10^{-4}$ mN s m^{-1} the modes are at resonance at $\varepsilon_o/\gamma_o = 0.07$ whereas following a further increases in to -2×10^{-4} mN s m^{-1} the modes appear to mix.

Clearly, this brief discussion indicates that the real frequencies of the dilational and capillary modes exhibit resonances beyond those predicted by the first order approximations which seem attributable to the influence of relatively large surface viscosities. Further simulations are required to get a more systematic understanding of how γ' and ε' jointly influence this behaviour. These simulations do indicate that it is perhaps a misleading to assume that in order for resonance to occur between the surface modes ε_o/γ_o must be 0.16.

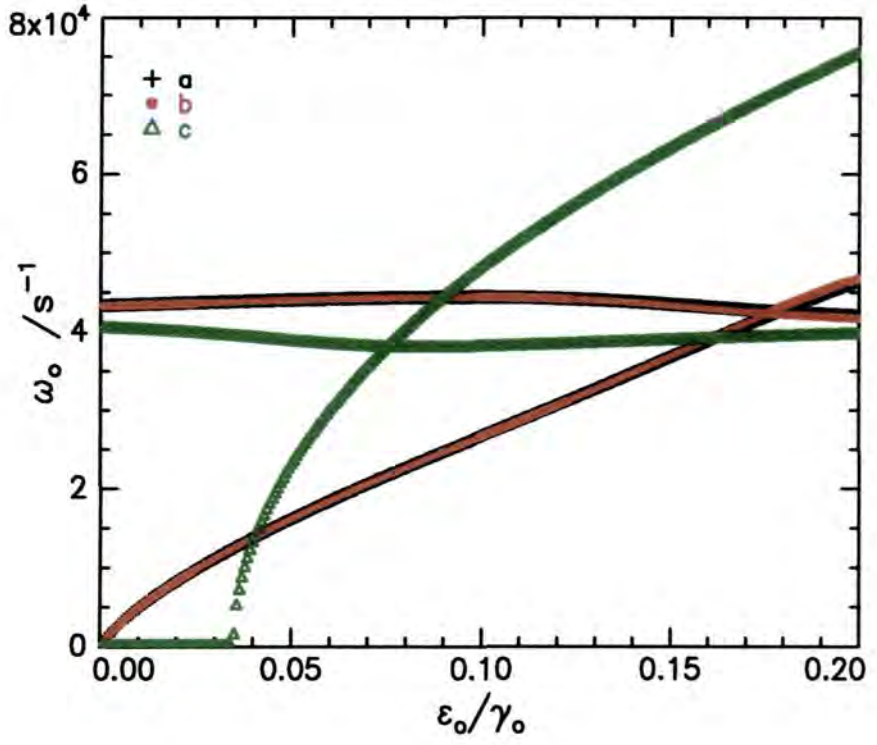

Figure 4.5.47 Simulations at q = 300 cm^{-1}, with γ_o = 70 mN m^{-1} and ε_o varying. For data set a) both γ' and ε' =0, set b)ε' =0, γ' = 1 $\times$ 10^{-4} mN s m^{-1}, set c γ' =0, ε' = -3 $\times$ 10^{-4} mN s m^{-1}.

4.5.48a.

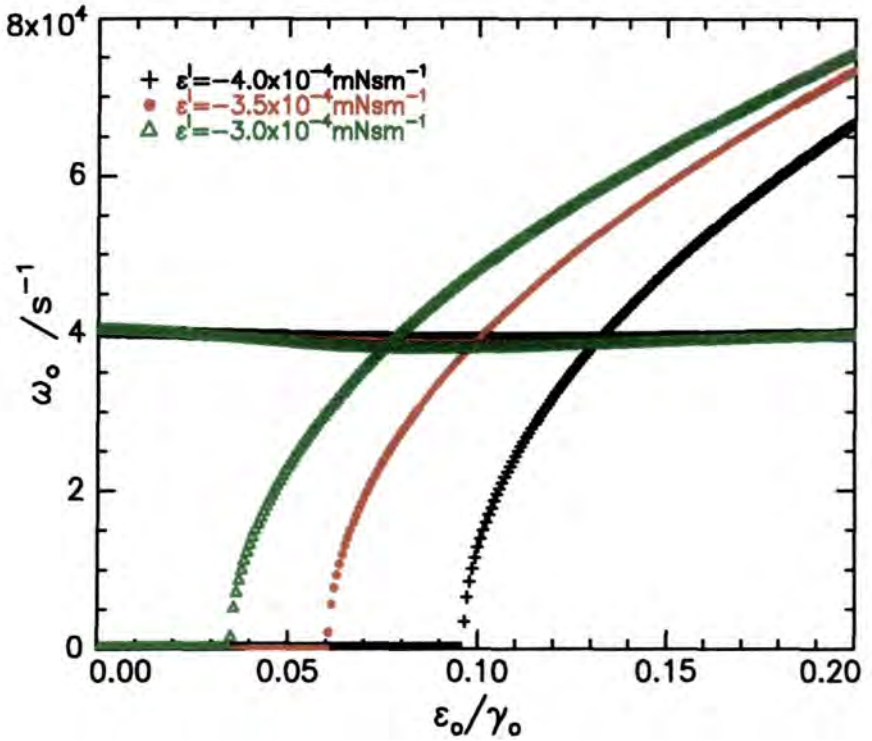

4.5.48b.

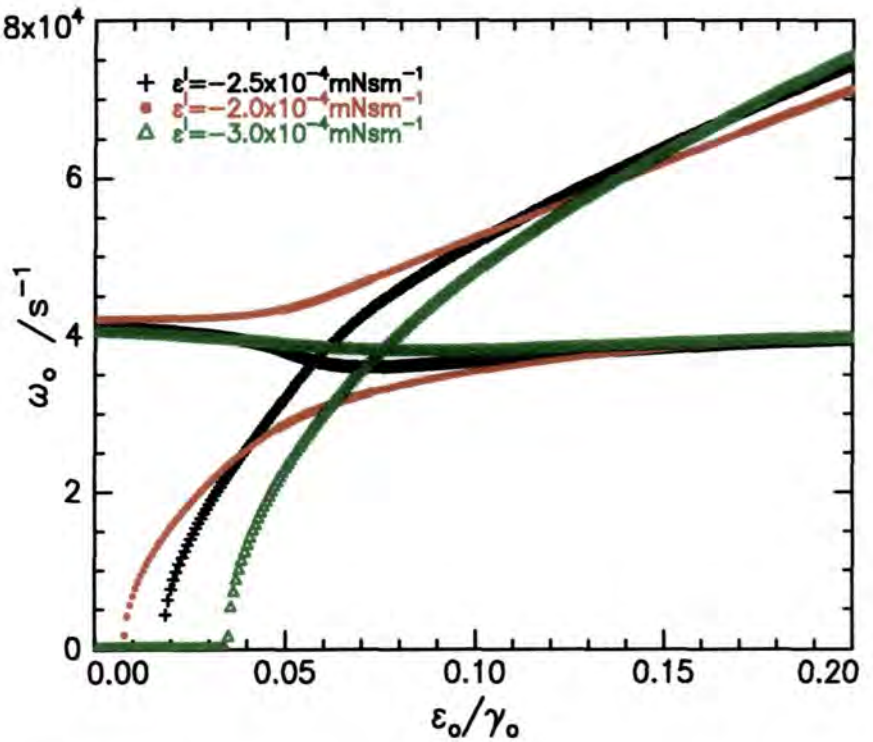

Figure 4.5.48 a) and b) illustrate the shift in the resonance for q = 300 cm^{-1}, γ_o = 70 mN m^{-1}, $\gamma' = 1 \times 10^{-4}$ mN s m^{-1} and ε' as given. See text for discussion.

This statement is particularly true for the graft copolymers and more generally the possibility of resonances corresponding to values of ε_o / γ_o other than 0.16 should be considered for any system where the surface viscosities are relatively large, more specifically where ε' is negative.

To confirm previous suggestions that for the 0.30 mg m^{-2} film of 10CP the surface modes are not mixed and in an attempt to reproduce the variation in the normalised damping, simulations have once again been used. Dispersions have been generated assuming that the viscoelastic parameters are q independent. Clearly this is rather a large assumption to make, especially given the rather marked frequency dependence shown by all the films of 10CP. However, it is believed that by using average values for γ_o , ε_o, γ' and ε' a reasonable attempt can be made to reproduce observed behaviour . This assumption is found to be borne out by the similarities between simulations and experimental data. This is demonstrated by comparing the behaviour of the experimentally determined normalised damping for 10CP at 0.30 mg m^{-2}, figure 4.5.42, with the values generated assuming average values of γ_o, γ', ε_o and ε', given in Table 4.5.5, see figure 4.5.49.

Polymer	Γ_s / mg m^{-2}	γ_o / mN m^{-1}	γ' / mN s m^{-1}	ε_o / mN m^{-1}	ε' / mN s m^{-1}
10CP	0.15	70	0.4×10^{-4}	1.0	-0.5×10^{-4}
10CP	0.30	80	1.5×10^{-4}	3.0	-1.0×10^{-4}
10CP	1.00	62	0.8×10^{-4}	1.0	-0.3×10^{-4}
60CP	0.25	72	1.0×10^{-4}	0.4	-0.7×10^{-4}
60CP	0.70	63	1.5×10^{-4}	0.8	-0.8×10^{-4}
60CP	1.25	55	1×10^{-4}	0.5	-0.6×10^{-4}

Table 4.5.5: The values of the surface parameters used to generate model dispersions.

The variation in the normalised damping is reproduced by the simulation indicating that 'mode jumping' is not an issue for this system. The generated capillary wave frequency and damping are also given in figure 4.5.50 with the first order approximations overlaid. These approximations are of great help in identifying the different modes and any mixed characteristics. This point is highlighted in figure 4.5.51 where the viscoelastic parameters have been chosen such that mode mixing occurs. Mode 1 is clearly dilational like at low q being coincident with the first order approximation.

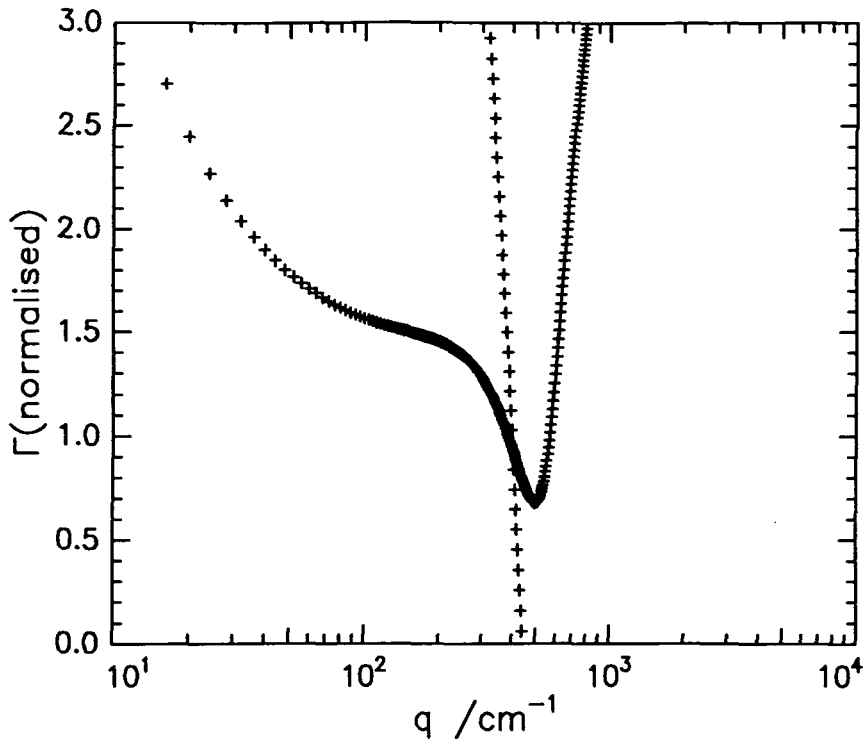

Figure 4.5.49 Generated dispersion data for 0.30 mg m^{-2} film of 10CP. The dilational mode exhibits the almost vertical decrease in damping with increasing q. The capillary mode shows much more variation and is discussed in the text.

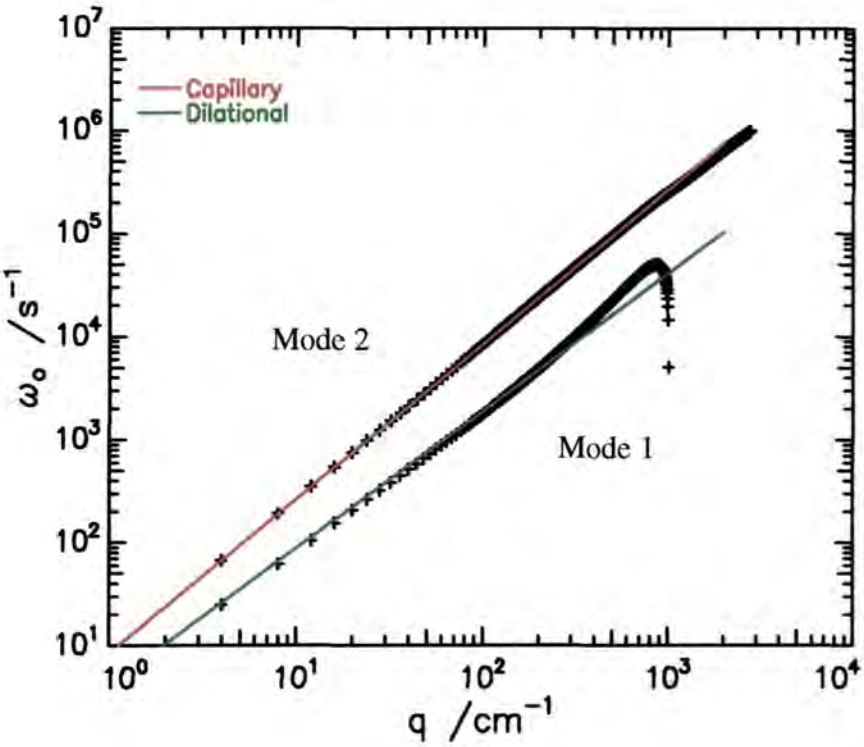

Figure 4.5.50 Generated dispersion data for 0.15 mg m^{-2} film of 10CP. The dilational wave is labelled mode 1, the capillary mode 2. Solid lines are first order approximations for the capillary and dilational as labelled.

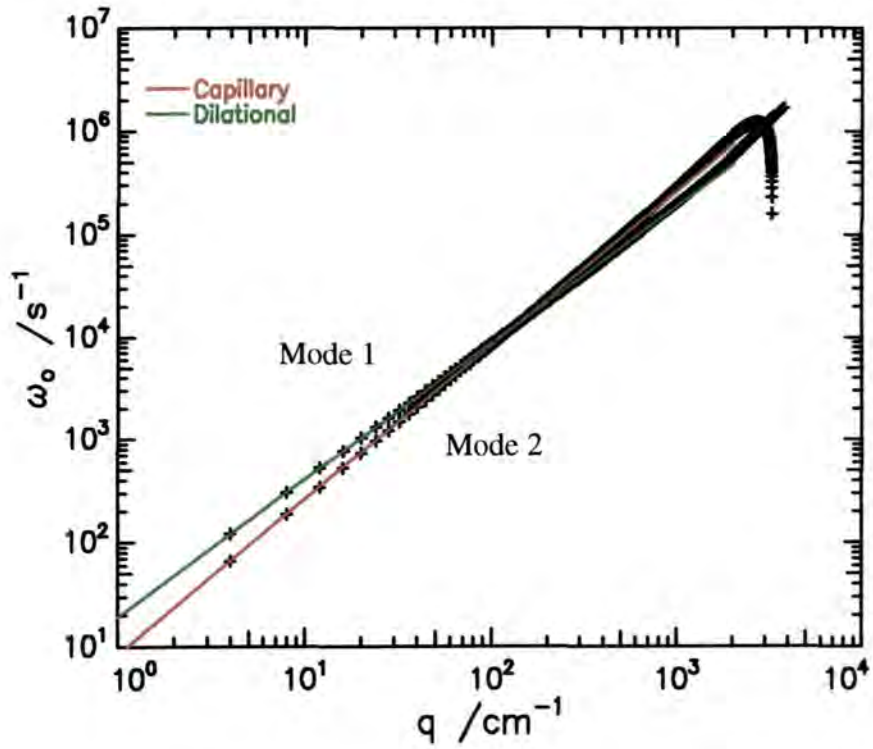

Figure 4.5.51 Generated dispersion data for mixed modes. First order approximations are overlaid.

However, at higher q the mode adopts capillary like behaviour exhibiting a q^2 variation. In contrast the other mode although initially capillary like at low q exhibits increasingly dilational like characteristics and turns over, the damping actually becoming negative which is symptomatic of destabilisation of the dilational modes when $\varepsilon' < 0$.

The simulations in figure 4.5.49 correspond to the 0.30 mg m^{-2} film of 10CP with mode 1 being dilational, the damping falling to negative values at high q while the frequency vanishes. In comparison the other mode demonstrates behaviour compatible with a capillary mode. Thus it is concluded that the surface modes for this particular surface concentration of 10CP are not mixed. The observed dip in the normalised wave damping, both the experimental and generated values, is associated with the collapse of the dilational waves and the capillary wave damping falling to its value in the absence of the dilational wave, see figure 4.5.49. The subsequent increase in the damping of this mode is attributed to γ', since $\Delta\Gamma \propto \gamma' q^3$ the influence of non zero γ' on Γ will cause a rapid increase at high q.

A similar approach has been applied to generate theoretical dispersions for each system using the values for the surface parameters given in Table 4.5.5. The resulting dispersions have been compared to the associated first order approximations, it was clear at a glance that none of the systems exhibited mixed modes.

Having identified the processes at the surface in terms of frequency and damping attention is now turned to the variation in the viscoelastic parameters. The viscoelastic parameters extracted for the two graft copolymers at different surface concentrations exhibit similar trends and are therefore discussed together. The values of γ_o for the films of 60CP do not exhibit a marked dependence on q, the lower concentration films giving values that are essentially constant. In contrast, for the highest concentration film, 1.00 mg m^{-2}, γ_o decreases with q. This trend is further exaggerated by the films of 10CP. This behaviour is rather unexpected; in previous studies γ_o was found to be either q independent or to increase with q and such behaviour could be reconciled by using phenomenological models.[27,5]

Turning now to the behaviour of γ' it is observed that the values extracted for 60CP are rather scattered with no obvious frequency dependence, whereas films of 10CP exhibit a marked dependence. For all the films of 10CP, γ' is found to decrease monotonically with increasing frequency down to a minimum negative value then, subsequently recover slightly, becoming positive again. A decrease in γ' with increasing frequency is predicted if the dissipative term in $\gamma = \gamma_o + i\omega\gamma'$ is not to become infinitely large. However, the appearance

of a minimum, negative values and the subsequent increase in γ' is not expected. Negative values of γ' have been reported previously for a study of alkanes[41] and were attributed to surface crystallisation and the associated reduction in conformational freedom. It is hard to draw any parallel between this behaviour and the observation of $\gamma' < 0$ for the graft copolymers. Negative values of γ' are only observed for the graft copolymer films at certain frequencies whereas for the study of the alkanes $\gamma' < 0$ was observed at all frequencies. The cause of $\gamma' < 0$ can be rationalised at a molecular level for the alkanes but since $\gamma' < 0$ is only observed at discrete frequencies for the graft copolymers it is unlikely to have such a straight forward explanation and may be associated with complex process occurring at the surface.

Negative values of ε' have been associated with energy being fed into the dilational waves. In the same manner it seems reasonable to suggest that similarly $\gamma' < 0$ may be associated with energy being fed into the capillary modes, essentially resulting in propagation of these modes. It may be that some other surface mode provides the energy; this may or may not correspond to the dilational mode. Since both γ' and ε' are negative it would appear that both the capillary and dilational surface modes are being heavily destabilised. Ideally one seeks to identify the source of destabilisation, which may arise due to a resonance with another surface mode or behaviour inherently linked to the structure of the system, i.e. molecular motion in the form of splay or twist feeding energy into these modes.

The minimum in γ' shifts with frequency, at 0.30 mg m^{-2} occurring at $\omega_0 = 2.2 \times 10^5$ s^{-1} corresponding to a process with a relaxation time of 4.5 μs, at 1.00 mg m^{-2} this increases to 7 μs. If the variation in γ' is due, at least in part, to some kind of molecular motion feeding energy into the system then the effect is clearly greatest where $\gamma' < 0$. Such process would presumably be correlated to surface concentration and may be envisaged as becoming more hindered at higher surface concentration thus taking longer and therefore occurring at lower frequencies. If the effect is attributable to contributions from some other surface mode then it must have a frequency of the order of that corresponding to $\gamma' < 0$. Taking the values for ε_0 and ε' determined at this point we find that the dilational wave cannot account for the behaviour observed, but this does not rule out the possibility of any other surface modes contributing, e.g. shear modes. This effect was first suggested by Kramer[26] and is specific to anisotropic films, otherwise for isotropic films the shear modes separate from the dilational and capillary modes which is an implicit assumption in the derivation of the dispersion equation applied here.

The behaviour of ε_0 with q is rather scattered and generally there is little systematic variation with frequency, some films indicating a vague increase in ε_0 with frequency. As in the study at constant q, ε_0 was hard to determine and typically a set of ten correlation functions at the same q and Γ_s could be fitted to obtain values for γ_0 , γ' and ε' all within experimental error whereas the values of ε_0 varied well outside the standard deviation. One suggestion is that in the presence of $\varepsilon' < 0$ the dilational parameters may both be so called effective parameters.

The most remarkable frequency dependence is that of ε', which is exhibited by all the polymers at each concentration. In fact all the films except 10CP at 0.30 mg m^{-2} give essentially the same value of ε', within error, at a particular ω_0. All the values of ε' extracted are found to be negative and, as in the earlier discussion, this is associated with the destabilisation of the dilational waves. The value of ε' at a given ω_0 is essentially the same for all but one of the surface concentrations studied, it follows that the dilational modes are all being destabilised by a similar amount. For simplicity this is assumed to arise from a single process. In the light of this observation it seems reasonable to suggest that the magnitude of ε' is fairly independent of subtle changes in molecular organisation which occur on compression and that all the systems simply fulfil a basic criterion leading to destabilisation. Given the fact that negative values of ε' have previously been observed for adsorbed films of low molecular weight surfactants and also for soluble polymers subphase penetration is anticipated to be important.

Attention is now turned to the variation of ε' with frequency. The increase in ε' with ω_0 to a constant, negative value is demonstrated by all the data and remarkably similar variations in ε' with ω_0 have been reported in the literature. A recent study of the liquid that drains from a commercial shaving foam[34] reported values of $\varepsilon' < 0$ and gave a frequency dependence very similar to that observed here. The dilational viscosity was found to increase from -9×10^{-5} mN s m^{-1} at a frequency of 2×10^4 s^{-1} to -0.5×10^{-4} mN s m^{-1} at $\omega_0 = 4 \times 10^4$ s^{-1}. The similarity in the values of ε' compared with those found for the graft copolymers is quite remarkable, especially when the chemical composition of the foam is considered. The shaving foam will contain a number of low molecular weight surfactants, fragrances, which may well have considerable surface activity, as well as stabilisers and most notably poly(ethylene glycol), a low molecular weight analogue of PEO.

A recent SQELS study of both spread[27] and adsorbed[42] films of PEO also reported instances where $\varepsilon' < 0$. When the spread film surface concentration exceeded 0.5 mg m^{-2} the dilational viscosity was found to become negative. Previous neutron reflectometry studies indicate that at this surface concentration the chains begin to penetrate the subphase. In contrast ε' was always negative for the adsorbed films. The negative values of ε' were found to exhibit the same type of frequency dependence as observed here, independent of whether the film was spread or adsorbed. Although only a small number of studies where $\varepsilon' < 0$ have been reported it is worth noting that this marked dependence of ε' on ω_0 is not always observed. A study of solutions of octanol and decanol found that although for both systems $\varepsilon' < 0$ there was only a slight dependence on ω_0, in no way as marked as for the systems mentioned previously.[43]

In an attempt to rationalise $\varepsilon' < 0$ features common to all the studies mentioned above are noted. All the molecules of interest, other then the graft copolymer, are soluble. The presence of a ethylene oxide units may be associated with the marked frequency dependence of ε'. However, the studies where ε' has been reported to be negative are currently rather few and far between and the presence of ethylene oxide segments may be coincidental. It may be suggested that the variation of ε' with frequency is correlated to the presence of strongly hydrophilic units, if not PEO itself. Clearly hydrophilic groups will interact favourably with the subphase and will seek to maximise these interactions. In the case of an adsorbed film this is easy to achieve but in the case of a insoluble spread monolayer the situation may be slightly different. In order for the hydrophilic groups to interact significantly with the subphase the chains seek to maximise interactions which may lead to subphase penetration. This leads to the suggestion that subphase penetration may be an important factor in the process causing $\varepsilon' < 0$. If the observed behaviour of ε' arises, at least in part, due to chains penetrating the subphase then one would expect to see the same type of behaviour for any films where strongly hydrophilic groups behave in this manner irrespective of their chemistry. No such studies are currently available to test this hypothesis although if it is correct ε' is predicted to be independent of surface concentration once the value corresponding to the onset of subphase penetration is exceeded.

If subphase penetration is always associated with $\varepsilon' < 0$ then it, or some process associated with it, must somehow cause energy to be transferred to the dilational waves. It is hard to imagine such a process arising due to subphase penetration and one suggestion already

mentioned is that when the PEO chains penetrate the subphase they undergo Rouse motion. However, it has already been shown that such movement is too rapid to contribute significantly to motion associated with either the capillary or dilational modes suggesting that the origin of the behaviour may be co-operative motion which would be considerably slower.

Any quantitative information available from the variation of ε' with both the capillary and dilational mode frequency is now considered. As the frequency of the capillary mode increases ε' becomes less negative and this implies that the higher frequency dilational waves, which are indirectly influencing the observed capillary modes, are less destabilised by ε' , i.e. are more stable. Detailed examination of the data shows that $|\varepsilon'|$ falls with increasing frequency, reaching an essentially constant value at $\omega_o = 0.5 \times 10^5\ s^{-1}$. This behaviour can be interpreted in two ways, either arising due to ε' experiencing a relaxation or a time dependence in the destabilisation process which actually causes ε' to be negative. If ε' experiences a relaxation it is only significant at frequencies below $1.5 \times 10^5\ s^{-1}$ indicating that the relaxation time is greater than 7 μs.

The other possible cause of the observed dependence of ε' on ω_o is a frequency dependent destabilisation process. Such a dependence would be consistent with destabilisation arising from a process linked to molecular motion, either at the level of a single chain or slower long range co-operative motion of the film. At capillary wave frequencies above $1.5 \times 10^5\ s^{-1}$ ε' reaches what appears to be a constant value indicating that the destabilisation process has reached a constant level and has become frequency independent. If the destabilisation of the dilational wave is due to a single process of finite frequency one would anticipate that once the wave frequency is sufficiently different the influence of the destabilisation process would become negligible and ε' would tend to positive values. It appears that ε' reaches a constant value at $\omega_o > 1.5 \times 10^5\ s^{-1}$ and it is assumed that this is because the destabilisation process no longer influences the wave evolution. However, in fact ε' remains negative over the whole frequency range indicating that the dilational waves always experience a level of destabilisation. This destabilisation may be in addition to frequency dependent effects which only influence behaviour over a finite range of ω_o. Alternatively ε' may be increasing very slowly with ω_o, although on the frequency scale available the values certainly appear to be constant. In this case ε' may reach positive values at frequencies well outside the accessible range. A possible explanation for a frequency independent

destabilisation process is that the waves are destabilised by a number of processes, all of which may be linked to subphase penetration with a frequency independent component.

It was noted that the values of ε' at a particular capillary wave frequency are very similar except for 10CP at 0.30 mg m^{-2} and 60CP at 0.50 mg m^{-2} where the values were particularly low. A rationale for this observation can be made by considering the propagation of the surface modes and how this alters with surface concentration. At 0.30 mg m^{-2} for 10CP, and generally at Γ_s* for each system, the study at q = 220 cm^{-1} indicated that the coupling between the dilational and capillary waves is at a maximum. As a consequence of this the capillary mode frequency is a maximum whereas the dilational mode frequency passes through a minimum. Calculations performed using the surface parameters determined at q = 220 cm^{-1} showed that the frequency of the dilational mode is fairly constant over the entire surface concentration range except within a band around Γ_s* where it decreases rapidly. The maximum in the capillary wave frequency is much less marked as is clearly demonstrated by referring back to figure 4.5.11. Consider a variable q study of three fixed surface concentration films, assuming that behaviour at q = 220 cm^{-1} is representative. If one of the surface concentrations studied is Γ_s* and the other two differ from this by at least 0.2 mg m^{-2} then only two different dilational modes frequencies will be sampled. This follows by examining figure 4.5.11 from which it is clear that the dilational wave frequency only exhibits a significant variation with Γ_s in the vicinity of Γ_s*. Otherwise the frequency of this mode remains essentially constant despite changes in Γ_s. Basically the import of this is that at a particular q the dilational mode frequency only differs for data recorded at Γ_s*. In contrast the frequency of the capillary mode at a single q value is assumed to be constant and given the scale of the change in the dilational mode this seems a valid approximation, again see figure 4.5.11.

It has already been stated that ε' scales with the frequency of the dilational mode and that the only significant change in the frequency of this mode occurs at Γ_s*. It follows then that due to the minimum in ω_{oD} the dilational viscosity will also exhibit a minimum value. Consistent with the constant value of ω_{oD} over the remainder of the concentration range at Γ_s away from Γ_s* the value of ε' is essentially the same. Since the capillary wave frequency remains constant at each q, despite variations in Γ_s, a plot of ε' against ω_o will be almost identical, within errors, for all film concentrations studied except Γ_s* where, due to the drop in the dilational wave frequency, ε' will be systematically low. This discussion provides an

explanation for the variation in ε' with ω_0 and is supported by both the variable frequency data and the fixed ω_0, variable surface concentration data.

Additional processes which may be coupling to the dilational waves and therefore contributing energy to them are now considered. To determine the relevance of possible processes it is instructive to compare the frequency with that of the mode of interest, the dilational mode. The values of γ_0, γ', ε_0 and ε' obtained from the direct spectral fit were used to solve the dispersion equation at each q value enabling the frequency and damping of the capillary and dilational waves to be extracted. The computed capillary wave frequencies were found to be in good agreement with the experimental values for all the films of both 10CP and 60CP, as were the damping constants. Thus, these calculations clearly reproduced the experimentally observed capillary wave behaviour indicating that the dispersion equation used does provide a good description of the dependence of the capillary wave propagation on γ_0 , γ' , ε_0 and ε'. This statement does not imply anything regarding the possibility of 'effective' viscoelastic parameters: it simply means that the values extracted from the spectral fits do reproduce the observed dispersion behaviour correctly.

The aim of this exercise is the determination of the dilational wave frequency and damping and since there is no alternative method of extracting this information from the current experiment the results of the calculation are assumed to be correct. There is some debate as to whether the dispersion equation used here is appropriate for this system. If it is not, by using it to fit the experimental correlation function the surface parameters extracted are open to the possibility of being 'effective' parameters, i.e. not having any direct physical significance. If this is the case then it would not necessarily follow that using these surface parameters to solve the dispersion equation in terms of frequency and damping would give meaningful results. Clearly, given that negative values of ε' have been observed and noting the discrepancies between static and dynamic values of γ_0 and ε_0 the appropriateness of the dispersion equation and whether it accounts for all the processes influencing the surface wave propagation, is in doubt. Although the capillary wave frequency and damping were reproduced successfully using this equation the characteristics of the dilational wave propagation are predominantly influenced by ε_0 and ε'. Given the anomalous nature of ε' it is the propagation characteristics of the dilational mode that are the most likely to be influenced and not be reproduced accurately whereas the capillary mode will be only effected indirectly.

4.5.52a.

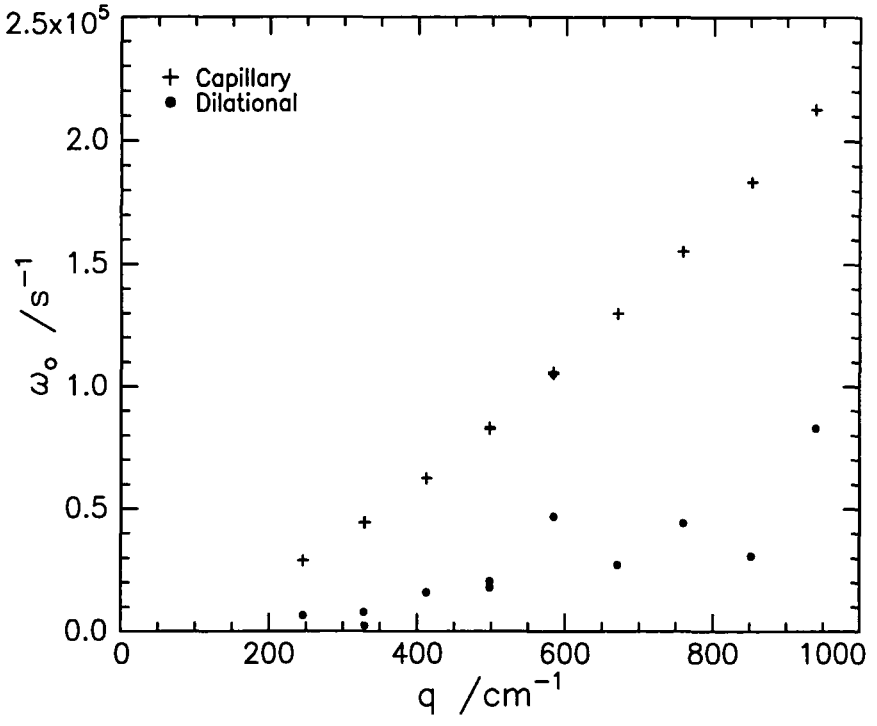

4.5.52b.

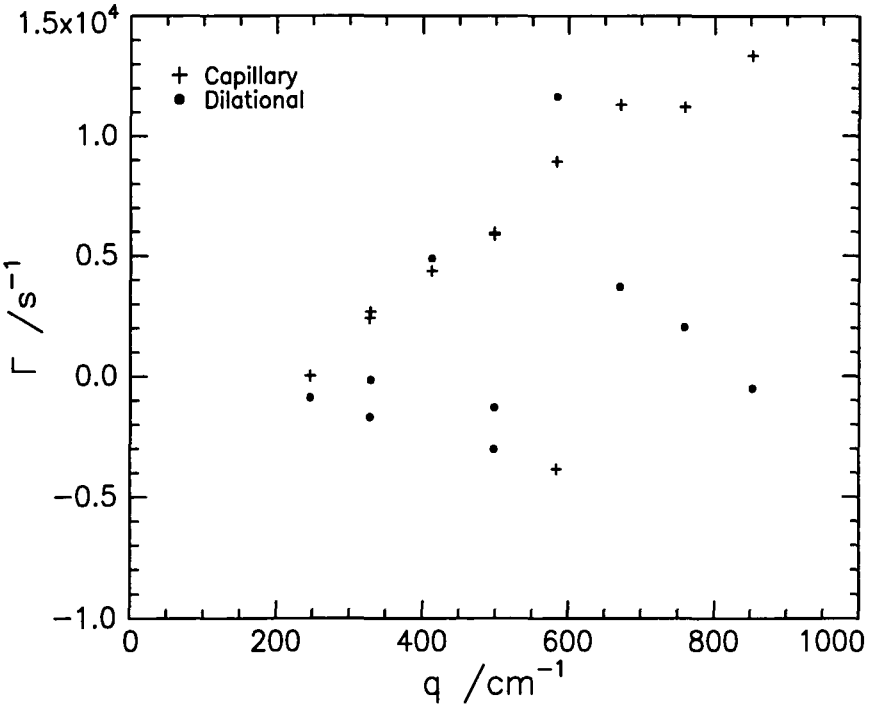

Figure 4.5.52 a) Comparison of capillary and dilational mode frequencies. b) comparison of the damping for the two modes.

Thus, it is possible that the dilational mode propagation is not correctly described but, given the absence of any other information, the results are used and assumed meaningful.

The calculated dilational wave frequencies were found to be finite and always less than the associated capillary wave frequency at a given q, this is illustrated in figure 4.5.52. The damping values were predominantly negative, this is attributed to the negative values of ε'. At first this may appear physically unrealistic but in fact can be associated with the behaviour of a maintained oscillator.

The characteristics of a maintained vibrator have been discussed in many texts, notably that by Pippard.[30] A damped simple harmonic oscillator which is being supplied with energy from an external source forms the simplest model system. Basically, as an increasing amount of energy is supplied to the oscillator the time taken for the amplitude of the oscillations to decay increases until the situation is reached where the internal dissipation is exactly matched and the vibrations are maintained at constant amplitude. If further energy is supplied the oscillations will begin to grow, and the damping appears to be negative because the oscillations are propagating. Such growth cannot be maintained indefinitely, in the case of waves on a water surface the result would be an increasingly turbulent surface and eventually water being thrown out of the surface! Although there will be a finite time over which the waves do propagate in this manner something in the system will change, the coupling may breakdown or the energy source fail, and the system becomes non linear. Although such a system is strictly non linear standard results for simple harmonic oscillators may be applied to the linear region and have the same solutions whether the damping is positive or negative.
The standard equation for simple harmonic motion is:

$$\ddot{x} + k\dot{x} + \omega_o^2 x = 0$$

Equation 4.5.38

where x is the displacement, ω_o is the natural frequency of the undamped oscillator and $k\dot{x}$ is the term representing the damping force. In the case of light damping, $k < 2\omega_o$ and the frequency of the oscillation is given by:

$$\omega'^2 = \omega_o^2 - \frac{k^2}{4}$$

Equation 4.5.39

Thus the negative damping values indicate that the waves are becoming less stable, although they do propagate to an extent with a finite frequency. This is consistent with a negative ε' which implies that energy is being supplied to the waves. The computed dilational wave behaviour is found to be consistent with the model above which predicts that $\omega'^2 \propto -k^2$ so that as $|k|$ ($|k| \propto \Gamma$) increases there should be an associated decrease in the wave frequency. The dilational wave frequency and damping that have been determined do vary in this manner, see figure 4.5.53, thus the dilational waves do appear to act as maintained simple harmonic oscillators.

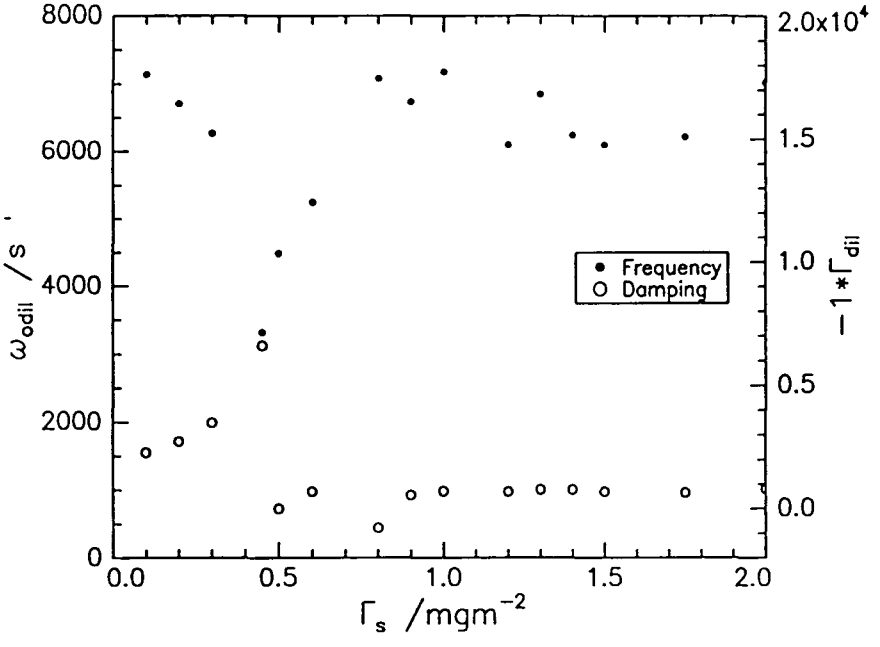

Figure 4.5.53 Variation in the dilational wave damping and frequency for 60CP with Γ_s at q = 220 cm^{-1}.

The frequencies of the dilational waves are of considerable interest as they offer information regarding the frequency of any harmonic processes which may be the source of the 'extra' energy being supplied. However, there is no a priori requirement for the extra energy source to be harmonic and a variety of possibilities will be considered in turn.

One possible source of energy is the inherent movement associated with solvated polymer chains. Many complex theoretical models have been developed to predict the characteristic times of the various types of motion associated with polymers in solution. The Rouse model in which a polymer chain is viewed as a number of beads linked by springs has

already been mentioned and is applicable here. The Rouse equation, equation 4.5.11, is repeated below and has been used to determine relaxation times for all the separate components, side chain, back bone and the entire chain.

$$\tau_r = 0.325\eta_s \frac{(\sqrt{N}a)^3}{k_B T}$$

As before the statistical step length for both the PEO and PMMA is taken as being to be 6 - 10 Å which should be sufficient to estimate the magnitude on the range of any molecular motion. In addition to this estimate it is stressed that this theory is strictly applicable to linear polymers in solution, a situation rather different to that of grafted chains at an interface. Given the approximate nature of this treatment it is important that the values extracted are taken as 'ball park' figures only.

System	τ_R / μs	Frequency / s^{-1}
PEO side chain	0.003 - 0.003	2.5×10^8 - 3×10^7
PMMA backbone: 10CP	0.4 - 0.08	2.5×10^5 - 1.2×10^7
PMMA backbone: 60CP	0.15 - 0.70	6.8×10^6 - 1.5×10^6
Entire Molecule: 10CP	1 5	2×10^5 - 10^6
Entire Molecule: 60CP	0.4 - 1.8	5.6×10^6 - 2.6×10^6

Table 4.5.6: Relaxation times and associated frequencies for Rouse type motion of the chains.

Table 4.5.6 reports the predicted ranges of τ_R and the associated frequencies for 10CP and 60CP, these representing the extremes in copolymer composition and therefore in relaxation times. The relaxation time was determined for the side chain, backbone and the entire molecule. Given that Rouse equation applies to chains in bulk solutions it is anticipated that the values are most relevant for the side chains when they are solvated. However, spread polymer monolayers have been treated as the two dimensional equivalents of solutions and so the behaviour is unlikely to be totally different. It is probable that, if anything, the chains actually move rather faster than given here, i.e. at higher frequencies. Neutron reflectometry studies indicate that the upper most layer of the surface contains PMMA, water and air. If the PMMA is considered to be in a mixed 'solvent' of air and water then the average viscosity

would fall leading to a reduction in τ_R and an even more rapid relaxation. Thus it seems reasonable to suggest that the timescales for motion given in Table 4.5.6 are lower bounds and it is feasible that the motion is actually more rapid.

Given that the dilational wave frequencies fall in the range 8000 - 2000 s^{-1} it appears that molecular motion is too fast to be due to a resonance. The slowest motion calculated is that involving the entire chain and since the chains are not linear, may be anticipated to be slower than that predicted by the Rouse equation. It is not clear how to envisage co-operative motion of the entire molecule, although of course any motion of the backbone will always impose some motion on the side chains and vice versa. The steric bulk of the grafted chains may hinder molecular motion and anchor sections of the hydrophobic backbone on the water surface. Conversely, it is known from neutron reflectometry that segments of the backbone do loop above the subphase and as a consequence it is anticipated that they will be able to move quite rapidly. Due to the complex nature of these graft copolymers it is unlikely that molecular motion will occur at discrete frequencies and a range of frequencies are expected to be associated with molecular motion. It may be that some of the motion is sufficiently slow to be at resonance with the dilational waves but there is no way of quantifying any effects and they are not anticipated to be significant.

Section 4.6 Conclusion

The behaviour of the graft copolymers has been shown to scale with composition, exhibiting certain features associated with the spread films of the separate homopolymers. The surface pressure isotherms in section 4.3 demonstrated that surface behaviour is highly dependent on copolymer composition. At low surface concentrations it was clear that the isotherms were dominated by the PEO side chains. The temperature dependence exhibited by the surface pressure isotherms was consistent with a subphase - side chain interaction becoming less favourable with increasing temperature. This behaviour was exhibited mainly at high Γ_s, see figure 4.3.4, implying that the PEO side chains penetrate the subphase increasingly as Γ_s increases. This inference was consistent with considerations of available surface area.

Using neutron reflectivity it was shown that, despite increases in Γ_s, the PMMA backbone of all the graft copolymers populates a constant width of the interface, about 15 - 17 Å. In contrast the PEO side chains have been shown to stretch into the subphase on compression of the films. This behaviour is believed to be directly analogous to the subphase penetration associated with spread films of PEO[19] above a critical surface concentration. Due to the presence of the insoluble PMMA backbone in the graft copolymers, which occupies surface area, the PEO side chains stretch into the subphase to reduce the number density at the surface. This behaviour has been compared to that of a polymer brush and by using brush theories it appears that the behaviour, although not totally consistent with the models, exhibits similar features, see figures 4.4.34 and 4.4.35.

The observation that the PMMA backbones adopt the same interfacial organisation irrespective of the PEO content in the copolymer is rather surprising. It was suggested that the PEO chains may act as anchors constraining the PMMA backbone to the interface. In this model it was anticipated that the higher the PMMA content of the copolymer, the longer the sections between anchors and the more freedom the PMMA would have to loop above the subphase. From the results of the neutron reflectometry study it can be concluded that this is not the case. Comparing the dimensions of the PMMA layer formed by the graft copolymers with that of spread films of PMMA lead to the conclusion that they were essentially identical, see section 4.4.6, figures 4.4.30 and 4.4.31. Despite the similarities in the layer structure normal to the interface the influence of this backbone on the surface pressure isotherm is quite

different to that of PMMA. It was shown in section 4.3.4.3 that, even accounting for the contribution from the PEO, the surface pressure isotherm did not converge to that associated with spread films of PMMA. From this result it is concluded that while the interfacial organisation normal to the surface is similar to that of homopolymer PMMA the interactions within the surface plane are very different. These lateral interactions will influence the characteristics of the surface pressure isotherms. It has been suggested that the lateral interactions are stronger the higher the PEO content of the graft copolymer. Such behaviour may arise due to favourable interactions between the PEO and PMMA which lead to stronger in plane interactions as the PEO content increases. Unfortunately, none of the experimental techniques available can provide any quantitative information on such interactions.

The capillary wave dynamics of this system have been shown to be very unusual and are different from the behaviour exhibited by films of either PEO or PMMA. One of the most significant observations was that of a negative dilational viscosity. The implication of this result is that there are additional forces in the system which are influencing the evolution of the dilational modes and somehow causing them to propagate. The origin of this behaviour has not been identified, although it has become clear that current surface wave theories do not suffice to describe this system fully. Modification of current theories with an emphasis on applications to polymeric systems is currently in progress.[44]

One of the aims of the work was to correlate dynamic behaviour with surface organisation. Clearly the surface organisation of the graft copolymers, at least normal to the interface, has been determined successfully. Unfortunately identifying correlations between these features and the surface viscoelastic parameters is not complete. Subphase penetration by the PEO side chains has been shown, albeit by circumstantial evidence, to be important in influencing the dilational parameters. It follows that processes directly linked to this structural organisation are thought to lead to the breakdown of the conventional surface wave propagation in this situation. Unfortunately this is currently the limit of the correlations. It can simply be concluded that the subphase penetration exhibited by the side chains dominates the surface wave propagation with some remarkable effects.

There are many extensions of this study which seem feasible and potentially informative. Clearly the study could be extended to liquid - liquid interfaces where a judicious choice of fluids could modify the coupling between the surface wave modes. Given

that ε′ is intimately linked with side chain - subphase penetration investigations into the dependence on the nature of the PEO seem valid. Considering graft copolymers of a constant PEO content, but containing very different chain lengths, may be informative. This would provide a more systematic study than that given here, where this behaviour was rather stumbled upon. Other polymeric systems also come to mind, perhaps the most pressing study being to consider a non PEO containing copolymer which is known to demonstrate subphase penetration, for example a poly(dimethylsiloxane) poly(styrene) diblock on ethyl benzoate.[45] Extending existing studies in this way should enable the origin of negative ε′ to be considered for a wide range of systems, enabling the role of PEO and subphase penetration to be separated. It is hoped that following this study continuing work in this field will enable a more quantitative evaluation of surface wave propagation for these, and other, more complex systems.

4.7 References

1. C. E Rehberg, C.H. Fisher, *J. Amer Chem Soc*, **66**, 1203, (1944).
2. H.S. Kaufmann, A. Sasher, T. Alfrey, J. Fankuchen, *J. Amer. Chem .Soc.*, **70**, 3147, (1948).
3. Y. Gallot, M. Leng, H. Benoit, P. Rempp, *J. Chim. Phys*, **62**, 821, (1965).
4. P. Dreyfuss, R. P. Quirk, *Encyclopedia of Polymer Science and Engineering*, **7**, Wiley Interscience, (1987).
5. B. R. Rochford, PhD Thesis, University of Durham, (1995).
6. K. Hatada, T. Kitayama, K. Ute, *Prog. Polym. Sci*, **13**, 189, (1988).
7. T.G. Fox, *Bull. Am. Phys Soc*, **1**, 123,(1952).
8. J. Brandrup, E.H. Immergut, *Polymer Handbook*, Wiley Interscience, (1989).
9. T.G. Fox, S. Loshaek, *J. Polym Sci.*, **15,** 371, (1955).
10. B.E. Read, *Polymer*, **3**, 529, (1962).
11. T.M. Connor, B.E. Read, G. Williams, *J. Appl. Chem*,**14**, 74, (1964).
12. J. A. Faucher, J.V. Kolveske, E.R. Santee, J.J. Sratta, C.W. Wilson, *J. Appl. Phys*, **37,** 3962, (1966).
13. J.A. Henderson, PhD Thesis, University of Durham, (1992).
14. J.A. Henderson, R.W. Richards, J. Penfold, R.K. Thomas, *Macromolecules*, **26**, 65, (1993).
15. J.A. Henderson, R.W. Richards, J. Penfold, R.K. Thomas, *Acta Polymer*, **44**, 184, (1993).
16. R.H.G Brinkhuis, A.J. Schouten, *Macromolecules*, **24**, 1487, (1991).
17. D. Poupinet, R. Vilanove, F. Rondelez., *Macromolecules*, **24**, 1496, (1989).
18. T.L. Crowley, *Physica A*, **195**, 354, (1993).
19. J.A. Henderson, R.W. Richards, J. Penfold, J.R. Lu, R.K. Thomas, *Macromolecules*, **26**, 4591, (1993).
20. S.V. Alexander, *J. Phys (Paris),* **38**. 983, (1977).
21. P.G. de Gennes, *Macrmolecules*, **13**, 1069, (1990).
22. S.T. Milner, T.A. Witten, M.E. Cates, *Macromolecules*, **21**, 2610, (1988).
23. G.N. Malcom, J.S. Rowlinson, *Trans. Faraday soc.*, **53**, 921, (1957).
24. P.J. Flory, *Statistical Mechanics of Chain Molecules*, Interscience Publishers, (1969).
25. E.H. Lucassen-Reynders, J. Lucassen, *Adv. Colloid. Interf Sci.*, **2**, 347, (1969).

26. L. Kramer, *J. Chem. Phys*, **55**, 2097, (1971).
27. R.W. Richards, M.R. Taylor, *J. Chem. Soc. Faraday Trans*, **92**, 601, (1996).
28. Y. Kambe, C. Honda, *Polymer Com.*, **24**, 208, (1983).
29. For a discussion of this model see: *Introduction to Polymer Physics*, M. Doi, Oxford, (1996).
30. A.B. Pippard, *The Physics of Vibration*, Vol 1, 379 - 381, Cambridge University Press, (1978).
31. For a discussion of the Marangoni effect see: L.E. Scriven, C.V. Sternling, *Nature*, **187**, 186, (1960).
32. X.L.Chu, M.G. Velarde, *PhysicoChem Hyrodynamics*, **10**, 72, (1988).
33. J.C Earnshaw, E. McCoo, *Langmuir*, **11**, 1087, (1995).
34. J.C. Earnshaw, D. J. Sharpe, *J. Chem Soc. Faraday Trans*, **92**, 611, (1996).
35. M. Hennenberg, X.L. Chu, A. Sanfield, M.G. Velarde, *J. Colloid Interf Sci.*, **150**, 7, (1992).
36. R.W. Richards, M.R. Taylor, unpublished results.
37. For polymers see: Ferry, *Viscoelastic Properties of Polymers*, Wiley,(1970).
38. J.C. Earnshaw, R.C. McGivern. P.J. Winch, *J. Phys. France*, **49**, 1271, (1988).
39. J.C. Earnshaw, A.C. McLaughlin, *Proc. R. Soc. Lond. A*, **433**, 663, (1991).
40. J.C. Earnshaw, A.C. McLaughlin, *Proc. R. Soc. Lond. A*, **440**, 519, (1993).
41. C.J. Hughes, J.C. Earnshaw, *Phys. Rev, E*, **47**, 3485, (1993).
42. R.W. Richards, M.R. Taylor, In preparation.
43. J.C. Earnshaw, A.C. McLauglin, Progr. *Colloid Polym. Sci.*, **79**, 155, (1988).
44. J.L.Jones, R.W.Richards, Unpublished results.
45. M.S. Kent, L.T. Lee, B.J. Factor, F. Rondelez, G.S. Smith, *J. Chem. Phys.*,**103**, 2320 (1995).

Chapter Five

Films of poly(methyl methacrylate) spread on PEO solution

Section 5.1 Introduction and Background

Although the monolayer behaviour of PMMA[1] and PEO[2] at the air water interface has been extensively studied there have been few studies of the effects of having both polymers at the interface. Those studies which have been reported have invariably involved copolymers, for example the graft copolymer whose behaviour has been reported in Chapter 4 and a recent study of a diblock copolymer.[3] The system which falls between the two extremes of the separate homopolymer films and the complex copolymers is one where both homopolymers are present at the surface but are not chemically linked, i.e. some kind of mixture. It is known that as well as forming a stable spread monolayer[4] when in aqueous solution PEO, having a lower surface energy than water, adsorbs at the surface to form a surface excess.[5] In contrast PMMA is insoluble and hydrophobic and only forms a monolayer when spread from solution. In this chapter the behaviour of the system where PEO has absorbed at the air water interface and PMMA is subsequently spread on to the surface, is considered.

As well as providing a useful comparison to the behaviour of the copolymers this study complements the small, but increasing, body of work in which the behaviour of monolayers spread on solutions has been reported. At this stage there are few, if any studies, of the behaviour of polymer films spread on polymer containing solutions. The bulk of the work in which polymers have been spread on solutions, rather than water, has so far involved low molecular weight solutes. The earliest of such work involved spreading poly(methyl vinyl ether) onto electrolyte solutions.[6,7] The aim of such experiments was to investigate any modifications to the polymer - subphase interactions and to correlate these to interactions between the subphase and the ions.

Recently Langevin has reported a study of a polymer films, poly(dimethyl siloxane), PDMS,[8,9] spread on various non ionic surfactant solutions. These particular systems are of interest as they have applications in commercial antifoaming and defoaming agents. The behaviour of this system was studied by means of surface pressure, capillary wave and ellipsometry experiments. It was found that whilst the PDMS spread on the surfactant solutions the ease with which it did so was correlated to the concentration of the solution. The more concentrated the surfactant solution the

more easily the film was observed to spread. It was suggested that this behaviour was correlated to the surface being more hydrophobic where there is a surface excess of surfactant. PDMS spreads more easily on a hydrophobic surface as it does not need to modify its chain configuration so radically as when spread on hydrophilic substrate.

As mentioned those studies where the solute has been polymeric, even if the monolayer is non polymeric, are relatively few. Motivated by a growing interest in the fabrication of Langmuir - Blodgett films incorporating polymeric layers Miyano et al[10] have reported work where such a film was formed as a polymer adsorbed from solution onto a pre-spread monolayer. The polymer of interest was potassium poly(styrene sulphonate) which adsorbed onto a monolayer of cationic amphiphiles, dioctadecyldimethylammonium bromide, DOABr. By application of attenuated total reflection this provided the first in situ measurement of polymer adsorption onto a Langmuir film. This general field of polymers adsorbing onto preformed monolayers appears to be continuing to attract interest. Charron et al[11] recently reported work in which the adsorption of a poly(styrene) poly(ethylene oxide), PS - PEO, diblock onto a lipid monolayer was studied. They demonstrated that the polymer adsorbs driving the lipid monolayer from the liquid expanded to the liquid condensed phase, essentially equivalent to mechanical compression of the monolayer. It appears that adsorption of the PS - PEO diblock caused nucleation of condensed domains. The extent of adsorption was considerable and the surface concentration appeared indistinguishable from that adsorbed from solution in the absence of a monolayer. In contrast, and in agreement with the proposed hypothesis for behaviour, no adsorption was observed where the monolayers were already in the liquid condensed phase.

From the increasing body of literature on these 'mixed' systems this is clearly an area of increasing interest. Such systems not only offer novel behaviour but are also anticipated to be of more direct relevance to the multicomponent systems which are of commercial importance.

The system of current interest is that of PMMA spread on solutions of PEO. To characterise the behaviour of this system three techniques have been used. The classic measurement was that of the surface pressure isotherm. Although experimentally the least demanding of the techniques used the surface pressure isotherm is very informative, containing information from which details regarding

structural organisation may be inferred. In addition this provides a simple comparison to the behaviour of the simple single component systems to establish whether the behaviour of the spread film differs significantly from that on water. Detailed information regarding film structure can be obtained using neutron reflectivity. This technique has been applied and, in principle, enables the number density distribution of species at the interface to be determined. By application of SQELS, information regarding the interfacial dynamics of the film is provided. In addition this technique can provide information regarding film structure which, as opposed to neutron reflectivity, may contain information regarding in plane properties The results of these experiments are presented and discussed in the following chapter.

Section 5.2 Materials

All the polymers used in this work were synthesised by F. T. Kiff. Brief details of the synthetic procedure are included for completeness.

The following abbreviations are used:

hPMMA	hydrogenous poly(methyl methacrylate)
dPMMA	perdeuterated poly(methyl methacrylate)
hPEO	hydrogenous poly(ethylene oxide)
dPEO	perdeuterated poly(ethylene oxide)

Generally where the terms PMMA and PEO are used without a prefix the hydrogenous version is referred to.

5.2.1 Poly(methyl methacrylate)

Both perdeuterated and hydrogenous syndiotactic poly(methyl methacrylate) were prepared in tetrahydrofuran (THF) solution at 195K using fluorenyl lithium as initiator. Addition of degassed methanol terminated the reaction. The product was purified by precipitation and dried under vacuum.

5.2.2 Poly(ethylene oxide)

The samples of poly(ethylene oxide) were prepared from the appropriate purified monomer at 340K using THF as a solvent and diphenyl methyl potassium as initiator. The reaction was terminated using ethanoic acid and the product precipitated into hexane and dried under vacuum.

5.2.3 Characterisation

The polymers were characterised using proton NMR and chloroform SEC using polystyrene standards. The molecular weights are given in Table 5.2.1.

Polymer	Code	M_w / g mol^{-1}	M_w/M_n
hPEO	TK62	89600	1.06
dPEO	TK222	83700	1.20
dPEO	TK223	86000	1.17
dPMMA	TK26	110600	1.21
hPMMA	TK76	121000	1.35

Table 5.2.1: Molecular weights of the polymers used in this work.

The behaviour of spread PMMA films on PEO solution has been studied using surface pressure isotherms, neutron reflectivity and SQELS. In all these experiments the same samples of hPMMA and hPEO were used, likewise in the neutron study the same sample of dPMMA, was used throughout. Two samples of dPEO were used in the reflectivity work. Initially TK222 was used however, for the final reflectivity experiment a different sample of dPEO, TK223, was used, there being insufficient of the original sample to complete the work. The molecular weights of the two samples are very similar, see Table 5.2.1, and are above the critical value at which monolayer properties lose their dependence on molecular weight. It follows that the use of different polymer samples should not pose any problems or influence the behaviour of the system.

NB: Throughout this Chapter where the symbol Γ_s is used the surface concentration of PMMA is implied.

Section 5.3 Surface Pressure Measurements

5.3.1 Introduction

In this Section experiments to investigate the properties of PMMA films spread on a 0.1 wt.% aqueous solution of PEO using surface pressure measurements are detailed.

It is important to know how the properties of both spread and adsorbed films vary with time. Film stability will be an important issue in the current study and in any subsequent applications where it is likely to be the long term properties of the film which are exploited. In the current context it is essential for both neutron reflectivity and SQELS experiments that the nature of the film and any possible changes with time are understood. With these issues in mind the relaxation behaviour of three fixed surface concentration films of 1 mg m^{-2}, 2 mg m^{-2} and 3 mg m^{-2} of PMMA has been studied by monitoring the surface pressure as a function of time.

5.3.2 Experimental

5.3.2.1 Surface Pressure Isotherms

The surface pressure isotherms for PMMA spread on a 0.1 wt.%. solution of PEO were recorded using a Nima trough and Wilhelmy plate technique which has been described earlier. Attempts to use the small rectangular Nima trough to reduce the volume of PEO solution used were unsuccessful. On compression the film became so stiff that the Wilhelmy plate was displaced in the direction of the single barrier movement. Typically the displacement was such that the plate became inclined at more than 10° to the vertical. In contrast the large circular Nima trough has two barriers which close symmetrically exerting an equal force either side of the plate and no further problems were encountered.

The same method was always used to prepare the PEO solution before the PMMA film was spread. The solution was carefully poured into the clean Langmuir trough and the surface swept and briefly aspirated to remove any surface

contamination. The barriers were then opened and the solution left for 10 minutes to come to equilibrium. Prior to recording the surface pressure isotherm the surface tension of the PEO solution was always measured using the Wilhelmy plate. The plate was zeroed in the solution and then removed, the resultant pressure reading gave the surface tension. This procedure was repeated ten times and the measured values averaged.

5.3.2.2 Relaxation Behaviour

The relaxation behaviour of three fixed surface concentration films of PMMA was studied, these being 1 mg m^{-2}, 2 mg m^{-2} and 3 mg m^{-2}. The difference in this approach to that used when recording the isotherms was that exactly the required amount of PMMA was spread over the entire surface area to achieve each surface concentration without using compression. This avoids having two different surfaces in the system, i.e. bare PEO solution and PMMA covered PEO solution, which could lead to complications due to preferential adsorption.

5.3.3 Results

The surface tension of the PEO solution was found to be 63.6 ± 0.2 mN m^{-1}.

5.3.3.1 Surface Pressure - Surface Concentration Isotherms

The surface pressure - surface concentration isotherm obtained for PMMA spread on a 0.1 wt.% solution of PEO is given in figure 5.3.1. The isotherm was found to be entirely reproducible over the concentration range 0 to 2 mg m^{-2}, whereas to reproduce the behaviour over the surface concentration range 2 to 4 mg m^{-2} was more difficult and considerable care was required. This is believed to be due to various phenomenon which are not entirely reproducible, such as relaxation processes which, as will be discussed, are most significant for high surface concentrations of PMMA. Other non reproducible effects which may influence film behaviour are

surface contamination and local deformations of the films. The surface pressure isotherm was found to be independent of the isotopic composition of the polymer.

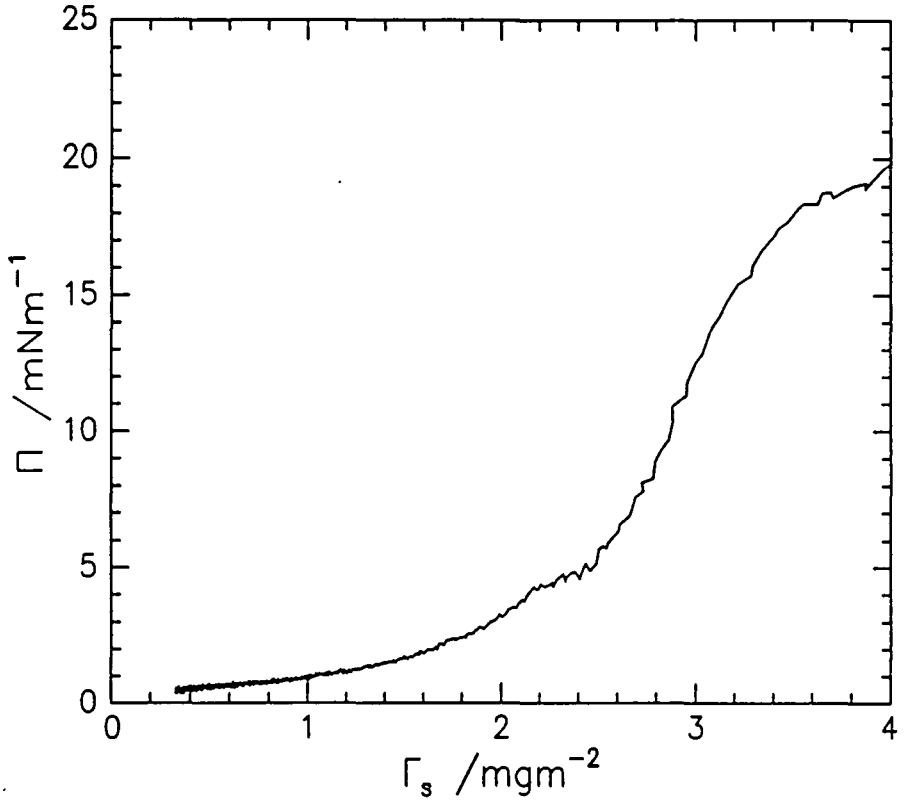

Figure 5.3.1 Surface Pressure Isotherm for PMMA spread on PEO solution

5.3.3.2 Relaxation Study

The surface pressure for a 1 mg m^{-2} film of PMMA on PEO solution did not exhibit any systematic change in the surface pressure. Over the entire duration of the experiments the surface pressure changed by only 0.2 mN m^{-1}. In contrast both the 2 mg m^{-2} and 3 mg m^{-2} films exhibit relaxation behaviour, see figure 5.3.2. Both films display a pseudo exponential relaxation over the first 40 to 50 minutes, thereafter the surface pressure is stable.

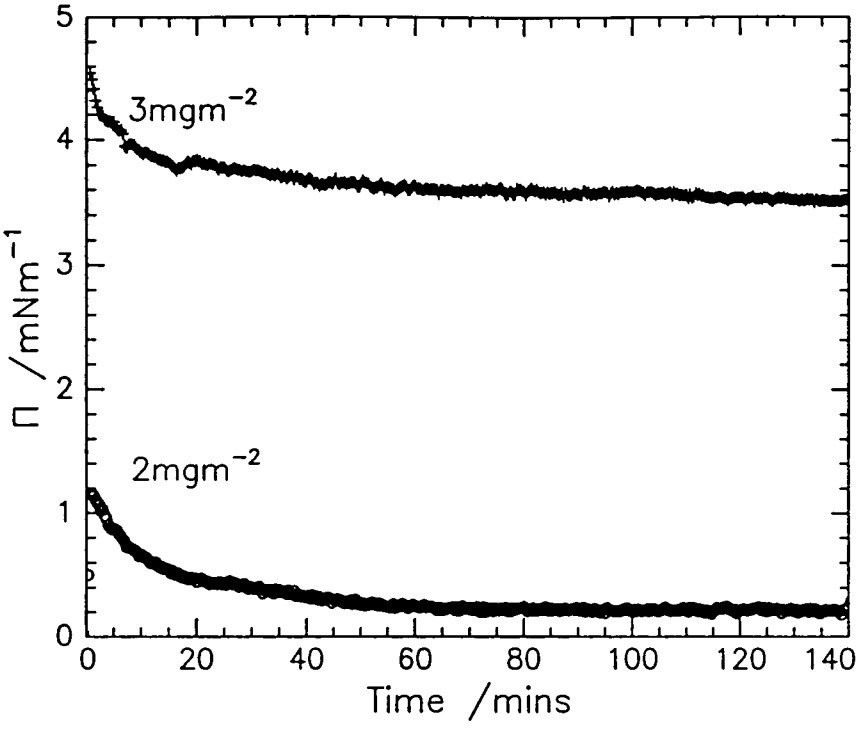

Figure 5.3.2 Relaxation in the surface pressure over time 2 mg m^{-2} and 3 mg m^{-2} PMMA on PEO solution.

5.3.4 Discussion

It was observed that the surface tension of the PEO solution was perfectly stable after only a few minutes, indicating that the system had come to equilibrium and a complete film had been formed. Although this observation is contrary to an early study of PEO solutions by Glass[5] it is in agreement with results reported by Lu et al[12]. This group attributed the discrepancies to the polydispersity of the samples studied by Glass.

Having established that a complete adsorbed layer of PEO was present prior to spreading the PMMA film the behaviour of the system when the PMMA is spread on the solution is now discussed in detail. Initially the surface pressure isotherm is compared to that of PMMA on water and for this reason the two isotherms are overlaid in figure 5.3.3.

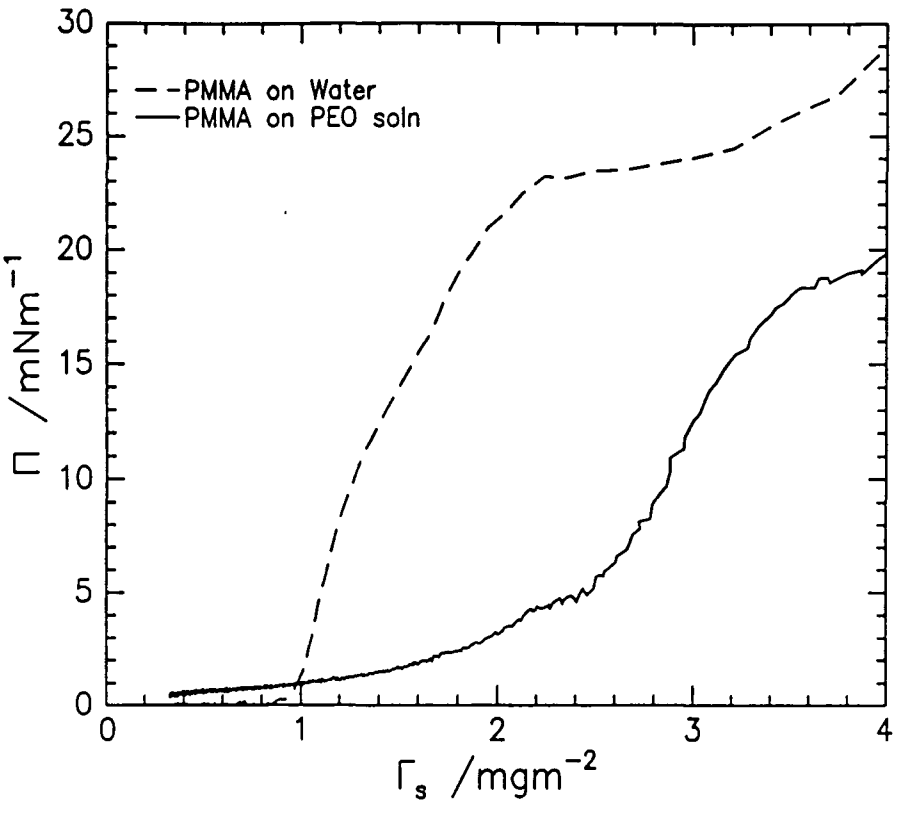

Figure 5.3.3 Surface Pressure for PMMA on water and PMMA on PEO solution.

It is clear from figure 5.3.3 that the characteristics of the surface pressure variation with Γ_s are very different for the two subphases. The surface pressure exhibited by a film of PMMA on water is negligible until an abrupt increase when a surface concentration of 1 mg m^{-2} is reached. There is analogous behaviour when the subphase contains PEO and the surface pressure increases gradually with surface concentration up to 2.5 mg m^{-2}. Thereafter Π increases more rapidly before reaching a plateau at 3.5 mg m^{-2}. The surface pressure for PMMA on water also reaches a plateau value, but the onset is at a lower surface concentration of approximately 2 mg m^{-2}.

The negligible surface pressure exhibited by a dilute, $\Gamma_s < 1$ mg m^{-2}, film of PMMA has been attributed to the presence of a non homogeneous film. Experimental evidence[13] suggests that at surface concentrations below 1 mg m^{-2} PMMA exists as islands on the water surface. The rapid increase in surface pressure above this surface concentration is associated with the formation of a homogeneous, condensed monolayer with strong lateral interactions. In the case of syndiotactic PMMA[14] this behaviour is associated with the sideways alignment of ester groups which is possible

at the water surface. Due to this alignment the dipolar interactions between the ester groups, which are not shielded by the water, contribute to the lateral forces in the monolayer.

The surface pressure for the film of PMMA on PEO solution increases gradually up to relatively high concentrations of 2 mg m^{-2}. This implies that there is a very different PMMA - subphase interaction and, quite possibly, different in plane structures in this situation. Clearly the film does not become as stiff as PMMA on water despite reaching surface concentrations where one would anticipate that the chains would be interacting strongly. This indicates that the lateral forces in the film are weaker than for PMMA on water. Such behaviour may be due to different alignment of the ester groups at the surface or, may be associated with other species, i.e. PEO, becoming incorporated in the film and weakening the interactions between the PMMA chains. Whatever the origin of these effects the results clearly indicate that the surface organisation adopted by the PMMA is very different when spread on a solution of PEO as opposed to a water subphase.

At this stage there are two approaches which may provide some information, albeit indirectly, on the structure adopted by the PMMA. Consider first the concept of the limiting area per segment. It is conventional to extrapolate the close packed region of the isotherm to zero pressure to determined a close packed, i.e. minimum, area per molecule. It has been argued[15] that the close packed area per molecule for polymers may be somewhat questionable because chain segments may coil or desorb on compression. Despite these possible effects it is considered of use to compare the values found for PMMA on water and PMMA on PEO solution.

The limiting area per molecule has been calculated from the isotherm, the values are given in Table 5.3.1 below.

System	Limiting Γ_s / mg m^{-2}	Limiting area per monomer / $Å^2$
PMMA	0.98 ± 0.02	17 ± 1
PMMA on PEO soln.	2.21 ± 0.03	8 ± 1

Table 5.3.1: Limiting surface concentration and area for PMMA films.

The limiting surface area is less for PMMA on PEO solution than for PMMA on water. This implies that the chains pack together to form a more compact film in the presence of the PEO. At the simplest level this could be interpreted by considering the limiting area as being controlled by the interactions between molecules on the surface. In the presence of just water the intermolecular interactions, which are contributed to by the dipolar interactions between the ester groups, are such that the molecules occupy a minimum of 17 $Å^2$. Since the minimum area falls in the presence of PEO this indicates that the interactions between the molecules are smaller and the chains can pack more tightly. It is conceivable that incorporation of PEO into the PMMA film could have such an effect if the chains were uniformly distributed in the interfacial layer hindering, and therefore disrupting, the interactions between the PMMA chains. This scenario is in agreement with the surface pressure isotherm which indicates reduced lateral interactions for PMMA spread on PEO solution over the entire surface concentration range.

It is instructive to consider how the surface tension of PMMA on PEO solution compares to the surface tension on water. Equation 5.3.1 can be applied to the surface pressure measurements and used to extract the surface tension for various film concentrations:

$$\Pi = \gamma_{sub} - \gamma_{oST}$$

Equation 5.3.1

where γ_{sub} is the surface tension of the bare subphase and γ_{oST} is the surface tension of the film covered subphase.

For water γ_{sub} = 72.3 mN m^{-1} at 296 K,[16] for the PEO solution γ_{sub} was determined to be 63.6 ± 0.2 mN m^{-1}. The surface tension for both PMMA on water, $\gamma_{water\text{-}PMMA}$, and PMMA on PEO solution, $\gamma_{PEO\text{-}PMMA}$, has been calculated at three surface concentrations of PMMA, 1 mg m^{-2}, 2 mg m^{-2} and 3 mg m^{-2}, see Table 5.3.2.

Γ_s / mg m^{-2}	Π / mN m^{-1}	$\gamma_{water-PMMA}$ / mN m^{-1}	Π / mN m^{-1}	$\gamma_{PEO-PMMA}$ / mN m^{-1}
1	1	71 ± 1	1	63 ± 1
2	20	51 ± 1	3	61 ± 1
3	23	48 ± 1	14	50 ± 1

Table 5.3.2: Surface Tensions for PMMA / water and PMMA / PEO at fixed Γ_s.

From the definition of surface tension it follows that the higher the surface tension of a material the more work is required to create a surface and the higher the energy of the molecules at that surface. Poly(ethylene oxide) molecules have a lower surface energy than water and so adsorb at the surface, reducing the surface tension of the system from approximately 72 mN m^{-1} to 64 mN m^{-1}. It is implicitly assumed in the calculation of the values in Table 5.3.2 that despite the presence of the PMMA film the surface excess of PEO remains constant over the course of the experiment. Basically this assumption means that for the PEO solution γ_{sub} is constant at 63.6 mN m^{-1} which may not necessarily be true. As the surface concentration of PMMA increases the balance of interactions at the surface may change, for example the PMMA may reduce the surface tension of the water to the same extent as the adsorption of PEO. In this situation there would no longer be a driving force favouring adsorption of the PEO. Since the PEO is already adsorbed before the PMMA is spread it is not clear how the system would react. Depending on the balance of forces there may be some desorption on standing, although the timescale of such effects is unknown. The other feasible alternative available to reduce the surface tension in the system is additional adsorption of PEO. If either of these processes occur the assumption of constant γ_{sub} may be a serious error. However, at this stage it is only by making such an assumption that any discussion regarding the variation in the surface pressure can be attempted.

The surface tension in the presence of a 1 mg m^{-2} film of PMMA on water is 71 mN m^{-1} whereas the equivalent film on a PEO solution has a surface tension of 63 mN m^{-1}. Given that the surface tensions of the two systems are so different it seems reasonable to suggest that there are very different interactions between the subphases

and the PMMA. Since the system with the lowest surface tension is PMMA on PEO solution it is assumed that the surface excess of PEO will be maintained at the same surface concentration. Subject to molecular rearrangements and reorientations the composition of the interfacial layer, as comprised of PEO, PMMA and water, is expected to be stable.

In contrast for a 2 mg m^{-2} film of PMMA the surface pressure is greater for a water subphase than for the PEO solution, being 20 mN m^{-1} as opposed to 3 mN m^{-1}. Correspondingly the surface tension is lowest for the water subphase being 51 mN m^{-1} rather than 61 mN m^{-1}. This indicates that, at this surface concentration, PMMA interacts more favourably with an aqueous subphase than with PEO solution. From consideration of surface tension arguments alone it is possible to suggest that, on standing, with this surface concentration of PMMA spread on the solution the surface concentration of PEO would change. In the extreme, desorption of PEO could lead to a surface layer where the concentration of PEO is depleted relative to that in the bulk solution. The interactions between the spread film and subphase would then become essentially the same as those for PMMA on water. Alternatively if PEO adsorbs to reduce the surface tension a PEO rich region would be formed at the interface. Unfortunately with this experiment it is not possible to determine which process, if either, occurs. Desorption of PEO relies on the PMMA having sufficient mobility to modify its orientation from that adopted on a PEO solution to the optimum arrangement for water so that the reduction in surface tension can be achieved. Although in bulk the T_g of PMMA is ~ 378 K evidence suggests that for thin films T_g is depressed.[17] This effect may also be contributed to by incorporation of water into the layer, possibly having the effect of a plasticiser. It is anticipated that these effects will combine so that the PMMA is relatively mobile at the surface.

If the surface concentration of the PEO does change in some way anomalous behaviour may be observed in the surface pressure - time study. If one of the processes outlined above dominated there would be an associated decrease in the surface tension. However, due to the method of determining surface pressure the overall effect on the reading given by the pressure sensor is not transparent. As described in chapter 3 zeroing the pressure sensor whilst fully wetted by the subphase accounts for the net force acting downwards on the Wilhelmy plate. Any subsequent

reduction in the surface tension will mean that the downward force on the plate is less than assumed and there will be a residual upward force acting on the plate.

If PEO desorbs from the surface the surface tension of what constitutes the bare subphase, albeit theoretically, will either fall or remain constant. If the surface tension of the subphase falls this will offset the upward forces from 'real' reductions in the surface tension of the system due to the spread film. Depending on the balance of these effects the measured surface pressure may appear lower than the true value. Due to the effects outlined desorption of PEO may be accompanied by a decrease in the apparent surface pressure of a system on standing. Alternatively if the surface tension of the system is reduced by desorption of the PEO, and this is the dominant effect, the measured surface pressure will increase. It follows from the above that, due to the measurement technique, desorption of PEO may be associated with either an increase or decrease in the apparent surface pressure. Recent work[18] suggests that competitive desorption of polymers, a process analogous to that occurring here, occurs over long timescales. Initially the process occurs rapidly, over 40 - 60 minutes, in an exponential manner. Subsequently the desorption occurs much more slowly and may not be complete for a number of days, possibly weeks. It follows that considerations of the timescales of any changes in the surface pressure may be important in establishing the nature of the processes occurring in this system.

The surface pressure of both the 2 mg m^{-2} and 3 mg m^{-2} films is observed to decrease on standing, see figure 5.3.2. Initially one may think this is vindication of the effects discussed above whereby desorption of PEO can be rationalised with a decrease in the surface pressure. However, in the discussion above no attempt was made to consider other relaxation effects which may be relevant. To consider such effects it is instructive to refer back to the behaviour of syndiotactic PMMA on water at the same surface concentration. Henderson[19] found that a 2 mg m^{-2} film did demonstrate a relaxation occurring over approximately 25 minutes, a 3 mg m^{-2} film behaves likewise. This behaviour was attributed to the film becoming increasingly stiff on compression but having the ability to relax over time to reduce the energy of the system. The relaxation is associated with an increase in the surface tension of the system and must be driven by the relative energies of the different film conformations rather than surface tension requirements. For the same concentration films on a

solution of PEO the surface pressure was not stable until at least 40 minutes had passed. The origin of this relaxation is not obvious, there may be rearrangements in the film analogous to those for PMMA on water as well as desorption of the PEO.

Table 5.3.2 demonstrated that there may be a driving force for desorption of PEO when a 2 mg m^{-2} film of PMMA is spread on the surface of the solution. In contrast when a 3 mg m^{-2} film of PMMA is spread on either water or PEO solution the surface tension is the same. Despite this the results of the stability study show that both films demonstrate a significant relaxation. The relaxations occur in a pseudo exponential manner and are complete after about 40 - 50 minutes. Clearly, the timescale for the relaxation is rather longer than for PMMA on water. However, it is believed that this reflects the presence of the PEO in the surface which may hinder the reorientation of the PMMA chains. Otherwise the characteristics of the relaxation are akin to those for PMMA on water. Given this observation, and the lack of a strong driving force for desorption, it is suggested that the dominant cause of the observed relaxations is reorientation within the film.

To establish the true nature of the relaxation behaviour and how substantial any desorption, or even adsorption effects, are both neutron reflectometry and SQELS results are essential. SQELS experiments should give an absolute surface tension, albeit not the static value. This will help to determine whether the surface tension is constant during the relaxation of the film, indicating that the change in surface pressure is due changes in the 'subphase' surface tension as discussed. In addition neutron reflectometry provides information about the distribution of species at the interface and should reflect any desorption by showing an absence of PEO at the interface.

In the light of the evidence suggesting that rearrangement of the polymers may be an issue at high film concentrations it seems reasonable to suggest that the recorded surface pressure isotherm will represent a film in a non-equilibrium state. Given that recording a surface pressure isotherm takes 30 minutes it is possible that the surface organisation will not be constant over the duration of the experiment. Continuous measurement of the surface pressure isotherm for PMMA spread on a PEO solution clearly corresponds to a complex system. There will be both film covered and bare PEO solution leading to regions of different chemical potentials which may

complicate behaviour. These effects are anticipated to be most significant at high Γ_s, 2 mg m^{-2} and above, possibly explaining why the high surface concentration region of the isotherm tended not to be reproducible.

On comparing figures 5.3.1 and 5.3.2 it is observed that films spread at the required surface concentration gave lower surface pressures than would be expected from the measured surface pressure isotherm. This is attributed to rapid relaxations at short times. The delay between starting the experiment and spreading the film was typically about 30 s which, given the rapid fall in Π initially, may explain the discrepancy in the values. For films spread at the required surface concentration, covering the entire surface area, both the initial surface pressure and the subsequent relaxation behaviour could be reproduced.

Despite the discrepancies mentioned above the major conclusion deduced from the surface pressure isotherm, the fact that the properties of the PMMA film are severely influenced by the presence of the PEO in the subphase, still stands. As can be seen from the isotherm, figure 5.3.3, once Γ_s exceeded 1 mg m^{-2} the surface pressure for a continuously compressed film was lower than for the same concentration of PMMA on water. Fully relaxed films gave even lower surface pressures and there is therefore no evidence to suggest that films of PMMA spread at the required surface concentration onto a PEO solution bear any more resemblance to films of PMMA on water than continuously compressed films. The other factor influencing the surface pressure isotherms is the assumption of constant γ_{sub}. This has been discussed and it was argued that erroneously low surface pressures could result. Unfortunately there is no way of quantifying such effects, but given the large differences in surface pressure over most of the surface concentration range covered they are not likely to be significant.

5.3.5 Conclusion

It is clear from the surface pressure isotherms that the behaviour of PMMA when spread on PEO solutions is different to that when the subphase is clean water. It is likely that the behaviour and surface organisation adopted by the polymers,

particularly the PEO, will change with Γ_s although the specific details are not known. Although stable at low surface concentrations of PMMA at higher values, 2 mg m^{-2} and 3 mg m^{-2}, the films relax. Similar behaviour is exhibited by films of PMMA on water but they tend to relax rather more rapidly. The discrepancy is believed to be correlated to the presence of additional species, i.e. PEO, in the interfacial region. Consistent with the latter statement and from a consideration of area per segment, it seems likely that the PEO and PMMA mix at the interface. Such behaviour also accounts for the reduction in the cohesive forces in the film. Although this suggestion seems feasible and is consistent with behaviour at low Γ_s there may be significant changes in the surface organisation as the film is compressed further. These features will be addressed in more detail in later sections where different experimental techniques offer direct means of probing such behaviour.

Section 5.4 Neutron Reflectometry

5.4.1 Introduction

Neutron reflectivity has been used to study the interfacial structure of PMMA films spread on a 0.1 wt.% solution of PEO. Studies on two surface concentrations of PMMA, 1 mg m^{-2} and 3 mg m^{-2}, have been completed and are reported. A third study where Γ_s = 2 mg m^{-2} was not completed due to beam loss. A limited data set is available and has been included where relevant.

The reflectometry data reported was collected over a series of experiments using CRISP. A full set of deuterated polymers were available for this study and by using both D_2O and NRW subphases six contrasts were available, enabling the kinematic approximation to be used in the analysis. Model fitting using the optical matrix analysis has also been used to confirm the models indicated using the kinematic approximation.

Although the overall aim of the neutron reflectometry experiments was to determine the structure and composition of the interfacial layer formed when a film of PMMA is spread on a solution of PEO it was considered important to study the interfacial structure of adsorbed layers for a bare PEO solution initially. The reasons for this were twofold. First, it is important to know the interfacial structure of the solution before a film is spread so that any changes can be related back to the initial state. Second, the structure of adsorbed films of PEO has been studied and reported so this experiment also acted as a check to ensure that the PEO solutions were initially in the same state as those studied by other groups.[12] Given this fact any unusual features observed once the PMMA films were introduced would, unquestionably, be due to the introduction of this species.

Previously PMMA films up to 2 mg m^{-2} have been studied using neutron reflectometry. Thus while the structure of the low concentration, 1 mg m^{-2}, film on water had been elucidated there was no similar data available for a 3 mg m^{-2} film. With the aim of providing comparisons to PMMA on PEO solution this experiment has also been performed. By taking advantage of all the different isotopic combinations of polymer and subphase this data has been analysed using the kinematic approximation.

The data is presented in three separate sections. The results of the study of the PEO solution are presented and discussed first, then the 3 mg m^{-2} film of PMMA and finally the results for PMMA on PEO solution. Brief experimental details are provided in each section.

5.4.2 Neutron Reflectometry Study of 0.1 wt.% Solution of PEO

5.4.2.1 Experimental

Samples of both dPEO and hPEO were available for this study, it has already been established by other workers[12] that aqueous solutions of dPEO and hPEO exhibit the same behaviour. Solutions of dPEO in D_2O and NRW and hPEO in D_2O were prepared a day before the reflectivity experiment. By collecting the reflectivity profiles for each of these solutions of differing isotopic content the full kinematic approximation could be applied to analysis of the data.

In an attempt to minimise the amount of deuterated chemicals used small troughs with a volume of approximately 100 ml were used in this experiment. These troughs were mounted on a sample changer and are available at the Rutherford Appleton Lab. The troughs were fabricated from PTFE but did not have any barriers and so can only be used for studying films adsorbing from solution.

5.4.2.2 Results

The reflectivity profiles for hPEO / D_2O and dPEO / D_2O are presented in figures 5.4.1 and 5.4.2. The reflectivity falls off very rapidly with increasing Q and by 0.25 $Å^{-1}$ the signal is within the background. The reflectivity for D_2O is overlaid and is higher than for the solution of hPEO. This is consistent with a species of low scattering length density adsorbing at the interface. In contrast the reflectivity for the dPEO solution is comparable, in fact almost identical, to D_2O. This is a symptom of the fact that dPEO and D_2O have similar scattering length densities, 6.32×10^{-6} $Å^{-2}$ and 6.35×10^{-6} $Å^{-2}$ respectively.

The reflectivity for the dPEO / NRW solution is very much lower than for the D_2O contrasts where the reflectivity is driven by the D_2O. When the subphase is NRW the only contribution to the reflectivity will come from the adsorbed polymer. For this system the reflectivity falls off rather slowly as Q increases, characteristic of a diffuse layer.

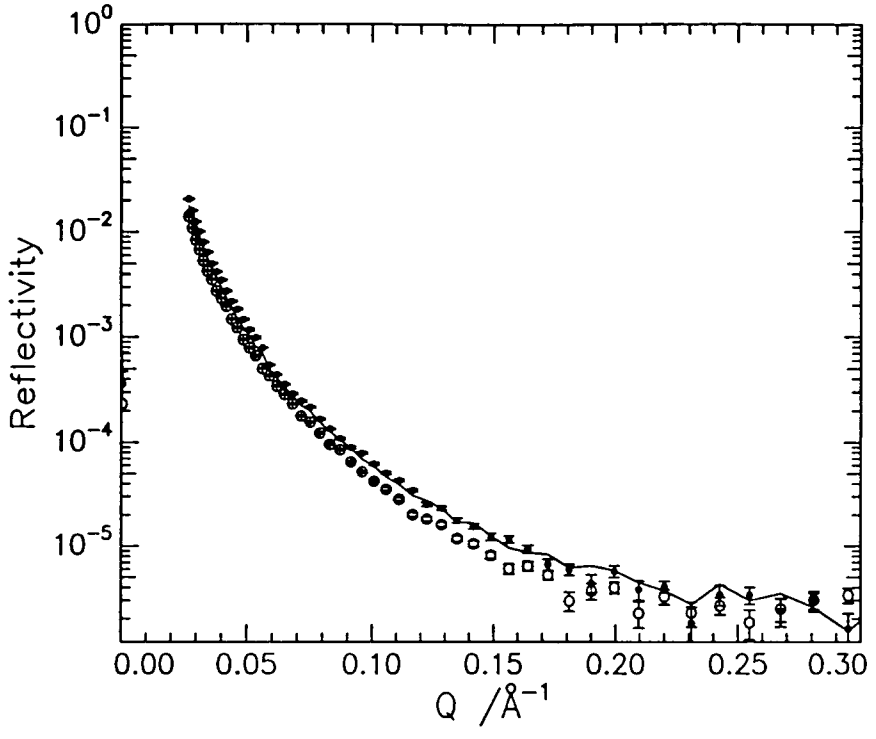

Figure 5.4.1 Reflectivity profiles for dPEO / D_2O, crosses, hPEO / D_2O, circles overlaid with that for D_2O.

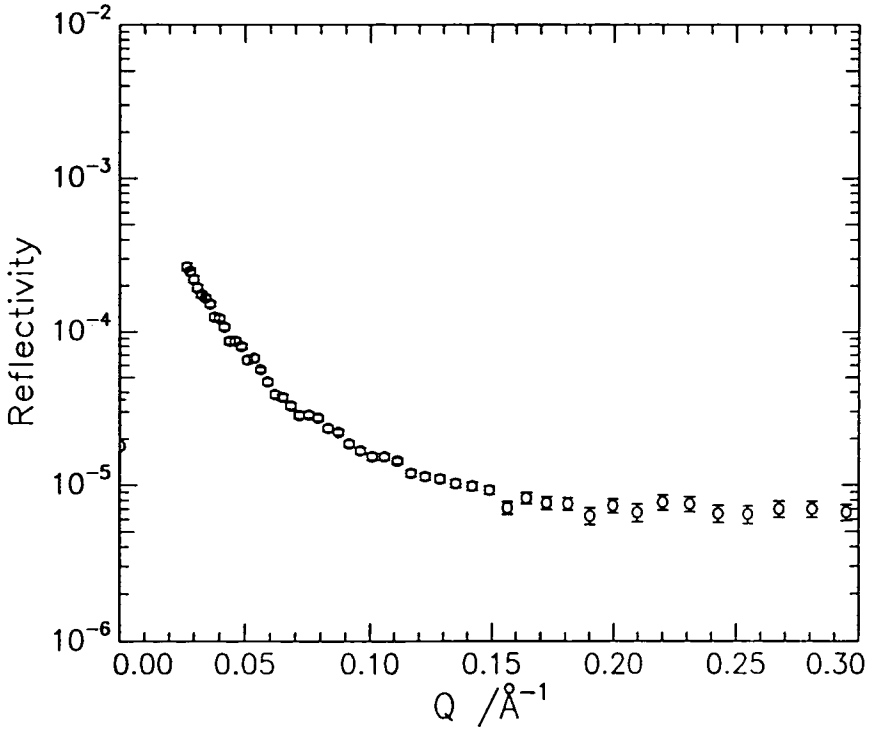

Figure 5.4.2 Reflectivity profile for dPEO / NRW.

5.4.2.3 The Kinematic Approximation Analysis

The structure of adsorbed layers of PEO has been established by Lu et al,[12] relying mainly on direct fitting techniques. Given these results, and since this study was only completed to form a base for discussion of PMMA on PEO solution, only the results of a kinematic analysis are reported here. It is noted that model fitting has been applied to this data and gave results consistent with those reported.

The kinematic approximation[20] is a highly informative way of interpreting neutron reflectometry data and will be used heavily both in this and subsequent sections. A full analysis of reflectivity data using this method relies on all the components in the system being deuterated selectively. In this system the components of interest are the water and PEO, both of which were available in different isotopic forms. In this method, which has already been discussed, the reflectivity profiles for each contrast are used to solve simultaneous equations at each Q to extract both the self and cross partial structure factors, $h_{ii}(Q)$ and $h_{ij}(Q)$ respectively. These are related to the reflectivity via:

$$R(Q) = \frac{16\pi^2}{Q^2}\left[b_1^2 h_1(Q) + b_2^2 h_2(Q) + 2b_1 b_2 h_{12}(Q)\right]$$

Equation 5.4.1

The self partial structure factors depend on the distribution of the different species at the interface, the cross terms depend on the relative positions of these distributions. Models are invoked to describe the distribution of each species at the interface. These are fitted to the experimentally determined partial structure factors to yield the parameters characterising the distributions. The cross term can also be fitted to give information regarding the separation of the distributions.

The self partial structure factors for PEO and water and the cross partial structure factor for PEO / water are considered over the Q range 0 - 0.2 $Å^{-1}$. A restricted range of Q is presented because at Q values above 0.20 $Å^{-1}$ the reflectivity falls to such a level that the coherent signal is lost in the background.

5.4.2.3A PEO Self Partial Structure Factor

There are two generally accepted models for the distribution of species spread or adsorbed at an interface. These are the uniform layer model and the Gaussian distribution. These models imply quite different distributions of the species at the interface. The uniform layer model represents a single block of the species whereas in the Gaussian model the layer is much more diffuse and the number density changes gradually. The differences are schematically illustrated in figure 5.4.3 where two such number density profiles are overlaid.

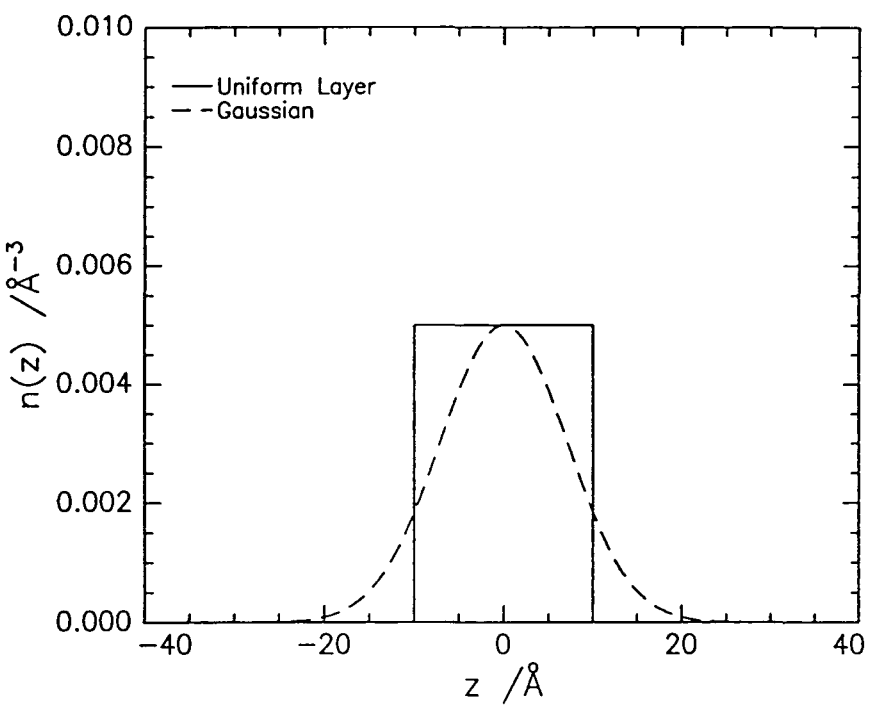

Figure 5.4.3 Number density profile for a uniform layer d= 20 Å, $n_{pl} = 0.5 \times 10^{-2}$ Å^{-3} and a Gaussian distribution, $\sigma = 20$ Å and $n_{pl} = 0.5 \times 10^{-2}$ Å^{-3}.

For a uniform layer of thickness d and number density n_{pl}

$$n_p(z) = n_{pl} \qquad -d/2 < z < d/2$$

$$n_p(z) = 0 \qquad \text{all other } z$$

Equation 5.4.2

For a Gaussian distribution where σ is the full width at n_{pl}/e

$$n_p(z) = n_{pl} \exp(-4z^2/\sigma^2)$$

Equation 5.4.3

The uniform layer model is considered initially. The expression for n(Q) is obtained by Fourier transformation of n(z). The partial structure factor, $h_{ii}(Q)$, is given by:

$$Q^2 h_{pp}(Q) = 4n_{pl}^2 \sin^2(Qd/2)$$

Equation 5.4.4

This function has been fitted to the data using a non linear least squares fitting routine with d and n_{pl} as variables, starting from initial values which are input by the user. The result of the fit is given in figure 5.4.4 and clearly the experimental self partial structure factor is fitted well by this model. The parameters of the fit are given in Table 5.4.1.

Model	n_{pl} / 10^{-2} Å^{-3}	**d / Å**	χ^2 / 10^{-11}
Uniform Layer	0.34 ± 0.01	20.13 ± 0.28	0.3628
Model	n_{pl} / 10^{-2} Å^{-3}	σ / Å	χ^2 / 10^{-11}
Gaussian Layer	0.44 ± 0.01	17.71 ± 0.29	0.3794

Table 5.4.1: Parameters of the fits to the PEO self partial structure factor

The alternative and, rather more realistic model, is that of a Gaussian distribution of species at the interface. In this model the self partial structure is given by:

$$Q^2 h_{ii}(Q) = \frac{n_{pl}^2 \pi Q^2 \sigma^2}{4} \exp(-Q^2\sigma^2/8)$$

Equation 5.4.5

Equation 5.4.5 has also been fitted to the experimental self partial structure factor using n_{pl} and σ as variables, see figure 5.4.4. Comparing the fits and values of χ^2 returned by the fitting routine* shows that there is little to chose between the two models, see Table 5.4.1. This observation is symptomatic of the fact that over the Q range accessible it is very difficult to differentiate between a Gaussian and uniform layer distribution. This is illustrated by putting the fitted parameters back into equations 5.4.4 and 5.4.5 and comparing the results, see figure 5.4.5. The models cannot be distinguished until Q values above 0.2 Å^{-1}. Due to these

* $\chi^2 = \sum_{0}^{npts} (y_{exp} - y_{fit})^2$ which is not the true statistical definition of chi squared.

effects it is often difficult to distinguish which model describes a particular system best. It is possible to calculate the surface concentration from the extracted parameters and this may help in deciding which model to adopt. The parameters defining the distributions can be related to the surface concentration and for a uniform layer give:

$$\Gamma = \frac{n_{pl}d}{N_A} M_i \times 10^{23} \text{ mg m}^{-2}$$

Equation 5.4.6

where M_i is the molar weight of a segment and N_A is Avogadro's number.

Whereas for a Gaussian layer:

$$\Gamma = \frac{\sigma n_{pl} \pi^{0.5} M_i}{2N_A} \times 10^{23} \text{ mg m}^{-2}$$

Equation 5.4.7

In reality these equations are generally only of use if the surface concentration of the species of interest is known. Although this is the case for spread films the problem is not trivial for adsorbed films. In the current study it is found that the parameters for a uniform layer indicate a surface concentration in the range 0.53 - 0.56 mg m^{-2} whereas the Gaussian model indicates a concentration in the range 0.54 - 0.56 mg m^{-2}, i.e. both models indicate basically the same surface concentration of PEO. Given the similarities between both the quality of the fit and the extracted surface concentrations the choice of which model to adopt to describe the distribution of PEO becomes rather subjective. Intuitively a Gaussian distribution of adsorbed species seems physically more realistic than a uniform layer, where the system is modelled as a slab of adsorbed polymer at the interface. Given such considerations a Gaussian distribution of PEO at the interface is the accepted model.

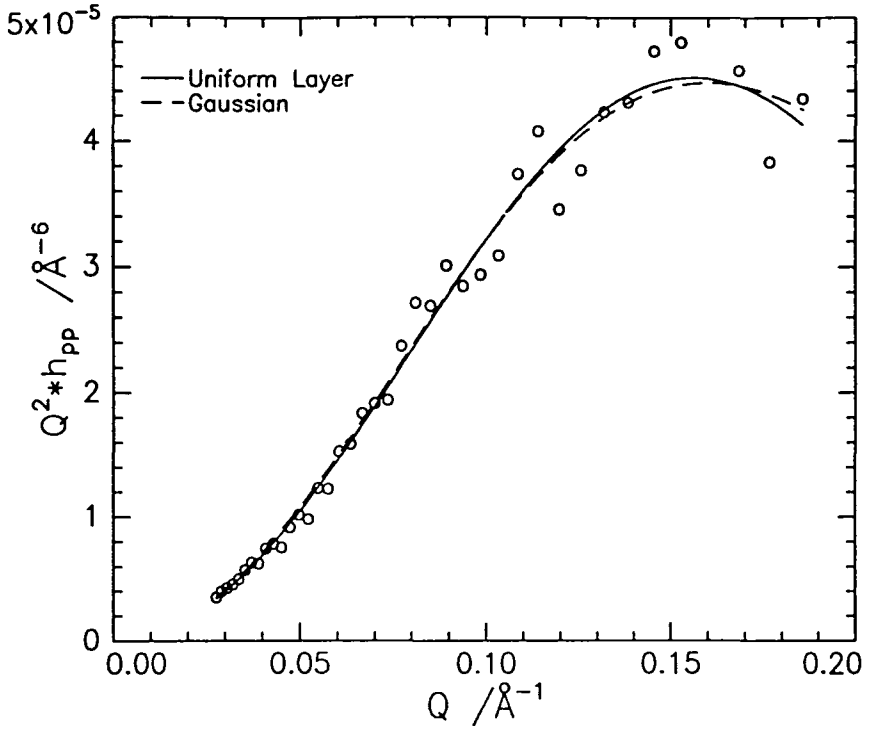

Figure 5.4.4 PEO self partial structure factor with the best uniform layer and Gaussian fit overlaid.

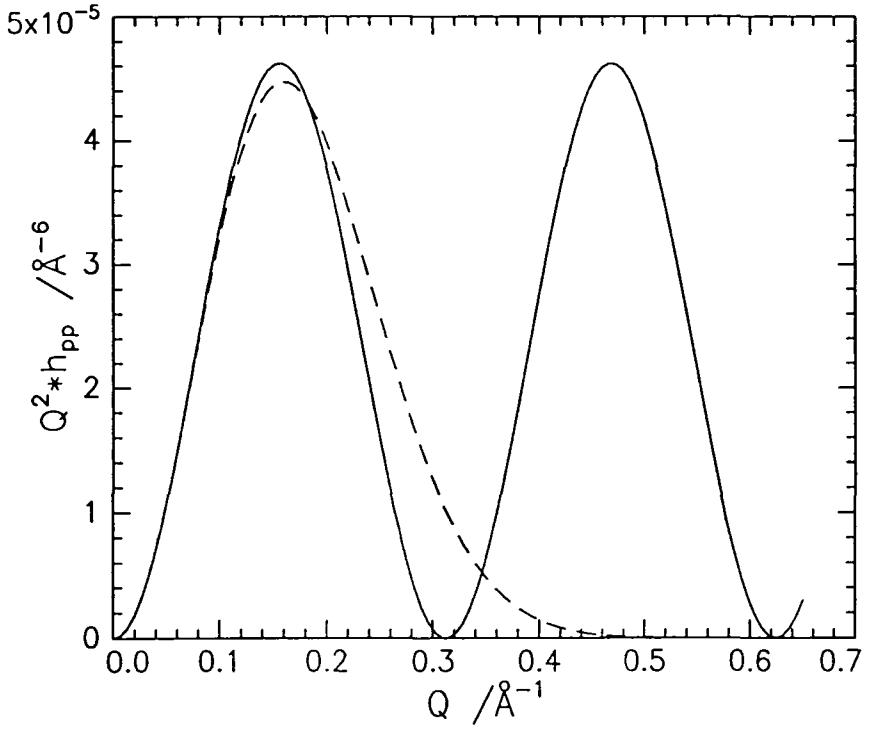

Figure 5.4.5 Generated self partial structure factors for a Gaussian distribution, solid line, and a uniform layer model, broken line. See text for further details.

5.4.2.3B The Water Partial Structure Factor

To describe the distribution of water a function is required which allows the number density to be zero away from the water, and the bulk number density of water, n_{wo}, at sufficient depths. Such models include a uniform layer where a slab is modelled in which the number density of the interfacial water layer differs from that of the bulk. Another useful function is that of a hyperbolic tangent. In this model the number density of water increases gradually to that of bulk water. The two profiles are schematically represented in figure 5.4.6.

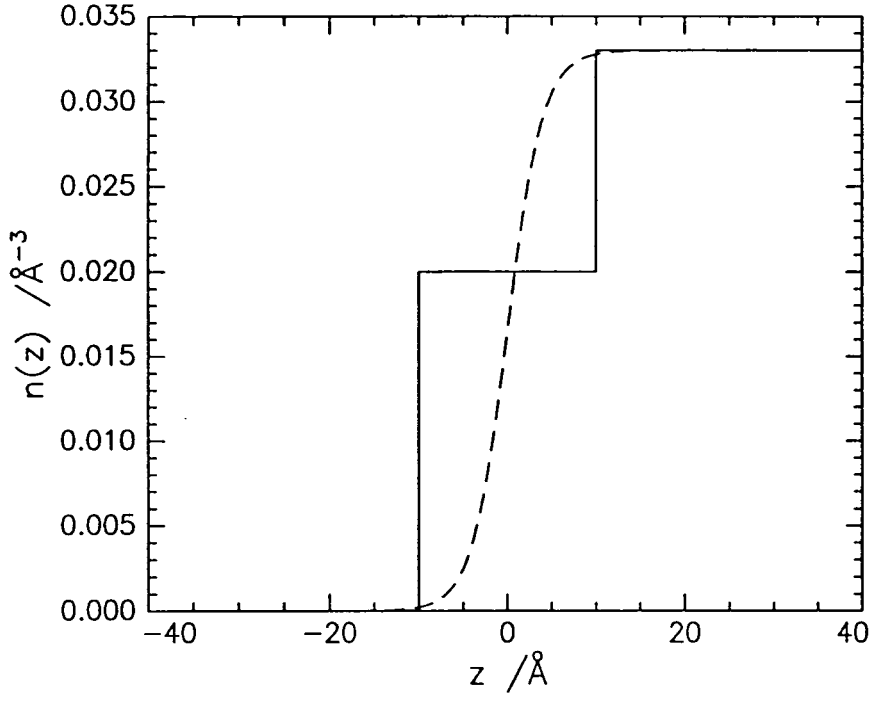

Figure 5.4.6 Number density profile for a uniform layer of water, d = 20 Å, n = 0.02 Å^{-3}, solid line, and a tanh profile, ζ = 5 Å, broken line.

The equations for a uniform layer model are modified relative to those for adsorbed or spread films. This is because, unlike film forming species, water has a finite bulk density of 0.033 Å^{-3}. In this case the number density, n(z) is described by:

$$n_w(z) = \begin{cases} 0 & z < -d/2 \\ n_W & -d/2 < z < d/2 \\ n_{wo} & z > d/2 \end{cases}$$

The partial structure factor becomes:

$$Q^2 h_{ww}(Q) = n_{wo}^2 + 4n_w(n_w - n_{wo})\sin^2(Qd/2)$$

Equation 5.4.8

where n_w is the number density of water in the interfacial layer. Equation 5.4.8 has been fitted to the water self partial structure factor using n_w and d as variables. The fit is given in figure 5.4.7 and the parameters in Table 5.4.2.

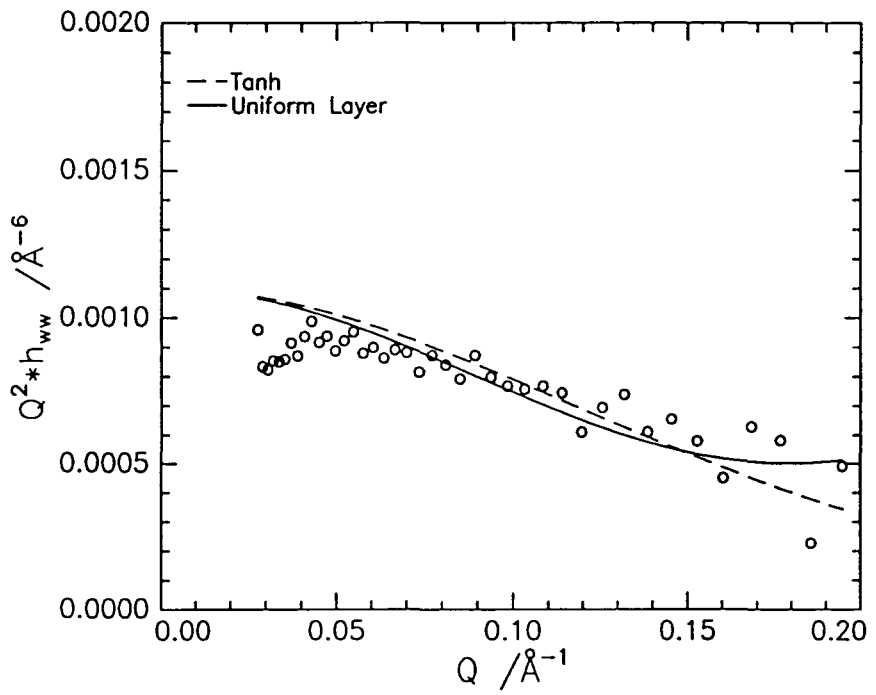

Figure 5.4.7 Best fits to the water self partial structure factor using the models outlined above.

Model	n_w / 10^{-2}	d / Å	χ^2 /10^{-7}
Uniform layer	0.54 ± 0.05	17.53 ± 1.38	0.1260
Model		ζ / Å	χ^2 /10^{-7}
Tanh		6.45 ± 0.26	0.1370

Table 5.4.2: Parameters for the best fits to the water self partial structure factors

The hyperbolic tangent model of the subphase distribution has also been used. In this model the number density increases gradually across the interface from zero to that for bulk water. The number density follows:

$$n_w(z) = n_{wo}(0.5 + 0.5\tanh(z/\varsigma))$$

Equation 5.4.9

and the partial structure factor is given by:

$$Q^2 h_{ww}(Q) = n_{wo}^2(\varsigma\pi Q/2)^2 \operatorname{cosech}^2(\varsigma\pi Q/2)$$

Equation 5.4.10

Equation 5.4.10 was fitted to the experimental partial structure factor by varying ζ. The results are presented in Table 5.4.2, the fit is overlaid in figure 5.4.7.

It is not necessarily straightforward to distinguish between a tanh and uniform layer fit especially if both give comparable fits, as seems to be the case here. The two models have a different number of fitting variables and, therefore, it is not a simple case of comparing the values of χ^2 to determine which gives the best fit. In this case the parabolic variation associated with the single layer fit is not evident in the experimental structure factor. This observation, coupled with the similarity in χ^2 despite the increased number of variables for a uniform layer fit, implies that the distribution of water at the interface is described better by a tanh profile rather than a block profile.

5.4.2.3C The Cross Partial Structure Factor

To reproduce the behaviour of the cross partial structure factor the functions fitted to the self partial structure factors must be reviewed. The PEO self partial structure factor was fitted with a Gaussian function, whereas a tanh distribution was assumed for the water profile at the interface. The latter function is predominantly odd, whereas the Gaussian function is even. As mentioned in chapter 2 for this situation the cross partial structure factor is given by:

$$h_{pw}(Q) = \pm\left(h_{ww}h_{pp}\right)^{0.5}\sin(Q\delta)$$

Equation 5.4.11

In this expression the dependence of h_{pp} and h_{ww} on Q has been omitted for clarity, generally where h_{ii} is written it is implicit that there is a Q dependence. This function can be fitted to the variation in the cross partial structure factor using δ, the centre-centre separation of the distributions, as the fitting variable.

The method employed to determine δ was generation of $Q^2h_{pw}(Q)$ varying δ each time. Experimental values were substituted into equation 5.4.11 to calculate the product $h_{pp}h_{ww}$. Substituting different values of δ into the equations demonstrates how sensitive the shape of the cross partial structure factors is to the separation of the distributions. The cross partial structure factors generated in this way were compared to the experimental cross partial structure factors, see figure 5.4.8.

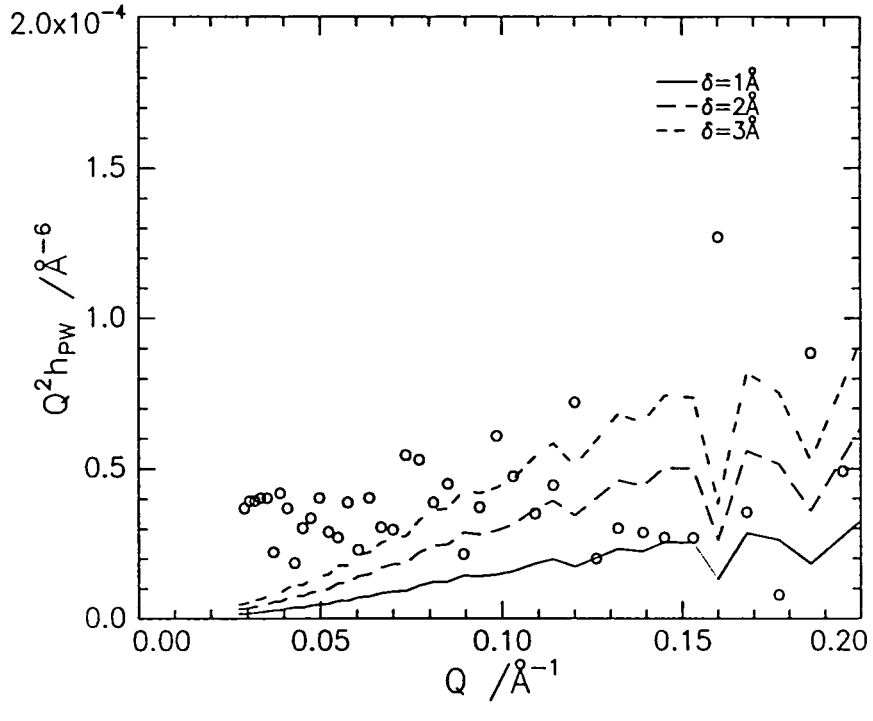

Figure 5.4.8 Cross partial structure factor compared to generated data with δ as given.

The results of this approach are given for δ = 1 Å, δ = 2 Å and δ = 3 Å. Clearly the separation, δ, is small. As δ increases the generated cross partial structure factor exhibits an increasing gradient whereas the experimental values barely exhibit a gradient. This is taken as indicative that the separation between the PEO / water distribution is negligible which, given that PEO is water soluble and is adsorbing from the bulk, is hardly surprising. It is clear from equation 5.4.11 that if the separation of the distributions really was zero the cross term should also be zero. Although this is not observed, probably because behaviour is not ideal, given that the values exhibit little dependence on Q assuming that δ is negligible seems fair.

5.4.2.4 Interpretation

From the analysis of the partial structure factors a number density profile of the species at the interface can be constructed. The centre of the water distribution is placed at z = 0 and since the separation between PEO and water distributions is zero the PEO distribution is also centred there. The resulting number density profile is given in figure 5.4.9.

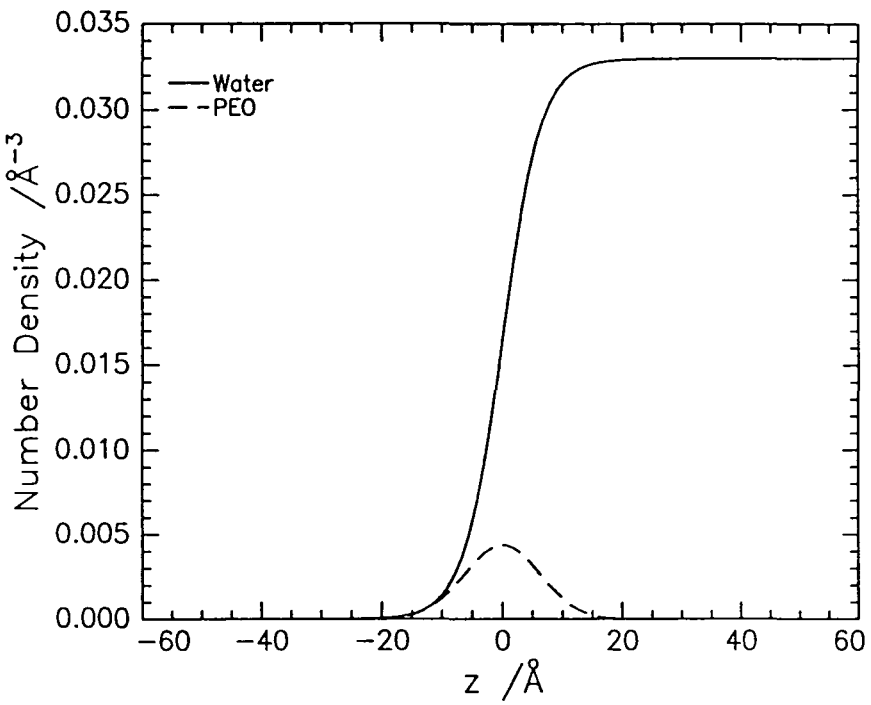

Figure 5.4.9 Number density profile for layers of PEO adsorbed at the air solution interface.

The models give a number density profile which seems perfectly feasible. The PEO adsorbs to form a diffuse layer which has a high water content, however there are certain limitations with this model. It is assumed that the number density of PEO is zero away from the interfacial layer whereas, in fact, since a PEO solution is being studied the bulk number density of PEO, although likely to be very small, will have a finite value. These effects, which are beyond the resolution of the experiment, are neglected.

5.4.2.5 Discussion

As mentioned the PEO layers adsorbed at the air water interface have been studied previously and only a brief discussion of behaviour is given here. The main reason for performing this experiment was to confirm that the PEO solution was in the same initial state as those studied by Lu et al.[12] This group analysed their results using both the optical matrix analysis and the kinematic approximation. They estimated the adsorbed surface concentration of PEO to fall in the range 0.53 - 0.57 mg m^{-2} from model fitting the reflectivity directly. This group also used a Gaussian to model the self partial structure factor for PEO, inferring a surface concentration of 0.6 ± 0.1 mg m^{-2} from the extracted parameters. These values are in excellent agreement with the results obtained here and it is concluded that the adsorbed layer of PEO has been successfully described and is equivalent to that studied by previously.

5.4.3 Neutron Reflectometry study of a 3 mg m^{-2} film of PMMA spread at the air / water interface.

Although there have been a number of studies of spread films of syndiotactic PMMA[1,19] on water neutron reflectometry has only been applied for film concentrations up to 2 mg m^{-2}. At the time of these studies the kinematic approximation had only recently been developed and its full application had not been realised. As a consequence of this only the self partial structure factors were analysed and this is the first study where the full analysis has been applied.

5.4.3.1 Experimental

Three reflectivity profiles were collected for dPMMA spread on both NRW and D_2O and for hPMMA on D_2O. These three profiles enabled the full kinematic approximation to be applied to the data. To be consistent with the method used for spreading PMMA on PEO solutions the PMMA films were spread so as to achieve a surface concentration of 3 mg m^{-2} when occupying the entire surface area of the trough.

5.4.3.2 Results

The profiles collected for a D_2O subphase are presented in figures 5.4.10 and 5.4.11 along with the profile for D_2O as comparison. The profiles exhibit the characteristic rapid fall off in reflectivity as Q increases and by Q = 0.25 $Å^{-1}$ the signal is within the background. Clearly the reflectivity is only slightly depressed when hPMMA is spread at the interface. The reflectivity for dPMMA / D_2O is of a comparable order to that for clean D_2O. In fact the reflectivity profiles for dPMMA / D_2O and D_2O cross one another, so that at Q values below about 0.05 $Å^{-1}$ the polymer film causes a reduction in the reflectivity compared to D_2O. At higher Q values the situation appears to be reversed.

The reflectivity for dPMMA on NRW is considerably lower than for any of the D_2O systems and the reflectivity falls off rather more gently, see figure 5.4.12.

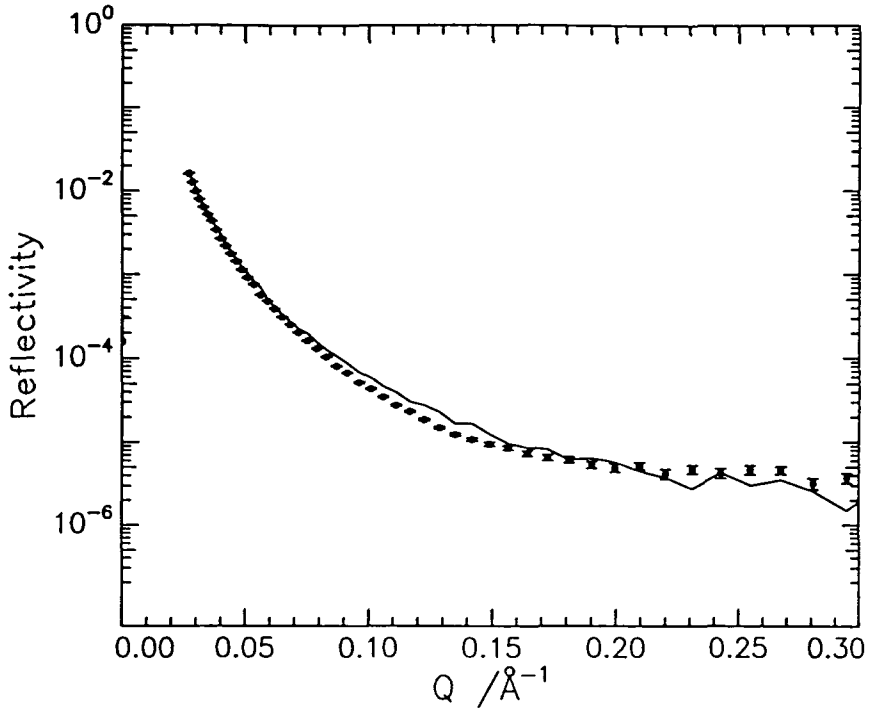

Figure 5.4.10 Reflectivity profile for hPMMA / D_2O, the profile for D_2O is overlaid.

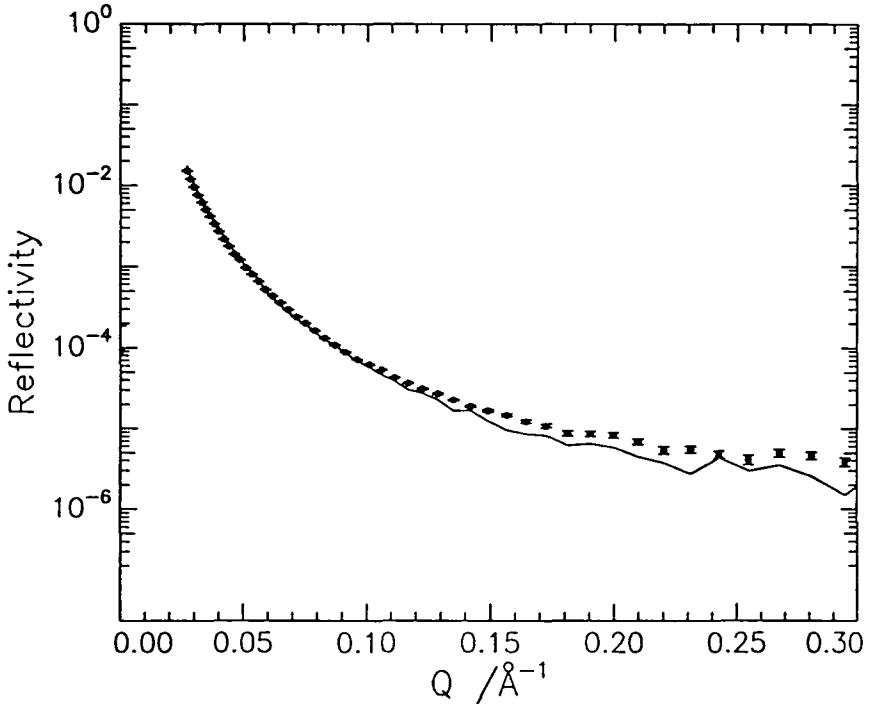

Figure 5.4.11 Reflectivity profile for dPMMA / D_2O. The profile for D_2O is overlaid, solid line.

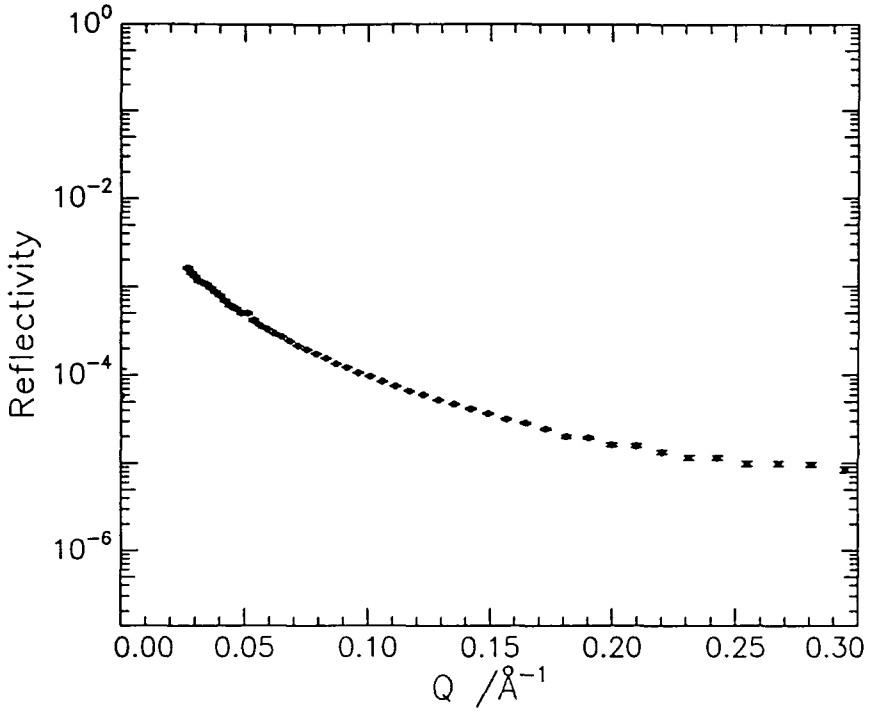

Figure 5.4.12 Reflectivity profile for dPMMA / NRW.

5.4.3.3 Data Analysis: The Kinematic Approximation

The data has been analysed by applying the full kinematic approximation.

5.4.3.3A PMMA Self Partial Structure Factor

The PMMA self partial structure factor increases with increasing Q exhibiting behaviour characteristic of a species adsorbed at the interface. The Gaussian distribution and a single uniform layer models have been considered and been fitted to the data, see figure 5.4.13. The parameters of the fits are given in Table 5.4.3.

Model	n_{pl} / 10^{-2} Å^{-3}	d / Å	χ^2 / 10^{-10}
Uniform Layer	0.51 ± 0.01	17.69 ± 0.13	0.1446
Model	**n_{pl} / 10^{-2} Å^{-3}**	**σ / Å**	**χ^2 / 10^{-10}**
Gaussian	0.66 ± 0.03	16.00 ± 0.14	0.1447

Table 5.4.3: Parameters of the best fits of the PMMA self partial structure factor.

As previously, to differentiate between the fits it is necessary to consider the surface concentration calculated from the fitted parameters and compare this to the spread concentration.

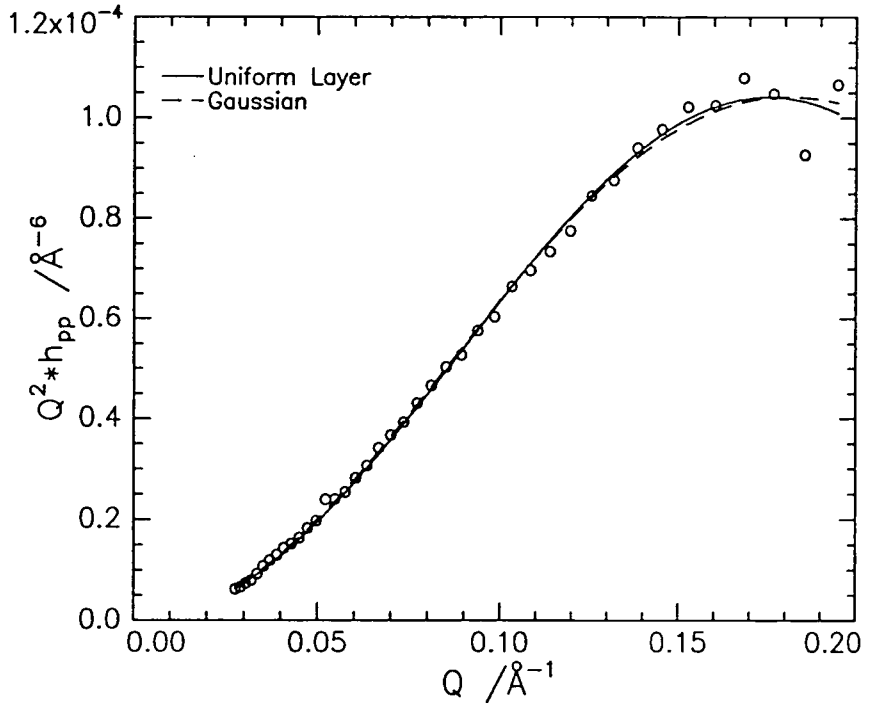

Figure 5.4.13 Fits to the self partial structure factor of PMMA, open circles experimental data

Using Equations 5.4.6 and 5.4.7 and the parameters given in Table 5.4.3 the surface concentrations have been calculated. The uniform layer model gave 1.58 - 1.66 mg m^{-2}, the Gaussian 1.64 - 1.72 mg m^{-2}. Clearly both models give surface concentrations in the same range, although both are considerably lower than the known spread amount. Given the discrepancies in surface concentrations apparent for both models it is not possible to chose one model over the other except by exercising physical intuition. As previously the Gaussian

model is considered a rather more appealing model and has the added advantage of extending to a slightly higher surface concentration.

5.4.3.3B Water Self Partial Structure Factor

The water self partial structure factor increases slowly as Q decreases exhibiting a characteristically flat variation. This is behaviour typical of a subphase structure factor and so the accepted models for a subphase distribution have been applied, see figure 5.4.14.

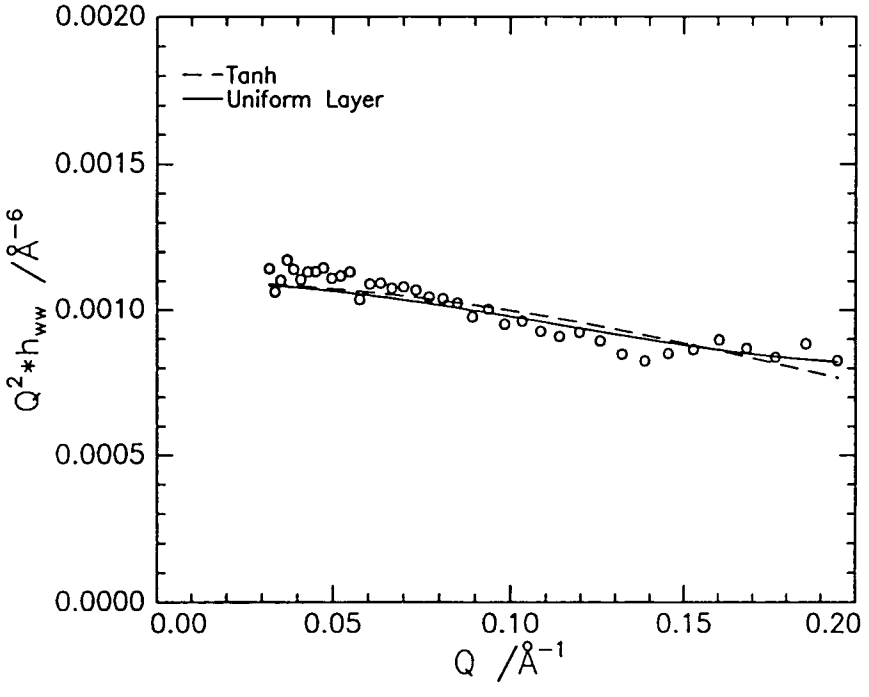

Figure 5.4.14 Water self partial structure factor, open circles, with the best fits for a uniform layer model and a tanh profile overlaid

The parameters of the fits are presented in Table 5.4.4 and, as for the polymer distribution, neither fit appears more suitable than the other. The effect of the number of fitting variables has already been mentioned, see section 5.4.2.3. Given this fact it is slightly surprising that there is not a larger difference in χ^2 for the two models, the two parameter fit gives only a marginally smaller χ^2. This fact, coupled with the more realistic image that a tanh profile portrays of a steadily increasing water distribution rather the step function associated with a uniform layer, leads to the suggestion that the true interfacial distribution of water is closer to a hyperbolic tangent profile than a uniform layer.

Model	n_{wl} / 10^{-2} Å^{-3}	d / Å	χ^2 / 10^{-8}
Uniform	0.23 ± 0.04	14.19 ± 2.00	0.2036
Model	**n_w / 10^{-2} Å^{-3}**	**ζ / Å**	**χ^2 / 10^{-8}**
Tanh		3.46 ± 0.11	0.2321

Table 5.4.4: Fitted parameters for water self partial structure factor.

5.4.3.3C The Cross Partial Structure Factor

The cross partial structure factor between water and PMMA is presented in figure 5.4.15 and contains information about the relative distribution of the PMMA and water distributions at the interface. The functions describing the polymer and water distributions are as for PEO and so Equation 5.4.11 applies here.

The product $h_{ii}h_{jj}$ was calculated from the experimentally determined self partial structure factors and by taking different values for δ, the model cross term was generated. In this manner a value of $\delta = 6 \pm 0.5$ Å was extracted. The fit to the cross partial structure factor data is given overlaid on the experimental data in figure 5.4.15. A change of only 1 Å in δ caused the fit to vary as demonstrated.

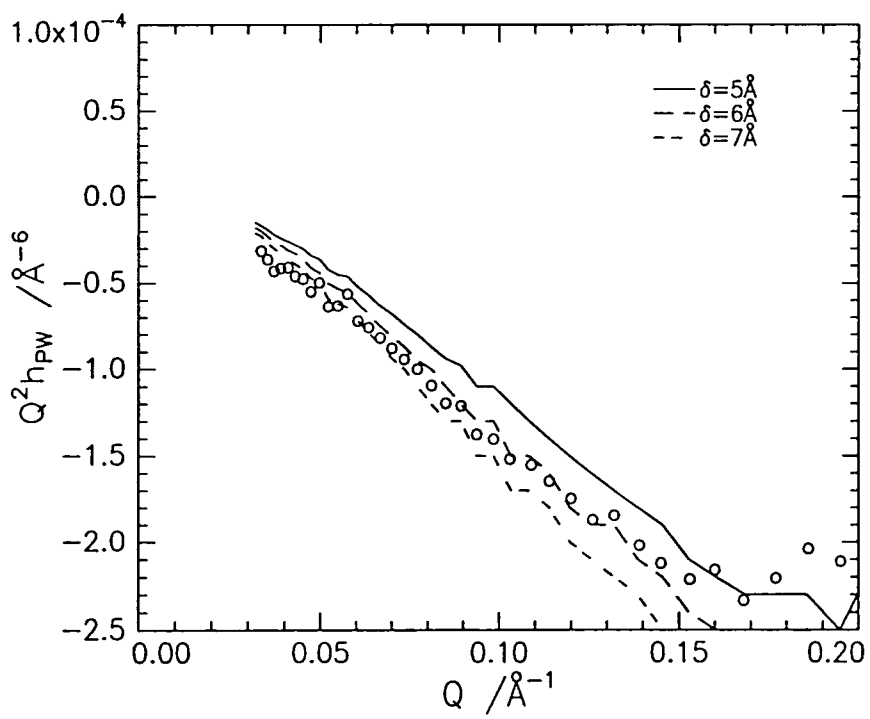

Figure 5.4.15 Cross partial structure factor, open circles, with the fits from equation 3.11 overlaid, δ is given in the figure.

A number density profile of the system can be constructed since the distribution of each species and their separations are known. To construct the profile the centre of the water distribution is placed at zero and the PMMA distribution is then placed relative to this. Since δ is just a dimension there is no information indicating whether the PMMA is in the water, i.e. 6 Å below the centre of the water distribution, or out of the water. Physical intuition is used and given the hydrophobicity of PMMA, the distribution is placed above the water, see figure 5.4.16.

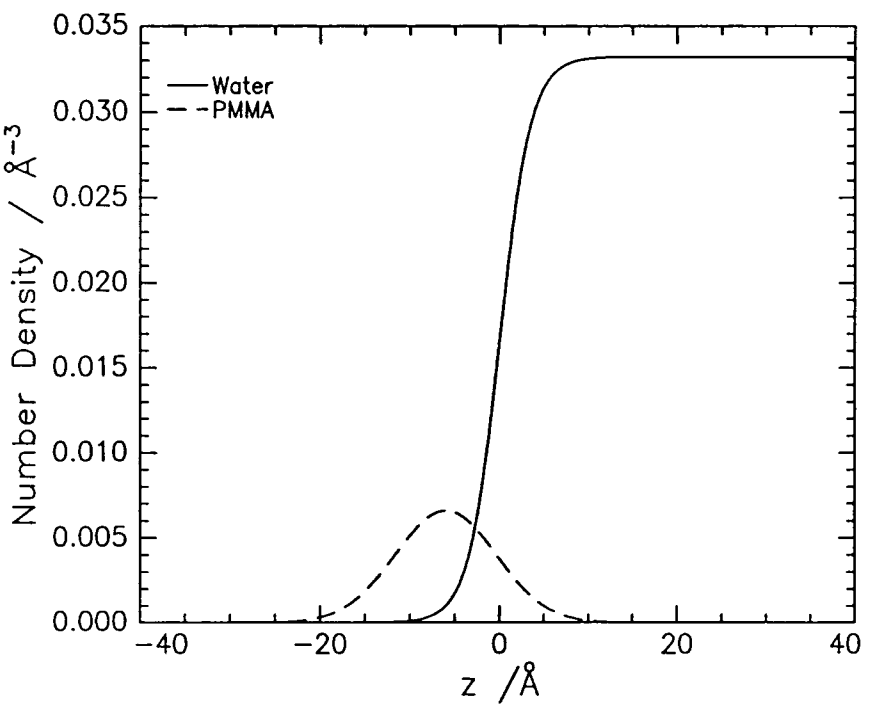

Figure 5.4.16 Number density profile for a 3 mg m^{-2} film of PMMA on water.

The number density profile clearly indicates that the majority of the PMMA remains in the air as one would expect. In total about 60% of the polymer extends into the air. There is some interpenetration between the PMMA and water, the PMMA extending about 10 Å into the water.

Although there have been previous studies of PMMA[1,19] on water there was no analysis of the cross terms as their relevance has only been realised since. It was therefore not possible to construct a number density profile of the system, although from the optical matrix analysis it was suggested that the PMMA forms a uniform layer at the air / water interface with a negligible fraction of polymer immersed in the aqueous subphase. This is consistent with the observations made here.

5.4.3.4 General Discussion

The interfacial structure of a 3 mg m^{-2} film of PMMA on water has been successfully characterised using neutron reflectometry. The distribution of the PMMA was described by a Gaussian layer, the water distribution by a tanh profile. In fact the PMMA self term seemed to be equally well described by either a uniform layer or a Gaussian distribution. Despite this, both models gave a calculated surface concentration which was much lower than the spread amount. Simulations show that despite the low surface concentration inferred from fitting the PMMA self term the parameters do reproduce the reflectivity profiles well. Consider a layer of dPMMA on NRW. Using the parameters in Table 5.4.3, the dPMMA is modelled as forming a layer 18 Å thick with a scattering length density of 5.06×10^{-6} $Å^{-2}$. As figure 5.4.17 illustrates this model is in excellent agreement with the experimental reflectivity.

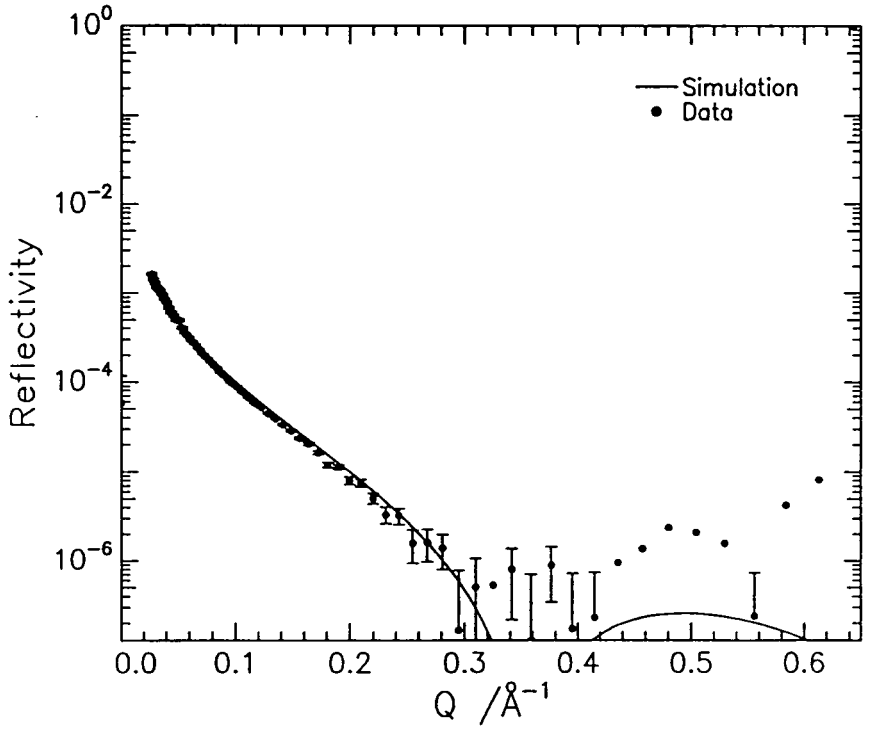

Figure 5.4.17 Simulated reflectivity overlaid on the experimental data for dPMMA / NRW.

From the evidence in figure 5.4.17 it is clear that the reflectivity profile is consistent with only 1.7 mg m^{-2} rather than 3 mg m^{-2} of PMMA contributing to the reflectivity. Thus it

is suggested that somehow some of the polymer is lost at the interface and not detected in the experiment.

Similar behaviour is evident in previous studies[1] where the surface concentration extracted for a uniform layer model fit to the self partial structure factor for a 2 mg m^{-2} was found to be 1.8 mg m^{-2}. The discrepancy is believed to originate as the surface concentration increases and the polymer chains begin to loop above, and possibly below, the subphase, becoming so dilute that they do not contribute significantly to the reflectivity.

The number density profile presented earlier provides a model for the system which can not be compared to any other data in the literature. However from the optical matrix analysis performed by Henderson et al[1] it was suggested that the PMMA forms a uniform layer at the air / water interface with a negligible fraction of polymer immersed in the subphase. The best uniform layer model of the system indicated a layer 18 Å thick. If the centre of this distribution is placed 6 Å above the water distribution about 3 Å of this will contain water, although the volume fraction of water is very low, being only 0.07. This 3 Å wide section of the distribution contains about 17 % of the PMMA at the surface so clearly the majority of the PMMA does remain in the air, avoiding interactions with the water.

Comparing the composition of the interfacial layers with those for lower concentration films shows some remarkable similarities. The volume fraction of water was found to be in the region 0.06 - 0.09 for all films over the concentration range 0.4 - 2 mg m^{-2}. This compares well with the value found here of 0.07. The volume fraction of polymer compares equally well. In this situation it was found to be 0.84, previous values for low concentration films vary from 0.2 - 0.95. The value of 0.95 was found for a 2 mg m^{-2} and since the value for a 3 mg m^{-2} is slightly less this will indicate a greater amount of air in the layer. This could be envisaged to be symptomatic of the polymer chains beginning to loop above the condensed layer and effectively being lost from the system. This mechanism may account for the low surface concentration inferred from the reflectivity data.

5.4.3.5 Conclusion

In conclusion the structural organisation of a 3 mg m^{-2} film of PMMA on water has been elucidated successfully. The characteristics of the organisation are consistent with early work by Henderson et al[1] and will provide an adequate comparison to data for the same concentration film on PEO solution.

5.4.4 Neutron Reflectometry Study of PMMA films spread on 0.1 wt.% PEO Solution

5.4.4.1 Experimental

Films of PMMA were spread on solutions of PEO at the required Γ_s in the manner outlined previously. Where the film concentration was such that a relaxation occurred the system was left for at least 40 minutes and the surface pressure continually monitored. Once the surface pressure had achieved a stable value data collection was started. Three film concentrations were studied in this way, 1 mg m^{-2}, 2 mg m^{-2} and 3 mg m^{-2}.

Reflectivity profiles for six different contrasts were required to perform a rigorous kinematic approximation analysis. These being:

hPMMA / hPEO / D_2O	dPMMA / hPEO / D_2O	dPMMA / hPEO / NRW
hPMMA / dPEO / D_2O	dPMMA /dPEO / NRW	hPMMA / dPEO / NRW

All the required profiles were collected for a 1 mg m^{-2} and 3 mg m^{-2} film of PMMA on PEO solution. These were recorded in the first set of experiments which were performed on CRISP. The 2 mg m^{-2} film of PMMA was studied as part of a subsequent experiment on SURF in the first round of beam allocation on that instrument. Unfortunately this latter experiment was plagued by beam loss and as a consequence only three contrasts were run, these were hPEO / hPMMA / D_2O, hPEO / dPMMA and dPEO / hPMMA on NRW. The first and last of these runs can be analysed using approximate methods giving an estimation of the partial structure factors for water and PEO respectively, but there is insufficient data available to perform either a full kinematic approximation analysis or have any confidence in a model obtained from model fitting methods.

5.4.4.2 Results

The reflectivity profiles following background subtraction are presented in figures 5.4.18 to 5.4.21. For the profiles where the subphase is D_2O the reflectivity is

dominated by the subphase. Where hydrogenous species are present the depletion in the scattering length density will cause the reflectivity to decrease below that for D_2O.

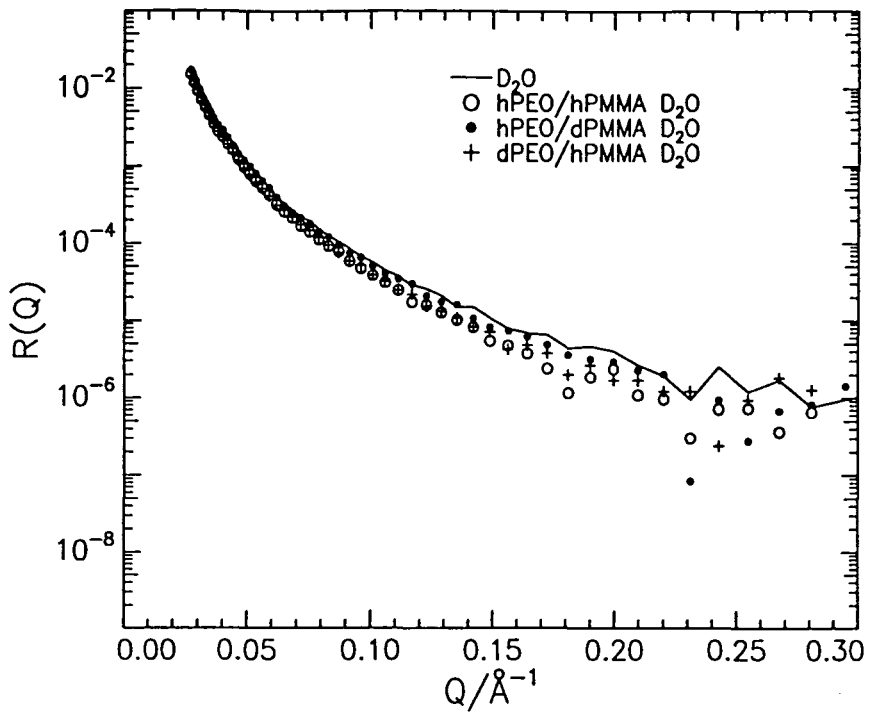

Figure 5.4.18 Reflectivity profile for Γ_s = 1 mg m^{-2} and a D_2O subphase.

The reflectivity profiles for Γ_s = 1 mg m^{-2} exhibit only a small variation as the isotopic composition changes, see figure 5.4.18. However, as would be expected, in all cases the reflectivity is depressed below that for D_2O. The greatest depression is for the hPEO / hPMMA system, consistent with this system having the highest hydrogen content. The reflectivity is slightly greater for dPEO / hPMMA suggesting that the PEO is in the interfacial region, contributing to the reflectivity. The contrast hPEO / dPMMA / D_2O has the greatest reflectivity, which is indicative of the PMMA having a substantial influence on the reflectivity.

This behaviour is confirmed by the profiles recorded on NRW which are easier to interpret directly than the D_2O profiles. This is because of the phase problem associated with neutron reflectometry. Due to this it is not possible to determine whether a film has a very high scattering length density, just less than D_2O, or whether the scattering length density is very low.

The reflectivity in figure 5.4.19 varies markedly with isotopic composition. The dPEO / dPMMA contrast exhibits the greatest reflectivity in accordance with

having the maximum deuteration. When the PEO is hydrogenous the reflectivity falls somewhat but the profile maintains the same shape. The most marked decrease in the reflectivity is when only the PEO is deuterated, i.e. dPEO / hPMMA. The decrease in the reflectivity from that of the dPMMA / dPEO system to dPEO / hPMMA is considerable. This indicates that it is the dPMMA that drives the reflectivity when the subphase is NRW. Such behaviour implies that the contribution from the PEO to the reflectivity is only small. This means that the product of the scattering length density of the layer occupied by the PEO and its thickness is small, assuming a simple layer structure. This statement implies that the PEO either forms a thin dense layer at the interface or a dilute thick layer. Given the rather gentle fall off in the reflectivity for dPEO / hPMMA / NRW the latter situation seems more likely.

Figure 5.4.20 illustrates that when the concentration of PMMA is increased to 3 mg m^{-2} the behaviour of the system changes markedly. Even the reflectivity from D_2O, where the subphase contributions dominate, varies considerably as the isotopic composition of the polymers changes. The greatest change is when both polymers are hydrogenous. Such a sharp decrease in the reflectivity of D_2O is quite remarkable.

The fact that the reflectivity profile for hPEO / dPMMA / D_2O is only very slightly depressed compared to D_2O indicates that the contribution of the PEO to the reflectivity is quite low. This is confirmed by the greater reduction in the reflectivity for hPMMA / dPEO D_2O.

The reflectivity profiles recorded for the high surface concentration of PMMA on NRW emphasise the fact that it appears to be the PMMA that is dominating behaviour, see figure 5.4.21. The reflectivity profile for dPMMA / hPEO / NRW exhibits only a very small decrease compared to that for dPMMA / dPEO / NRW and over much of the Q range the two profiles are coincident. The difference is mainly at the low Q region indicating that the influence of the PEO is most marked at low Q, consistent with significant subphase penetration. This behaviour contrasts to that when Γ_s = 1 mg m^{-2} where the reflectivity exhibits a significant decrease as the isotopic composition

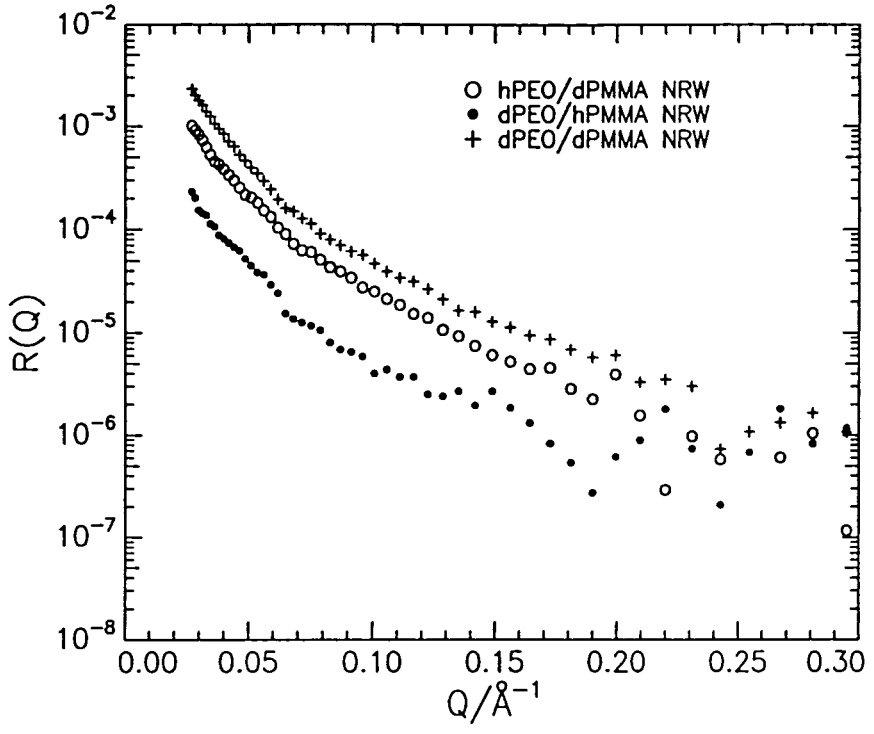

Figure 5.4.19 Reflectivity profiles for Γ_s = 1 mg m^{-2} where the subphase is NRW.

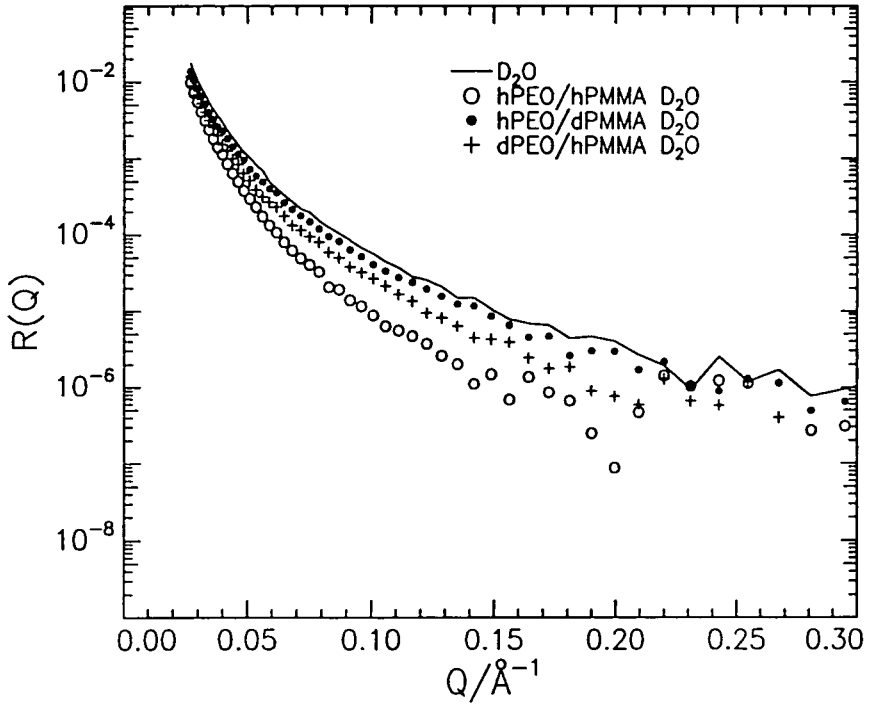

Figure 5.4.20 Reflectivity profiles for Γ_s = 3 mg m^{-2} where the subphase is D_2O.

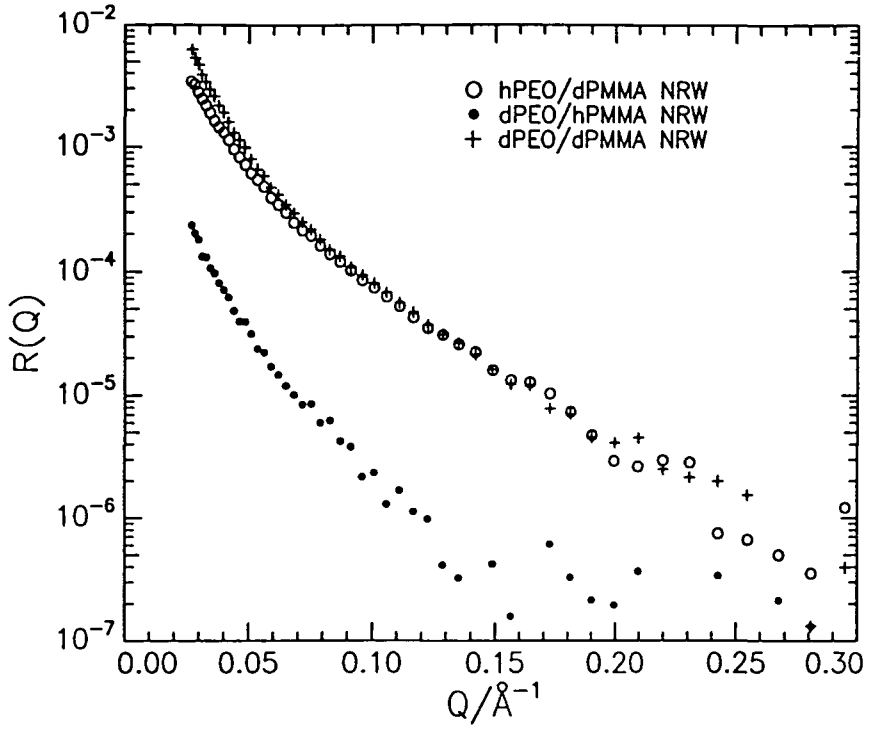

Figure 5.4.21 Reflectivity profiles for $\Gamma_s = 3$ mg m^{-2} where the subphase is NRW.

changes from dPMMA / dPEO / NRW to dPMMA / hPEO / NRW. This difference indicates that the contribution from the PEO is much greater when $\Gamma_s = 1$ mg m^{-2} than 3 mg m^{-2}. This implies different surface organisations in the two situations. The reflectivity of the hPMMA / dPEO / NRW contrast when $\Gamma_s = 3$ mg m^{-2} is very low and falls off rapidly so that by Q values as low as 0.15 Å^{-1} the signal is within the background. This behaviour is consistent with a relatively thick, diffuse layer of low scattering length density, confirming that the adsorbed layer of PEO may be forced to adopt a different interfacial organisation in the presence of a 3 mg m^{-2} film of PMMA.

The reflectivity profiles for a 2 mg m^{-2} film of PMMA are given in figure 5.4.22. Of the profiles collected only those for hPMMA / hPEO / D_2O and hPMMA / dPEO / NRW can be analysed and so only these are given.

The behaviour exhibited in figure 5.4.22, namely the marked decrease in the reflectivity compared to D_2O for the hPMMA / hPEO contrast is similar to the behaviour exhibited when $\Gamma_s = 3$ mg m^{-2}. The reduction is not quite so marked in this situation and it seems that the reduction in the reflectivity of this contrast, compared

to D_2O is directly correlated to the PMMA content. This is further emphasised by overlaying the profiles for this contrast, see figure 5.4.23.

It is clear from figure 5.4.23 that, although the decrease in reflectivity for the hPMMA / hPEO / D_2O contrast appears to be correlated to the concentration of PMMA present, the relationship is not linear. Increasing Γ_s to 3 mg m^{-2} leads to a marked reduction in the reflectivity of the system. Presumably this behaviour reflects changes in the interfacial organisation which, given that no similar behaviour was exhibited for hPMMA / D_2O at 3 mg m^{-2}, is particular to this system.

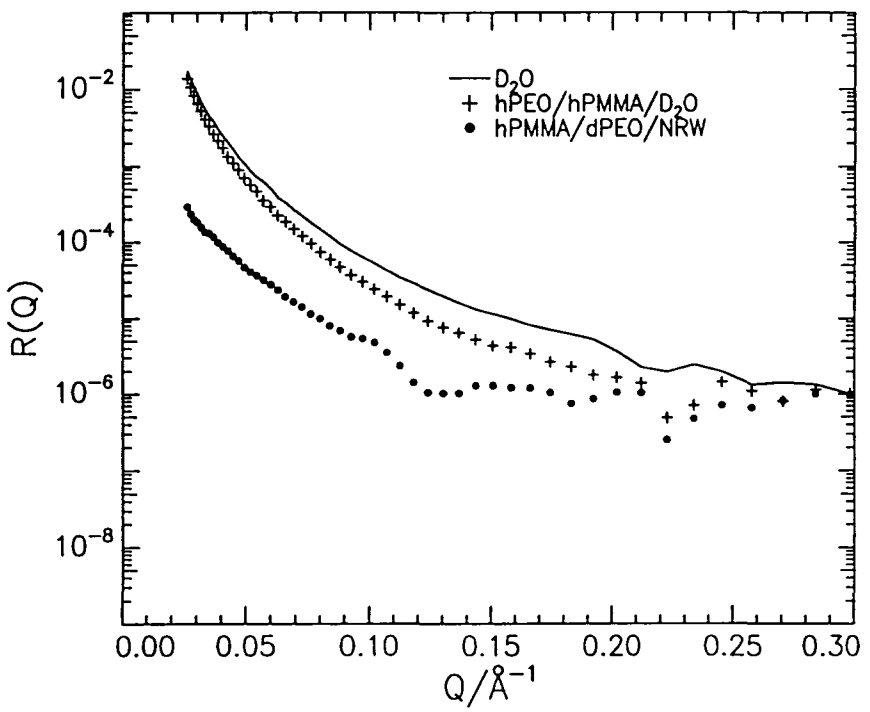

Figure 5.4.22 Reflectivity profiles for $\Gamma_s = 2$ mg m^{-2} contrasts as indicated.

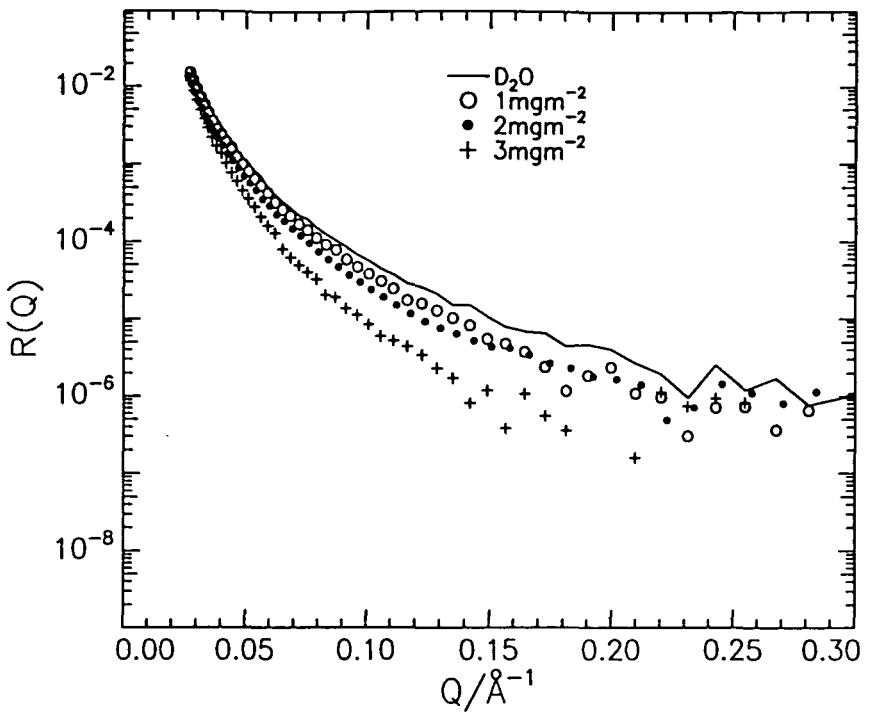

Figure 5.4.23 Comparison of the reflectivity profiles for hPMMA / hPEO / D_2O as a function of Γ_s.

5.4.4.3 Data Analysis: Self Partial Structure Factors

Emphasis is placed on data analysis using the kinematic approximation. The self partial structure factors are each considered in turn in this section.

5.4.4.3A The PEO Self Partial Structure Factor

The self partial structure factors for PEO adsorbed at the surface of a solution in the presence of a spread film of PMMA are presented in figure 5.4.24. Clearly the self partial structure factors are both very small. The values in the presence of a 1 mg m^{-2} film of PMMA are scattered around zero, being predominantly negative at low Q. Despite this systematic variation over this limited Q range consideration of a wider range indicates that the points are scattered such that the average value is zero.

Turning to the partial structure factor in the presence of a 3 mg m^{-2} film of PMMA, again the values are very small. In contrast to the self term at 1 mg m^{-2} the values in the

presence of a 3 mg m^{-2} film are predominately negative. On examination it is clear that the values are not scattered around zero but are systematically negative.

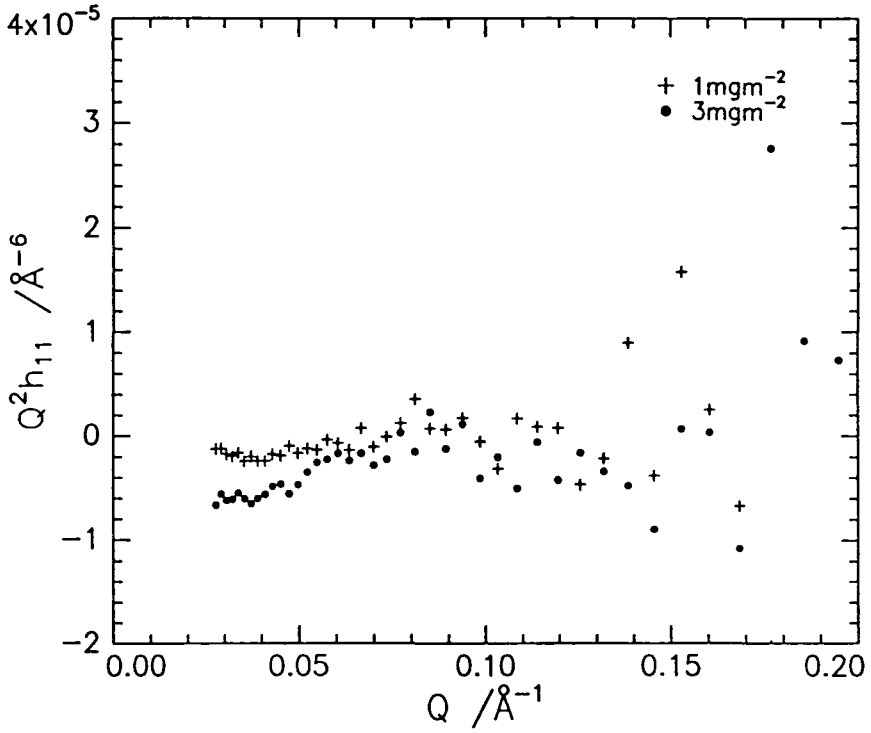

Figure 5.4.24 PEO self partial structure factors, the spread surface concentration of PMMA is indicated.

The self partial structure factor is related to the modulus of the number density of a species by:

$$h_{ii}(Q) = |n_{ii}(Q)|^2$$

Equation 5.4.12

It follows from equation 5.4.12 that h_{ii} cannot be negative. This leads to the suggestion that the observed self partial structure factor is erroneous. To consider how such values may be returned from the kinematic analysis the reflectivity profiles for the system must be considered in detail.

The reflectivity profile which most significantly contributes to the determination of this self partial structure factor is that for dPEO / hPMMA on NRW. The reflected signal for this system was observed to be very low. As will be discussed later, it is believed that the supposedly negative self partial structure factor values are a symptom of this. The low

reflectivity of this system indicates that only a small amount of deuterated species is present at the interface. A comparison of the reflectivity profiles for this contrast in the presence of the two different concentration PMMA films and for a clean solution of PEO shows that the reflectivity falls markedly when a film of PMMA is spread at the interface, see figure 5.4.25

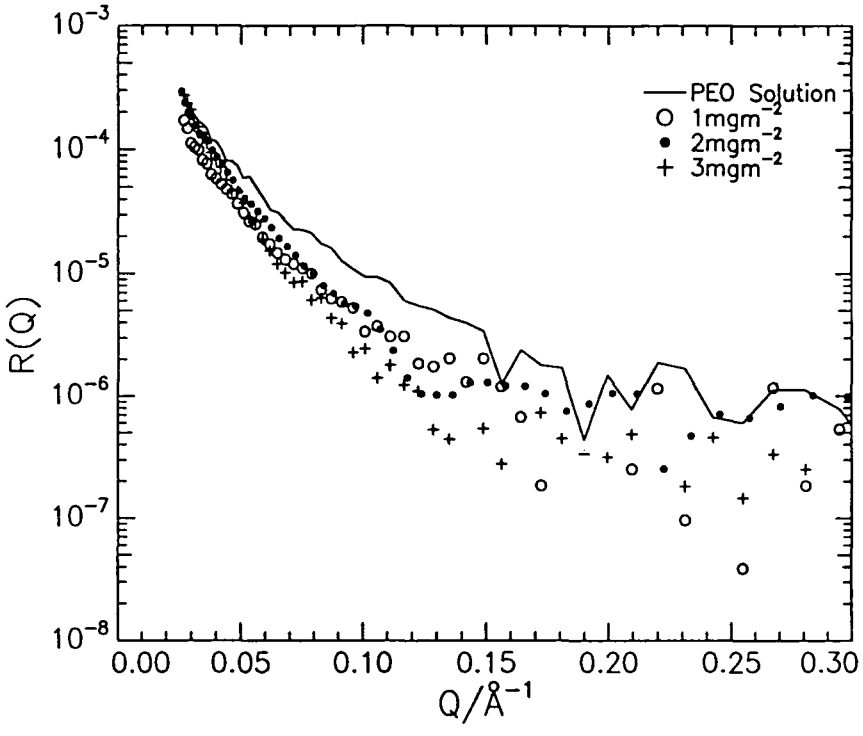

Figure 5.4.25 Reflectivity profiles for PEO solution and hPMMA / dPEO / NRW where the surface concentration of PMMA is as indicated.

The reflected signal falls off very rapidly with Q in the present of a spread film of PMMA, reaching background by around Q = 0.2 Å^{-1}. Such behaviour indicates that the surface organisation of the deuterated species, i.e. PEO, changes on spreading the PMMA. The decrease in the reflectivity appears to be correlated to the presence of PMMA but not explicitly to the surface concentration of the PMMA. Such behaviour indicates that, although the organisation of the PEO is markedly influenced by the presence of PMMA, this behaviour change is not linked continuously to the surface concentration of PMMA. This follows from the fact that the reflectivity exhibits little variation despite the three fold increase in the surface concentration of PMMA.

The reflectivity profiles are consistent with the suggestion that the organisation of the PEO in the interfacial layer is different to that in solution. It is possible that the decrease in reflectivity actually corresponds to depletion of PEO from the interface. In such

circumstances the self partial structure factor for the PEO would be very small. It is also possible that the self term is zero and the PEO is totally desorbed from the surface. This suggestion is consistent with the finite reflectivity exhibited by hPMMA / dPEO / NRW which could arise from the hPMMA in the system. Whatever its true origin the reflected signal is clearly quite low and will be subject to errors in data collection and reduction. Such factors, although generally small, may have a relatively large effect on this particular contrast, possibly causing the extracted value to appear negative rather than being low or zero.

There is an alternative method available which, by making a number of assumptions, allows the self partial structure factors to be estimated directly from the reflectivity profiles. The reflectivity profile for dPEO / hPMMA / NRW is used and is assumed to be influenced only by the dPEO in the system. Basically, the assumption is made that for hydrogenous PMMA the scattering length is negligible and there is no contribution to the reflectivity from the PMMA. In this case the reflectivity can be expressed:

$$R(Q) = \frac{16\pi^2}{Q^2} b_{PEO}^2 h_{pp}(Q)$$

Equation 5.4.13

Clearly, the assumptions made to express the reflectivity in this way are not strictly correct, especially given the high concentration of PMMA at the interface in one case. Therefore it must be acknowledged that this method may lead to an over estimation of the self partial structure factor. Despite these limitations the partial structure factor for PEO in the presence of a 1 mg m^{-2} and 3 mg m^{-2} film of PMMA have been determined. The values extracted in this way are best viewed as representing the upper bounds of the self terms whereas the 'true' partial structure factors in figure 5.4.24 represent lower bounds. The incomplete data set recorded in the presence of a 2 mg m^{-2} film of PMMA has also be analysed in this way. The results of the calculations are presented in figure 5.4.26.

The self partial structure factors extracted in the way described above are still small but finite. The values are given in figure 5.4.26 with the 'real' self partial structure factor for a solution of PEO overlaid for comparison, i.e. that from a full kinematic analysis. The self terms in the presence of a PMMA film are essentially coincident up to Q values around 0.04 $Å^{-1}$ above which they diverge increasingly. The self term remains lowest in the presence of a 3 mg m^{-2} film of PMMA, the values are almost flat and become scattered as Q increases. In contrast, the PEO self terms where the PMMA film is more dilute exhibit a positive gradient

both increasing with Q up to 0.1 $Å^{-1}$. These two self terms are similar, and are almost parallel up to Q values of around 0.1 $Å^{-1}$, although the values are rather larger where the spread film concentration is 2 mg m^{-2}. This self partial structure factor exhibits some very unusual behaviour as Q increases above 0.1 $Å^{-1}$ falling sharply and experiencing a minimum at about 0.13 $Å^{-1}$. In contrast the self term where Γ_s = 1 mg m^{-2} continues to increase.

Although the absolute values of the self terms presented in figure 5.4.26 may be slightly overestimated the results imply that the surface organisation adopted by the PEO differs markedly from that of the adsorbed layers of a bare solution. Despite earlier indications the surface excess of PEO, although modified, does not appear to be completely desorbed. In addition the surface organisation of the PEO appears similar, at least over the low Q range, in the presence of both the 1 mg m^{-2} and 2 mg m^{-2} film of PMMA. The most significant change occurs when the concentration of PMMA increases to 3 mg m^{-2} and the self partial structure factor becomes flat.

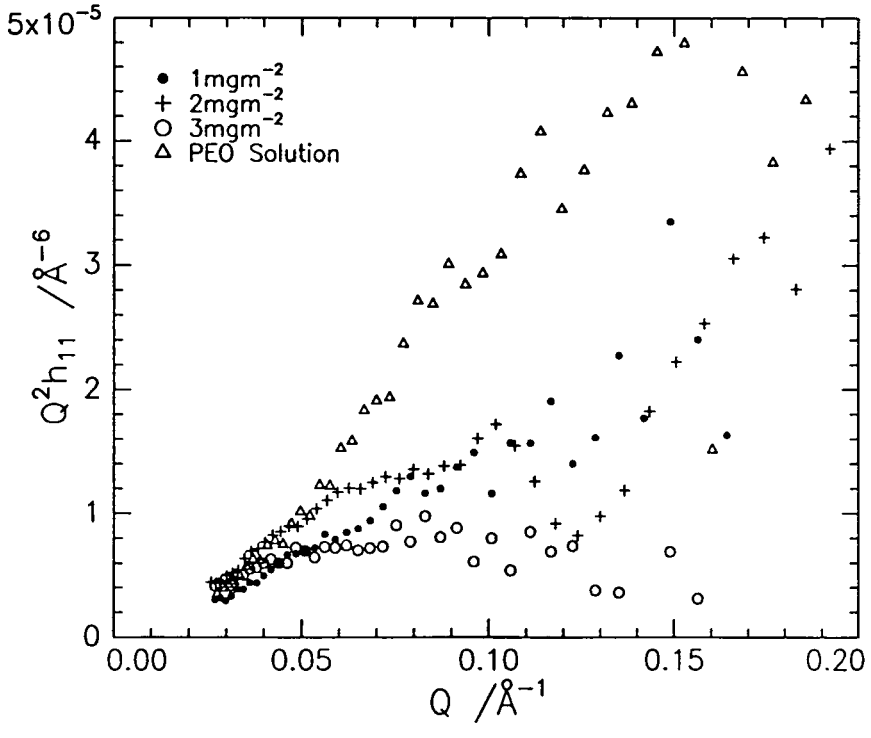

Figure 5.4.26 PEO self partial structure factors in the presence of PMMA films, surface concentrations as indicated. These self terms have been extracted directly from the reflectivity profiles. The 'real' self term for a PEO solution is also overlaid.

Initially uniform layer profiles were fitted to the self terms. The application of a uniform layer model to the PEO self term in the presence of a 1 mg m^{-2} and 2 mg m^{-2} film of PMMA is considered first. As illustrated in figures 5.4.27 and 5.4.28 this model did not fit either self term. The self term where Γ_s = 2 mg m^{-2} was particularly badly fitted. For the lower concentration film of PMMA the self term is fitted rather better at high Q but the values at low Q are systematically underestimated. A Gaussian model gave much the same fit, the discrepancies being exactly as discussed for the uniform layer fits. Clearly an alternative model is required to model the behaviour of these systems.

Uniform Layer Model

Γ_S / mg m^{-2}	n_{pl} /10^{-2} Å^{-3}	d / Å	χ^2	Γ_s / mg m^{-2}
1	0.23 ± 0.01	21 ± 1	0.8682×10^{-11}	0.39 ± 0.03
2	0.28 ± 0.02	14 ± 2	0.2948×10^{-10}	0.32 ± 0.06

Gaussian Segment Distribution

Γ_S / mg m^{-2}	n_{pl} /10^{-2} Å^{-3}	σ / Å	χ^2	Γ_s / mg m^{-2}
1	0.30 ± 0.01	18 ± 1	0.8508×10^{-11}	0.39 ± 0.04
2	0.37 ± 0.03	13 ± 2	0.2902×10^{-10}	0.34 ± 0.08

Table 5.4.5: Parameters of the fits given in figures 5.4.27 and 5.4.28.

One model that has been mentioned in the literature,[21] but only sparingly used, is that of a species existing in two uniform layers at the interface. In such a model the polymeric species is envisaged to form two uniform layers at the interface each with different number densities. A typical example of such a profile is given in figure 5.4.29.

For two uniform layers: $n(z) = n_A \quad 0 < z < d_A$

$n(z) = n_B \quad d_A < z < d_B$

Equation 5.4.14

In this model there are two layers one d_A Å thick and one $d_B - d_A$ Å thick. The surface concentration is given by the sum of the contributions for each of the layers.

$$\Gamma_i = n_A d_A + n_B(d_B - d_A)$$

Equation 5.4.15

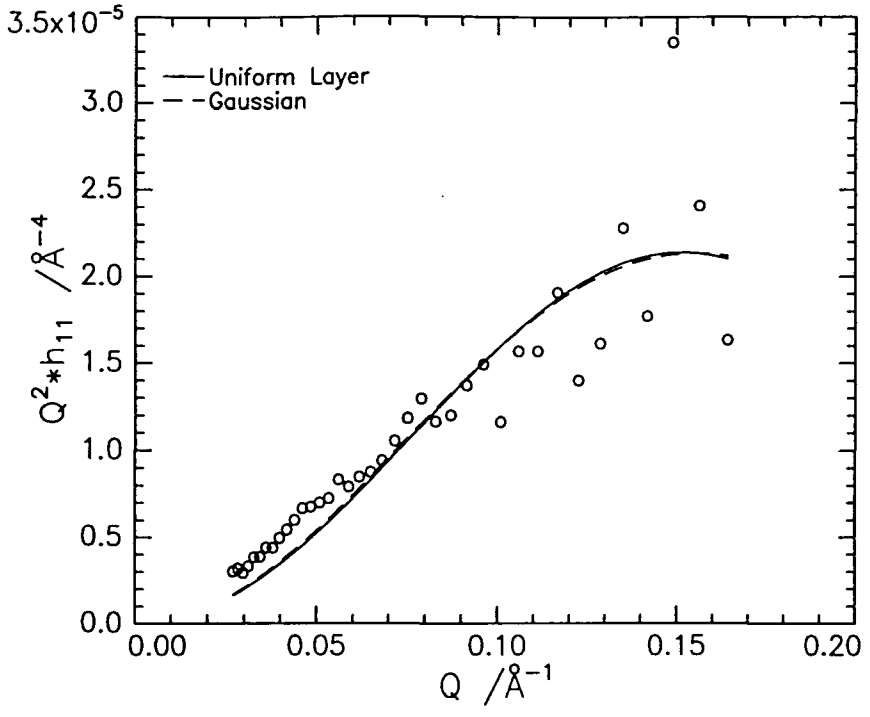

Figure 5.4.27 Estimated PEO self partial structure when Γ_{sPMMA} = 1.0 mg m^{-2} with the best fit for both a uniform layer model and Gaussian overlaid.

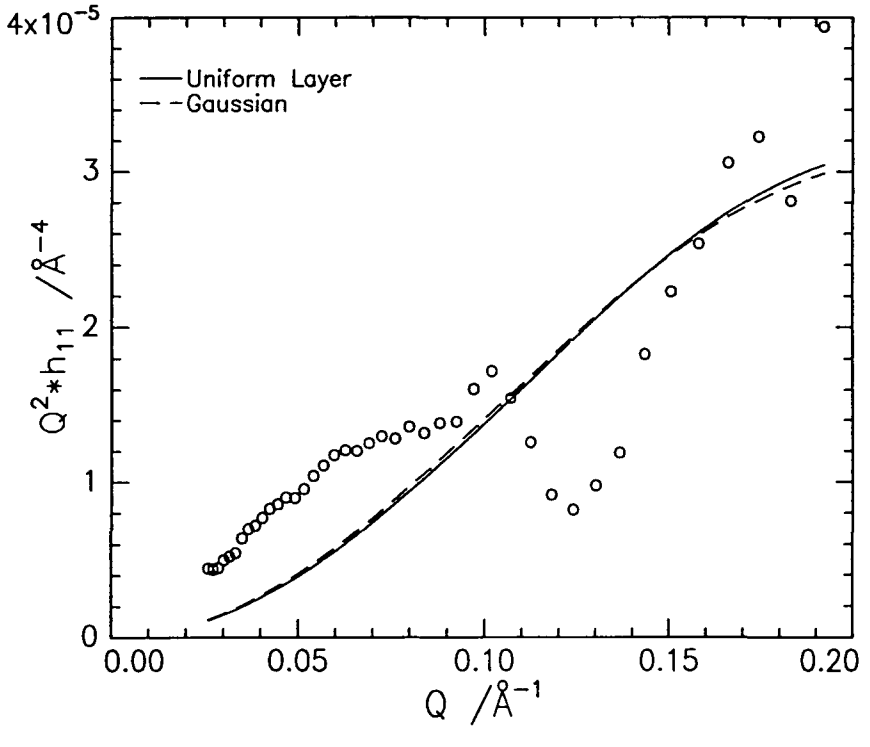

Figure 5.4.28 Estimated PEO self partial structure when Γ_{sPMMA} = 2.0 mg m^{-2} with the best fit for both a uniform layer model and Gaussian overlaid.

Note that this is the correct form for the surface concentration, that given by Thomas[21] in the paper in which this model was first suggested is incorrect.

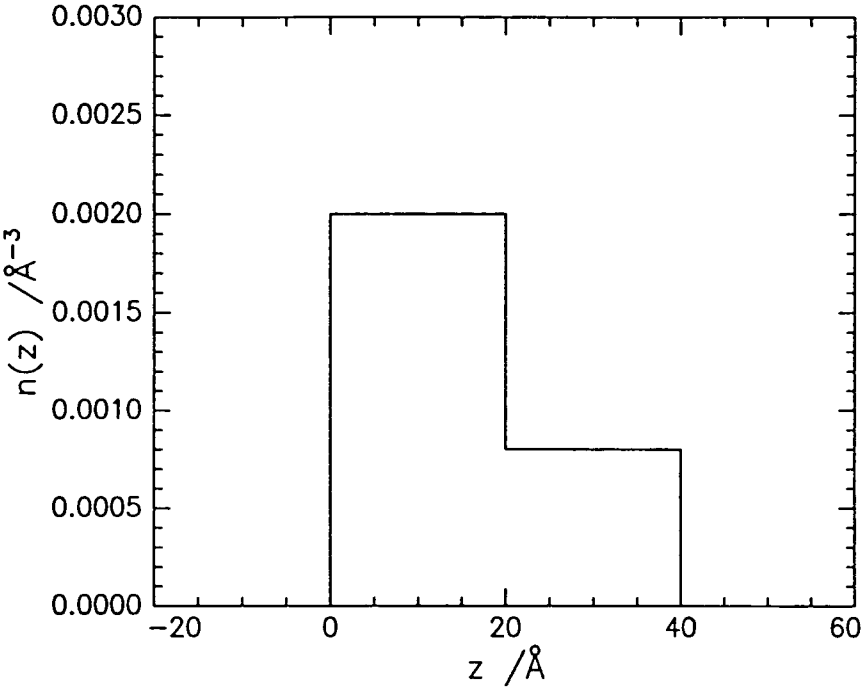

Figure 5.4.29 Typical number density profile for two uniform layers both of width 20 Å, $n_A = 0.002$ Å^{-3}, $n_B = 0.0008$ Å^{-3}.

Fourier Transform of n(z) gives:

$$n(Q) = \frac{n_B}{iQ}\left(\exp(-iQd_B) - \exp(-iQd_A)\right) + \frac{n_A}{iQ}\left(\exp(-Qd_A) - 1\right)$$

Equation 5.4.16

The partial structure factor can be obtained from this and gives:

$$Q^2h(Q) = 4\left[n_A(n_A - n_B)\sin^2\left(\frac{Qd_A}{2}\right) + n_An_B\sin^2\left(\frac{Q(d_A + d_B)}{2}\right) - n_B(n_A - n_B)\sin^2\left(\frac{Qd_B}{2}\right)\right]$$

Equation 5.4.17

To fit this model to the experimental self partial structure factor four fitting parameters, n_A, n_B, d_A and d_B are used. Unfortunately, other than the thicknesses being positive, there are no physical limits which one can realistically impose on any of the

variables. This model was originally suggested in the context of a study on the interfacial distribution of surfactant molecules.[21] In such circumstances other relationships within the system can be used to constrain the fitted parameters. For example in surfactant systems is often possible, and highly advantageous, to deuterate head and tail groups selectively. Thus it is implicit that the models used to describe the distributions of these species must yield the same total surface concentration and such a requirement can be used to constrain the fitting parameters. Unfortunately, there is no parallel in the present system and the only option available was to allow both thicknesses and number densities to float unrestrained. Once a fit was obtained the parameters were expected to yield a reasonable surface concentration, although given that an adsorbed film is being studied the definition of a reasonable surface concentration is somewhat vague. Clearly, it is possible that non unique solutions may be returned by the fitting, however it is hoped that by exercising intuition the models extracted provide a fair representation of the system.

As illustrated in figure 5.4.30 this model fits the PEO self partial structure factor for Γ_s = 1 mg m^{-2} well. When the concentration of PMMA is increased to 2 mg m^{-2} the self term is quite unusual exhibiting a definite minimum. Although this feature is not reproduced exactly, the general form of the fit using this model is much improved compared to a single layer fit: compare figure 5.4.31 with figure 5.4.28. The low Q features of the data are reproduced faithfully, something which was not possible when a single layer was used. The extracted parameters for both fits are presented in Table 5.4.6.

The double uniform layer model does have certain limitations: although each layer is characterised by both a thickness and a number density there is no information on their positions relative to one another, i.e. which one is uppermost at the surface. This is a manifestation of the phase problem associated with neutron reflectivity.

From the values in Table 5.4.6, and the quality of the fits obtained, it follows that surface organisation of the PEO can be described adequately by two layers. When Γ_s = 1 mg m^{-2} the layers thicknesses are 22 Å and 15 Å, the latter corresponds to the more diffuse layer.

Γ_{Ss} / mg m^{-2}	d_A / Å	n_A / 10^{-2} Å^{-3}	d_B / Å	n_B / 10^{-2} Å^{-3}	χ^2 /10^{-11}	$\Gamma_{s\,calc}$ / mg m^{-2}
1	22 ± 1	0.24 ± 0.01	37 ± 3	0.034 ± 0.001	0.6778	0.46 ± 0.05
2	16 ± 1	0.31 ± 0.01	30 ± 1	0.094 ± 0.001	0.4596	0.51 ± 0.06

Table 5.4.6: Parameters for the double uniform layer fits.

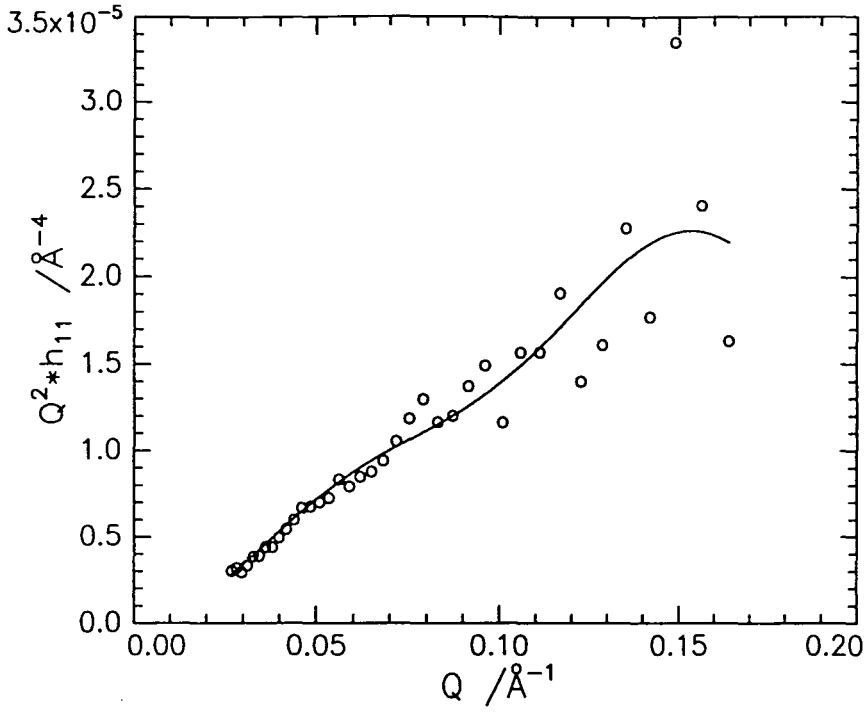

Figure 5.4.30 Double uniform layer model fitted to the self partial structure factor for PEO where Γ_{sPMMA} = 1.0 mg m^{-2}.

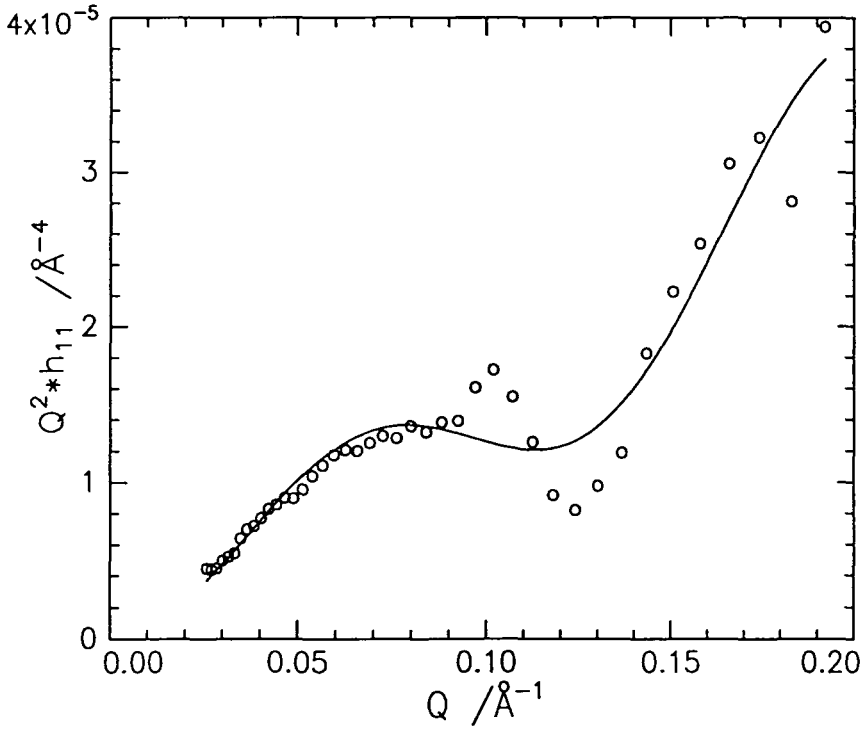

Figure 5.4.31 Double uniform layer model fitted to the self partial structure factor for PEO where Γ_{sPMMA} = 2.0 mg m^{-2}.

The layer dimensions change only slightly when the Γ_s is increased to 2 mg m^{-2}. The dense layer becomes slightly narrower at 16 Å whilst the dimensions of the lower layer remain much the same at 14 Å. Within error the concentration of PEO contained in this upper layer is the same for both models, the reduction in the thickness of the denser layer when Γ_s = 2 mg m^{-2} being compensated for by an accompanying increase in the number density. In contrast, whilst the thickness of the diffuse layer, layer B, remains the same the number density of PEO increases with Γ_s. As a consequence of this the concentration of PEO in this layer is only 0.04 ± 0.01 mg m^{-2} at the lower concentration of PMMA and 0.11 ± 0.02 mg m^{-2} for Γ_s = 2 mg m^{-2}. From this result it would appear that changing the amount of PMMA spread on a solution of PEO results in a number of changes. It is clear that for Γ_s = 1 mg m^{-2} and above the surface organisation adopted by the PEO is very different to that at the surface of a clean solution, requiring a different model to be adopted. The dimensions of the two layers at the interface do not vary greatly with Γ_s and the surface excess of PEO remains much the same. In fact, referring back to section 5.4.2 demonstrates that the surface excess is essentially the same as for a PEO solution.

Modelling the surface excess of PEO as existing in two uniform layers much improved the fits to the self partial structure factors. Whilst the structure adopted by the PEO at the interface is quite different from that of adsorbed layers of PEO the surface concentration is very similar. From this result it is concluded that the adsorbed PEO which is present at the surface before the PMMA is spread is forced to adopt a different structure when the film is spread. Despite this change in structure there does not appear to be significant desorption, or adsorption, of PEO at the interface. When the concentration of PMMA is increased to 2 mg m^{-2} the layers of PEO become denser, each being narrower with an increased number density. Despite these changes the total surface concentration of PEO remains the same.

It is noted that there is an alternative two layer model which has also been considered, particularly in reference to the PMMA self terms. This model is comprised of two Gaussian layers and has five fitting parameters. Given that the double uniform layer model fitted the PEO self partial structure factors adequately it was not necessary to introduce this more complex model. A full description of the details and application are given in the subsequent section.

A full analysis of the cross terms should enable the relative positions of all the species to be determined so that it is possible to establish which of the two layers is uppermost. This, combined with a basic knowledge of the polymers, should help to resolve the ambiguity

associated the two layer model. The details of this analysis are left until the cross terms are explicitly considered and analysed.

The parameters fitted to the PEO self term when Γ_s = 1.0 mg m^{-2} imply that the surface concentration of PEO is the same as that for surface excess formed for a solution of PEO although the organisation of the PEO in the two situations is very different. As has been previously discussed, the results of monitoring the surface pressure of this system over time implied there were no significant relaxations. However, reorganisation of the PEO at the interface may not cause a change in the surface pressure and so this observation does not provide any information about the timescale over which the structural reorganisation changes. Van der Beek et al[18] suggest that, certainly for polymers adsorbing from solution, diffusion and reorientation processes occurring in the surface region are rapid.

From the results in Table 5.3.2 it was noted that the surface tension of the PEO - PMMA system when Γ_s = 2.0 mg m^{-2} was found to be higher than for PMMA- water. From this result either additional adsorption, or complete desorption, of the PEO could be rationalised as, in principle, either would lead to a system of lower surface energy. The fitted parameters indicate clearly that the total surface concentration of PEO remains unchanged. It is therefore assumed that the system manages to achieve a low energy surface without the surface excess of PEO changing. This suggests that by adopting a surface organisation of PEO different to that of the adsorbed layer the system reaches a stable configuration. Unfortunately, as noted earlier, this data set is currently incomplete and as a consequence it is not possible to determine the interfacial structure in any further detail.

The conclusion that the total surface concentration of PEO remains unchanged from that for a bare solution implies that the observed relaxation is not due to any desorption / adsorption processes. Neither is the relaxation likely to be linked to the reorganisation of PEO into a two layer structure. If this were the case a relaxation would be anticipated for a 1 mg m^{-2} film. It is therefore concluded that the observed relaxation is due to processes in the film akin to those exhibited by films of PMMA on water.[19]

Attention is now turned to the PEO self term for Γ_s = 3 mg m^{-2}. The values are low and rather scattered. Despite the scatter in the points attempts have been made to fit the behaviour. There is little to chose between the Gaussian and uniform layer model as illustrated in figure 5.4.32.

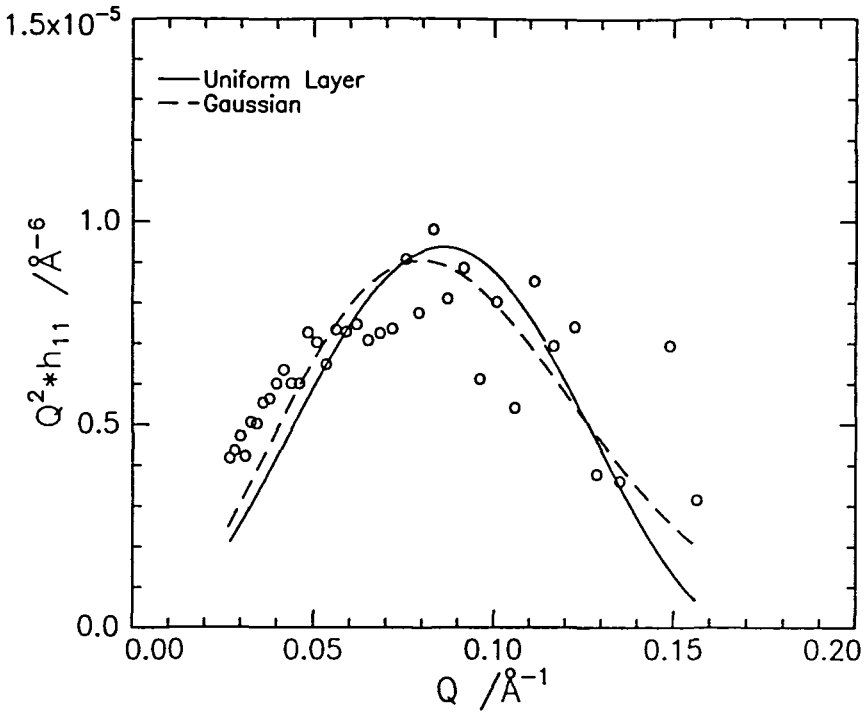

Figure 5.4.32 Best Gaussian and uniform layer fits to PEO self partial structure factor when $\Gamma_s = 3.0$ mg m^{-2}. Open circles are experimental values.

Given the scatter in the self term the implications of the parameters in table 5.4.7 are uncertain. It appears that the surface concentration of PEO is not significantly different to that adsorbed at the surface of a clean solution. However, the thickness of the layer, or width of the distribution depending which model is accepted, is considerably greater than for a PEO solution. In addition the number density is almost halved compared to that for the same model applied to PEO solution, see Section 5.4.2 and the parameters in table 5.4.7.

a: Uniform Layer

Γ_s / mg m^{-2}	n /10^{-2} Å^{-3}	d / Å	χ^2 / 10^{-11}	Γ_s / mg m^{-2}
3	0.15 ± 0.01	37 ± 1	0.3165	0.44 ± 0.04

b: Gaussian Distribution

Γ_S/ mg m^{-2}	n /10^{-2} Å^{-3}	σ / Å	χ^2 / 10^{-11}	Γ_s / mg m^{-2}
3	0.20 ± 0.01	35 ± 1	0.2000	0.56 ± 0.04

Tables 5.4.7a & b : Fitted parameters for PEO self partial structure factor.

It appears then that the PEO still populates the surface but forms a thicker, more diffuse layer. Once again it is observed that neither the uniform layer, nor the Gaussian model, reproduce the low Q variation of the self terms well. A double uniform layer model has purposely not been fitted to the data. Fitting a four parameter function to such scattered data is not justifiable.

Although only a very rough idea of the interfacial structure adopted by the PEO in the presence of the most concentrated film of PMMA has been gleaned the results do seem to be consistent with other data, primarily the surface pressure relaxation study. As for Γ_s = 2 mg m^{-2}, although the PEO may be reorienting itself at the interface this is not expected to have any effect on the surface pressure measurement. Instead the observed relaxation in the surface pressure is expected to be associated predominantly with relaxations and reorientations of the PMMA at the interface.

Following from the discussion above it can be concluded that on spreading a film of PMMA onto a solution of PEO the interfacial organisation of adsorbed PEO is modified. It seems that the surface excess of PEO spreads itself over a wide interfacial region with a lower number density.

Consideration of the area available for the species at the interface provides additional evidence for the existence of very different surface organisation for PMMA / PEO solution compared to the analogous polymer on water systems. The limiting area per monomer unit for PMMA on water and PMMA on PEO solution have been determined and for subsequent comparison the values are repeated here, along with that for spread PEO films as reported by Henderson,[19] see Table 5.4.8.

The limiting area per MMA segment is very low in the presence of PEO solution. In fact, from a very basic estimation of the area occupied if one PMMA unit was to sit flat on the liquid surface occupying a rectangle of the surface an area of 24 $Å^2$ was extracted.[16] It would appear that in the presence of PEO solution the units of PMMA occupy far less space, so much so that it is not likely to be just through increased packing but rather reflects the fact that not all the MMA groups are in contact with the water surface.

System	Area per monomer unit / Å^2
PMMA on water	17
PMMA on PEO solution	8
Spread PEO	43

Table 5.4.8: Area occupied per monomer unit.

Taking the limiting area occupied by spread PMMA on water it transpires that 1 m^2 of surface will be exactly occupied by PMMA when Γ_s = 1.00 mg m^{-2} and the molecules are at their limiting area. This result appears to be consistent with indications from the neutron data that the surface excess of PEO is forced to reside in a rather thicker layer than it would normally occupy at the surface of a solution. Presumably this behaviour reflects the fact that there is less free area available for the PEO to occupy in the presence of the PMMA film. Since PEO is water soluble, it seems reasonable to suggest that this polymer may relinquish at least some of the area it occupies prior to deposition of the PMMA. Given the relative solubilities of PEO and PMMA in water it seems reasonable to expect that PEO, rather than PMMA, will form a layer heavily diluted by the subphase. From this discussion it appears that consideration of the area available at the surface, in addition to surface tension differences, will be important in determining the organisation of species at interfaces. To consider such effects further it would be interesting to study a 0.5 mg m^{-2} film of PMMA on PEO solution. At this concentration the PMMA is not expected to occupy the entire surface so it is possible that a mixed layer of PEO and PMMA would form. In such circumstances the surface organisation of the two polymers would be expected to retain characteristics associated with the individual polymers on water. Although this experiment was planned, due to beam loss it has not been possible to do it.

5.4.4.3B The PMMA Self Partial Structure Factor

The self partial structure factors for PMMA, like those of PEO, do not conform to the basic models of either a single uniform layer or a Gaussian distribution of segments. As observed for PEO the self terms exhibit behaviour at low Q which the simple models fail to reproduce. This tendency is greatest when the self term for the concentrated film is considered, see figure 5.4.33.

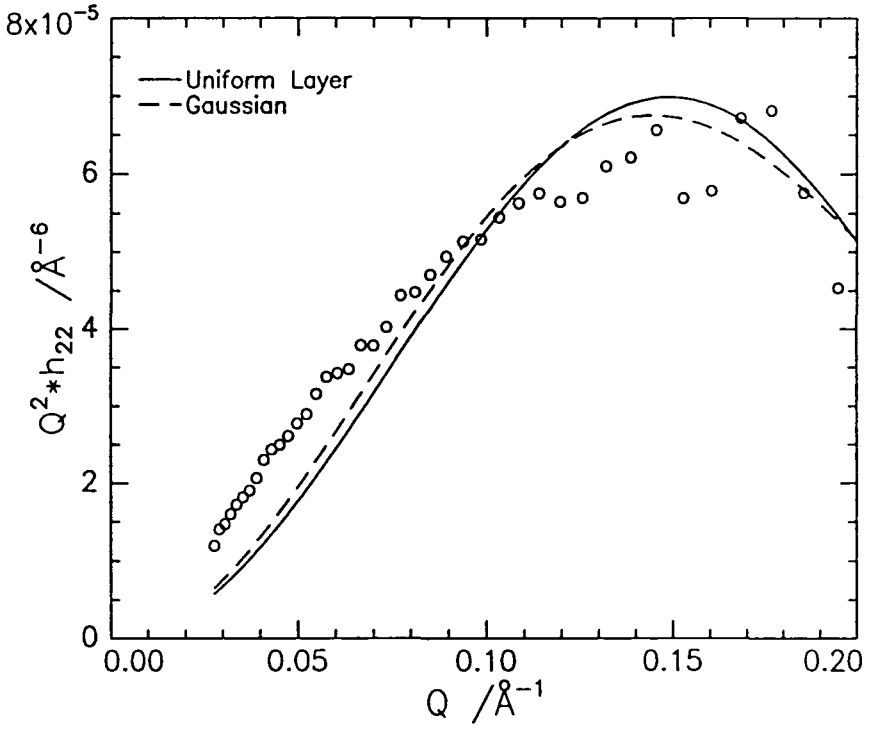

Figure 5.4.33 'Best' fits to the PMMA self partial structure factor for a 3 mg m^{-2} film using the models indicated. Open circles represent experimental values.

In an attempt to fit the PMMA self partial structure factors models for two distinct layers at the interface have been adopted. As well as the previously discussed double uniform layer model the concept of two Gaussian segment distributions has also been considered. The results for a double uniform layer model are considered first.

Equation 5.4.17 was fitted to the data to extract the number density and thickness of each layer. The fits were much improved as can be seen by comparing figure 5.4.34 and figure 5.4.33. The parameters of the fits are given in Table 5.4.9

System / mg m^{-2}	d_A / Å	n_A / 10^{-2} Å^{-3}	d_B / Å	n_B / 10^{-3} Å^{-3}	χ^2 /10^{-11}	Γ_{scalc} / mg m^{-2}
1	22 ± 1	0.25 ± 0.01	28 ± 2	0.24 ± 0.04	0.1408	1.01 ± 0.24
3	26 ± 1	0.43 ± 0.01	32 ± 1	0.57 ± 0.04	0.2292	2.06 ± 0.23

Table 5.4.9: Parameters of the double uniform layer fits.

Modelling the polymer distribution as a double uniform layer appears to fit both the self partial structure factors at high and low Γ_s satisfactorily. The PMMA remains predominantly in layer A, layer B is only 6 Å thick and is thought to represent a rough layer of PMMA between the dense layer and the bulk continuous phase, water or air. Given the dimensions of this layer it is anticipated to correspond to chains of PMMA looping out of layer A. The surface concentration calculated from the fitted parameters is in good agreement with the known spread amount for the case of the dilute film. In contrast, for the 3 mg m^{-2} film the surface concentration is calculated to be 2.06 mg m^{-2}, which is significantly lower than the spread amount. Film inhomogeneity is sometimes suggested to account for such discrepancies but this is not anticipated to be such an issue for high concentration films. Although there is evidence to suggest that dilute films of PMMA on water exist as islands studies indicate that as the surface concentration is increased the films become uniform.[13]

Assuming that the film has in plane uniformity the means by which polymer could be 'lost' are now considered. The highest surface concentration film of syndiotactic PMMA previously studied on water was 2 mg m^{-2}. The PMMA self term was fitted using a uniform layer and the surface concentration obtained was 1.8 mg m^{-2}, the only spread film of the seven studied by Henderson et al[1] for which fits to the neutron reflectivity data gave a concentration lower than the known spread amount. Of more direct relevance is the study of the 3 mg m^{-2} film of PMMA on water, see section 5.4.3, for which the surface concentration implied by neutron reflectivity is significantly lower than the spread amount. In this case the self term was fitted well using a Gaussian distribution, the parameters of which indicated a surface concentration of 1.7 mg m^{-2}. The reason for the discrepancy was attributed to detachment of polymer chains from the surface, possibly with the formation of loops. Given this result it is perhaps not too surprising that the same observation is made for PMMA on PEO solution. However, it is noted that in the latter case the discrepancy in Γ_s between the spread and calculated surface concentration is less. This result is significant since it confirms the

suggestion that the presence of PEO at the water surface not only changes the interfacial structure adopted by the PMMA. In addition it appears that more PMMA remains at the immediate surface indicating that when PEO populates the water surface it becomes a more favourable environment for PMMA. As a consequence of this, less of the PMMA detaches itself from the surface and is 'lost'.

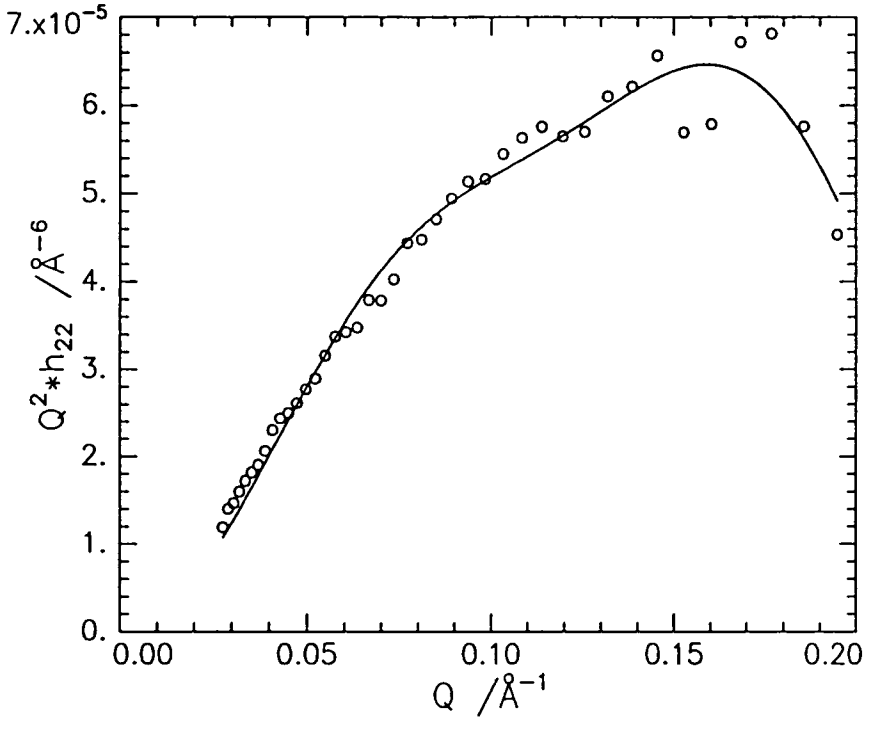

Figure 5.4.34 Double uniform layer fit for 3.0 mg m^{-2} film of PMMA. Solid line represents the fit, open circles the experimental data.

The low surface concentrations inferred from neutron reflectivity data for PMMA on water, and in turn for PMMA on PEO solution, have been rationalised to an extent, albeit in a rather qualitative manner. However, an alternative explanation worth considering is that the double uniform layer model is not a good description of the distribution of PMMA at the interface in this case. If this is correct, any other model must contain specific features. The presence of the shoulder in the self term at low Q indicates that the distribution of PMMA at the interface is likely to be asymmetric and this must be incorporated into any model. In view of this, the model which has been considered is that of two Gaussian layers.

The number density of two Gaussian layers at the interface one centred at z = 0 and one centred at d_g is given by:

$$n(z) = n_{i1} \exp\left(\frac{-4z^2}{\sigma_1^2}\right) + n_{i2} \exp\left(\frac{-4(z+d_g)^2}{\sigma_2^2}\right)$$

Equation 5.4.18

A typical number density profile described by this equation is represented schematically in figure 5.4.35.

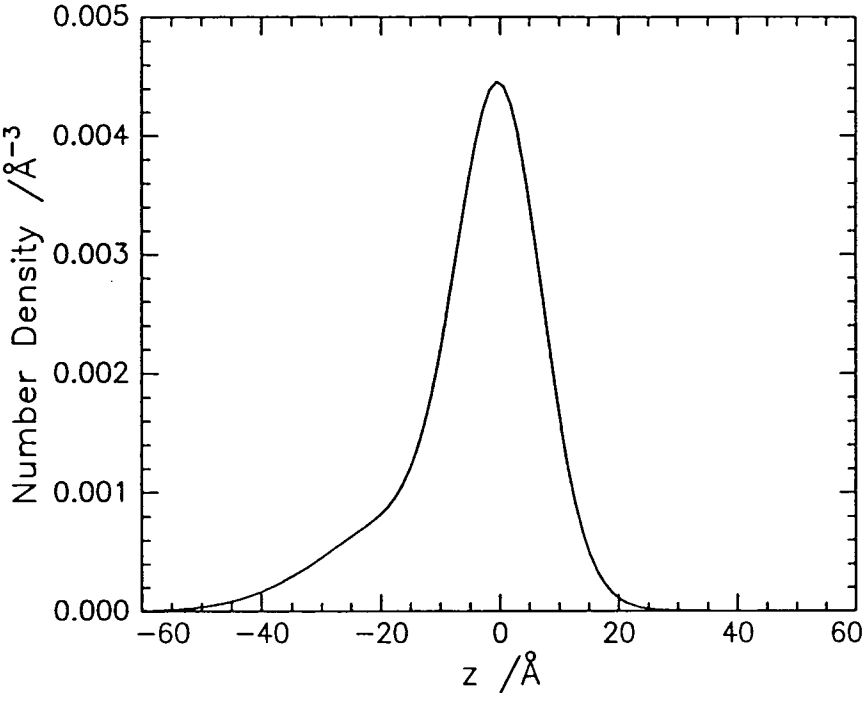

Figure 5.4.35 Number density profile for a double Gaussian layer, $n_1 = 0.4 \times 10^{-2}$ Å^{-3}, $n_2 = 0.8 \times 10^{-3}$ Å^{-3}, $\sigma_1 = 20$ Å, Å $\sigma_2 = 40$ Å and $d_g = -15$ Å.

As illustrated in figure 5.4.35 this approach provides another way, in addition to two uniform layers, by which an asymmetric distribution of polymer at the interface can be described. The Fourier Transform of equation 5.4.18 gives $n_p(Q)$,

$$n(Q) = \frac{\sqrt{\pi}}{2}\left(n_1\sigma_1 \exp\left(\frac{-Q^2\sigma_1^2}{16}\right) + n_2\sigma_2 \exp\left(\frac{-Q^2\sigma_2^2}{16}\right)\exp\left(-id_gQ\right)\right)$$

Equation 5.4.19

The self partial structure factor can also be determined and is given by:

$$h(Q) = \frac{\pi}{4}\left(n_1^2\sigma_1^2 \exp\left(\frac{-Q^2\sigma_1^2}{8}\right) + n_2^2\sigma_2^2 \exp\left(\frac{-Q^2\sigma_2^2}{8}\right) + 2n_1n_2\sigma_1\sigma_2 \cos\left(Qd_g\right)\exp\left(\frac{-Q^2(\sigma_1^2+\sigma_2^2)}{16}\right)\right)$$

Equation 5.4.20

Equation 5.4.20 describes the self partial structure factor for a double Gaussian distribution of polymers at the interface and contains five variables, these being the width and number density of each distribution and their separation, d_g.

Given the large number of variables it is highly unlikely that equation 5.4.20 would not fit the data. However, whether parameters of real physical significance can be extracted from such a fit is another question. There is undoubtedly going to be some interplay between all the parameters and the results of such a fit should be treated with caution. With these considerations in mind the PMMA self terms have both been fitted by this model, the results are presented below in Table 5.4.10, an example of a fit is given in figure 5.4.36.

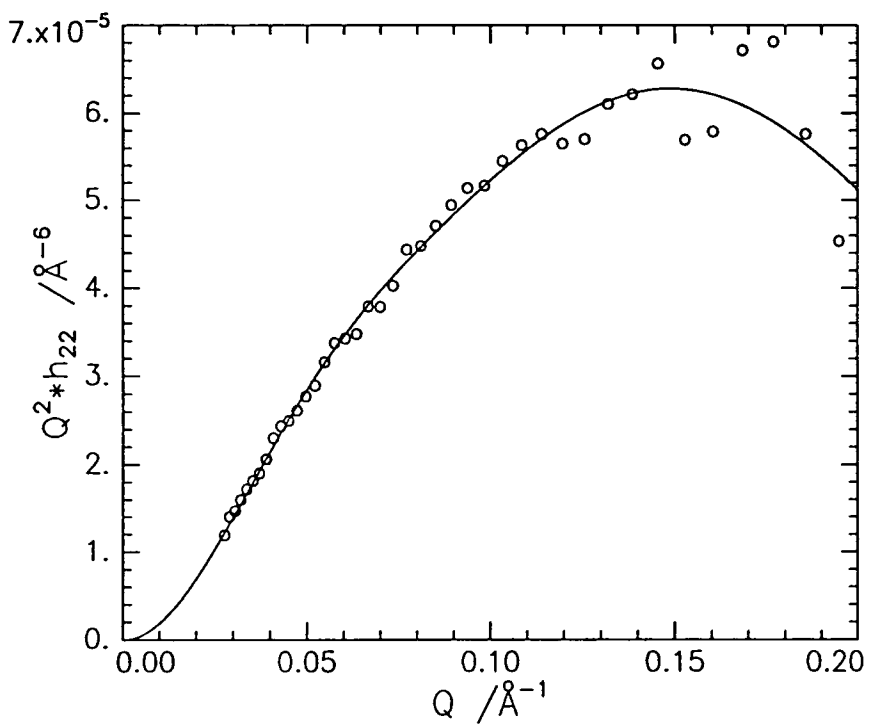

Figure 5.4.36 Double Gaussian fit to the PMMA self partial structure factor, Γ_s = 3 mg m^{-2}. Solid line represents fit, open circles experimental data.

System Γ_s / mg m^{-2}	σ_1 / Å	n_1 / 10^{-2} Å^{-3}	σ_2 / Å	n_2 / 10^{-2} Å^{-3}	d_g / Å	χ^2 /10^{11}
1	15 ± 1	0.49 ± 0.01	71 ± 4	0.085 ± 0.005	-0.1 ± 10	0.276
3	8 ± 7	0.80 ± 0.54	49 ± 5	0.16 ± 0.04	-0.2 ± 10	0.223

Table 5.4.10: Parameters from double Gaussian fits.

The parameters extracted from these fits are subject to large uncertainties, in particular the term d_g, see Table 5.4.10. This behaviour can be rationalised by generating $Q^2h_{pp}(Q)$ for the double Gaussian layer using $n_1 = 0.2 \times 10^{-2}$ Å^{-3}, $n_2 = 0.5 \times 10^{-3}$ Å^{-3}, $\sigma_1 = 20$ Å and $\sigma_2 = 30$ Å. The separation of the two distributions, d_g, is varied from 0 - 30 Å and the results are given in figure 5.4.37.

There is only a subtle change in $Q^2h_{pp}(Q)$ as d_g increases from 5 Å to 10 Å and over the low Q range, 0 - 0.15 Å^{-1}, where the experimental self partial structure factors are most reliable, there is barely any difference. The asymmetry arising due to the presence of a second distribution is identifiable only by access to Q values above 0.15 Å^{-1} and unfortunately over this range the experimental values are scattered as the reflected signal is lost in the background.

The data in figure 5.4.37 demonstrates that the influence of d_g is unlikely to be correctly accounted for until its value exceeds 10 Å. Any effects on the experimental self terms that are due to small d_g values can be fitted by a combination of other variables. This will mask the influence of d_g and the extracted values will not have any physical significance. As d_g increases to larger values , 20 and 30 Å, which are of the same magnitude as the width of the distribution, the self term exhibits characteristic behaviour at low Q which could only be accounted for by assuming a significant separation between the two distributions.

From the discussion above it follows that the larger the separation between the distributions the easier it will be to fit the data and extract a reliable value of d_g. This was confirmed, albeit rather crudely, by attempting to fit the generated self partial structure factors given in figure 5.4.37 for $d_g = 5$ Å and $d_g = 30$ Å. The same starting points were used for both fits, with the initial guess for d_g being 17 Å. This value was chosen as it is intermediate between the separate values for the two systems. The 'best' parameters for the fit to the data generated from $d_g = 5$ Å are presented in Table 5.4.11 below.

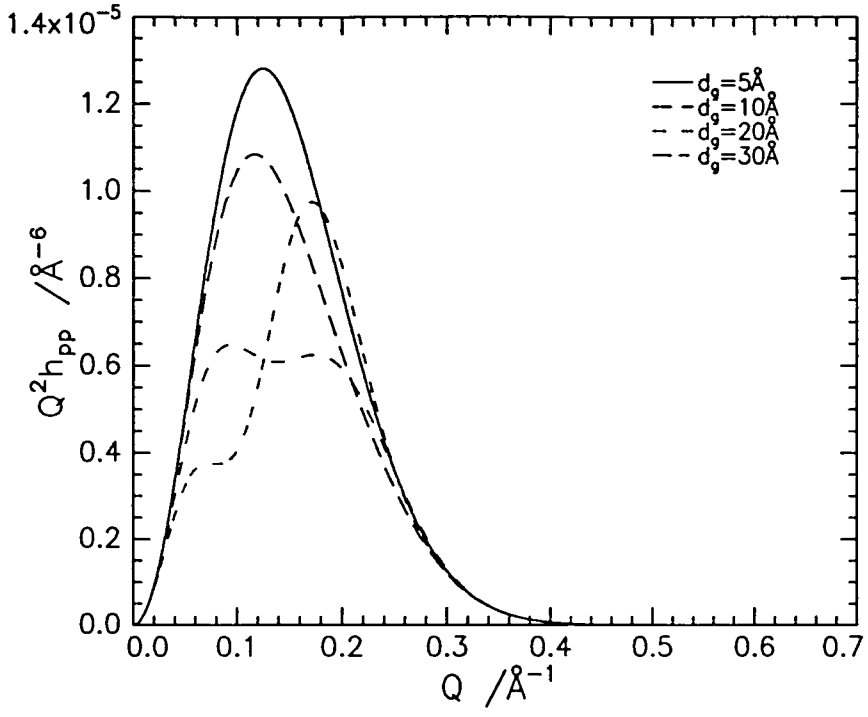

Figure 5.4.37 Generated self partial structure factors for a double Gaussian layer varying d as given, see text for details of the parameters.

σ_1 / Å	n_1 / 10^{-2} Å^{-3}	σ_2 / Å	n_2 / 10^{-2} Å^{-3}	d_g / Å	χ^2 / 10^{-16}
24 ± 1	0.23 ± 0.01	0.9 ± 0.2	0.0062 ± 0.0001	86 ± 1	0.6705

Table 5.4.11: Parameters for a double Gaussian layer fit to generated data.

Clearly, these values are not even close to those used to generate the data. In fact if different starting parameters were used it was found to be very hard to get the program to fit this data and frequently the fitting routine became stuck and failed. In contrast the data generated for d = 30 Å fitted very well and gave exactly the same parameters as those used to generate the data with uncertainties of less than 0.1%.

These results confirm that $Q^2h_{pp}(Q)$ will only reflect the influence of d_g sufficiently to give fitted parameters of good confidence when d is relatively large, i.e. comparable with the width of the separate distributions. Consider the fact that the self partial structure factors for PMMA were fitted by a double uniform layer model. In this model the layers are essentially back to back, i.e. d = 0. It has already been demonstrated that fits to experimental

self terms using single uniform layers and Gaussian distributions are often very difficult to distinguish and the fitted parameters are generally found to be very similar. Assuming that this behaviour translates to the 'double' equivalents of these models it is expected that, similarly, the fitted parameters of these models should also return similar parameters. If this is the case the centres of the two Gaussian distributions, like the uniform layers, are expected to be relatively close to one another. As demonstrated, attempting to fit such behaviour with equation 5.4.20 will yield unrealistic parameters. This rationalises the observation made previously that, although the Gaussian model did fit the self partial structure factors, the uncertainties on the parameters are such that they are unrealistic and the model is therefore abandoned.

The discussion above suggests that whatever the true nature of the distribution of the PMMA segments normal to the interface it is continuous and the model of two distributions separated appreciably from one another is not valid. Since the PMMA was spread at the interface this is not very surprising. Models where the distributions are separated necessarily imply that some of the spread film has diffused a significant distance from the rest to form a separate layer. In contrast the double uniform layer model describes a finite width of the interface in which the PMMA resides with a continuous distribution. This is intuitively more acceptable than the type of double Gaussian distribution which can be reliably identified by this technique.

It is concluded that the preferred model for describing the distribution of PMMA at the interface is the double uniform layer model. Having accepted this model the details of the surface organisation for the two surface concentrations of PMMA are now considered. Referring back to table 5.4.9 it becomes clear that the dimensions of the two layers of PMMA remain very similar despite the large increase in surface concentration, this change being reflected in the number densities of the two layers. What is not clear from either fit is which layer is uppermost at the surface. Considering the behaviour of the PMMA on water, and the known hydrophobicity of this species, it seems fair to assume at this stage that the layer with the greatest number density sits on top of the water. The diffuse layer may represent PMMA chains just looping beyond the defined layer on one side, penetrating either the air or the water. More detailed information regarding the relative positions of all the species at the interface is required to determine the most likely structure. This is available from the cross partial structure factors and will be reconsidered in the relevant section.

To summarise, it is clear that the surface organisation of both a 1 mg m^{-2} and 3 mg m^{-2} film of PMMA spread on an aqueous solution of PEO can be adequately described by a double uniform layer. The thicknesses of the layers barely change with surface concentration, the most marked changes occur in the number densities of the layers. This may indicate that it is preferable for the polymer to pack more tightly in the volume rather than attempt to create more space at the interface. Such behaviour is consistent with a relatively confined interface. Consideration of the cross terms and the behaviour of all the species should resolve the remaining ambiguities regarding the details of surface organisation.

5.4.4.3C The Water Self Partial Structure Factor

The self partial structure factors for water exhibits remarkable behaviour, see figure 5.4.38. It has already been noted that as Q approaches zero the self partial structure factor for water should always tend to n^2_{W0} i.e. 0.0011 $Å^{-6}$. This follows because there is an inverse dependence between penetration depth, d_p, and Q so that as Q tends to zero d_p tends to infinity which corresponds to the bulk. This is also clearly indicated by either of the models used to describe the distribution of water, equations 5.4.8 and 5.4.10.

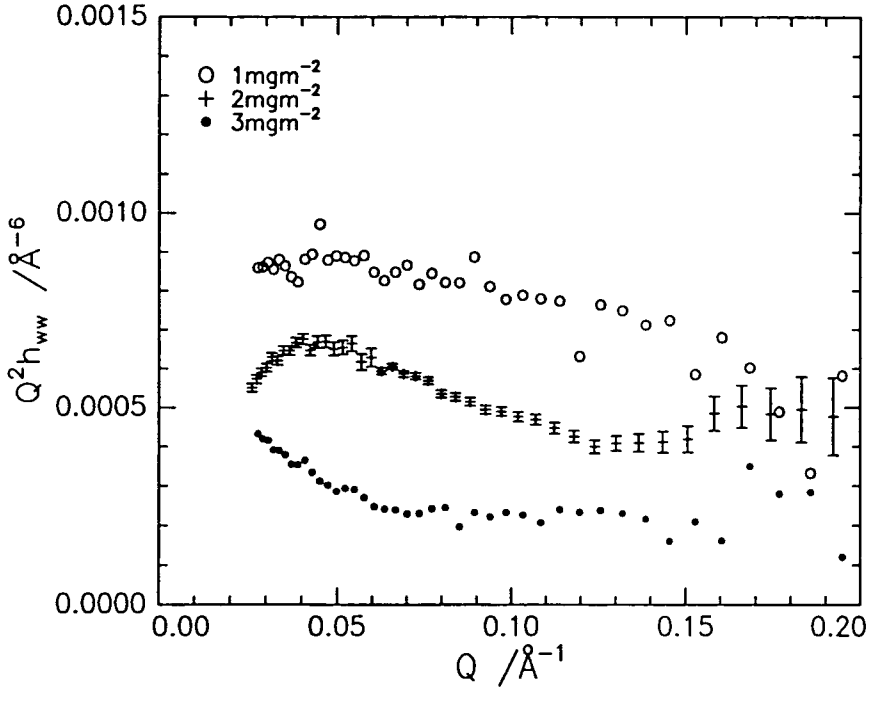

Figure 5.4.38 Water self partial structure factors, the concentration of PMMA is indicated.

Consider the form of $Q^2h_{ww}(Q)$ described by the tanh and single uniform layer profiles which have been used to model subphase distributions successfully. The anticipation is that the water self partial structure factors determined for PMMA on PEO solution would be similar, i.e. relatively flat with a gradual increase to a value of 0.0011 $Å^{-6}$ as Q approaches zero. This is the behaviour exhibited by the water self partial structure factor when a 1 mg m^{-2} film of PMMA is spread. As can be seen in figure 5.4.38, $Q^2h_{ww}(Q)$ increases very slowly with decreasing Q in the presence of the low concentration film of PMMA; in fact the values are almost flat. A rather puzzling feature of the behaviour is the slight downturn exhibited at the lowest Q. It has been observed that for a number of polymeric systems the water self partial structure factor exhibits this kind of downturn at low Q. This appears to be particularly so for systems which contain PEO,[2,3] although such behaviour is also evident in an early study of isotactic PMMA by Henderson et al.[22] No explanation has been put forward to account for this behaviour. Currently there are suggestions that PEO somehow causes the water to become more structured. This fails to explain the observation rigorously and offers no rationale for the behaviour of PMMA films. As Q decreases, i.e. as larger penetration depths are probed, the number density should become that of bulk water. If the self term does not intercept the y axis at the bulk number density of water, the implication is that the bulk properties of water are being altered by the presence of a monolayer at the surface. This does not seem very credible, particularly if the spread monolayer is insoluble as in the case of PMMA.

In this particular study PEO is a bulk solute and the idea of changes in the bulk properties of water due to the presence of the solute are slightly more acceptable. Since the solution is dilute, only 0.1 wt.%, it seems surprising that such low concentrations of PEO would influence the water structure so drastically. Unfortunately, this study does not appear to offer any further clues as to the origin of this effect and its presence is simply noted.

When a 3 mg m^{-2} film is spread the behaviour of the self partial structure factor is totally different to that for the dilute film, see figure 5.4.38. The values are very low and do not exhibit any of the classical behaviour associated with subphase self terms. If the values are to be extrapolated towards 0.0011 $Å^{-6}$ as Q approaches zero a very rapid increase is required. No such behaviour has been exhibited by any of the other systems studied here. Given the unusual nature of these values the possibility of errors in data reduction has been

addressed. To this end the water self partial structure factor has been calculated from the reflectivity data.

As for the PEO system, the water self partial structure factor can be calculated from a reflectivity profiles. In this case the profile for the hPEO / hPMMA / D_2O contrast was used. A flat background was subtracted from the data and it was then corrected as appropriate for a D_2O subphase. Assuming that R(Q) for this system is due to the D_2O present gives:

$$R(Q) = \frac{16\pi^2}{Q^2} b_w^2 h_{ww}(Q)$$

Equation 5.4.21

The self partial structure factor determined in this way exhibited exactly the same behaviour as the true partial structure factor. Within error the estimated values agreed with the 'true' values. This confirms that the self partial structure factor observed does represent real behaviour of the system. This result was so surprising that it was considered wise to repeat the measurement to ensure that the result is reproducible. The repeat reflectivity data for the hPEO / hPMMA D_2O system was obtained on SURF. The result was reproducible in all respects indicating that a real effect was being observed. The data was combined with the previously collected spectra and used to solve PARTIAL3. In addition, generation of the $R(Q) \times Q^4$ data file enabled a quick estimation of the self partial structure factor, Q^2h_{ww}. The self partial structure factor was found to be reproduced well indicating not only that the observed partial structure factor is 'real', but also the reassuring result that the reflectometers SURF and CRISP give equivalent data.

The reflectivity profile for hPEO / hPMMA / D_2O in the presence of a 2 mg m^{-2} film of PMMA was also available. Unfortunately it was not possible to perform a full kinematic approximation analysis for this concentration, but using the method described above the water self partial structure factor has been estimated directly from the reflectivity data. The resulting self term is also plotted in figure 5.4.38 and is found to be very low over the entire Q range, falling between the self terms for the extremes of the PMMA surface concentrations studied. Similar to the self term for the most concentrated film of PMMA, this term is clearly much lower than one would anticipate. Since this term was extracted using approximations the question arises as to whether this behaviour could be a symptom of the fact that a number of approximations have been used to extract the values. Due to the way in which this self

term was extracted it is likely to be slightly over estimated rather than underestimated. Basically, all the reflectivity has been attributed to the D_2O despite the fact that the hydrogenous polymers may contribute. Given this consideration it is clear that even the 'real' self term will not approach the more generally accepted behaviour exhibited by the self term for Γ_s = 1 mg m^{-2}. This result implies that increasing the concentration of the PMMA film causes a progressive change in the structure of the water layer at the interface. In addition this particular self term exhibits some unique behaviour, in contrast to the other water self terms in figure 5.4.38 that for Γ_s = 2 mg m^{-2} decreases in a linear manner with increasing Q between 0.05 - 0.10 $Å^{-1}$. Meanwhile the other water self terms, for a 1 mg m^{-2} and 3 mg m^{-2} film, are essentially flat over the same interval. The downturn in Q^2h_{ww} at the lowest Q values, mentioned in reference to the low concentration behaviour, is even more pronounced in this system.

In the presence of a 1 mg m^{-2} film of PMMA the water self partial structure factor was observed to exhibit classical behaviour. As a consequence the tanh and uniform layer models have both been used to model behaviour, see figure 5.4.39.

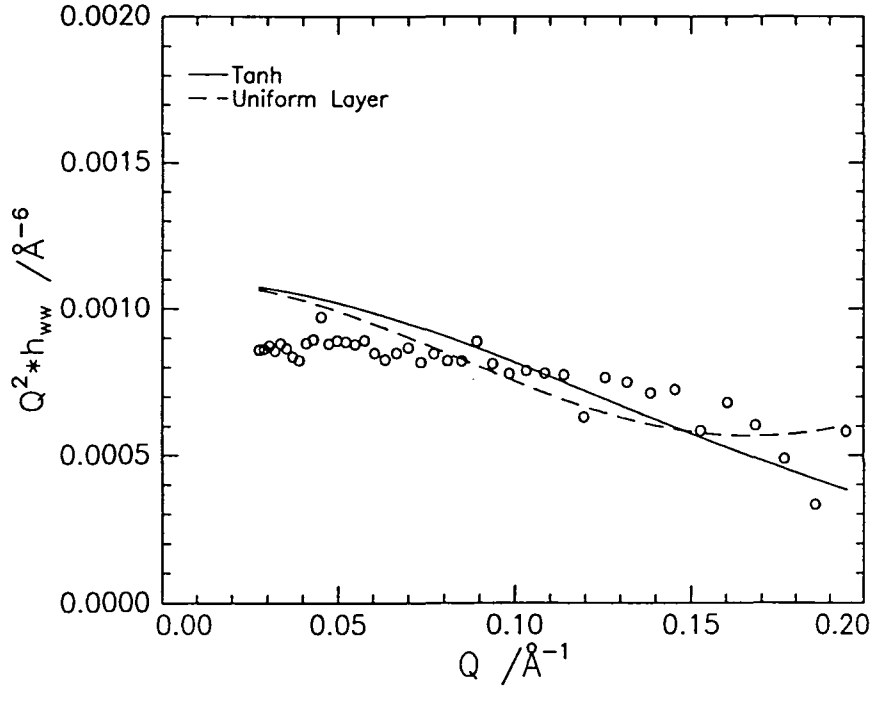

Figure 5.4.39 Fits to the water self partial structure factor in the presence of a 1 mg m^{-2} film of PMMA. Open circles represent data, lines fits as indicated.

Clearly neither of the models reproduces the experimental self partial structure factor. Such behaviour is often observed for polymeric systems. Given that the discrepancies between experiment and theory are not specific to this system the approach used by in a number of studies[12,1,9] is applied and the tanh model is adopted. This model represents a gradually changing number density profile and intuitively seems more acceptable than a the step profile associated with a uniform layer model. The parameters of both the fits are given in Table 5.4.12.

Model	**d / Å**	**n_w / 10^{-2} Å^{-3}**	**χ^2 / 10^{-7}**
Uniform layer	19 ± 1	0.47 ± 0.04	0.1147
Model	**ζ / Å**		**χ^2 / 10^{-7}**
Tanh	6.11 ± 0.29		0.1742

Table 5.4.12: Fitted parameters to water self partial structure factor

It is instructive to compare the water self partial structure factor in the presence of a 1 mg m^{-2} film of PMMA to that for a solution of PEO, see figure 5.4.40. There is barely any difference between the two self terms and the values are almost coincident. This seems to indicate that, certainly at this concentration of PMMA, it is the PEO that primarily influences the structure adopted by the water in the interfacial layer.

Similar data exists for a 1 mg m^{-2} film of PMMA on water, although the experiment and analysis were performed relatively early in the development of the kinematic approximation and only uniform layer models were used to interpret the data. On comparison it appears that the water self partial structure factor is similar to that reported here which may indicate that, within the resolution of the experiment, the type of structure adopted by the water is influenced simply by the presence of the polymeric species rather than being discretely influenced by specific functionalities. At this stage there is insufficient evidence to suggest any hypothesis about exactly how and why certain polymers cause such behaviour, it is simply concluded that the water self partial structure factor for a 1 mg m^{-2} film of PMMA spread on a PEO solution is consistent with studies of the individual systems.

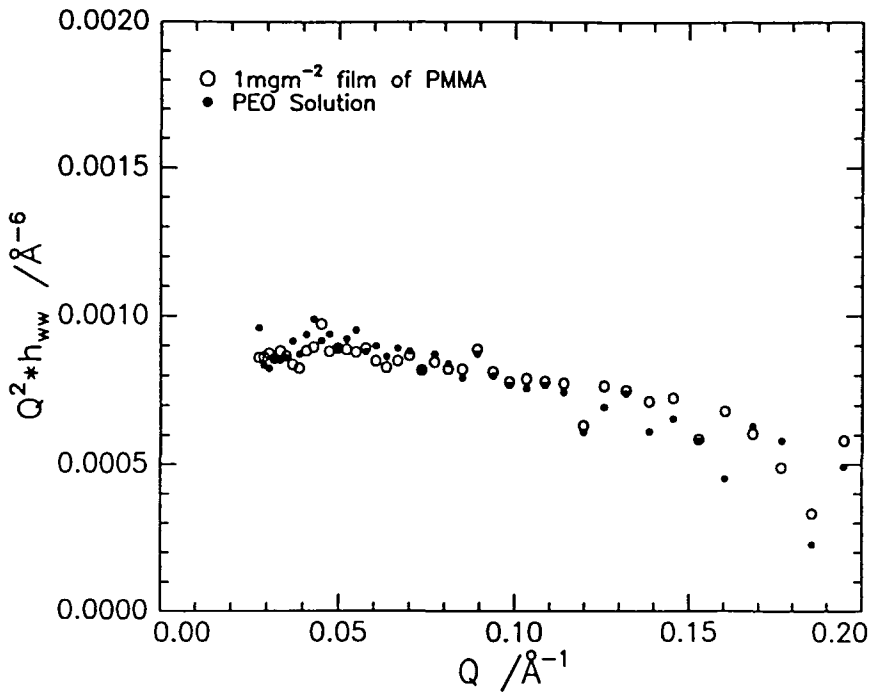

Figure 5.4.40 Comparison of the water self partial structure factors for PEO solution and with a 1 mg m^{-2} film of PMMA.

Attention is now turned to the rather more bizarre self partial structure factors obtained in the presence of a 3 mg m^{-2} and 2 mg m^{-2} film of PMMA. The behaviour of these self terms is quite remarkable. The values are exceptionally low over the entire Q range. This is particularly true for the highest concentration PMMA film for which between 0.10 - 0.15 Å^{-1} the number density of water is extremely small, about 0.00015 Å^{-6}, less than a tenth of the value for bulk water. Taken at face value this observation implies that there is a significant depletion of water in the interfacial layer. Similar behaviour is exhibited when the film concentration is 2 mg m^{-2}, although the values are slightly higher than for a 3 mg m^{-2} film. More amazing still is the extraordinary behaviour exhibited by both self terms at low Q. For both self terms to extrapolate to 0.0011 Å^{-6} a rapid increase is required at low Q. For the self term where Γ_s = 2 mg m^{-2} this involves a total change in character since extrapolation of the values at the lowest Q would be in the wrong direction! The fact that Q^2h_{ww} is so low at the lowest Q for both these terms indicates that the number density is far from that of bulk water. This suggests very long range ordering of the solvent, extending over hundreds of Ångstroms, resulting from the changes caused by a spread film of PMMA. Nothing of comparable scale has been observed for either corresponding polymer / water systems or indeed any polymer

systems. Clearly neither a single uniform layer or tanh model will successfully fit this behaviour.

The unusual partial structure factors are entirely consistent with the reflectivity profiles for the three systems. The profiles are overlaid in figure 5.4.41 and it is clear that as the concentration of PMMA increases the reflectivity falls quite rapidly.

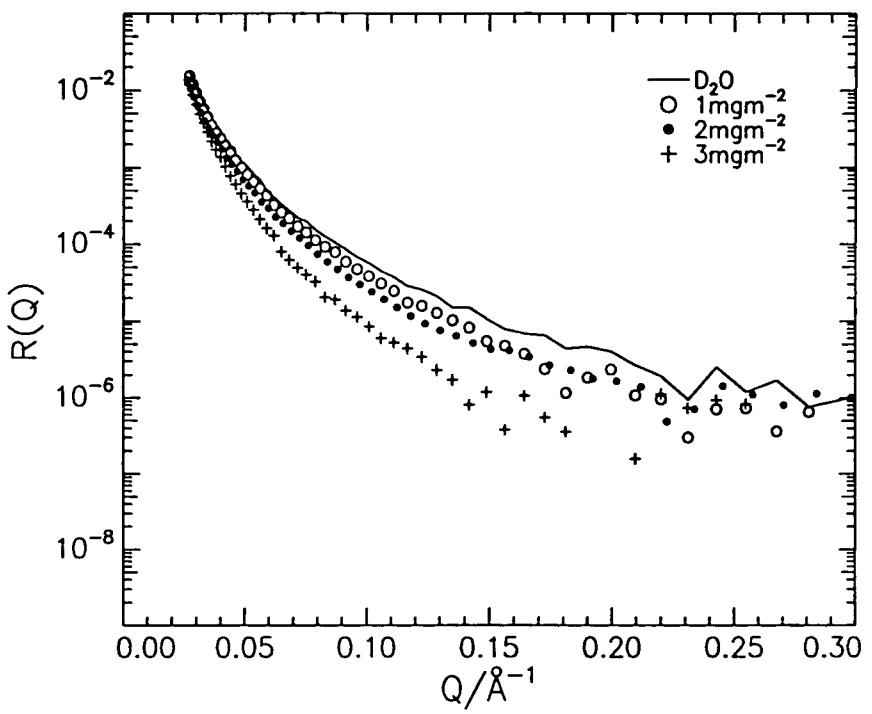

Figure 5.4.41 Reflectivity profiles for hPMMA / hPEO / D_2O where the surface concentration of PMMA is as indicated.

The decrease in the reflectivity is most noticeable for the situation where Γ_s = 3 mg m^{-2}. Attempts to fit this behaviour using a model where the surface was divided into a maximum of three layers failed to reproduce this behaviour. The only way in which the profile could be fitted directly was to include roughness into the fit. It was found that the best fit was given by floating the roughness at both the air / water interface and between the layer and the subphase. Roughness decreases the specular reflectivity. It has been shown[23] that the intensity scattered from a surface is reduced by roughness by a Debye - Waller type factor of the form:

$$I = I_0 \exp\left(-Q^2\sigma_r^2\right)$$

Equation 5.4.22

where σ_r is the root mean square roughness. It is possible to include these effects into the fitting program used. Allowing the roughness at both interfaces to float and applying a single layer fit gave the result in figure 5.4.42. The parameters describing this fit are presented in Table 5.4.13. The estimated water self partial structure factor for Γ_s = 2 mg m^{-2} was also observed to be rather low. It was possible to fit the reflectivity profile of the same contrast for this system again by allowing for substantial roughening of the air / water surface.

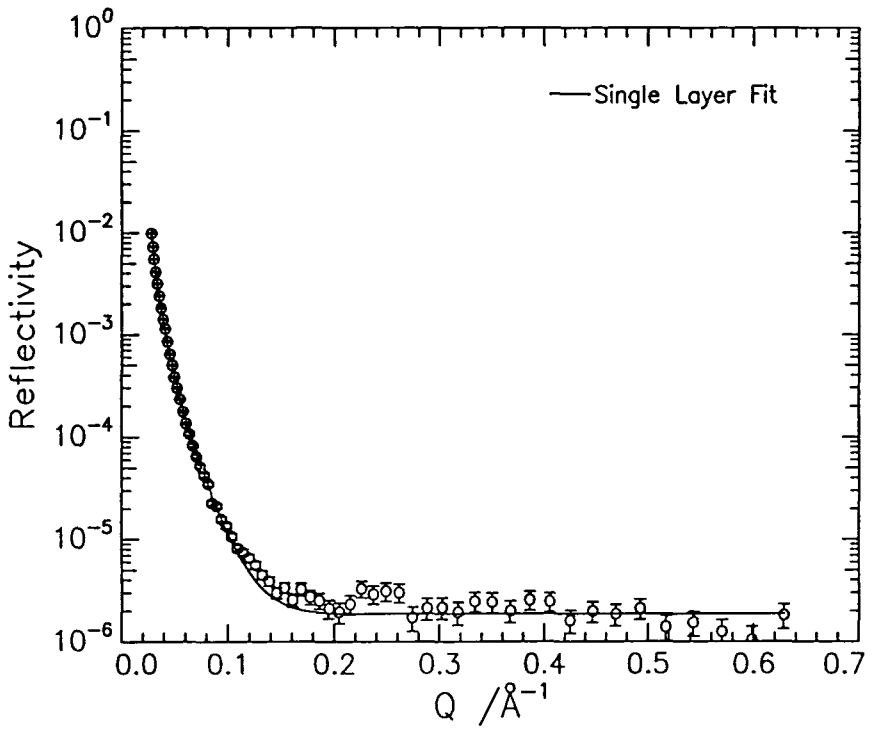

Figure 5.4.42 Reflectivity profile for hPMMA / hPEO / D_2O Γ_s = 3 mg m^{-2}.

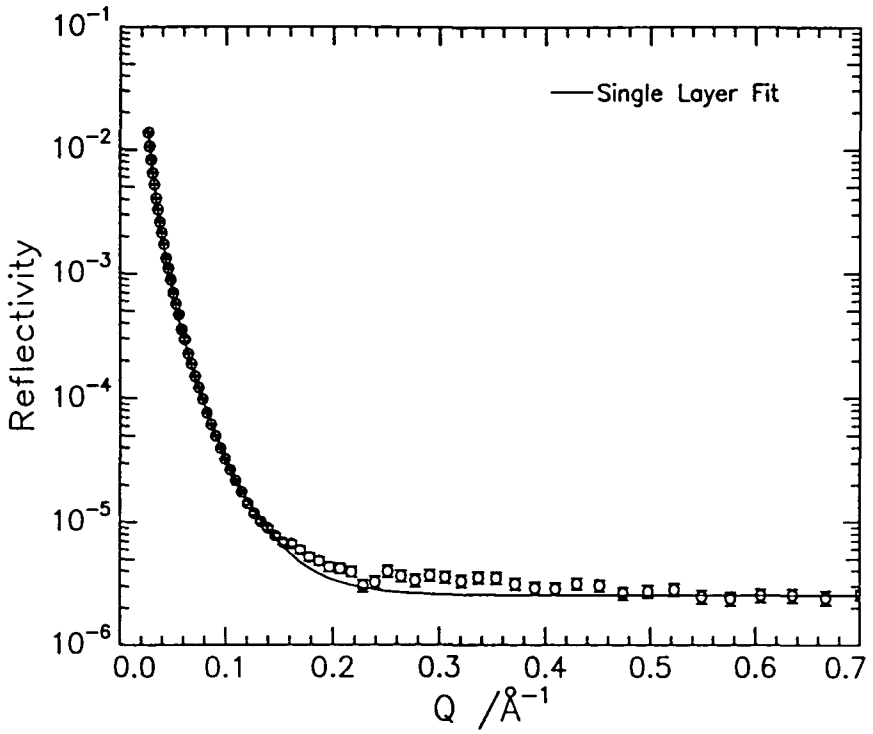

Figure 5.4.43 Reflectivity profile for hPMMA / hPEO / D_2O $\Gamma_s = 2$ mg m^{-2}.

Γ_s / mg m^{-2}	Layer thick. / Å	ρ /10^{-6} Å^{-6}	$\sigma_{air-water}$ / Å	$\sigma_{layer-bulk}$ /Å
2	16 ± 1	1.65 ± 0.36	67 ± 2	4 ± 1
3	13 ± 2	2.44 ± 0.39	59 ± 2	10 ± 1

Table 5.4.13: Single layer fits to hPMMA / hPEO / D_2O reflectivity profiles.

In isolation these parameters are not easy to interpret directly into the number density profile and for this reason the number density profiles are presented in figure 5.4.44.

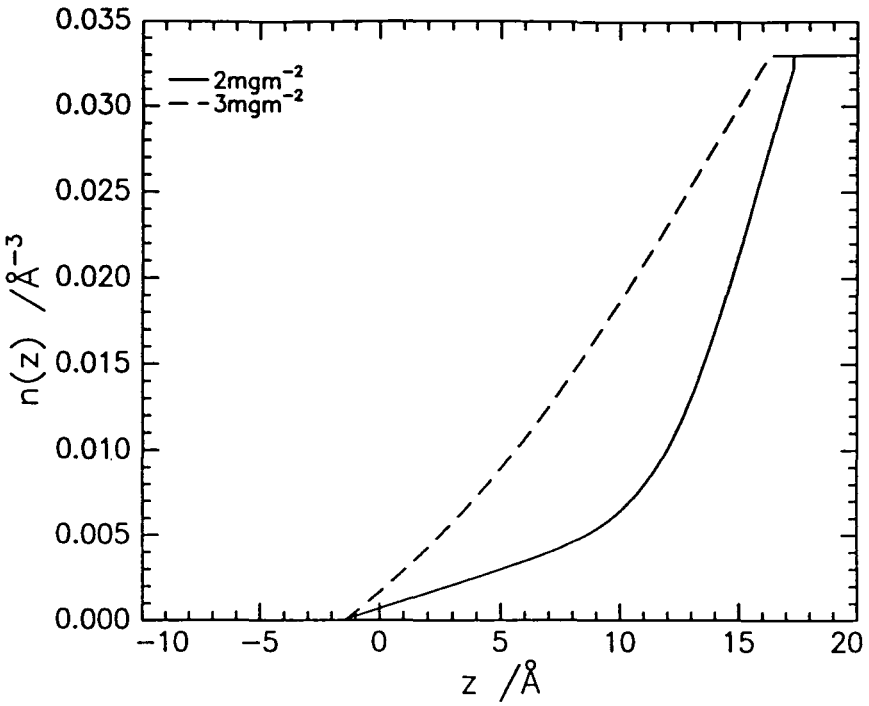

Figure 5.4.44 Number density profiles for water where the surface concentration of PMMA is as indicated.

Figure 5.4.44 implies that the number density of water gradually increases to the bulk value over a width of about 15 Å in both cases. In the only standard model which allows for a diffuse interface of water, the tanh, the number density increases much more rapidly and generally over a narrower interfacial width. This appears to be the first example in which a solvent number density increases so gradually. To establish that this behaviour is consistent with the partial structure factor the fitted reflectivity has been used to generate the partial structure factor, i.e. $Q^4R(Q)$. The generated reflectivity profile with background subtraction was used. The Crowley correction was applied and the structure factor generated using the approximate method of calculation, equation 5.4.21.

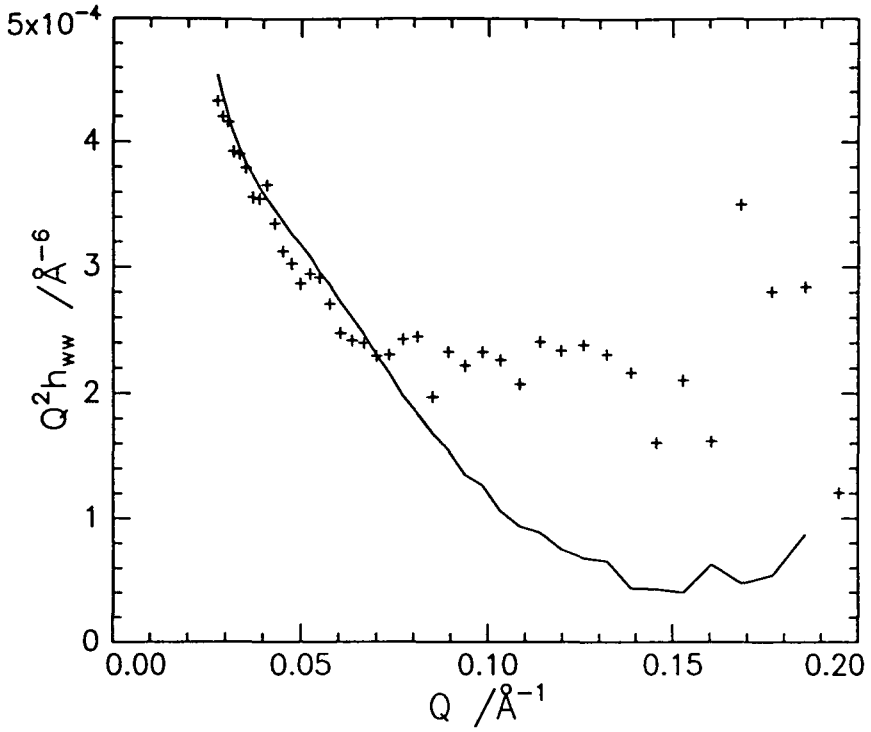

Figure 5.4.45 Generated partial structure factor for water, solid line, overlaid with the experimental values, $\Gamma_s = 3$ mg m^{-2}, crosses.

The fitted reflectivity clearly reproduces the experimental partial structure factor well at low Q. As Q increases the deviations between the experimental and calculated partial structure factor become larger although the general trend of the values being very low is retained. These deviations may actually reflect errors in the data reduction and scatter on the experimental points, such factors will be magnified by plotting in the form of $R(Q) \times Q^4$. Thus the generated reflectivity does seem to model behaviour adequately and it is concluded that the strange behaviour observed in the partial structure factor for water can be attributed to the formation of a diffuse layer of water. From now on the layer will be referred to as diffuse rather than rough which is rather misleading when the dimensions of the layers are as large as this.

A similar approach has been applied to the reflectivity data in the presence of 1 mg m^{-2} film. Although it was possible to fit the data satisfactorily the self term generated in the method described above did not reproduce the data any better than the tanh model in figure 5.4.39, see figure 5.4.46.

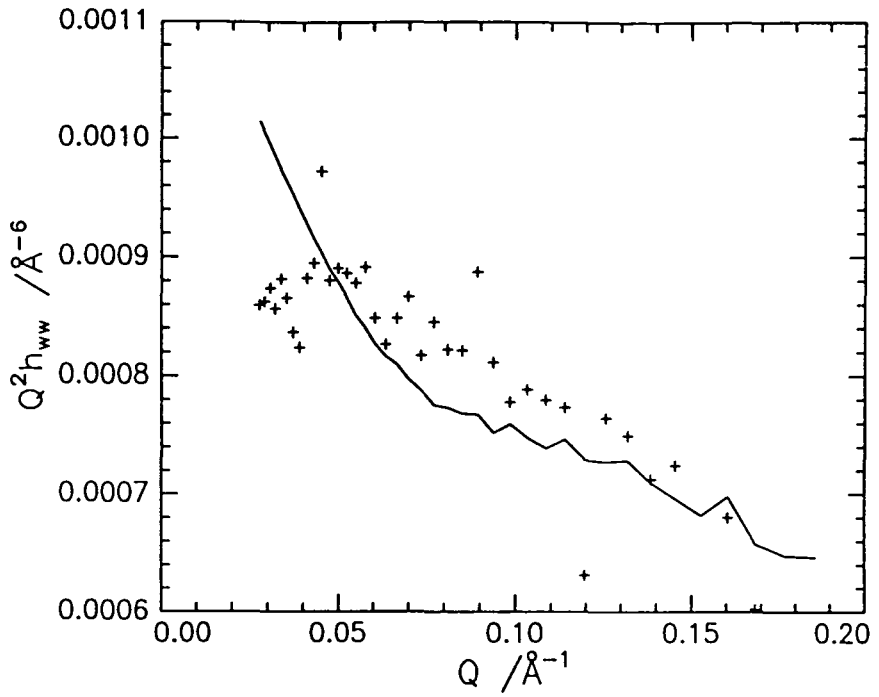

Figure 5.4.46 Generated self term, solid line, overlaid with experimental self partial structure factor, crosses. $\Gamma_s = 1$ mg m^{-2}.

The tanh layer failed to reproduce behaviour Q values below 0.1 Å^{-1}. Similarly application of direct model fitting, including contributions from roughness, fails to generate a self term which reproduces the marked downturn at low Q. Directly fitting the reflectivity profiles and generating the self term as described involves more variables than a tanh fit. Despite this the quality of the fit to the self partial structure factor did not improve significantly and the tanh distribution is retained as the best model for this system. In addition to the reasons cited above this model is consistent with the models applied to the water self partial structure factor for PEO solution and enables comparisons to be drawn between the two systems.

The self terms in figure 5.4.38 exhibit certain systematic variations. The value of the water self term at any particular Q decreases progressively as the surface concentration of PMMA increases. From this observation it is suggested that as more PMMA is spread on the surface water is driven out of the uppermost layer. This leads to the formation of a diffuse layer where the number density of water gradually increases to the bulk value just as observed here. The behaviour can be rationalised by considering the interface before the PMMA is spread. It is known that the adsorbed PEO remains in the water and is heavily diluted. It

seems feasible to suggest that when the PMMA is spread on to this surface it may want to mix with the PEO chains, such behaviour being consistent with the favourable interaction parameter observed for the two polymers in the bulk.[24,25] The presence of water may modify this interaction, as well as being another species occupying space in the interfacial region. Due to these combined effects it would be quite reasonable that some water will be expelled from the region so that the polymers maximise their interactions. This scenario is consistent with the observed number density profile for water which spans a thickness comparable to that of the dense layer of PMMA at this surface concentration, i.e. 26 Å. Comparison with the behaviour of PEO is not so straight forward. When the surface concentration of PMMA increases to 3 mg m^{-2} the PEO self partial structure factor becomes scattered. This behaviour is consistent with the PEO occupying a thicker, much more dilute layer at the surface. Analysis demonstrated that compared to a dense layer thickness of 22 Å for Γ_s = 1 mg m^{-2}, the PEO layer thickness increased to around 37 Å as Γ_s = 3 mg m^{-2}. It is evident that, as the surface concentration of PMMA increases, the width of the interfacial water layer also increases. Given that the PEO is expected to be incorporated in this layer the behaviour of the PEO and water self terms are consistent with this.

It is clear that the interfacial layer of water in this system exhibits some very unusual behaviour which seems to be inherently linked to the concentration of PMMA at the interface. The water self terms are consistent with the water layer becoming progressively more diffuse as the PMMA concentration increases. These changes cannot be attributed solely to the PMMA, otherwise one would expect to observed similar behaviour for PMMA on water. Clearly there are complex interactions between all three components at the interface which, as yet, are not fully appreciated.

Summary

From the discussion of the self terms it is clear that the behaviour of both PEO and PMMA is completely different to that of the simple polymer / water systems. At both 1 mg m^{-2} and 3 mg m^{-2} the PMMA appears to populate a greater width of the interfacial region than if the subphase were just pure water. The presence of a spread film of PMMA causes drastic changes in the surface organisation of PEO. The surface excess of PEO remains constant but occupies a wider region of the interface and is more diffuse. If the PEO forms a relatively structured layer at the interface then it seems plausible that the water incorporated in this layer

may have a structure imposed on it by the PEO. This may account for the strange behaviour of the water self terms. The problem with this model is that the structure adopted by the PEO does not seem to be significantly different in the presence of a 1 mg m^{-2} film of PMMA to that in the presence a 2 mg m^{-2} film. If the origin of the behaviour observed in the water self terms was caused directly by structuring due to the presence of the PEO one would expect to observe it in all the self terms whereas that for the dilute film appears to be barely influenced by the presence of the PMMA. A more successful model for the behaviour occurring as Γ_s increases is that where the water layer is considered to become increasingly diffuse at the surface. This has been modelled by incorporating roughness into model fitting and generating self partial structure factors from the fitted reflectivity. Although this does not provide an ideal fit to the experimental self term no other model has come anywhere near reproducing the behaviour.

5.4.4.4 The Cross Partial Structure Factors

It is clear, from the preceding discussions, that the behaviour of the species distributed at the interface when PMMA is spread on PEO is complex. Not all the self terms were successfully fitted, nor were they rationalised. For those that were fitted, in many cases different models had to be invoked to describe the distributions. This will have implications on the cross partial structure factors. In the cases where the self partial structure factors have been satisfactorily described, it should be possible to fit the cross partial structure factors to determine δ, the separation between the centres of the distributions. Depending on the model fitted to the relevant self terms the relationship for the cross partial structure factor, in terms of the parameters of the separate distributions and δ, may become quite complex.

Where a self term was not fitted satisfactorily it may not be possible to fit any of the cross terms in which the species is involved. This follows because the equation that links the self partial structure factors and δ to the cross terms depends explicitly on the form of the distribution of the species involved, in the simplest case whether n(z) is odd or even. For the most simple systems the relationship between the self partial structure factors and the cross terms is of the form:

$$h_{ij}(Q) = \pm\left(h_{ii}(Q)h_{jj}(Q)\right)^{0.5} f(Q,\delta)$$

Equation 5.4.23

where the function $f(Q,\delta)$ is a either the sine or cosine of the product $Q\delta$.

When the number densities of species i and j, $n(z)$, are both described by even functions $f(Q,\delta)=\cos(Q\delta)$, when one of the distributions is odd and one even, $f(Q,\delta)=\sin(Q\delta)$. Since δ is tied into a sinusoidal function it is impossible to infer the relative sizes of the separation by simply comparing the cross partial structure factors. In addition, until the form of the relationship between the cross term and $Q\delta$ is known, even basic qualitative information such as whether δ is non zero cannot be inferred. Where the relevant self partial structure factors are fully analysed attempts have been made to fit the cross partial structure factors. Where a term of the form h_{ii} appears the experimental self partial structure factor was used.

5.4.4.4A The PEO / Water Cross Partial Structure Term

In the presence of a 1 mg m^{-2} film of PMMA the best fit to the PEO self partial structure factor was given by a double uniform layer, whereas the water self term was consistent with a tanh layer. The expression for the cross term between two such distributions has been derived, the details are given in Appendix A, and the relation is:

$$Q^2 h_{ij} = (h_{ww})^{0.5}\left((n_B - n_A)\cos Q(d_A - \delta) - n_B \cos Q(d_B - \delta) + n_A \cos Q\delta\right)$$

Equation 5.4.24

Initially this equation was fitted to the cross term by varying δ, using experimental values for the water self partial structure factor and the fitted parameters for n_A, n_B, d_A and d_B. Equation 5.4.24 exhibits a weak dependence on δ with the calculated cross term changing only very slowly despite large changes in δ. This is illustrated by comparison of the generated cross terms and the experimental values as in figure 5.4.47. The sensitivity of equation 5.4.24 to changes in δ is anticipated to depend on the values of the other parameters and the weak dependence exhibited may be particular to this system.

An improved fit was obtained by using the expression given by equation 5.4.11 for the cross term where one number density distribution is odd and one even. For clarity this equation is repeated here:

$$h_{ij}(Q) = \pm(h_{ii}h_{jj})^{0.5} \sin Q\delta$$

Equation 5.4.11

This equation was applied by substituting in the experimental values for the self partial structure factors. The values of the PEO self partial structure factor obtained by solving the kinematic approximation had an average value of zero which, given that this cross term is non zero, are clearly not consistent. This confirms the suspicions that the 'true' PEO self term is subject to errors. As previously the partial structure factors calculated directly from the reflectivity profiles were used.

The assumption necessary in applying equation 5.4.11 to the experimental cross term is that the self partial structure factor of PEO is even. This basically means that the dilute lower layer of PEO is ignored. Neglecting this layer of PEO, which was absolutely central to fitting the self partial structure factor of PEO, may seem like an unrealistic approximation. In fact this is not believed to be the case. To understand the reason for this it is necessary to consider the reflectivity profile which contributes to the determination of the cross partial structure factor. The reflectivity profile for hPMMA / dPEO / D_2O contributes most significantly to the determination of the PEO - water cross partial structure factor. The scattering length density of dPEO is very similar to that of D_2O and it is possible that the lower layer of PEO is so dilute that it does not contribute significantly to the reflectivity for this contrast. Although there is some dPEO at these depths there may not be sufficient to depress the reflectivity noticeably from that of D_2O and, within the resolution of the experiment, this layer appears no different from D_2O. As a consequence of these effects, as far as determination of the cross term is concerned, the PEO forms a single uniform layer at the interface.

The discussion above is supported by comments made by Thomas[21] who has stated that although the distribution of species at the interface may not follow a wholly even or odd function the resolution of the experiment is not sufficient to detect deviations from equations based on 5.4.23. Experimentally this is supported by the fact that the fit obtained from equation 5.4.11 is considerably better than that given by 5.4.24 which would seem to be the more rigorous description of the system. Clearly, although equation 5.4.24 is strictly the correct form for the distribution of PEO and water at the interface, the subtle differences that would be expected in the cross term from equation 5.4.24 are not resolvable.

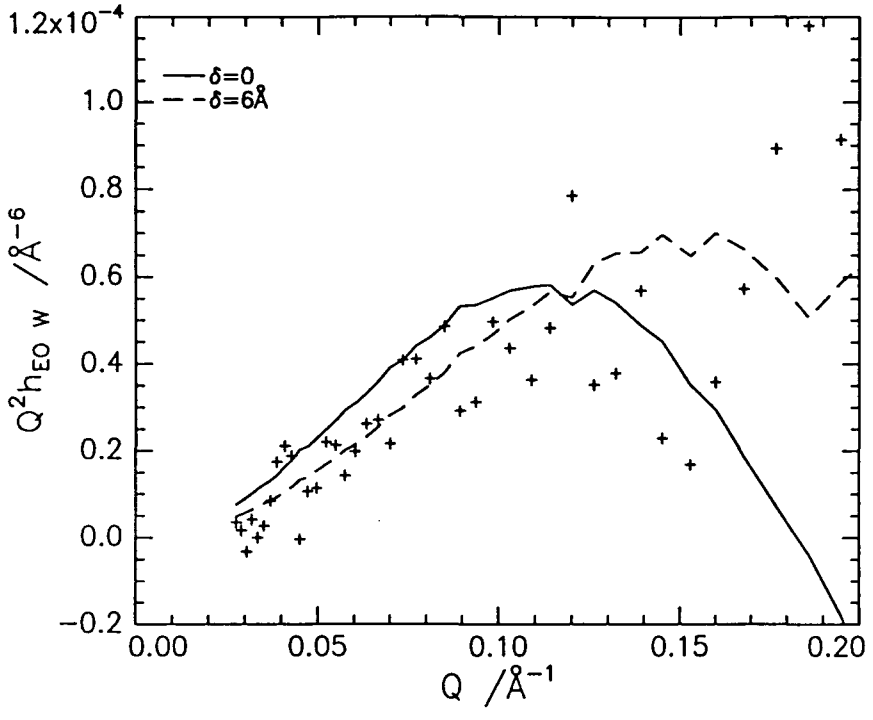

Figure 5.4.47 PEO - Water cross partial structure factor. Experimental values are indicated by the crosses. Equation 5.4.24 has been used to generate the cross terms for values of δ as indicated.

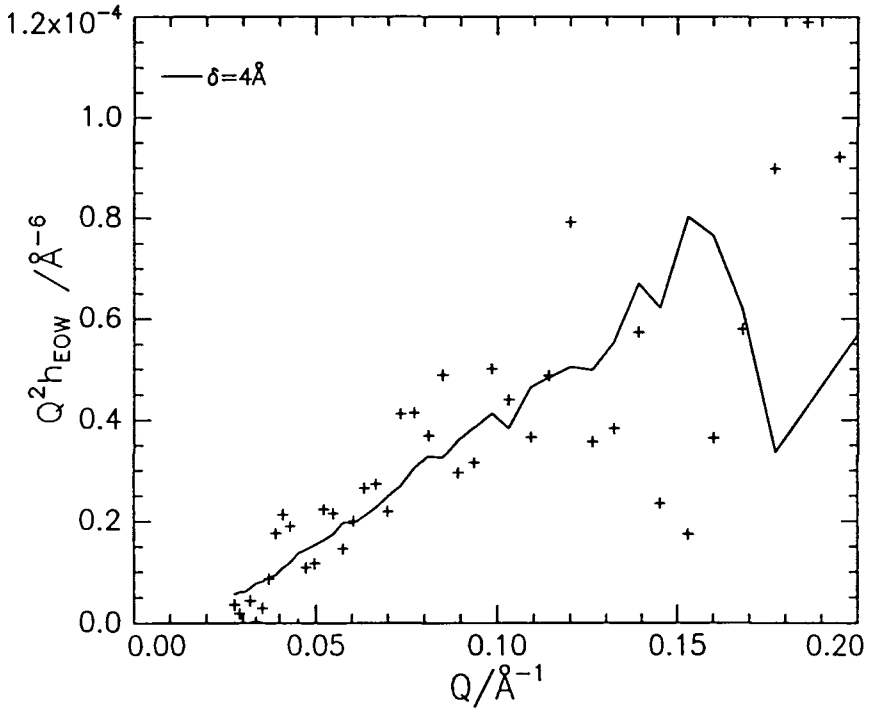

Figure 5.4.48 Fit to PEO - water cross partial structure factor using equation 5.3.11.

The best fit obtained using equation 3.11 gave δ = 4 Å indicating that the PEO and water distributions are slightly offset from one another, see figure 5.4.48. In contrast, the separation between the centre of the PEO and water distribution for a PEO solution was negligible. From this comparison it is concluded that spreading a PMMA film onto PEO solution not only modifies the surface organisation adopted by the PEO but also alters the relative positions of the PEO and water distributions.

A similar analysis was applied to the data obtained in the presence of a 3 mg m^{-2} film of PMMA. Unfortunately this situation is rather more complicated. The water self partial structure factor at this concentration is very unusual and all efforts to fit it using a 'conventional' kinematic analysis have failed. To fit the cross term requires an assumption to be made regarding the number density distribution of the water. The method adopted is to assume that the water distribution is odd. The number density of the subphase must increase from zero to the bulk value over the width of the interfacial region and, whatever the true nature of the distribution, this behaviour will not be described by a totally even function. The single uniform layer has also been used to describe subphase distributions and is somewhat more complex than this, not being a true odd function.[21] Despite these possible complications, in the absence of any other information, equation 5.4.11 was assumed to apply and has been fitted to the cross term.

As illustrated in figure 5.4.49 the cross partial structure factor was not fitted very successfully by this approach. The best attempt is given in figure 5.4.49 for which δ = 16 Å, and, although reproducing the form of the behaviour, the generated cross term is too low over the entire Q range. This may be symptomatic of the approximations made in determining the PEO self partial structure factor which is likely to be overestimated . Although one might originally think that this would lead to a generated cross term larger then the 'true' value the factor cosQδ will have a modulating effect and will bring the values down. However, if the problem lay solely in miscalculation of the product $h_{ii}h_{jj}$ then, in principle, the term $\cos Q\delta$ should compensate for this, with the result being an erroneous calculation of δ. The fact that this behaviour is not observed and that the generated cross term cannot be fitted to the experimental values suggests that the problem is rather more fundamental. If the distribution of water is more complex than assumed by this simple model extra terms would be required to describe the cross term. If this is true then similar discrepancies should be observed for all the cross terms involving water, i.e. also the PMMA / Water cross term. If the PMMA water

cross term can be described adequately by the simple model which has failed here it would suggest that the observed behaviour is attributable to the self partial structure factor for PEO.

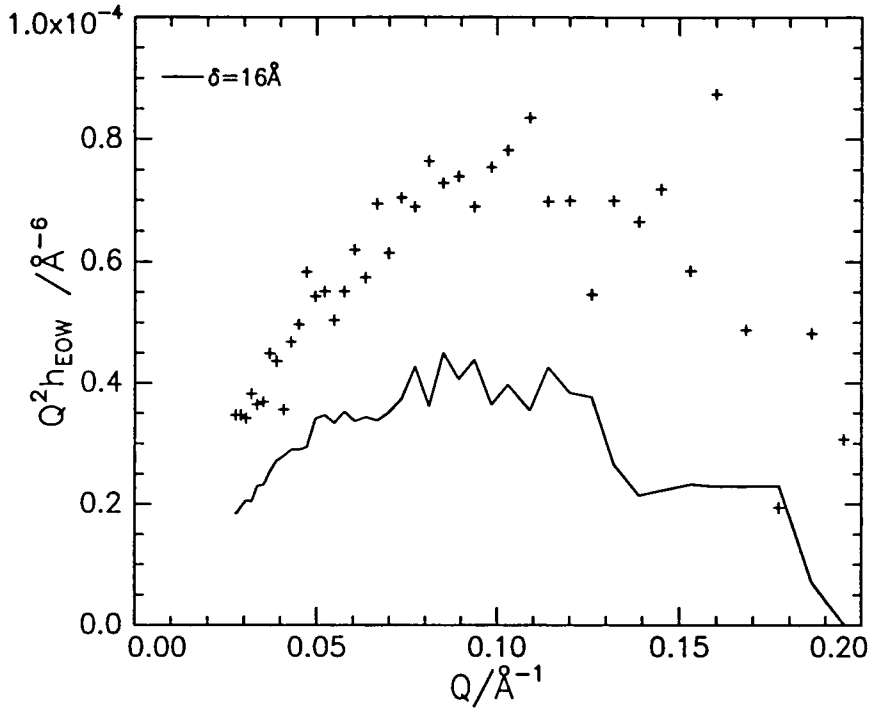

Figure 5.4.49 Fit to PEO - water cross partial structure factor using equation 3.11, Γ_s = 3 mg m^{-2}.

None of the above can be quantified in anyway and in the absence of a better model it is suggested that the separation between the centre of the water distribution and the PEO distribution increases with the surface concentration of PMMA although the value of δ is not known . This is consistent with changes in the surface organisation adopted by the PEO as Γ_s increases, i.e. the formation of a thick, dilute layer. The suggestion that such a structural change is associated with an increase in the distance between the centre of its distribution and the water distribution seems perfectly feasible.

5.4.4.4B The PMMA / Water Cross Term

From the preceding discussion it is clear that despite the sophisticated models which have been required to fit the self partial structure factors the basic equations of the form

$$h_{ij} = \pm(h_{ii}h_{jj})^{0.5} f(Q\delta)$$

are the most successful at fitting the cross terms. This behaviour was rationalised for the PEO / water cross term by suggesting that the reflectivity profile for the contrast which contributes most directly to determination of the cross term is not sensitive to the lower layer of PEO. It is only because of this lower layer that the distribution of polymer appears to be more complex than that described by the more usual functions, i.e. the single uniform layer and the Gaussian.

Similar behaviour is anticipated in this situation. The reflectivity profile with the dominant influence on the cross term is that for dPMMA / hPEO / D_2O. Once again the scattering length density of the subphase and the deuterated polymer are sufficiently similar that the diffuse lower layer will not contribute significantly to the reflectivity. Therefore the behaviour of the cross term approaches the simple limit for an odd function, the water distribution, and an even function, i.e. equation 5.4.11 applies here.

For a 1 mg m^{-2} film of PMMA applying equation 5.4.11 gives $\delta = 4 \pm 1$ Å, increasing to 8 ± 1 Å as the concentration increases to 3 mg m^{-2}, see figures 5.4.50 and 5.4.51. This suggests that the separation between the PMMA and water distributions is very similar in the two situations. In the study of a 3 mg m^{-2} film of PMMA on water a similar separation between the water and PMMA distributions was observed, in this system $\delta = 6$ Å. At the time of the early study by Henderson[1,22] the importance of the cross terms had not been realised and so no other comparisons can be made.

The implications of the results above are twofold. It is already known that similar interfacial structures are adopted by the two different concentration PMMA films spread on PEO solution. In both instances the surface organisation has been modelled successfully using a double uniform layer. The results above indicate that whilst the structure of the PMMA layer may remain much the same, the separation between the PMMA and the water increases with surface concentration. In addition to this the water self partial structure factor changed markedly with increasing PMMA concentration. These results indicate that while the PMMA adopts the same structure at the interface the other components, notably the water, are forced to adopt organisations which depend on the amount of PMMA present. Both the water and PEO have the freedom to react to changes in the surface environment. If necessary the PEO can desorb and the structure of the interfacial water layer can change. In contrast the PMMA films are insoluble and once spread at the interface have little alternative but to remain there.

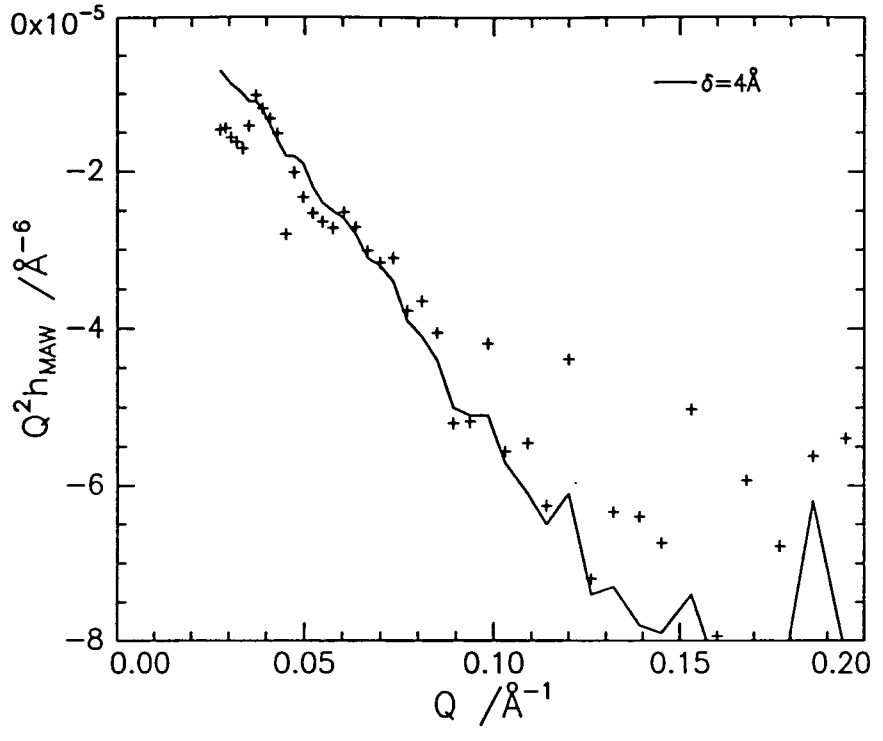

Figure 5.4.50 Fit to the cross partial structure factor for PMMA - water cross term, Γ_s = 1 mg m^{-2}, solid line. Crosses represent the experimental cross term.

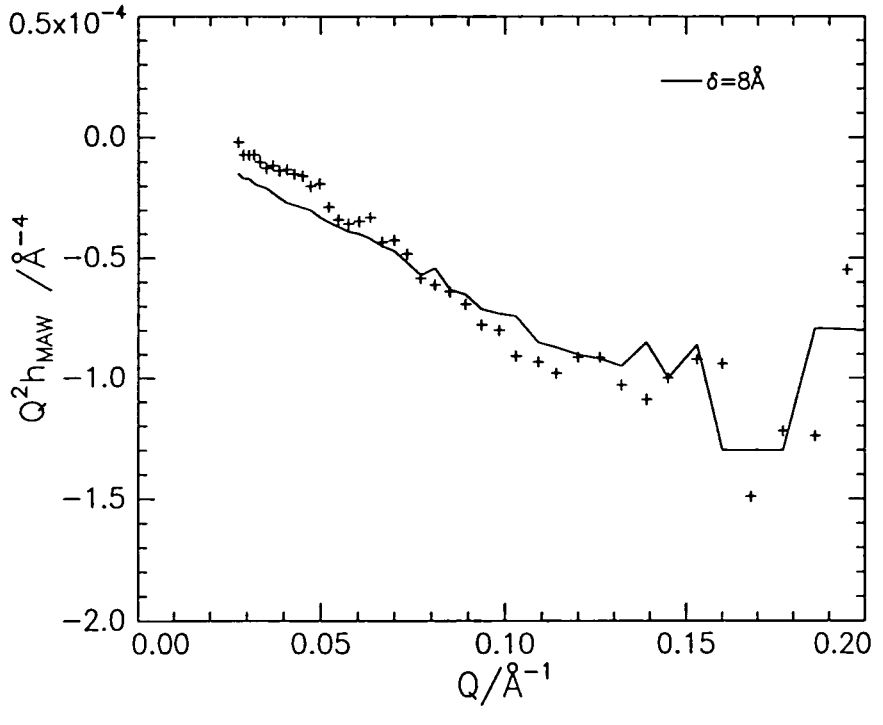

Figure 5.4.51 Fit to the cross partial structure factor for PMMA - water cross term, Γ_s = 3 mg m^{-2}, solid line. Crosses represent the experimental cross term.

5.4.4.4C The PMMA / PEO Cross Partial Structure Factor

To interpret the cross partial structure factor between PEO and PMMA in the presence of the 1 mg m^{-2} film it is necessary to consider the distributions which have been used to model the individual self terms. Although a double uniform layer was required to fit the self terms of both the polymers it has been demonstrated that the cross terms are not sensitive to both layers. Thus as previously the experimental cross term is fitted using a simple equation of the form given in 5.4.23. For two even functions this becomes:

$$h_{ij}(Q) = \pm\left(h_{ii}h_{jj}\right)^{0.5}\cos(Q\delta)$$

Equation 5.4.25

It was not possible to achieve a satisfactory fit to the low concentration cross term using equation 5.4.25. Despite varying δ over a wide range attempts to generate a cross term of a similar magnitude to the experimental values failed. In all cases the generated cross term was too low. In an attempt to extract some idea of the separation between these components, their separations from water have been considered. Both polymer distributions are positioned 4 Å from the centre of the water distribution. Thus, to be consistent with the separation between the PEO and PMMA distributions δ must be either 8 Å or 0. Cross terms have been generated for both values of δ and are overlaid in figure 5.4.52 with the experimental values. It seems that $\delta = 0$ gives a cross term closer to the experimental values, but even so it can hardly be termed a fit. However, in the absence of any other information $\delta = 0$ is taken as the separation and will subsequently be used to generate the number density profiles.

The same method was applied to generate the cross term for a 3 mg m^{-2} film of PMMA. In contrast to behaviour when Γ_s = 1 mg m^{-2} it was possible to achieve a reasonable fit to the data for δ = 13 Å, see figure 5.4.53.

It is therefore concluded that a reasonable model of this system is one in which the polymer distributions are separated by 13 Å. This is a considerably larger separation than for a 1 mg m^{-2} film of PMMA. To confirm this the generated cross term for δ = 13 Å is overlaid on figure 5.4.52 and clearly it does not reproduce the experimental cross term any better than $\delta = 0$.

From the extracted values of δ it is suggested that when a 1 mg m^{-2} film of PMMA is spread on the PEO solution the polymers mix. In contrast when the film concentration increases the distributions become further apart, behaviour consistent with the PEO adopting a

broader distribution predominantly beneath the PMMA layer. It was suggested earlier that the formation of a diffuse layer of water with increasing Γ_s was associated with the repulsion of water from the polymer film. The rationale being that the PEO and PMMA could interact more favourably in the absence of water. Clearly the result above shows that this is not the case. In addition to the water being repelled from the interfacial region the distribution of the PEO also separates from the PMMA. A more consistent model for the system is that where, following compression, the PMMA forms a condensed film expelling the other components of the system.

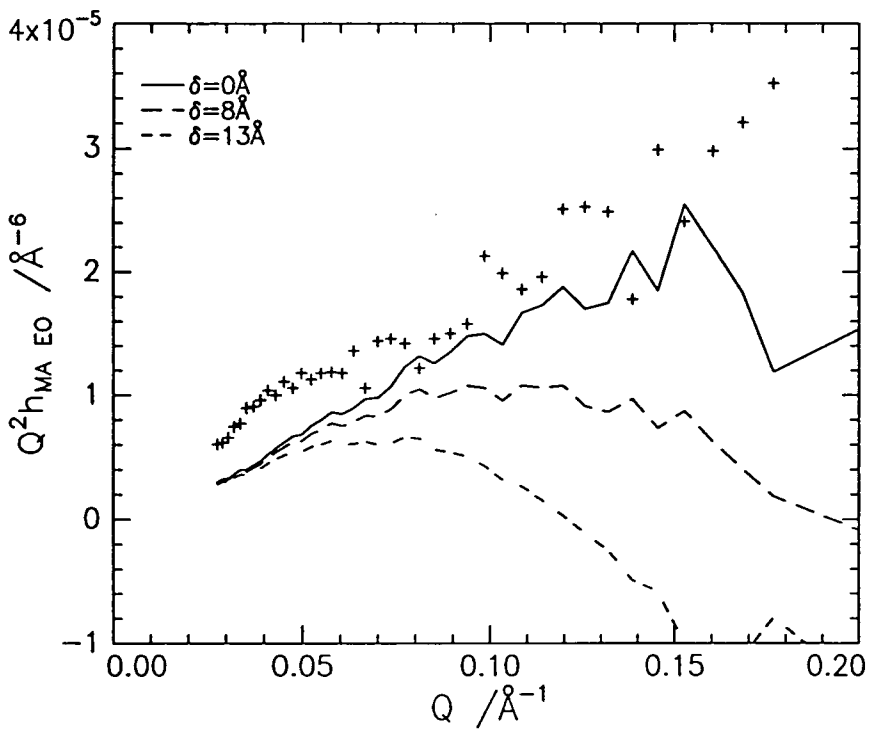

Figure 5.4.52 Generated cross terms for PMMA - PEO overlaid with the experimental values, $\Gamma_s = 1$ mg m^{-2}, represented by crosses.

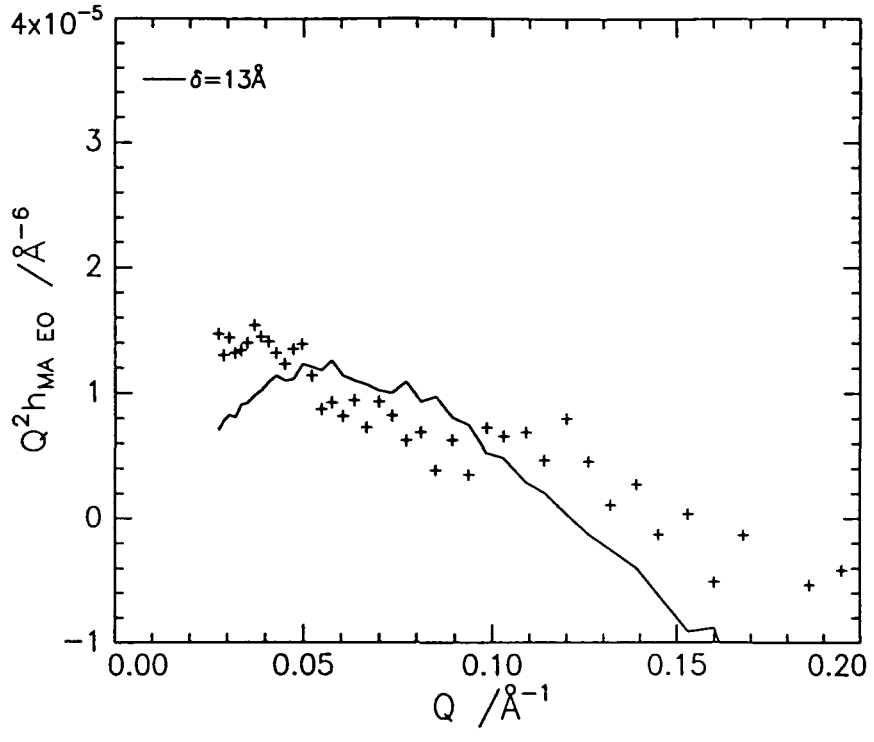

Figure 5.4.53 Generated cross terms for PMMA - PEO overlaid with the experimental values, $\Gamma_s = 3$ mg m^{-2}

5.4.4.5 Discussion

In principle, knowing the separation between the centres of the distributions and the form of the distributions for each component enables a number density profile of the interfacial components to be constructed.

System, Γ_s of PMMA	δ PMMA - water / Å	δ PEO - water / Å	δ PMMA - PEO / Å
1 mg m^{-2}	4 ± 1	0 ± 1	4 ± 1
3 mg m^{-2}	8 ± 1	16 ?	13 ± 1

Table 5.4.14: Centre - centre separations for the components at the interface

The separations determined in the preceding analysis are presented in Table 5.4.14. Consider the behaviour in the presence of a 1 mg m^{-2} film of PMMA. The distribution of each species has been fitted satisfactorily so that a complete description of the interface should be possible. To construct the number density profile one distribution must be arbitrarily

placed at zero and the other distributions placed relative to it. It is the general practice to define the centre of the water distribution as zero and this is the approach adopted here. The next issue is that δ is a scalar quantity so there is no way of knowing where any of the distributions are relative to water, i.e. do they fall above or below the centre of the water distribution. In practise physical intuition is exercised in determining whether a distribution is placed δ Å into the water or δ Å out of the water.

Given that PMMA is insoluble in water and predominantly hydrophobic, the PMMA layer is placed 4 Å above the centre of the water distribution. The cross terms were not sensitive to the 6 Å thick diffuse layer of PMMA and its position is not obvious. Reflectivity profiles have been simulated for all the possible structures but on examination it became obvious that this approach is not sensitive to such effects. The profile most sensitive to the two layer structure of PMMA is that for dPMMA / hPEO / NRW has the most significant influence on determination of the self term. To determine which way up the layers are the profiles on D_2O are required. Unfortunately, if the diffuse / dilute PMMA layer is placed in the water it is so diluted that its influence on the reflectivity is negligible. Alternatively if the layer is placed in the air it is so diluted by this null scattering component that, as opposed to the dominant reflectivity from the D_2O subphase, once again its contribution to the reflectivity is negligible. In the light of these observations it is necessary to rely on physical intuition rather than hard scientific fact to determine the relative positions of the layers. Following similar arguments to those exercised above it was decided to position the diffuse layer at the top face of the dense layer such that it protrudes into the air phase.

From Table 5.4.14 it is evident that at Γ_s = 1 mg m^{-2} the layers of polymer are almost coincident indicating a mixed layer of PMMA and PEO at the surface. As for the PMMA there is no evidence regarding the positioning of the dilute layer of PEO relative to the denser layer. Given that the PEO is contained in solution it is anticipated that this layer represents a diffuse layer over which the concentration of PEO tails off from the surface excess value to the bulk solution concentration. Consistent with this logic the dilute layer of PEO is placed below the dense layer in the aqueous phase.

The number density profile constructed in this way is presented in figure 5.4.54. In fitting the cross partial structure factors it was assumed that the polymeric species existed in a single layer. As a result of this, although the distributions of the polymeric species in figure 5.4.54 are actually represented as consisting of two layers, they are positioned such that the centre of the first layer is δ Å away from the centre of the water distribution.

The finite separation between the PEO and water distribution in figure 5.4.54 is quite striking. In contrast for PEO solution the centres of the two distributions are coincident, see figure 5.4.9. It is believed that spreading the PMMA has had the effect of forcing the water distribution back. This can be rationalised by considering the space requirements at the interface and assuming that the water originally occupies space required by the PMMA. In addition to this the PMMA - water interactions will not be favourable and where possible these two components will seek to minimise their interactions.

Constructing a number density profile for a 3 mg m^{-2} film of PMMA is not straightforward. While it was not possible to fit the water self partial structure factor, by assuming considerable roughening of the interface a model was fitted to the reflectivity data and a number density profile extracted. It was decided to use this profile in an attempt to construct a number density profile for this system, although it is stressed that the resulting profile of all the components at the interface should be treated with extreme caution. Clearly, the partial structure factor analysis failed to provide a complete model of the water distribution and it may be that the profiles of the polymers, and more likely the cross terms will also be influenced by the origin of this behaviour. Unfortunately the number density profile of water is determined only over the interfacial region with no interpolation to the bulk phase either side. As a consequence of this the profile is very angular, particularly at the transition to bulk water. This is not expected to represent physical reality and much smoother behaviour is anticipated.

To construct the approximate number density profile the centre of the water distribution must be identified. This was calculated by approximating the number density profile to a straight line such that the profile can be drawn as a triangle. The centre of the distribution was defined as that point on the z axis where the area of this triangle is exactly halved. This position was found to correspond to a distance 11 Å along the x axis.

The PMMA water cross term was fitted well giving a separation of 8 Å, see figure 5.4.51. Again given the hydrophobicity of PMMA this layer is positioned above the subphase distribution, similarly for the diffuse layer.

It now becomes clear that the values of δ in Table 5.4.14 do not combine to give a consistent number density profile. The cross term between PMMA and PEO at this concentration inspires the most confidence as it should be free from any adverse effects from the strange water distribution. This is almost certainly correct since the reflectivity profile which dominates this cross term is that for dPMMA / dPEO / NRW, i.e. the water is null scattering. The separation of the two polymers was found to be 13 Å. Given the solubility of

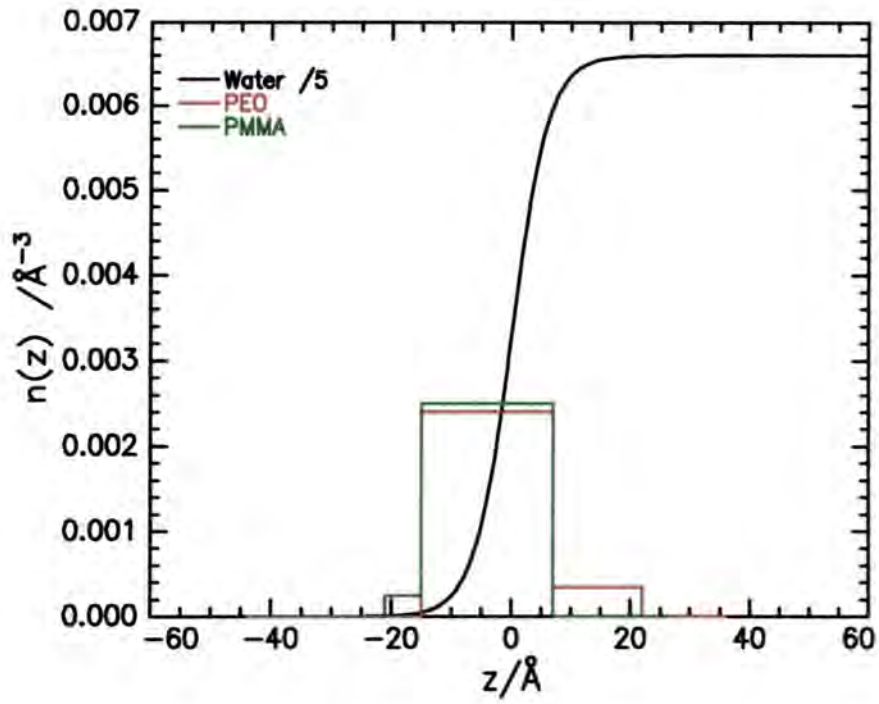

Figure 5.4.54 Number density profile when Γ_s = 1 mg m^{-2}

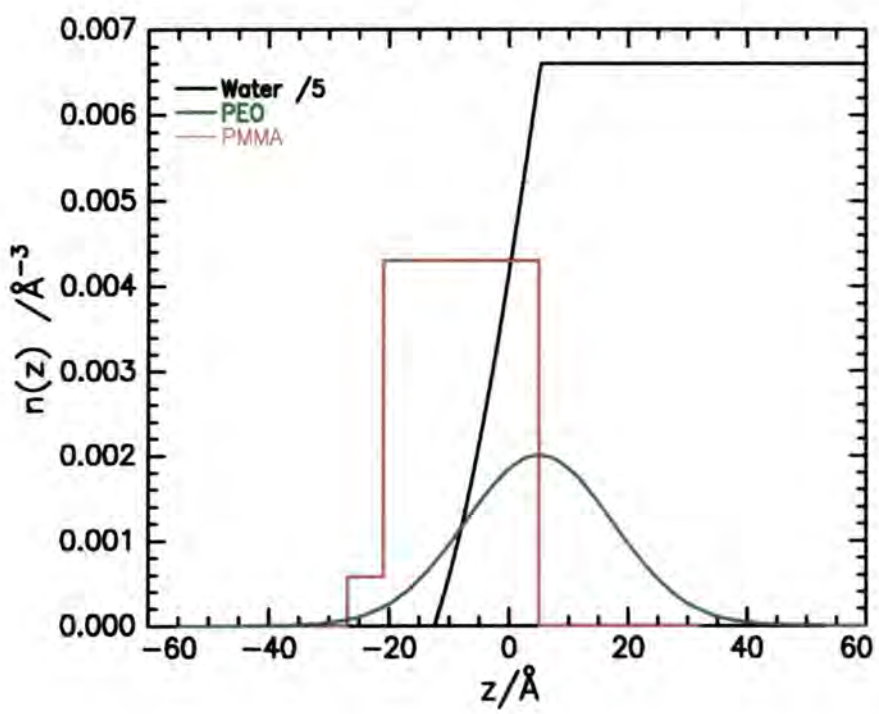

Figure 5.4.55 Number density profile when Γ_s = 3 mg m^{-2}

PEO it seems most likely that this distribution will be below the PMMA layer and immersed in the aqueous phase. Placing the distribution in this position it is clear that the separation between the water and PEO distribution is considerably lower than anticipated at 4 Å rather than around 16 Å.

The large discrepancy in the inferred separation between the water and PEO distribution is believed to be a symptom of the coarse models applied to both these self terms. At this concentration of PMMA not only is the water self partial structure factor unusual but, in addition, the PEO self term was very scattered and could barely be fitted. It seems highly likely that these effects will combine such that no sensible interpretation can be made of the cross term. This is consistent with the reported difficulties in fitting this cross term. Following this discussion the number density profile is tentatively presented in figure 5.4.55 but should be treated with caution.

Assuming that the number density profiles presented in figures 5.4.54 and 5.4.55 are representative of behaviour their implications are considered. It is clear that the surface organisation at the two concentrations of PMMA studied are quite different. At low concentrations of PMMA, 1 mg m^{-2}, a mixed film of PEO and PMMA forms at the surface. As the concentration of PMMA increases the PEO is forced out of the surface layer. Although the two polymers remain mixed at Γ_s = 3 mg m^{-2} the separation between their distributions clearly increases and proportionally less of the PEO at the surface is mixed with the PMMA. It is evident that at Γ_s = 1 mg m^{-2} the entire dense layer of PEO is mixed with PMMA whereas at Γ_s = 3 mg m^{-2} only about 50 % of the PEO mixes with the PMMA. The remainder of the PEO forms a diffuse tail into bulk water. Such behaviour is associated with the formation of a dense layer of PMMA. It is envisaged that on compression of the PMMA film, due to the constraints imposed by the limited surface area, the PEO is forced out of the upper surface and resides below the immediate surface.

The behaviour of the water layer which forms at the interface when Γ_s = 3 mg m^{-2} is more difficult to reconcile. At 1 mg m^{-2} a block or tanh layer gave an adequate fit to the water self term. However, as the surface concentration of PMMA increases the behaviour of this near surface water layer changes considerably. A diffuse layer of water appears to form where the number density increases gradually from zero to the bulk value in a pseudo linear manner over an interfacial width of about 15 Å. A clear picture of how and why such behaviour arises is not forthcoming. It is suggested tentatively that this behaviour is correlated to partial

expulsion of PEO from the dense surface layer of PMMA. At 1 mg m^{-2} the two polymers are mixed in a layer that also contains a considerable amount of water. As the PEO is forced out of this surface layer it is reasonable to expect that the organisation of the water would change as well. Given that PMMA is hydrophobic one would hardly expect a dense layer of PMMA to be mixed with water. Thus it is suggested that on compression of the PMMA film both the water and PEO are forced out of the uppermost surface leading, ultimately, to a layer of PMMA. At Γ_s = 3 mg m^{-2} this transition is not complete and as a consequence a diffuse layer of water exists at the interface.

Despite all attempts it seems that only a rather primitive understanding of the high concentration system has been achieved. This is unfortunate since this system exhibits some remarkable behaviour and qualities. If complete data were available for surface concentrations intermediate between 1 mg m^{-2} and 3 mg m^{-2} of PMMA this would aid understanding of the system, enabling the evolution of the marked change in properties at the extreme concentrations to be followed.

5.4.4.6 Optical Matrix Model Fitting

A number of attempts have been made to fit the reflectivity data directly using the optical matrix method described earlier. These attempts have not been very successful and attempts to fit all six profiles to obtain a description of the entire system have failed.

Consider first the reflectivity profiles where the PMMA surface concentration is 1 mg m^{-2}. Attempts were initially made to fit these profiles using a single uniform layer, each layer being characterised by a thickness d_i and a scattering length density ρ_i. Although it was possible to fit the data for a D_2O subphase adequately, the parameters of the fits were inconsistent across the series, see Table 5.4.15. When the profiles for a NRW subphase were considered it was found that the single layer fit failed to fit the features of the profiles. This is illustrated in figure 5.4.56 where the fit clearly fails to reproduce behaviour over the Q range 0.1 - 0.2 $Å^{-1}$.

The values in table 5.4.15 do not give consistent scattering length densities. This is not immediately obvious but becomes clear when calculating the layer composition. Despite this the thicknesses do exhibit similar behaviour. The parameters for dPMMA / hPEO /NRW indicate a PMMA layer thickness which is in good agreement with the values found using the

kinematic approximation. Likewise where the scattering length density of the PEO differs significantly from that of the subphase the layer thickness increases consistent with the suggestion that the surface excess of PEO contains a diffuse layer which penetrates the subphase.

Contrast	d_1 / Å	ρ_1 / 10^{-6} Å^{-2}
hPMMA / hPEO / D_2O	25 ± 1	0.80
dPMMA / hPEO / D_2O	30 ± 1	5.81
hPMMA / dPEO / D_2O	19 ± 3	6.22
dPMMA / hPEO / NRW	28 ± 1	2.20
hPMMA / dPEO / NRW	40 ± 1	0.81
dPMMA / dPEO / NRW	33± 1	2.89

Table 5.4.15: Parameters of the single layer fit for Γ_s = 1 mg m^{-2}.

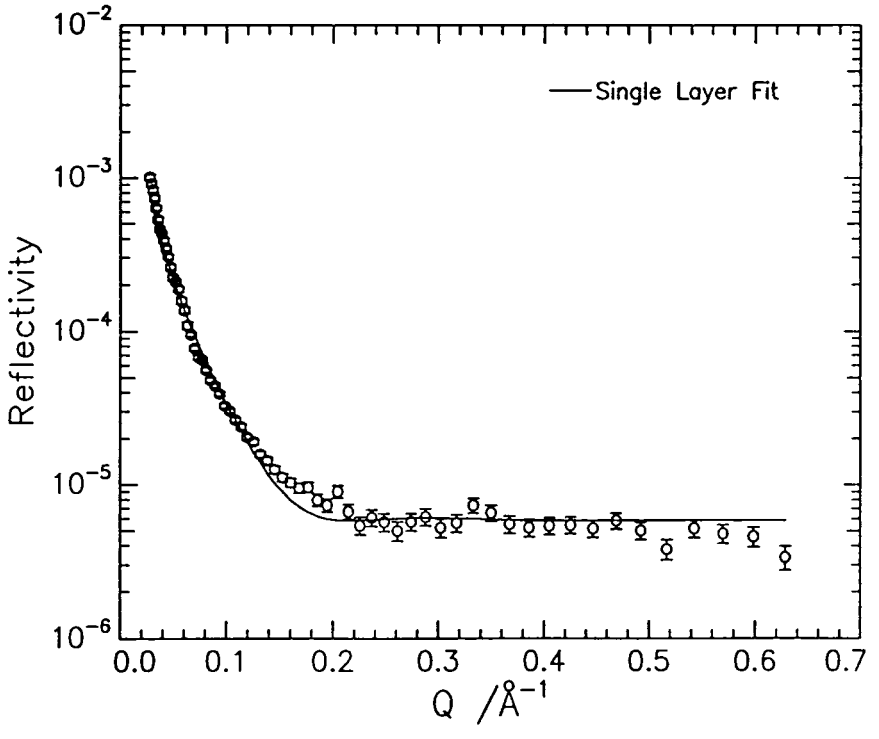

Figure 5.4.56 Single layer fit to profile for dPMMA / hPEO / NRW, Γ_s = 1 mg m^{-2}

When the surface concentration of PMMA is 3 mg m^{-2}, single layer fits failed to provide a consistent picture of the system. Despite these problems the parameters are presented in Table 5.4.16 for comparison with those for Γ_s = 1 mg m^{-2}.

Contrast	d_1 / Å	ρ_1 / 10^{-6} $Å^{-2}$
hPMMA / hPEO / D_2O	-	-
dPMMA / hPEO / D_2O	54 ± 2	5.91
hPMMA / dPEO / D_2O	39 ± 2	6.01
dPMMA / hPEO / NRW	34 ± 1	3.69
hPMMA / dPEO / NRW	52 ± 1	0.69
dPMMA / dPEO / NRW	39 ± 1	3.78

Table 5.4.16: Parameters of the single layer fit for Γ_s = 3 mg m^{-2}

A comparison of the values in the tables 5.4.15 and 5.4.16 indicates, in agreement with the kinematic approximation, that the width of the interfacial region that the polymers occupy increases with Γ_s. This observation is consistent with the result inferred from the kinematic approximation analysis that, although the PMMA and PEO form a mixed layer at low Γ_s, as Γ_s increases they begin to separate.

When a second layer was introduced the fits to the reflectivity profiles for Γ_s = 1 mg m^{-2} were much improved. The features of the profiles for both subphases were reproduced successfully with this model. One such fit is presented in figure 5.4.56 and can be compared directly with figure 5.4.57 which is the same data fitted by a single layer model. It is clear that the quality of the fit is improved considerably by inclusion of another layer. The parameters of the two layer fits are presented in table 5.4.17, on examination it becomes clear that the layer thicknesses are consistent for all the contrasts.

The top layer thickness falls in the range 21 - 26 Å which is in good agreement with the layer thickness found using the kinematic approximation. This latter analysis gave a layer thickness of around 22 Å which is well within the range found here.

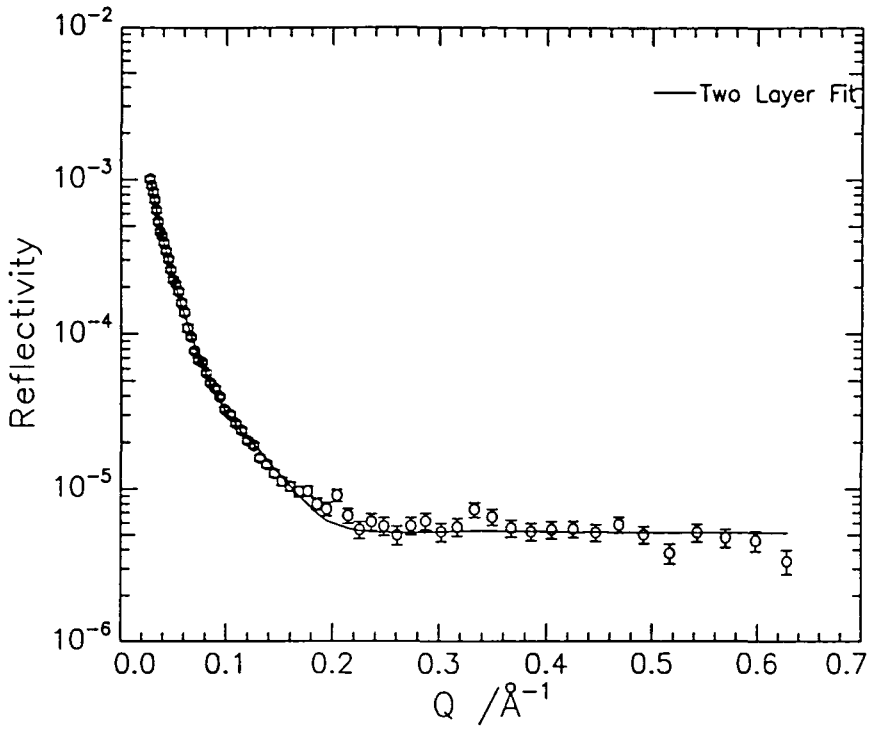

Figure 5.4.57 Two layer fit to profile for dPMMA / hPEO / NRW, Γ_s = 1 mg m^{-2}

Contrast	d_1 / Å	ρ_1 /10^{-6} Å^{-2}	d_2 / Å	ρ_2 /10^{-6} Å^{-2}
hPMMA / hPEO / D_2O	23 ± 1	0.62	66 ± 5	6.15
dPMMA/ hPEO/ D_2O	24 ± 1	5.66	61 ± 2	6.11
hPEO / dPMMA / D_2O	23 ± 2	0.58	60 ± 1	6.34
dPMMA / hPEO / NRW	24± 1	2.55	38 ± 3	0.34
hPMMA / dPEO / NRW	24 ± 1	1.15	37 ± 2	0.21
dPMMA / dPEO / NRW	24 ± 1	3.63	39 ± 1	0.64

Table 5.4.17: Parameters of the two layer fits for Γ_s = 1 mg m^{-2}

The composition of the layers can be determined taking the scattering length densities for the contrasts on NRW:

For dPMMA / hPEO / NRW

$$6.02\phi_{MA} + 0.57\phi_{EO} = 2.55 \qquad \mathbf{A}$$

For hPMMA / dPEO / NRW

$$0.90\phi_{MA} + 6.33\phi_{EO} = 1.15 \qquad \mathbf{B}$$

For dPMMA / dPEO / NRW

$$6.02\phi_{MA} + 6.33\phi_{EO} = 3.63 \qquad \mathbf{C}$$

Subtracting B from C, the volume fraction of PMMA in the layer is found to be 0.48, subtracting A from C gives the volume fraction of PEO as 0.19. From these values the number densities of the components can be calculated and in turn the surface concentration. It can be shown that the surface concentration of PMMA comes out at 1.1 ± 1 mg m^{-2} whereas that for PEO is found to be 0.50 ± 0.04 mg m^{-2}. These agree not only with the spread amount, in the case of PMMA, but also with the surface concentrations inferred from the kinematic approximation.

The lower layer is clearly mainly composed of PEO, albeit considerably diluted by water. There is also some evidence of PMMA in this layer, the volume fractions are, ϕ_{MA} = 0.08, ϕ_{EO} = 0.05 indicating surface concentrations of 0.3 mg m^{-2} and 0.22 mg m^{-2} respectively. These values do not agree with previous models particularly well but this is not too alarming. It was generally observed in the fitting that whilst the parameters of the top layer were quite 'robust', and even when started far from the optimum fit returned there quite rapidly, in contrast the parameters returned for the lower layer were rather more variable. This behaviour is attributed to the fact that the species in this layer are heavily diluted and is difficult to characterise fully.

When the parameters for the two layer fits for the contrasts on D_2O subphase are compared to those on NRW certain discrepancies arise. While the thickness of the top layer is essentially the same across the series the lower layer thickness appears to be considerably greater on D_2O. This can be reconciled with the penetration depths of the adsorbed PEO. The reason that this is not observed for NRW is that in this case the reflectometry is driven predominantly by the deuterated polymer. As they become increasing diluted by the null scattering component their contribution to the reflectivity will become lost in the incoherent background. In contrast, when the subphase is D_2O it dominates the reflectivity. If the scattering length density of the subphase is reduced by the presence of hydrogenous polymer then this will cause a detectable reduction in the reflectivity. The reduction in the reflectivity in the latter situation will be greater than the contribution to the reflectivity made by a heavily

diluted deuterated polymer. As a direct result of this the lower layer may appear thicker where the subphase is D_2O than when it is NRW. There may also be some structuring of the subphase due to the presence of PEO which could cause the scattering length density to differ from that of the bulk. Again this would manifest in such a way that the layer thickness was greater for a D_2O subphase than NRW.

Having rationalised this difference another problem is encountered. When the scattering length densities obtained for D_2O are considered in more detail the extracted parameters are found to be inconsistent. This is believed to be due to the water present. The water self partial structure factor was 'fitted' using a tanh profile but in reality the values appeared uncharacteristically low. This behaviour seems consistent with a diffuse water layer being formed at the surface. To fit these data fully it would be necessary to introduce many more layers into the model to describe the water distribution.

The behaviour of the water in the interfacial layer complicates attempts at model fitting both sets of data. Whilst the two layer model was reasonably successful for the 1 mg m^{-2} data it failed to fit the 3 mg m^{-2}, as did a three layer model. No further layers have been incorporated into the models, and given the very diffuse nature of the water distribution it seems likely that a complete description would only be achieved with a large number of layers. The problem associated with incorporating more than two or three layers into the fit is that of constraining the fits. In this situation the only thing known about the system is the surface concentration of PMMA. Unfortunately there are no parameters which can justifiably be limited or set to a specific value. The concern was that by introducing extra layers although the quality of the fits would undoubtedly improve, the physical implications of the extracted parameters would be questionable. It follows that although model fitting has confirmed that at 1 mg m^{-2} the PEO and PMMA are mixed in a layer about 22 Å wide, to improve on this and to fit the 3 mg m^{-2} data requires a more sophisticated fitting procedure. Ideally a fitting program is required such that the profiles for all the contrasts would be fitted simultaneously with the constraint that all the layer dimensions must be the same within a specified tolerance. Such software was not available, nor was there the time to modify existing programs. Despite these limitations the results of the model fitting confirm that the kinematic approximation does provide an adequate description of the interfacial structure. As a result the kinematic analysis is relied upon to describe the 1 mg m^{-2} system. Clearly the behaviour exhibited by the 3 mg m^{-2} film is rather unusual and not easily interpreted by either model.

Section 5.5: Surface Quasi Elastic Light Scattering

5.5.1 Introduction

SQELS has been applied to the study of PMMA films on a PEO solution. Although only a limited number of experiments have been performed, using a single low q value of 276 cm^{-1}, insight into film relaxation and behaviour has been obtained.

Two different SQELS experiments have been performed. One experiment was performed at fixed q while varying Γ_s by compressing the film, essentially tracking along the surface pressure isotherm. In the other experiment two fixed concentration films were studied at fixed q over a period of roughly two hours. The aim of these experiments was to see whether time dependent processes in the films influence capillary wave evolution.

5.5.2 Experimental

The details of the experiments performed are given below. During both experiments the subphase temperature was 294K.

5.5.2.1. Variable Surface Concentration of PMMA

The PEO solution was prepared as described earlier and the PMMA film was spread. Ten correlation functions were recorded at the most dilute surface concentration, i.e. as spread. The film was then compressed to the next surface concentration, using a barrier speed of 30 cm^2 min^{-1}, and a further ten correlation functions recorded. This cycle was repeated to cover a range of surface concentrations. The q value was fixed at 276.5 cm^{-1} during the study.

5.5.2.2. Fixed Surface Concentration of PMMA

Films were spread to cover the entire surface area at the required surface concentration as in the study of the film stability. Following deposition of the film data collection was started and correlation functions were subsequently recorded over a period of approximately 2 hours. Two film concentrations were studied in this way, 0.25 mg m^{-2} and 3 mg m^{-2}, again q

was fixed at 276.5 cm^{-1}. For the low concentration film it took 60 s to collect each correlation function, for the high surface concentration it took 30 s. Clearly the data collection time limits the timescale of the processes that the experiment is sensitive to.

To analyse the SQELS data using the spectral fitting method it is necessary to know the density and viscosity of the PEO solution. These quantities had been determined for the sample of PEO used in this work by Dr. Mark Taylor. The density was found to be the same as water whereas the viscosity was 1.099 mN s m^{-2} at 293 K and 0.991 mN s m^{-2} at 298 K. The value for 294 K was calculated by linear extrapolation between the points.

5.5.3 Results

5.5.3.1 Results: Capillary wave frequency and damping

The results from the experiment in which Γ_s was varied, essentially tracking along the isotherm, are presented and discussed first.

The characteristics of the capillary wave propagation are presented in figures 5.5.1 and 5.5.2. It is clear that on spreading the film of PMMA the wave frequency shows an immediate decrease relative to the value for a bare solution which is given at $\Gamma_s = 0$. This sets a general trend of decreasing wave frequency over the entire surface concentration range studied. When the surface concentration of PMMA reaches 0.5 mg m^{-2} there is a further marked decrease in the wave frequency. This second decrease is larger than that observed on spreading the film which suggests a significant change in the film properties at this point. Thereafter ω_o remains essentially constant until a surface concentration of 1.5 mg m^{-2} is reached, after which there is a steady decline in the frequency.

The variation of the damping with Γ_s is considerably more scattered than the frequency and is subject to larger errors. The wave damping appears to increase very slightly on spreading the film and continues to exhibits a general trend of increasing as Γ_s is incremented. The values appear to plateau out when the film concentration exceeds 1.5 mg m^{-2} then fall slightly at the highest surface concentrations studied. The largest increase in the damping, compared to the value for a bare PEO solution, is quite low, being less than 400 s^{-1}.

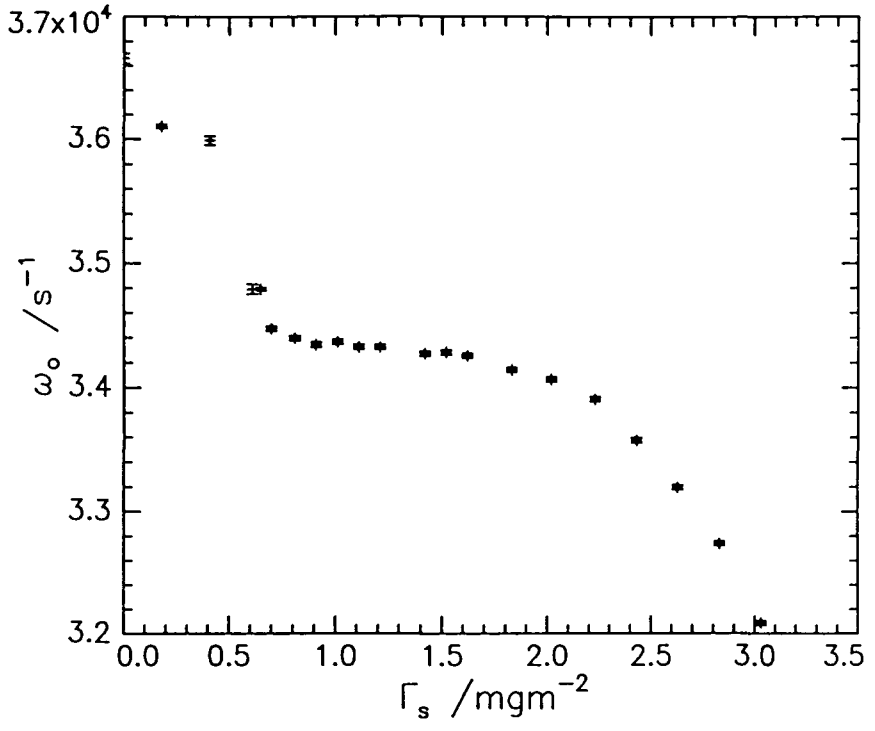

Figure 5.5.1 Capillary wave frequency as a function of Γ_s.

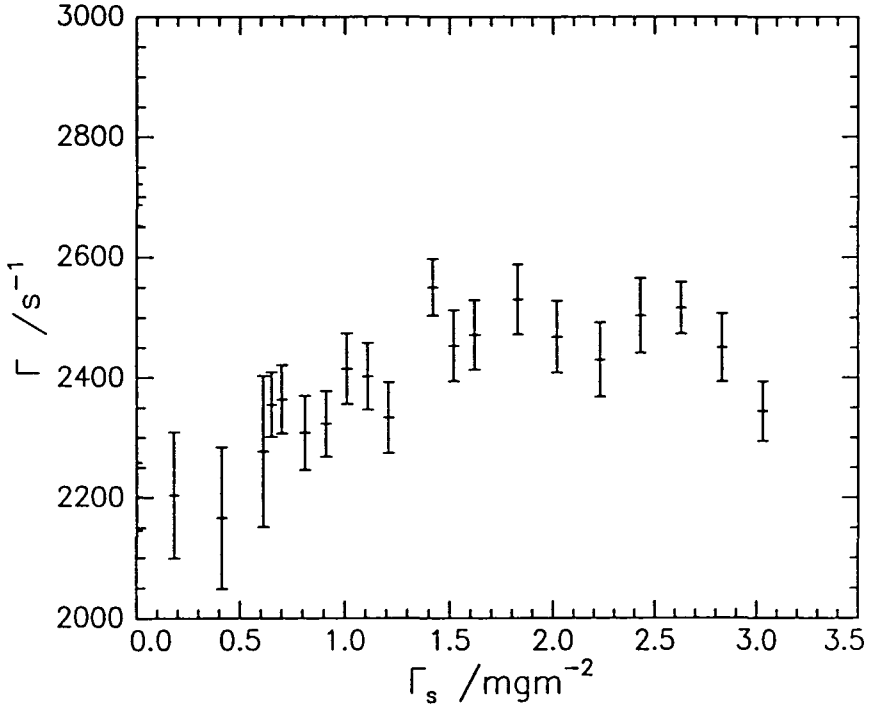

Figure 5.5.2 Capillary wave damping as a function of Γ_s, q = 276.5 cm^{-1}.

5.5.3.2 Results of Spectral Fitting

The results of analysing the data using a direct spectral fit are given in figures 5.5.3 to 5.5.7. Data for a clean solution of PEO were also collected and fitted, the results are plotted at $\Gamma_s = 0$. Each of the four surface parameters is considered in turn.

5.5.3.2A Surface Tension

The surface tension predictably exhibits the same dependence on Γ_s as the capillary wave frequency, see figure 5.5.4.

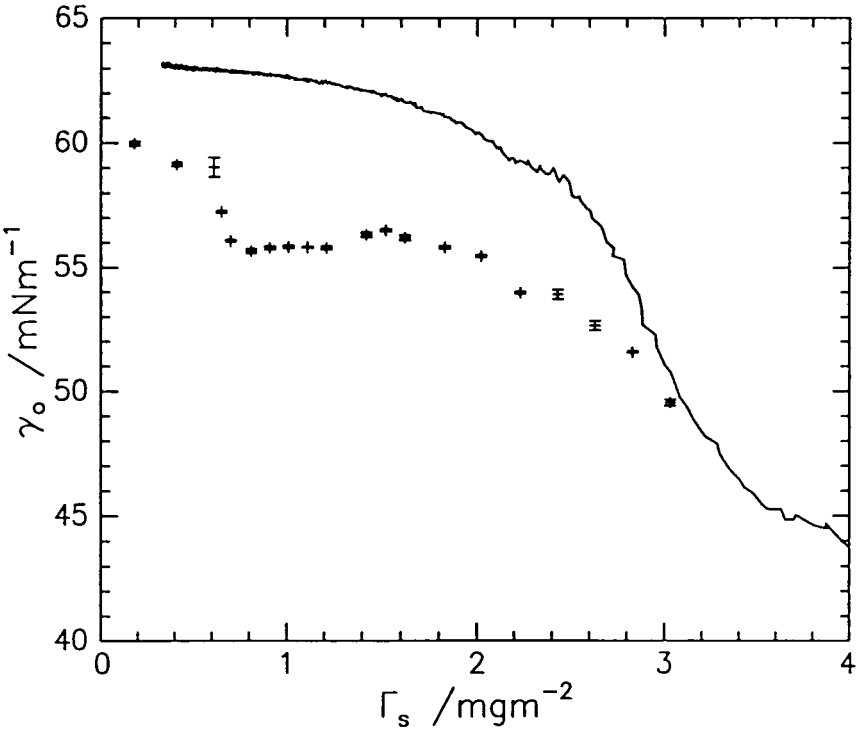

Figure 5.5.3 Dynamic surface tension as a function of Γ_s, crosses, q = 276.5 cm^{-1}. The solid line represents the static measurements.

As the surface concentration increases to 0.5 mg m^{-2} the surface tension falls rapidly to a value which remains essentially constant over the concentration range 0.8 - 1.00 mg m^{-2}. Thereafter, following a slight increase, γ_o falls steadily from 56 mN m^{-1} at 1.5 mg m^{-2} to 49 mN m^{-1} at 3 mg m^{-2}. The 'rate' of the decrease in the surface tension with increasing surface concentration is different for the two regions and it is clear that the decrease in γ_o per unit surface concentration is greatest at low surface concentrations.

The surface tension from static measurements is also plotted in figure 5.5.3 and clearly, despite the difference in the absolute values, both the dynamic and static surface tension exhibit broadly similar trends. However, the marked decrease in γ_o between 0 - 0.5 mg m^{-2} and the subsequent plateau up to surface concentrations of about 1.5 mg m^{-2} is not reproduced in the static measurement.

5.5.3.2B The Transverse Shear Viscosity

The values for the transverse shear viscosity are very scattered and do not exhibit a systematic dependence on Γ_s, see figure 5.5.4. The values are all round 2×10^{-4} mN s m^{-1} which is very similar to the value determined for clean PEO solution. There appears to be an increase in γ' when the surface concentration of PMMA exceeds 0.5 mg m^{-2}.

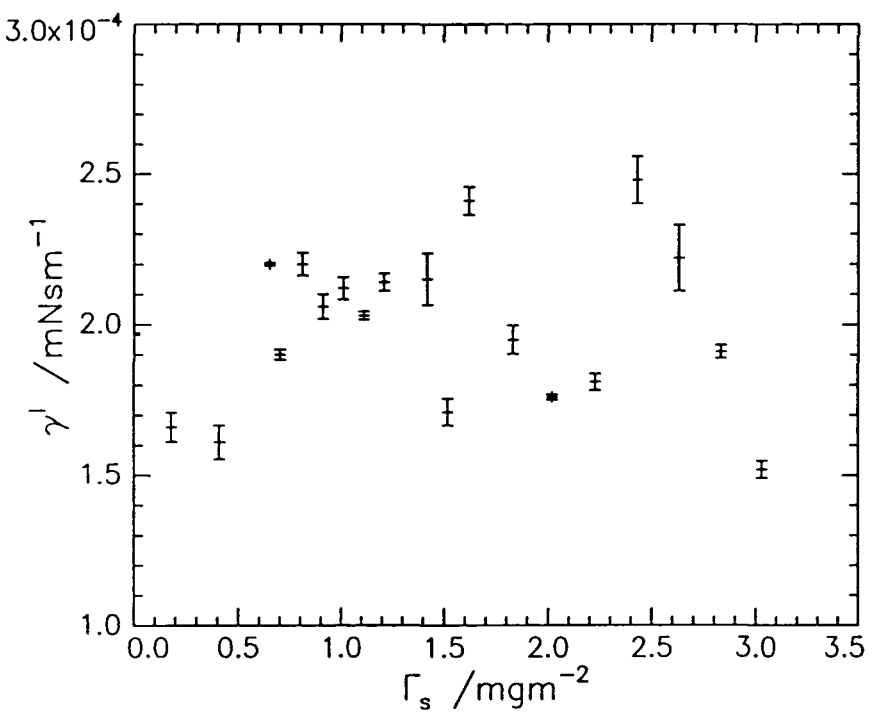

Figure 5.5.4 Transverse shear viscosity as a function of Γ_s, q = 276.5 cm^{-1}.

5.5.3.2C The Dilational Modulus

A glance at the data in figure 5.5.5 demonstrates the rather surprising result that ε_o appears to be independent of surface concentration. Other than the values at low surface concentrations, which are subject to very large errors, the values are always around 0.5 mN m^{-1}. This is consistent with the value of ε_o for a bare PEO solution which was found to be 0.5 $\pm$ 0.1 mN m^{-1}. Although there is some scatter on the points there is no disputing the indication that, within error, ε_o does not vary significantly as Γ_s of PMMA increases.

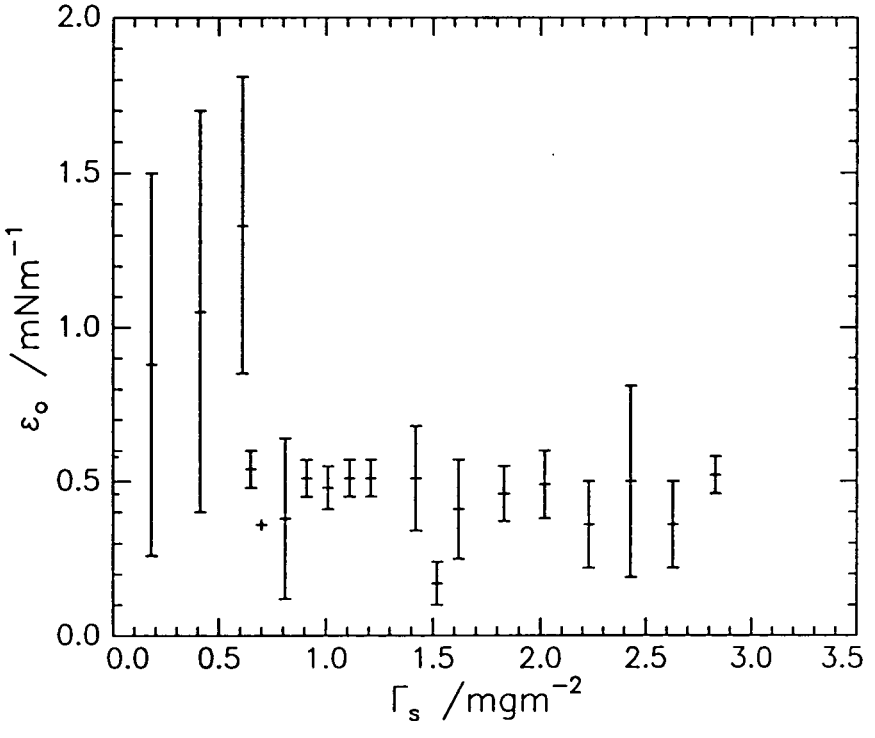

Figure 5.5.5 Dilational modulus as a function of Γ_s for q = 276.5 cm^{-1}.

The values of the dilational modulus are lower than one would expect by comparison to the static values. These are computed from the surface pressure isotherm for PMMA on PEO solution using:

$$\varepsilon_{oST} = \Gamma_s \frac{d\Pi}{d\Gamma_s}$$

The differential $d\Pi/d\Gamma_s$ was calculated by fitting a polynomial function to the surface pressure surface concentration isotherm, as described for the graft copolymers. This function was differentiated and its value calculated over the entire surface concentration range studied. The values were then multiplied by Γ_s, the results are plotted in figure 5.5.6 and are clearly very different to those determined by light scattering. As well as differences in the absolute values of ε_o and ε_{oST} at each surface concentration the dependence on surface concentration is also totally different. In an attempt to rationalise the differences the static elastic moduli have been calculated for the components as independent systems, i.e. PMMA on water and a PEO solution. The motivation for this is to see if the observed behaviour of ε_o bears a particular resemblance to one of the single systems.

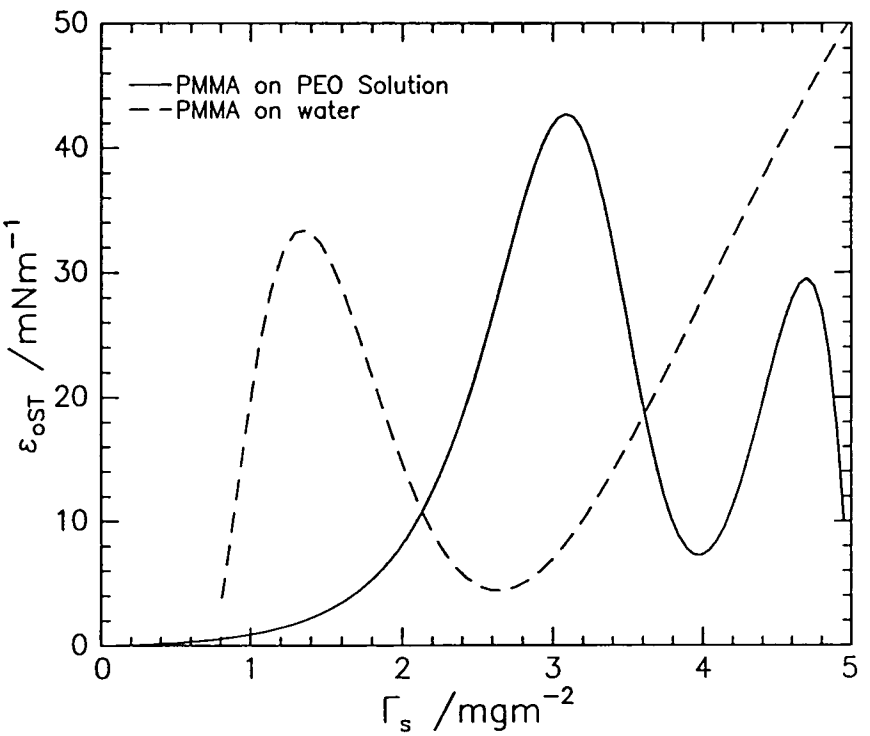

Figure 5.5.6 Static dilational modulus for PMMA on water and PMMA on PEO solution.

The static elastic moduli for an adsorbed film, which will be applicable to PEO solutions is given by:

$$\varepsilon_{oST} = \frac{d\gamma_{oST}}{d \ln A}$$

Equation 5.4.1

where γ_{oST} is the static surface tension and A is the area per monomer unit.

As remarked by Sauer and Yu[26] the problem with the use of equation 5.4.1 for adsorbed films is determination of A since this requires knowledge of the surface concentration rather than the bulk concentration. Following the recent application of neutron reflectometry to the study of adsorbed films such information is becoming accessible. Despite this, in order to apply equation 5.4.1 surface tension data for a range of different (bulk) concentration solutions of PEO are required, both γ_{oST} and A will vary with solution concentration. Although there are data available in the literature[12] giving A for solutions of PEO concentrations varying from 0.1 - 0.04 wt. % there are no accompanying surface tension data. In work primarily studying a 0.1 wt. % solution of PEO[12] surface tension data for other concentration films were also reported and it was shown that the surface tension is essentially constant over the range 0.1 - 0.0001 wt %. Consequently although A is known and therefore dlnA can be determined over this concentration range $d\gamma_o$ is very low, almost zero, and it is not possible to calculate ε_{oST} which undoubtedly would be small.

In comparison no such problems were encountered for the PMMA water system. Being a spread film the approach outlined above can be used. As previously the surface pressure isotherm was fitted with a functional form and the first differential calculated. The values are overlaid given in figure 5.5.6 with the same data for the PMMA / PEO system overlaid. Clearly the elastic moduli are quite different for the two systems. For PMMA on water ε_{oST} is negligible until Γ_s = 0.7 mg m^{-2}, where the value rises rapidly to a local maximum of 34 mN m^{-1}. For the same concentration of PMMA on PEO the value increases steadily, only reaching about 10 mN m^{-1} over the same concentration range. These values continue to increase, reaching a maximum of 40 mN m^{-1} at 3 mg m^{-2} and, at a very similar concentration, the value for PMMA / water falls to a minimum. Thereafter the values for PMMA on water increase linearly with Γ_s and, for all surface concentrations above 3.6 mg m^{-2}, are higher than for the PMMA / PEO system. Although both of the systems demonstrate quite different behaviour generally the values of ε_{oST} are high, an observation which is rather at odds with the values of ε_o extracted using light scattering.

5.5.3.2D The Dilational Viscosity

In a similar manner to the dilational modulus the dilational viscosity, ε', does not appear to show any dependence on surface concentration, certainly not within experimental error, see figure 5.5.7. The values are negative and, within error, remain the same as for the bare solution of PEO, for which $\varepsilon' = -1.3 \times 10^{-4}$ mN s m^{-1}. This behaviour is exhibited despite the increasing surface concentration of spread PMMA.

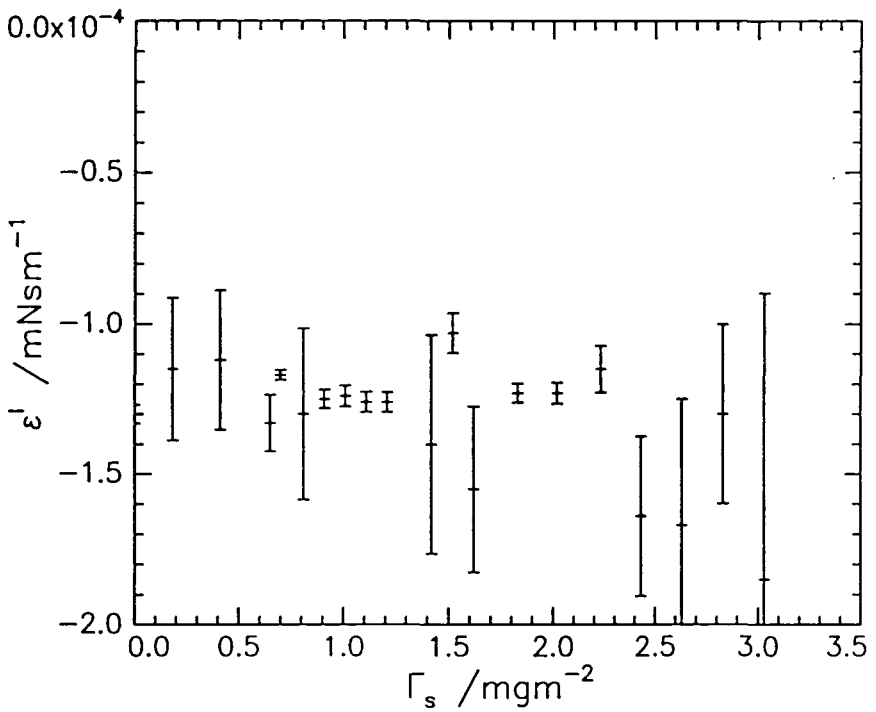

Figure 5.5.7 Dilational Viscosity as a function of Γ_s, q = 276.5 cm^{-1}.

5.5.4 Discussion

In this discussion the behaviour exhibited by PMMA on PEO solution is compared and contrasted to that of the homopolymer films.[13] It was anticipated that the behaviour would have characteristics of both components which could provide information regarding surface composition and organisation. Initially the capillary wave propagation is considered and discussed.

5.5.4.1 Capillary Wave Propagation

The observed capillary wave propagation when PMMA is spread on a solution of PEO bears similarities to both the homopolymer films. Spread layers of PEO[13] exhibit a rapid decrease in wave frequency at low surface concentrations, thereafter remaining approximately constant at surface concentrations above 0.4 mg m^{-2}, up to 1.0 mg m^{-2}. In contrast the wave frequency for PMMA remains as for pure water until Γ_s = 1 mg m^{-2}. This is consistent with reports[27] that at low surface concentrations PMMA does not form a homogenous film but rather exists as discrete islands. The patchy nature of the film is associated with the seemingly negligible influence that the PMMA exerts on the capillary wave propagation at low surface concentrations.

Consideration of the capillary wave propagation for the two homopolymer films spread on water leads to a number of suggestions for the behaviour of the present system. Clearly, the capillary wave frequency increases at low surface concentrations where, from comparisons with the behaviour of PMMA on water, one would not anticipate an influence. This behaviour may be symptomatic of the different surface organisation of PMMA in the two situations.

The capillary wave damping even for a bare PEO solution is greater than for water which at the same q was determined to be 937 ± 34 s^{-1}. This result would be anticipated from a consideration of first order approximations for a pure liquid since:

$$\Gamma = \frac{2\eta q^2}{\rho}$$

Equation 5.4.2

Capillary waves are more heavily damped on PEO solution than on water because of the viscosity of the solution, the density remaining the same as for water. The surface viscosities associated with an adsorbed layer may cause additional increases in Γ above that due to the change in viscosity. When a PMMA film is spread on the PEO solution it is anticipated that additional energy dissipation processes are introduced into the system and thus an additional increase in Γ is expected.

It was observed that the capillary wave damping does increase with Γ_s. Although the data were rather scattered they exhibited a maximum value of about 2500 s^{-1} at Γ_s = 1.7 mg m^{-2}. Previous studies[13] have revealed that the capillary wave damping for films of PMMA is

of a similar order, about 2300 s^{-1}. Spread films of PEO[13] exhibit similar behaviour when the surface concentration exceeds 0.4 mg m^{-2}. The damping for waves on the surface of spread films of PEO follow a roughly arc shaped variation as Γ_s increases, tailing off at high Γ_s. The variation in the wave damping with increasing Γ_s for PMMA[13] films is rather more complicated due to large oscillations in Γ at low Γ_s which are attributed to the previously mentioned patchy nature of the film.

Although Γ is fairly scattered for the PMMA / PEO system, like ω_o, the values do not exhibit the marked oscillations seen for PMMA on water. From this observation it is concluded that the film does not exist in the form of discrete islands, at least not comparable to the size of those formed by PMMA on water. It follows that the film is either more homogenous than PMMA on water or that the domains are of a smaller size. Smaller domains would mean that at any one time the beam sees both film and subphase and consequently the results represent an average of this view. Either of the two proposed structures imply that the PMMA - subphase interaction is more favourable than that for PMMA - water. Favourable PMMA - subphase interactions reduce the driving force to minimise the contacts between the PMMA and the subphase, i.e. form large islands where the PMMA just interacts with itself. The bulk miscibility of PMMA and PEO[24,25] has already been alluded to and it seems reasonable to suggest that the presence of PEO at the water surface would make it more attractive to the spread PMMA, having the action of a compatibiliser. Such effects may suppress the tendency of PMMA to form patchy films, leading to a more homogeneous film. These characteristics are also evident in the neutron reflectivity study.

Clearly, the capillary wave damping is not significantly different from the value for either of the homopolymers. In an attempt to rationalise this, the viscoelastic surface parameters which contribute to the damping are considered. The surface viscosities for films of PMMA on water are quite different to those for PEO films. The transverse shear viscosity is ~ 10^{-5} mN s m^{-1} for PMMA[13] compared to 10^{-4} mN s m^{-1} for PEO[13] whereas the dilational viscosity could not be determined for any concentration of PMMA. The latter fact implies that either the dilational parameters are very small or that the coupling between the dilational and capillary waves is particularly weak for PMMA. From a consideration of γ' alone it is perhaps rather surprising that the capillary wave damping is found to be fairly similar for both PMMA and PEO spread on water. For PEO γ' is an order of magnitude greater than for PMMA and it would be expected that correspondingly Γ would be larger. In fact as seen for

the graft copolymers ε′ for PEO[13] is large in magnitude but negative and acts to offset the increase in Γ that would be caused by the action of γ′ alone, see chapter 4, section 4.5.4.2. From a consideration of the homopolymers' behaviour one would expect the capillary wave damping to be larger for the 'dual' system being studied here. Making the drastic assumption that viscoelastic behaviour of the PMMA / PEO system is additive, contributions to the overall γ′ from both PEO and PMMA would be anticipated to be offset to a lesser extent by the same negative ε′. This comment is supported by the observation that ε′ does not exhibit any variation from the value for a PEO solution despite the presence of PMMA, see figure 5.5.7. In addition the subphase viscosity is greater than for the case of either of the spread films which would be predicted to cause Γ to increase even more. Given all the above considerations it would be expected that the waves on the PMMA / PEO system would be considerably more damped than for either of the homopolymers on water. This is at odds with the experimental data and in fact the values are comparable. This may indicate that assuming additivity of the separate surface viscosities is incorrect. This is not particularly surprising, especially given that the experimental data indicate surface organisations and behaviour different from either of the components. Clearly, the viscoelastic behaviour of the PMMA / PEO system is rather more complicated than can be explained by simply adding influences of the separate systems. Thus the relatively low damping, despite the presence of two components, is unexpected and cannot be accounted for. Further consideration of the viscoelastic parameters may assist understanding but at this stage it is concluded that rather unexpectedly the damping is not significantly different to a PMMA /water system.[13] Despite the ambiguities regarding the details of the behaviour it is clear that both ω_o and Γ exhibit behaviour which shows characteristics of PMMA and PEO. This is entirely consistent with the results of the neutron reflectometry study which shows that, certainly up to $\Gamma_s = 3$ mg m^{-2}, the two polymers form a mixed film at the interface.

5.5.4.2 The Surface Viscoelastic Parameters

Attention is now turned to the results of the spectral fits, again concentrating on comparisons with the separate polymers.

It has already been mentioned that there is a significant discrepancy between the static and dynamic surface tensions. This in itself, is not necessarily unexpected and has been

observed for other systems where such behaviour has been attributed to frequency dependent relaxation processes.[13,28] Generally, in such situations the dynamic surface tension value is predicted to be greater than the static value. In contrast, for this system the dynamic value of the surface tension is actually lower than the static value. This appears to indicate that there must be a 'negative' relaxation process, so that the zero frequency value is largest. The physical interpretation of this observation is not understood at this stage. At the simplest level it suggests that, as for the graft copolymers, phenomenological models do not suffice to explain the behaviour of these systems.

The dilational parameters ε_o and ε' both appear to be independent of the surface concentration of PMMA on the PEO solution. From the calculation of the static elastic moduli, figure 5.5.6 it was expected that the dynamic values would also vary quite markedly with Γ_s and generally exceed the value of 0.5 mN m^{-1} found using light scattering. As well as appearing independent of PMMA surface concentration, the dilational viscosity is negative having a value of -1.3×10^{-4} mN s m^{-1}. This is essentially the same value found for bare PEO solution, as is the dilational modulus, see the data for $\Gamma_s = 0$. Thus, it seems that the presence of PMMA has a negligible influence on the dilational parameters. This is consistent with a study of PMMA on water in which it was reported that it was not possible to extract the dilational parameters.[13] This may be interpreted in two ways. It is possible that the dilational parameters are very small and beyond the experimental sensitivity, although static measurements of ε_{oST} do not support this. A more plausible explanation is that the difficulties in determining ε_o and ε' are symptomatic of the capillary and dilational waves being particularly weakly coupled in the presence of PMMA. This is consistent with the high values of ε_{oST} for PMMA with the consequence that the capillary waves are only weakly influenced by the dilational waves, hence the difficulties in extracting ε_o and ε'.

The fact that the dilational parameters were successfully determined for the PMMA / PEO system indicates that, in contrast to the PMMA water system,[13] the coupling between the dilational and capillary waves is appreciable. This is assumed to be a consequence of the different surface organisation of the PMMA in the two environments, as well as the presence of PEO. The combination of these effects is such that the capillary waves retain their sensitivity to the dilational parameters. This is consistent with the different static moduli of the two systems. For PMMA on water the values reach up to 34 mN m^{-1} at surface

concentrations up to 2 mg m^{-2}. For the same concentration range when PMMA is spread on PEO the values are less than 10 mN m^{-1}.

The fact that the dilational parameters are as for PEO solution implies that the dilational modes are predominantly influenced by PEO. Assuming that this is correct, it is clear from the results presented here, combined with the neutron reflectometry results, that both ε_0 and ε' are independent of changes in the surface organisation of the PEO. Thus, it is suggested that, as for the graft copolymers, provided one factor is satisfied, ε_0 and ε' will not change. Given the emphasis put on the influence of subphase penetration for the graft copolymers this may also apply here. This suggestion is highly applicable to this system given that the PEO is contained in the subphase and given the observation that negative ε' are only observed when the spread PEO films are known to penetrate the subphase. The static dilational modulus is calculated from the surface pressure isotherm which is intimately linked to changes in the surface structure and so the suggestion that the corresponding dynamic parameter, ε_o, is independent of surface organisation seems quite extraordinary. It is believed that the explanation again lies in the concept of 'effective' parameters. Negative dilational viscosities have already been discussed in considerable detail and are viewed as effective parameters, a description which may also apply to the dilational modulus under the same circumstances. The implication of such terminology is that additional processes, which are not parameterised in the current dispersion equation, are influencing the dilational surface modes.

The implication of the SQELS results for PMMA on PEO solution are rather muddled. Despite the unusual discrepancy with the static values, the trends exhibited by γ_0 are in broad agreement with the surface pressure isotherm data. This evidence indicates that γ_0 represents the behaviour of the entire system. The transverse shear viscosity, being rather scattered, is rather more difficult to discuss. The values for PMMA films on water are about a tenth of those for PMMA / PEO and it is not possible to determine whether γ' appears to be influenced by both components. Given that γ_0 represents the behaviour of the system as a whole it is anticipated that γ' will too. Conversely the dilational parameters seem totally oblivious of the presence of the PMMA film and are typical of the values for PEO solution.

To summarise this discussion, it is concluded that the capillary waves are influenced by all the components in the system whereas the dilational waves are influenced predominantly by the PEO.

5.5.5 Stability Study: Introduction

A stability study was also completed using SQELS. In this experiment the PMMA was spread at the required surface concentration covering the entire surface of the PEO solution, films of 3 mg m^{-2} and 0.25 mg m^{-2} were studied.

The aim of this experiment was to investigate in plane inhomogeneity and film stability. If the films were patchy and consisted of condensed islands of polymer moving in and out of the beam, depending on their size, fluctuations in the capillary wave propagation would be seen. If the islands were sufficiently large, with dimensions greater than the illuminated area, only water or film would be contributing to the signal at any one time. Consequently ω_o and Γ would oscillate between the values for pure subphase and film covered subphase. Alternatively if the islands had small dimensions ω_o and Γ would be averaged between the two extremes.

Other effects which may be observed are time dependent relaxations. The films exhibit relaxations which are observed in surface pressure measurements. This translates to changes in the surface tension which will be reflected in the capillary wave frequency.

5.5.6 Results

5.5.6.1. 0.25 mg m^{-2} Film

The capillary wave frequency and damping are presented in figures 5.5.8 and 5.5.9 and clearly neither vary significantly with time. The small scatter on the points is attributed to disturbances in the laboratory over the course of the experiments and appears in a random manner over a discrete time interval. Since the results of analysing each correlation function separately are given, rather than averaging the values for 10 fits as is usual, the effect of any spurious data values will not be averaged out. However there do not appear to be any systematic fluctuations in either ω_o or Γ.

5.5.6.2. 3 mg m^{-2} film

In contrast to the lower concentration film, as figures 5.5.10 and 5.5.11 indicate, there does appear to be some change in the propagation of the capillary wave with time. Within

error the damping is constant at 2500 s^{-1}, although given the rather large errors which accompany the damping subtle variations may be masked. In contrast, there is a marked change in the wave frequency with time. Over the first 500 s, 8 minutes, the frequency increases up to values comparable to those for a clean PEO solution. Subsequently, the variation of the frequency appears to follow an almost sinusoidal variation with a long period. The capillary wave frequency does not become as stable as for the 0.25 mg m^{-2} film even after an hour. Given the variations in frequency it is perhaps surprising that the damping is constant over the entire range.

5.5.7 Discussion

The low concentration film, 0.25 mg m^{-2}, appears to be stable and does not exhibit a relaxation. This is consistent with the results of the stability study on a 1 mg m^{-2} film for which the surface pressure was found to be perfectly stable with time. Given this result it would be expected that any less concentrated films would also be stable. In addition the stability of the frequency and damping indicates that any film homogeneity is either at a smaller scale than the area illuminated by the beam, about 0.03 cm^2, or moves so quickly that over the time of the measurement that the effect is averaged.

The variation in the capillary wave frequency for 3 mg m^{-2} film warrants a more detailed discussion. There does not appear to be a marked random variation in ω_o or Γ indicating, subject to the limitations mentioned above, that the film is homogenous. It is known that the film exhibits an almost exponential relaxation in surface pressure over the first 40 minutes and since, $\Pi = \gamma_{sub} - \gamma_{oST}$ this implies that the surface tension of the interface increases. The dependence of the capillary wave frequency on surface tension is:

$$\omega_o = \left(\frac{\gamma q^3}{\rho} \right)^{0.5}$$

Equation 5.4.3

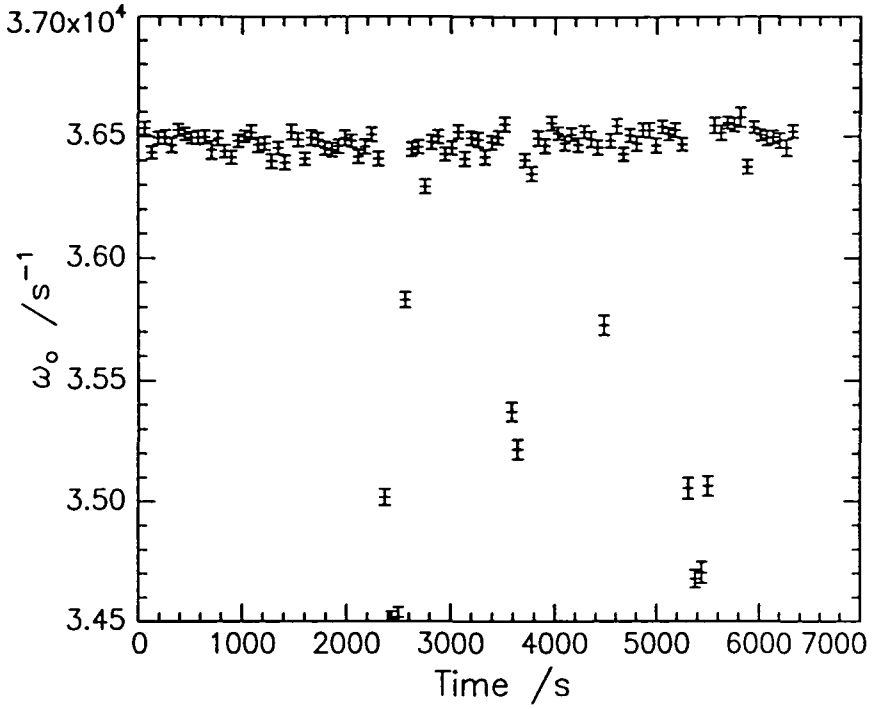

Figure 5.5.8 Variation in the capillary wave frequency for 0.25 mg m^{-2} with time.

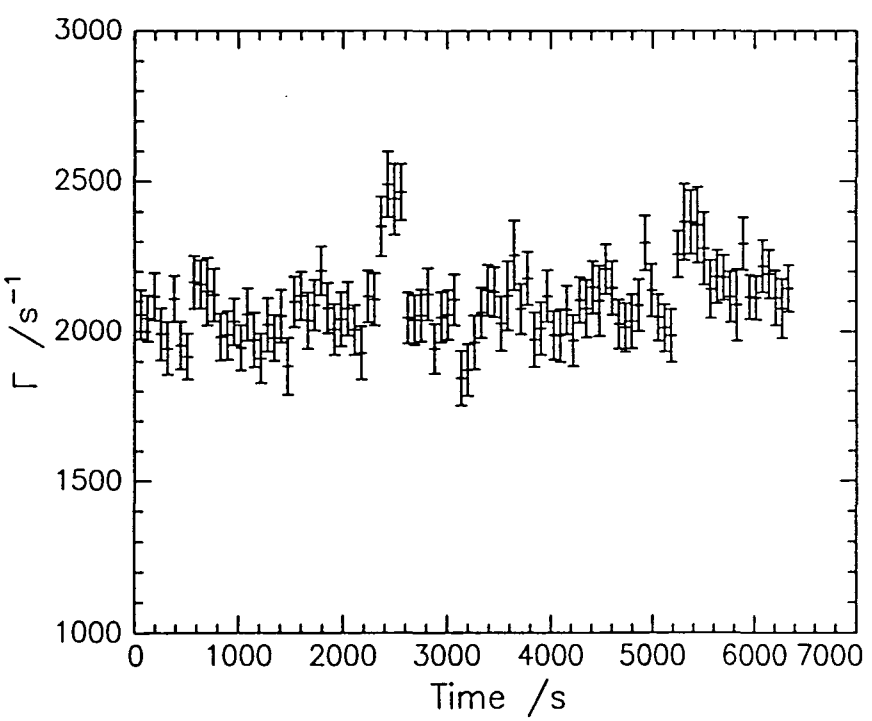

Figure 5.5.9 Variation in the capillary wave damping for 0.25 mg m^{-2} with time.

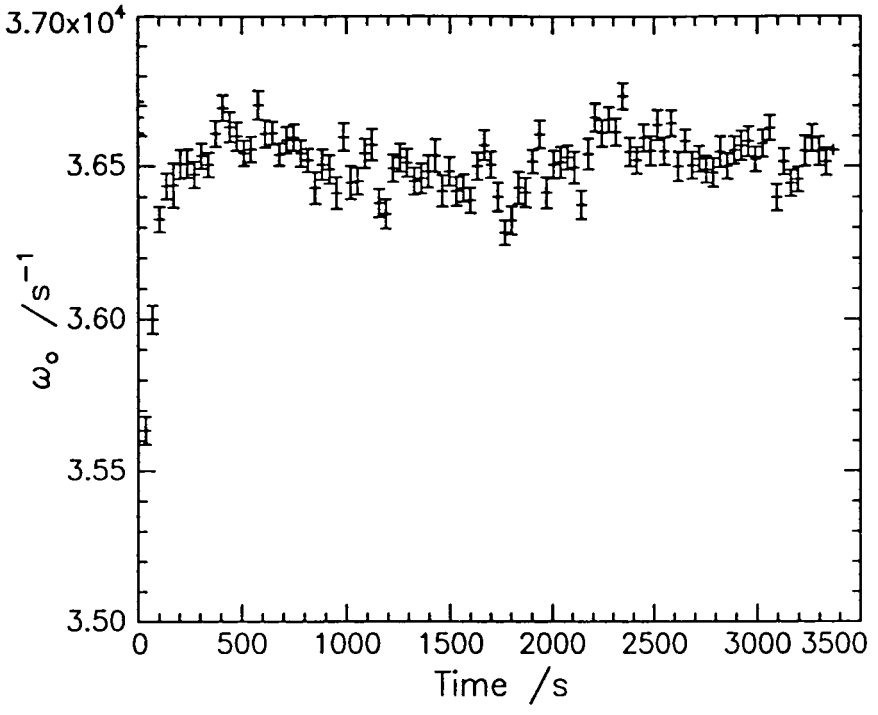

Figure 5.5.10 Variation in the capillary wave frequency for 3 mg m^{-2} with time.

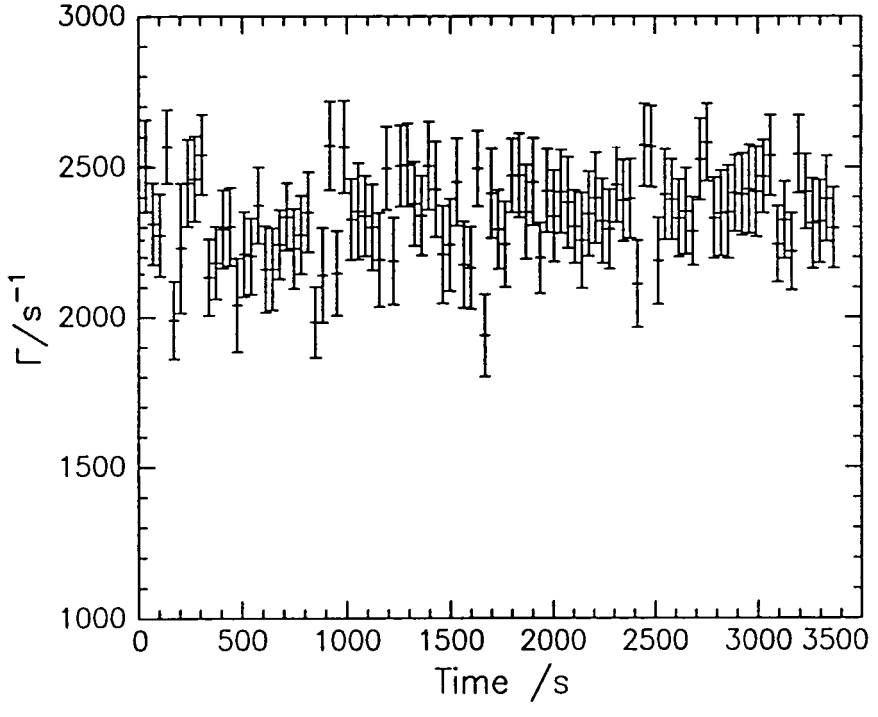

Figure 5.5.11 Variation in the capillary wave damping for 3 mg m^{-2} with time.

It follows from the above that an increase in ω_o is predicted as the film relaxes. The observed increase in the frequency can be rationalised in this way but the anomaly is that the relaxation in the surface pressure occurs over a 40 minute period whereas the marked increase in ω_o only occurs over the first 600 s. Application of the first order approximations enables the frequency change to be expressed in terms of the changes in the surface tension from γ_1 to γ_2:

$$\Delta\omega_o = \omega_2 - \omega_1 = \left(\frac{\gamma_2 q^3}{\rho}\right)^{0.5} - \left(\frac{\gamma_1 q^3}{\rho}\right)^{0.5}$$

$$\Delta\omega_o = \left(\frac{q^3}{\rho}\right)^{0.5} (\gamma_2 - \gamma_1)$$

Equation 5.4.4

When $q = 276\ cm^{-1}$ and $\rho = 997.5\ kg\ m^{-3}$

$$\Delta\omega_o = 141(\gamma_2 - \gamma_1)^{0.5}$$

From the relation above it follows that a change in the capillary wave frequency will only be observed if the increment in the surface tension is significant. In order for the change in the frequency to be outside experimental error $\Delta\omega_o$ must be greater than 100. Substituting $\Delta\omega_o = 100\ s^{-1}$ into equation 5.4.4 it is found that the increment in the surface tension must be 0.5 mN m^{-1}. It follows that a relatively large increase in the surface tension is required if the capillary wave frequencies determined from two successive correlation functions are to show an increase. Given this, it is not surprising that a systematic increase in the surface tension is only observed over the first 500 - 600 s, 8 - 10 minutes, whereas from surface pressure measurements it is known that the surface tension values are not stable until after about 2400 s, 40 minutes. Since the film relaxes exponentially, the largest increment in surface tension will happen over a short time and, it follows, that at sufficiently long times the change in the surface tension will not be sufficient to cause a marked change in the frequency. Hence the observation that the increase in wave frequency occurs over a shorter timescale than the film relaxation can be rationalised.

The subsequent variation in the wave frequency for times greater than 600 s is more complex. There is a systematic decrease in the wave frequency which would indicate a fall in the surface tension. This is not consistent with the surface pressure relaxation data and may indicate a slow change in the film structure. This may correspond to a very slow desorption of the PEO, although there is no other evidence.

Although all the facets of the behaviour of this system are far from being fully understood or reconciled, it is clear that the behaviour exhibited is different from that of the graft copolymers. There was no evidence of any resonant behaviour comparable to that exhibited by the graft copolymers. The transverse shear viscosity was far more scattered in this system and was much smaller than for any of the graft copolymers, for which the values varied between 3 - 5 $\times$ 10^{-4} mN s m^{-1}. In contrast, for PMMA spread on a PEO solution the values did not exceed 2.5 $\times$ 10^{-4} mN s m^{-1}. Despite these differences the most noticeable similarities are between the dilational parameters of the two systems. Ignoring the resonance response behaviour exhibited by the graft copolymers the dependence of ε' at Γ_s above 0.5 mg m^{-2} could be approximated by a horizontal line through -1.4 - 1.7 $\times$ 10^{-4} mN s m^{-1}, see chapter 4 figure 4.5.9. This is not unlike the behaviour exhibited by PMMA on PEO solution. Likewise the values of ε_o for both systems were very low, rather scattered and subject to relatively large errors. These observations appear to confirm the inference that the dilational properties are predominantly influenced by the PEO in these systems. Assuming the latter statement is correct, it is concluded that the magnitude of the dilational properties is independent of the molecular weight of the PEO. This follows since ε' and ε_o are of similar magnitude for the two systems despite the fact that in the graft copolymers the side chains are only 54 units long as opposed to around 2200 units in the PEO used here.

To summarise, it is clear that both the wave propagation and surface viscoelastic parameters are consistent with the presence of both PEO and PMMA. Behaviour of this system is not that unlike the graft copolymers studied, further details of this comparison will be outlined in chapter 6.

Section 5.6 Conclusion

The results of the surface pressure isotherm, neutron reflectometry and SQELS experiments prove that the behaviour of PMMA films spread on a 0.1 wt.% solution of PEO is unique to that of PMMA spread on water. The presence of the PMMA film causes changes in the surface organisation of the PEO which have not been observed elsewhere. The unusual behaviour is not confined to the polymeric species and there are clear indications of an unusual water layer being formed at the surface.

The surface pressure isotherm measurements demonstrated that, on compression, the film does not become as stiff as PMMA on water. In contrast the relaxations exhibited by the films at and above 2 mg m^{-2} are analogous to the behaviour of PMMA on water. The neutron reflectometry study has demonstrated that both the PMMA and PEO occupy a wider region of the interface than when separately spread, or adsorbed, there. At low surface concentrations of PMMA, 1 mg m^{-2}, the polymers mix to form a surface film of PEO, PMMA and water. It was noted in section 5.3 that the onset of surface pressure occurred at lower surface concentrations than for PMMA on water. This indicates that a more homogenous film is formed which, given the evidence from the neutron reflectivity study, can be attributed to incorporation of PEO into the surface film. This is also consistent with the results of the SQELS study where a 1 mg m^{-2} film of PMMA on PEO solution exhibited a constant ω_0 and Γ. This is in contrast to the behaviour of PMMA on water for which the surface wave propagation has been observed to vary between that of water and film covered surface due to 'patchy' films.[13]

When the surface concentration of PMMA increases to 3 mg m^{-2} some of the PEO is squeezed out of the surface film and the water content also falls. This behaviour is consistent with the formation of a dense layer of PMMA. Again, the results of the SQELS stability study are consistent with the formation of a uniform surface film.

The results of the SQELS experiments have been reconciled by the suggestion that whilst the transverse properties, i.e. γ_0 and γ', reflect influences of both PMMA and PEO the dilational properties, ε_0 and ε', are dominated by the PEO. These dilational parameters seem unaffected by the subtle changes in surface organisation and are constant over the surface concentration range 0 - 3 mg m^{-2} of PMMA.

Earlier it was suggested that the presence of PEO at the surface of water when the PMMA is spread may have the action of a compatibiliser. To rationalise the very different behaviour of PMMA spread on PEO solution and PMMA on water it is important to consider the properties of the surface that the PMMA encounters. Due to the presence of adsorbed PEO the surface of the solution will be less hydrophilic than a pure water surface. Given that PMMA is predominantly a hydrophobic polymer, the surface of the solution is anticipated to offer a more favourable environment than a pure water surface. Favourable interactions between PEO and PMMA in bulk[24,25] may translate to additional contributions at the surface. In reality it is likely that a number of contributions combine so that the PMMA mixes with the PEO and populates a wider region of the interface than if spread on water. The fact that PEO solution provides a more favourable interface for PMMA than water was confirmed in the neutron reflectometry study. When a 3 mg m^{-2} film of PMMA is spread on water the parameters fitted to self terms indicate a concentration considerably lower than the amount spread, circa. 1.7 mg m^{-2}. In contrast when the subphase contains PEO the inferred surface concentration is 2 mg m^{-2}. Although the reasons for the substantial discrepancies from amount spread are not understood fully, it is clear that in the presence of PEO more PMMA remains in the interfacial region. This evidence confirms that the PMMA - subphase interactions are rather more favourable in the presence of PEO.

From the discussion above it is clear that spreading a film of PMMA on a solution of PEO results in some unusual behaviour. In addition to providing a useful comparison to more complex copolymers this system exhibits many properties which make it quite fascinating it its own right.

5.7 References

1. J.A. Henderson, R.W. Richards, J. Penfold, R.K. Thomas, *Macromolecules*, **26**, 65, (1993).
2. J.A. Henderson, R.W. Richards, J. Penfold, J.R. Lu, R.K. Thomas, *Macromolecules*, **26**, 4591, (1993).
3. R.W. Richards, B.R. Rochford, J.R.P. Webster, *Faraday Discuss*, **98**, 263, (1994).
4. R.L. Shuler, W.A. Zisman, *J. Phys. Chem.*, **74**, 1523, (1970).
5. J.E. Glass, *J. Phys. Chem*, **27**, 4459, (1968).
6. D.D. Eley, M.J. Hey, J.M. Speight, *J. Chem. Soc., Faraday Trans. 1*, **79**, 755, (1983).
7. D.D. Eley, M.J. Hey, J.M. Speight, *J. Chem. Soc., Faraday Trans. 1*, **84**, 2069, (1988).
8. E.K. Mann, D. Langevin, *Langmuir*, **7**, 112, (1991).
9. V. Bergeron, D. Langevin, *Macromolecules*, **29**, 306, (1996).
10. K. Miyano, K. Asano, *Langmuir*, **7**, 444, (1991).
11. J.R. Charron, R.D. Tilton, *J. Phys. Chem*, **100**, 3179, (1996).
12. J.R. Lu, T.J. Su, R.K. Thomas, J. Penfold, R.W. Richards, *Polymer*, **37**, 263, (1996).
13. R.W. Richards, M.R. Taylor, *J. Chem. Soc. Faraday Trans*, **92**, 601, (1996).
14. R.H.G Brinkhuis, A.J. Schouten, *Macromolecules*, **24**, 1487, (1991).
15. M.S. Aston, *Chem. Soc. Rev.*, **66**, 67, (1993).
16. *Handbook of Chemistry and Physics*, CRC Press Inc., (1988).
17. J.L. Keddie, R.A.L. Jones, R.A. Cory, *Faraday Discuss.*, **98**, 214, (1994).
18. G.P. van der Beek, M.S. Cohen Stuart, G.J. Fleer, *Macromolecules*, **24**, 3553, (1991).
19 J.A. Henderson, PhD Thesis, University of Durham, (1992).
20. T.L. Crowley, E.M. Lee, E.A. Simister, R.K. Thomas, *Physica B*, **173**, 143, (1991).
21. E.A.Simister, E.M. Lee, R.K. Thomas, J. Penfold, *J. Phys. Chem*, **96**, 1373, (1992).
22. J.A. Henderson, R.W. Richards, J. Penfold, R.K. Thomas, *Acta Polymer*, **44**, 184, (1993).
23. L. Nevot, P. Croce, *Phys. Appl*, **15**, 761, (1980).
24. H. Ito, T.P. Russell, G.D. Wignall, *Macromolecules*, **20**, 2213, (1987).
25. I. Hopkinson, F.T. Kiff, R.W. Richards, S.M. King, T. Farren, *Polymer*, **36**, 3523, (1995).
26. B.B. Sauer, H. Yu, *Macromolecules*, **22**, 786, (1989).
27. B.B. Sauer, H. Yu, M. Yazdanian, G. Zografi, M.W. Kim, *Macromolecules*, 22, 2332, (1989).
28. R.W. Richards, B.R. Rochford, M.R. Taylor, *Macromolecules*, **29**, 1980, (1996).

Chapter Six

Conclusions and Further Work

6.1 Conclusions

The motivation for studying films of PMMA on PEO solutions was, primarily, to provide a system intermediate between studies on the individual homopolymers and more complex copolymer systems. Given this it is valuable to compare the behaviour exhibited by this system and the graft copolymers.

Consider the surface pressure isotherms of the graft copolymers, section 4.3, chapter 4. On inspection it was possible to identify behaviour associated with the constituent homopolymers. At low Γ_s behaviour was PEO like, the PMMA characteristics increasing with Γ_s. By comparison with the isotherm of spread films of PEO it has been shown that the graft copolymers exhibit behaviour which is correlated to PEO content. In contrast the isotherms of PMMA on PEO solution, certainly up to 2.5 mg m^{-2}, are quite unlike those of spread films of PMMA or PEO, see section 5.3, chapter 5. The only correlation is observed at high surface concentrations, above 3 mg m^{-2}, where the surface pressure exhibits a rapid increase, behaviour analogous to PMMA on water at 1 mg m^{-2}. It follows that the isotherm behaviour of the graft copolymers is unique to that of PMMA on PEO solution. The difference in behaviour may be associated to the different surface organisations adopted by the components. In addition to these effects in plane structure, notably the lateral forces, also have an influence on the isotherm. Given the totally different molecular architectures of the two systems the latter effect is anticipated to be significantly different for the two systems.

Comparison of the results of the neutron reflectivity studies confirms that the systems adopt very different surface organisations. The most direct comparison is provided by considering the self partial structure factor of PMMA for 20CP at Γ_s = 2 mg m^{-2}, Γ_{sMA} = 0.8 mg m^{-2}, and that for a 1 mg m^{-2} film of PMMA on PEO solution.

It is clear from figure 6.1.1 that the self terms exhibit completely different features. Clearly the differences cannot be accounted for by the slight discrepancy in surface concentration of PMMA as the self terms do not scale in the correct manner. The PMMA self term of the graft copolymer was fitted adequately using a single uniform layer, see section 4.4.6, chapter 4. For films of PMMA spread on PEO solution a rather more sophisticated double uniform layer model was required, see section 5.4.4, chapter 5. The behaviour of the self term exhibited by the PMMA backbone of the graft copolymer was shown to be similar to that of the same concentration spread film of PMMA on water. In contrast the organisation

adopted by PMMA spread on PEO solution is very different to that on water and the PMMA occupies a much wider region of the interface.

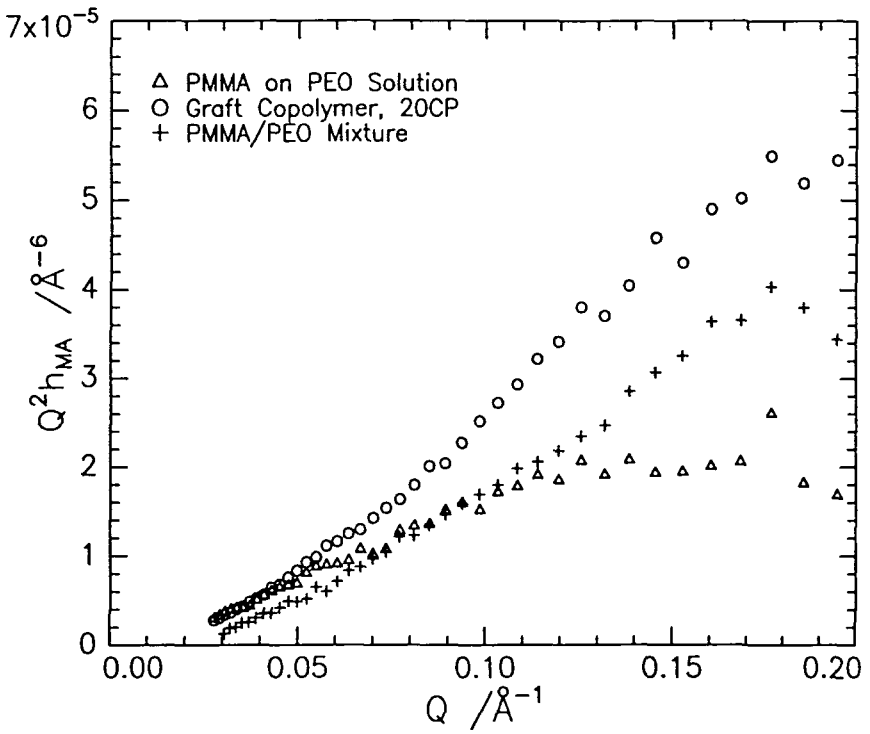

Figure 6.1.1 Comparison of PMMA self partial structure factors for 20CP and PMMA on PEO solution, Γ_{sMA} circa. 1 mg m^{-2}. Also overlaid is the self term for a mixed spread film of PMMA and PEO, see text for discussion.

The very different surface organisation adopted by the PMMA in the two systems is attributed to the fact that the interface presented to spread films of the graft copolymers is different to that when spreading PMMA on PEO solution. In the case of the graft copolymer a clean water surface is encountered. Given the hydrophobic nature of the PMMA it appears reasonable that the backbone of the graft copolymer should behave in essentially the same way as spread films of PMMA and adopt a very similar surface organisation. In comparison when PMMA is spread on a PEO solution the presence of adsorbed PEO will give the surface a different, partially hydrophobic, character. It is believed that the effect is sufficient to cause the PMMA to adopt different interfacial structures in the two circumstances.

The suggestion above can be confirmed, at least in part, by reference to a similar study. Mixed films of PMMA and PEO, where both components are spread at the interface, have also been studied using neutron reflectivity.[1] Consider the PMMA self partial structure factor

for a system containing 70 % by mass of PMMA. When this mixture is spread so that the surface concentration of PMMA is 0.7 mg m^{-2} the partial structure factor is not unlike that for the graft copolymer, see figure 6.1.1. The self terms exhibit the same characteristics, the difference in their magnitude reflecting the lower surface concentration of PMMA in the mixture. This result implies that for a spread mixture of PMMA and PEO, the self term is much like that for PMMA on water at the same surface concentration. This is confirmation that joint occupancy of the surface by PEO and PMMA is not sufficient to modify the behaviour of PMMA. For a marked change in the surface organisation adopted by the PMMA it is essential that the PEO is present in advance of spreading the film.

Comparing the surface organisation adopted by the PEO in the graft copolymer and in the presence of a spread film of PMMA is not so straightforward. It was not possible to determine the self partial structure factor for the PEO side chains in the graft copolymer. Despite this limitation there is evidence to show that the PEO side chains stretch on compression of the copolymer monolayers, particularly when the surface concentration of PEO exceeds 0.5 mg m^{-2}, see section 4.4.6, chapter 4. Compression of the graft copolymer monolayers may be considered to be directly analogous to increasing the spread surface concentration of PMMA on PEO solution. Examining the fitted parameters in table 5.4.6, in chapter 5, it is clear that for a spread PMMA concentration of 1 mg m^{-2} the PEO populates a region approximately 37 Å thick in the interfacial region. When the surface concentration of PMMA is doubled to 2 mg m^{-2} the dimensions barely change, 30 Å, and at 3 mg m^{-2} of PMMA a layer approximately 37 Å thick is formed. Similarly, the total surface excess of PEO remained the same in all the situations at 0.5 mg m^{-2}. These results are consistent with the hypothesis that the PEO side chains of the grafts stretch in an attempt to maintain the number density of the PEO at the value where $\Gamma_{sEO} = 0.5$ mg m^{-2}.

At a more general level this observation provides information about the behaviour of PEO at a water surface. Considering a number of PEO systems a surface concentration of 0.5 mg m^{-2} recurs as representing a transition in behaviour. Not only is this the surface excess formed at the surface of a solution, certainly up to bulk concentrations of 0.1 wt.%, but in addition it is the surface concentration that, for spread films of PEO, corresponds to penetration of the subphase.[2] For films of PMMA on PEO solution, although the details of the surface organisation adopted by the PEO are different to that of 'normal' adsorbed layers, the surface excess is exactly the same. This is despite the fact that spreading PMMA on the surface clearly modifies the surface organisation, leading to the formation of two layers, one

dense and one diffuse. It is suggested that the similarities in the width of the interface occupied by the PEO are coincidental. The more fundamental parameter is believed to be the surface concentration and maintaining a surface excess of 0.5 mg m^{-2}. Presumably the increasingly diffuse layers of PEO are formed as the PMMA occupies the interface. However, despite the PMMA occupying the uppermost surface the PEO maintains the same Γ_s. The motivation for such behaviour is not clear. From a consideration of the surface tension for PMMA on PEO solution one would predict, or could at least rationalise, desorption of PEO, see section 5.3, chapter 5, evidently this is not the case. It appears that consideration of surface tension alone is not sufficient to explain behaviour.

Comparison of the water self partial structure factors for the graft copolymer and PMMA on PEO solution at Γ_s = 1 mg m^{-2}, as would be expected, leads to the observation that the values are rather different. This is believed to reflect the behaviour of the PEO in the two systems. For PMMA on PEO solution the surface excess of PEO will be in a dynamic equilibrium with the solution. In comparison because the PEO side chains are forced to remain at the interface the water layers reflect the behaviour of the system as it attempts to reduce Γ_{sEO}.

Having established the main features of the surface organisation adopted by these systems the rather more ambiguous characteristics of surface wave propagation are considered. Rather than highlight the differences in the behaviour exhibited by the two systems, attention is focused on the similarities.

Consider first the capillary wave propagation. It was clear that in both systems the parameters which influence this behaviour most directly, γ_o and γ', are consistent with the surface pressure isotherm data and the influence of both PEO and PMMA. The most notable features exhibited by both the systems studied are the dilational parameters. Only a limited comparison is possible because data are only available at a single q for PMMA on PEO solution.

To make this comparison the dilational parameters, ε_o and ε', have been overlaid and are given in figures 6.1.2 and 6.1.3. Note that the values for PMMA on PEO solution were determined at q = 276 cm^{-1}. The values for 60CP at q = 220 cm^{-1} are overlaid and the surface concentration have been expressed in terms of PMMA surface concentration.

Examination of figures 6.1.2 and 6.1.3 demonstrates that the dilational parameters are of the same order for the two systems. In both cases ε' is negative and ε_o low. In fact given the discrepancy in the q values which these data correspond to, it is concluded that the values

are essentially the same. From the frequency dependent study of the graft copolymers it was observed that ε' becomes less negative as the frequency increases, the increase being most rapid at lower frequencies. Similar behaviour is exhibited in frequency dependent studies of PEO solutions.[3] It is therefore assumed that this behaviour translates to films of PMMA on PEO solution. Thus the observation that ε' is less negative for PMMA on PEO solution than for the graft copolymers is attributed to the different q values. It follows that, apart from the resonant response observed in the dilational parameters for the graft copolymer, the two systems exhibit similar characteristics. This observation seems to be consistent with the suggestion, which has already been made in regard to both systems separately, that it is the PEO which predominantly influences the evolution of the dilational parameters. This is supported by the fact that for spread films of PMMA it is not possible to even extract ε_0 and ε'.[3] It should be noted that the above discussion relies on the tacit assumption that the parameters extracted and called ε_0 and ε' represent the same processes in all the systems mentioned. It has been suggested that where ε' is negative the parameters are 'effective' in which case this may invalidate comparisons with PMMA on water.

The implications of the behaviour observed in this study are summarised briefly below. It is clear that very different interfacial organisations may be formed, even when essentially the same species populate the interface. It is concluded that, not surprisingly, the interfacial structure is inherently linked to the molecular architecture of the species. The capillary wave propagation also seems to be linked to these features, and is clearly influenced by all the species at the interface. Conversely, ignoring the resonance type behaviour exhibited by the graft copolymers, the characteristics of the dilational wave propagation are very similar for both systems. This implies that where processes are linked to these parameters either system would respond in much the same way. Thus ε_0 and ε' are not sensitive to the quite marked changes in surface organisation either between the two systems or on compression of the films. This indicates that it may be possible to modify surface organisation, for example by the presence of an adsorbed layer, without compromising features of dilational wave propagation.

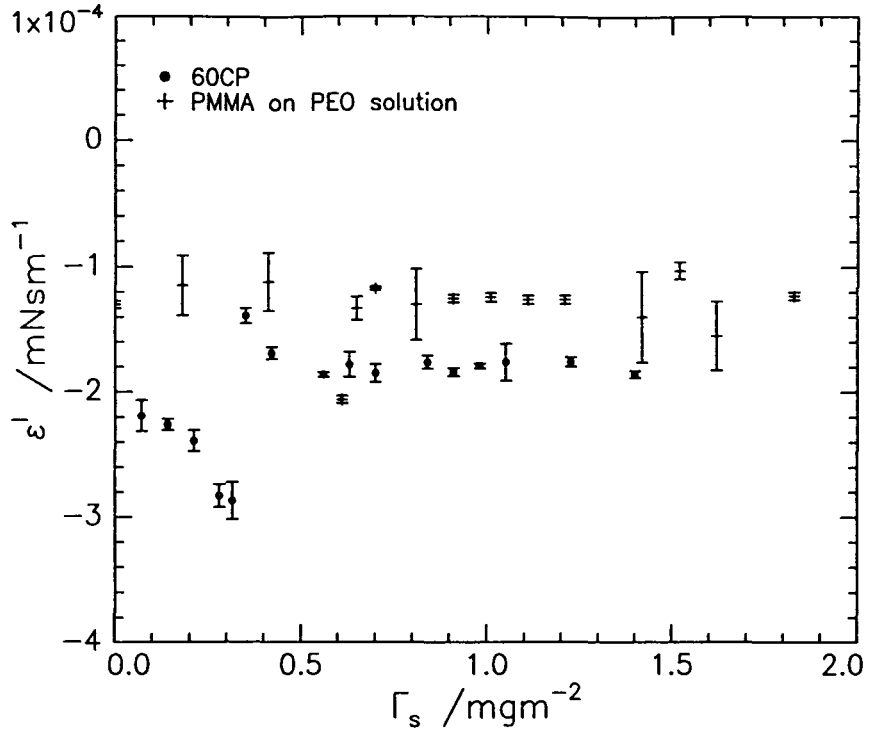

Figure 6.1.2 Dilational viscosity for 60CP as a function of PMMA surface concentration overlaid with the values for PMMA on PEO solution.

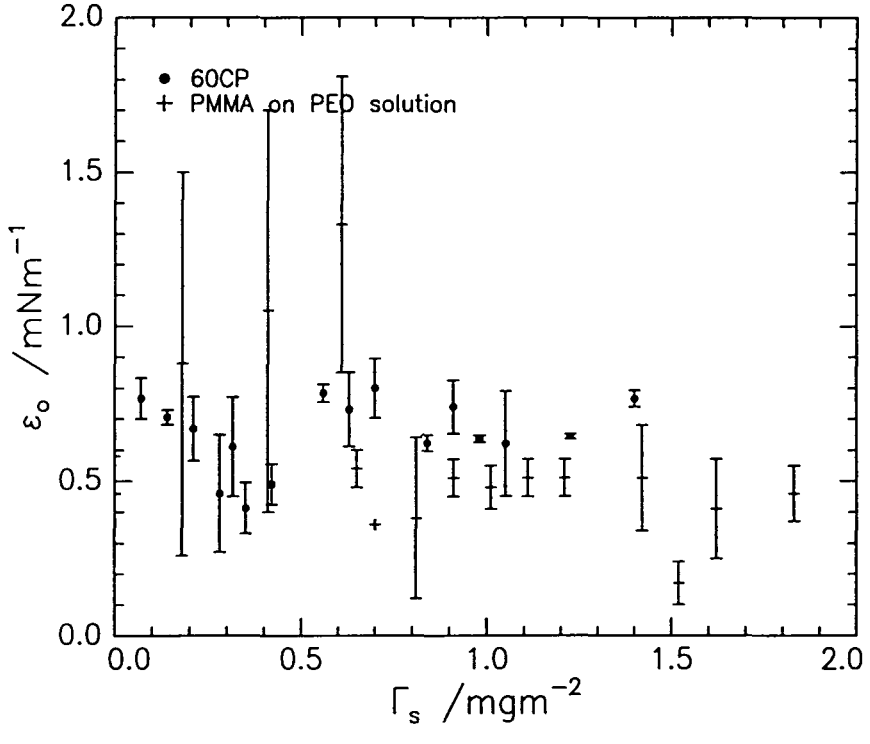

Figure 6.1.3 Dilational modulus for 60CP as a function of PMMA surface concentration overlaid with the values for PMMA on PEO solution.

6.2 Further Work

Clearly there remains some speculation regarding some of the effects mentioned above. Questions arise as to whether the surface organisation adopted by the PMMA could be enforced by the presence of a low molecular weight surfactant, how important is the fact that PEO and PMMA are miscible in the bulk? Studies of this nature, especially if they can be extended to liquid - liquid interfaces, may have direct application to industrial uses of polymeric stabilisers where there are likely to be a variety of components.

In addition to these questions, which are perhaps rather specific, are those regarding the surface wave propagation. It is clear that processes are occurring at the surface which are influencing the surface waves in a manner which is not understood currently. Recent work[3,4,5,6] has shown that similar effects are being discovered in a number of other systems. This study adds to this growing body of work and it is hoped that in the near future these ambiguities will be resolved.

6.3 References

1. S.K. Peace, R.W. Richards, unpublished results.
2. J.A. Henderson, R.W. Richards, J. Penfold, R.K. Thomas, *Macromolecules*, **26**, 65, (1993).
3. R.W. Richards, M.R. Taylor, *J. Chem. Soc. Faraday Trans*, **92**, 601, (1996).
4. J.C Earnshaw, E. McCoo, *Langmuir*, **11**, 1087, (1995).
5. M.R. Taylor, R.W. Richards, in preparation.
6 J.C. Earnshaw, D. J. Sharpe, *J. Chem Soc. Faraday Trans*, **92**, 611, (1996).

Appendices

Appendix A: Cross Term between a double uniform Layer and tanh profile

For two uniform layers: $n(z) = n_A \quad 0 < z < d_A$

$n(z) = n_B \quad d_A < z < d_B$

Otherwise $n(z) = 0$

It follows that

$$n(Q) = \int_0^{d_A} n_A \exp(iQz)dz + \int_{d_A}^{d_B} n_B \exp(iQz)dz$$

Equation A1.2

$$n(Q) = \frac{-n_A}{iQ}\left[\exp(iQd_A) - 1\right] - \frac{n_B}{iQ}\left[\exp(iQd_B) - \exp(iQd_A)\right]$$

Equation A1.3

The tanh layer is sufficiently odd to assume that it's Fourier transform, $n_T(Q)$, is imaginary:

Let $n_T(Q) = in_{TA}(Q)$

It follows that the water partial structure factor is given by:

$$h_w = |n_T(Q)|^2$$

The Q dependence of h_w has been omitted for clarity

The cross term is defined by: $h_{ij}(Q) = \mathrm{Re}\left|n_i(Q).n^*_j(Q)\exp(iQ\delta)\right|$

Equation A1.4

Using Euler's Formula, $\exp(i\theta) = \cos\theta + i\sin\theta$, Equation A1.3 can be written:

$$n(Q) = \frac{-n_A}{iQ}\left[\cos(Qd_A) + i\sin(Qd_A) - 1\right] - \frac{n_B}{iQ}\left[\cos(Qd_B) + i\sin(Qd_B) - \cos(Qd_A) + i\sin(Qd_A)\right]$$

Equation A1.5

Let $n(Q) = n_j(Q)$, $n_T(Q) = n_i(Q)$

$$n^*_j(Q) = -\frac{n_B}{Q}\sin Qd_B + \frac{n_B}{Q}\sin Qd_A - \frac{n_A}{Q}\sin Qd_A + \frac{n_B}{Q}\cos Qd_A - \frac{n_B}{Q}\cos Qd_B + \frac{n_A}{iQ} - \frac{n_A}{Q}co$$

Equation A1.6

Substitute for n*j(Q) and $n_i(Q)$ in Equation A1.4 and expand exp(iQδ) using Euler's formula. Taking real parts only:

$$Q^2 h_{ij} = (h_W)^{\frac{1}{2}}\begin{pmatrix}\cos(Qd_A)\cos(Q\delta)(n_B - n_A) + (n_B - n_A)\sin(Qd_A)\sin(Q\delta) - n_B\cos(Qd_B)\cos(\\ -n_B\sin(Qd_B)\sin(Q\delta) + n_A\cos(Q\delta)\end{pmatrix}$$

Equation A1.7

$$Q^2 h_{ij} = (h_W)^{\frac{1}{2}}\begin{pmatrix}(n_B - n_A)\big(\cos(Qd_A)\cos(Q\delta) + \sin(Qd_A)\sin(Q\delta)\big) + n_A\cos(Q\delta)\\ -n_B\big(\cos(Qd_B)\cos(Q\delta) + \sin(Qd_B)\sin(Q\delta)\big)\end{pmatrix}$$

Equation A1.8

Using the Trig identity: Cos(A – B) = cos A cos B + sin A sin B

Gives the result:

$$Q^2 h_{ij} = (h_w)^{\frac{1}{2}}\big((n_B - n_A)\cos Q(d_A - \delta) - n_B\cos Q(d_B - \delta) + n_A\cos Q\delta\big)$$

Equation A1.9

Appendix B: Conferences, Publications, Lectures and courses attended

B1: Conferences Attended

September 1993	Neutron Beam Users Meeting, Sheffield University.
September 1993	IRC Club Meeting, Durham University.
September 1993	Polymers at Interfaces, Bristol University.
December 1993	RSC Faraday Division, Colloid and Interface Science Group. Dynamics of Surfactant Monolayers, London.
April 1994	Macro Group (U.K.) Family Meeting, Birmingham University.
April 1995	IRC Polymer Physics Course, Leeds.
April 1995	Neutron Beam Users Meeting, Manchester University.*
April 1995	RSC Annual Chemical Congress, Herriot Watt University.*
September 1995	IRC Club Meeting, Durham University.*
September 1995	Intersociety Polymer Meeting, Baltimore, USA.*
November 1995	Highlights of UK Chemistry Research 1995.**
April 1996	Macro Group Family Meeting, Manchester University.**
April 1996	ICI Colloid and Surface Science Symposium.*

* indicates poster presentation by the author.

** indicates oral presentation by the author.

B2: Publications

S.K. Peace, R.W. Richards, to be published in Polymer 1996

B3: Lectures Attended

Only lectures attended by the author are shown.

Academic Year 1993 / 1994

October 4	Prof. F.J. Feher, University of California, Irvine, USA Bridging the Gap between Surfaces and Solution with Sessilquioxanes
October 14	Dr. P. Hubberstey, University of Nottingham Alkali Metals: Alchemist's Nightmare, Biochemist's Puzzle and Technologist's Dream
October 20	Dr. P. Quayle, University of Manchester Aspects of Aqueous ROMP Chemistry
November 10	Prof. M.N.R. Ashfold, University of Bristol High Resolution Photofragment Translational Spectroscopy : A New Way to Watch Photodissociation
January 26	Prof. J. Evans, University of Southampton Shining Light on Catalysts
February 23	Prof. P.M. Maitlis, University of Sheffield Across the Border : From Homogeneous to Heterogeneous Catalysis
March 9	Prof. F. Wilkinson, Loughborough University of Technology Nanosecond and Picosecond Laser Flash Photolysis
March 2	Dr. C. Hunter, University of Sheffield Noncovalent Interactions between Aromatic Molecules

Academic Year 1994 / 1995

October 5	Prof. N. L. Owen, Brigham Young University, Utah, USA Determining Molecular Structure - the INADEQUATE NMR way
October 19	Prof. N. Bartlett, University of California Some Aspects of Ag(II) and Ag(III) Chemistry
November 2	Dr P. G. Edwards, University of Wales, Cardiff The Manipulation of Electronic and Structural Diversity in Metal Complexes - New Ligands
November 9	Dr G. Hogarth, University College, London New Vistas in Metal-imido Chemistry

December 7	Prof. D. Briggs, ICI and University of Durham Surface Mass Spectrometry
March 1	Dr M. Rosseinsky, Oxford University Fullerene Intercalation Chemistry
March 22	Dr M. Taylor, University of Auckland, New Zealand Structural Methods in Main-group Chemistry
April 26	Dr M. Schroder, University of Edinburgh Redox-active Macrocyclic Complexes : Rings, Stacks and Liquid Crystals

Academic Year 1995 / 1996

October 11	Prof. P. Lugar, Frei Univ Berlin, FRG Low Temperature Crystallography
November 17	Prof. David Bergbreiter, Texas A&M, USA Design of Smart Catalysts, Substrates and Surfaces from Simple Polymers
November 22	Prof. I Soutar, Lancaster University A Water of Glass? Luminescence Studies of Water-Soluble Polymers.
November 29	Prof. Dennis Tuck, University of Windsor, Ontario, Canada New Indium Coordination Chemistry
January 31	Dr J. Penfold, Rutherford Appleton Laboratory, Soft Soap and Surfaces
February 28	Prof. E. W. Randall, Queen Mary & Westfield College New Perspectives in NMR Imaging
February 21	Dr C R Pulham , Univ. Edinburgh Heavy Metal Hydrides - an exploration of the chemistry of stannanes and plumbanes
March 12	RSC Endowed Lecture - Prof. V. Balzani, Univ of Bologna Supramolecular Photochemistry

B4 First Year Induction Courses

The course consists of ten one hour lectures on the services available in the Chemistry Department at Durham University.

Examined Lecture Courses: October 1993 - April 1994

Three courses were attended.

1. X-Ray Diffraction
   Prof. Tanner
   Physics Department

2. FORTRAN Programming
   Six two hour workshops
   Physics Department

3. The Physics of Polymers
   Prof. Richards
   Chemistry Department